

Bulletin of the Geological Society of Denmark



VOLUME 66 | 2018 | COPENHAGEN





Bulletin of the Geological Society of Denmark

is published by the Geological Society of Denmark
(DGF, Dansk Geologisk Forening), founded in 1893

Chief editor

Lotte Melchior Larsen, Geological Survey of Denmark and Greenland (GEUS), Øster Voldgade 10, DK-1350 Copenhagen K, Denmark.
Tel: +45 91333889; E-mail: lml@geus.dk

Erik Thomsen, Department of Geoscience, University of Aarhus, Høegh-Guldbergs Gade 2, DK-8000 Aarhus C, Denmark. Tel: +45 87156443; E-mail: erik.thomsen@geo.au.dk; (palaeontology and stratigraphy).

Scientific editors

Lars B. Clemmensen, Department of Geosciences and Natural Resource Management, University of Copenhagen, Øster Voldgade 10, DK-1350 Copenhagen K, Denmark.
Tel: +45 35322449; E-mail: larsc@ign.ku.dk; (clastic sedimentology, sedimentary basins and palaeoclimatology).

Henrik Tirsgaard, Mærsk olie og Gas AS, Esplanaden 50, DK-1263 Copenhagen K, Denmark. Tel: +45 61209140; E-mail: Henrik.tirsgaard@maerskoil.com; (carbonate sedimentology, petroleum geology and sedimentary basins).

Nicolaj Krog Larsen, Department of Geoscience, Aarhus University, Høegh-Guldbergs Gade 2, DK-8000 Aarhus C, Denmark. Also Natural History Museum of Denmark, University of Copenhagen, Øster Voldgade 5–7, DK-1350 Copenhagen K, Denmark. E-mail: nkl@geo.au.dk; (Quaternary geology).

J. Richard Wilson, Department of Geoscience, University of Aarhus, Høegh-Guldbergs Gade 2, DK-8000 Aarhus C, Denmark. Tel: +45 25321169; E-mail: jrw@geo.au.dk; (igneous petrology and geochemistry).

Jesper Milàn, Geomuseum Faxe, Østsjællandss Museum, Østervej 2, DK-4640 Faxe, Denmark.
Tel: +45 23319488; E-mail: jesperm@oesm.dk; (palaeontology).

The *Bulletin* publishes contributions in all fields of geological sciences on results of new work on material from Denmark, the Faroes and Greenland. Contributions based on foreign material may also be submitted to the *Bulletin* if the subject is relevant for the geology of the area of primary interest. The rate of publishing is one volume per year. All articles are published as pdf-files immediately after acceptance and technical production.

Lars Nielsen, Department of Geosciences and Natural Resource Management, University of Copenhagen, Øster Voldgade 10, DK-1350 Copenhagen K, Denmark.
Tel: +45 35322454; E-mail: ln@ign.ku.dk; (geophysics).

Scientific editing and reviewing are done on an unpaid collegial basis; technical production expenses are covered by the membership fees.

Stig Schack Pedersen, Geological Survey of Denmark and Greenland (GEUS), Øster Voldgade 10, DK-1350 Copenhagen K, Denmark.
Tel: +45 21252733; E-mail: sasp@geus.dk; (structural geology, tectonics).

The bulletin is freely accessible on the web page of the Geological Society of Denmark:
<http://2dggf.dk/publikationer/bulletin/index.html>

Jan Audun Rasmussen, Museum Mors, Fossil- og Molermuseet, Skarrehagevej 8, DK-7900 Nykøbing Mors, Denmark.
Tel: +45 42149792;
E-mail: jan.rasmussen@museummors.dk; (palaeontology).

Instructions to authors:

See inside the back cover and also <http://2dggf.dk/publikationer/bulletin/vejledning.html>

Mette Elstrup Steeman, Museum Sønderjylland, Naturhistorie og Palæontologi, Lergravsvej 2, DK-6510 Gram, Denmark. Tel: +45 73820909; E-mail: mese@museum-sonderjylland.dk; (palaeontology)

Cover photo: Landsat image of the Øresund region with the cities Copenhagen in Denmark and Malmö in Sweden, and the bridge and tunnel connecting them. The two countries have common interests in the geothermal potential in the region. See this volume pp. 123–149: M. Erlström *et al.*: Stratigraphy and geothermal assessment of Mesozoic sandstone reservoirs in the Øresund Basin – exemplified by well data and seismic profiles. Image credit: NASA/GSFC/METI/ERSDAC/JAROS, and U.S./Japan ASTER Science Team.

Stratigraphy and geochemical composition of the Cambrian Alum Shale Formation in the Porsgrunn core, Skien–Langesund district, southern Norway

NIELS HEMMINGSEN SCHOVSBO, ARNE THORSHØJ NIELSEN, ANDREAS OLAUS HARSTAD
& DAVID L. BRUTON



Schovsbo, N.H., Nielsen, A.T., Harstad, A.O. & Bruton, D.L. 2018. Stratigraphy and geochemical composition of the Cambrian Alum Shale Formation in the Porsgrunn core, Skien–Langesund district, southern Norway. © 2018 by Bulletin of the Geological Society of Denmark, Vol. 66, pp. 1–20. ISSN 2245-7070. (www.2dgf.dk/publikationer/bulletin).

The fully cored BHD-03-99 borehole (hereafter referred to as the Porsgrunn borehole and core) penetrated Ordovician and Cambrian strata in the Skien–Langesund district, southern part of the Oslo region in Norway. Hand-held X-ray fluorescence (HH-XRF) measurements combined with spectral gamma ray and density core scanning of the Middle Cambrian – Furongian Alum Shale Formation have been made and compared with similar measurements obtained on Alum Shale cores from Scania (southernmost Sweden) and Bornholm (Denmark). The Porsgrunn drill site is located in an area that was only mildly overprinted by Caledonian tectonics and represents one of the few sites in the Oslo area where a nearly untectonised sedimentary succession can be studied in terms of thickness and geochemistry. The Alum Shale Formation is 28.8 m thick in the Porsgrunn core, excluding the thickness of five 0.9–5.5 m thick dolerite sills of assumed Permian age.

In the Alum Shale Formation the bulk densities are around 2.7 g/cm³ with a slightly decreasing trend up through the formation. The shale has total organic carbon (TOC) values up to 14 wt%, which is comparable to the TOC levels for the Alum Shale elsewhere in the Oslo area and for dry gas matured Alum Shale in Scania and Bornholm. The basal Furongian is characterised by a gamma ray low and an increase in Mo interpreted to reflect the Steptoean Positive Carbon Isotope Excursion (SPICE) event. The Porsgrunn core data suggest that the Mo concentration remained high also after the SPICE event.

Characteristic, readily identified features in the gamma log motif are named the Andrarum gamma low (AGL), base Furongian gamma low (BFGL), *Olenus* triple gamma spike (OTGS) and the *Peltura* gamma spike (PGS). No Lower Ordovician Alum Shale is present. The 14.8 m thick Furongian part of the Alum Shale represents the *Olenus*, *Parabolina*, *Leptoplastus*, *Protopeltura* and *Peltura* trilobite superzones judging from log-stratigraphic correlations to Scania and Bornholm. The Middle Cambrian interval is 14.0 m thick and includes the Exsulans Limestone Bed and 1.4 m of quartz sandstone. A 0.3 m thick primary limestone bed may be an equivalent to the Andrarum Limestone Bed. The succession represents the *Paradoxides paradoxissimus* and *P. forchhammeri* superzones. The Alum Shale Formation rests atop the 13.0 m thick Lower Cambrian Stokkevannet sandstone (new informal name) that in turn directly overlies the basement. Overall, the stratigraphic development of the comparatively thin Alum Shale Formation resembles the condensed sequence seen on Bornholm.

Keywords: Porsgrunn, Alum Shale, Cambrian, Correlation, Scandinavia, Geochemistry.

Niels Hemmingsen Schovsbo [nsc@geus.dk], Geological Survey of Denmark and Greenland (GEUS), Øster Voldgade 10, DK-1350 Copenhagen K, Denmark. Arne Thorshøj Nielsen [arnet@ign.ku.dk], Department of Geosciences and Natural Resource Management, University of Copenhagen, Øster Voldgade 10, DK-1350 Copenhagen K, Denmark. Andreas Olaus Harstad [aoh@ngi.no], Norges Geotekniske Institutt (NGI), Sognsveien 72, N-0806 Oslo, Norway. David L. Bruton [d.l.bruton@nhm.uio.no], Natural History Museum (Geology), University of Oslo, Postboks 1172 Blindern, NO-0318 Oslo, Norway.

Received 13 December 2016
Accepted in revised form
18 June 2017
Published online
5 February 2018

Nowhere in the Oslo region are the Palaeozoic sedimentary rocks more dramatically displayed than in the Skien–Langesund area. High cliffs and local fjord sections expose fossiliferous Cambrian and Ordovician rocks preserved in a series of fault-controlled horsts, which fascinated Brøgger (1884) and his predecessors such as Forbes (1856), Dahl (1856) and Kjerulf (1857). All produced local stratigraphic schemes that were followed in subsequent years by Kiær (1897, 1906), Strand (1934) and Størmer (1953). The succession includes a comparatively thin Alum Shale Formation, briefly referred to by Henningsmoen (1957), based on a cored shallow borehole at Rognstranda (Fig. 1).

Investigation of the Alum Shale Formation in Norway is hampered by the fact that the unit is strongly tectonised in most areas, as the shale acted as decollement level during the Caledonian Orogeny (Ramberg & Bockelie 1981; Bockelie & Nystuen 1985; Nilssen 1985; Owen *et al.* 1990). As a consequence few areas

exist where a detailed undeformed stratigraphy can be studied. The aim of this paper is to examine the cored Porsgrunn borehole that penetrated the entire Alum Shale in the Skien–Langesund district. The examination is based on hand-held X-ray fluorescence (HH-XRF) measurements and spectral gamma and density logs derived from scanning of the core (Figs 1, 2). The paper also demonstrates that long-distance correlation of the Alum Shale is possible, based on consistent gamma log-patterns.

In this paper we use the traditional terms Early/Lower Cambrian (\approx Terreneuvian and Cambrian provisional series 2) and Mid/Middle Cambrian (\approx Cambrian provisional series 3), pending the introduction of formal names for the new Cambrian global series. The Furongian corresponds to the traditional Late/Upper Cambrian except that the *Agnostus pisiformis* Zone is now assigned to the Middle Cambrian.

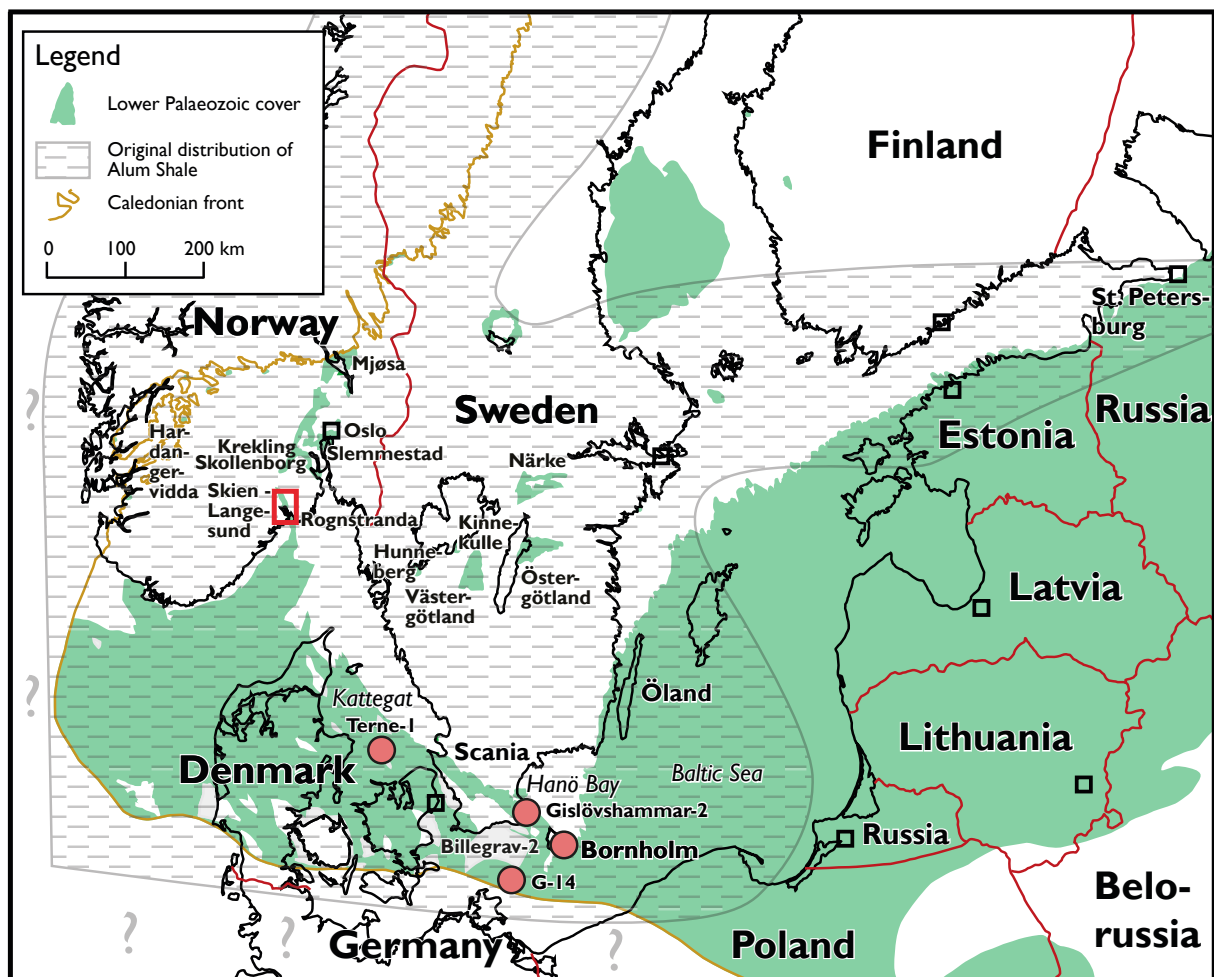


Fig. 1. Outline of approximate original distribution of the Alum Shale Formation and present day occurrence of lower Palaeozoic strata in southern Scandinavia. Boreholes referred to in this work are indicated with red dots. Red square outlines the Eidanger peninsula where the Porsgrunn core is drilled (Fig. 2). The occurrence of lower Palaeozoic strata is modified from Nielsen & Schovsbo (2015) with respect to interpretation of the Hanö Bay area as presented by Sopher *et al.* (2016).

Geological Setting

During the Cambrian, Baltica was positioned at intermediate latitudes in the southern hemisphere, and siliciclastic deposition prevailed (Torsvik *et al.* 1991; Nielsen & Schovsbo 2011). The sea level rose stepwise through the Early Cambrian and eventually all of Scandinavia became covered by a relatively shallow epicontinental sea (Nielsen & Schovsbo 2011, 2015). From the early Mid Cambrian through to the

Tremadocian (Early Ordovician), the offshore parts of this epicontinental sea became characterised by low-oxygen conditions, i.e. from about the storm wave base and deeper. Here the slowly accumulating Alum Shale mud was deposited, comprising dark organic-rich mudstone with abundant disseminated pyrite (for a general discussion of the Alum Shale facies, see Nielsen & Schovsbo 2015 and references therein). Deposition of the Alum Shale took place in an area that extended for more than 800 000 km² across the

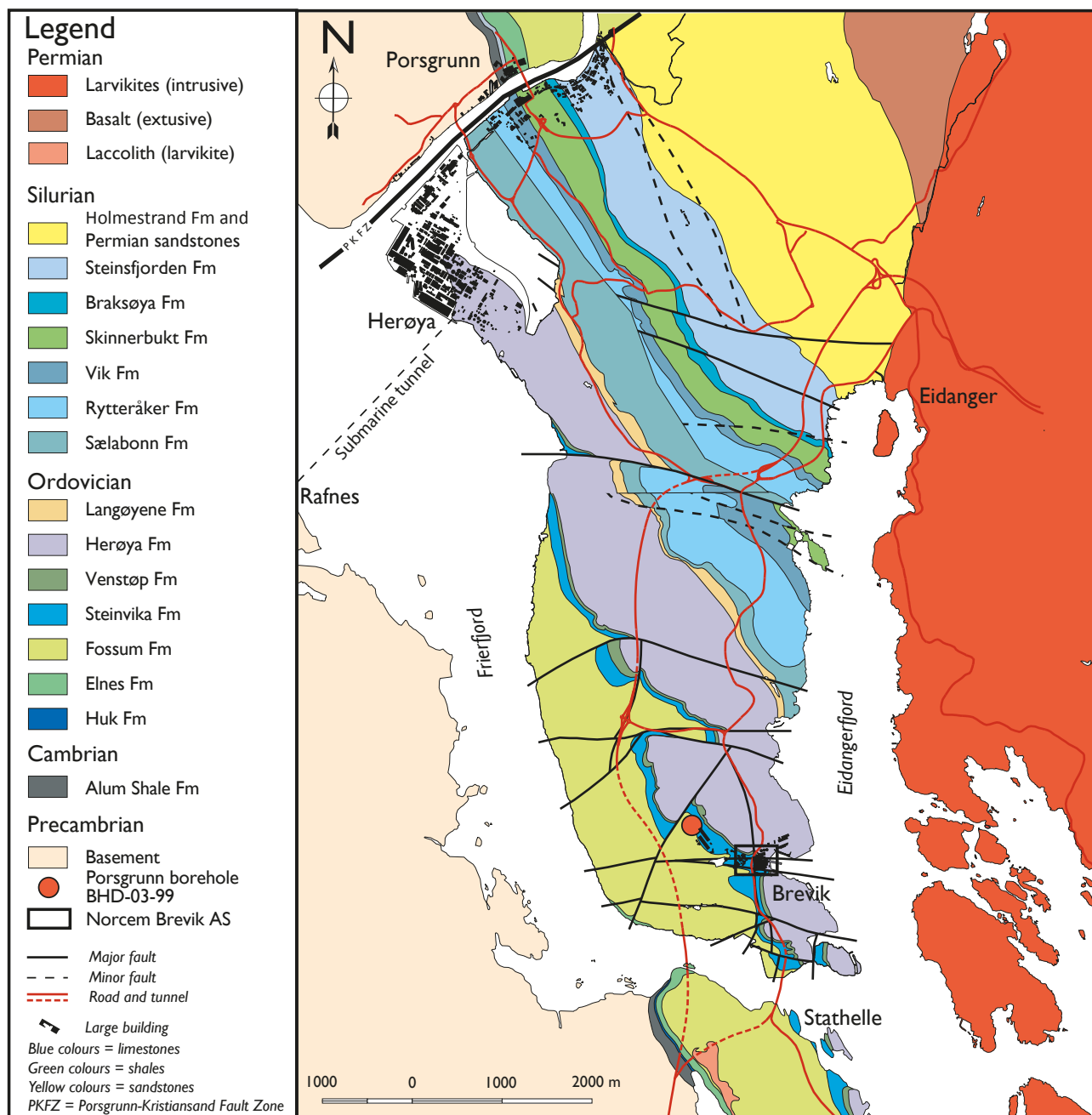


Fig. 2. Geological map of the Eidanger peninsula with the location of the Porsgrunn borehole (BHD-03-99). The surface coordinates for the borehole are 59°03'59.63" N, 9°40'37.19" E and the elevation is 63 m above sea level. Modified from Harstad (2005). Location of tunnel from Lien *et al.* (1978).

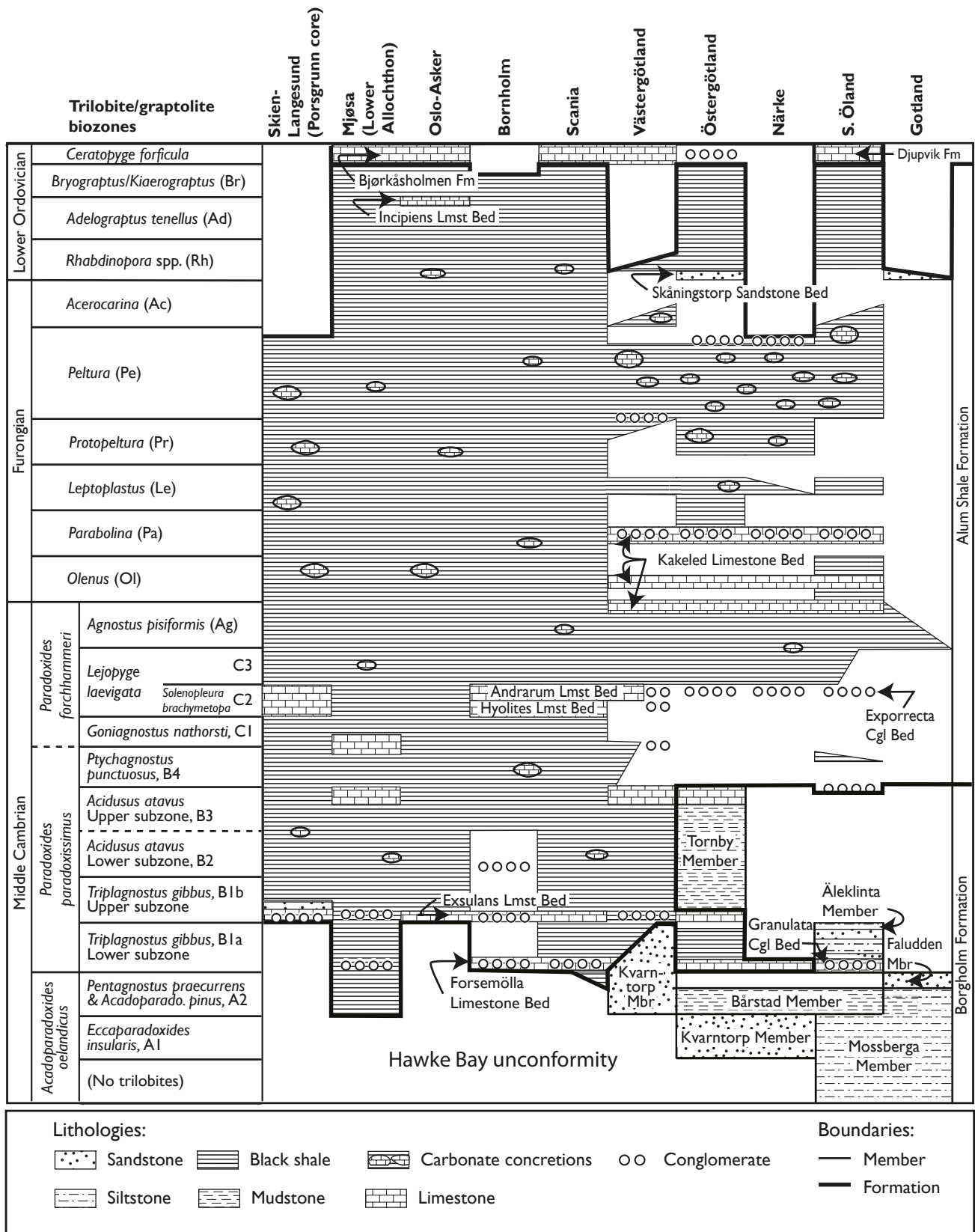


Fig. 3. Stratigraphic development of the Alum Shale in various districts of Scandinavia. For locations, see Fig. 1. The Furongian trilobite stratigraphy is updated according to Nielsen *et al.* (2014). Modified from Nielsen & Schovsbo (2007).

western part of Baltica (Fig. 1; Nielsen & Schovsbo 2015). Throughout this vast area the Alum Shale lithology is remarkably uniform although a mid shelf and an outer shelf facies (termed platform and shelf facies, respectively, by Buchardt *et al.* 1997) have been recognised, based on the abundance of carbonate concretions and stratigraphic completeness (Buchardt *et al.* 1997; Schovsbo 2002; Nielsen & Schovsbo 2007). Buchardt *et al.* (1997) assigned the Alum Shale in the Skien–Langesund area to the platform facies whereas the Alum Shale in the Oslo–Asker area was assigned to the shelf facies. They inferred a local south Norwegian topography referred to as the Telemark Shoal and the Oslo Trough (cf. Buchardt *et al.* 1997, fig. 9). The assignment of the Skien–Langesund Alum Shale to the platform facies was at the time only based on the local thinness of the unit. However, it does not contain much limestone (c. 12%) and no intraformational limestone conglomerate levels and is here considered as a thin outer shelf facies type.

The unit varies considerably in thickness across Scandinavia. In south-central Sweden the Alum Shale is mostly around 20–25 m thick, whereas in Scania and the central Oslo area it varies between 80 and 100 m. The greatest thickness, 178 m, has been encountered in the Danish offshore well Terne-1 (Nielsen & Schovsbo 2007; Schovsbo *et al.* 2016). The shale thins towards the southern margin of Baltica and measures only some 27–34 m on Bornholm (Schovsbo *et al.* 2011, 2015b) and 32 m in the offshore German well G-14 (Piske & Neumann 1993). The Alum Shale apparently also thins towards the western margin of Baltica, being some 30–40 m thick in the Hardangervidda area (Andresen 1978). As reported in the present paper the unit is only 29 m in the Skien–Langesund district located in the southernmost part of the Oslo area (excluding the combined thickness of 15 m of dolerite sills intruded into the formation). The thickness variation reflects repeated erosive events in south-central Sweden linked to sea level lowstands in combination with uplifts of the margins of Baltica. The latter condition may have created a silled basin leading to poor ventilation of the Alum Shale sea (Nielsen & Schovsbo 2015).

The Alum Shale deposited on the southern and western fringes of Baltica became deeply buried in the Caledonian foreland basin during the late Silurian – Early Devonian (e.g. Buchardt & Lewan 1990; Samuelsson & Middleton 1998; Pedersen *et al.* 2007). The Alum Shale acted as decollement level during Caledonian thrusting and the unit is usually strongly tectonised in the Caledonides, including most of the Oslo area. However, the southern part of the Skien–Langesund area, where the Porsgrunn borehole was made, is located outside the Caledonian deformation zone (Bruton *et al.* 2010), but here the lower Palaeozoic

strata have been affected by igneous larvikite intrusions and dolerite sills during the Permian rifting that created the Oslo Graben (Jamtveit *et al.* 1997; Fig. 2).

Despite being deposited under low oxygen conditions, the Cambrian part of the Alum Shale contains a low-diverse, but highly abundant trilobite fauna. This fauna has facilitated the definition of a high-resolution biostratigraphic zonation comprising three Middle Cambrian superzones subdivided into eight zones and six Furongian superzones subdivided into 26 zones (Fig. 3); for review and latest updates, see Terfelt *et al.* (2008), Weidner & Nielsen (2014), Nielsen *et al.* 2014) and Rasmussen *et al.* (2016).

The Alum Shale lithology is remarkably uniform across Scandinavia with a fairly simple lithostratigraphy including several widespread thin event beds (Fig. 3). The unit is enriched in a variety of trace elements, notably U, V and Mo (Armands 1972; Andersson *et al.* 1985; Leventhal 1991; Buchardt *et al.* 1997; Schovsbo 2001, 2002; Dahl *et al.* 2013; Hammer & Svensen 2017). Of these elements the radioactive U has been especially studied both for economic reasons and stratigraphic purposes (Gee 1972; Edling 1974; Hessland & Armands 1978; Andersson *et al.* 1985; Schovsbo 2002).

The gamma ray (Gr) log pattern of the Alum Shale is readily correlated between boreholes (Pedersen & Klitten 1990; Michelsen & Nielsen 1991; Erikson 2012; Schovsbo *et al.* 2015a, 2016; Nielsen *et al.* manuscript in submission 2018). The unique nature of the gamma response of the formation has been used for lithostratigraphic correlation within local areas such as the Oslo Region (Siggerud 1955; Skjeseth 1958; Elvebakk 2011), Bornholm (Pedersen & Klitten 1990; Schovsbo *et al.* 2016), central Sweden (Armands 1972; Hessland & Armands 1978, Andersson *et al.* 1985; Dypvik 1993) and the Caledonian mountain chain (Snäll 1988).

The Porsgrunn core

The investigated core was made available by Norcem Brevik AS. The company is Norway's largest producer of cement and part of the Heidelberg Cement Group. It is situated in the community of Porsgrunn, Telemark County (Fig. 2). The core was drilled in 1999 as part of a work program associated with the establishment of a regional geological stratigraphic reference model. Brevik is situated in the southern end of the Oslo region (Størmer 1953; Bruton *et al.* 2010). Palaeozoic rocks in the area outcrop in a NNW–SSE belt delimited by Precambrian rocks to the west and Permian igneous rocks to the east (Fig. 2). A series of dolerite sills of assumed Permian age intruded into the lower Palaeozoic strata have given rise to low-grade contact metamor-

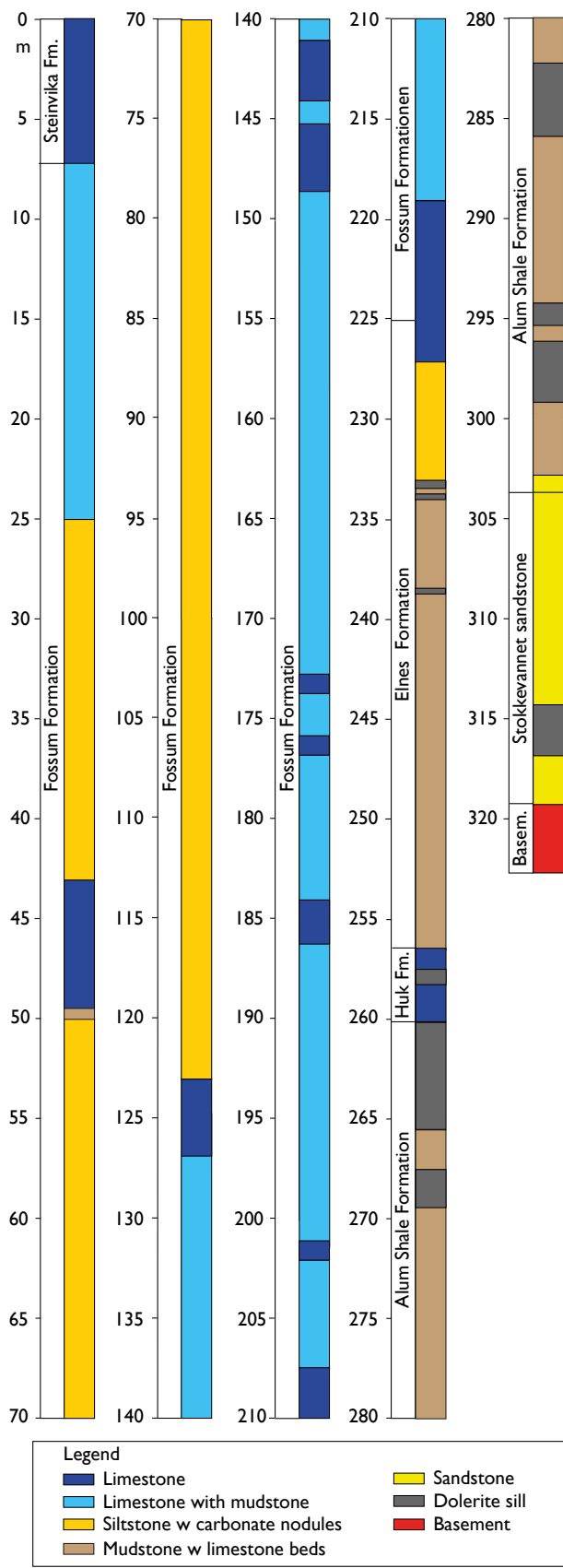


Fig. 4. Overview log of the Porsgrunn (BHD-03-99) core. Based on unpublished log provided by Norcem Brevik AS.

phism. Tectonism caused a general regional tilting to the east; for local details, see Ramberg & Bockelie (1981), Bockelie & Nystuen (1985) and Nilssen (1985).

The Porsgrunn borehole was drilled using conventional mining exploration equipment which provided a continuous 1 inch diameter core. The surface borehole location is in the northern part of the Dalen open pit limestone mine some 900 m north-east of the Norcem cement plant in Brevik, on the southern part of the Eidanger Peninsula (Fig. 2). The borehole was drilled to a total depth of 322.6 m with full core recovery (Fig. 4). Sedimentological logging of the core suggested that none of the known faults in the area intersected the well. Thus, it is assumed that the borehole represents the true stratigraphic thickness of the penetrated rock units. Stratigraphically, the surface location of the borehole is situated 7.2 m above the base of the Middle Ordovician Steinvika Formation (see Owen *et al.* 1990). Below the Steinvika Formation the borehole encountered the Fossum, Elnes, Huk and Alum Shale formations (Fig. 4). The Alum Shale rests on Lower Cambrian sandstone, here informally referred to as the Stokkevannet (named so after Stokkevannet, South of Brevik) sandstone, which in turn overlies the Precambrian gneiss basement (Fig. 4).

Methods

Hand-held XRF core measurements

Concentrations of elements were determined at 365 levels in the core, corresponding to approximately every 15 cm in the interval 322.6–260.0 m. Measuring was done using a hand held Niton™ XI3t Gold+ XRF device (HH-XRF) at the Geological Survey of Denmark and Greenland (GEUS's) Core Analysis Laboratory in Copenhagen, Denmark. The device is equipped with an Ag anode that measures at 6–50 kV and up to 200 μ A and provides semi-quantitative element concentrations. The measuring area is about 5 mm in diameter, and the measuring time was 2 minutes per measuring point, applying the “test all geo filter” that measured dually on low and high filters. Measurements were performed both directly on the curved core surface and on bedding planes where the core had split. Measurements of both in-house and certified powder samples were made to ensure data quality and reliability.

The HH-XRF has proved to be a reliable and stable tool (Dahl *et al.*, 2013; Hammer & Svensen 2017), provided that matrix effects are eliminated by comparison with reference samples with similar matrix (Esbensen & Johansson 2013). For this study the HH-

XRF element concentrations of Si, Al, Ca, Fe, K, Mg, Mn, P, Ti, S, As, Ba, Cu, Mo, Nb, Ni, Pb, Rb, Sr, Th, U, V, Zn, and Zr were compared to element concentrations determined by ICP-MS (inductively coupled plasma mass spectrometry) analysis of a set of eleven representative in-house lower Palaeozoic shale samples. The ICP-MS analyses were carried out on an Elan 6100 ICP-MS instrument at GEUS. Crushed samples were dissolved in HF and HNO₃ acid for two days at 130°C and element concentrations were determined using the Perkin Elmer TotalQuant software that provides semi-quantitative concentrations for 66 elements.

The element concentrations determined by HH-XRF and ICP-MS methods are highly correlated, as reflected in Pearson correlation coefficient (r^2) values generally >0.9 (n=11, Table 1, Fig. 5). Lowest correlation coefficients between the two methods are seen for Mg (no relationship could be established) and for Al (not statistically significant at the calculated probability < 0.1, Table 1). For comparison with literature data, the HH-XRF element concentrations were recalculated using the regression lines for the interdependence of the HH-XRF and ICP-MS results; nine examples are presented in Fig. 5.

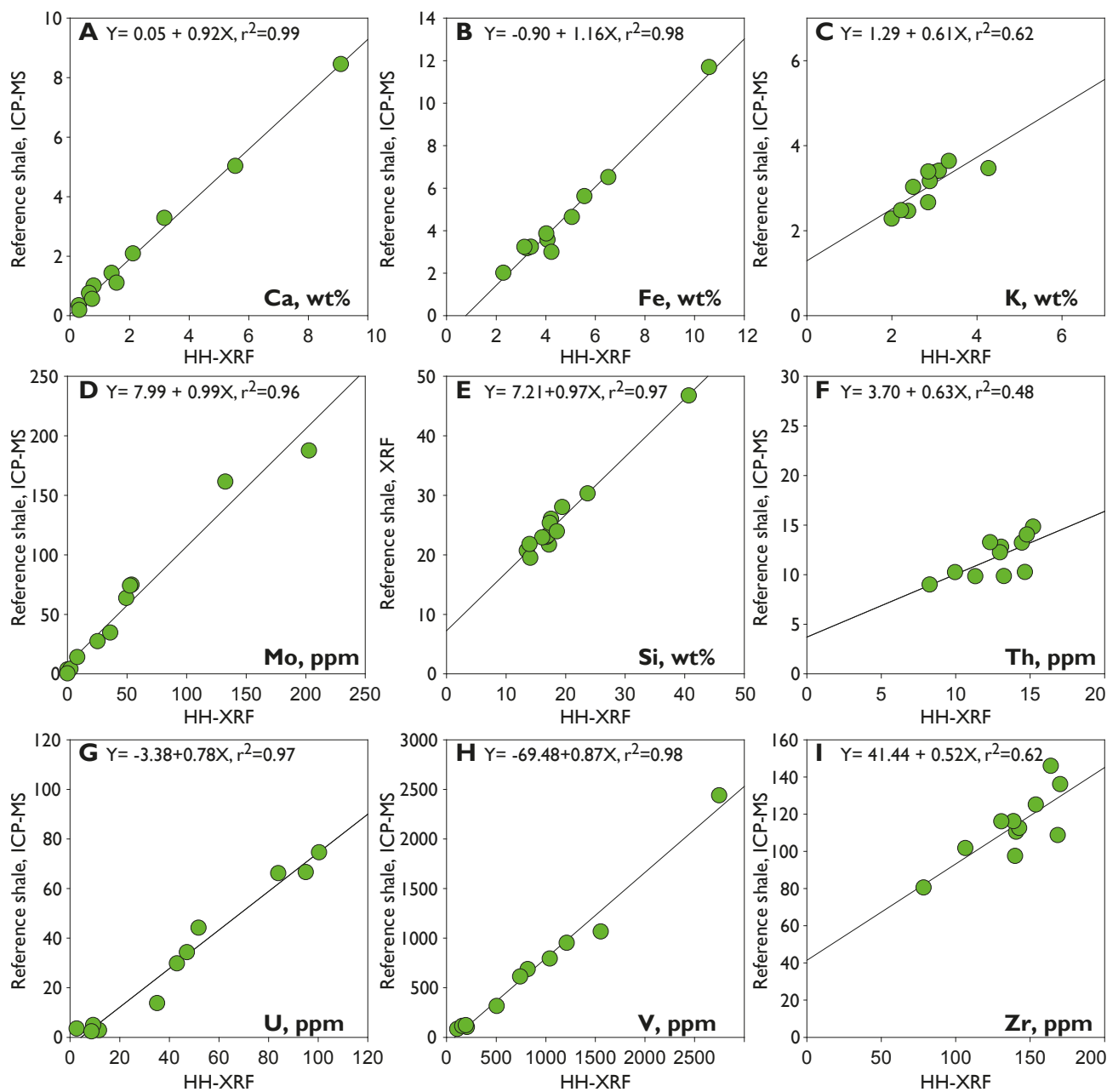


Fig. 5. HH-XRF vs ICP-MS (Total Quant method) comparison for powdered samples.

Table 1. Correlation coefficients and statistical significance levels for correlations between elements determined by HH-XRF and ICPMS analysis of 11 Palaeozoic shale samples from Denmark.

Element	R ² for linear regression	Significant at
	line*	p < 0.10
Al	0.19	no
As	0.99	yes
Ba	0.52	yes
Ca	0.99	yes
Cu	0.98	yes
Fe	0.98	yes
K	0.62	yes
Ni	0.96	yes
Nb	0.23	no
Mn	0.97	yes
Mo	0.96	yes
P**	0.93	yes
Pb	0.91	yes
Rb	0.70	yes
Si***	0.97	yes
Sr	0.99	yes
Th	0.48	yes
Ti	0.48	yes
U	0.97	yes
V	0.98	yes
Zn	0.98	yes
Zr	0.62	yes

* linear conversions used. see Fig. 5 for selected elements.

** for P >200 ppm; N=4.

*** Determined by conventional XRF.

Formation bulk density

The Porsgrunn core interval between 322.6 and 260.0 m was scanned at the GEUS Core Analysis Laboratory using a density scanner equipped with a Cs source for determining the bulk density. The vertical resolution is 1 cm core length. The scanning was performed at a speed of 1 cm/min. Calibration of the scanner was made by running in-house standards with known densities. The scanned density measurements are very sensitive to imperfections such as cracks, fractures, drilling-induced damages, and to poor alignment of the core within the scanner. Generally the core is in very good condition and extra care was taken to align it directly under the sensor and to fit the core pieces together to minimise any effects on the measurements.

Determination of the bulk density was done on 33 core samples, each consisting of an approximately 1 cm long full core. Measurements were done by normalising the weight of the sample relative to the bulk volume measured by submersion of the sample in a

Hg bath using Archimedes' principle. The porosity was determined on the same samples by subtraction of the measured grain volume from the measured bulk volume. The He technique, employing Boyle's Law, was used for grain volume determination, applying a double-chambered helium porosimeter with digital readout. For each measurement stable He volumes were reached in more than 15 minutes to ensure complete filling of the pore volume. For more detailed descriptions of methods, instrumentation and principles of calculation, see American Petroleum Institute (API)'s recommended practice for core analysis procedure (API 1998).

Spectral gamma ray scanning

Spectral gamma ray scanning of the core was done at the GEUS Core Analysis Laboratory in a scanner equipped with two 15 cm NaI (Tl) crystals. Due to the size of the crystals, the U, K, and Th signals are averaged over 15 cm core lengths. Calibration of the spectral gamma ray scanner was made by running in-house standards with known U, K and Th concentrations. After calibration, the core measurements of U, K and Th were rescaled by comparing with the HH-XRF measurements. The gamma ray activity measured by the scanner (counts per second) was converted to Sum gamma ray (SGr) in American Petroleum Institute (API) units according to the algorithm by Ellis & Singer (2007): Sum gamma ray (API units) = 4 × Th (ppm) + 8 × U (ppm) + 16 × K (wt%).

Carbon and sulphur core measurements

Total organic carbon (TOC), total carbon (TC) and total sulphur (TS) contents were measured on 63 acid treated samples in a LECO CS-200 carbon/sulphur analyser at GEUS's Source Rock Laboratory. Dissolution of carbonate was done by treating 0.05 g dried sample with 2M HCl solution at 65°C for 2 hours. The powdered samples were placed together with iron accelerator material in an induction furnace and heated to 1300°C, and the evolved gases were measured by infrared absorption.

Results

Lithostratigraphy

Dolerite sills intrude the section from the basement and up to the base of the Middle Ordovician Huk Formation with an accumulated thickness of 17.5 m. The true thickness of the Alum Shale Formation is

Table 2. Stratigraphic depths and thicknesses of intervals and dolerite sills in the Porsgrunn well

	Depth in core. m	Restored depth below top	
		Alum Shale. m	Thickness. m
Base Huk Formation	260.0	0.0	
Top Alum Shale / base dolerite	265.5	0.0	
<i>Peltura</i> gamma spike (PGS)	275.0	7.5	
Top <i>Olenus</i> triple gamma spike (OTGS)	280.0	12.5	
Base <i>Olenus</i> triple gamma spike (OTGS)	281.3	13.8	
Base Furongian gamma low (BFGL)	282.3	14.8	
? Andrarum Lmst Bed gamma low (AGL)	296.0	24.0	
Base Exsulans Lmst Bed	303.7	28.8	
Base Alum Shale Formation	303.7	28.8	
Base Stokkevannet sandstone	319.2	41.7	
Alum Shale. restored			28.8
Furongian. Alum Shale			14.8
Middle Cambrian. Alum Shale			14.0
Stokkevannet sandstone			13.0
Dolerite in Furongian (2.00 + 3.54 + 5.50 m)			11.0
Dolerite in M. Cambrian (0.93 + 2.91 m)			3.8
Dolerite in Stokkevannet sst (2.58 m)			2.6

The borehole was terminated at 322.6 m in basement gneiss

thus 28.8 m (Table 2). Due to magmatic heating the cored rock is very hard and brittle. The basal 3.4 m of the core (322.6–319.2 m) consist of gneissic basement, in turn overlain by 13.0 m of fine-grained quartzitic sandstone (319.2–303.7 m) intruded by a 2.6 m thick dolerite sill (Fig. 6). The fine-grained sandstone is here informally termed the Stokkevannet sandstone. It likely represents a tongue of the Swedish File Haidar Formation (Nielsen & Schovsbo 2007, 2011) and for simplicity it could be contemplated using that term in Norway also.

The topmost part of the Stokkevannet sandstone between 303.7–304.9 m is dark stained and includes a matrix-supported conglomerate between 304.7–304.5 m. The matrix consists of fine-grained quartz sand; the clasts are up to 3 cm in diameter, typically around 1 cm, sub-angular to sub-rounded, dark coloured and probably consist of phosphorite. Unfortunately, none of the HH-XRF measuring points covered these clasts. The upper boundary of the conglomerate may represent an unconformity; here a crust of assumed phosphorite is developed with a sharp upper boundary. The sandstone between 304.5–303.7 m is very fine-grained and bioturbated (dark-stained mottled).

The basal 6 cm of the Alum Shale Formation (303.67–303.61 m) is developed as a conglomeratic limestone with a primary bioclastic fabric, and this horizon likely represents the Exsulans Limestone Bed (Fig. 3). The lower boundary to the Stokkevannet sandstone is sharp but irregular and is overlain by phosphorite nodules up to 1×1.5 cm in size. The lime-

stone grades into very fine to fine-grained sandstone, in part carbonate cemented (303.6–302.2 m). The upper boundary is sharp. The overlying interval (302.2–265.5 m) is developed as black shale with limestone beds and concretions that in total amount to about 3.6 m or approximately 12% of the formation thickness. Macroscopic pyrite occurs in veins. In the interval 299.0–294.3 m, 0.4 m of shale and a 0.30 m thick limestone bed are sandwiched between two dolerite sills (Fig. 6). The carbonate bed (296.0–295.7 m) has in part a clear limestone texture and does not resemble the diagenetic limestone commonly present in the shale. The interval above the dolerite sill at 294.3–265.5 m represents the main upper part of the Alum Shale Formation and consists of shale with scattered black limestone nodules. Dolerite sills with sharp boundaries to the Alum Shale occur at 285.8–282.2, 269.4–267.4 and 265.5–260.0 m. The top dolerite sill is directly overlain by the Middle Ordovician Huk Formation at 260.0 m, suggestive of a major unconformity at this level.

Formation bulk density

The formation bulk density ranges between 2.0 and 3.3 g/cm³ with the lowest values measured in the shales and the highest in the dolerite sills (Fig. 6). The bulk density of the Lower Cambrian sandstone is close to 2.65 g/cm³ in the interval 314.0–309.0 m, which is the density of pure quartz (Ellis & Singer 2007). Slightly higher densities occur in the interval 307.0–305.5 m where also the K₂O content is slightly raised, suggest-

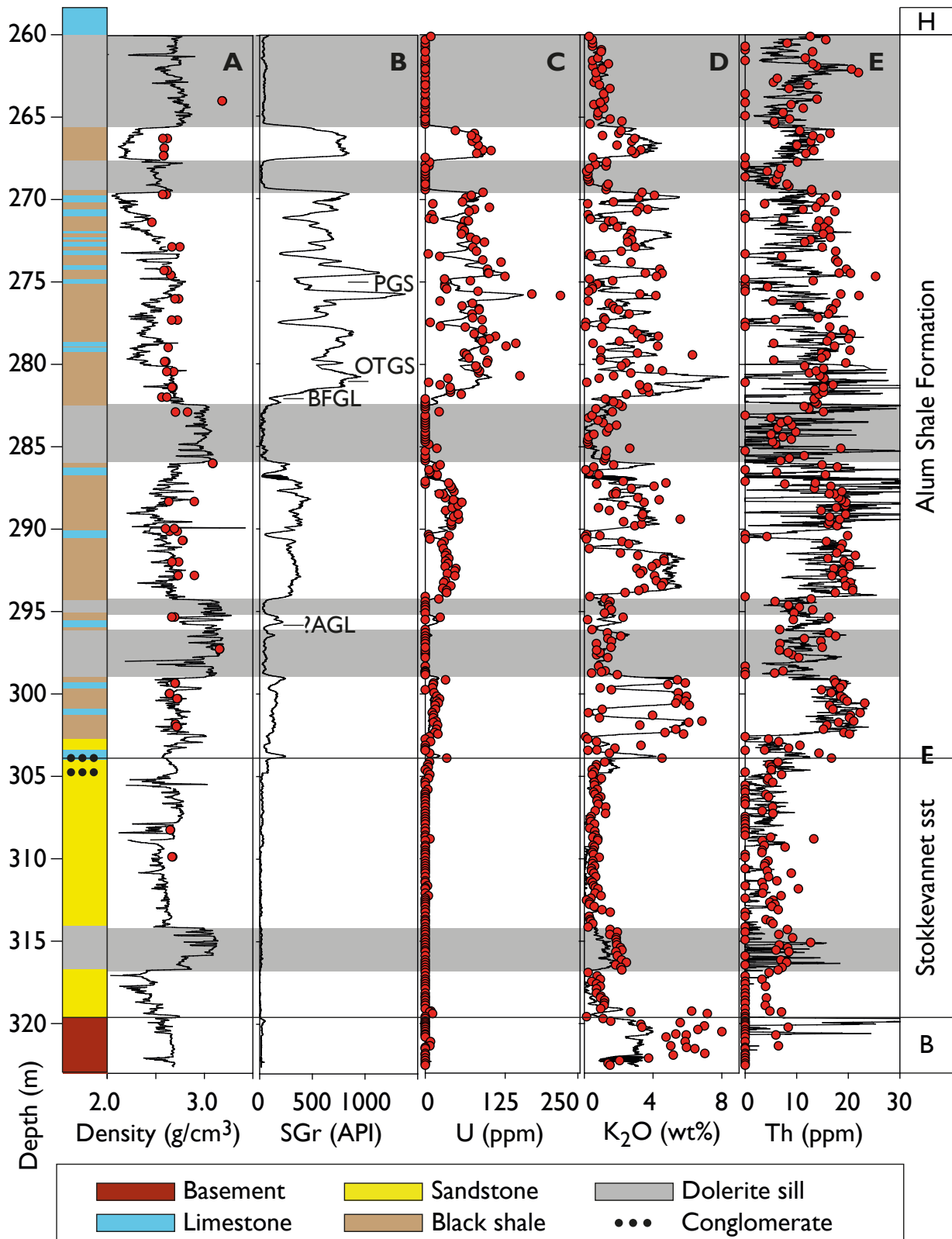


Fig. 6. Lithology, core scanning and core measurements of the Porsgrunn core (BHD-03-99) in the interval 322.6–260.0 m. A 5 cm running average was calculated through the density data. U, K₂O and Th determined by HH-XRF. Black lines: core scanning measurements. Red dots: core sample measurements. H: Huk Formation. B: Basement. E: Exsulans Limestone Bed. Sst: sandstone. PGS: *Peltura* gamma spike (central position). OTGS: *Olenus* triple gamma spike (central position). BFGl: Base Furongian gamma low. AGL: Andrarum gamma low.

ing the presence of other components besides quartz in the sand (Fig. 6). The low bulk values in the interval 320.0–316.7 m may reflect poor alignment of the core in the scanner.

In the Alum Shale Formation the bulk densities are around 2.7 g/cm³ with a slightly decreasing trend up through the formation. The highest densities in the Alum Shale (>2.7 g/cm³) are associated with carbonate beds (Fig. 6). Very low densities were measured by the scanner in the intervals 279.3–276.0, 271.6–269.6, and 267.4–265.5 m that cannot be reproduced by the core bulk density measurements (Fig. 6), and we suspect that the measured densities reflect poor alignment of the rather slim core (diameter 2.5 cm) in the scanner.

The dolerite sills have a density of about 2.8–3.2 g/cm³. The highest densities were measured in the dolerite sills in the basal part (316.7–314.1 m) and the lowest in the topmost part of the core (265.5–260.0 m).

Spectral gamma scanning

The Sum gamma ray (SGr) log ranges from 0 to 1500 API units with the highest readings in the Alum Shale and the lowest in the dolerite sills and the Stokkevannet sandstone (Fig. 6). The latter unit has <40 API units in agreement with the general non-radioactive mineralogy present here. A slight increase in API units is seen from 310.0 m and upwards and again in the topmost part of the sandstone around 305 m. In both cases the increase is related to higher K₂O and Th contents suggesting that clay minerals are present in the sand.

In the Alum Shale the API values increase in a stepwise manner from 230 API units in the interval 305.0–300.0 m, to 420 API units in the interval 294.0–286.0 m, and to about 800 API values in the interval 282.0–265.0 m which shows a quite fluctuating pattern (Fig. 6). The high API values in the Alum Shale reflect the U content with concentrations up to 220 ppm in parts of the core (Fig. 6). Low API values were measured in intervals with carbonate beds as these are characterised by low U, K₂O and Th concentrations. The K₂O content in the Alum Shale varies between 0 and 8 wt%. The K₂O content exhibits an overall upwards decrease in concentrations from around 7 wt% at the base of the shale to about 4 wt% in the topmost part. A similar decrease in Th concentrations can be seen from about 20 ppm in the basal part of the formation to about 15 ppm in the topmost parts.

The SGr response of the dolerite sills varies between 50 and 100 API units and is thus slightly higher than the SGr response of the basal sandstone. The K₂O content varies around 1–2 wt% with the highest content in the basal dolerite sills and the lowest content in the topmost sill (Fig. 6). This, together with the differences

in densities of the sills, may indicate compositional differences caused either by primary variation or differences in reactions between the sills and the surrounding sediment.

The U, K and Th concentrations measured by HH-XRF were used to rescale the spectral gamma log readings (see section on methods), and thus they have similar ranges in values (Fig. 6). The core scanning and the HH-XRF measurements generally track each other quite well despite the fact that the core-scanner readings were measured with a 15 cm wide crystal sensor where the radioactive signal is representative for the whole core volume, whereas the HH-XRF measurements are representative of only discrete spots. The Th variation seen in Fig. 6 even suggests that the HH-XRF measured a more stable signal in the Alum Shale, which implies that the Th calibration of the core-scanner drifted slightly during measurement.

Mo, V, TOC and SiO₂ content

In the Stokkevannet sandstone and the dolerite sills, only a few samples have a measurable Mo content (Fig. 7). In the Alum Shale, the Mo concentrations increase in a stepwise manner that tends to follow the pattern exhibited by the U concentrations (Fig. 6). In the Alum Shale the section between 304.0 and 295.0 m has 0–20 ppm Mo, the section between 294.5 and 286.0 m has on average 150 ppm Mo and the section above 280.0 m has up to 450 ppm Mo. The Mo content decreases from about 290.0 m and upwards to the sill contact at 285.7 m and increases again above the sill contact at 282.1 m up to about 280 m (Fig. 7A). No decrease in Mo concentration is observed near any other contact to sills, i.e. at 294.0 m, 269.2 m and 265.5 m, suggesting that the Mo variation is not controlled by the occurrence of sills.

The Stokkevannet sandstone has V contents generally lower than 20 ppm (Fig. 7). The V content in the dolerite sill in the sandstone ranges up to 800 ppm. In the dolerite sills in the Alum Shale the V content is slightly lower, in the range 500–800 ppm. The V content in the Alum Shale is in the range of 100–500 ppm for most of the section, without a clear stratigraphic trend (Fig. 7). This enrichment pattern thus deviates from the stepwise upwards increase in U and Mo concentrations.

The TOC content has only been measured in the shale lithology of the Alum Shale Formation (Fig. 7). The TOC content varies between 1 and 14 wt%, with the lowest content in the basal section between 304.0 and 300.0 m where values of 1–4 wt% are found. Higher up in the formation the TOC content varies between 7 and 14 wt% with the highest values measured in the interval between 275.0–272.0 m. In the

intervals 294.0–288.0 m and 275.0–272.0 m, the TOC content exhibits upward increasing trends (Fig. 7).

The SiO₂ content in the Stokkevannet sandstone is overall very high, as expected for a pure sandstone (Fig. 7). The SiO₂ concentrations exceed, however, 100

wt% because a powdered quartz standard was used for calibration (see section on methods), and thus the denser nature of the core resulted in a slightly higher content. The dolerite sills have SiO₂ contents around 40 wt% with no clear stratigraphic variation.

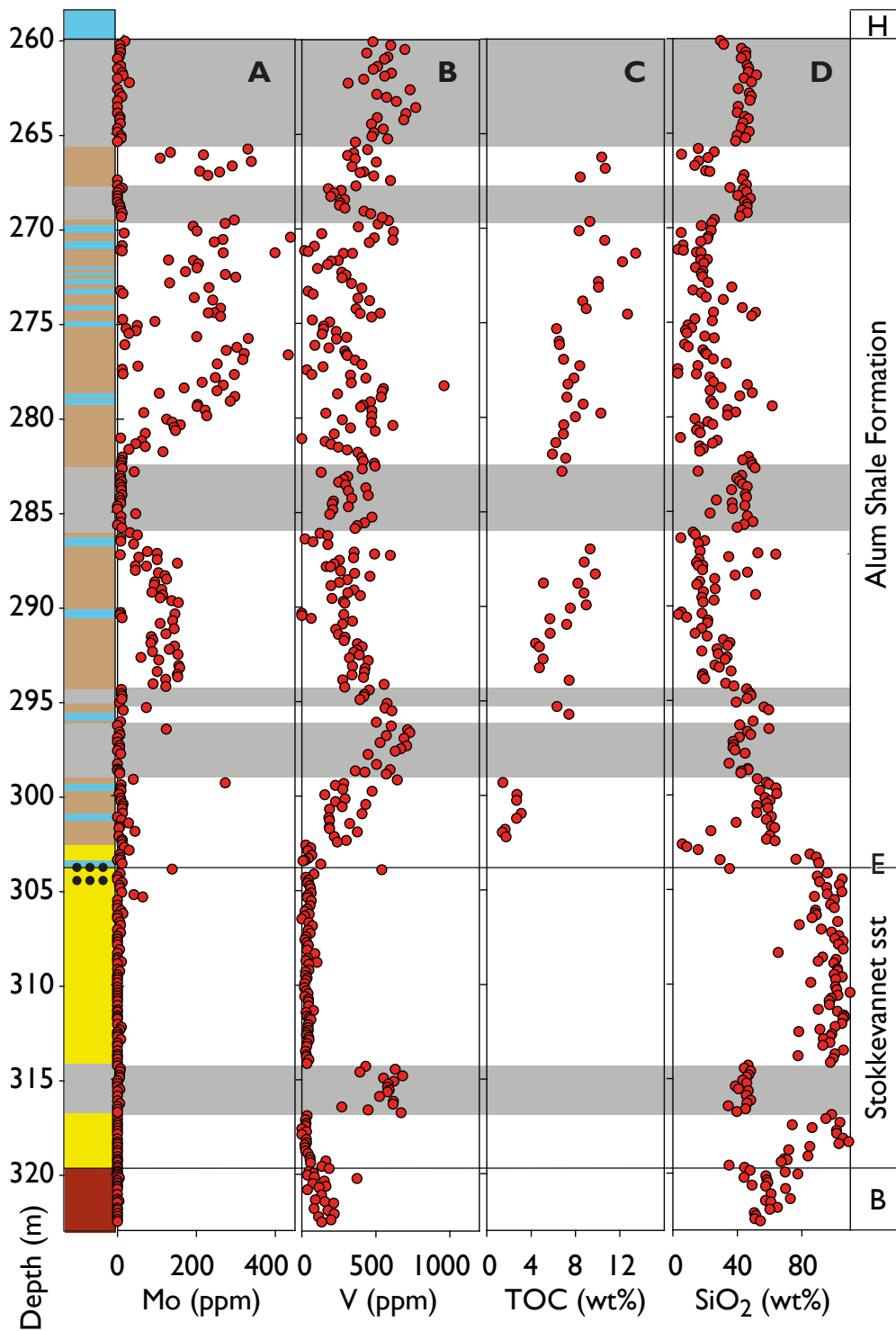


Fig. 7. Measurements of the Porsgrunn core (BHD-03-99) in the interval 322.6–260.0 m. Mo, V and SiO₂ by HH-XRF. Other explanations as in Fig. 6.

The basal Alum Shale Formation in the interval 303.6–302.7 m has a SiO₂ content >80 wt%, similar to the Stokkevannet sandstone and in agreement with the sandy to silty lithology of the interval. Above this level the SiO₂ content decreases up to the 290.0 m level; at higher levels the SiO₂ content is stable around 20 wt% (Fig. 7). However, a few samples in the shale show SiO₂ concentrations exceeding 40 wt%.

Discussion

Correlation

The stratigraphic motif of the restored SGr log (excluding the sills) compares well with results from boreholes through the Alum Shale in Scania and on Bornholm, where the log intervals to some extent have been dated based on the occurrence of trilobites (Fig. 8) (Nielsen & Buchardt 1994; Pedersen & Klitten 1990; Lauridsen 2000; Christensen *et al.* 2002; Schovsbo 2002).

In the Gislövshammar-2 well, located in south-eastern Scania (Fig. 1), the Andrarum Limestone Bed is identified on the gamma ray log as a characteristic low peak termed the Andrarum gamma low (AGL) (Fig. 8). The AGL separates higher Gr active shale belonging to the *Lejopyge lavigata* Zone (C3) from rather low Gr active parts of the underlying shale belonging to the *Goniagnostus nathorsti* (C1) and *Paradoxides paradoxissimus* (B1–B4) superzones (Fig. 8). In the Porsgrunn core the AGL level is not unequivocally identified but may be located at either 296.0 m, corresponding to 24.0 m (restored) below the top of the Alum Shale, or at 290.2 m, corresponding to 19.1 m (restored) below the top of the Alum Shale (Fig. 8). At 296.0 m a limestone bed with a primary bio-clastic fabric occurs that may be a representation of the Andrarum Limestone Bed, whereas the limestone at 290.2 m is clearly of diagenetic origin. Hence, the 296.0 m level is the most likely candidate for the AGL.

In the Gislövshammar-2 and in the Billegrav-2 wells located in Scania and on Bornholm, respectively (Fig. 1), the base of the Furongian is characterised by a transient minimum in the Gr log (termed base Furongian gamma low, BFGL) underlying an interval with very high responses that characterises the upper part of the *Olenus* Superzone (termed *Olenus* triple gamma spike, OTGS; see also Schovsbo 2002). In the Porsgrunn core the BFGL log pattern is observed at 282.3 m in the core (14.8 m below top of the Alum Shale) and the OTGS is observed between 280.0–281.3 m in the core (13.8–12.5 m below the top of the Alum Shale), see Fig. 8 and Table 2. This interpretation is also supported by the stratigraphic distribution of Mo in the Porsgrunn

core (Fig. 7) which is known to increase in the lower part of the *Olenus* Superzone associated with the Steptoean Positive Carbon Isotope Excursion (SPICE) event (Gill *et al.* 2011). The increase in Mo content seen at 283.3–281.0 m (15.8–13.5 m below top of the Alum Shale) in the Porsgrunn core (Fig. 7) is suggested to reflect this event. The Porsgrunn core data suggest that the Mo concentration remained high also after the SPICE event at least to the mid-Furongian *Peltura* Superzone (see below). Dahl *et al.* (2013) observed that the Mo content remained high at least until the *Parabolina* Superzone at Andrarum in SE Scania they did not investigate higher levels.

The most prominent gamma-ray spikes in the Furongian occur at 274.2 and 276.3 m core depth (at 6.7 m and 8.8 m below the top of the Alum Shale, respectively). However, the lowering of the U content between these peaks reflects the presence of a diagenetic carbonate concretion and thus the original spike was not twinned. This spike is easily identified as the gamma ray spike that occurs in the lower part of the *Peltura* Superzone (termed the *Peltura* gamma spike, PGS) in the Gislövshammar-2 core (Fig. 8). This horizon is one of the most characteristic of all gamma ray spikes within the Furongian. The PGS can thus be identified in wells penetrating the Alum Shale Formation in Denmark and Sweden (Andersson *et al.* 1985; Pedersen & Klitten 1990; Michelsen & Nielsen 1991; Schovsbo 2002; Eriksson 2012; Schovsbo *et al.* 2011, 2015a, b, 2016) as well as in Norway (Skjeseth 1958; Elvebakk 2011; present study).

Compared with the Gislövshammar-2 and Billegrav-2 cores there is no suggestion that the Porsgrunn core contains any Lower Ordovician Alum Shale. This would have been seen as consistent lower gamma ray readings compared to those of the Furongian. This interpretation is corroborated by the absence of a V anomaly in the topmost part of the Alum Shale in the Porsgrunn core, which is elsewhere characteristic of the topmost Furongian and Lower Ordovician Alum Shale (Andersson *et al.* 1985; Berry *et al.* 1986; Schovsbo 2001; Gautneb & Sæther 2009). The Furongian is thus interpreted to be 15.8 m thick in the Porsgrunn core (Table 2).

Effect of diagenesis

The Alum Shale Formation in the Skien–Langesund district has experienced early diagenetic, catagenetic and contact metamorphic effects during the Palaeozoic. This caused changes in the mineralogy and may possibly also have led to mobilisation of certain elements. Thus the original trace element signature may in theory have been altered in the Porsgrunn core. However, the Alum Shale is known to retain its

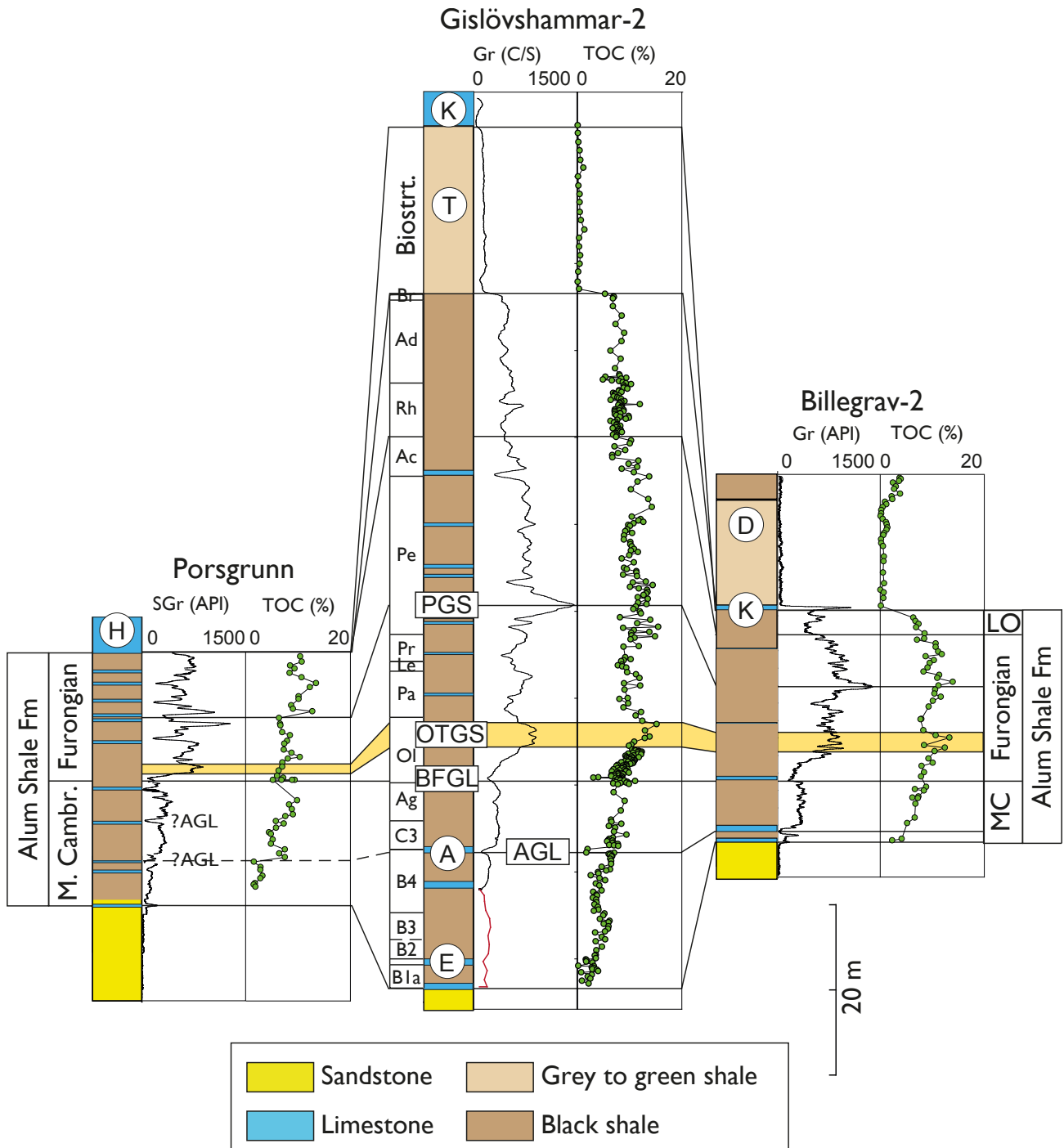


Fig. 8. Gamma ray log and TOC correlation between the Porsgrunn, Gislövshammar-2 and Billegrav-2 cores, including data from Schovsbo (2001, 2002) and Schovsbo *et al.* (2011). The biostratigraphy of Gislövshammar-2 is based on Nielsen & Buchardt (1994) and modified according to Nielsen *et al.* (2014). The lowest part of the Gr curve (in red) in the Gislövshammar-2 core is calculated from core measurements. Abbreviations: TOC: Total Organic Carbon. SGr: Spectral gamma ray. Gr: Gamma ray. API: America Petroleum Institute units. C/S: counts pr second. K: Komstad Limestone. T: Tøyen Shale. D: Dicellograptus Shale. H: Huk Formation. MC: Middle Cambrian. M. Cambr.: Middle Cambrian. LO: Lower Ordovician (Tremadocian). A: Andrarum Limestone Bed. E: Exsulans Limestone Bed. PGS: *Peltura* gamma spike. OTGS: *Olenus* triple gamma spike (interval shown with pale orange colour). BFGL: Base Furongian gamma low. AGL: Andrarum gamma low. Biostr.: Biostratigraphy in the Alum Shale Formation. For biostratigraphical abbreviations, see Fig. 3. Two possible positions for the AGL are shown; the preferred correlation is shown with a dashed line.

geochemical characteristics even in metasediments, and radioactive elements such as K, Th and U are in general considered to be immobile during diagenesis (Gee 1981; Olerud 1984; Snäll 1988, Lecomte *et al.* 2017). The presence of high concentrations of U and V in Alum Shale of presumed Furongian and Early Ordovician age in the Caledonian Mountain belt (Gee 1981; Sundblad & Gee 1985) also suggest that the trace element signature is very robust.

The new data from the Porsgrunn core compare rather well with previous geochemical studies of the Alum Shale in the Oslo area presented by Gautneb & Sæther (2009) and Pabst *et al.* (2016). The U values found in the Porsgrunn core are also comparable to those observed elsewhere in other outer shelf Alum Shale facies, see Schovsbo (2002). Hence we do not anticipate a significant tectonic overprint on the geochemistry in the core.

The organic carbon levels are lowered as thermal maturation increases due to hydrocarbon generation and expulsion, and it is expected that the TOC content is lowered in the Porsgrunn core. Thermal maturation probably took place during deep burial of the shale and/or thrust loading during the Caledonian Orogeny, but subsequent local heating also occurred in association with Permo–Carboniferous magmatic activity during the extensional phase of the Oslo Graben (Buchardt & Lewan 1990; Samuelsson & Middleton 1998; Pedersen *et al.* 2007). Any organic carbon originally present is now converted to graphite. Due to the proximity to the sills the maturity of the Alum Shale in the Porsgrunn core is assumed to correspond to at least 5% graptolite reflectance values (cf. Buchardt & Lewan 1990; Olsson 1999).

The Alum Shale kerogen is a type II with hydrogen index of about 500 mg HC per g TOC, capable of generating hydrocarbons (Dahl *et al.* 1989; Więclaw *et al.* 2010; Sanei *et al.* 2014). In the Porsgrunn core, TOC values up to 14 wt% occur, which is comparable to the TOC levels reported by Gautneb & Sæther (2009) for the Alum Shale elsewhere in the Oslo area. This level is also similar to the values seen in dry gas matured Alum Shale sections (graptolite reflectance values of 2–2.3%; Petersen *et al.* 2013) in Scania and Bornholm (Fig. 8). The TOC content in immature Alum Shale may exceed 20 wt% (Schovsbo 2002) and it is likely that the TOC content has been somewhat reduced in all thermally mature Alum Shale sections throughout Scandinavia. In Scania and on Bornholm the TOC content increases in a step-wise manner up through the Alum Shale Formation to the *Peltura* Superzone from where it gradually decreases again (Fig. 8). In the Porsgrunn core this trend can still be recognised although in a rather scattered condition, which suggests that some remobilisation of C has occurred.

Stratigraphy

The established gamma ray log-stratigraphy of the Porsgrunn core is in good agreement with previous knowledge of the Cambrian succession in and around the Skien–Langesund district. In the Slemmestad and Krekling areas farther north and northeast (Fig. 1), an up to 3 m thick, basal interval of conglomerates, sand, silt and shale overlies the basement and marks the regional Early Cambrian transgression (Høyberget & Bruton 2008; Nielsen & Schovsbo 2011). This basal succession is thicker in the Skien–Langesund district; Vogt (1929) reported a section of 15.5–17.5 m of sandstone at Stokkevannet, and this interval was c. 6 m thick in a borehole at Rognstranda c. 5 km south of Porsgrunn studied by Henningsmoen (unpublished). The Lower Cambrian is 13.0 m thick in the Porsgrunn core, i.e. essentially intermediate in thickness between the two previous reports. It is likely that some of the thickness variation of the basal strata reflects undulations of the Subcambrian Peneplane, but a general thickening southwards is anticipated. We here informally refer to this unnamed succession as the Stokkevannet sandstone, but it may be envisaged as a tongue of the File Haidar Formation in south-central Sweden and this term could perhaps also be used in Norway (cf. Nielsen & Schovsbo 2011). These beds are unconformably overlain by Middle Cambrian shales with a phosphorite-bearing limestone at the base. This basal limestone is assumed to represent the Exsulans Limestone Bed, as in the classical outcrop just south of the centre of Slemmestad described by Spjeldnæs (1955, 1962). At Slemmestad a very thin arkosic sandstone bed occurs intercalated in the Alum Shale a few centimetres above the Exsulans Limestone Bed (Høyberget & Bruton 2008); in the Porsgrunn core there is intercalated 1.4 m of quartz sandstone, in part with lime cement, between the assumed Exsulans Limestone Bed and the base of the shale (Fig. 6 at 303.6–302.2 m). It may be discussed whether this sandstone should be separated as a member of its own within the Alum Shale Formation. Thin sandstone units of similar thickness are known to overlie the Hawke Bay unconformity farther north in the Caledonian Mountain chain, see Marklund (1952) and Nielsen & Schovsbo (2015).

The trilobites reported by Brøgger (1878) from the lower part of the Alum Shale in the Skien–Langesund area (see alternatively Strand 1929) are characteristic of the Middle Cambrian *Aciducus atavus* Zone (upper part equivalent to the *Hypagnostus parvifrons* Zone sensu Westergård 1946), the *Ptychagnostus punctuosus* Zone and the *Goniagnostus nathorsti* Zone. According to Brøgger's measurements the *Paradoxides paradoxissimus* Superzone is 5 to 6 m thick and overlain by c. 6

m of shale belonging to the *P. forchhammeri* Superzone, whereupon follow the “upper” Cambrian shales. In the Porsgrunn core the Middle Cambrian is 14.0 m thick, i.e. in good accordance with Brøgger’s measurements; note that we here assign the pre-Furongian *Agnostus pisiformis* Zone to the Middle Cambrian.

According to Henningsmoen (1957) the thickness of the Upper Cambrian (~ Furongian) is not more than 12 m in the Skien–Langesund area owing to the absence not only of the *Acerocarina* Superzone but also of the upper part of the *Peltura* Superzone. The 12 m thickness derives from a borehole at Rognstranda where the Alum Shale is penetrated by numerous sills (unpublished), and it is uncertain whether the succession includes the *A. pisiformis* Zone. The Furongian is close to 15 m thick in the Porsgrunn core. Conglomeratic levels of possible regional distribution as observed in Sweden (see e.g. review by Martinsson 1974) have not been described from the Furongian of the Skien–Langesund district and are not identified in the Porsgrunn core. The biostratigraphy of the Furongian in the district was investigated by Henningsmoen (1957, 1958), but due to the intense Permian heating fossils are difficult to extract from the baked Alum Shale which is hard and splintery.

The Cambrian-Ordovician hiatus

Central to work in the area has been a discussion of the local unconformity between the Cambrian and Ordovician. In the borehole at Rognstranda the Furongian part of the Alum Shale Formation consists of only 12 m of strata lacking parts of the *Peltura* Superzone and all of the *Acerocarina* Superzone (Henningsmoen 1957; Strand & Henningsmoen 1960). The Alum Shale is here directly overlain by the Middle Ordovician Rognstranda Member of the Huk Formation (Owen *et al.* 1990).

Rønning (1976, 1978; personal communication 1/12/2014 to D. Bruton) identified the Tremadocian Zone of *Rhabdinopora* in a submarine tunnel used for a pipeline for Norsk Hydro from their chemical plant at Rafsnes to Herøya, extending under Frierfjord (see also Lien *et al.* 1978; for location see Fig. 2). Rønning made collections of well-preserved dendroid graptolites (*Rhabdinopora*) and obolid brachiopods, proving beyond doubt the presence of Tremadocian Alum Shale in the now flooded tunnel.

The interpretation of the local unconformity is controversial; it was interpreted as a thrust contact by Ramberg & Bockelie (1981, fig. 2) and Bockelie & Nystuen (1985) and as an erosional unconformity by Nilssen (1985). The former authors suggested that a sole thrust might be present within the Alum Shale Formation to explain the lack of Lower Ordovician at almost all localities in the district.

Bockelie & Nystuen (1985, p. 76, fig. 4I), referring to Rønning’s work, preferred to invoke a frontal ramp to explain the absence of Tremadocian Alum Shale, rather than local non-deposition or erosion as favoured by Strand & Henningsmoen (1960). The Alum Shale is stratigraphically complete at Krekling some 75 km to the north (Høyberget & Bruton 2008) where it includes the Tremadocian followed by the Bjørkåsholmen Formation (0.6 m thick) and a thin Tøyen Shale (ca. 5 m), while further west, south of Skollenborg and near Flata, these units are absent and the Alum Shale (middle part of the *Peltura* Superzone) is directly overlain by the Huk Formation (see Fig. 1 for locations). Elsewhere in Scandinavia are also seen gaps between the Furongian and the Tremadocian. A classic example is Hunneberg in Västergötland, south-central Sweden, where pockets of thin Tremadocian Alum Shale directly overlie the *Peltura* Superzone (Westergård 1922). Reworked trilobites from the *Peltura* Superzone were recorded in the *Acerocarina* Superzone at nearby Kinnekulle by Weidner & Nielsen (2013), which is taken to indicate late Furongian uplift and erosion of Västergötland. Tremadocian Alum Shale is absent across most of this district. On southern Öland only the middle part of the Tremadocian is represented (Westergård 1922). We conclude that there appears to have been widespread crustal unrest in Scandinavia in the late Furongian associated with local uplift. As a result the terminal Furongian *Acerocarina* Superzone has a rather limited distribution (see recent map in Weidner & Nielsen 2013). We thus support Strand & Henningsmoen (1960) in proposing the local absence of the Tremadocian in most of the Skien–Langesund district to be the result of non-deposition.

Conclusions

The described core section represents the interval 322.6–260.0 m (TD) in the BHD-03-99 Porsgrunn borehole. This drill site is located in an area of southern Norway that did not undergo Caledonian tectonic deformation and thus represents one of the few sites in the Oslo region where it is possible to study a nearly untectonised sedimentary sequence in terms of thickness and geochemistry. The succession is, however, penetrated by numerous sills of assumed Permian age. The Alum Shale Formation is 28.8 m thick in the Porsgrunn core, excluding the thickness of five 0.9–5.5 m thick dolerite sills.

The Middle Cambrian interval is 14.0 m thick and includes the Exsulans Limestone Bed (0.06 m thick) and 1.4 m of quartz sandstone immediately overlying this limestone. A 0.3 m thick primary limestone at

296.0–295.7 m may represent the Andrarum Limestone Bed but interpretation of the gamma log-motif in this interval is ambiguous. The Alum Shale Formation rests atop a 13.0 m thick lower Cambrian sandstone, informally referred to as the Stokkevannet sandstone, that in turn rests directly on the basement.

The upper 14.8 m thick Furongian part of the Alum Shale represents the *Olenus*, *Parabolina*, *Leptoplastus*, *Protopeltura* and *Peltura* trilobite superzones, judging from log-stratigraphic correlations to Scania and Bornholm. No Ordovician Alum Shale is present and the *Acerocarina* Superzone also appears to be absent. This is ascribed to local uplift as also seen elsewhere in Scandinavia at that time.

The stratigraphic development of the comparatively thin Alum Shale Formation resembles the condensed sequence seen on Bornholm except for the absence of Ordovician strata.

Acknowledgments

The authors would like to thank Norcem Brevik AS for allowing access to the BHD-03-99 core. The study was part of a Geocenter Denmark project awarded to Niels H. Schovsbo and Arne Thorshøj Nielsen. Hans-Jørgen Lorentzen, Marga Jørgensen and Lisbeth Løvig Nielsen at the GEUS Core Analysis Laboratory are thanked for assistance with the core measurements. Trond Kaasa, present manager of the Mining and Quarrying Division at Norcem Brevik AS, is thanked for permission to publish the BHD-03-99 results. Hans Arne Nakrem is thanked for help with storage of the core, and Knut Rønning, Statoil, Bergen, and Tor Løken, formerly of the Norwegian Geotechnical Institute, Oslo, are thanked for sharing data from their work during construction of the Rafsnes–Herøya submarine tunnel. The Porsgrunn core is now deposited in the collections of the Natural History Museum (Geology), University of Oslo, under accession number PMO 231.430. Constructive comments by the journal referees David Gee and Christian Bjerrum and careful editorial handling by Bulletin editor Lotte Melchior Larsen improved the final version of the paper.

References

American Petroleum Institute (API) 1998. Recommended Practices for Core Analysis. American Petroleum Institute. Recommended Practices 40, 2nd edition, February 1998. API Publishing Services, 1220 L Street, N.W., Washington, D.C. 20005, 236 pp.

Andersson, A., Dahlman, B., Gee, D.G. & Snäll, S. 1985: The

Scandinavian alum shales. *Sveriges Geologiska Undersökning Serie Ca 56*, 1–50.

Andresen, A. 1978: Lithostratigraphy of the autochthonous/parautochthonous Lower Palaeozoic metasediments on Hardangervidda, South Norway. *Norges Geologiske Undersøkelse 338*, 59–69.

Armands, G. 1972: Geochemical studies of uranium, molybdenum and vanadium in a Swedish alum shale. *Stockholm Contributions in Geology, University of Stockholm 27*, 148 pp.

Berry, W.B.N., Wilde, P., Quinby-Hunt, M.S. & Orth, C.L. 1986: Trace element signatures in Dictyonema Shales and their geochemical and stratigraphic significance. *Norsk Geologisk Tidsskrift 66*, 45–51.

Bockelie, J.F. & Nystuen, J.P. 1985: The southeastern part of the Scandinavian Caledonides. In: Gee, D.G. & Sturt, B.A. (eds), *The Caledonide Orogen – Scandinavia and Related Areas*. John Wiley, Chichester, 69–88.

Brøgger, W.C. 1878: Om Paradoxidesskifrene ved Krekling. *Nyt Magazin for Naturvidenskaberne 24*, 18–88. [In Norwegian].

Brøgger, W.C. 1884: Spaltungsverwerfungen in der Gegend Langesund–Skien. *Nyt Magazin for Naturvidenskaberne 28*, 253–419. [In German].

Bruton, D.L., Gabrielsen, R.H. & Larsen, B.T. 2010: The Caledonides of the Oslo region, Norway – stratigraphy and structural elements. *Norwegian Journal of Geology 90*, 93–121.

Buchardt, B. & Lewan, M.D. 1990: Reflectance of vitrinite-like macerals as a thermal maturity index for Cambrian–Ordovician alum shale, southern Scandinavia. *American Association of Petroleum Geologists Bulletin 74*, 394–406.

Buchardt, B., Nielsen, A.T. & Schovsbo, N.H. 1997: Alun skiferen i Skandinavien. *Geologisk Tidsskrift 3*, 1–30. [In Danish].

Christensen, C.D., Nielsen, A.T. & Schovsbo, N.H. 2002: Completion report - Fågeltofta 2. Unpublished report, Geological Museum, University of Copenhagen, 55 pp.

Dahl, J., Chen, R.T. & Kaplan, I.R. 1989: Alum shale bitumen maturation and migration: implications for Gotland's oil. *Journal of Petroleum Geology 12*, 465–476.

Dahl, T. 1856: Profile durch die Gegend von Skien, Porsgrund und Langesund. *Nyt Magazin for Naturvidenskaberne 9*, 306–333. [In German].

Dahl, T.W., Ruhl, M., Hammarlund, E.U., Canfield, D.E., Rosing, M.T. & Bjerrum, C.J. 2013: Tracing euxinia by molybdenum concentrations in sediments using handheld X-ray fluorescence spectroscopy (HHXRF). *Chemical Geology 360*, 241–251.

Dypvik, H. 1993: Natural gamma activity - a possible aid in sedimentological fieldwork. *Norsk Geologisk Tidsskrift 73*, 58–62.

Edling, B. 1974: Distribution of Uranium in the Upper Cambrian Alum Shale from Randstad, Billingen, Västergötland. *Publications from the Paleontological Institution of the University of Uppsala, Special 2*, 118 pp. [In Swedish].

Ellis, D.V. & Singer, J.M. 2007: *Well logging for earth scientists*. 2nd edition. Springer, Dordrecht, the Netherlands, 687 pp.

- Elvebakk, H. 2011: Geofysisk logging av borehull ved Arnestad skole, Asker. Norges Geologiske Undersøgelse, Rapport 2011.016, 19 pp. [In Norwegian].
- Eriksson, M. 2012: Stratigraphy, facies and depositional history of the Colonus Shale Trough, Skåne, southern Sweden. Dissertation in Geology at Lund University, master thesis no. 310. Department of Geology, Lund University. 40 pp.
- Esbensen, K.H. & Johansson, L. 2013. Portable XRF vs the geo-analytical laboratory – a first foray assessment of sampling errors. Sixth World Conference on Sampling and Blending (WCSB6), Lima, Peru, 19–22 November 2013, 163–171.
- Forbes, D. 1856: On the relations of the Silurian and metamorphic rocks of the South of Norway. The Edinburgh New Philosophical Journal III new series, 79–89.
- Gautneb, H. & Sæther, O.M. 2009: A compilation of previously published geochemical data on the lower Cambro-Silurian sedimentary sequence, including the alum shales in the Oslo region. Geological Survey of Norway, Report 2009.053, 25 pp.
- Gee, D.G. 1972: The regional geological context of the Tåsjo uranium project, Caledonian Front, Central Sweden. Sveriges Geologiska Undersökning Serie C 671, 1–36.
- Gee, D.G. 1981: The Dictyonema-bearing phyllites at Nordaunevoll, eastern Trøndelag, Norway. Norsk Geologisk Tidsskrift 61, 93–95.
- Gill, B.C., Lyons, T.W., Young, S.A., Kump, L.R., Knoll, A.H. & Saltzman, M.R. 2011: Geochemical evidence for widespread euxinia in the Later Cambrian ocean. *Nature* 469, 80–83.
- Hammer, Ø. & Svensen, H.H. 2017: Biostratigraphy and carbon and nitrogen geochemistry of the SPICE event in Cambrian low-grade metamorphic black shale, Southern Norway. *Palaeogeography, Palaeoclimatology, Palaeoecology* 468, 216–227.
- Harstad, A.O. 2005: Dissolution, growth and recrystallisation of calcite and limestone: Effects of impurities. Dissertation for the degree of dr. scient, Faculty of Mathematics and Natural Sciences, University of Oslo, 124 pp.
- Henningsmoen, G. 1957: The trilobite family Olenidae with descriptions of Norwegian material and remarks on the Olenid and Tremadocian Series. Skrifter utgitt av Det Norske Videnskaps-Akademi i Oslo I. Matematisk-Naturvidenskabelig Klasse 1, 303 pp.
- Henningsmoen, G. 1958: The Upper Cambrian Faunas of Norway with descriptions of non-olenid invertebrate fossils. *Norsk Geologisk Tidsskrift* 38, 179–196.
- Hessland, I. & Armands, G. 1978: Alunskiffer-Underlagsmateriale Geologi. Utredning från statens industriverk. SIND PM 1978: 3, Stockholm, 1–146. [In Swedish]
- Høyberget, M. & Bruton, D.L. 2008: Middle Cambrian trilobites of the suborders Agnostina and Eodiscina from the Oslo Region, Norway. *Palaeontographica, Abteilung A* 286, 1–87.
- Jamtveit, B., Dahlgren, S. & Austrheim, H. 1997: High-grade contact metamorphism of calcareous rocks from the Oslo rift, Southern Norway. *American Mineralogist* 82, 1241–1254.
- Kiær, J. 1897: Faunistische Uebersicht der Etage 5 des norwegischen Silursystems. Videnskabselskabets Skifter I, Matematisk-Naturvidenskabelig Klasse no 3, 76 pp. [In German].
- Kiær, J. 1906: Das Obersilur im Kristianiagebiete: eine stratigraphisch-faunistische Untersuchung. Videnskabselskabets Skifter I, Matematisk-Naturvidenskabelig Klasse B II, 595 pp. [In German].
- Kjerulf, T. 1857: Ueber die Geologie des südlichen Norwegens. Christiania. Verlag von Johan Dahl, 141 pp. [In German].
- Lauridsen, B.W. 2000: The Cambrian–Tremadoc interval of the Albjåra-1 drill-core, Scania, Sweden. Unpublished Cand. Scient. Thesis, Geological Institute, University of Copenhagen, Copenhagen. Denmark. 28 pp.
- Lecomte, A., Cathelineau, M., Michels, R., Peiffert, C. & Brönnimann, M. 2017: Uranium mineralization in the Alum Shale Formation (Sweden): evolution of a U-rich marine black shale from sedimentation to metamorphism, *Ore Geology Reviews*, doi: <http://dx.doi.org/10.1016/j.oregeorev.2017.04.021>
- Leventhal, J.S. 1991: Comparison of organic geochemistry and metal enrichment in two black shales: Cambrian alum shale of Sweden and Devonian Chattanooga shale of United States. *Mineralium Deposita* 26, 104–112.
- Lien, R., Garshol, K. & Løken, T. 1978: Submarine tunnel Rafsnes–Herøya, southern Norway. Norsk forening for fjellsprengningsteknikk. Publikation 01: Hard Rock Tunneling, 68–73.
- Martinsson, A. 1974: The Cambrian of Norden. In: Holland, C.H. (ed.), *Cambrian of the British Isles, Norden and Spitsbergen*, 185–283. Lower Palaeozoic Rocks of the World 2. London: John Wiley and Sons.
- Marklund, N. 1952: A Cambro–Ordovician type-section in the Sarvas Region SE of Nasafjäll, Lapland, and problems suggested thereby. *Geologiska Föreningens i Stockholm Förhandlingar* 74, 353–384.
- Michelsen, O. & Nielsen, L.H. 1991: Well records on the Phanerozoic stratigraphy in the Fennoscandian Border Zone, Denmark: Sæby-1, Hans-1 and Terne-1 wells. *Danmarks Geologiske Undersøgelse Serie A* 29, 37 pp.
- Nielsen, A.T. & Buchardt, B. 1994: Gislövshammar-2 shallow drill-hole in eastern Scania, Sweden: stratigraphy and geochemistry of the cored Lower Ordovician–Lower Cambrian strata. Unpublished Final report II, Pre-Westphalian Source Rocks in northern Europe, Geological Institute, University of Copenhagen, 1–44.
- Nielsen, A.T. & Schovsbo, N.H. 2007: Cambrian to basal Ordovician lithostratigraphy in southern Scandinavia. *Bulletin of the Geological Society of Denmark* 53, 47–92.
- Nielsen, A.T. & Schovsbo, N.H. 2011: The Lower Cambrian of Scandinavia: Depositional environment, sequence stratigraphy and palaeogeography. *Earth Science Reviews* 107, 207–310.
- Nielsen, A.T. & Schovsbo, N.H. 2015: The regressive Early – Mid Cambrian ‘Hawke Bay Event’ in Baltoscandia: Epeirogenic uplift in concert with eustasy. *Earth Science Reviews* 151, 288–350.
- Nielsen, A.T., Weidner, T., Terfelt, F. & Høyberget, M. 2014: Upper Cambrian (Furongian) biostratigraphy in Scandinavia

- revisited: definition of superzones. *GFF* 136, 193–197.
- Nilssen, I.R. 1985: Kartlegging av Langesundshalvøyas kambro-ordoviciske avsetningslagrekke, intrusiver og forkastningstektonikk, samt fullført lithostratigrafisk inndeling av områdets mellom-Ordovicium. Unpublished Master thesis in geology. Paleontologisk Museum, Tøyen, Universitetet i Oslo. 176 pp. [In Norwegian]. Available from <https://www.telemarkskilder.no/handle/123456789/2618>
- Olsson, I. 1990: Regional burial heating *vs* local magmatic heat influence of the Röstånga area, Scania, southern Sweden. *GFF* 121, 209–214.
- Olerud, S. 1984: Metallogeny of the Elsjø area, northern Oslo region, Norway. *Norsk Geologisk Tidsskrift* 64, 325–334.
- Owen, A.W., Bruton, D.L., Bockelie, J.F. & Bockelie, T. 1990: The Ordovician successions of the Oslo region, Norway. *Norges geologiske undersøkelse Special Publication* 4, 3–54.
- Pabst, T., Sørmo, E. & Endre, E. 2016: Geochemical characterisation of Norwegian Cambro-Ordovician black mudrocks for building and construction use. *Bulletin of Engineering Geology and the Environment* 76, 1577–1592.
- Pedersen, G.K. & Klitten, K. 1990: Anvendelse af gamma-logs ved korrelasjon af marine skifre i vandforsyningsboringer på Bornholm. *Dansk Geologisk Forening Årsskrift 1987–89*, 21–35. [In Danish].
- Pedersen, J.H., Karlsen, D.A., Spjeldnæs, N., Backer-Owe, K., Lie, J.E. & Brunstad, H. 2007: Lower Paleozoic petroleum from southern Scandinavia: Implications to a Paleozoic petroleum system offshore southern Norway. *AAPG Bulletin* 91, 1189–1212.
- Petersen, H.I., Schovsbo, N.H. & Nielsen, A.T. 2013: Reflectance measurements of zooclasts and solid bitumen in Lower Palaeozoic shales, southern Scandinavia: correlation to vitrinite reflectance. *International Journal of Coal Petrology* 114, 1–18.
- Piske, J. & Neumann, E. 1993: Tektonische Gliederung des prävariszischen Untergrundes in der südwestlichen Ostsee. *Geologisches Jahrbuch A* 131, 361–388. [In German].
- Ramberg, I.B. & Bockelie, J.F. 1981: Geology and tectonics around Oslo. In: Larsen, B. T. (ed.), *Guide to excursions B-4*, 4th International Conference on Basement Tectonics, Oslo, August 1981. *Nytt fra Oslofeltgruppen* 7, 81–100.
- Rasmussen, B.W., Rasmussen, J.A. & Nielsen, A.T. 2016: Biozonation of the Furongian (upper Cambrian) Alum Shale Formation at Hunneberg, Sweden. *GFF* 138, 467–489.
- Rønning, K. 1976: Geologiske undersøkelser av Kambro-Silur-sedimentene i tunnel under Friefjorden. Unpublished report, 14 pp, Geologisk Institutt avd. A, University of Bergen. [In Norwegian].
- Rønning, K. 1978: Kambro-Silur sedimentene. In: Bering, B. & Olsen, R. (eds), *Geologisk fører for Grenland*. 23–33. Telemark Geologiforening (Printer: Wegerland-Porsgrunn). [In Norwegian].
- Samuelsson, J. & Middleton, M.F. 1998: The Caledonian foreland basin in Scandinavia: constrained by the thermal maturation of the Alum Shale. *GFF* 120, 307–314.
- Sanei, H., Petersen, H.I., Schovsbo, N.H., Jiang, C. & Goodsite, M.E. 2014: Petrographic and geochemical composition of kerogen in the Furongian (U. Cambrian) Alum Shale, central Sweden: reflections on the petroleum generation potential. *International Journal of Coal Petrology* 132, 158–169.
- Schovsbo, N.H. 2001: Why barren intervals? A taphonomic case study of the Scandinavian Alum Shale and its faunas. *Lethaia* 34, 271–285.
- Schovsbo, N.H. 2002: Uranium enrichment shorewards in black shales: A case study from the Scandinavian Alum Shale. *GFF* 124, 107–116.
- Schovsbo, N.H., Nielsen, A.T., Klitten, K., Mathiesen, A. & Rasmussen, P. 2011: Shale gas investigations in Denmark: Lower Palaeozoic shales on Bornholm. *Geological Survey of Denmark and Greenland Bulletin* 23, 9–12.
- Schovsbo, N.H., Esbensen, K.H., Nielsen, A.T., Derbez, E., Gaucher, E.C., Poirier-Coutansais, X., Riou, A., Tallone, P. & Milton-Taylor, D. 2015a: Rock types in the Scandinavian Alum Shale resource play: Definitions and predictions. 77th EAGE Conference & Exhibition 2015, IFEMA, Madrid, Spain 1–4 June 2015. Extended abstract Th N101 13, 5 pp.
- Schovsbo, N.H., Nielsen A.T. & Klitten, K. 2015b: The Lower Palaeozoic now fully cored and logged on Bornholm. *Geological Survey of Denmark and Greenland Bulletin* 33, 9–12.
- Schovsbo, N.H., Nielsen, A.T. & Erlström, M. 2016: Middle–Upper Ordovician and Silurian stratigraphy and basin development in southernmost Scandinavia. *Geological Survey of Denmark and Greenland Bulletin* 35, 39–42.
- Siggerud, T. 1955: Tillegg til statsgeolog Skjeseths rapport for uranundersøkelser i kambriske alunskifer i Oslofeltet og tilgrensende områder sommeren 1954. *Bergvesenet, Rapportarkivet, Trondheim, Norway*, BV 3570, 33 pp., 7 Figs. [In Norwegian].
- Skjeseth, S. 1958: Uran i kambrisk alunskifer i Oslofeltet og tilgrensende områder. *Norges Geologiske Undersøkelse Bulletin* 203, 100–111. [In Norwegian].
- Snäll, S. 1988: Mineralogy and maturity of the alum shales of south-central Jämtland, Sweden. *Sveriges Geologiska Undersökning C* 818, 49 pp.
- Sopher, D., Erlström, M., Bell, N. & Juhlin, C. 2016: The structure and stratigraphy of the sedimentary succession in the Swedish sector of the Baltic Basin: New insights from vintage 2D marine seismic data. *Tectonophysics* 676, 90–111.
- Spjeldnæs, N. 1955: Middle Cambrian stratigraphy in the Røyken area, Oslo Region. *Norsk Geologisk Tidsskrift* 34, 105–121.
- Spjeldnæs, N. 1962: The Middle Cambrian at Slemmestad, Oslo region. *Norsk Geologisk Tidsskrift* 42, 196–197.
- Størmer, L. 1953: The Middle Ordovician of the Oslo Region, Norway. 1. Introduction to stratigraphy. *Norsk Geologisk Tidsskrift* 31, 37–141.
- Strand, T. 1929: The Cambrian beds of the Mjøsen in Norway. *Norsk Geologisk Tidsskrift* 10, 307–365.
- Strand, T. 1934: The Upper Ordovician cephalopods of the Oslo Area. *Norsk geologisk Tidsskrift* 14, 1–117.
- Strand, T. & Henningsmoen, G. 1960: Cambro–Silurian stratig-

- raphy. In: Høltedahl, O. (ed.), The Geology of Norway. Norges Geologiske Undersøkelse Bulletin 208, 128–169.
- Sundblad, K. & Gee, D.G. 1985: Occurrence of a uraniferous-vanadiniferous graphitic phyllite in the Kōli Nappes of the Stekenjokk area, central Swedish Caledonides. GFF 106, 269–274.
- Terfelt, F., Eriksson, M.E., Ahlberg, P. & Babcock, L.E. 2008: Furongian Series (Cambrian) biostratigraphy of Scandinavia – a revision. Norwegian Journal of Geology 88, 73–87.
- Torsvik, T.H., Ryan, P.D., Trench, A. & Harper, D.A.T. 1991: Cambrian–Ordovician paleogeography of Baltica. Geology 19, 7–10.
- Vogt, T. 1929: Undersøkelser over den kambriske sandsten ved Langesundsfjorden. Norges Geologiske Undersøkelse 133, 52–57. [In Norwegian].
- Weidner, T. & Nielsen, A.T. 2013: The late Cambrian (Furongian) *Acerocarina* Superzone (new name) on Kinnekulle, Västergötland, Sweden. GFF 135, 30–44.
- Weidner, T. & Nielsen, A.T. 2014: A highly diverse trilobite fauna with Avalonian affinities from the Middle Cambrian *Acidusus atavus* Zone (Drumian Stage) of Bornholm, Denmark. Journal of Systematic Palaeontology 12, 23–92.
- Westergård, A.H. 1922: Sveriges olenidskiffer. Sveriges Geologiska Undersökning Ca 18, 205 pp. [In Swedish].
- Westergård, A.H. 1946: Agnostidea of the Middle Cambrian of Sweden. Sveriges Geologiska Undersökning C 477, 141 pp.
- Więclaw, D., Kotarba, M.J. & Lewan, M.D. 2010: Estimation of hydrous-pyrolysis kinetic parameters for oil generation from Baltic Cambrian and Tremadocian source rocks with Type-II kerogen. Geological Quarterly 54, 217–226.

A review of Palaeozoic and Mesozoic tetrapods from Greenland

MARCO MARZOLA, OCTÁVIO MATEUS, JESPER MILÀN & LARS B. CLEMMENSEN



Marzola, M., Mateus, O., Milàn, J. & Clemmensen, L.B. 2018. A review of Palaeozoic and Mesozoic tetrapods from Greenland. © 2018 by Bulletin of the Geological Society of Denmark, Vol. 66, pp. 21–46. ISSN 2245-7070. (www.2dgf.dk/publikationer/bulletin).

Received 1 December 2016
Accepted in revised form
27 October 2017
Published online
3 March 2018

This article presents a synthesis of Palaeozoic and Mesozoic fossil tetrapods from Greenland, including an updated review of the holotypes and a new photographic record of the main specimens. All fossil tetrapods found are from East Greenland, with at least 30 different known taxa: five stem tetrapods (*Acanthostega gummari*, *Ichthyostega eigili*, *I. stensioi*, *I. watsoni*, and *Ymeria denticulata*) from the Late Devonian of the Aina Dal and Britta Dal Formations; four temnospondyl amphibians (*Aquiloniferus kochi*, *Selenocara groenlandica*, *Stoschiosaurus nielseni*, and *Tupilakosaurus heilmani*) from the Early Triassic of the Wordie Creek Group; two temnospondyls (*Cyclotosaurus naraserluiki* and *Gerrothorax cf. pulcherrimus*), one testudinatan (cf. *Proganochelys*), two stagonolepids (*Aetosaurus ferratus* and *Paratypothorax andressorum*), the eudimorphodontid *Arcticodactylus*, undetermined archosaurs (phytosaur and both sauropodomorph and theropod dinosaurs), the cynodont *Mitredon cromptoni*, and three mammals (*Haramiyavia clemmenseni*, *Kuehneotherium*, and cf. *?Brachyzostrodon*), from the Late Triassic of the Fleming Fjord Formation; one plesiosaur from the Early Jurassic of the Kap Stewart Formation; one plesiosaur and one ichthyosaur from the Late Jurassic of the Kap Leslie Formation, plus a previously unreported Late Jurassic plesiosaur from Kronprins Christian Land. Moreover, fossil tetrapod trackways are known from the Late Carboniferous (morphotype *Limnopus*) of the Mesters Vig Formation and at least four different morphologies (such as the crocodylomorph *Brachychirotherium*, the sauropodomorph *Eosauropus* and *Evazoum*, and the theropodian *Grallator*) associated to archosaurian trackmakers are known from the Late Triassic of the Fleming Fjord Formation. The presence of rich fossiliferous tetrapod sites in East Greenland is linked to the presence of well-exposed continental and shallow marine deposits with most finds in terrestrial deposits from the Late Devonian and the Late Triassic.

Keywords: Greenland, tetrapoda, marine reptiles, archosauria, trace fossils.

Marco Marzola [m.marzola@campus.fct.unl.pt], GeoBioTec, Departamento de Ciências da Terra, Faculdade de Ciências e Tecnologia, Universidade Nova de Lisboa, Quinta da Torre, 2829-516 Caparica, Portugal; also Department of Geosciences and Natural Resource Management, Øster Voldgade 10, DK-1350 Copenhagen K, Denmark; also Museu da Lourinhã, Rua João Luís de Moura, 95, 2530-158 Lourinhã, Portugal; also Geocenter Møns Klint, Stengårdsvej 8, DK-4751 Borre, Denmark. Octávio Mateus [omateus@fct.unl.pt], GeoBioTec, Departamento de Ciências da Terra, Faculdade de Ciências e Tecnologia, Universidade Nova de Lisboa, Quinta da Torre, 2829-516 Caparica, Portugal; also Museu da Lourinhã, Rua João Luís de Moura, 95, 2530-158 Lourinhã, Portugal. Jesper Milàn [jesperm@oesm.dk], Geomuseum Faxe, Østsjælland Museum, Østervej 2, DK-4640 Faxe, Denmark; also Natural History Museum of Denmark, Øster Voldgade 5–7, DK-1350 Copenhagen K., Denmark. Lars B. Clemmensen [larsc@ign.ku.dk], Department of Geosciences and Natural Resource Management, Øster Voldgade 10, DK-1350 Copenhagen K, Denmark.

Corresponding author: Marco Marzola

The Devonian to Triassic strata of East Greenland are preserved in well-exposed terrestrial basins which have been extensively examined for terrestrial fossil remains since the 19th century. The first tetrapod discoveries in Greenland are recorded from the Devonian of Ymer Ø (East Greenland, Fig. 1), found during an expedition in 1899 led by the Swedish naturalist and Arctic explorer Alfred Gabriel Nathorst (Nathorst

1900, 1901; Woodward 1900). From the late 1920s until at least 1955, the Devonian of East Greenland was the target of several palaeontological expeditions (Heintz 1930, 1932; Koch 1930; Orvin & Heintz 1930; Stensiö 1931; Säve-Söderbergh 1932; Ries 2002; Blom *et al.* 2007). The Devonian outcrops of East Greenland also shed light on the first stem tetrapod ever found and described from Greenland: *Ichthyostega* Säve-Söderbergh

1932, a milestone fossil recovered in 1929 (Stensiö 1931). A few years later, the Devonian of East Greenland provided vertebrate palaeontologists with a second milestone stem tetrapod for understanding the transition from fishes to tetrapods: *Acanthostega gunnari* Jarvik 1952. New expeditions also took place during the early 1970s, one of which, led by P.F. Friend from the University of Cambridge, discovered new tetrapod material (Friend *et al.* 1976). These were followed by expeditions in 1987 and 1998 which recovered much more material (Clack 1988a, b; Bendix-Almgreen *et al.* 1990, Marshall *et al.* 1999, Clack & Neiningen 2000; Clack *et al.* 2012) (Fig. 1D). During the earliest expeditions, tetrapod fossils were discovered in the Early Triassic of the Wordie Creek Group (e.g. Säve-Söderbergh 1935; Nielsen 1954, 1967). Extensive stratigraphical studies of the Mesozoic strata in the Jameson Land area were carried out in the late 1960s and early 1970s and led to the discovery of a few vertebrate fossils, including temnospondyl remains in Middle and Late Triassic strata (e.g. Clemmensen 1980b). Moreover, at

the beginning of the 1970s the Mesozoic sediments of the eastern Milne Land were mapped and a couple of Late Jurassic neodiapsid marine reptiles were reported (Håkansson *et al.* 1971).

From the late 1980s, East Greenland saw new explorative initiatives aimed at recovering fossil tetrapod material by Harvard University (Massachusetts, USA) in collaboration with the University of Copenhagen (Denmark). These expeditions, led by the late Farish Jenkins, took place from 1988 to 2001 and explored the Late Triassic of the Jameson Land Basin (Fig. 1F); they acquired a plethora of unique tetrapods such as temnospondyls, testudinians, pterosaurs, dinosaurs and the early mammal *Haramiyavia clemmenseni* Jenkins *et al.* 1997 (see also Jenkins *et al.* 1994, 2001, 2008; Gatesy *et al.* 1999; Shapiro & Jenkins 2001; Sulej *et al.* 2014; Clemmensen *et al.* 2016).

The latest expeditions that collected fossil tetrapods from Greenland were undertaken in 2012 and 2016 by the GeoCenter Møns Klint Dinosaur Expeditions, and in 2014 by a Polish-Danish team, recovering tes-

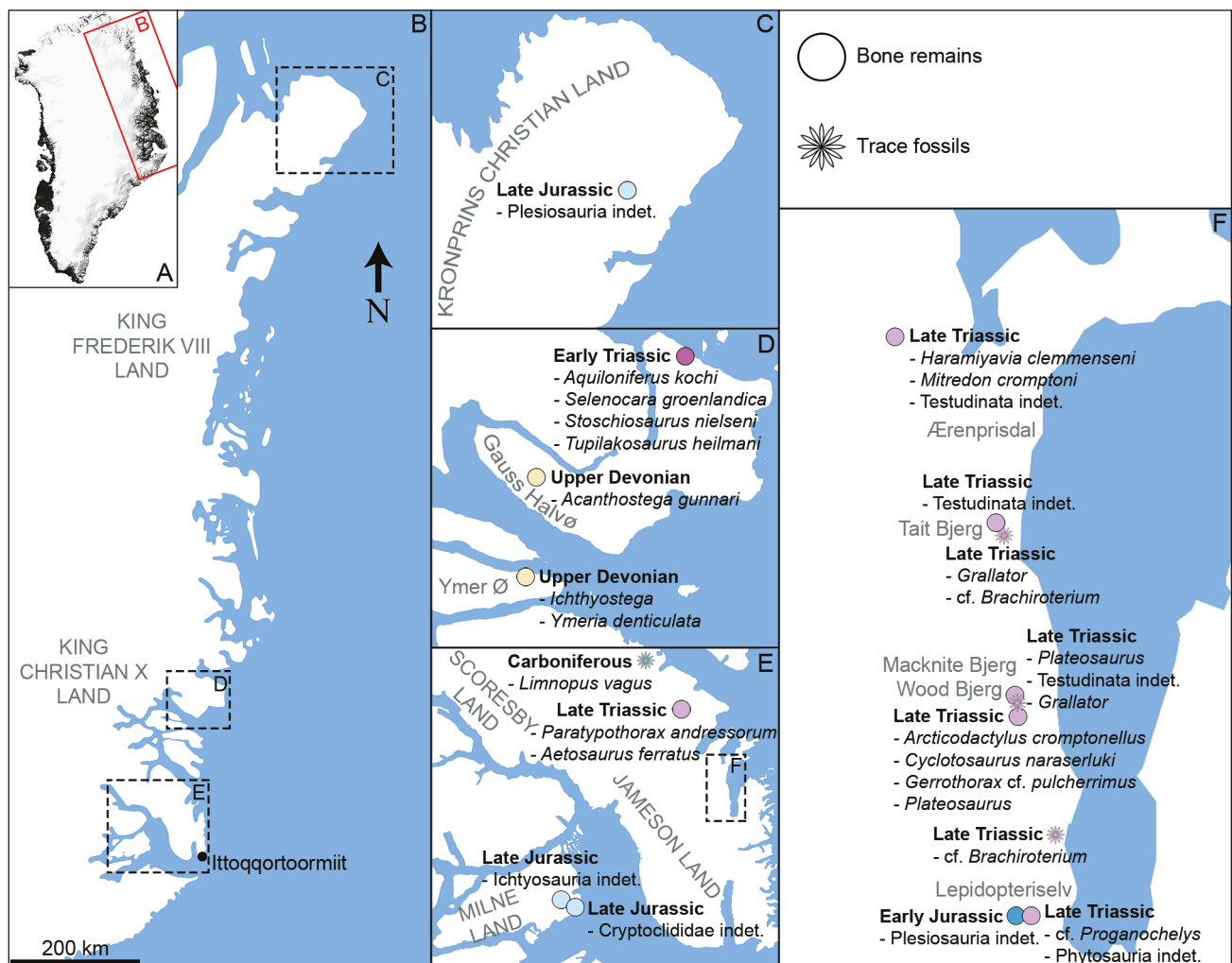


Fig. 1. A–F: Maps showing the position of the main fossil tetrapod sites of Greenland.

tudinatans, phytosaurs, dinosaurs, stem mammals and various vertebrate tracks from the Late Triassic of different fossiliferous sites in the Jameson Land Basin (Milàn *et al.* 2004, 2006, 2012; Mateus *et al.* 2014; Sulej *et al.* 2014; Clemmensen *et al.* 2016; Hansen *et al.* 2016; Kear *et al.* 2016a; Klein *et al.* 2016; Marzola *et al.* 2016, 2017a; Lallensack *et al.* 2017; Niedzwiedzki & Sulej 2017). Expeditions to the Celsius Bjerg Group, Wordie Creek Group and Fleming Fjord Formation of East Greenland were also launched by Uppsala University (Sweden) in 2015 and 2016, with vertebrate fossils recovered from various sites (Benjamin Kear, personal communication 2017).

We use the lithostratigraphical schemes by Clack & Neinger (2000) for the Celsius Bjerg Group (Fig. 1D),

Surlyk *et al.* (2017) for the Wordie Creek Group (Fig. 1D), and Clemmensen (1980b) for the Fleming Fjord Formation (Fig. 1E–F).

This article aims to give an updated systematic list and photographic review of the known Palaeozoic and Mesozoic fossil tetrapod occurrences from Greenland (Figs. 1–2). We also give the first formal report on plesiosaur remains from the Late Jurassic Kuglelejet Formation (Dypvik *et al.* 2002) at Kilen, Kronprins Christian Land (Fig. 1C).

Abbreviations. MCZ, Museum of Comparative Zoology, Harvard University (Massachusetts, USA); MGUH, Geological Museum, Copenhagen, Denmark; NHMD, Natural History Museum of Denmark, Copenhagen.

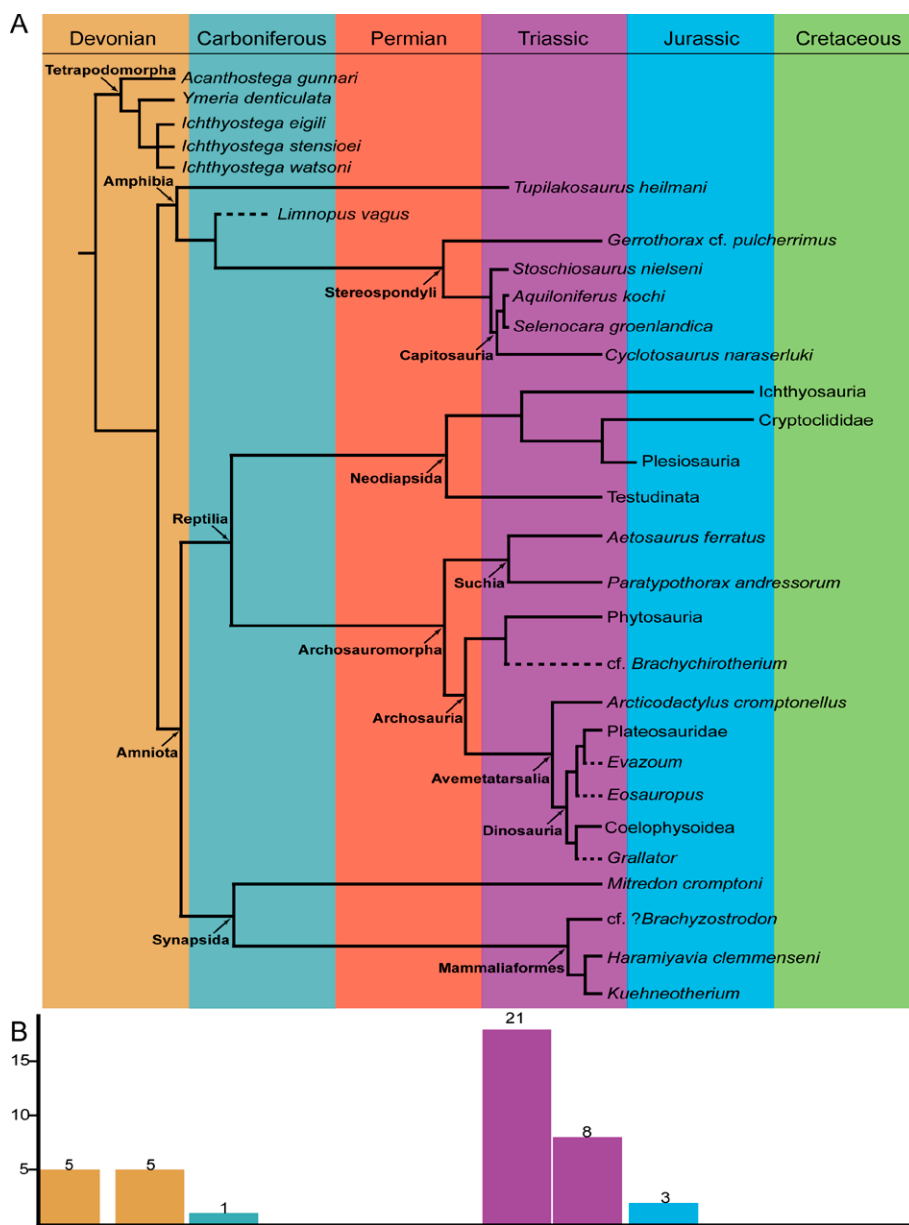


Fig. 2. Main fossil tetrapod taxa of Greenland. **A:** Time calibrated phylogenetic cladogram with major nodes enlightened with arrows and bold headings (for major clades relationships see Ruta *et al.* 2007; Schoch 2008; Brusatte *et al.* 2011; Clack *et al.* 2012; Benton 2014). Dashed lines stand for ichnotaxa. **B:** Alpha diversity (number of taxa per period). Left bars indicate the number of taxa in the fossil record; when present, right bars indicate the number of endemic species of Greenland.

Environmental context

Tetrapod fossils were recovered from at least three main sedimentary basins in Greenland, all of which are connected to extensive tectonic events and successive sedimentary infills. The Late Devonian Celsius Bjerg Group is the fourth and youngest stratigraphic division of the continental Old Red Sandstone Basin in East Greenland. This basin was formed during the Middle to Late Devonian, mainly by extensional collapse of an over-thickened Caledonian crustal welt (Larsen *et al.* 2008). Fossil-bearing horizons include the Aina Dal Formation, characterised by meandering river deposits, and the Britta Dal Formation, distinguished by ephemeral stream and flood basin deposits (Larsen *et al.* 2008).

During the Middle to Late Devonian, East Greenland was located around 5–10°N, forming part of the equatorial Laurasia continent, and likely included a trade wind belt with monsoonal climate during the summer (Olsen 1990; Larsen *et al.* 2008). Greenland drifted north during the entire Palaeozoic era, and during the Early–Middle Triassic the East Greenland basins were situated at a latitude of ~25°N and were characterised by an arid paleoclimate (Kent & Clemmensen 1996). Northward drift continued, and in the Late Triassic the Jameson Land Basin reached 40°N and was situated at the boundary between a subtropical arid and a winter-wet, warm temperate climate belt (Kent & Clem-

mensen 1996; Clemmensen *et al.* 1998; Kent & Tauxe 2005). Continued northward drift during the Jurassic changed the climate in the Jameson Land and nearby basins to warm temperate and humid.

The Triassic continental Jameson Land Basin is situated in the southern part of the East Greenland rift system and has been interpreted as an open embayment with a N–S orientation. The basin developed by extension and subsidence episodes during both the Late Permian to Early Triassic and the Late Triassic (Clemmensen 1980a, b; Price & Whitham 1997; Wignall & Twitchett 2002; Larsen *et al.* 2008). Characterised during the first stages of the Early Triassic by marine conditions, the Jameson Land Basin records regressions and continental emergence later in the Early Triassic (Clemmensen 1980a, b; Wignall & Twitchett 2002; Nøttvedt *et al.* 2008). Tetrapod fossils are found in the Jameson Land Basin in the mainly marine Early Triassic Wordie Creek Group, in the Late Triassic Fleming Fjord Formation characterised by freshwater lake deposits, and in the Late Triassic to Jurassic Kap Stewart Formation interpreted as a lacustrine depositional system (Clemmensen 1980a; Dam & Surlyk 1992; Clemmensen *et al.* 1998, 2016; Wignall & Twitchett 2002; Larsen *et al.* 2008).

Milne Land (Fig. 1E) is characterised by Jurassic marine sediments that directly overlie the Caledonian crystalline basement; the sediments were deposited during the Bathonian, due to the opening of the proto-



Fig. 3. The stem tetrapod *Acanthostega gunnari* Jarvik 1952, holotype NHMD 74758 (previously MGUH VP 6033 (MGUH A33 in Coates 1996 and previously MGUH VP 6264): partial skull in dorsolateral view, from the Late Devonian of the Britta Dal Formation. Scale bar: 5 cm.

Atlantic seaway between Greenland and Norway (Callomon & Birkelund 1980). Fossil tetrapods have been found in the Kap Leslie Formation, which is composed of marine sandstones and shales (Callomon & Birkelund 1980).

Devonian

Skeletal fossils

Acanthostega gunnari Jarvik 1952 (Stegocephali: Acanthostegidae)

Holotype. NHMD 74758 (previously MGUH A33 in Coates 1996 and previously MGUH VP 6264), a partial skull (Fig. 3).

Localities. Wiman Bjerg & Stensiö Bjerg, Gauss Halvø (Fig. 1D).

Horizon. Britta Dal Formation, Celsius Bjerg Group, fluvial deposits; low-latitude monsoonal climate.

Age. Late Devonian (Famennian).

Selected bibliography. Clack (1988a, 1989, 1992, 1994, 1998, 2002a, b); Coates (1996); Ahlberg & Clack (1998); Marshall *et al.* (1999); Clack *et al.* (2003); Larsen *et al.* (2008); Neenan *et al.* (2014).

Comments. We report here only the holotype. Coates (1996) reported at least 14 different specimens ascribed to *Acanthostega*.

Ichthyostega Säve-Söderbergh 1932 (Tetrapodomorpha: Ichthyostegidae)

Holotypes. *I. eigili* Säve-Söderbergh 1932 - MGUH VP 6004, an almost complete skull (Fig. 4); *I. stensioi* Säve-Söderbergh 1932 - MGUH VP 6001, a partial skull with skull roof and anterior palate (Fig. 5); *I. watsoni* Säve-Söderbergh 1932 - MGUH VP 6003, an almost complete skull (Fig. 6).

Locality. East Plateau at the north side of Celsius Bjerg, Ymer Ø (Fig. 1D).

Horizon. Aina Dal Formation and Britta Dal Formation, Celsius Bjerg Group, fluvial deposits; low-latitude monsoonal climate.

Age. Late Devonian (Famennian).

Selected bibliography. Jarvik (1952, 1996); Marshall *et al.* (1999); Ahlberg *et al.* (2005); Blom (2005); Ahlberg & Clack (2006); Larsen *et al.* (2008); Pierce *et al.* (2012, 2013).

Comments. We report here only the holotypes' depository numbers. As noted by Blom (2005) over 300 specimens are referred to *Ichthyostega*. The species name for *I. stensioi* is given following the spelling of Snitting & Blom (2009).

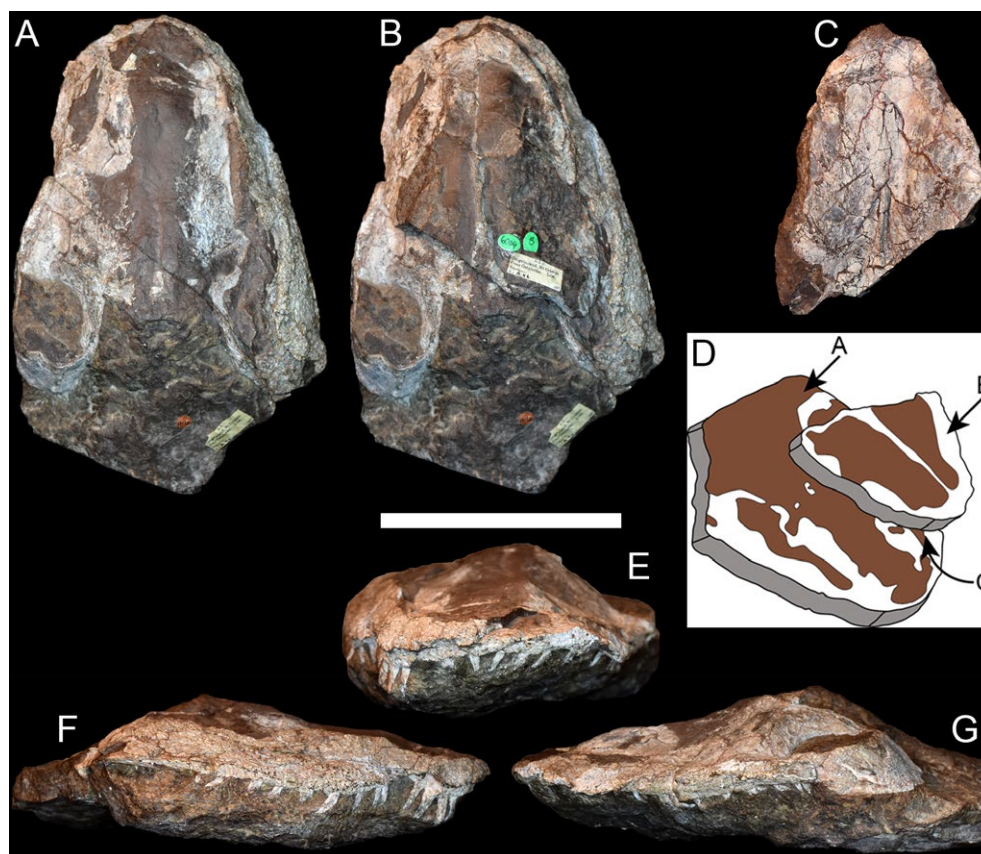


Fig. 4. The stem tetrapod *Ichthyostega eigili* Säve-Söderbergh 1932, holotype MGUH VP 6004 from Late Devonian of the Aina Dal and Britta Dal Formations. **A–B:** Dorsal views **C:** Ventral view. **D:** Schematic drawing of MGUH VP 6004 with correspondent views of **A**, **B**, and **C**, out of scale and with exaggerated thickness. **E:** Frontal view. **F:** Right lateral view. **G:** Left lateral view. Scale bar **A–C**, **E–G:** 10 cm.

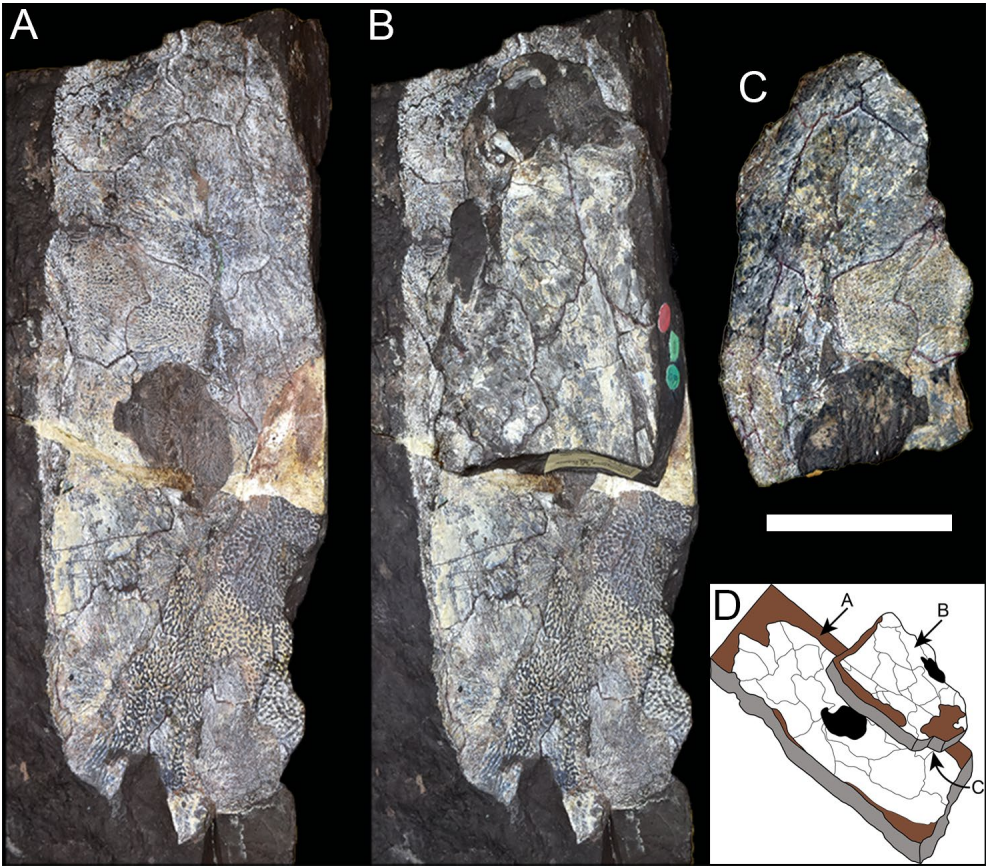


Fig. 5. The stem tetrapod *Ichthyostega stensioi* Säve-Söderbergh 1932, holotype MGUH VP 6001: partial skull from Late Devonian of the Aina Dal and Britta Dal Formations. **A–B:** Dorsal views. **C:** Ventral view. **D:** Schematic drawing of MGUH VP 6001 with correspondent views of A, B, and C, out of scale and with exaggerated thickness. Scale bar A–C: 5 cm.

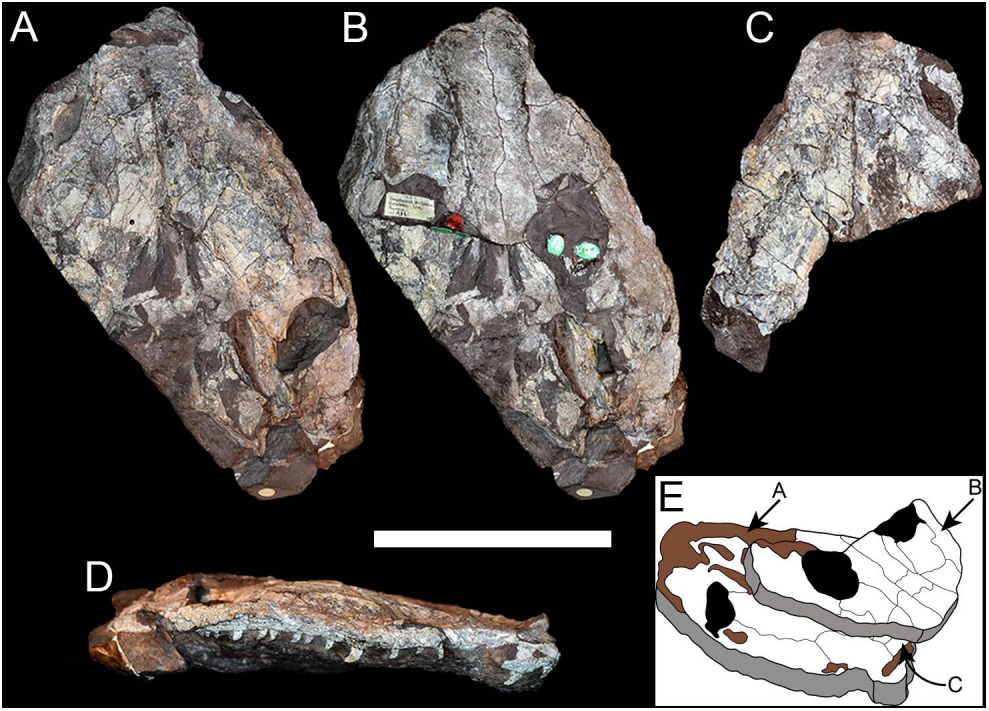


Fig. 6. The stem tetrapod *Ichthyostega watsoni* Säve-Söderbergh 1932, holotype MGUH VP 6003: partial skull from Late Devonian of the Aina Dal and Britta Dal Formations. **A–B:** Dorsal views. **C:** Ventral view. **D:** Right lateral view. **E:** Schematic drawing of MGUH VP 6001 with correspondent views of A, B, and C, out of scale and with exaggerated thickness. Scale bar A–D: 10 cm.

Ymeria denticulata Clack *et al.* 2012 (Tetrapodomorpha: Tetrapoda)

Holotype. NHMD 74759 (previously MGUH VP 6088), a partial skeleton with cranial elements (lower jaws, maxillae, premaxillae, partial palate) and postcranial shoulder girdle (Fig. 7).

Locality. South side of Celsius Bjerg, Ymer Ø (Fig. 1D).

Horizon. Celsius Bjerg Group, scree (fluvial deposits); low-latitude monsoonal climate.

Age. Late Devonian (Famennian).

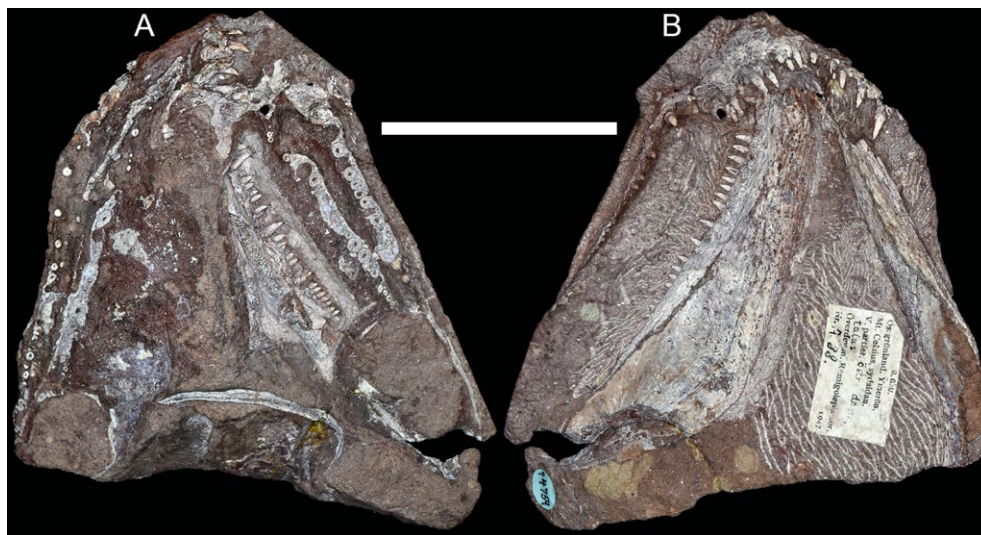


Fig 7. The stem tetrapod *Ymeria denticulata* Clack *et al.* 2012, holotype NHMD 74759 (previously MGUH VP 6088), a partial skull with lower jaws from Late Devonian of the Britta Dal Formation. **A:** Dorsal view. **B:** Ventral view. Scale bar: 5 cm.

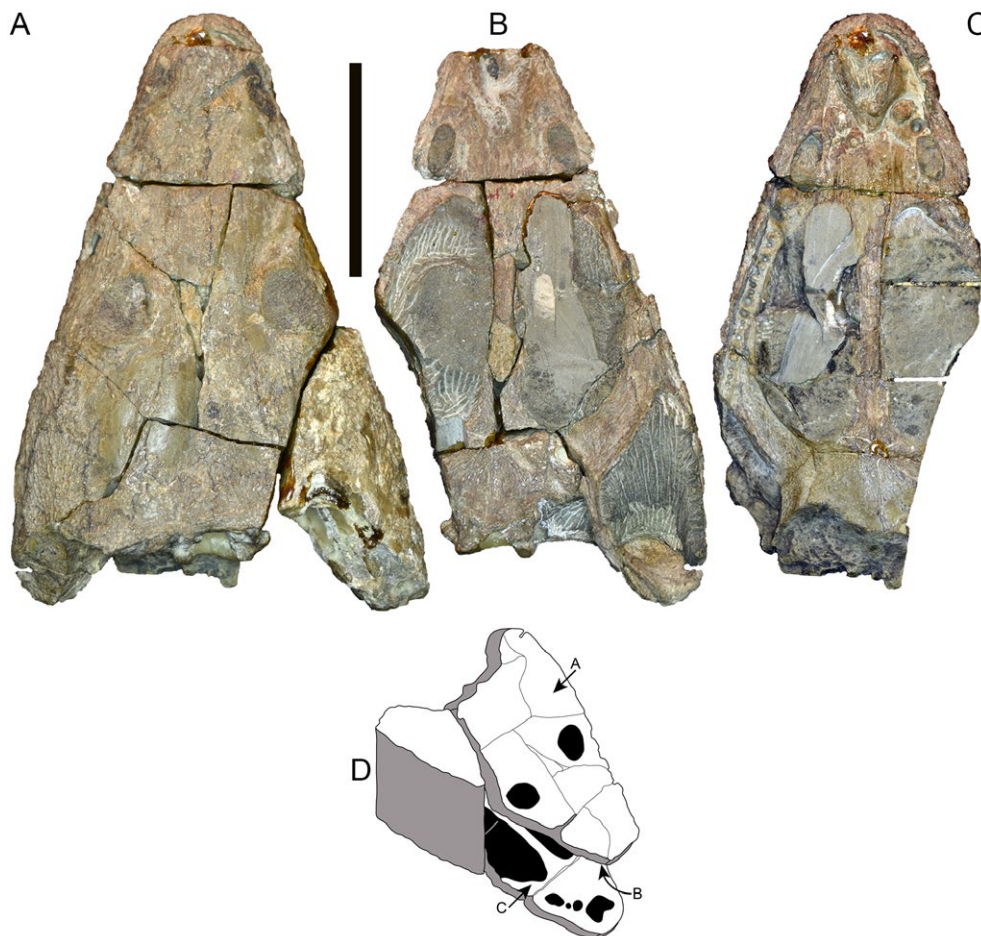


Fig. 8. The capitosauroid *Aquiloniferus kochi* Bjerring 1999, holotype MGUH VP 3357 (previously MGUH VP At.1): a skull from the Early Triassic of the Wordie Creek Group. **A, C:** Dorsal views. **B:** Ventral view. **D:** Schematic drawing of MGUH VP 3357 with correspondent views of A, B, and C (out of scale and with exaggerated thickness). Scale bar A–C: 5 cm.

Carboniferous

Trace fossil

Limnopus vagus Marsh 1894

Referred material. MGUH 31556, a slab preserving at least 12 tracks (isolated and three as pes-manus couples) on average 50 to 55 mm long and 55 to 70 wide.

Locality. Langelinie mountain, Mesters Vig, northern Scoresby Land, 72°09 N, 24°07 W (Fig. 1E).

Horizon. Non-marine dark brown, fine- to medium-grained sandstone from floodplain deposits of either Blyklippen or Profilbjerget Member of the Mesters Vig Formation, Traill Ø Group.

Age. Late Carboniferous (late Bashkirian to early Moscovian).

Selected bibliography. Bendix-Almgreen (1976); Milàn *et al.* (2016a).

Comments. The tracks were originally found by E. Witzig during field work in 1950. These tracks, together with additional material, were first depicted by Bendix-Almgreen (1976, p. 553, fig. 425D) and described as casts of tetrapod trails. However, Bendix-Almgren (1976) erroneously reported them as Lower Permian. Gilberg (1992) re-mentioned them briefly in a firsthand account from the fieldwork in 1950. Milàn *et al.* (2016a) indicated eryopoid temnospondyls as the potential track makers.

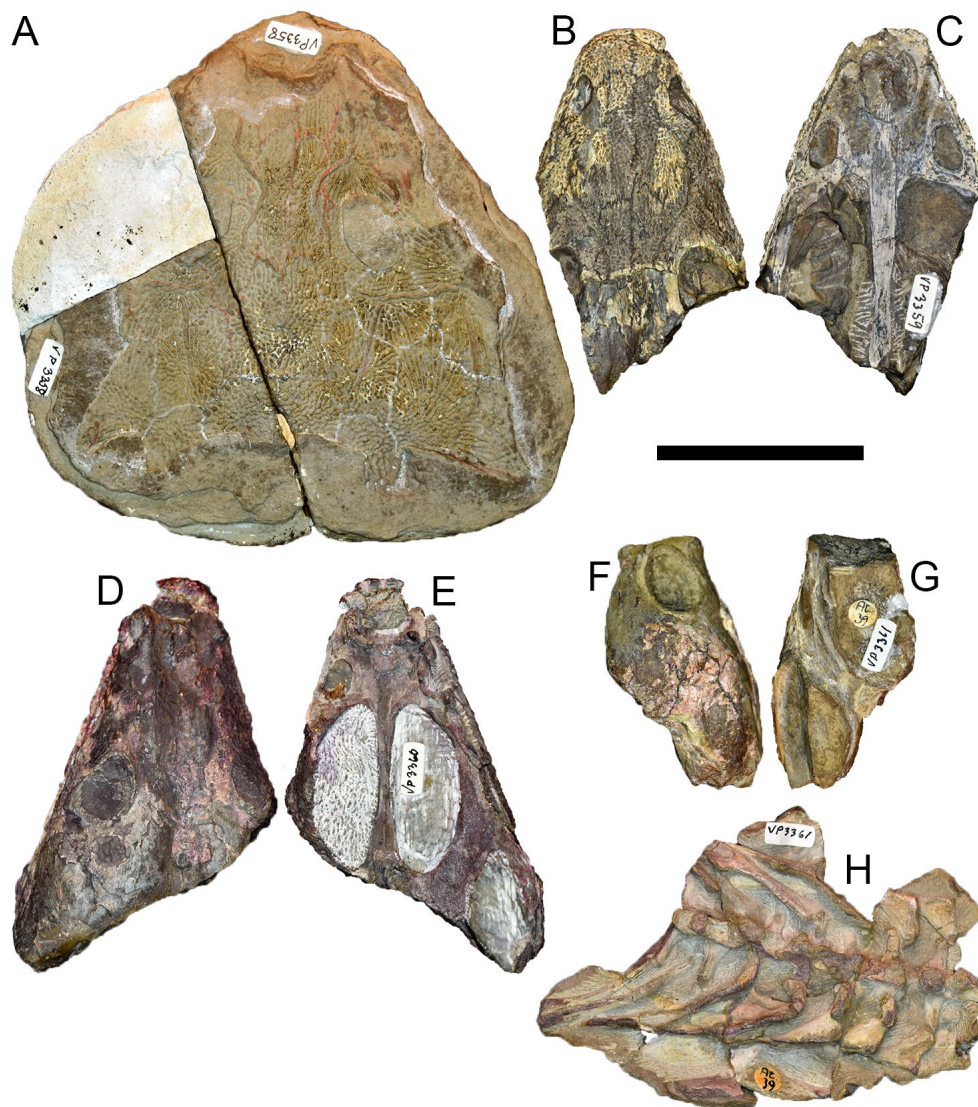


Fig. 9. The capitosauroid *Aquiloniferus kochi* Bjerring 1999: specimens from the Early Triassic of the Wordie Creek Group. **A:** Dorsal view of MGUH VP 3358 (previously MGUH VP At. 3), natural internal cast of a partial skull. **B–C:** Dorsal and ventral views of MGUH 3359 (previously MGUH VP At. 28), a partial skull. **D–E:** Dorsal and ventral views of MGUH 3360 (previously MGUH VP At. 29), a partial skull. **F–H:** MGUH 3361 (previously MGUH VP At. 39), as a partial skull, in dorsal (F) and ventral (G) views, and seven cervical vertebrae (H). Scale bar: 5 cm.

Triassic

Skeletal fossils

Aquiloniferus kochi Bjerring 1999 (Temnospondyli: Capitosauroida)

Holotype. MGUH VP 3357 (previously MGUH VP At.1), a skull (Fig. 8).

Referred material. MGUH VP 3358 (previously MGUH VP At. 3), a natural internal cast of a partial skull; MGUH 3359 (previously MGUH VP At. 28), a partially preserved anterior half of a skull; MGUH 3360 (previously MGUH VP At. 29), a partially preserved skull; MGUH 3361 (previously MGUH VP At. 39), a partially preserved skull associated to seven cervical vertebrae (Fig. 9).

Locality. South-east of Kap Stosch, Stensiö Plateau and Spath Plateau, Hold With Hope (Fig. 1D).

Horizon. *Myalina kochi* horizon, Wordie Creek Group, shallow marine deposits; warm tropical climate.

Age. Early Triassic (Induan).

Selected bibliography. Cosgriff (1984); Lucas (1998); Bjerring (1999).

Comments. These specimens were originally attributed to *Luzocephalus johanssoni* Säve-Söderbergh 1935.

Selenocara groenlandica Bjerring 1997 (Temnospondyli: Capitosauroida)

Holotype. MGUH VP 3339 (previously MGUH VP At. 2), posterior part of a skull (Fig. 10).

Referred material. MGUH VP 3340 (previously MGUH VP At. 17), a natural cast of a partial skull.

Locality. South-east of Kap Stosch, ridge VIII-IX of the north-east slope of Stensiö Plateau, Hold With Hope (Fig. 1D).

Horizon. *Myalina kochi* horizon, Wordie Creek Group, shallow marine deposits; warm tropical climate.

Age. Early Triassic (Induan).

Selected bibliography. Bjerring (1997); Lucas (1998).

Comments. These specimens were originally

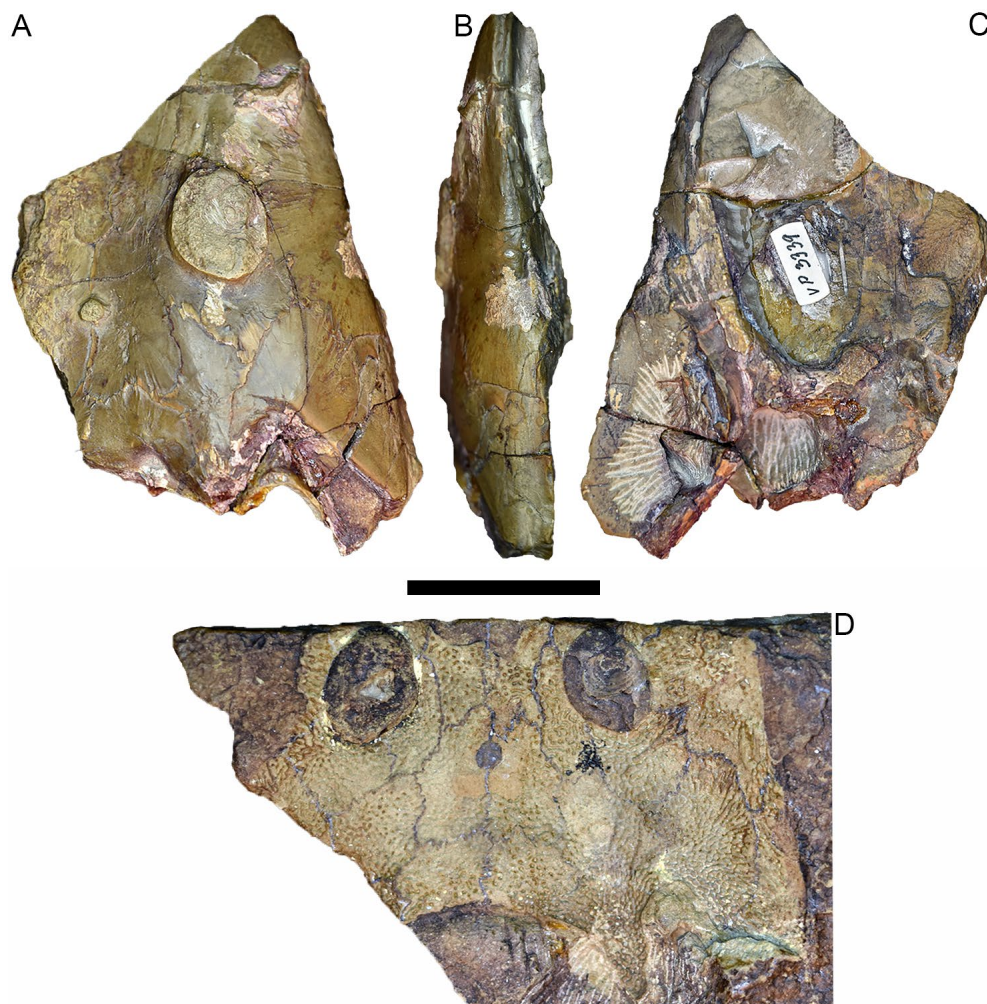


Fig. 10. The capitosaurid *Selenocara groenlandica* Bjerring 1997, holotype MGUH VP 3339 (previously MGUH VP At. 2): a partial skull from the Early Triassic of the Wordie Creek Group, in **A**: Dorsal views, **B**: Lateral right view, and **C**: Ventral views; and natural cast of partial skull MGUH VP 3340 (previously MGUH VP At. 17) (**D**), from the Early Triassic of the Wordie Creek Group in **D**: dorsal view. Scale bar: 3 cm.

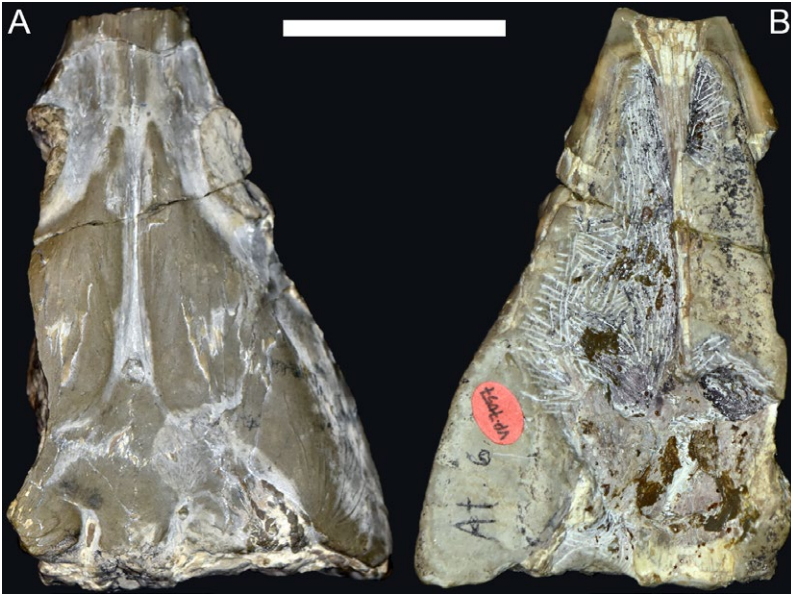


Fig. 11. The trematosaurid *Stoschiosaurus nielsenii* Säve-Söderbergh 1935, holotype MGUH VP 7057 (previously MGUH VP At.6): a partial skull. **A:** Dorsal view. **B:** Ventral view. Scale bar: 3 cm.

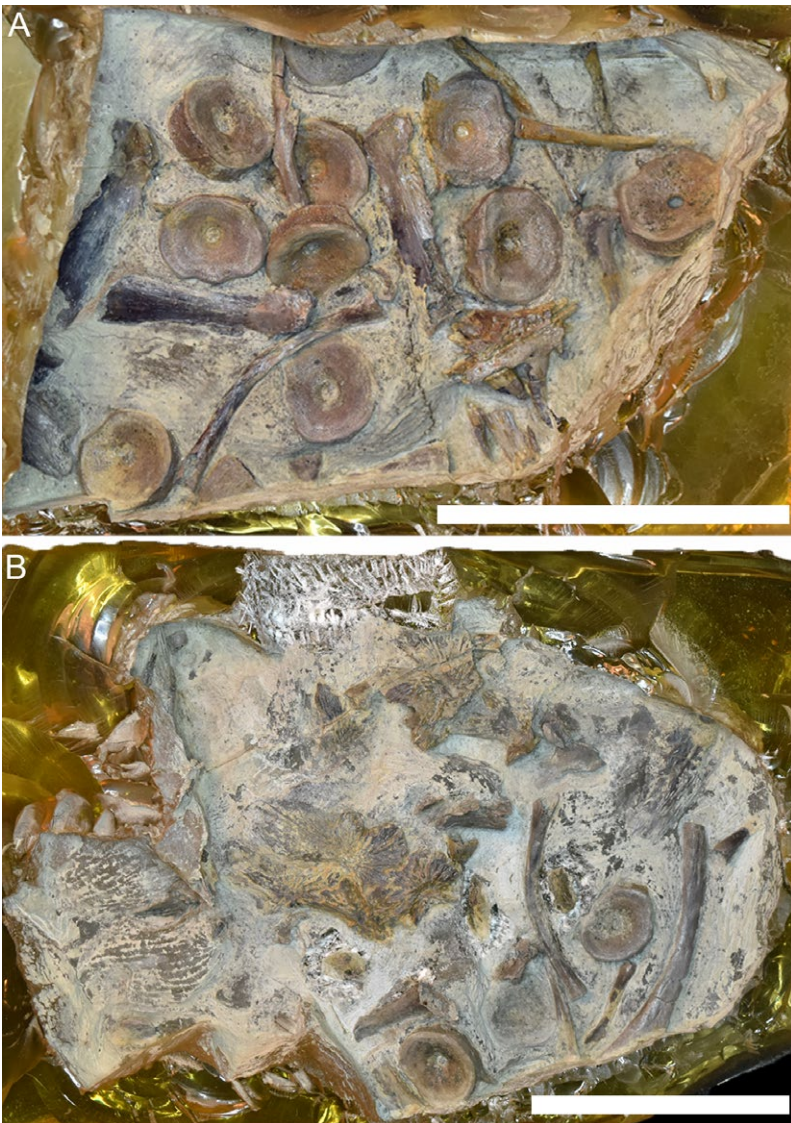


Fig. 12. The tupilakosaurid *Tupilakosaurus heilmanni* Nielsen 1954, holotype MGUH VP 3328 (specimen A): two separate blocks containing postcranial material (including vertebrae, ribs, tooth) from the Early Triassic of the Wordie Creek Group. **A:** Block A. **B:** Block B. Scale bars: 5 cm.

identified as *Wetlugasaurus groenlandicus* by Säve-Söderbergh (1935).

***Stoschiosaurus nielseni* Säve-Söderbergh 1935** (Temnospondyli: Trematosauridae)

Holotype. MGUH VP 7057 (previously MGUH VP At.6), a partial skull (Fig. 11).

Locality. South-east of Kap Stosch, ridge VIII–IX of the north-east slope of Stensiö Plateau, Hold With Hope (Fig. 1D).

Horizon. *Myalina kochi* horizon, Wordie Creek Group, coastal claystone/sandstone, shallow marine deposits; warm tropical climate.

Age. Early Triassic (Induan).

***Tupilakosaurus heilmani* Nielsen 1954** (Temnospondyli: Tupilakosauridae)

Holotype. MGUH VP 3328 (specimen A), a partial skeleton (Fig. 12).

Locality. South-east of Kap Stosch, north-east slope of Stensiö Plateau, Hold With Hope (Fig. 1D).

Horizon. *Myalina kochi* horizon, Wordie Creek Group, shallow marine deposits; warm tropical climate.

Age. Early Triassic (Induan).

Selected bibliography. Nielsen (1954, 1967).

***Cyclotosaurus naraserluiki* Marzola et al. 2017b** (Temnospondyli: Cyclotosauridae)

Holotype. MGUH.VP 9522, a nearly complete skull (Fig. 13A).

Referred material. Two vertebral intercentra, MGUH.VP 9523 and MGUH.VP 9524.

Locality. Macknight Bjerg, Jameson Land, 71°22.30' N, 22°33.14' W (Fig. 1F).

Horizon. Ørsted Dal Member (Carlsberg Fjord beds), Fleming Fjord Formation, lacustrine deposits; subtropical arid to winter-wet, warm temperate climate.

Age. Late Triassic (late Norian to early Rhaetian).

Selected bibliography. Jenkins et al. (1994); Marzola et al. (2017b).

***Gerrothorax* cf. *pulcherrimus* Fraas 1913** (Temnospondyli: Plagiosauridae)

Referred material. At least sixty-four specimens of *G. pulcherrimus* have been recovered from the Fleming Fjord Formation. The main specimens used for the descriptions in Jenkins et al. (2008) are MGUH 28916, MGUH 28917, MGUH 28918, MGUH 28919, MGUH 28921, MGUH 28923 and MGUH 28925 for skull anatomy and interclavicles; MGUH 28922 and MGUH 28924 for vertebral structure and dermal armour.

Locality. Macknight Bjerg, Jameson Land, 71°22.30' N, 22°33.14' W (Fig. 1F).

Horizon. Ørsted Dal Member (Carlsberg Fjord beds), Fleming Fjord Formation, lacustrine deposits; subtropical arid to winter-wet, warm temperate climate.

Age. Late Triassic (late Norian to early Rhaetian).

Selected bibliography. Jenkins et al. (1994, 2008); Schoch & Witzmann (2012); Sulej et al. (2014).

cf. *Proganochelys* Baur 1887 (Testudinata: Proganochelyidae)

Referred material. NHMD 190349 (previously MCZ Field no. 22/88G), partially preserved carapace and plastron, caudal vertebrae, and incomplete limb bones (right humerus, right ulna, right radius, both femora, and left tibia) (Fig. 13C).

Locality. Lepidopteriselv, Jameson Land, 71°15.760' N, 22°32.682' W, 285 m a.s.l. (Fig. 1F)

Horizon. Upper part of the Ørsted Dal Member (Carlsberg Fjord Beds), Fleming Fjord Formation, lacustrine deposits; subtropical arid to winter-wet, warm temperate climate.

Age. Late Triassic (late Norian to early Rhaetian).

Selected bibliography. Jenkins et al. (1994); Marzola et al. (2016).

Comments. This specimen was originally described by Jenkins et al. (1994) as cf. *Proganochelys*, based on two presumed autapomorphies for the genus *Proganochelys*: (1) the presence of a pair of gular and intergular projections and (2) the presence of the dorsal epiplastral process. Paired gular projections are now also known in the Late Triassic *Odontochelys semitestacea* Li et al. (2008) from China, while dorsal epiplastral processes are known both in *O. semitestacea* and the Early Jurassic *Kayentachelys aprix* Gaffney et al. (1987) from Arizona, USA. An expedition to the Jameson Land Basin in the summer of 2016 (Marzola et al. 2017a) revisited the source locality and collected additional components of the specimen including two fragmentary vertebrae.

Testudinata indet.

Referred specimen. NHMD 163391–163417, a fragmentary specimen including carapace, plastron, scapular and pelvic girdles, and limb bones; NHMD 74737, a fragmentary specimen including carapace, plastron, and pelvic girdle.

Locality. NHMD 163391–163417 was found during the US-Danish expedition in 1995 at Ærenprisdal, Jameson Land, 71°32.611' N, 22°55.307' W; NHMD 74737 was found during the Danish expedition in 2012 by one of us (OM) in solifluction at Wood Bjerg–Macknight Bjerg, Jameson Land, 71°22.965' N, 22°33.216' W (Fig. 1F).

Horizon. NHMD 163391–163417 and NHMD 74737 both come from the Ørsted Dal Member (Carlsberg Fjord beds) of the Fleming Fjord Formation, lacustrine deposits; subtropical arid to winter-wet, warm temperate climate.

Age. Late Triassic (late Norian to early Rhaetian).

Selected bibliography. Mateus *et al.* (2014); Clemmensen *et al.* (2016); Marzola *et al.* (2016).

Comments. Both specimens are unpublished and are currently under study. Another specimen has been found by the Cambridge expedition in 2015, from the Malmros Klint or Ørsted Dal Member of the Fleming Fjord Formation (Steven Andrews, personal communication 2016).

Aetosaurus ferratus Fraas 1877 (Archosauria: Stagonolepididae)

Referred material. NHMD 190375–190379 (previously MCZ Field no. 22/92G), a skull associated with dermal armor, limb bones, vertebrae, and a partial sacrum (Fig. 13B).

Locality. Sydkronen, northern Jameson Land, 71°49.65' N, 23°30.83' W (Fig. 1E).

Horizon. Ørsted Dal Member (Bjergkronerne beds), Fleming Fjord Formation, fluvial deposits; subtropical arid to winter-wet, warm temperate climate.

Age. Late Triassic (late Norian to early Rhaetian).

Selected bibliography. Jenkins *et al.* (1994); Schoch (2007); Parker (2016).

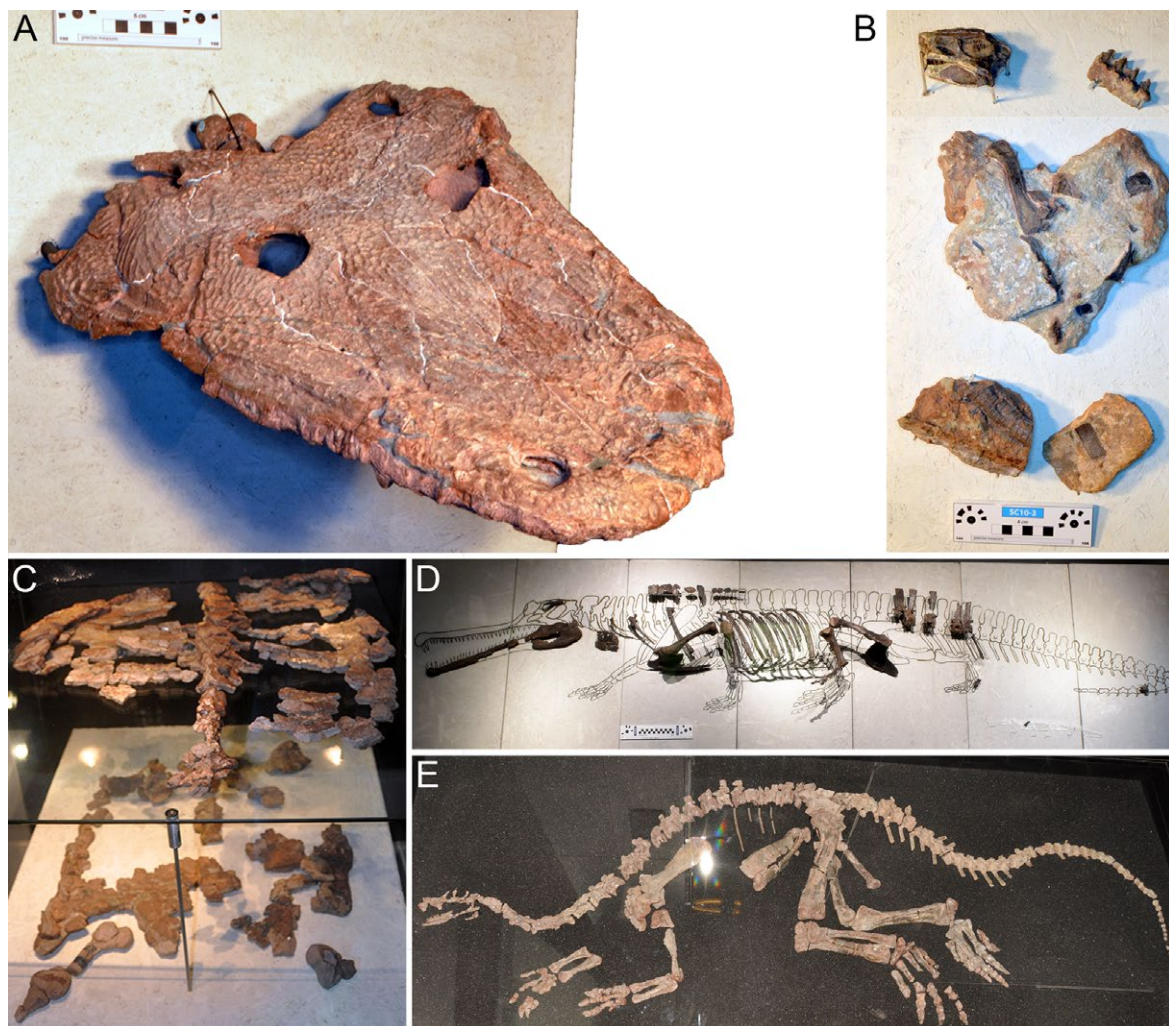


Fig. 13. Fossil tetrapods from the Late Triassic of Jameson Land Basin in exhibition at the GeoCenter of Møns Klint, Denmark, as of 2016. **A:** Oblique photograph of the holotype of the capitosaurid *Cyclotosaurus naraserluiki* Marzola *et al.* 2017b MGUH.VP 9522. **B:** The stagonolepidid *Aetosaurus ferratus* Fraas 1877 NHMD 190375–190379 (previously MCZ Field no. 22/92G). **C:** Oblique photograph of the testudine NHMD 190349 (previously MCZ Field no. 22/88G) (top layer: carapace; bottom layer: plastron and limb bones). **D:** Adult and juvenile (bottom right corner) phytosaurs, respectively NHMD 74733 and NHMD 74736. **E:** Sauropodomorph plateosauridae NHMD 164734 (previously 4/88/G and GM.V 2013-683). C and E not scaled. Scale bars, A–B: 6 cm; D: 15 cm.

Comments. Despite being incomplete, this specimen has been attributed to *A. ferratus* by most recent studies (Schoch 2007; Parker 2016).

***Paratypothorax andressorum* Long & Ballew 1985** (Archosauria: Stagonolepididae)

Referred material. MCZ Field no. 23/92G, one paramedian (mostly preserved as a natural mold) and two lateral dermal scutes.

Locality. Sydkronen, northern Jameson Land.

Horizon. Uncertain, potentially Ørsted Dal Member, Fleming Fjord Formation, fluvial deposits; subtropical arid to winter-wet, warm temperate climate.

Age. Late Triassic (late Norian to early Rhaetian).

Selected bibliography. Jenkins *et al.* (1994); Lucas *et al.* (2006).

Phytosauria indet. (Archosauriformes: Crurotarsi)

Referred specimen. Four incomplete phytosaurs (two adults, one subadult and one juvenile) collected during the 2012 GeoCenter Møns Klint expedition (NHMD 74733–74736, Fig. 13D).

Locality. ‘Mateus’ site, Lepidopteriselv, Jameson Land, 71°15.584’ N, 22°31.785’ W (Fig. 1F).

Horizon. Middle Malmros Klint Member, Fleming Fjord Formation, lacustrine and overbank fluvial deposits; subtropical arid to winter-wet, warm temperate climate.

Age. Late Triassic (late Norian to early Rhaetian).

Selected bibliography. Mateus *et al.* (2014); Clemensen *et al.* (2016).



Fig. 14. The eudimorphodontid *Arcticodactylus cromptonellus* (Jenkins *et al.* 2001), holotype NHMD 74799 from the Late Triassic of the Fleming Fjord Formation. **A:** block exposed in the GeoCenter (as for 2016). **B:** counter block at NHMD. Scale bar: 3 cm.

***Arcticodactylus cromptonellus* (Jenkins *et al.* 2001)**
(Pterosauria: Eudimorphodontidae)

Holotype. NHMD 74799, a disarticulated skeleton preserving numerous cranial and postcranial elements (Fig. 14).

Locality. Macknight Bjerg, Jameson Land, 71°22.277' N, 22°33.341' W (Fig. 1F).

Horizon. Ørsted Dal Member (Carlsberg Fjord beds), Fleming Fjord Formation, lacustrine deposits; subtropical arid to winter-wet, warm temperate climate.

Age. Late Triassic (late Norian to early Rhaetian).

Selected bibliography. Jenkins *et al.* (1994); Dalla Vecchia (2003, 2014); Kellner (2015).

Comments. Originally attributed by Jenkins *et al.* (1994) to the genus *Eudimorphodon* Zambelli 1973, this specimen was later described as a new genus, *Arcticodactylus*, by Kellner (2015).

Plateosauridae indet. (Dinosauria: Sauropodomorpha)

Referred material. At least four individuals: NHMD 164734 (previously 4.88.G and GM.V 2013-683), an unreported and unpublished complete individual with cranial and postcranial material (Fig. 13E); NHMD 164741 (previously MCZ Field no. 61/91G), a skull reported in Jenkins *et al.* (1994, fig. 11, p. 14); NHMD 164758 (previously 1/G95 or 1/95/G), an unreported and unpublished individual with cranial and postcranial material, probably a sub-adult; NHMD 164775, unpublished and partially unprepared material excavated during the 2012 Danish expedition.

Locality. NHMD 164734 is from Lepidopteriselv,

Jameson Land; NHMD 164741 and NHMD 164758 are from the north side of Macknight Bjerg, Jameson Land, with the former located at 71°23.010' N, 22°34.114' W and the latter stratigraphically slightly above it, at 71°22.993' N, 22°33.972' W; NHMD 164775 is from the 'Iron Cake' Site, Wood Bjerg–Macknight Bjerg, Jameson Land, 71°22.262' N, 22°33.381' W (Fig. 1F).

Horizon. NHMD 164734 is from the Ørsted Dal Member (Carlsberg Fjord beds), Fleming Fjord Formation, NHMD 164741 and 164758 from the uppermost Malmros Klint Member, Fleming Fjord Formation, lacustrine deposits; subtropical arid to winter-wet, warm temperate climate.

Age. Late Triassic (late Norian to early Rhaetian).

Selected bibliography. Jenkins *et al.* (1994); Clemmensen *et al.* (2016).

Comments. As of August 2017, NHMD 164734 is exhibited at GeoCenter Møns Klint, Denmark (Fig. 13E); NHMD 164741 and the skull of NHMD 164758 are under restoration and final preparation at Museu da Lourinhã (Portugal), while the postcranial material of NHMD 164758 is in storage at GeoCenter Møns Klint; a partially prepared rib cage of NHMD 164775 is also exhibited at GeoCenter Møns Klint, while the rest of the material from the 2012 expedition is stored and under preparation at Dino-Park Münchehagen (Germany).

Jenkins *et al.* (1994) associated NHMD 164741 to *Plateosaurus engelhardti*. We suggest that this association is considered with caution because preliminary phylogenetic studies by our team indicate that this specimen belongs to the clade Plateosauria, though presenting distinct and unique morphological characters that distinguish it from *Plateosaurus*.



Fig. 15. The cynodont *Mitredon cromptoni* Shapiro & Jenkins 2001, holotype MGUH VP 3392: a left dentary from the Late Triassic of the Fleming Fjord Formation. **A:** lingual view. **B:** labial view. Scale bar: 1 cm.

Mitredon cromptoni Shapiro & Jenkins 2001 (Therapsida: Cynodontia)

Holotype. MGUH VP 3392, an incomplete left mandible with teeth (Fig. 15).

Locality. North of Ærenprisdal at its junction with Pingel Dal, Jameson Land, 71°32.929' N, 22°55.450' W (Fig. 1F).

Horizon. Uppermost dolostone in Ørsted Dal Member (Tait Bjerg Beds), Fleming Fjord Formation, lacustrine deposits; subtropical arid to winter-wet, warm temperate climate.

Age. Late Triassic (late Norian to early Rhaetian).

Selected bibliography. Shapiro & Jenkins (2001).

cf. *?Brachyzostrodon* Sigogneau-Russell 1983 (Mammalia: Morganucodontidae)

Referred specimen. MCZ Field no. 64/91 G 4, a mammalian tooth.

Locality. Western slope of Tait Bjerg, Jameson Land, bounded by Passagen to the south, Buch Bjerg to the north, and Carlsberg Fjord to the east.

Horizon. Dolomitic limestone of the Tait Bjerg Beds, Ørsted Dal Member of the Fleming Fjord Formation, lacustrine deposits; subtropical arid to winter-wet, warm temperate climate.

Age. Late Triassic (late Norian to early Rhaetian).

Selected bibliography. Jenkins *et al.* (1994).

Haramiyavia clemmenseni Jenkins *et al.* 1997 (Mammalia: Haramiyidae)

Holotype. MCZ 7/95, partially associated cranial elements and postcranial bones, including dentaries, premaxilla, vertebrae, and limb bones (Fig. 16A–B).

Referred specimen. MCZ 10/95, a left mandible with teeth (Fig. 16C).

Locality. North side of Ærenprisdal, at the junction with Pingel Dal, Jameson Land, 71°32.958' N, 22°55.188' W, 670 m a.s.l. (Fig. 1F).

Horizon. Ørsted Dal Member (Tait Bjerg Beds), Fleming Fjord Formation, lacustrine deposits; subtropical arid to winter-wet, warm temperate climate.

Age. Late Triassic (late Norian to early Rhaetian).

Selected bibliography. Jenkins *et al.* (1994); Luo *et al.* (2015).

Kuehneotherium Kermack *et al.* 1968 (Mammalia: Kuehneotheriidae)

Referred specimen. MCZ Field no. 62/91 G 1–2 and 64/91 G 3–8 and 10: ten mammalian teeth.

Locality. Western slope of Tait Bjerg, Jameson Land, bounded by Passagen to the south, Buch Bjerg to the north, and Carlsberg Fjord to the east.

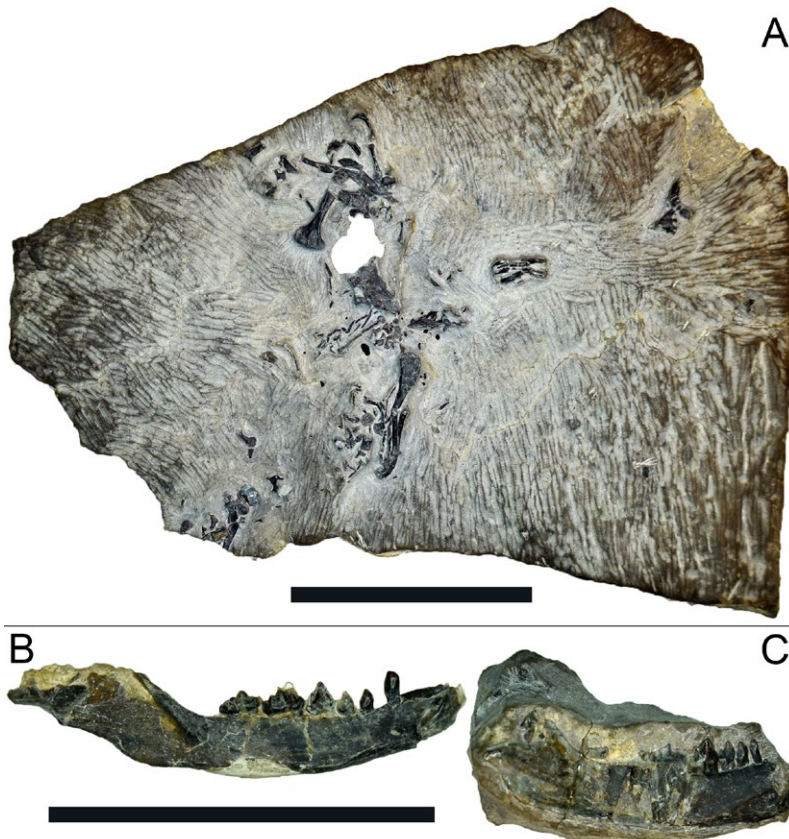


Fig. 16. The haramiyid *Haramiyavia clemmenseni* Jenkins *et al.* 1997, holotype MCZ 7-G95 from the Late Triassic of the Fleming Fjord Formation. **A:** Main block with cranial and postcranial elements. **B:** Right mandible in labial view. **C:** Left mandible in lingual view. Scale bars, A: 5 cm; B and C: 2 cm.

Horizon. Ørsted Dal Member (Tait Bjerg Beds, dolomitic limestone), Fleming Fjord Formation, lacustrine deposits; subtropical arid to winter-wet, warm temperate climate.

Age. Late Triassic (late Norian to early Rhaetian).

Selected bibliography. Jenkins *et al.* (1994).

Comments. Two teeth (MCZ 62/91 G 1–2) were found in the lowermost Ørsted Dal Member (Carlsberg Fjord beds), while the remaining eight teeth (MCZ 64/91 G 3–8, 10) were found in the uppermost Ørsted Dal Member (Tait Bjerg Beds).

Sulej *et al.* (2014) reported abundant Late Triassic vertebrate material from the Malmros Klint and Ørsted Dal Members of the Fleming Fjord Formation. To date, this material has not been described. Among the most significant vertebrate fossils reported from the 2014 expedition were archosaur bone remains including fragmentary limbs and pelvis associated with dinosauriforms and theropod dinosaurs from Macknight Bjerg, the latter including part of a maxilla, two isolated teeth, two cervical vertebrae, fragmentary tibia, fibula, pubis, ischium, dorsal and caudal vertebrae and tentatively attributed to a coelophysoid theropod (Niedzwiedzki & Sulej 2017). There are also sauropodomorph and theropod dinosaur tracks and trackways from Macknight Bjerg, remains of stem turtles and a potential pterosaur, an incomplete mandible and associated dentition of a stem mammal from Liasryggen (Jameson Land) and pentadactyl tracks, possibly of stem mammal affinity.

Trace fossils

***Eosauropus* isp. Lockley *et al.* 2006a**

Referred specimens. Trackways S1 and S2 described in Lallensack *et al.* (2017, figs. 2–3).

Locality. ‘Track Mountain’, on a north-east slope of Wood Bjerg–Macknight Bjerg, Jameson Land (Trackway S1: 71°24.853' N, 22°33.322' W and 534 m a.s.l.; Trackway S2: 71°24.955' N, 22°32.952' W; Fig. 1F).

Horizon. Ørsted Dal Member (lowermost Tait Bjerg Beds), Fleming Fjord, lacustrine deposits; subtropical arid to winter-wet, warm temperate climate.

Age. Late Triassic (late Norian to early Rhaetian).

Selected bibliography. Sulej *et al.* (2014); Lallensack *et al.* (2017).

Comments. The *Eosauropus* trackways described in Lallensack *et al.* (2017) are the largest tracks known for this morphotype and were potentially made by sauropod dinosaurs; the tracks represent the first evidence of the clade Sauropoda from Greenland and extend their presence back to the Late Triassic.

***Evazoum* isp. Lockley *et al.* 2006b**

Referred specimens. Trackways S3 as described by Lallensack *et al.* (2017, fig. 4).

Locality. ‘Track Mountain’, on a north-east slope of Wood Bjerg–Macknight Bjerg, Jameson Land, 71°24.857' N, 22°33.334' W (Fig. 1F).

Horizon. Ørsted Dal Member (lowermost Tait Bjerg Beds), Fleming Fjord, lacustrine deposits; subtropical arid to winter-wet, warm temperate climate.

Age. Late Triassic (late Norian to early Rhaetian).

Selected bibliography. Sulej *et al.* (2014); Lallensack *et al.* (2017).

Comments. The *Evazoum* trackway described in Lallensack *et al.* (2017) was made by a bipedal trackmaker, potentially a non-sauropod sauropodomorph dinosaur, and are the largest known tracks ascribed to this morphotype.

***Grallator* Hitchcock 1858**

Referred specimens. MGUH 27811–27915 described by Milàn *et al.* (2006) and further tracks described by Gatesy *et al.* (1999, p. 142, fig. 1), Gatesy (2001, p. 139, fig. 1), Milàn *et al.* (2004, p. 289, fig. 4), and Clemmensen *et al.* (2016, p. 42, fig. 8).

Locality. Different localities at Tait Bjerg and Wood Bjerg, Jameson Land (Fig. 1F).

Horizon. Malmros Klint and Ørsted Dal Member, Fleming Fjord Formation, lacustrine deposits; subtropical arid to winter-wet, warm temperate climate.

Age. Late Triassic (late Norian to early Rhaetian).

Selected bibliography. Jenkins *et al.* (1994); Gatesy *et al.* (1999); Gatesy (2001); Milàn *et al.* (2004); Sulej *et al.* (2014); Clemmensen *et al.* (2016).

Comments. The *Grallator* tracks have an average foot size of 23.5 cm length and 8 cm width; trackways have an average pace of 61 cm and step of 119 cm (Clemmensen *et al.* 2016). They were attributed to ceratosaurid theropod dinosaurs by Gatesy *et al.* (1999). The record is extremely rich, including thousands of tracks from multiple horizons in the middle and upper part of the Malmros Klint Member, the overlying Carlsberg Fjord beds (the most abundant source) and the lowermost Tait Bjerg Beds of the Ørsted Dal Member (Milàn *et al.* 2014; Sulej *et al.* 2014; Clemmensen *et al.* 2016).

cf. *Brachychirotherium* Beurlen 1950

Referred specimens. MGUH 31233a–c and MGUH 31234, two slabs preserving tracks as concave epireliefs (true tracks); MGUH 31235, a slab bearing tracks as convex hyporeliefs (natural casts).

Locality. Tait Bjerg (MGUH 31235) and north of Lepidopteriselv (MGUH 31233a–c and MGUH 31234,

71°15.687' N, 22°32.326' W, 242 m a.s.l.), Jameson Land (Fig. 1F).

Horizon. Ørsted Dal Member (Carlsberg Fjord beds), Fleming Fjord Formation, fluvial and lacustrine deposits; subtropical arid to winter-wet, warm temperate climate.

Age. Late Triassic (late Norian to early Rhaetian).

Selected bibliography. Klein *et al.* 2016.

Comments. Klein *et al.* (2016) attributed these footprints to crocodylomorph archosaurs.

Other tracks

Sulej *et al.* (2014) reported at least nine provisional morphologies among the tracks recovered from different beds of the Fleming Fjord Formation, including cf. *Brachychirotherium* isp., cf. *Apatopus* isp., cf. *Atreipus* isp., *Chirotheriidae* indet., *Grallator* isp., *Eubrontes* isp.,

cf. *Evazoum* isp., *Eosauropus* isp. and cf. *Tetrasauropus* isp.. Hansen *et al.* (2016) reported vertebrate coprolites of which many could be of tetrapod origin.

Jurassic

Skeletal fossils

Plesiosauria indet. (Diapsida: Sauropterygia)

Referred specimens. Two partial vertebrae NHMD 74795 and NHMD 74796; a partial rib NHMD 74797 (Fig. 17).

Locality. East slope of a mountain near Lepidopteriselv, 71°15.761' N, 22°34.287' W, 498 m a.s.l., Jameson Land (Fig. 1F).

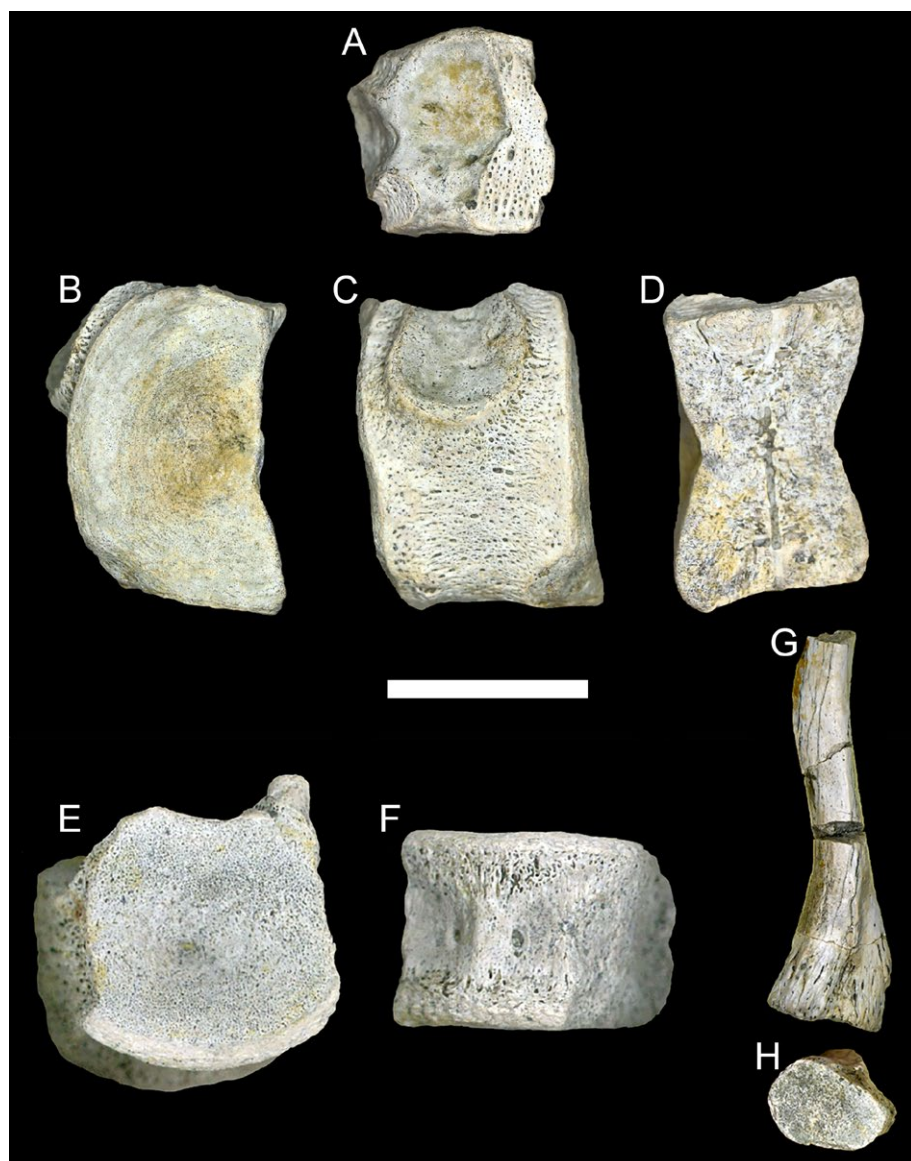


Fig. 17. Early Jurassic plesiosaur from the Kap Stewart Formation of the Jameson land Basin: two vertebrae NHMD 74795 (A–D), NHMD 74796 (E–F) and a rib NHMD 74797 (G–H). A: Dorsal view. B, E, G: Frontal views. C: Lateral right view. D: Lateral left view; F: Ventral view; H: Medial view. Scale bar: 2 cm.



Fig 18. The cryptoclidid plesiosaur MGUH VP 28378: partial skeleton from the Kimmeridgian (Late Jurassic) of East Milne Land, Scoresby Sund. Scale bar: 20 cm.

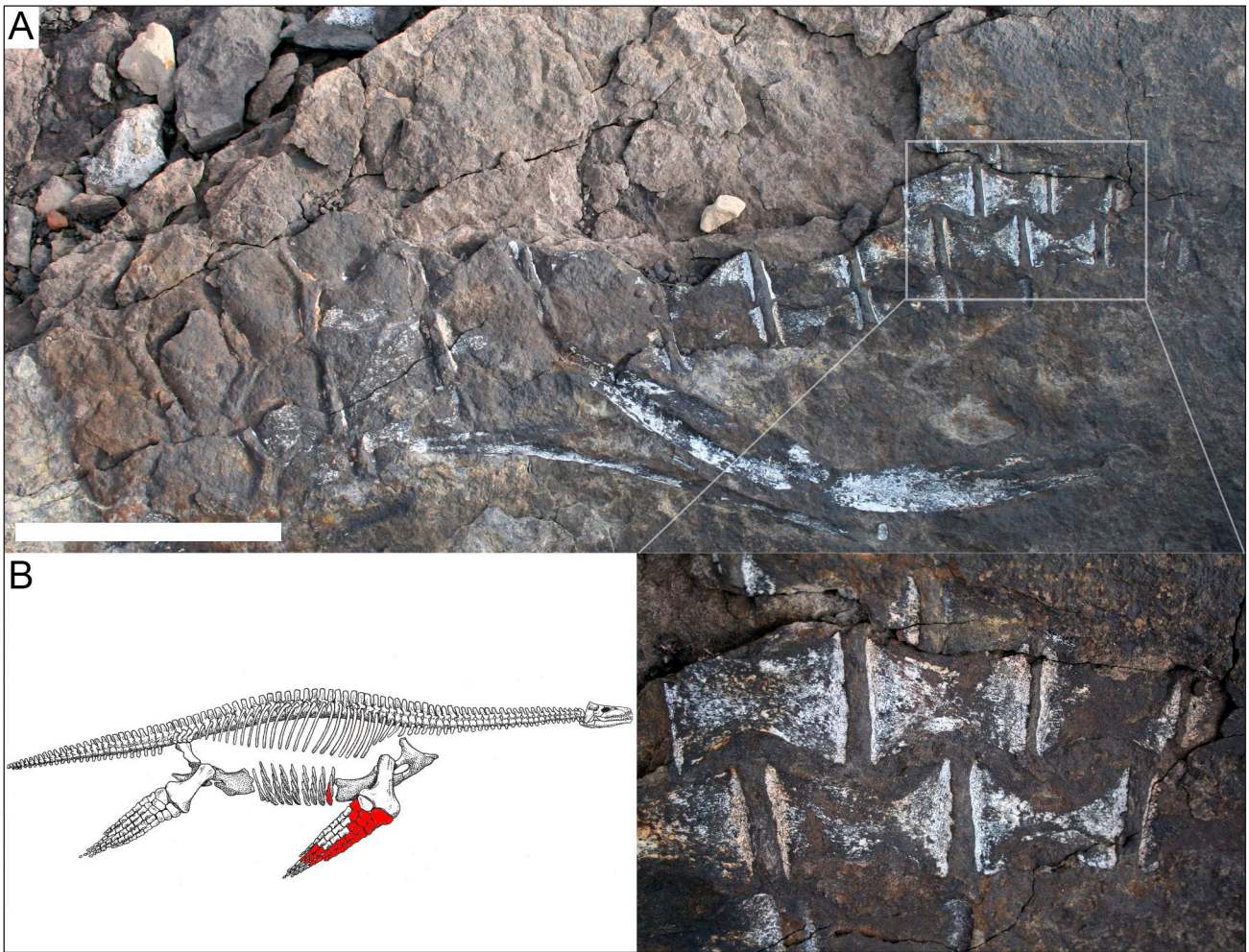


Fig 19. Late Jurassic plesiosaur from Kilen. **A:** The frontal right paddle as found on the field. **B:** reconstruction of the surveyed material using *Cryptoclidus* from Andrews (1910) as model. Scale bar in A: 20 cm.

Horizon. Middle part of the Kap Stewart Formation, delta front sheet sandstone; warm temperate humid climate.

Age. Early Jurassic (Hettangian).

Selected bibliography. Milàn *et al.* (2016b).

Comments. This material was collected during the GeoCenter Møns Klint expedition in the summer of 2016 and comprises small amphicoelous vertebral centra with a diameter of 2 cm that bear paired ventral nutritive foramina and unfused neurocentral sutures. The finds record marine tetrapods in the Kap Stewart Formation prior to the complete transgression in the Pliensbachian (see Dam & Surlyk 1992).

Cryptoclididae indet. (Sauropterygia: Plesiosauria)

Referred specimen. MGUH 28378, a partial skeleton consisting of dorsal and cervical vertebrae and ribs, part of scapular girdle, and forelimb (Fig. 18).

Locality. East of Milne Land, Scoresby Sund, 70°40.61' N, 25°22.83' W (Fig. 1E).

Horizon. Krebsedal Member, Kap Leslie Forma-

tion, offshore shelf deposits; warm temperate humid climate.

Age. Late Jurassic (Kimmeridgian).

Selected bibliography. von Huene (1935); Bendix-Almgreen (1976); Smith (2007).

Comments. Originally ascribed to *Cryptoclidus* (*Apractocleidus*) *aldingeri* von Huene 1935, this specimen was re-evaluated by Smith (2007) as an indeterminate cryptoclidid.

Plesiosauria indet. (Diapsida: Sauropterygia)

Locality. Kilen (near Station Nord), Kronprins Christian Land, 81°15.623' N, 13°57.007' W (Fig. 1C).

Horizon. Wandel Hav Basin, Kuglelejet Formation. The Kuglelejet Formation comprises a fine- to medium-grained sandstone succession which is sporadically bioturbated (Dypvik *et al.* 2002).

Age. Late Jurassic (Upper Kimmeridgian/Middle Volgian).

Comments. This specimen was initially discovered in

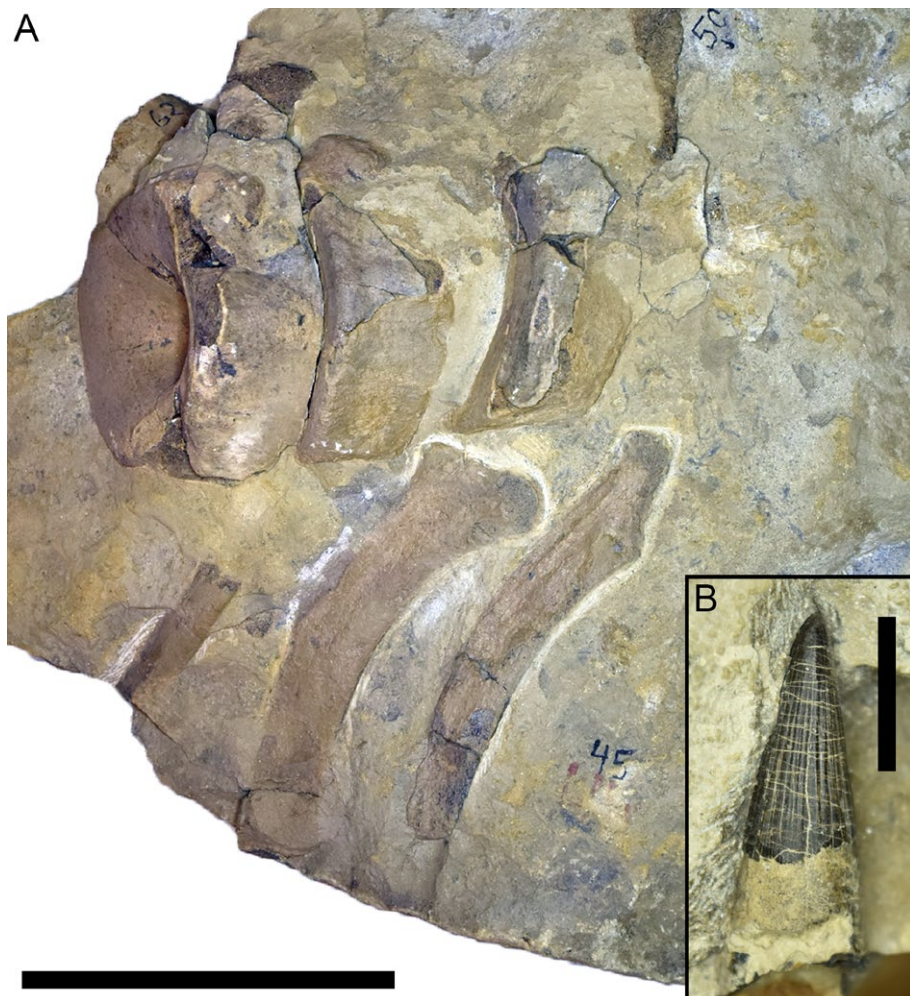


Fig. 20. Undetermined ichthyosaur NHMD 74798 from the Upper Kimmeridgian (Late Jurassic) of the Kap Leslie Formation, in Milne Land, Scoresbysund. **A:** Block including three vertebrae and ribs. **B:** Tooth. Scale bars, A: 10 cm; B: 1 cm.

1998 by a team of Danish and Norwegian geologists exploring for tsunami deposits from a meteor impact in the Barents Sea around the Jurassic–Cretaceous boundary. It has been described briefly by Bruhn (1999) and Dypvik *et al.* (2002) as “... well preserved skeletal material probably belonging to *Plesiosaurus*”. The site was revisited in 2008 by one of us (JM) to evaluate if an excavation would be feasible (Milàn 2009). The original remains consist of impressions of two gastralia and a partial articulated limb (Fig. 19).

Ichthyosauria *indet.* (Diapsida: Ichthyopterygia)

Referred specimen: NHMD 74798, includes fragmentary blocks that preserve three vertebrae with ribs and a tooth (Fig. 20).

Locality. Pernaryggen, Milne Land, Scoresbysund, 70°43.033' N, 25°24.050' W (Fig. 1E).

Horizon. Krebsedal Member, Kap Leslie Formation, offshore shelf deposits; warm temperate humid climate.

Age. Late Jurassic (Upper Kimmeridgian).

Selected bibliography. Håkansson *et al.* (1971).

Comments. This specimen was mentioned by Håkansson *et al.* (1971) but has never been formally described.

Faunal correlations

The Devonian tetrapod fauna of Greenland is characterised by five endemic stem tetrapod species. Though the phylogeny of Late Devonian stem tetrapods is still ambiguous, the taxa closest to *Acanthostega*, *Ichthyostega* and *Ymeria* are *Metaxygnathus* Campbell & Bell 1977 from Australia, *Ventastega* Ahlberg *et al.* 1994 from Latvia, *Densignathus* Daeschler 2000 from USA, *Elginerpeton* Ahlberg 1995 from Scotland, and *Elpistostege* Westoll 1938 and *Tiktaalik* Daeschler *et al.* 2006 from Canada (see also Ruta *et al.* 2003; Ruta & Coates 2007; Neenan *et al.* 2014).

The Early Triassic temnospondyls in the Wordie Creek Group show an affinity to coeval faunas from Central Europe, Russia, and Gondwana. *Aquiloniferus* was originally ascribed to *Lyrocephalus* Wiman 1914, and we consider *Aquiloniferus* as belonging to, or as being very closely related to, the Early Triassic clade of the Lydekkerinidae known from Antarctica, Australia, India, Madagascar, Russia and South Africa (Jeannot *et al.* 2006). *Selenocara* is known from the Early Triassic of Russia and belongs to the Wetlugosaurinae, a clade distributed in Eastern Europe (Novikov 2016). *Stoschiosaurus* belongs to the clade of the Trematosauridae from the Early Jurassic of Europe, Africa,

Asia, Australia and North America (Welles 1969, 1993; Damiani *et al.* 2000; Damiani & Welman 2001; Schoch 2006; Maganuco & Pasini 2009; Warren 2012). *Tupilakosaurus* is recognised from the Early Triassic of Russia, and the clade Tupilakosauridae is recorded in the Early Triassic of Greenland, Russia and South Africa (Shishkin & Novikov 1992; Warren 1998).

Even though Greenland is part of the North American plate, its Late Triassic tetrapod fauna has more affinities with coeval faunas of Europe than to any other areas; among Amphibia, *Cyclotosaurus* Fraas 1889 is restricted to Europe (Germany, Poland, and the Svalbard archipelago), with *C. naraserluki* being the westernmost and northernmost of the known species, endemic to East Greenland (Marzola *et al.* 2017b). The taxa closest to *Cyclotosaurus* are *Quasicyclotosaurus* Schoch 2000 from the Middle Triassic of Arizona and *Eocyclotosaurus* Ortlam 1970 from the Middle Triassic of Central Europe, UK, Algeria, and southern USA (Arizona and New Mexico) (Schoch 2008; Witzmann *et al.* 2016). The European origin of the Capitosauria can be pinpointed to Central East Europe, with its most primitive taxon, *Eryosuchus* Ochev 1966 from the Middle Triassic of Russia (Lehman 1971; Lucas & Hunt 1987; Morales 1987; Ochev & Shishkin 1989; Milner *et al.* 1990; Sulej & Majer 2005; Schoch 2008; Witzmann *et al.* 2016; Kear *et al.* 2016b).

The plagiosaurid *Gerrothorax* Nilsson 1934 is reported from the Middle and Late Triassic of Germany and Sweden, with the clade Plagiosauridae recorded throughout the Triassic of Europe, Australia and Brazil (see Bartholomai 1979; Hellrung 2003; Dias-Da-Silva & Ramos Ilha 2009; Witzmann *et al.* 2012). Among Stagonolepididae, the closest relatives to the Greenlandic *Aetosaurus* are the Late Triassic *Stagonolepis* Agassiz 1844 from Germany, Poland and UK, and *Aetosauroides* Casamiquela 1960 from Argentina and Brazil. The Late Triassic *Paratypothorax* is the only Greenlandic tetrapod taxon with a North American origin: it is documented also from Germany and southern USA, it is closely related to *Rioarribasuchus* Lucas *et al.* (2006) and *Tecovasuchus* Martz & Small 2006 from the Late Triassic of Arizona, Mexico and Texas (Long & Ballew 1985; Heckert & Lucas 1999, 2000; Schoch 2007).

Among Archosauria, the relationships of the pterosaur *Arcticodactylus* is still under debate; however, recent analyses (Kellner 2015; Upchurch *et al.* 2015) propose a close relationship to Italian taxa *Carniadactylus* Dalla Vecchia 2009 and *Eudimorphodon* Zambelli 1973. A preliminary analysis of the sauropodomorph dinosaur remains briefly described in Jenkins *et al.* (1994) allows for the correlation between Greenlandic specimens and Plateosauridae, however differentiating it from *Plateosaurus*. Plateosauridae are recorded from Eurasia and South America (Lapparent 1967;

Galton 1986, 2001; Kellner & Campos 2000; Hurum *et al.* 2006; Klein & Sander 2007; Novas *et al.* 2010).

Shapiro & Jenkins (2001) proposed that the closest relative to the Greenland cynodont *Mitredon* is *Meurthodon* Sigogneau-Russell & Hahn (1994) from the Triassic of France. The clade Haramiyidae is distributed throughout the Late Triassic and includes *Haramiyavia* from Greenland, *Theroteinus* Sigogneau-Russell *et al.* (1986) from France and some undetermined remains from Switzerland (Clemens 1980).

Conclusions

The complete known Palaeozoic and Mesozoic tetrapod fossil record of Greenland includes at least 30 taxa, comprising the Late Devonian stem tetrapods *Acanthostega gunnari*, *Ichthyostega eigili*, *I. stensioi*, *I. watsoni* and *Ymeria denticulate*; the Early Triassic temnospondyls *Aquiloniferus kochi*, *Selenocara groenlandica*, *Stoschiosaurus nielseni* and *Tupilakosaurus heilmanni*; the Late Triassic temnospondyls *Cyclotosaurus naraserluki* and *Gerrothorax cf. pulcherrimus*, the stagonolepids *Aetosaurus ferratus* and *Paratypothorax andressorum*, the eudimorphodontid *Arcticodactylus*, the cynodont *Mitredon cromptoni* and the three mammals *Haramiyavia clemmenseni*, *Kuehneotherium* and *cf. ?Brachyzostrodon*. Undetermined remains are represented by Late Triassic testudinatanans, archosaurs (such as phytosaurs and both sauropodomorph and theropod dinosaurs), and Early and Late Jurassic plesiosaurs and ichthyosaurs. Fossil tracks associated to tetrapod trackmakers are reported from the Late Carboniferous (eryopoid temnospondyls morphotype *Limnopus*) and from the Late Triassic (crocodylomorph morphotype *Brachychirotherium*, sauropodomorph morphotypes *Eosauropus* and *Evazoum*, and theropodian morphotype *Grallator*). Tetrapod coprolites have also been found from the Jameson Land Basin. The two most productive stratigraphical sections are the Devonian, with five recorded taxa and as many unique species, and the Triassic, with 18 recorded taxa and at least eight endemic species.

The richness and diversity of Late Devonian and Triassic tetrapods is due to the formation of terrestrial deposits and their later preservation and exposure during uplift. Through both the Late Devonian and the Triassic, East Greenland was characterised by extensional subsidence, followed by rapid filling of the resulting basins. These events can be linked to the Caledonian crustal welt collapse during the Middle to Late Devonian and the various Triassic rifting phases during the initial breakup of Pangaea (Larsen *et al.* 2008; Clemmensen 1980a, b; Nøttvedt *et*

al. 2008). Synrift sediment deposition and subsequent preservation of vertebrate fossils are well documented worldwide during different epochs and contributed to the existence of fossil vertebrate lagerstätten (Hallam 1971; Feibel *et al.* 1989; Clemmensen *et al.* 1998; Mateus 2006; Larsen *et al.* 2008; Wood & Leakey 2011).

Further studies will clarify the phylogenetic position of the yet poorly reported tetrapod material from Greenland, focusing on the origin of the Late Triassic biota of the Jameson Land Basin and on the different influences of climate and geography on the distribution of life on Earth during the Late Triassic.

Acknowledgments

We wish to thank Bent Lindow (NHMD) for critical comments on an early version of the manuscript, as well as for access to the holotypes and referred specimens pictured in this work. The original manuscript was significantly improved thanks to the reviews by Benjamin Kear (Uppsala University, Sweden) and Jennifer Clack (University of Cambridge, UK), as well as to James Neenan (University of the Witwatersrand, South Africa) who improved the English of the entire manuscript. We are thankful to Eckart Håkansson and Peter Willumsen for sharing information on the ichthyosaur material found during the expedition in 1970. Special thanks also go to Nils Natorp and Eliza Jarl Estrup (GeoCenter Møns Klint) whose friendship and support made this research possible.

MM is supported by the Fundação para a Ciência e a Tecnologia doctoral fellowship SFRH/BD/99580/2014 (Ministério da Ciência, Tecnologia e Ensino superior, Portugal). MM was also supported by the 2015 European Association of Vertebrate Palaeontologists' Research Grant (EAVP-ERG) and by the 2015 Stan Wood Award of The Palaeontological Association (PA-SW201502). Field work in Greenland by LBC was supported by the Carlsberg Foundation.

References

- Agassiz, L. 1844: Monographie des poisons fossiles du vieux grès rouge ou Système Dévonien (Old Red Sandstone) des Isles Britanniques et de Russie. 171 pp. Jent et Gassman, Neuchâtel.
- Ahlberg, P.E. 1995: *Elginerpeton pancheni* and the earliest tetrapod clade. *Nature* 373, 420–425.
- Ahlberg, P.E. & Clack, J.A. 1998: Lower jaws, lower tetrapods – a review based on the Devonian genus *Acanthostega*. *Transactions of the Royal Society of Edinburgh* 89, 11–46.
- Ahlberg, P.E. & Clack, J.A. 2006: Palaeontology: a firm step from water to land. *Nature* 440, 747–749.

- Ahlberg, P.E., Luksevics, E. & Lebedev, O. 1994: The first tetrapod finds from the Devonian (Upper Famennian) of Latvia. *Philosophical Transactions of the Royal Society B: Biological Sciences* 343, 303–328.
- Ahlberg, P.E., Clack, J.A. & Blom, H. 2005: The axial skeleton of the Devonian tetrapod *Ichthyostega*. *Nature* 437, 137–140.
- Andrews, C.W. 1910: A descriptive catalogue of the marine reptiles of the Oxford Clay. Part I, 205 pp. British Museum (Natural History), London.
- Bartholomai, A. 1979: New lizard-like reptiles from the Early Triassic of Queensland. *Alcheringa* 3, 225–234.
- Bendix-Almgreen, S.E. 1976: Palaeovertebrate faunas of Greenland. In: Esher A. & Watt, W.S. (eds): *Geology of Greenland*, 536–573. Grønlands Geologiske Undersøgelse.
- Bendix-Almgreen, S.E., Clack, J.A. & Olsen, H. 1990: Upper Devonian tetrapod palaeoecology in the light of new discoveries in East Greenland. *Terra Nova* 2, 131–137.
- Benton, M.J. 2014: *Vertebrate Palaeontology*. 4th ed., 480 pp. Wiley-Blackwell, Oxford.
- Beurlen, K. 1950: Neue Fahrtenfunde aus der fränkischen Trias. *Neues Jahrbuch für Geologie und Paläontologie, Monatshefte*, 308–320.
- Bjerring, H.C. 1997: The question of the Eotriassic tetrapod genus *Wetlugasaurus* in Greenland and thoughts on the fossa coniformis entopterygoidea. *Meddelelser om Grønland, Geoscience* 34, 25 pp.
- Bjerring, H.C. 1999: A new amphibious tetrapod from the Greenlandic Eotriassic. *Meddelelser om Grønland, Geoscience* 38, 42 pp.
- Blom, H. 2005: Taxonomic revision of the Late Devonian tetrapod *Ichthyostega* from East Greenland. *Palaeontology* 48, 111–134.
- Blom, H., Clack, J.A., Ahlberg, P.E. & Friedman, M. 2007: Devonian vertebrates from East Greenland: a review of faunal composition and distribution. *Geodiversitas* 29, 119–141.
- Bruhn, R. 1999: Plesiosaurer og andet godtfolk på Nordgrønland. *Varv* 1999(4), 109–112.
- Brusatte, S.L., Benton, M.J., Lloyd, G.T., Ruta, M. & Wang, S.C. 2011: Macroevolutionary patterns in the evolutionary radiation of archosaurs (Tetrapoda: Diapsida). *Earth and Environmental Science Transactions of the Royal Society of Edinburgh* 101, 367–382.
- Callomon, J.H. & Birkelund, T. 1980: The Jurassic transgression and the mid-late Jurassic succession in Milne Land, central East Greenland. *Geological Magazine* 117, 211–226.
- Campbell, K.S.W. & Bell, M.W. 1977: A primitive amphibian from the Late Devonian of New South Wales. *Alcheringa* 1, 369–381.
- Casamiquela, R.M. 1960: Noticia preliminar sobre dos nuevos estagonolepoideos Argentinos. *Ameghiniana* 2, 3–9.
- Clack, J.A. 1988a: New material of the early tetrapod *Acanthostega* from the Upper Devonian of East Greenland. *Palaeontology* 31, 699–724.
- Clack, J.A. 1988b: Pioneers of the land in East Greenland. *Geology Today* 4, 192–194.
- Clack, J.A. 1989: Discovery of the earliest-known tetrapod stapes. *Nature* 342, 425–427.
- Clack, J. A. 1992: The stapes of *Acanthostega gunnari* and the role of the stapes in early tetrapods. In: Fay, R.R. *et al.* (eds): *The Evolutionary Biology of Hearing*, 405–420. New York: Springer Verlag.
- Clack, J.A. 1994: *Acanthostega gunnari*, a Devonian tetrapod from Greenland: the snout, palate and ventral parts of the braincase, with a discussion of their significance. *Meddelelser om Grønland, Geoscience* 31, 24 pp.
- Clack, J.A. 1997: Devonian tetrapod trackways and trackmakers; a review of the fossils and footprints. *Palaeogeography, Palaeoclimatology, Palaeoecology* 130, 227–250.
- Clack, J.A. 1998: The neurocranium of *Acanthostega gunnari* Jarvik and the evolution of the otic region in tetrapods. *Zoological Journal of the Linnean Society* 122, 61–97.
- Clack, J.A. 2002a: A revised reconstruction of the dermal skull roof of *Acanthostega gunnari*, an early tetrapod from the Late Devonian. *Earth and Environmental Science Transactions of the Royal Society of Edinburgh* 93, 163–165.
- Clack, J.A. 2002b: The dermal skull roof of *Acanthostega gunnari*, an early tetrapod from the Late Devonian. *Earth and Environmental Science Transactions of the Royal Society of Edinburgh* 93, 17–33.
- Clack, J.A., Ahlberg, P.E., Blom, H. & Finney, S.M. 2012: A new genus of Devonian tetrapod from North-East Greenland, with new information on the lower jaw of *Ichthyostega*. *Palaeontology* 55, 73–86.
- Clack, J.A., Ahlberg, P.E., Finney, S.M., Alonso, P.D., Robinson, J. & Ketcham, R.A. 2003: A uniquely specialized ear in a very early tetrapod. *Nature* 425, 65–69.
- Clack, J.A. & Neiningner, S.L. 2000: Fossils from the Celsius Bjerg Group, Upper Devonian sequence, East Greenland: significance and sedimentological distribution. *Geological Society, London Special Publication* 180, 557–566.
- Clemens, W.A. 1980: Rhaeto-Liassic mammals from Switzerland and West Germany. *Zitteliana*, 5, 51–92.
- Clemmensen, L.B., 1980a: Triassic rift sedimentation and palaeogeography of central East Greenland. *Grønlands Geologiske Undersøgelse Bulletin* 136, 1–72.
- Clemmensen, L.B., 1980b: Triassic lithostratigraphy of East Greenland between Scoresby Sund and Kejsers Franz Josephs Fjord. *Grønlands Geologiske Undersøgelse Bulletin* 139, 1–56.
- Clemmensen, L.B., Kent, D.V. & Jenkins, F.A. 1998: A Late Triassic lake system in East Greenland: facies, depositional cycles and palaeoclimate. *Palaeogeography, Palaeoclimatology, Palaeoecology* 140, 135–159.
- Clemmensen, L.B., Milàn, J., Adolfssen, J.S., Estrup, E.J., Frobøse, N., Klein, N., Mateus, O. & Wings, O. 2016: The vertebrate-bearing Late Triassic Fleming Fjord Formation of central East Greenland revisited: stratigraphy, palaeoclimate and new palaeontological data. *Geological Society, London, Special Publications* 434, 31–47.
- Coates, M.I. 1996: The Devonian tetrapod *Acanthostega gunnari* Jarvik: postcranial anatomy, basal tetrapod interrelationships and patterns of skeletal evolution. *Transactions of the Royal Society of Edinburgh: Earth Sciences* 87, 363–421.
- Cosgriff, J.W. 1984: The temnospondyl labyrinthodonts of the earliest Triassic. *Journal of Vertebrate Paleontology* 4, 30–46.
- Daeschler, E.B. 2000: Early tetrapod jaws from the Late Devonian of Pennsylvania, USA. *Journal of Paleontology* 74, 301–308.
- Daeschler, E.B., Shubin, N.H. & Jenkins, F.A. 2006: A Devonian tetrapod-like fish and the evolution of the tetrapod body plan. *Nature* 440, 757–763.
- Dalla Vecchia, F.M. 2003: New morphological observations on Triassic pterosaurs. *Geological Society, London, Special Publications* 217, 23–44.
- Dalla Vecchia, F.M. 2009: Anatomy and systematics of the pterosaur *Carniadactylus* gen. n. *rosenfeldi* (Dalla Vecchia, 1995).

- Rivista Italiana di Paleontologia e Stratigrafia 115, 159–188.
- Dalla Vecchia, F.M. 2014: Gli pterosauri triassici. Museo friulano di storia naturale 54, 319 pp. Museo Friulano di Storia Naturale, Udine.
- Dam, G. & Surlyk, F. 1992: Forced regressions in a large wave- and storm-dominated anoxic lake Rhaetian-Sinemurian Kap Stewart Formation, East Greenland. *Geology* 20, 749–752.
- Damiani, R.J. & Welman, J. 2001: A long-snouted trematosaurid amphibian from the Early Triassic of South Africa. *South African Journal of Science* 97, 318–320.
- Damiani, R.J., Neveling, J., Hancox, J. & Rubidge, B. 2000: First trematosaurid temnospondyl from the Lystrosaurus Assemblage Zone of South Africa and its biostratigraphic implications. *Geological Magazine* 137, 659–665.
- Dias-Da-Silva, S. & Ramos Ilha, A.L. 2009: On the presence of a postulated temnospondyl in the Lower Triassic of southern Brazil. *Acta Palaeontologica Polonica* 54, 609–614.
- Dypvik, H., Håkansson, E. & Heinberg, C. 2002: Jurassic and Cretaceous palaeogeography and stratigraphic comparisons in the North Greenland-Svalbard region. *Polar Research* 21, 91–108.
- Feibel, C.S., Brown, F.H. & McDougall, I. 1989: Stratigraphic context of fossil hominids from the Omo Group deposits: northern Turkana Basin, Kenya and Ethiopia. *American Journal of Physical Anthropology* 78, 595–622.
- Fraas, E. 1889: Die Labyrinthodonten der schwäbischen Trias. *Palaeontographica* 36, 1–158.
- Fraas, E. 1913: Neue Labyrinthodonten aus der schwäbischen Trias. *Palaeontographica* 60, 275–294.
- Fraas, O. 1877: *Aetosaurus ferratus*, Die gepanzerte Vogel-Echse aus dem Stubensandstein bei Stuttgart. Jahreshefte des Vereins für vaterländische Naturkunde in Württemberg 33, 1–21.
- Friend, P.F., Alexander-Marrack, P.D., Nicholson, J. & Yeats, A.K., 1976: Devonian sediments of East Greenland II, Sedimentary structures and fossils: Meddelelser om Grønland 206 (2), 1–91.
- Gaffney, E.S., Hutchison, J.H., Jenkins, F.A. & Meeker, L.J. 1987: Modern turtle origins: the oldest known cryptodire. *Science* 237, 289–291.
- Galton, P. M. 1986: Prosauropod dinosaur *Plateosaurus* (= *Gresslyosaurus*) (Saurischia: Sauropodomorpha) from the Upper Triassic of Switzerland. *Geologica et Palaeontologica* 20, 167–183.
- Galton, P. M. 2001: The prosauropod dinosaur *Plateosaurus* Meyer, 1837 (Saurischia: Sauropodomorpha; Upper Triassic). II. notes on the referred species. *Revue de Paléobiologie* 20, 435–502.
- Gatesy, S.M. 2001: Skin impressions of Triassic theropods as records of foot movement. *Bulletin of the Museum of Comparative Zoology* 156, 137–149.
- Gatesy, S.M., Middleton, K.M., Jenkins, F.A. & Shubin, N.H. 1999: Three-dimensional preservation of foot movements in Triassic theropod dinosaurs. *Nature* 399, 141–144.
- Gilberg, A. 1992: Blyminen ved Mestersvig i Østgrønland. *Tidsskriftet Grønland* 1992, 289–311.
- Håkansson, E., Birkelund, T., Heinberg, C. & Willumsen, P. 1971: Preliminary results of mapping the Upper Jurassic and Lower Cretaceous sediments of Milne Land. *Rapport Grønlands Geologiske Undersøgelse* 37, 32–41.
- Hallam, A. 1971: Mesozoic geology and the opening of the North Atlantic. *The Journal of Geology* 79, 129–157.
- Hansen, B.B., Milàn, J., Clemmensen, L.B., Adolfssen, J.S., Estup, E. J., Klein, N., Mateus, O. & Wings, O. 2016: Coprolites from the Late Triassic Kap Stewart Formation, Jameson Land, East Greenland: morphology, classification and prey inclusions. *Geological Society, London, Special Publications* 434, 49–69.
- Heckert, A.B. & Lucas, S.G. 1999: A new aetosaur (Reptilia: Archosauria) from the Upper Triassic of Texas and the phylogeny of aetosaurs. *Journal of Vertebrate Paleontology* 19, 50–68.
- Heckert, A.B. & Lucas, S.G. 2000: Taphonomy, phylogeny, biostratigraphy, biochronology, paleobiogeography, and evolution of the Late Triassic Aetosauria (Archosauria: Crurotarsi). *Zentralblatt für Geologie und Paläontologie* 11–12, 1539–1587.
- Heintz, A. 1930: Oberdevonische Fischreste aus Ost-Grønland. *Skrifter om Svalbard og Ishavet* 30, 30–46.
- Heintz, A. 1932: Beitrag zur Kenntnis der devonischen Fischfauna Ost-Grønlands. *Skrifter om Svalbard og Ishavet* 42, 5–27.
- Hellrung, H. 2003: *Gerrothorax pustuloglomeratus*, ein Temnospondyle (Amphibia) mit knöcherner Branchialkammer aus dem Unteren Keuper von Kupferzell (Süddeutschland). *Stuttgarter Beiträge zur Naturkunde B* 330, 1–130.
- Hitchcock, E. 1858: *Ichnology of New England*. A report on the sandstone of the Connecticut Valley especially its fossil footmarks. 199 pp. W. White, Printer to the State of Boston.
- Hurum, J.H., Bergan, M., Muller, R., Nystuen, J.P. & Klein, N. 2006: A Late Triassic dinosaur bone, offshore Norway. *Norsk Geologisk Tidsskrift* 86, 117–123.
- von Huene, F.R.F. 1935: Ein plesiosaurier-rest aus grönländischem oberem jura. *Meddelelser om Grønland* 99 (4), 1–11.
- Jarvik, E. 1952: On the fish-like tail in the ichthyostegid stegocephalians, with descriptions of a new stegocephalian and a new crossopterygian from the Upper Devonian of East Greenland. *Meddelelser om Grønland* 114 (12), 1–90.
- Jarvik, E. 1996: The Devonian tetrapod *Ichthyostega*. *Fossils and Strata* 40, 1–213.
- Jeannot, A.M., Damiani, R. & Rubidge, B.S. 2006: Cranial anatomy of the Early Triassic stereospondyl *Lydekkerina huxleyi* (Tetrapoda: Temnospondyli) and the taxonomy of South African lydekkerinids. *Journal of Vertebrate Paleontology* 26, 822–838.
- Jenkins, F.J., Shubin, N.H., Amarel, W.W., Gatesy, S.M., Schaff, C.R., Clemmensen, L.B., Downs, W. R., Davidson, A.R., Bonde, N.C. & Osbaeck, F. 1994: Late Triassic continental vertebrates and depositional environments of the Fleming Fjord Formation, Jameson Land, east Greenland. *Meddelelser om Grønland, Geoscience* 35, 25 pp.
- Jenkins, F.A., Gatesy, S.M., Shubin, N.H. & Amaral, W.W. 1997: Haramiyids and Triassic mammalian evolution. *Nature* 385, 715–718.
- Jenkins, F.A., Shubin, N.H., Gatesy, S.M. & Padian, K. 2001: A diminutive pterosaur (Pterosauria: Eudimorphodontidae) from the Greenlandic Triassic. *Bulletin of the Museum of Comparative Zoology* 156, 151–170.
- Jenkins, F.A., Shubin, N. H., Gatesy, S. M. & Warren, A. 2008: *Gerrothorax pulcherrimus* from the Upper Triassic Fleming Fjord Formation of East Greenland and a reassessment of head lifting in temnospondyl feeding. *Journal of Vertebrate Paleontology* 28, 935–950.
- Kear, B.P., Lindgren, J., Hurum, J.H., Milàn, J. & Vajda, V. 2016a: An introduction to the Mesozoic biotas of Scandinavia and its Arctic territories. *Geological Society, London, Special Publications* 434, 1–14.

- Kear, B.P., Poropat, S.F. & Bazzi, M. 2016b: Late Triassic capitosaurian remains from Svalbard and the palaeobiogeographical context of Scandinavian Arctic temnospondyls. Geological Society, London, Special Publications 434, 113–126.
- Kellner, A.W. 2015: Comments on Triassic pterosaurs with discussion about ontogeny and description of new taxa. Anais da Academia Brasileira de Ciências 87 (2), 669–689.
- Kellner, A.W. & Campos, D.A. 2000: Brief review of dinosaur studies and perspectives in Brazil. Anais da Academia Brasileira de Ciências 72, 509–538.
- Kent, D.V. & Clemmensen, L.B. 1996: Paleomagnetism and cycle stratigraphy of the Triassic Fleming Fjord and Gipsdalen formations of East Greenland. Bulletin of the Geological Society of Denmark 42, 121–136.
- Kent, D.V. & Tauxe, L. 2005: Corrected Late Triassic latitudes for continents adjacent to the North Atlantic. Science 307, 240–244.
- Kermack, D.M., Kermack, K.A. & Mussett, F. 1968: The Welsh pantothere *Kuehneotherium praecursoris*. Journal of the Linnean Society of London, Zoology 47, 407–423.
- Klein, H., Milàn, J., Clemmensen, L.B., Frobøse, N., Mateus, O., Klein, N., Adolfssen, J. S., Estrup, E. J. & Wings, O. 2016: Archosaur footprints (cf. *Brachychirotherium*) with unusual morphology from the Upper Triassic Fleming Fjord Formation (Norian–Rhaetian) of East Greenland. Geological Society, London, Special Publications 434, 71–85.
- Klein, N. & Sander, P.M. 2007: Bone histology and growth of the prosauropod dinosaur *Plateosaurus engelhardti* von Meyer, 1837 from the Norian bonebeds of Trossingen (Germany) and Frick (Switzerland). Special Papers in Palaeontology 77, 1–169.
- Koch, L. 1930: Preliminary Report of the Danish Expedition to East Greenland in 1929. Meddelelser om Grønland 74, 173–206.
- Lallensack, J.N., Klein, H., Milàn, J., Wings, O., Mateus, O. & Clemmensen, L.B. 2017: Sauropodomorph dinosaur trackways from the Fleming Fjord Formation of East Greenland: Evidence for Late Triassic sauropods. Acta Palaeontologica Polonica 62(4), 833–843. doi:https://doi.org/10.4202/app.00374.2017
- Larsen, P.H., Olsen, H. & Clack, J.A. 2008: The Devonian basin in East Greenland—Review of basin evolution and vertebrate assemblages. Geological Society of America Memoirs 202, 273–292.
- Lapparent, A.F. de. 1967: Les dinosaures de France. Sciences 51, 4–19.
- Lehman, J.P. 1971: Nouveaux Vertèbres fossiles du Trias de la sene de Zarzaytine. Annales de Paleontologie (Vertèbres) 57, 71–113.
- Li, C., Wu, X.-C., Rieppel, O., Wang, L.-T. & Zhao, L.-J. 2008: An ancestral turtle from the Late Triassic of southwestern China. Nature 456, 497–501.
- Lockley, M.G., Lucas, S.G. & Hunt, A.P. 2006a: *Eosauropus*, a new name for a Late Triassic track: Further observations on the Late Triassic ichnogenus *Tetrasauropus* and related forms, with notes on the limits of interpretation. New Mexico Museum of Natural History and Science Bulletin 37, 192–198.
- Lockley, M.G., Lucas, S.G. & Hunt, A.P. 2006b. *Evazoum* and the renaming of northern hemisphere “*Pseudotetrasauropus*”: implications for tetrapod ichnotaxonomy at the Triassic–Jurassic boundary. New Mexico Museum of Natural History and Science Bulletin 37, 199–206.
- Long, R.A. & Ballew, K.L. 1985: *Aetosaur* dermal armor from the Late Triassic of southwestern North America, with special reference to material from the Chinle Formation of Petrified Forest National Park. Museum of Northern Arizona Bulletin 47, 45–68.
- Lucas, S.G. 1998: Global Triassic tetrapod biostratigraphy and biochronology. Palaeogeography, Palaeoclimatology, Palaeoecology 143, 347–384.
- Lucas, S.G. & Hunt A.P. 1987: Stratigraphy of the Anton Chico and Santa Rosa formations, Triassic of east-central New Mexico. Journal of the Arizona-Nevada Academy of Science 22, 21–33.
- Lucas, S.G., Hunt, A.P. & Spielmann, J.A. 2006: *Rioarribasuchus*, a new name for an aetosaur from the Upper Triassic of north-central New Mexico. New Mexico Museum of Natural History and Science Bulletin 37, 581–582.
- Luo, Z.-X., Gatesy, S.M., Jenkins, F.A., Amaral, W.W. & Shubin, N.H. 2015: Mandibular and dental characteristics of Late Triassic mammaliaform *Haramiyavia* and their ramifications for basal mammal evolution. Proceedings of the National Academy of Sciences 112, E7101–E7109.
- Maganuco, S. & Pasini, G. 2009: A new specimen of trematosaurian temnospondyl from the Lower Triassic of NW Madagascar, with remarks on palatal anatomy and taxonomic affinities. Atti della Società Italiana di Scienze Naturali e del Museo Civico di Storia Naturale di Milano 150, 91–112.
- Marsh, O.C. 1894: Footprints of Vertebrates in the Coal Measures of Kansas. American Journal of Science 48, 81–84.
- Marshall, J.E.A., Astin, T.R. & Clack, J.A. 1999: East Greenland tetrapods are Devonian in age. Geology 27, 637–640.
- Martz, J.W. & Small, B.J. 2006: *Tecovasuchus chatterjeei*, a new aetosaur (Archosauria: Stagonolepididae) from the Tecovas Formation (Carnian, Upper Triassic) of Texas. Journal of Vertebrate Paleontology 26, 308–320.
- Marzola, M., Mateus O., Milàn J. & Clemmensen L.B. 2017a: The 2016 Dinosaur Expedition to the Late Triassic of the Jameson Land Basin, East Greenland, pp. 249–253. In: Barrios de Pedro S. *et al.* (eds): A Glimpse of the Past. Abstract book of the XV Encuentro de Jóvenes Investigadores en Paleontología/ XV Encontro de Jovens Investigadores em Paleontologia. 428 pp. Pombal.
- Marzola, M., Mateus, O., Shubin, N.H. & Clemmensen, L.B. 2017b: *Cyclotosaurus naraserluki*, a new Late Triassic cyclotosaurid (Amphibia, Temnospondyli) from the Fleming Fjord Formation of the Jameson Land Basin (East Greenland). Journal of Vertebrate Paleontology. DOI:10.1080/02724634.2017.1303501.
- Marzola, M., Mateus, O., Wings, O., Klein, N., Milàn, J. & Clemmensen, L.B. 2016: The Late Triassic herpetofauna of the Jameson Land Basin (East Greenland): review and updates. In: Holwerda, *et al.* (eds): Programme and Abstract Book of the XIV Annual Meeting of the European Association of Vertebrate Paleontologists, p. 177. Haarlem, The Netherlands.
- Mateus, O. 2006: Late Jurassic dinosaurs from the Morrison Formation (USA), the Lourinhã and Alcobaça formations (Portugal), and the Tendaguru Beds (Tanzania): a comparison. New Mexico Museum of Natural History and Science Bulletin 36, 223–231.
- Mateus, O., Clemmensen, L.B., Klein, N., Wings, O., Frobøse, N., Milàn, J., Adolfssen, J.S. & Estrup, E.J. 2014: The Late Triassic of Jameson Land revisited: new vertebrate findings and first phytosaur from Greenland. Journal of Vertebrate Paleontology 34 (Program and Abstracts), 182 only.
- Milàn, J. 2009: På svaneøglejagt 81° nord - gensyn med et 155 millioner år gammelt fossil. Geologisk Nyt 2009 (1), 10–5.

- Milàn, J., Clemmensen, B.L. & Bonde, N. 2004: Vertical sections through dinosaur tracks (Late Triassic lake deposits, East Greenland)–undertracks and other subsurface deformation structures revealed. *Lethaia* 37, 285–296.
- Milàn, J., Avanzini, M., Clemmensen, L.B., Garcíá-Ramos, J.C. & Piñuela, L. 2006: Theropod foot movement recorded from Late Triassic, Early Jurassic and Late Jurassic fossil footprints. *New Mexico Museum of Natural History and Science Bulletin* 37, 352–364.
- Milàn, J., Clemmensen, L.B., Adolffsen, J.S., Estrup, E.J., Frobøse, N., Klein, N., Mateus, O. & Wings, O. 2012: A preliminary report on coprolites from the Late Triassic part of the Kap Stewart Formation, Jameson Land, East Greenland. *New Mexico Museum of Natural History and Science Bulletin* 57, 203–206.
- Milàn, J., Klein, H., Voigt, S. & Stemmerik, L. 2016a: First record of tetrapod footprints from the Carboniferous Mesters Vig Formation in East Greenland. *Bulletin of the Geological Society of Denmark* 64, 69–76.
- Milàn, J., Mateus, O., Marzola, M. & Clemmensen, L.B. 2016b: Plesiosaur remains from the Lower Jurassic part of the Kap Stewart Formation, Jameson Land, East Greenland – evidence of the earliest marine incursion. *The Palaeontological Association 60th Annual Meeting, 14th–17th December 2016. Programme, Abstracts and AGM papers.* p. 95–96.
- Milner, A.R., Gardiner, B.G., Fraser, N.C. & Taylor, M.A. 1990: Vertebrates from the Middle Triassic Otter Sandstone Formation of Devon. *Palaeontology* 33, 873–892.
- Morales, M. 1987: Terrestrial fauna and flora from the Triassic Moenkopi Formation of the southwestern United States. *Journal of the Arizona-Nevada Academy of Science* 22, 1–19.
- Nathorst, A.G. 1900: Två somrar i Norra Ishafvet. 2. Stockholm: Beijer Bokförlagsakt.
- Nathorst, A.G. 1901: Bidrag till nordöstra Grönlands geologi. *GFF* 23, 275–306.
- Neenan, J.M., Ruta, M., Clack, J.A. & Rayfield, E.J. 2014: Feeding biomechanics in *Acanthostega* and across the fish–tetrapod transition. *Proceedings of the Royal Society of London B: Biological Sciences* 281, 20132689.
- Niedzwiedzki, G. & Sulej, T. 2017: A Norian coelophysoid tetrapod from Fleming Fjord Formation, East Greenland. 77th Annual Meeting of the Society of Vertebrate Paleontology, Calgary, Canada, August 23–26, 2017, At Calgary, Canada, Abstract book, 169.
- Nielsen, E. 1954: *Tupilakosaurus heilmani* n. g. et n. sp. an interesting batrachomorph from the Triassic of East Greenland. *Meddelelser om Grønland* 72 (8), 1–33.
- Nielsen, E. 1967: New observations on the skull-roof of the holotype of *Tupilakosaurus heilmani* Nielsen. *Journal of the Linnean Society of London, Zoology* 47, 225–229.
- Nilsson, T. 1934: Vorläufige mitteilung über einen Stegocephalenfund aus dem Rhät Schonens. *GFF* 56, 428–442.
- Nøttvedt, A., Johannessen, E.P. & Surlyk, F. 2008: The Mesozoic of western Scandinavia and East Greenland. *Episodes* 31, 59–65.
- Novas, F.E., Ezcurra, M.D., Chatterjee, S. & Kutty, T.S. 2010: New dinosaur species from the Upper Triassic Upper Maleri and Lower Dharmaram formations of central India. *Earth and Environmental Science Transactions of the Royal Society of Edinburgh* 101, 333–349.
- Novikov, I.V. 2016: New temnospondyl amphibians from the basal Triassic of the Obshchii Syrt Highland, Eastern Europe. *Paleontological Journal* 50, 297–310.
- Ochev, V.G. 1966: [Systematics and phylogeny of capitosauroid labyrinthodonts.] 181 pp. Saratov State University Press, Saratov. [Russian].
- Ochev, V.G. & Shishkin, M.A. 1989: On the principles of global correlation of the continental Triassic on the tetrapods. *Acta Palaeontologica Polonica* 34, 149–173.
- Olsen, H. 1990: Astronomical forcing of meandering river behaviour: Milankovitch cycles in Devonian of East Greenland. *Palaeogeography, Palaeoclimatology, Palaeoecology* 79, 99–115.
- Ortlam, D. 1970: *Eocyclotossaurus woschmidti* n. g. n. sp. ein neuer Capitosauride aus dem Oberen Buntsandstein des nördlichen Schwarzwaldes. *Neues Jahrbuch für Geologie und Paläontologie, Monatshefte* 1970, 568–580.
- Orvin, A.K. & Heintz, A. 1930: Beiträge zur Kenntnis des Oberdevons Ost-Grönlands. *Skrifter om Svalbard og Ishavet* 30. Oslo.
- Parker, W.G. 2016: Osteology of the Late Triassic aetosaur *Scutarx deltatylus* (Archosauria: Pseudosuchia). *PeerJ* 4: e2411. <https://doi.org/10.7717/peerj.2411>
- Pierce, S.E., Clack, J.A. & Hutchinson, J.R. 2012: Three-dimensional limb joint mobility in the early tetrapod *Ichthyostega*. *Nature* 486, 523–526.
- Pierce, S.E., Ahlberg, P.E., Hutchinson, J.R., Molnar, J.L., Sanchez, S., Tafforeau, P. & Clack, J.A. 2013: Vertebral architecture in the earliest stem tetrapods. *Nature* 494, 226–229.
- Price, S.P. & Whitham, A.G. 1997: Exhumed hydrocarbon traps in East Greenland: analogs for the Lower-Middle Jurassic play of Northwest Europe. *AAPG bulletin* 81, 1960150–221.
- Ries, C.J. 2002: Retten, magten og æren. Lauge Koch Sagen – en strid om Grønlands geologiske udforskning. 366 pp. Lindhardt of Ringhoff.
- Ruta, M. & Coates, M.I. 2007: Dates, nodes and character conflict: addressing the lissamphibian origin problem. *Journal of Systematic Palaeontology* 5, 69–122.
- Ruta, M., Jeffery, J.E. & Coates, M.I. 2003: A supertree of early tetrapods. *Proceedings of the Royal Society of London B: Biological Sciences* 270, 2507–2516.
- Ruta, M., Pisani, D., Lloyd, G.T. & Benton, M.J. 2007: A supertree of Temnospondyli: cladogenetic patterns in the most species-rich group of early tetrapods. *Proceedings of the Royal Society of London B: Biological Sciences* 274, 3087–3095.
- Säve-Söderbergh, G. 1932: Preliminary note on Devonian stegocephalians from East Greenland. *Meddelelser om Grønland* 94, 1–107.
- Säve-Söderbergh, G. 1935: On the dermal bones of the head in labyrinthodont stegocephalians and primitive reptilia: with special reference to Eotriassic stegocephalians from east Greenland. *Meddelelser om Grønland* 98 (3), 1–211.
- Shishkin, M.A. & Novikov, I.V. 1992: [Relict anthracosaurs in the early Mesozoic of Eastern Europe.] *Transactions (Doklady) of the U.S.S.R. Academy of Sciences: Earth Science Sections* 326, 219–223. [in Russian]
- Schoch, R.R. 2000. The status and osteology of two new cyclo-tosaurid amphibians from the Upper Moenkopi Formation of Arizona (Amphibia: Temnospondyli; Middle Triassic). *Neues Jahrbuch für Geologie und Paläontologie Abhandlungen* 216, 387–411.
- Schoch, R.R. 2006: A complete trematosaurid amphibian from the Middle Triassic of Germany. *Journal of Vertebrate Paleontology* 26, 29–43.
- Schoch, R.R. 2007: Osteology of the small archosaur *Aetosaurus* from the Upper Triassic of Germany. *Neues Jahrbuch für*

- Geologie und Paläontologie, Abhandlungen 246, 1–35.
- Schoch, R.R. 2008: The Capitosauria (Amphibia): characters, phylogeny, and stratigraphy. *Palaeodiversity* 1, 189–226.
- Schoch, R.R. & Witzmann, F. 2012: Cranial morphology of the plagiosaurid *Gerrothorax pulcherrimus* as an extreme example of evolutionary stasis. *Lethaia* 45, 371–385.
- Shapiro, M.D. & Jenkins, F.A. 2001: A cynodont from the Upper Triassic of East Greenland: tooth replacement and double-rootedness. *Bulletin of the Museum of Comparative Zoology* 156, 49–58.
- Sigogneau-Russell, D. 1983: Nouveaux taxons de Mammifères rhétiens. *Acta Palaeontologica Polonica* 28, 233–249.
- Sigogneau-Russell, D. & Hahn, G. 1994: Late Triassic microvertebrates from central Europe. In: Fraser, N.C. & Sues, H.-D. (eds): *In the Shadow of the Dinosaurs: Early Mesozoic Tetrapods*; Cambridge (Cambridge University Press), 197–213.
- Sigogneau-Russell, D., Frank, P., & Hemmerlé, J. 1986. A new family of mammals from the lower part of the French Rhaetic. In: Pandian, K. (eds): *The beginning of the age of dinosaurs: Faunal change across the Triassic-Jurassic boundary*. Cambridge: Cambridge Univ. Press, 99–108.
- Smith, A.S. 2007: The back-to-front plesiosaur *Cryptocleidus* (*Apractocleidus*) *aldingeri* from the Kimmeridgian of Milne Land, Greenland. *Bulletin of the Geological Society of Denmark* 55, 1–7.
- Snitting, D. & Blom, H. 2009: Correcting taxon names containing diacritics – examples from Paleozoic vertebrates. *Journal of Vertebrate Paleontology* 29, 269–270.
- Stensiö, E.A. 1931: Upper Devonian Vertebrates from East Greenland: Collected by the Danish Greenland Expeditions in 1929 and 1930. *Meddelelser om Grønland* 86, 1–212.
- Sulej, T. & Majer, D. 2005: The temnospondyl amphibian *Cyclotosaurus* from the Upper Triassic of Poland. *Palaeontology* 48, 157–170.
- Sulej, T., Wolniewicz, A., Bonde, N., Błazejowski, B., Niedźwiedzki, G. & Tałanda, M., 2014: New perspectives on the Late Triassic vertebrates of East Greenland: preliminary results of a Polish–Danish palaeontological expedition. *Polish Polar Research* 35, 541–552.
- Surlyk, F., Bjerager, M., Piasecki, S. & Stemmerik, L. 2017: Stratigraphy of the marine Lower Triassic succession at Kap Stosch, Hold with Hope, North-East Greenland. *Bulletin of the Geological Society of Denmark* 65, 87–123.
- Upchurch, P., Andres, B., Butler, R. J., & Barrett, P.M. 2015: An analysis of pterosaurian biogeography: implications for the evolutionary history and fossil record quality of the first flying vertebrates. *Historical Biology* 27, 697–717.
- Warren, A. 1998: Karoo tupilakosaurid: a relict from Gondwana. *Transactions of the Royal Society of Edinburgh: Earth Sciences* 89, 145–160.
- Warren, A. 2012: The South African stereospondyl *Microposaurus* from the Middle Triassic of the Sydney Basin, Australia. *Journal of Vertebrate Paleontology* 32, 538–544.
- Welles, S.P. 1969: Collecting Triassic vertebrates in the Plateau Province. *Journal of the West* 8, 231–246.
- Welles, S.P. 1993: A review of lonchorhynchine trematosaur (Labryrithodontia), and a description of a new genus and species from the lower Moenkopi Formation of Arizona. *PaleoBios* 14, 1–24.
- Westoll, T.S. 1938: Ancestry of the tetrapods. *Nature* 141, 127–128.
- Wignall, P.B. & Twitchett, R.J. 2002: Permian–Triassic sedimentology of Jameson Land, East Greenland: incised submarine channels in an anoxic basin. *Journal of the Geological Society* 159, 691–703.
- Wiman, C. 1914: Über die Stegocephalen aus der Trias Spitzbergens. *Bulletin of the Geological Institutions of the University of Uppsala* 13, 1–34.
- Witzmann, F., Schoch, R.R., Hilger, A. & Kardjilov, N. 2012: Braincase, palatoquadrate and ear region of the plagiosaurid *Gerrothorax pulcherrimus* from the Middle Triassic of Germany. *Palaeontology* 55, 31–50.
- Witzmann, F., Sachs, S. and Nyhuis, C.J. 2016: A new species of *Cyclotosaurus* (Stereospondyli, Capitosauria) from the Late Triassic of Bielefeld, NW Germany, and the intrarelationships of the genus. *Mitteilungen Aus Dem Museum Für Naturkunde in Berlin. Fossil Record* 19, 83–100.
- Wood, B. & Leakey, M. 2011: The Omo–Turkana Basin Fossil Hominins and Their Contribution to Our Understanding of Human Evolution in Africa. *Evolutionary Anthropology: Issues, News, and Reviews* 20, 264–292.
- Woodward, S.A.S 1900: Notes on Some Upper Devonian Fish-remains Discovered by Prof. AG Nathorst in East Greenland. *Bihangtill Kungliga Vetenskapsakademiens Handlingar* 26, 1–10.
- Zambelli, R. 1973: *Eudimorphodon ranzii* gen. nov., sp. nov., uno pterosauro Triassico. *Rendiconti Scienze di Istituto Lombardo*, B 107, 27–32.

New fossil fish microremains from the Upper Carboniferous of eastern North Greenland

GILLES CUNY & LARS STEMMERIK



Cuny, G. & Stemmerik, L. 2018. New fossil fish microremains from the Upper Carboniferous of eastern North Greenland. © 2018 by Bulletin of the Geological Society of Denmark, vol. 66, pp. 47–60. ISSN 2245-7070. (www.2dgf.dk/publikationer/bulletin).

The Moscovian of eastern North Greenland has yielded an assemblage dominated by teeth and dermal denticles of chondrichthyans with rarer teeth of actinopterygians. The rather poor preservation of the material precludes precise identification but the following taxa have been recorded: *Adamantina foliacea*, *Bransonella* spp., *Denaea* sp., “*Stemmatias*” *simplex*, *Lagarodus specularis*, *Actinopterygii* indet., as well as teeth probably belonging to new genera of Heslerodidae, ?Protacrodontidae and Hybodontiformes. This fauna appears therefore quite endemic. The abundance of *Bransonella* and durophagous chondrichthyans is in accordance with the shallow marine depositional environment. The record of a ?protacrodontid is possibly the youngest one for this taxon.

Keywords: Greenland, Carboniferous, Moscovian, Foldedal Formation, sharks, euchondrocephals.

Gilles Cuny [gilles.cuny@univ-lyon1.fr], Université de Lyon, UCBL, ENSL, CNRS, LGL-TPE, F-69622 Villeurbanne, France. Lars Stemmerik [lars.stemmerik@snm.ku.dk], Natural History Museum of Denmark, University of Copenhagen, Øster Voldgade 5–7, DK-1350 København K, Denmark; also The University Centre in Svalbard (UNIS), Longyearbyen, Norway.

Received 27 January 2017
Accepted in revised form
27 October 2017
Published online
6 March 2018

In Greenland, marine Carboniferous sediments are restricted to the Wandel Sea Basin of eastern North Greenland where shallow marine siliciclastics, carbonates and CaSO₄ evaporites of Moscovian to Gzhelian age unconformably overlie Lower Carboniferous (Visean) non-marine sediments and older rocks (Stemmerik & Håkansson 1989). The Upper Carboniferous sediments belong to the Kap Jungersen and Foldedal Formations of the Mallemuk Mountain Group and are part of a widely distributed succession of warm-water shelf sediments that were deposited along the northern margin of Pangea during the late Carboniferous and earliest Permian (Stemmerik 2000). During the time of deposition, North Greenland was located at around 35°N in a region characterized by warm and arid climate. The marine biota in the shelf carbonates belong to the late Palaeozoic warm-water chloroforam association recorded from Arctic Canada in the west across North Greenland, Svalbard and the Barents Shelf to Arctic Russia in the east (e.g. Beauchamp 1994; Stemmerik 2000). Records of fossil sharks from this vast warm-water shelf succession are few. Four taxa have been reported from North Greenland (Bendix-Almgreen 1976) and recently the occurrence

of *Lagarodus* was expanded to also include Svalbard (Cuny *et al.* 2016). The only records of fossil sharks from the Moscovian of Arctic Russia are from Novaya Zemlya and North Timan and include dermal denticles of ctenacanth, hybodont and neoselachian sharks, “*Stemmatias*”-like denticles, teeth of *Cooleyella* sp. and fragments of “bradyodont” toothplates (Ivanov 1999).

This paper describes a fish fauna from a carbonate bed in an otherwise shale-dominated interval in the lower part of the Foldedal Formation at Kap Jungersen, southern Amdrup Land (Fig. 1). The interval occurs in the lower part of sequence S5 in section 6 in Davydov *et al.* (2001, fig. 3). The well-exposed coastal cliff sections at Kap Jungersen are dated by fusulinids and correlated to the Russian type sections (Davydov *et al.* 2001). The fish fauna is from sediments belonging to the lower Moscovian (Kashirian) *Citrinoides paraozawai* zone of Davydov *et al.* (2001). Altogether around 100 chondrichthyan teeth and denticles and more than 50 actinopterygian microremains were recovered. The new material thus adds to our understanding of the fish fauna and diversity of the northern warm-water province during the late Carboniferous.

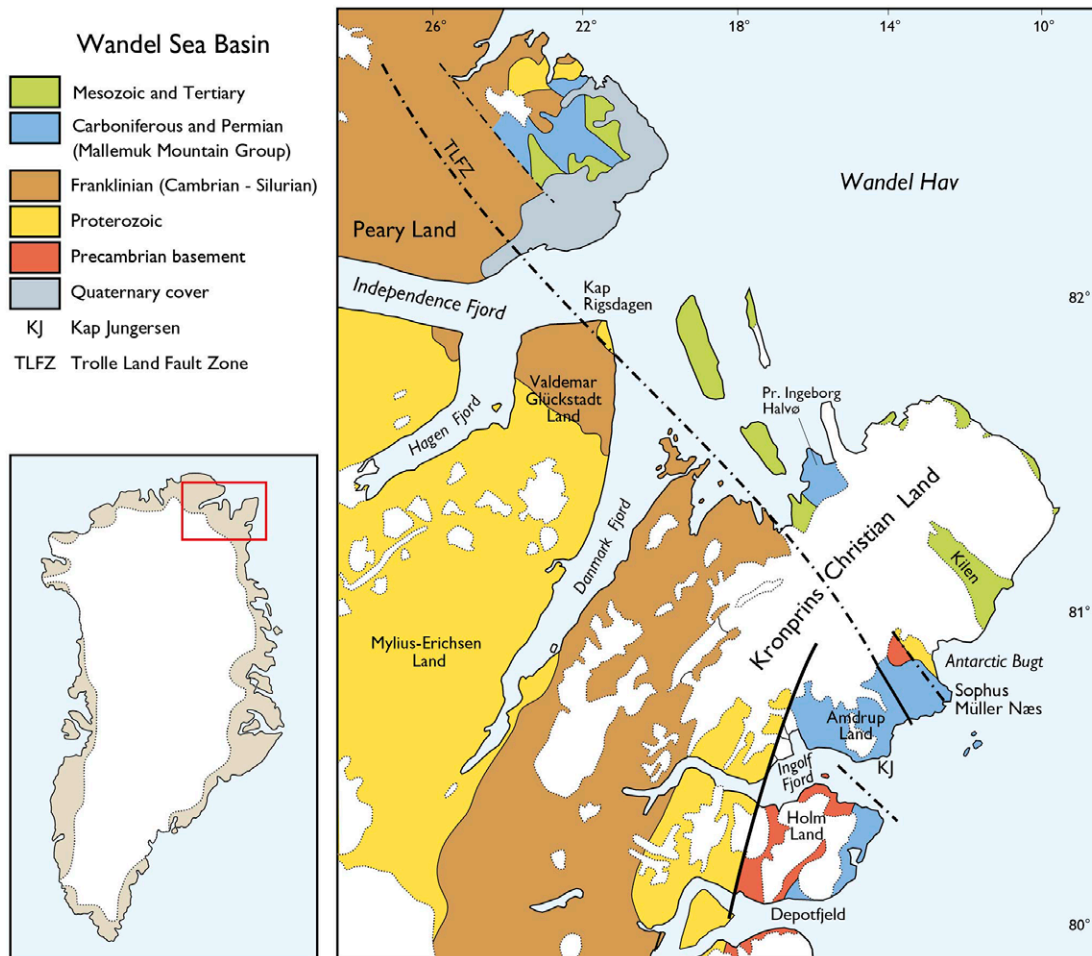


Fig. 1. Map of eastern North Greenland showing the distribution of marine Upper Palaeozoic sediments in the Wandel Sea Basin and location of the study locality (KJ).

Methods

The microremains were retrieved by dissolving approximately 250 g of limestone in 10% acetic acid, which resulted in *c.* 90 g of non-carbonate material. This material was sieved using 1 mm and 63 μm sieves and the fraction <1 mm and >63 μm was density separated; the light fraction, approximately 10 g, was then sorted for fish microremains using a microscope.

The systematic scheme used here follows Ginter *et al.* (2010). The use of the term 'root' in the following descriptions does not imply direct homology with the root of the teeth of other gnathostomes (Underwood *et al.* 2015).

All the specimens are housed at the Natural History Museum of Denmark, University of Copenhagen (abbreviation: MGUH).

Systematic palaeontology

Class Chondrichthyes Huxley 1880

Subclass Elasmobranchii Bonaparte 1838

Family Jalodontidae Ginter, Hairapetian & Klug 2002

Genus *Adamantina* Bendix-Almgreen 1993

***Adamantina foliacea* Ivanov 1999**

Fig. 2Q-T

Material. One tooth, NHMD 189710.

Description. NHMD 189710 is a tricuspid tooth measuring 1 mm mesio-distally. The three cusps are damaged, but the main cusp was probably a little higher than the mesial and distal ones. The bases of the cusps are fused. The crown is quite asymmetric, the mesial

(?) cusp being broader than the distal(?) one. The ornamentation of the labial face is chevron-shaped, whereas the lingual one displays faint and scarce ridges on the side of the cusps, but their central part is smooth.

The root is short and projected lingually, its basal face being perpendicular to the crown. There is a large central foramen at its lingual extremity. Additional foramina are present mainly at the base of the crown

lingually. There is a pair of well-developed labiobasal projections, one on each side of the central cusp of the crown, separated by a basolabial depression.

Comparisons. The tricuspid crown and chevron-shaped labial ornamentation of NHMD 189710 are reminiscent of teeth of *Bransonella*, but the absence of a central labial basal tubercle, replaced by a pair of labiobasal projections, allows easy separation of these two kinds

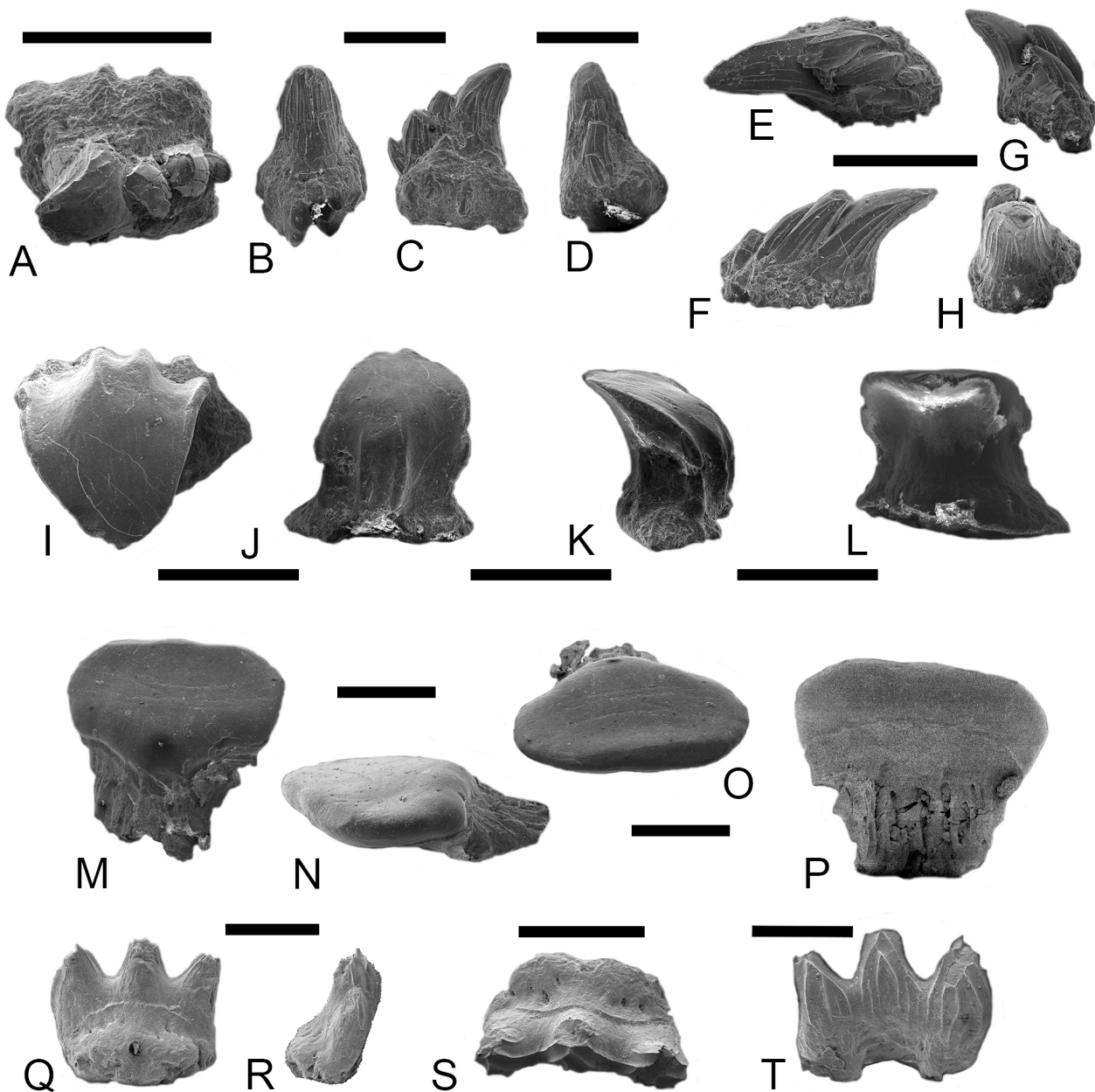


Fig. 2. A–H: “*Stemmatias simplex*”. A–D: NHMD 189706; A: apical view. B: anterior view. C: lateral view. D: posterior view. E–H: NHMD 189707; E: apical view. F: lateral view. G: posterior view. H: anterior view. I–P: dermal denticles of indeterminate chondrichthyans. I–L: NHMD 189708; I: apical view. J: anterior view. K: lateral view. L: posterior view. M–P: NHMD 189709; M: anterior view. N: lateral view. O: apical view. P: posterior view. Q–T: *Adamantina foliacea*, NHMD 189710; Q: lingual view. R: mesial or distal view. S: apical view. T: labial view. All scale bars represent 500 μm .

of teeth. A similar chevron-shaped ornamentation, as well as the presence of two labiobasal projections separated by a depression, is also encountered in jalodontids (Ivanov 1999; Ivanov *et al.* 2012). Many characters (a short root, the presence of a deep and wide labio-basal depression with prominent rounded tubercles, cusps labio-lingually compressed with their base fused, sub-equal in height and width, showing sub-parallel axes and ornamented by rare weak ridges on their lingual side) suggest that NHMD 189710 is better attributed to *Adamantina foliacea* (Ivanov 1999). *A. benedictae* differs from NHMD 189710 by a spirally

curved ornamentation and central cusp shorter than the lateral ones (Bendix-Almgreen 1993).

Superorder Xenacanthimorpha Nelson 1976

Order Bransonelliformes Hampe & Ivanov 2007

Genus *Bransonella* Harlton 1933

Bransonella spp.

Fig. 3

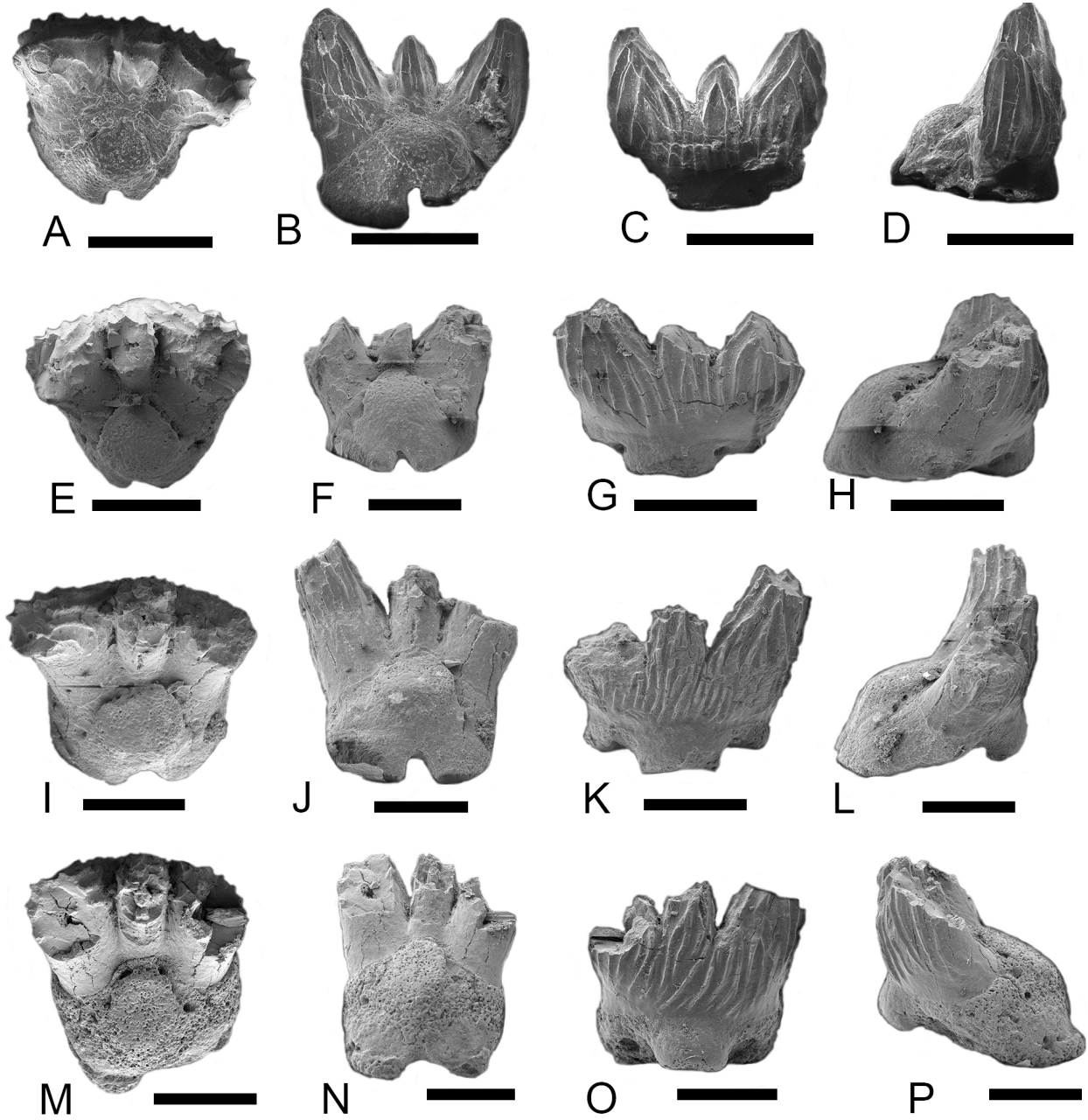


Fig. 3. *Bransonella* spp. A–D: NHMD 189711. E–H: NHMD 189713. I–L: NHMD 189715. M–P: NHMD 189716. A, E, I, M: apical views. B, F, J, N: lingual views. C, G, K, O: labial views. D, H, L, P: mesial or distal views. All scale bars represent 500 μ m.

Material. Six teeth, NHMD 189711 to NHMD 189716, and approximately 20 fragments.

Description. The crown of the best preserved specimen (NHMD 189711, Fig. 3A–D) is tricuspid and measures 1 mm mesio-distally. The mesial and distal cusps are twice the size of the intermediate one. The cross-section of the base of the mesial and distal cusps are almost circular, whereas the one of the intermediate cusp is more compressed mesio-distally. On the labial face, the ridges ornamenting the cusps anastomose to form chevrons. Some less well-preserved teeth, especially NHMD 189712 and NHMD 189716 (Fig. 3M–P), show an ornamentation denser and more oblique than that of NHMD 189711. The ornamentation on the lingual face is less developed than the one on the labial face with only two ridges on each cusp in NHMD 189711, whereas the lingual face of NHMD 189716 appears to be completely smooth. In addition, all three cusps possess well-developed cutting edges.

The root is projected lingually, perpendicularly to the crown. It shows a well-developed orolingual button, circular in outline. It covers most of the lingual surface of the root, except in NHMD 189711 where it is reduced in size and does not contact any of the cusps. On the lingual extremity of the root there is a notch corresponding to the opening of an unroofed vascular foramen. There are some additional foramina scattered irregularly on the surface of the root both labially and lingually. A basal tubercle is present on the labial margin, often with a foramen opening mesially and distally to it.

Comparisons. The following features allow these teeth to be attributed to the genus *Bransonella* (Ginter *et al.* 2010): The tricuspid crown has an intermediate cusp smaller than the mesial and distal ones, its labial ornamentation is chevron-shaped, the lingually extended root has a large orolingual button, and there are a labial basal tubercle and labial foramina. The intermediate cusp in the Greenland specimens appears smaller than that of the older (Tournaisian) teeth of *Bransonella* sp. described from Arctic Russia (Ivanov 1999). The Greenland teeth also differ from the ones of *B. tribula* by the lack of a pentagonal orolingual button elongated labio-lingually (Elliott & Hodnett 2013). The Greenland teeth are, however, quite disparate and may represent several species. When preserved, their rather low intermediate cusp and the presence in some teeth of a dense and strongly sigmoidal labial ornamentation are reminiscent of *B. lingulata*, but their orolingual button does not always reach the lingual rim of the root and some teeth show ridges on the lingual side of the crown. These two latter characters are more reminiscent of *B. nebraskensis* (Ivanov & Ginter 1996;

Johnson & Thayer 2009). Based on the morphology of its orolingual button and its smooth lingual crown, NHMD 189716 is the only tooth that would be better attributed to *B. lingulata* than to *B. nebraskensis*, but the labial ornamentation of the crown is more similar to that of *B. tribula* than to that of *B. lingulata*. In addition, the small lingual button of NHMD 189711, not in contact with the crown, is reminiscent of *B. tridentata*, but as this species is only known from a single, incomplete specimen, comparisons are difficult (Harlton 1933; Zidek 1973; Johnson 1984; Johnson 2005; Johnson & Thayer 2009).

Superorder Cladodontomorphi Ginter,
Hampe & Duffin 2010

Order Symmoriiformes Zangerl 1981

Family Falcatidae Zangerl 1990

Genus *Denaea* Pruvost 1922

Denaea sp.

Fig. 4A–H

Material. Two teeth, NHMD 189717 and NHMD 189718.

Description. NHMD 189717 measures 1.2 mm mesio-distally, whereas NHMD 189718 is larger with a mesio-distal length of 2 mm. The crown consists of a main cusp strongly arched lingually and flanked by two pairs of diverging lateral cusplets. The outer cusplets are larger than the inner ones and have a rounded cross-section. The main cusp is biconvex, with the lingual side more convex than the labial one. The labial face is ornamented by 8 to 13 non-anastomosing ridges and the lingual face by 14 to 16 similar ridges, some of which are restricted to the lower part of the cusp. The main cusp and lateral cusplets are connected by a faint lateral carina.

The root is projected lingually, showing a triangular outline in apical view. The orolingual ridge is elongated mesio-distally and displays a shallow concavity in its central part, separating a mesial and a distal button. The labial outline of the root shows a convexity at the level of the main cusp. One foramen corresponding to the main vascular canal opens on the lingual rim and there are smaller foramina irregularly distributed all over the root.

Comparisons. NHMD 189717 and 189718 are quite similar to the teeth of *Squatinactis*, except that they are more densely ornamented and that the labial convexity at the base of the main cusp is not as well developed (Ivanov 1996; Ginter *et al.* 2010). The fact that cusp and cusplets

are connected by a faint lateral carina could suggest that NHMD 189717 and 189718 belong to a ctenacanthiform rather than to a symmoriiform (Ginter *et al.* 2010). However, as pointed out by M. Ginter and A. Ivanov during the review process of this manuscript, faint carina between the cusps are quite often observed in teeth of *Denaea* (Ginter *et al.* 2015). NHMD 189717 and 189718 also share a similar rounded cross-section of the cusps with *Denaea*. In addition, teeth of *Denaea* display roots with weakly developed articulation devices and an orolingual ridge almost split in two by the opening of the main basal canal. Moreover, their outline in apical view is similar to that of NHMD 189717 and 189718 (Ginter *et al.* 2015). The quite robust cusps of the two teeth from Greenland are reminiscent of the teeth attributed to *Denaea* sp. by Ginter *et al.* (2015).

Symmoriiformes incertae sedis

“Stemmatias” simplex (St. John & Worthen 1875)

Fig. 2A–H

Material. Two denticles, NHMD 189706 and NHMD 189707.

Description. NHMD 189706 consists of four crowns forming a whorl over a fused base. The crowns decrease regularly in size posteriorly and are arched anteriorly. They are compressed antero-posteriorly. Their anterior faces are ornamented with numerous irregular ridges, whereas the posterior faces are almost smooth. The base is not very well preserved and shows a bulbous shape. It is almost as high as the main crown and is wider than the base of the crowns. Anteriorly, just under the base of the crowns, there is a row of foramina which fades posteriorly.

NHMD 189706 is very similar to NHMD 189707, except that the four crowns are not as well-aligned antero-posteriorly and the base appears less deep (Fig. 2E–H).

Comparisons. Specimens very similar to NHMD 189706 and 189707 were described from the Late Devonian and Late Carboniferous of Arctic Russia (Ivanov 1999), the Permian of Russia (Ivanov & Lebedev 2014) and the Late Devonian/Early Carboniferous of New Mexico (Ivanov & Lucas 2011). The latter specimens show a shallower base than the Greenland specimens, whereas the ones from Arctic Russia display a badly preserved base, making comparisons difficult. Ivanov (1999), Ivanov & Lucas (2011) and Ivanov & Lebedev (2014) attributed all these specimens to the genus *“Stemmatias”* and interpreted them as being buccopharyngeal denticles of Symmoriiformes. A similar single ‘coxcorn’ variety

was attributed to the species *“Stemmatias” simplex* by Williams (2001). Similar buccopharyngeal denticles were also described *in situ* in several Symmoriiformes: *Cobelodus aculeatus* (Zangerl & Case 1976), *Stethacanthus* cf. *altonensis* (Zidek 1993) and *Stethacanthus* (*Akmonistion*) *zangerli* (Coates & Sequeira 2001). Koot *et al.* (2013) described similar specimens from the Permian of Oman but attributed them to *Gunnelloodus bellistriatus* and interpreted them as buccopharyngeal denticles of Hybodontiformes, mostly because Symmoriiformes teeth were not recovered from the Permian of Oman. There is little morphological reason to separate *“Stemmatias” simplex* from *Gunnelloodus bellistriatus* at genus level, and as *Stemmatias* Hay 1899 has priority over *Gunnelloodus* Wilimovsky 1954, we refer our specimens as *“Stemmatias” simplex* buccopharyngeal denticles.

Zidek (1993) noted that pharyngeal whorls of denticles possess a thicker base in *Cobelodus* than in *Stethacanthus*, which might suggest that NHMD 189706 and 189707 belong to two different taxa.

Order Ctenacanthiformes Glickman 1964

Family Heslerodidae Maisey 2010

Heslerodidae indet.

Fig. 4I–P

Material. Two teeth, NHMD 189719 and NHMD 189720, and approximately 50 fragments.

Description. NHMD 189720 measures 1.8 mm mesio-distally, whereas NHMD 189719 is larger, measuring 3.2 mm mesio-distally with one of the extremities of the tooth lacking. The crown consists of a main cusp flanked by three pairs of lateral cusplets for NHMD 189719 and four pairs for NHMD 189720. The main cusp has a weakly convex labial face and a strongly convex lingual face. The labial face is ornamented with a few ridges of variable length, whereas the lingual ornamentation is denser, made of non-rectilinear ridges of variable length. In NHMD 189720 there are two ridges that anastomose to form a single ridge in the upper part of the labial face of the cusp, with a short ridge in between the two branches of the main ridge. The main cusp shows well-developed cutting edges. In NHMD 189719 only one of the lateral cusplets is partially preserved (Fig. 4J–K). In NHMD 189720 the outer pair of cusplets is the largest, the second pair the second largest, whereas the first and third pairs are the smallest (Fig. 4N–O). The outer pair was probably about half the height of the main cusp. The ornamentation of the labial faces of the cusplets is less dense than that of the lingual faces.

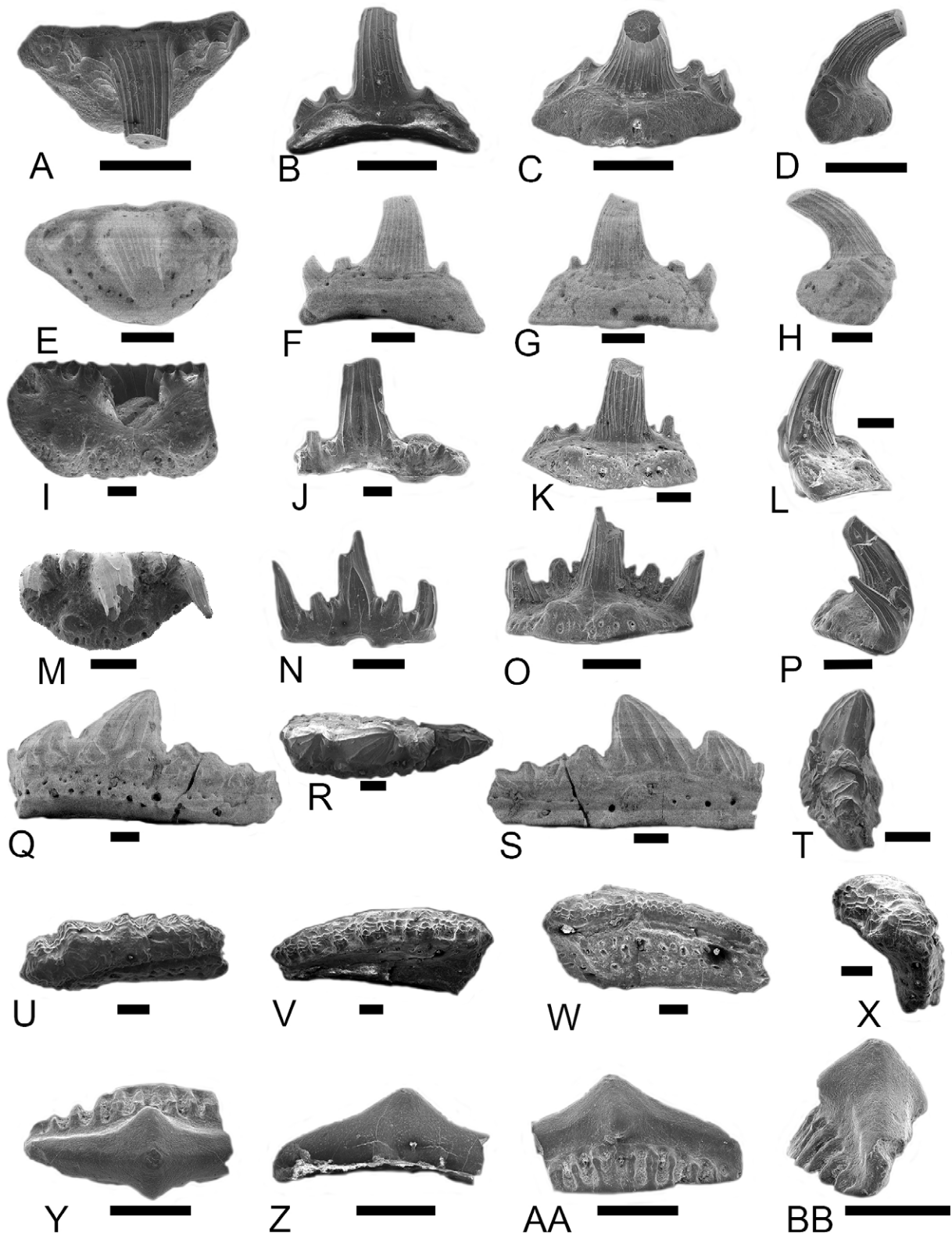


Fig. 4. A–H: Falcatidae indet. A–D: NHMD 189717. E–H: NHMD 189718. A, E: apical views. B, F: labial views. C, G: lingual views. D, H: mesial or distal views. I–P: ?Heslerodidae indet. I–L: NHMD 189719. M–P: NHMD 189720. I, M: apical views. J, N: labial views. K, O: lingual views. L, P: mesial or distal views. Q–X: Protacrodontidae indet. Q–T: anterior tooth NHMD 189721; Q: labial view. R: apical view. S: lingual view. T: distal view. U–X: posterior tooth NHMD 189722; U: apical view. V: labial view. W: lingual view. X: mesial view. Y–BB: Hybodontiformes indet. NHMD 189723; Y: apical view. Z: labial view. AA: lingual view. BB: mesial or distal view. All scale bars represent 500 μm .

The root is shallow and projected lingually, perpendicularly to the crown. In apical view it shows an almost quadrangular outline in NHMD 189719, but it is more semi-circular in NHMD 189720. There is a pair of well-separated orolingual buttons and labiobasal projections, one on each side of the main cusp of the crown. The orolingual buttons are almost circular in apical view. The root shows many foramina scattered over the whole surface, although they concentrate on its lingual margin. There are two paired enlarged foramina between the orolingual buttons in NHMD 189719 and a single one in NHMD 189720.

Comparisons. NHMD 189719 and NHMD 189720 differ from NHMD 189717 and NHMD 189718 by an ornamentation less dense on the labial side of the main cusp and a shallower root, not triangular in apical outline. The orolingual buttons are also clearly separated from each other, whereas this is not the case in NHMD 189717 and NHMD 189718. The presence of two separate orolingual buttons and two basolabial projections on each side of the main cusp suggests that NHMD 189719 and NHMD 189720 are closely related to the clade grouping *Kaibabvenator*, *Nanoskalme*, *Glickmanius* and *Heslerodus* as defined by Hodnett *et al.* (2012), although the orolingual buttons are not always completely separated in the teeth of *Heslerodus* (Ginter 2002). The presence of the same characters in the teeth of "*Ctenacanthus*" *costellatus* strongly suggests that this taxon also belongs to the same monophyletic group (Ivanov & Lebedev 2014). NHMD 189719 appears indeed quite similar to a fragmentary tooth from the Viséan of Derbyshire attributed to "*Ctenacanthus*" *costellatus* by Ginter *et al.* (2015), although it lacks a well-developed basolabial depression at the level of the main cusp. The lack of such a depression in NHMD 189719 and NHMD 189720 indicates that they are probably closer to *Kaibabvenator* + *Nanoskalme* than to *Glickmanius* + *Heslerodus* + "*Ctenacanthus*" *costellatus*.

Cohort Euselachii Hay 1902

Superfamily Protacrodontoidea Zangerl 1981

Family Protacrodontidae Cappetta, Duffin & Zidek 1993

?Protacrodontidae indet.

Fig. 4Q–X

Material. Two teeth, NHMD 189721 and NHMD 189722, and approximately 10 fragments.

Description. There are two different morphotypes of

protacrodont teeth in the material. The first is represented by NHMD 189721 (Fig. 4Q–T) which measures 3.9 mm mesio-distally but is broken mesially. The crown shows a main cusp oriented distally, flanked by at least one mesial cusplet and three distal ones. The mesial cusplet is larger than the distal ones, giving the crown a marked asymmetric aspect. The main cusp and the mesial cusplet are ornamented by three to five ridges reaching the apices on the labial and lingual faces. There are one to two ridges on the distal cusplets on each face. The ridges ornamenting the mesial and distal cusplets are more irregular than those on the main cusp. They bifurcate basally and join together, forming a reticulate ornamentation at the base of the crown. A longitudinal crest, forming moderately developed carinae, joins all cusp and cusplets together. At the base of the labial face there is a row of nine small accessory labial cusplets.

The root is half the height of the crown and is separated from the latter by a moderately developed groove. Foramina of various sizes are scattered on the lingual and labial sides of the root. On the labial side, the larger foramina are positioned at the base of the root and can be unroofed basally, forming short grooves. The basal part of the lingual side is devoid of foramina and the larger ones are concentrated on the middle part of the face. The root is slightly inclined lingually.

The second morphotype, NHMD 189722 (Fig. 4U–X), is very asymmetric and 4.3 mm long mesio-distally. There are eight very low cusp and cusplets. The main cusp is flanked by one mesial cusplet and six distal ones. There are one or two well-developed labial nodes in front of each cusp and cusplet. The ornamentation of the crown is complex, made of fine, reticulated ridges with a mesio-distal main orientation and restricted to the lower part of the crown. In apical view the ornamentation forms irregular, concentric rings around the crown. The labial part of the crown overhangs the root. Lingually, the root is separated from the crown by a well-defined groove. The labial face of the root is concave in mesial or distal view, whereas the lingual face is straight under the crown. Foramina of variable sizes are scattered on the upper two-thirds of the root.

Comparisons. NHMD 189721 is reminiscent of teeth of *Sphenacanthus*, but in the latter labial accessory cusplets are generally lacking at the level of the main cusp (Soler-Gijón 1997; Ginter *et al.* 2010) and the teeth are more symmetric, except for some teeth of *S. carbonarius* (Ginter *et al.* 2010, fig. 94A). However, in the latter species the lingual projection of the root is more developed and the labial foramina tend to form a horizontal row (Soler-Gijón 1997; Ginter 2016). As

noted by Ginter *et al.* (2010), it is almost impossible to separate isolated teeth of protacrodonts from those of Palaeozoic hybodonts, and as a convention teeth from the Devonian have generally been attributed to protacrodonts, whereas Carboniferous teeth are more often attributed to hybodonts. However, NHMD 189721 shares features with teeth of *Deihim* such as a similar root vascularization, the presence of a row of accessory labial cusplets and a reticulate ornamentation at the base of the crown. The main difference to the latter genus is that the root appears less projected lingually and the base of the crown is almost flat and not as convex as in the teeth of *Deihim*, without diverging cusplets (Ginter *et al.* 2002; Roelofs *et al.* 2016). A tooth from the Devonian of Morocco attributed to cf. *Deihim mansureae* by Ginter *et al.* (2002, plate 6 I–K) shows completely fused cusps and a complex reticulated ornamentation, at least on the lingual face, which is quite similar to what can be seen on NHMD 189722. A reticulated ornamentation at the base of the crown has also been observed in teeth of *Protacrodus* sp. from the Early Carboniferous of Iran (Habibi & Ginter 2011, pl. 2B) as well as in the teeth of a Protacrodontidae? indet. from the Tournaisian of China, which also share with the Greenland specimens a highly asymmetric crown (Ginter & Sun 2007). Several Devonian protacrodontids also display a reticulated ornamentation at the base of the crown (Long & Hairapetian 2000; Ginter & Sun 2007; Roelofs *et al.* 2015). Hence, the presence of a row of labial accessory cusplets and reticulate ornamentation at the base of the crown lead us to attribute NHMD 189722 and NHMD 189721 to a protacrodontid rather than to a hybodont shark. The morphology of NHMD 189722 is also reminiscent of non-symphysial teeth of Eugeneodontiformes, but to the authors' best knowledge a reticulated ornamentation at the base of the crown is unknown among this order. If we are correct, this would extend the stratigraphic range of the protacrodonts to the Middle Pennsylvanian; they are currently considered to disappear in the Early Carboniferous (Ginter *et al.* 2010).

Order Hybodontiformes Patterson 1966

Hybodontiformes indet.

Fig. 4Y–BB

Material. One tooth, NHMD 189723.

Description. The crown is elongated mesio-distally, devoid of ornamentation, with a blunt main cusp. At the base of the main cusp there is a well-developed labial and lingual peg. The root is compressed labio-lingually and projected lingually. On the lingual face

there is a series of nine furrows, with a foramen opening in the upper part of each furrow. As the mesial or distal part of the tooth is lacking, the total number of furrows was at least eleven, depending on whether the tooth was asymmetric or not. There is a row of large foramina in the uppermost part of the labial face of the root.

Comparisons. The root is of euselachian type according to Ginter *et al.* (2010). Its morphology, compressed labio-lingually, inclined lingually with well-developed furrows on the lingual face, is reminiscent of what can be observed in the enchondrocephalian *Cristatodens sigmoidalis* and the hybodont *Cassisodus margaritae* from the Tournaisian of China (Ginter & Sun 2007). However, the apparent lack of tubular dentine in the crown does not favour a relationships of NHMD 189723 to the Euchondrocephali. It is closer to *Cassisodus* and the Hybodontiformes, although its crown morphology is much simpler than in the latter genus. They share, however, the presence of a labial and lingual peg at the base of the main cusp, a character also found in other Palaeozoic Hybodontiformes such as *Omanoselache*, *Reesodus* and *Teresodus* (Koot *et al.* 2013). Furrows on the lingual side of the root are, however, not as well developed in these three taxa as in NHMD 189723. The latter therefore probably represents a new taxon closely allied to *Cassisodus*, but more material is necessary to test this hypothesis.

Elasmobranchii *incertae sedis*

Dermal denticles

Fig. 2I–P

Material. Two denticles, NHMD 189708 and NHMD 189709.

Description. NHMD 189708 is 0.7 mm high. Its crown is leaf-shaped and arched caudally. It shows two well-developed carinae that reach the apex of the crown, and two parallel ridges delimiting a mesial platform with a slightly concave surface that stops at the level of the caudal flexure. The subcrown is smooth. The pedicle is truncate (Johns *et al.* 1997) with at least six canal openings on its side.

The crown of NHMD 189709 is set almost horizontally, with a slightly concave surface. It is ovoid in shape, smooth, 1.8 mm long and 0.5 mm thick. Its anterior face shows a well-developed mesial protrusion. The subcrown is smooth with a well-developed halo. The pedicle is badly preserved and projected anteriorly. The anterior face presents two rows of canal openings. The subpedicle shows a series of furrows,

although this is likely to be an artefact due to post-mortem wear.

Comparisons. The shape of the crown of NHMD 189709 and its nearly horizontal position is reminiscent of the paragenus *Glabrisubcorona* Johns, Barnes & Orchard 1997 from the Late Triassic of Canada. However, its pedicle is much more projected anteriorly than in the latter. The presence of a double row of foramina openings on the pedicle is very unusual.

Subclass Euchondrocephali Lund & Grogan 1997

Order indet.

Family Lagarodontidae Lebedev 2008

Genus *Lagarodus* Jaekel 1898

Lagarodus specularis (Trautschold 1874)

Fig. 5

Material. One tooth, NHMD 189724.

Description. This tooth is strongly arched and asymmetric, with the reduced mesial part of the cusp per-

pendicular to the distal part, forming a transversely elongated tubercle. It measures 12 mm mesio-distally, 6 mm labio-lingually and is 5 mm at its maximum height. The crown is quadrangular in apical view, the mesial extremity being slightly wider than the distal one. The apical surface shows a dense network of circular depressions corresponding to the opening of the dentinal canals of the tubular dentine (orthotrabeculine). The labial and lingual faces of the crown are ornamented by irregular ridges parallel to each other and running mesio-distally. The labial ornamentation is better developed than the lingual one. The labial face overhangs the root and is separated from the latter by a constriction.

The root is rhomboid in outline in basal view and is not projected lingually. It displays small foramina scattered over all faces except the basal one. There is a tendency for the foramina to be larger on the distal part than on the mesial part.

Comparisons. The following features allow identification of this tooth as the *angustus* morphotype of *Lagarodus specularis* (Lebedev 2008): The mesial part of the tooth is strongly reduced with its surface perpendicular to that of the distal one, the central tubercle is transversely elongated, and the ornamentation at the base of the crown is made of irregular and parallel

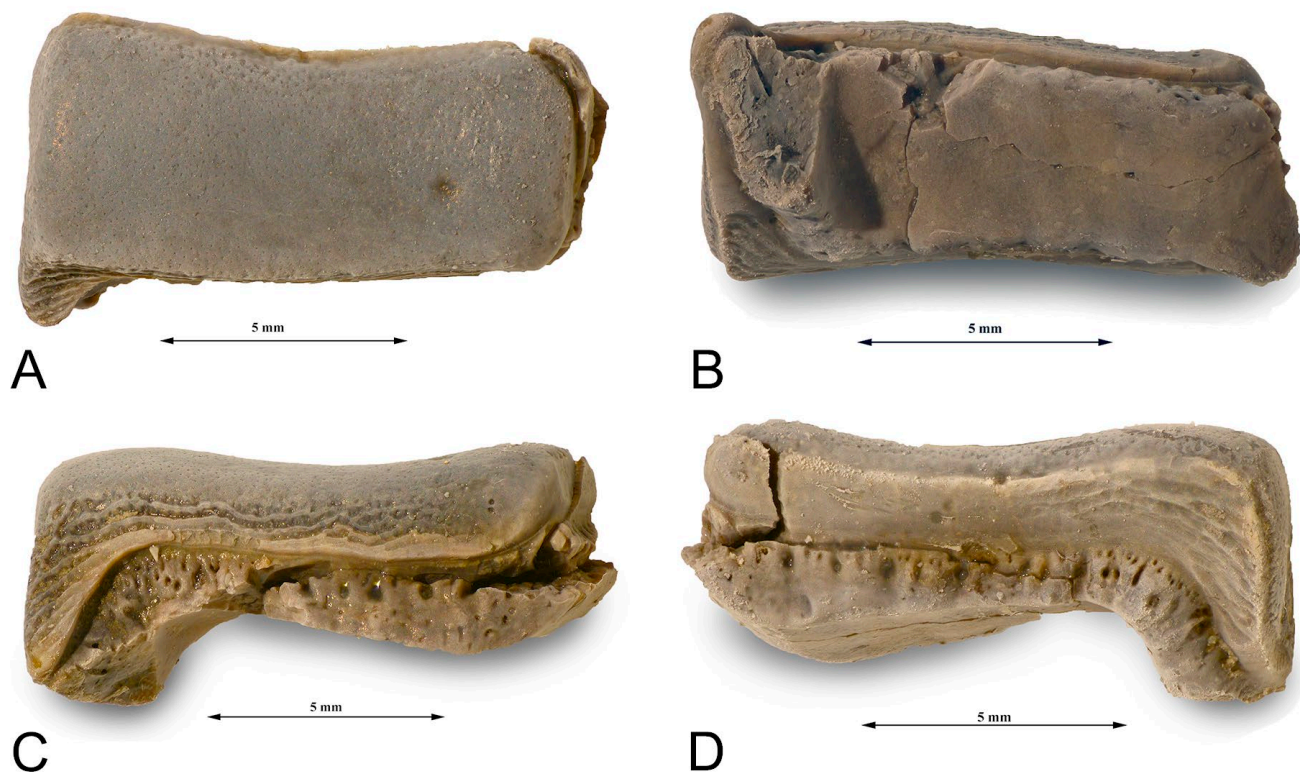


Fig. 5. *Lagarodus specularis*, NHMD 189724; A: apical view. B: basal view. C: labial view. D: lingual view.

mesio-distal ridges. The tooth therefore represents a parasymphysial tooth. Bendix-Almgreen (1975) described another parasymphysial tooth he attributed to *Lagarodus* sp. from the Upper Carboniferous of Amdrup Land. The latter is broken and more worn than the present specimen, but it shows no difference to it and is likely to belong to the same species.

It should be noted, however, that Cuny *et al.* (2016) recently suggested that a second species of *Lagarodus* might have existed in the northern hemisphere, but this was based on the description of a lateral tooth from Svalbard. The parasymphysial teeth of Greenland, on the other hand, fit perfectly the ones of *Lagarodus specularis*, and as no lateral teeth have yet been found in Greenland, the presence of this putative second species there cannot be tested for the time being.

Lebedev (2008) attributed the family Lagarodontiidae to elasmobranchs rather than to euchondrocephals, but at the same time pointed out similarities with both orodontiforms and eugeneodontiforms, which are enchondrocephals (Ginter *et al.* 2010). We therefore follow a more conventional point of view and maintain this family in the Subclass Euchondrocephali, pending a more detailed analysis of the phylogenetic affinities of this family.

Class Osteichthyes Huxley 1880

Actinopterygii Klein 1885

Actinopterygii indet.

Fig. 6

Material. Several isolated teeth (>50), including NHMD 189725.

Description. NHMD 189725 is 1.7 mm high with a conical, slightly sigmoidal shape. The acrodine cap is smooth and represents 22% of the total height of the tooth. The ganoine covering the shaft of the tooth is ornamented by a dense network of very short, irregular ridges (Fig. 6B).

Comparisons. NHMD 189725 presents a shape and an ornamentation of the ganoine similar to the actinopterygian type D teeth described from the Upper Carboniferous of Brazil by Richter *et al.* (1999), and similar to the teeth of Actinopterygii indet. A described from the Kasimovian of Illinois by Carpenter *et al.* (2011). However a similar pattern of ganoine ornamentation is known as early as the Devonian/Carboniferous boundary (Derycke *et al.* 1995).

Discussion

Very few fossil sharks have until now been described from the Carboniferous of Greenland and only four taxa have been known from isolated teeth and fin spines: *Ctenacanthus* sp. (fin spine), *Petalodus* sp., *Lagarodus* sp. and a cochlodontid or menaspid (Bendix-Almgreen 1976). As for *Adamantina*, it was so far restricted to the Permian in Greenland (Bendix-Almgreen 1993). This is therefore the first record of symmoriiform, protacrodont and hybodont sharks, as well as *Bransonella*, from this part of the world. Although the material recovered so far is not well preserved, some taxa appear to be new: the teeth of the Heslerodidae and Hybodontiformes do not fit any known genera. It suggests a rather high endemism of this fauna. Furthermore, East Greenland might have

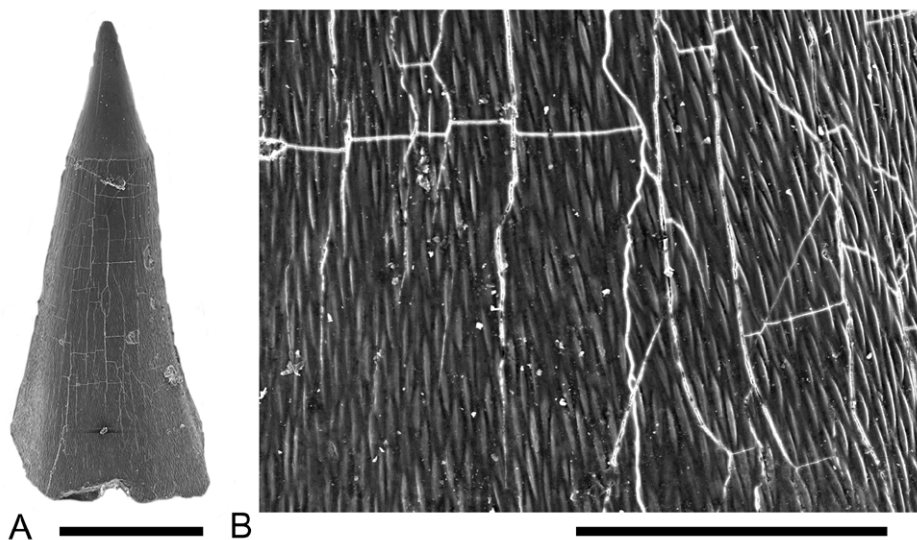


Fig. 6. Actinopterygii indet. NHMD 189725; **A:** tooth in lateral view. **B:** detail of the ornamentation of the ganoine. Scale bars represent 500 μm for **A** and 100 μm for **B**.

been a refuge area for the last protacrodonts as their putative record in Greenland represents their youngest known occurrence.

The fact that *Bransonella* could be represented by three species in Greenland (*B. lingulata*, *B. nebraskensis* and *B. tridentata*) is a bit surprising, as *B. lingulata* is currently unknown in rocks younger than the Bashkirian (Johnson & Thayer 2009). The poor quality of the material does not allow a deciphering of the relationships of the *Bransonella* teeth from Greenland at species level, but it is nonetheless interesting to note that they represent the most abundant teeth in the assemblage, whereas the genus is unknown from Arctic Russia after the Tournaisian (Ivanov 1999). According to Johnson & Thayer (2009), this genus may have preferred shallow marine water. Its association in Greenland with taxa possessing crushing dentition (*Lagarodus*, indeterminate protacrodont and hybodont) is in accordance with such a hypothesis and fits the overall depositional setting of the Amdrup Land succession (e.g. Stemmerik 2003). The disappearance of *Bransonella* in Arctic Russia after the Tournaisian may therefore be the result of a depositional environment too deep for this genus.

As discussed above, the quality of the material does not allow precise identification of the recovered taxa, and their biostratigraphical value is therefore limited. However, apart from the protacrodont, all of them are compatible with the Moscovian age of the site indicated by the fusulinids (Davydov *et al.* 2001).

Conclusion

The Moscovian Greenlandic fossil fish assemblage comprises several teeth that do not fit any hitherto described taxa. The assemblage encompasses possible new genera belonging to the Heslerodidae and Hybodontiformes, and also provides the youngest record of a protacrodontid. The abundance of *Bransonella* in the assemblage is in stark contrast with contemporaneous records in Arctic Russia, suggesting that the Greenland fauna represents a shallower marine setting.

Acknowledgements

We thank Jakob B. Kristensen and Line Skøtt for help with preparation and sorting. Jakob B. Kristensen also photographed most of the figured specimens under the SEM. We also thank Sten Lennart Jakobsen who took the photographs for Fig. 5 and Lotte Melchior Larsen for her help during the editorial process.

The material was collected during GEUS mapping of the area. Finally our most sincere thanks go to the reviewers of the manuscript, Michał Ginter and Alexander Ivanov, who corrected some of our original misidentifications and greatly improved the quality of this work.

References

- Beauchamp, B. 1994: Permian climatic cooling in the Canadian Arctic. In: Klein, G.D. (ed), *Pangea: Paleoclimate, Tectonics and Sedimentation during accretion, zenith and breakup of a supercontinent*. Geological Society of America Special Paper 288, 229–246.
- Bendix-Almgreen S.E. 1975: Fossil fishes from the marine Late Palaeozoic of Holm Land–Amdrup Land, North-East Greenland. *Meddelelser om Grønland* 195(9), 38 pp. + 3 plates.
- Bendix-Almgreen S.E. 1976: Palaeovertebrate faunas of Greenland. In: Escher, A. & Watt, W.S. (eds), *Geology of Greenland*, 536–573. Copenhagen: Geological Survey of Greenland.
- Bendix-Almgreen, S.E. 1993: *Adamantina benedictae* n.g. et sp. – a new elasmobranch from the marine Upper Permian of East Greenland. In: Johnsen O. (ed.), *Geologisk Museum – 100 år på Østervold*, 48–58. Copenhagen: Rhodos.
- Bonaparte, C.L.J.L. 1838: *Iconografia della fauna italica per le quarto classi degli animali vertebrati*. Tomo III: Pesci, 266 pp. Roma: Salviucci.
- Cappetta, H., Duffin, C. & Zidek, J. 1993: Chondrichthyes. In: Benton, M.J. (ed.), *The Fossil Record* 2, 593–609. London: Chapman and Hall.
- Carpenter, D., Falcon-Lang, H.J., Benton, M.J. & Nelson, W.J. 2011: Fishes and tetrapods in the Upper Pennsylvanian (Kasimovian) Cohn coal Member of the Mattoon Formation of Illinois, United States: Systematics, Paleoeology, and paleoenvironments. *Palaios* 26, 639–657.
- Coates, M.I. & Sequeira, S.E.K. 2001: A new stethacanthid chondrichthyan from the Lower Carboniferous of Bearsden, Scotland. *Journal of Vertebrate Paleontology* 21, 438–459.
- Cuny, G., Kristensen, J.B. & Stemmerik, L. 2016: First record of *Lagarodus* (Chondrichthyes: Euchondrocephali) from the Carboniferous of Svalbard, Arctic Norway. *Norwegian Journal of Geology* 96, 1–5.
- Davydov, V.I., Nilsson, I. & Stemmerik, L. 2001: Fusulinid zonation of the Upper Carboniferous Kap Jungersen and Foldedal Formations, southern Amdrup Land, eastern North Greenland. *Bulletin of the Geological Society of Denmark* 48, 25–72.
- Derycke, C., Blicq, A. & Turner, S. 1995: Vertebrate microfauna from the Devonian/Carboniferous boundary stratotype at La Serre, Montagne Noire (Hérault, France). *Bulletin du Muséum national d'Histoire naturelle* 17, 461–485.
- Elliott, D.K. & Hodnett, J.-P. 2013: A new species of *Bransonella* (Chondrichthyes, Xenacanthimorpha, Bransonelliformes)

- from the Middle Permian Kaibab Formation of Northern Arizona. *Journal of Paleontology* 87, 1136–1142.
- Ginter, M. 2002: Taxonomic notes on “*Phoebodus heslerorum*” and *Symmorium reniforme* (Chondrichthyes, Elasmobranchii). *Acta Palaeontologica Polonica* 47, 547–555.
- Ginter, M. 2016: The heterodonty in euselachian sharks from the Pennsylvanian of Nebraska. *Acta Geologica Polonica* 66, 299–312.
- Ginter, M. & Sun, Y. 2007: Chondrichthyan remains from the Lower Carboniferous of Muhua, southern China. *Acta Palaeontologica Polonica* 52, 705–727.
- Ginter, M., Hairapetian, V. & Klug, C. 2002: Famennian chondrichthyan remains from the shelves of North Gondwana. *Acta Geologica Polonica* 52, 169–215.
- Ginter, M., Hampe, O. & Duffin, C.J. 2010: Chondrichthyes, Palaeozoic Elasmobranchii: Teeth. *Handbook of Paleichthyology* vol. 3D, 168pp. München: Verlag Dr. Friedrich Pfeil.
- Ginter, M., Duffin, C.J., Dean, M.T. & Korn, D. 2015: Late Viséan pelagic chondrichthyan remains from northern Europe. *Acta Palaeontologica Polonica* 60, 899–922.
- Glikman, L.S. 1964: Sharks of the Paleogene and their stratigraphic significance. Moscow: Doklady Akademii Nauk Soyuz Sovetskikh Respublik. 228 pp. [In Russian].
- Habibi, T. & Ginter, M. 2011: Early Carboniferous chondrichthyan remains from the Mobarak Formation, central Alborz Mountains, Iran. *Acta Geologica Polonica* 61, 27–34.
- Hampe, O. & Ivanov, A. 2007: Bransonelliformes – a new order of the Xenacanthimorpha (Chondrichthyes, Elasmobranchii). *Fossil Record* 10, 190–194.
- Harlton, B.H. 1933: Micropaleontology of the Pennsylvanian Johns Valley Shale of the Ouachita Mountains, Oklahoma, and its relationship to the Mississippian Caney Shale. *Journal of Paleontology* 7, 3–29.
- Hay, O.P. 1899: On some changes in the names, generic and specific, of certain fossil fishes. *The American Naturalist* 33, 783–792.
- Hay, O.P. 1902: Bibliography and catalogue of the fossil vertebrata of North America. United States Geological Survey Bulletin 179, 868 pp.
- Hodnett, J.-P., Elliott, D.K., Olson, T.J. & Wittke, J.H. 2012: Ctenacanthiform sharks from the Permian Kaibab Formation, northern Arizona. *Historical Biology* 24, 381–395.
- Huxley, T. 1880: A manual of the anatomy of vertebrated animals, 431 pp. New York: D. Appleton & Co.
- Ivanov, A. 1996: The Early Carboniferous chondrichthyan remains of the South Urals, Russia. In: Strogon, P., Somerville, I.D. & Jones, G.L. (eds), *Recent advances in Lower Carboniferous Geology*. Geological Society, London, Special Publication 107, 417–425.
- Ivanov, A. 1999: Late Devonian – Early Permian chondrichthyan remains of the Russian Arctic. *Acta Geologica Polonica* 49, 267–285.
- Ivanov, A. & Ginter, M. 1996: Early Carboniferous xenacanthids (Chondrichthyes) from Eastern Europe. *Bulletin de la Société Géologique de France* 167, 651–656.
- Ivanov, A.O. & Lebedev, O.A. 2014: Permian chondrichthyan remains of the Kanin Peninsula, Russia. *Paleontological Journal* 48, 1030–1043.
- Ivanov, A. & Lucas, S.G. 2011: Fish fossils from the Paleozoic Sly Gap Formation of southern New Mexico, USA. *New Mexico Museum of Natural History and Science Bulletin* 53, 52–69.
- Ivanov, A., Nestell, M. & Nestell, G. 2012: New jalodontid chondrichthyan remains from the Middle Permian of West Texas, USA. *Historical Biology* 24, 359–368.
- Jaekel, O. 1898: Über die verschiedenen Rochen-Typen. *Sitzungsberichte der Gesellschaft Naturforschender Freunde zu Berlin* 5, 44–53.
- Johns, M.J., Barnes, C.R. & Orchard, M.J. 1997: Taxonomy and biostratigraphy of Middle and Late Triassic elasmobranch ichthyoliths from northeastern British Columbia. *Geological Survey of Canada Bulletin* 502, 235 pp.
- Johnson, G.D. 1984: A new species of *Xenacanthodii* (Chondrichthyes, Elasmobranchii) from the late Pennsylvanian of Nebraska. *Special publication Carnegie Museum of Natural History* 9, 178–186.
- Johnson, G.D. 2005: An unusual tricuspid chondrichthyan tooth from the Lower Permian of Texas, USA. *Revista Brasileira de Paleontologia* 8, 159–164.
- Johnson, G.D. & Thayer, D.W. 2009: Early Pennsylvanian xenacanth chondrichthyan remains from the Swisshelm Mountains, Arizona, USA. *Acta Palaeontologica Polonica* 54, 649–668.
- Klein, E.F. 1885: Beiträge zur Bildung des Schädels der Knochenfische 2. *Jahreshefte Vereins Vaterländischer Naturkunde in Württemberg* 42, 205–300.
- Koot, M.B., Cuny G., Tintori A. & Twitchett R.J. 2013: A new diverse fauna from the Wordian (Middle Permian) Khuff Formation in the interior Haushi-Huqf area, Sultanate of Oman. *Palaeontology* 56, 303–343.
- Lebedev, O.A. 2008: Systematics and dental system reconstruction of the durophagous chondrichthyan *Lagarodus* Jaekel 1898. *Acta Geologica Polonica* 58, 199–204.
- Long, J. & Hairapetian, V. 2000: Famennian microvertebrates from the Dalmeš area, central Iran. *Records of the Western Australian Museum, Supplement* 58, 211–221.
- Lund, R. & Grogan, E.D. 1997: Relationships of the Chimæriiformes and the basal radiation of the Chondrichthyes. *Reviews in Fish Biology and Fisheries* 7, 65–123.
- Maisey, J.G. 2010: *Heslerodidae* (Chondrichthyes, Elasmobranchii), a new family of Paleozoic phalacanthous sharks. *Kirtlandia* 57, 13–21.
- Nelson, J.S. 1976: *Fishes of the World*, 416 pp. Wiley and Sons, New York.
- Patterson, C. 1966: British Wealden sharks. *Bulletin of the British Museum (Natural History), Geology* 11, 283–350.
- Pruvost, P. 1922: Description de *Denaea fournieri*, sélacien nouveau du Marbre noir de Denée. Part 2 of Fournier, G. & Pruvost, P. : Découverte d’un poisson nouveau dans le marbre noir de Denée. *Bulletin de l’Académie Royal de Bruxelles Série* 5(8), 213–218.
- Richter, M., Neis, P.A. & Smith, M.M. 1999: Acanthodian and

- actinopterygian fish remains from the Itaituba Formation, Late Carboniferous of the Amazon Basin, Brazil, with a note on acanthodian ganoin. *Neues Jahrbuch für Geologie und Paläontologie Monatshefte* 1999, 728–744.
- Roelofs, B., Playton, T., Barham, M. & Trinajstić, K. 2015: Upper Devonian microvertebrates from the Canning Basin, Western Australia. *Acta Geologica Polonica* 65, 69–100.
- Roelofs, B., Barham, M., Mory, A.J. & Trinajstić, K. 2016: Late Devonian and Early Carboniferous chondrichthyans from the Fairfield Group, Canning Basin, Western Australia. *Palaeontologia Electronica* 19, 1–28.
- Soler-Gijón, R. 1997: Euselachian sharks from the Late carboniferous of the Puertollano basin, Spain: biostratigraphic and palaeoenvironmental implications. *Modern geology* 21, 137–169.
- St. John, O. & Worthen, A.H. 1875: Description of fossil fishes. *Geological Survey of Illinois, Paleontology* 6, 245–488.
- Stemmerik, L. 2000: Late Palaeozoic evolution of the North Atlantic margin of Pangea. *Palaeogeography, Palaeoclimatology, Palaeoecology* 161, 95–126.
- Stemmerik, L. 2003: Controls on localization and morphology of Moscovian (Late Carboniferous) carbonate buildups, southern Amdrup Land, North Greenland. In: Ahr, W.M., Harris, P.M., Morgan, W.A. & Somerville, I.D. (eds), *Permo-Carboniferous Carbonate Platforms and Reefs*, SEPM Special Publication 78, 253–265.
- Stemmerik, L. & Håkansson, E. 1989: Stratigraphy and depositional history of the Upper Palaeozoic and Triassic sediments in the Wandel Sea Basin, central and eastern North Greenland. *Rapport Grønlands Geologiske Undersøgelse* 143, 21–45.
- Trautschold, H. 1874: Die Kalkbrüche von Mjatschkova. Eine Monographie des oberen Bergkalks. Erste Hälfte. *Nouveaux Mémoires de la Société Impériale des Naturalistes de Moscou* 13(19), 276–324.
- Underwood, C.J., Johanson, Z., Welten, M., Metscher, B., Rasch, L.J., Fraser, G.J. & Smith, M.M. 2015: Development and evolution of dentition pattern and tooth order in the skates and rays (Batoidea; Chondrichthyes). *PLoS One* 10, 1–19.
- Wilimovsky, N.J. 1954: *Gunnelloodus*, a new name for *Idiacanthus* Gunnell. *Journal of Paleontology* 28, 693 only.
- Williams, M.E. 2001: Tooth retention in cladodont sharks: with a comparison between primitive grasping and swallowing, and modern cutting and gouging feeding mechanisms. *Journal of Vertebrate Paleontology* 21, 214–226.
- Zangerl, R. 1981: Chondrichthyes I. Paleozoic Elasmobranchii. *Handbook of paleoichthyology*, 3A, 114 pp. Stuttgart: Gustav Fischer Verlag.
- Zangerl, R. 1990: Two new stethacanthid sharks (Stethacanthidae, Symmoriida) from the Pennsylvanian of Indiana, U.S.A. *Palaeontographica A* 213, 115–141.
- Zangerl, R. & Case, G.R. 1976: *Cobelodus aculeatus* (Cope), an anacanthous shark from Pennsylvanian black shales of North America. *Palaeontographica A* 154, 107–157.
- Zidek, J. 1973: Oklahoma Paleoichthyology part II: Elasmobranchii (*Cladodus*, minute elements of cladoselachian derivation, *Dittodus*, and *Petrodus*). *Oklahoma Geology notes* 33, 87–104.
- Zidek, J. 1993: A large stethacanthid shark (Elasmobranchii: Symmoriida) from the Mississippian of Oklahoma. *Oklahoma Geology* 53(1), 4–15.

The Jurassic–Cretaceous lithostratigraphy of Kilen, Kronprins Christian Land, eastern North Greenland

JUSSI HOVIKOSKI, GUNVER K. PEDERSEN, PETER ALSEN, BODIL W. LAURIDSEN, KRISTIAN SVENNEVIG, HENRIK NØHR-HANSEN, EMMA SHELDON, KAREN DYBKJÆR, JØRGEN BOJESEN-KOEFOED, STEFAN PIASECKI, MORTEN BJERAGER & JON INESON



Hovikoski, J., Pedersen, G.K., Alsen, P., Lauridsen, B.W., Svennevig, K., Nøhr-Hansen, H., Sheldon, E., Dybkjær, K., Bojesen-Koefoed, J., Piasecki, S., Bjerager, M. & Ineson, J. 2018. The Jurassic–Cretaceous lithostratigraphy of Kilen, Kronprins Christian Land, eastern North Greenland. © 2018 by Bulletin of the Geological Society of Denmark, Vol. 66, pp. 61–112. ISSN 2245-7070. (www.2dgf.dk/publikationer/bulletin).

Received 19 May 2017
Accepted in revised form
15 September 2017
Published online
18 June 2018

Kilen, Kronprins Christian Land, contains the thickest and stratigraphically most complete Jurassic and Cretaceous sediment succession in North Greenland. This study revises and formalises the lithostratigraphic framework of these deposits. The work is based on recent extensive stratigraphic field work supplemented by photogeological mapping and biostratigraphic studies, and builds on the earlier stratigraphic work conducted mainly in the 1980s and 1990s. According to the new stratigraphic scheme, the more than 500 m thick Jurassic succession is divided into four formations. The poorly dated Gletscherport Formation comprises lagoonal heterolithic sandstones. The Mågensfjeld and Birkelund Fjeld Formations consist of shallow marine fine-grained sandstones of Bajocian–Bathonian and Kimmeridgian age, respectively. The Kuglelejet Formation comprises mainly shallow marine sandy mudstone and sandstone of Volgian age and includes the mudstone-dominated Splitbæk Member. The Lower Cretaceous interval is estimated to be more than 1500 m thick and is divided into three formations. The Dromedome Formation comprises deep shelf to offshore transition, black mudstones of late Ryazanian to Hauterivian age. It is erosively overlain by unfossiliferous, fluvial and estuarine sandstones of the Lichenryg Formation. The overlying, late Aptian to middle Cenomanian Galadriel Fjeld Formation comprises six members, of which the Tågekyst and Kangoq Ryg Members occur in the Gåseslette area, whereas the Pil, Valmue, Stenbræk and Hondal Members occur in the Kilen Fjelde area. The Galadriel Fjeld Formation is characterised by interbedded mudstones and sandstones from offshore–shoreface environments. The 650 m thick Upper Cretaceous succession is assigned to the Sølvbæk Formation, which is undivided in the Gåseslette area and divided into the Skalbæk and Scaphitesnæse Members in the Kilen Fjelde area. The Sølvbæk Formation is dominated by marine mudstones and sandstone–mudstone heteroliths of late Cenomanian to Santonian age. The new lithostratigraphic framework and significant biostratigraphic advances allow a closer correlation of the Mesozoic units between North Greenland and other Arctic basins.

Keywords: Lithostratigraphy, Mesozoic, Jurassic, Cretaceous, Kilen, North Greenland, Wandel Sea Basin.

Jussi Hovikoski [jhov@geus.dk], Gunver K. Pedersen [gkp@geus.dk], Peter Alsen [pal@geus.dk], Kristian Svennevig [kso@geus.dk], Henrik Nøhr-Hansen [hnh@geus.dk], Emma Sheldon [es@geus.dk], Karen Dybkjær [kd@geus.dk], Jørgen Bojesen-Koefoed [jbk@geus.dk], Morten Bjerager [mbj@geus.dk], Jon Ineson [ji@geus.dk], all Geological Survey of Denmark and Greenland (GEUS), Øster Voldgade 10, DK-1350 Copenhagen K, Denmark. Bodil W. Lauridsen [bwl@geus.dk], GEUS and Natural History Museum of Denmark, University of Copenhagen, Øster Voldgade 5–7, 1350 Copenhagen K, Denmark. Stefan Piasecki [stefan.piasecki@smn.ku.dk], Natural History Museum of Denmark, University of Copenhagen, Øster Voldgade 5–7, 1350 Copenhagen K, Denmark.

The Wandel Sea Basin (WSB) is a fault-bounded Carboniferous–Lower Tertiary sedimentary basin in North Greenland (Dawes & Soper 1973; Håkansson & Stemmerik 1989; Stemmerik *et al.* 1998; Fig. 1), which forms a key area for the understanding of the Meso-

zoic stratigraphy of the Arctic. The basin contains a more than 3.1 km thick Mesozoic sedimentary succession (Svennevig *et al.* 2016), which records sedimentation on the western margin of the Svalbard–Western Barents Sea Basins and on the north-western flank

of the Danmarkshavn Basin. Therefore, the area links the stratigraphy of North-East Greenland to the Svalbard and Sverdrup Basins and forms one of the closest onshore stratigraphic analogues for the offshore Danmarkshavn Basin and the north-western Barents Sea basin.

The WSB covers a number of geographical areas, from south-east to north-west: Holm Land, Kronprins Christian Land (including Amdrup Land, Kilen and Prinsesse Ingeborg Halvø), and eastern Peary Land (Fig. 1). The WSB contains a nearly continuous Middle Jurassic to Upper Cretaceous succession (Håkansson &

Stemmerik 1984) that forms one of the most complete upper Mesozoic onshore sedimentary records in the Arctic region. In particular, the presence of onshore Upper Cretaceous deposits is exceptional, considering that such deposits do not crop out elsewhere north of Hold with Hope in North-East Greenland (Kelly *et al.* 1998) and are absent on Svalbard (Dallman *et al.* 1999). However, due to the remote location and arctic conditions, the area has remained one of the least studied Mesozoic onshore sedimentary basins in the Arctic.

Pioneering stratigraphic works on the Mesozoic deposits in the WSB were conducted by E. Håkansson

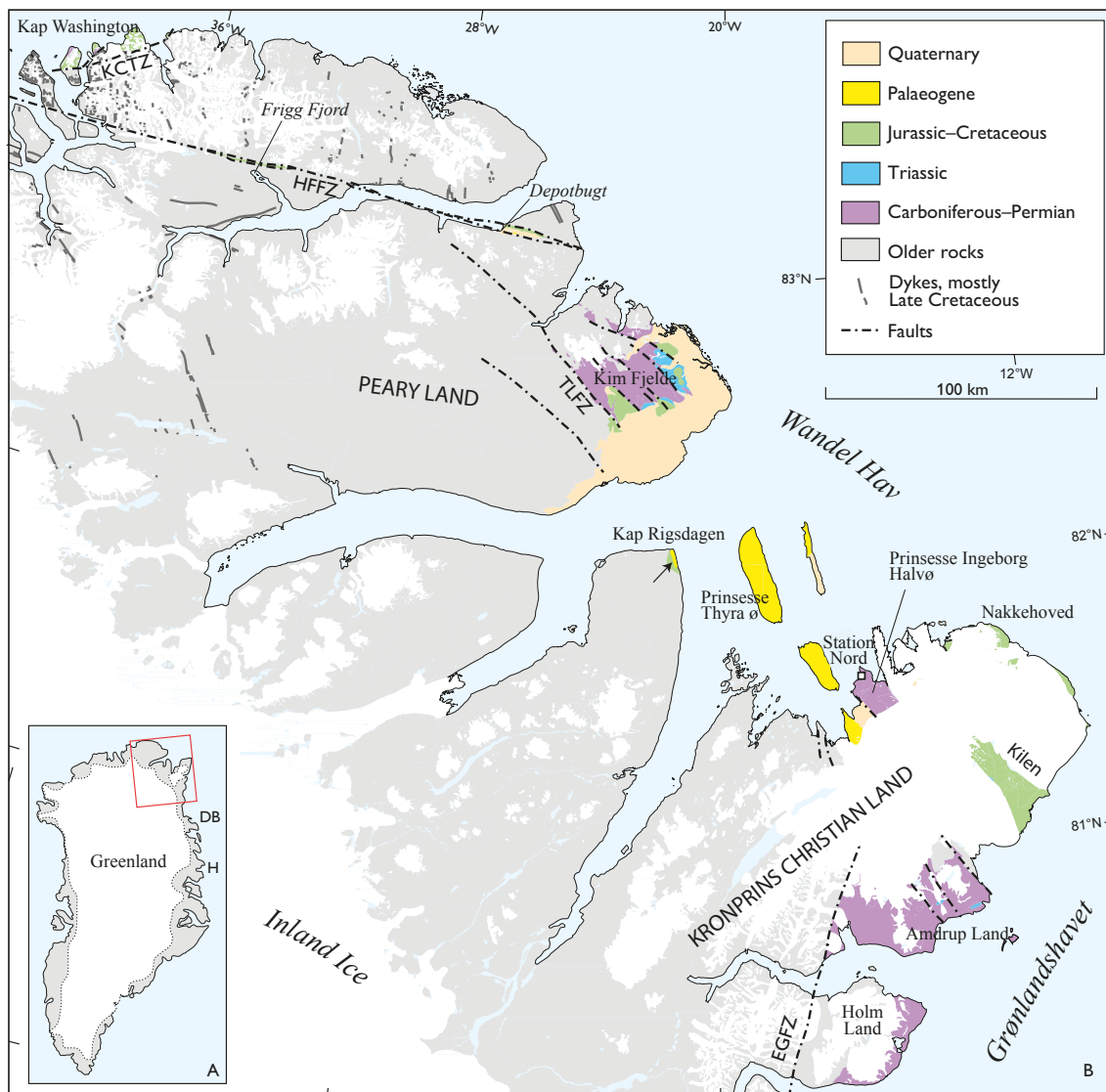


Fig. 1. **A:** Map of Greenland showing the position of the Wandel Sea Basin (framed area), the Danmarkshavn Basin (DB) and Hold with Hope (H). **B:** Map of the Wandel Sea Basin showing the main Mesozoic outcrop areas. The faults of the Wandel Sea Basin are oriented NW-SE. Kilen is located in Kronprins Christian Land and is bounded by an ice cap and the Greenland Sea (Grønlandshavet). The Carboniferous-Permian deposits in Amdrup Land are bounded eastwards by the East Greenland Fault Zone (EGFZ). TLFZ: Trolle Land Fault Zone. North of Peary Land: HFFZ: Harder Fjord Fault Zone. KCTZ: Kap Cannon Thrust-fault Zone. Map based on Håkansson & Pedersen (1982), Bengaard & Henriksen (1986) and Henriksen (2003).

son and his co-workers (Håkansson 1979; Håkansson *et al.* 1981b, 1991, 1993, 1994; Pedersen 1991; Heinberg & Håkansson 1994; Dypvik *et al.* 2002). These studies mapped the main Jurassic–Cretaceous exposures and

erected preliminary biostratigraphic and lithostratigraphic divisions for these rocks. The main outcrop areas were identified at Kilen (Kronprins Christian Land) and in eastern Peary Land. In addition, several

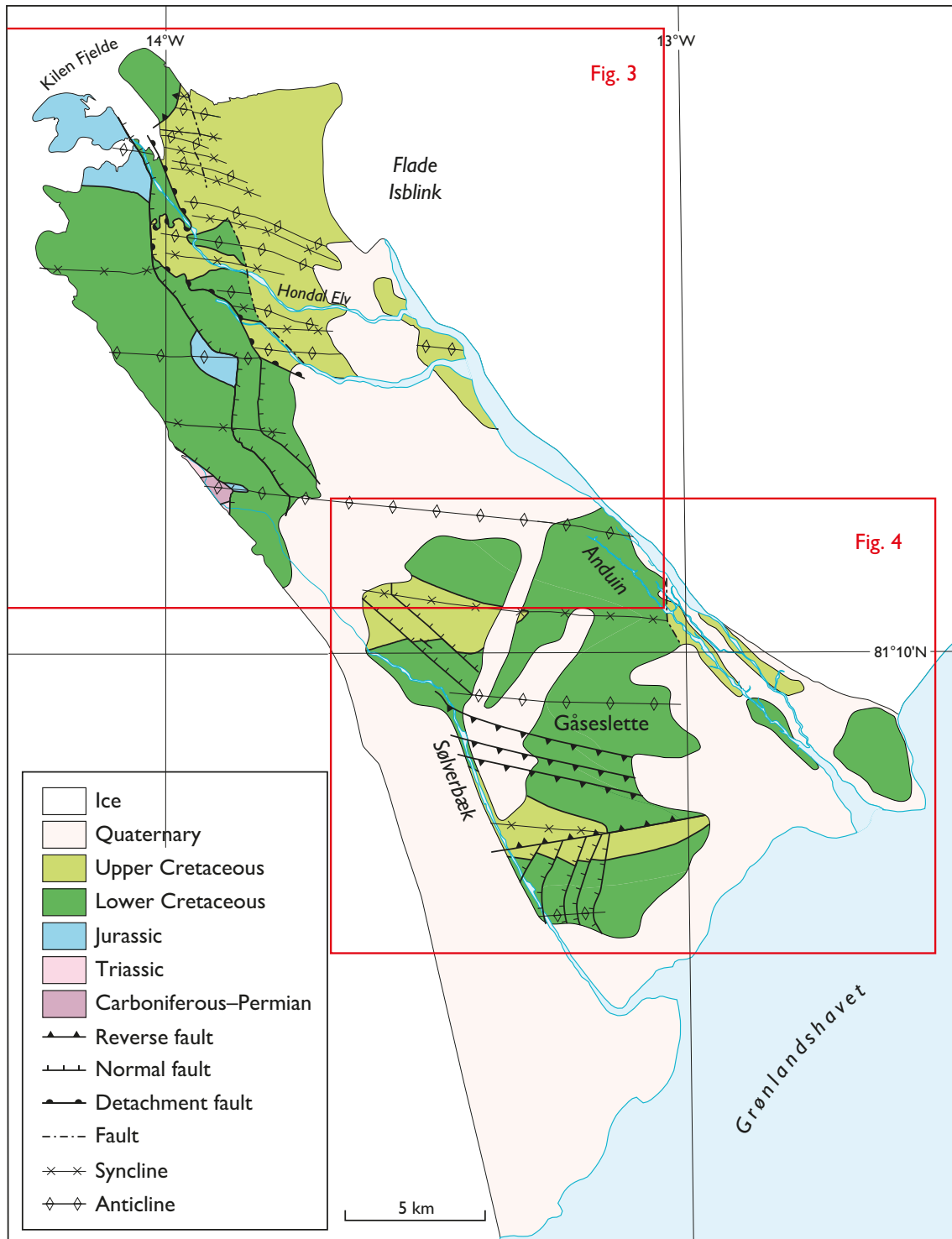


Fig. 2. Simplified geological map of Kilen showing the main faults. Kilen Fjelde is the hilly area to the north-west (Fig. 3) and Gåseslette is the plain to the south-east (Fig. 4). Locations of the detailed maps (Figs 3, 4) are indicated. Modified from Svennevig *et al.* (2016).

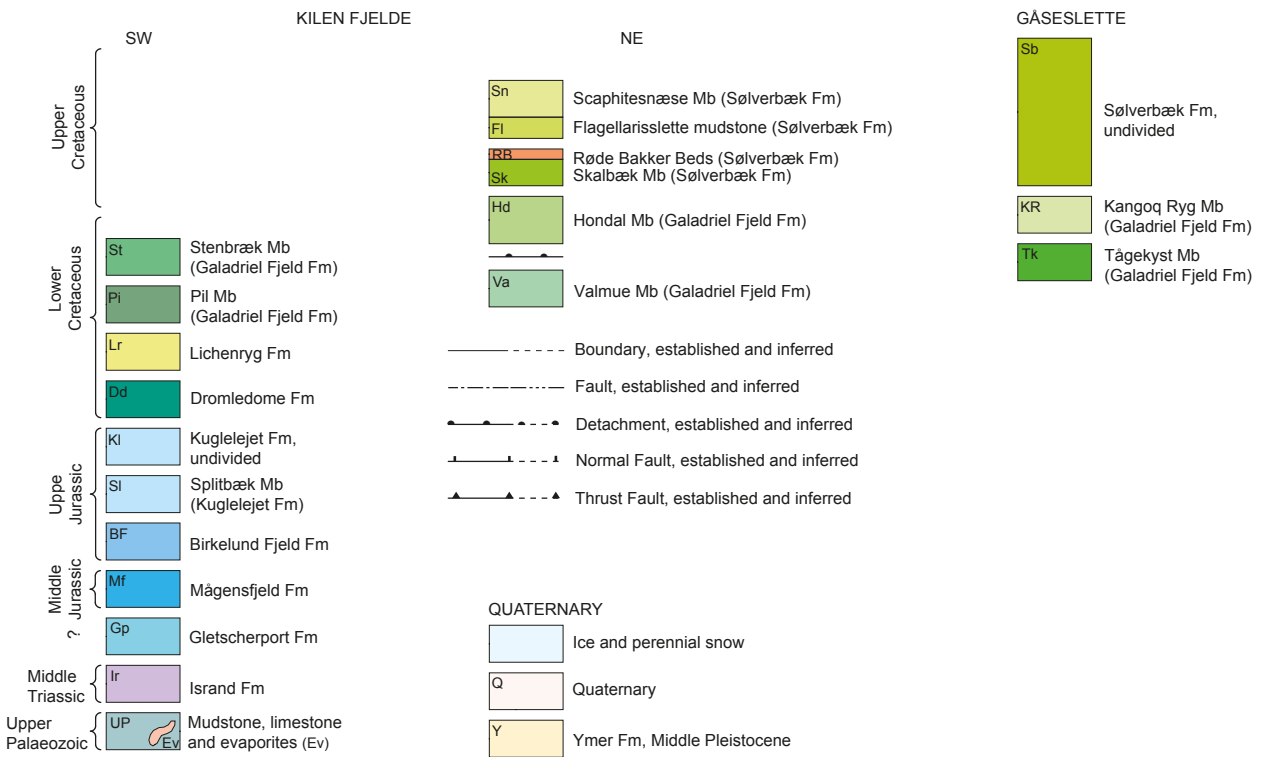
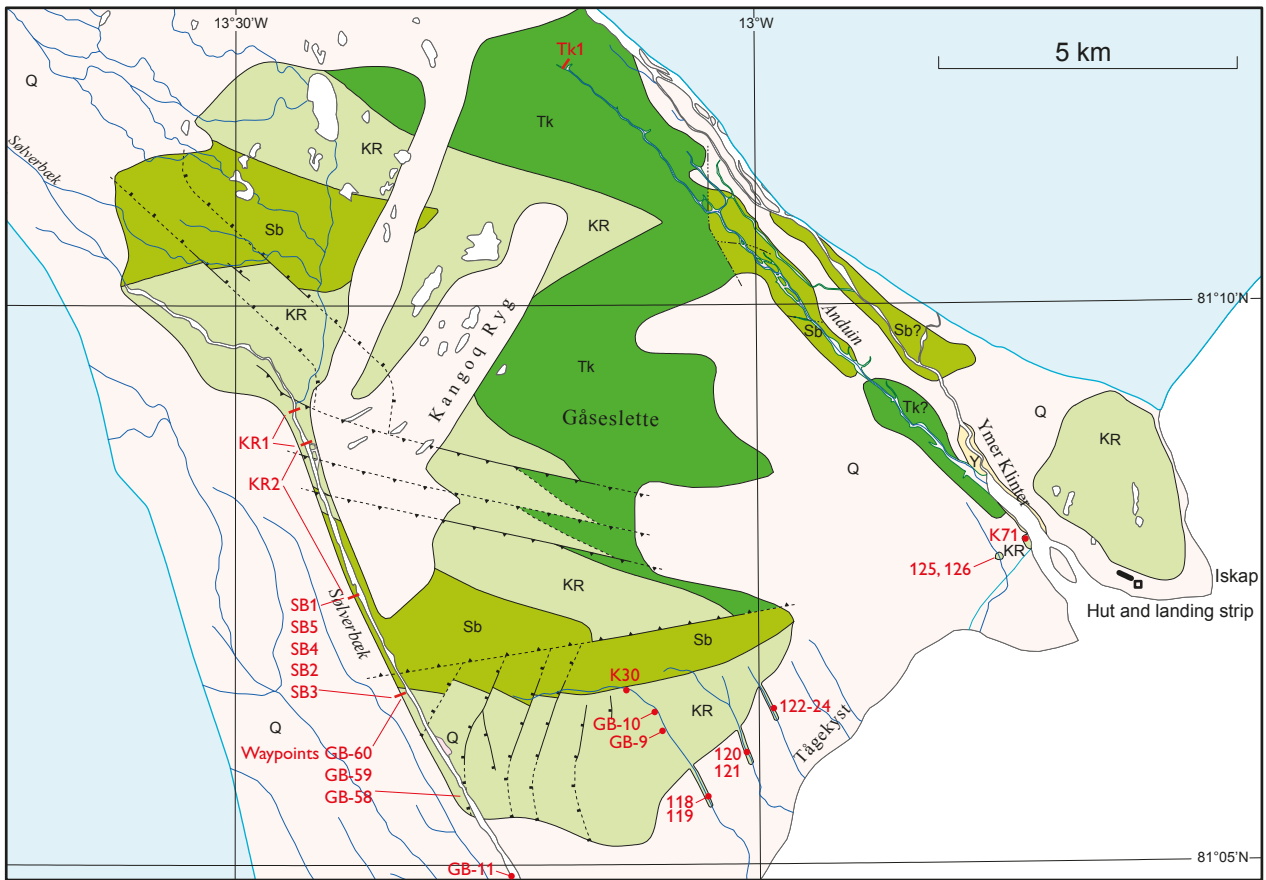


Fig. 4. Legend and detailed geological map of the Gåseslette area showing the positions of the studied sections referred to in the text. Place names in Figs 2–4 are field names. Modified from Svennevig (2018a).

m a.s.l. in the north-west, and the Gåseslette area, the lowlands bordering the sea in the south-east (Figs 3–4).

Kilen is dominated by Jurassic and Cretaceous sediments, although Triassic strata have recently

been recognised locally and are referred to the Isrand Formation (Alsen *et al.* 2017). The Jurassic and Cretaceous deposits have been subjected to intense tectonic deformation (Pedersen 1991; Pedersen & Håkansson

Pedersen 1991; Håkansson *et al.* 1994

This Study

		Kilen Fjelde		Gåseslette		Kilen Fjelde		Gåseslette					
		Formation		Formation		Formation		Member					
Cretaceous	Kilen Group	Dipperne*	Sølverbæk	Gåseslette Group	Kangoq Ryg	Sølverbæk	Undivided	Sølverbæk	Undivided				
		Mågensfjeld											
		Saddelfjeld											
		Scaphitesnæse											
		Flagellarislette											
		Røde Bakker											
		Skalbæk											
		Anduin											
		Hondal*											
	Flade Isblink Group	Galadriel Fjeld*	Upper*	Tågekyst*	Galadriel Fjeld	Galadriel Fjeld	Tågekyst*	Tågekyst*	Galadriel Fjeld	Kangoq Ryg**			
Middle*													
Lower*													
Lichenryg*		Lichenryg	Dromledome	Lichenryg	Dromledome	Kuglelejet	Undivided	Kuglelejet	Splitbæk				
Dromledome													
Kuglelejet													
Jurassic	Flade Isblink Group	Birkelund Fjeld	Iver Pynt	Birkelund Fjeld	Mågensfjeld	Gletscherport*	Gletscherport*	Birkelund Fjeld	Mågensfjeld				
										Splitbæk	Gletscherport*	Gletscherport*	Gletscherport*
										Kuglelejet	Gletscherport*	Gletscherport*	Gletscherport*

* undated; ** includes strata formerly referred to the Iver Pynt Formation; *** includes strata formerly referred to the Dipperne Formation. RB: Røde Bakker Beds. Fmd: Flagellarislette mudstone.

Fig. 5. Comparison between the lithostratigraphic subdivisions of the Jurassic and Cretaceous successions at Kilen by Pedersen (1991) and Håkansson *et al.* (1994) and the revised and formalised framework presented in this paper. The revised lithostratigraphy includes no groups and fewer formations. Tectonic boundaries separate the four members of the Galadriel Fjeld Formation in most of the Kilen Fjelde area (Figs 3, 6). Depositional boundaries between the Pil and Stenbræk Members, and between the Hondal and Skalbæk Members, are indicated in Figs 18, 23. See text for further discussion.

2001; Håkansson & Pedersen 2015; Svennevig *et al.* 2015, 2016, 2017; Svennevig 2018a). The sedimentary succession at Kilen has been variably exposed to thermal alteration that has commonly destroyed the dinocyst content, e.g. in Kilen Fjelde (Pedersen & Håkansson 2001; Svennevig *et al.* 2017, Pedersen *et al.* 2018). The absence of dinocysts complicates the correlations within different parts of Kilen, and to other sedimentary basins.

The Kilen area was affected by post-Cretaceous N–S compression, which folded the strata and divided the deposits into two thrust sheets (Svennevig *et al.* 2016). As a result, many of the lithostratigraphic units at Kilen are fault-bounded and intensively faulted. Some formations comprise coeval members that belong to different allochthonous thrust sheets (Svennevig *et al.* 2016; but see e.g. Håkansson & Pedersen (2015) for an alternative interpretation).

Previous work

The pioneering stratigraphic work in Kilen produced a geological map that shows the distribution of 19 formations in three groups of Jurassic and Cretaceous age (Fig. 5; Pedersen 1991). The map was accompanied by brief descriptions of lithology, thickness and age of the formations (Håkansson *et al.* 1993, 1994; Heineberg & Håkansson 1994), whereas type sections and boundaries of the formations were not described. The biostratigraphic framework based on the early collections of inoceramids and ammonites indicated that the formations range from the Kimmeridgian to the early Coniacian. Nine of the 19 formations were found to represent the middle Turonian to lower Coniacian (Håkansson 1994; Håkansson *et al.* 1994).

This study

This work is based on extensive field work by the Geological Survey of Denmark and Greenland (GEUS) on Kilen in 2012 and 2013, with supplementary data collection in 2016. A total of 30 sedimentological sections, 17 to 430 m thick, were studied in variable detail. The thicknesses indicated on the sedimentological logs are true thicknesses, with the exception of Fig. 31. The geographical coordinates of the type sections are based on WGS84. The geological ages of the formations are based on biostratigraphic work on ammonites, inoceramids and other bivalves, palynomorphs (dinoflagellate cysts) and foraminifera (Fig. 6). The photogeological mapping supported the identification of the tectonic boundaries between the formations, and the structural model provided estimates of formation thicknesses in areas without sedimentological logs (Svennevig *et al.* 2015, 2016, 2018).

Many of the lithostratigraphic units at Kilen are fault-bounded and intensively faulted, and the age determination for some units is dependent on limited macrofauna. Moreover, some formations comprise coeval members that belong to different allochthonous thrust sheets, which may have brought strata representing different depositional environments closer together than they were at the time of deposition. The members of the Galadriel Fjeld Formation exemplify such relationships (Svennevig *et al.* 2016, 2017, 2018). Due to these complicating factors, the nature of the formation boundaries, the thickness of the stratigraphic units and their correlation cannot always be stated.

In the revised lithostratigraphy, the deposits are assigned to eight formations of which one has six members, one has two members and one has a single member (Figs 5–6). The previous lithostratigraphic names have been retained where possible, but the use of four previous lithostratigraphic unit names, namely Iver Pynt, Anduin, Dipperne and Saddelfjeld, is discontinued. Definition of groups is not undertaken here. This awaits an improved understanding of the genetic stratigraphy of the entire succession, as well as correlations to the successions in other parts of the Wandel Sea Basin.

The terminology of open coast wave- and storm-influenced environments follows Pemberton *et al.* (2012). According to their scheme, the environment located below storm wave base is termed the shelf. The depositional environment located between storm and fair-weather wave-base is termed the offshore. The shoreface environment is located above fair-weather wave base.

Finally, detailed documentation of depositional environments is beyond the scope of this paper, and only brief generalised summaries of depositional settings are presented here. Therefore, features such as facies and facies association divisions, detailed ichnological descriptions and palaeocurrent data will be addressed elsewhere.

Gletscherport Formation

New formation

Name and history. The formation is named after a nearby mouth of a glacier.

Distribution. The unit has a single exposure on the east side of the hill Mågensfjeld in Kilen Fjelde (Fig. 3).

Type section. The east side of Mågensfjeld constitutes

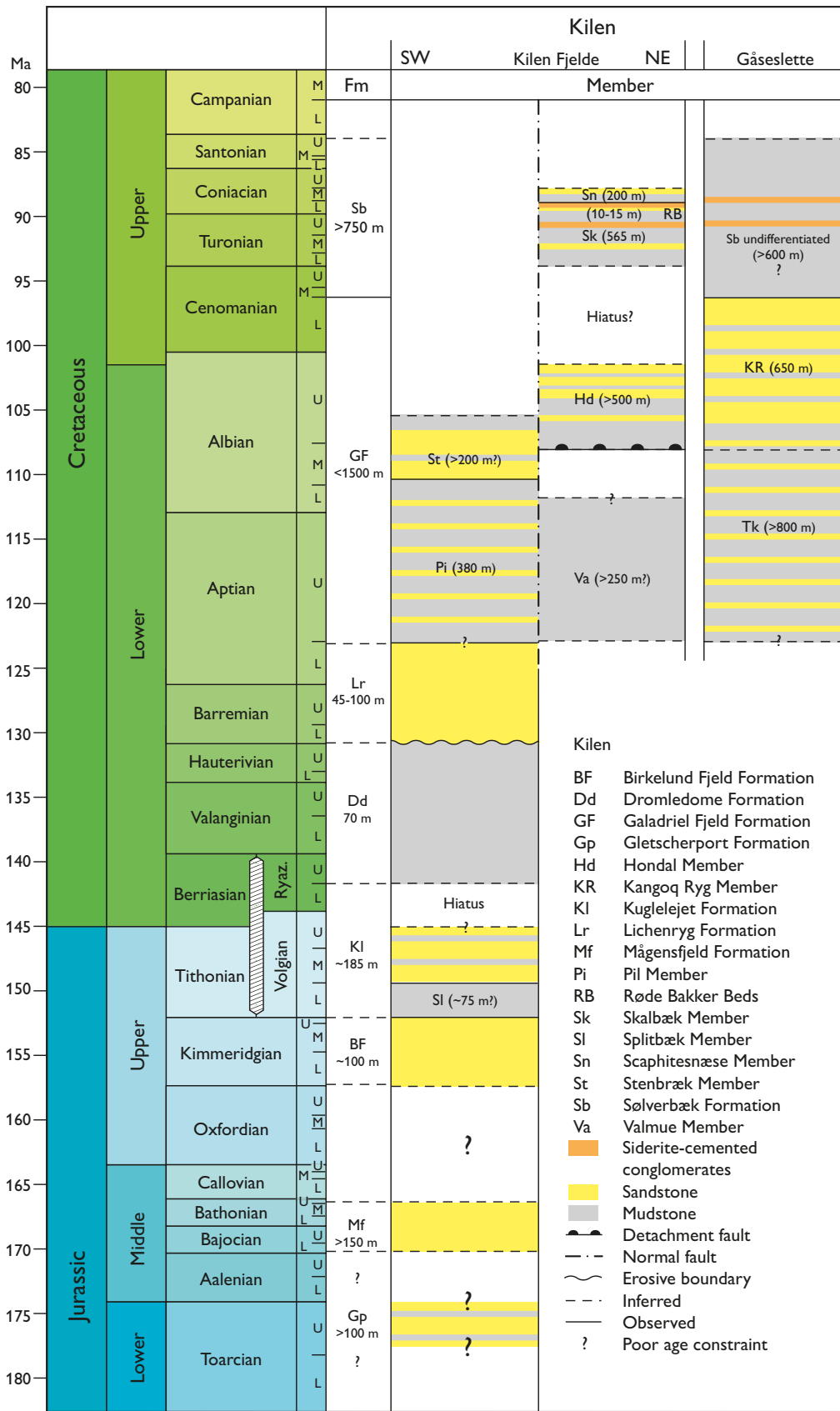


Fig. 6. A: Chronostratigraphic chart of the Jurassic and Cretaceous deposits in Kilen. Note that the Gletscherport Formation is undated. Numerical ages to the left follow the International Chronostratigraphic Chart 2017 (Cohen *et al.* 2013, updated 2017).

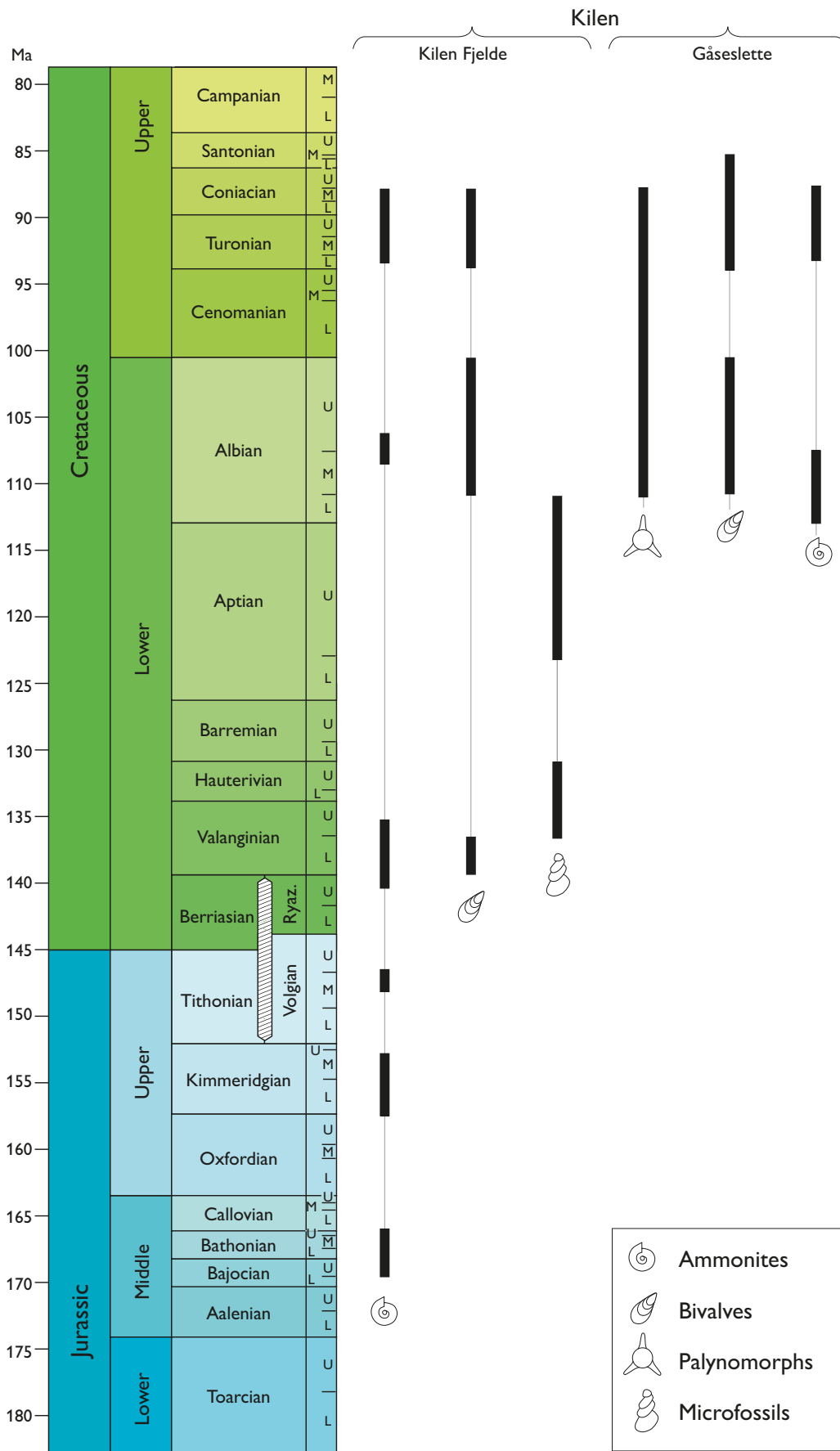


Fig. 6. B: Stratigraphic distribution of the main fossil groups used for biostratigraphic dating. See text for the main age-diagnostic taxa. The occurrence of additional fossils is included in the descriptions of the relevant lithostratigraphic units.

the type section (Fig. 7). The exposed part of the type section is covered by the log Gp1 (Fig. 8A). The base of the exposure is located at 81°18'51.2"N, 014°03'26.3"W.

Thickness. The thickness of the formation is unknown. Photogeological mapping suggests that the formation continues below the scree and is >100 m thick (Svennevig *et al.* 2016; Fig. 6A). The outcrop exposure is ~70 m thick.

Boundaries. The boundaries are not observable.

Fossils and age. Plant fragments, but no marine fossils have been found. A pre-Late Bajocian age is tentatively suggested based on the stratigraphic relationship with the overlying Mågensfjeld Formation.

Lithological description. The formation outcrops as a poorly exposed tectonic sliver at the east-side foot of Mågensfjeld. The deposits consist of heterolithic sandstone showing variously developed wave-ripple cross-stratification, combined-flow ripple cross-lamination, mudstone drapes and interbeds. Terrestrial

organic matter, such as leaf and coal fragments, is very common. Synaeresis cracks occur locally. The deposits are unbioturbated or variably bioturbated with a low-diversity trace fossil assemblage. Typical trace fossils include *Lockeia* isp., *Planolites* isp. and *Palaeophycus* isp.. Escape and equilibrium structures are also found.

Depositional environment. Sediment structures suggest common wave influence with superimposed non-oscillatory currents. Herringbone cross-lamination coupled with common heterolithicity suggest the presence of tidally modulated currents. The lack of bioturbation in many relatively low-energy facies indicates the presence of environmental stresses that commonly limited infaunal colonisation. The repeated occurrence of low-diversity trace fossil suites, which mainly comprise morphologically simple burrows such as *Planolites*, suggests that the main stress is related to low and/or fluctuating salinity. The inferred depositional environment is a wave- and tide-influenced, low-salinity to freshwater environment in a restricted setting such as a lagoon or bay.

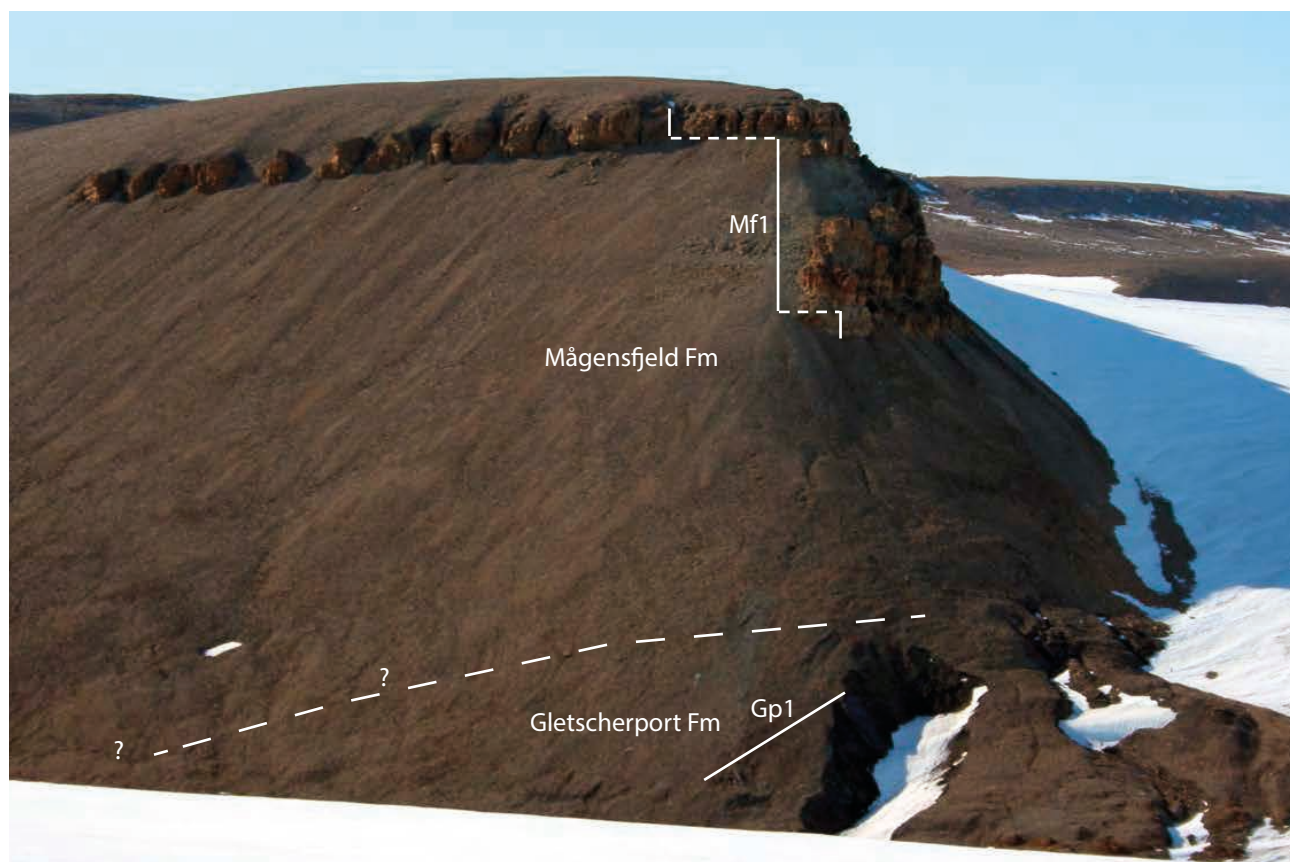


Fig. 7. Type sections of the Gletscherport and Mågensfjeld formations. The Gletscherport Formation is a tectonic sliver exposed at the foot of the Mågensfjeld hill, Kilen Fjelde. Approximate locations of the logs Gp1 and Mf1 are indicated. The exposed cliff of the Mågensfjeld Formation is ~100 m high. View towards the west.

Mågensfjeld Formation

Name and history. The unit was mapped by Pedersen (1991) and described by Håkansson *et al.* (1994) as an Upper Cretaceous formation. The name is derived from a prominent hill formed by this rock unit in Kilen Fjelde. The unit is here formalised and dated to the Middle Jurassic.

Distribution. The formation has a single exposure at Mågensfjeld, Kilen Fjelde (Fig. 3).

Type section. Mågensfjeld constitutes the type section (Figs 7, 9). The exposed part of the type section is shown in the sedimentological log Mf1 (Fig. 8B). The base of the exposure is located at 81°18'47.5"N, 014°04'07.9"W.

Boundaries. The boundaries of the formation are not exposed.

Thickness. The thickness of the formation is unknown, but estimated to be more than 150 m based on the photogeological interpretation (Svennevig *et al.* 2016; Fig. 6). The outcrop exposure is *c.* 100 m thick.

Fossils and age. The fossils include ammonites, belemnites, bivalves, plant fragments and coalified tree trunks. The formation is Middle Jurassic (upper Bajocian – Bathonian) based on ammonites, which include late Bajocian *Cranocephalites cf. pompeckji* and *C. furcatus* and Bathonian *Arctocephalites sp. cf. delicatus* or *arcticus*, *Arcticoceras crassiplicatum*, *Cadoceras calyx*, *C. apertum* and *Kepplerites sp. cf. traillensis* or *tenuicostatus*. Numerous large belemnites are commonly dissolved, leaving cavities sometimes filled with secondary calcite. Such belemnites were probably mistakenly interpreted as Late Cretaceous baculitids by Håkansson *et al.* (1993, their 'Unit 7'). Bivalves include the inoceramid *Retroceramus sp.*, that was probably likewise mistaken for a Late Cretaceous (early Coniacian) inoceramid (Håkansson *et al.* 1993).

Lithological description. A uniform sandstone succession comprising thinly bedded, fine-grained sandstone. Parallel lamination, ripple cross-lamination and cross-bedding are locally observed. The rock surface is typically weathered, which prevents observation of sediment structures. The sandstones are variably bioturbated with a low to moderately diverse trace fossil assemblage. Typical trace fossils include *Diplocraterion isp.*, *Phoebichmus isp.* and *Thalassinoides isp.* Terrestrial organic matter such as complete leaves occur in places.

Depositional environment. The sedimentological, ich-

nological and fossil data point to an overall shallow marine environment. The commonly high bioturbation intensity and rarity of preserved wave- or storm-generated structures suggest a confined setting, where oscillation currents were subdued. The interpreted depositional environments include protected lower-middle shoreface environments and deltaic intervals.

Birkelund Fjeld Formation

Name and history. The unit was mapped by Pedersen (1991) and described by Håkansson *et al.* (1994) and Dypvik *et al.* (2002). Birkelund Fjeld is a hill named after the late professor Tove Birkelund, University of Copenhagen. The formation is here formalised.

Distribution. The main outcrop area of the formation is in the Dromledome and Birkelund Fjeld areas, Kilen Fjelde (Fig. 3).

Type section. The Dromledome anticline constitutes the type section. The exposed part of the type section is covered by the log BF1 (Figs 8C and 10). The base of the exposure is located at 81°15'15.5"N, 013°54'46.6"W.

Boundaries. The lower boundary is not exposed. The upper boundary is partially covered by scree but is seen as a sharp change in lithology from sandstone to the mudstones of the Splitbæk Member of the Kuglelejet Formation (Fig. 10).

Thickness. Photogeological mapping indicates that the formation may reach a thickness of ~100 m below a scree slope (Svennevig *et al.* 2016; Fig. 6). The exposed part of the formation is more than 45 m thick.

Fossils and age. The fossils include ammonites, belemnites and plant material. The formation is upper Jurassic (Kimmeridgian), based on ammonites which include the early Kimmeridgian *Rasenia cymodoce* (Håkansson *et al.* 1994) and the late middle Kimmeridgian *Amoeboceras (Amoebites) elegans* (Fig. 6).

Lithological description. A uniform, dark grey to black, very fine- to fine-grained sandstone. Weathered rock surfaces show a pale coating that locally obscures sedimentary structures. The deposits, where visible, show parallel lamination, faint undulatory lamination, ripple cross-lamination and rare dune-scale cross-bedding. Plant fragments are common, belemnites and ammonites occur locally. The lower part of the formation is characterised by the trace fossil *Thalassinoides isp.*, whereas the top part contains common

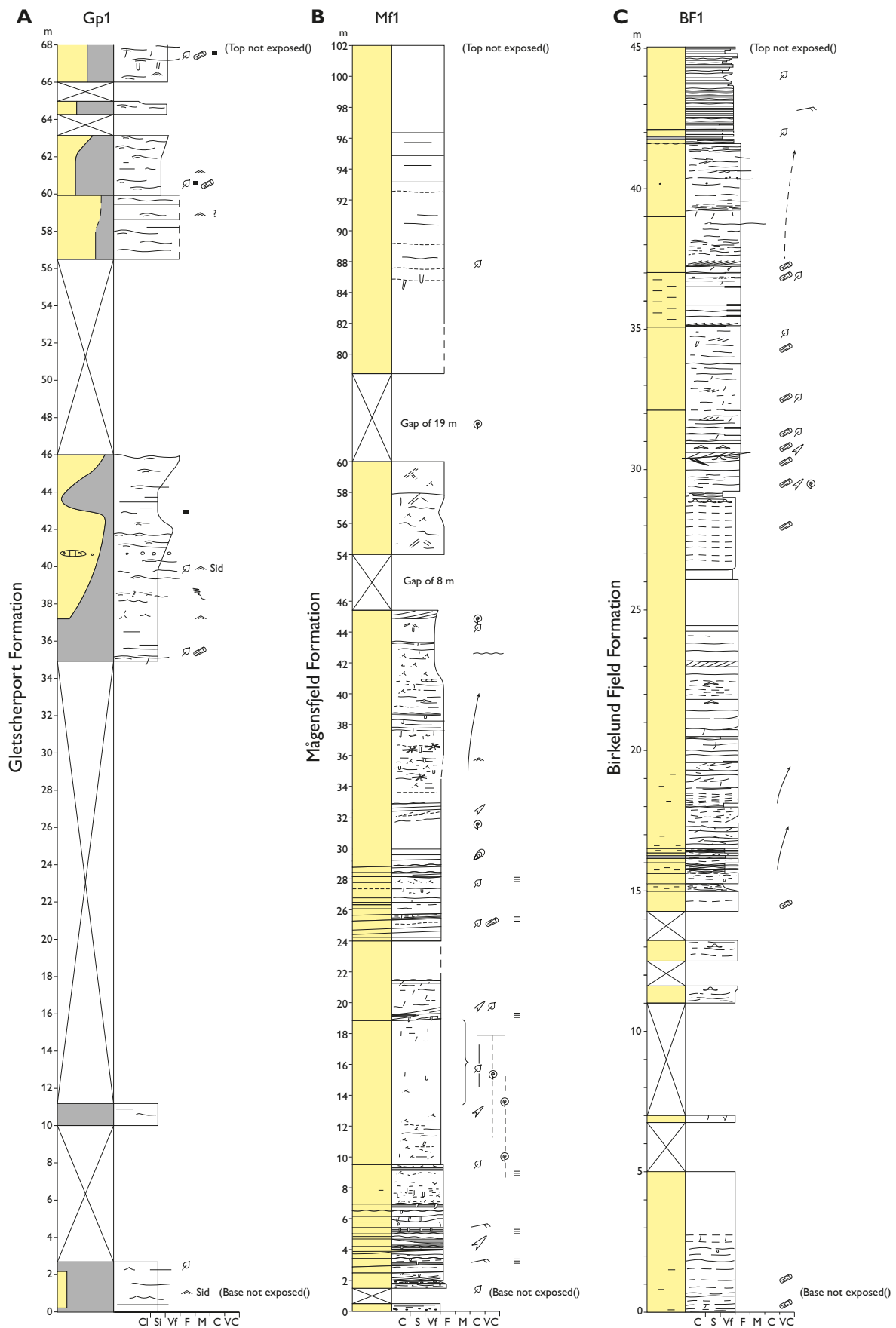


Fig. 8. A: Sedimentological log Gp1 of the type section of the Gletscherport Formation. **B:** Sedimentological log Mf1 covering the exposed part of the type section of the Mågensfjeld Formation. **C:** Sedimentological log BF1 covering the exposed part of the type section of the Birkelund Fjeld Formation. The logs are located in Figs 3, 7, 10.



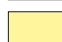


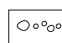







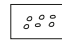

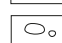

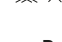

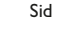
Rhizocorallium isp. (see also Heinberg & Håkansson 1994; Håkansson *et al.* 1994; Dypvik *et al.* 2002).

Depositional environment. The fossil and trace fossil contents point to an overall shallow marine depositional environment. The deposits lack wave-generated sedimentary structures and comprise unidirectional

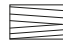

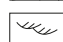
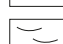
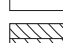






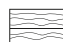



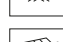




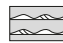

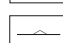


current-generated structures, which could point to a sheltered setting such as an embayment or a bay. The sporadically bioturbated, stacked parallel laminated beds may point to a gravity flow origin and a proximal prodelta-like environment, particularly in the top part of the formation.

D Legend




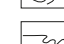
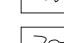

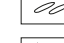

Lithology

	Mudstone
	Sandy mudstone
	Sandstone
	Heterolithic mudstone/sandstone
	Conglomerate
	Coarse-grained sand to granules
	Coal
	Coal clasts
	Mudstone drapes and clasts
	Mudstone clasts
	Sandstone clasts
	Intraformational clasts
	Extraformational clasts
	Concretion
	Concretions
	Concretion with cone-in-cone structures
	Pyrite
	Siderite
	Glauconite
	Glendonite



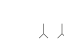

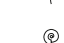







Sedimentary structures

	Low angle cross-stratification
	Trough cross-stratification
	
	Planar cross-bedding
	
	Planar lamination/bedding
	Parallel lamination
	Hummocky cross-stratification
	Swaley cross-stratification
	Hummocky and swaley cross-stratification
	Hummocky cross-stratified bed
	Ripple cross-lamination
	Wave-ripple cross-lamination
	Climbing ripple cross-stratification
	Herringbone cross-stratification
	Erosive sandstone bed
	Flaser bedding
	Heterolithic bedding (mud dominated)
	Heterolithic bedding (sand dominated)
	Sand streak
	Thin sand streak
	Weak lamination
	Indistinct lamination (often mottled heterolith)
	Structureless
	

Sedimentary structures

	Synaeresis crack
	Ptygmatic fold
	Slump fold
	Slump structure
	Load structure
	Imbrication
	Biomottled
	Sole mark

Fossils

	Fragment
	Belemnite
	Rootlets
	Plant fragments
	Ammonite
	Wood
	Dentalium
	Bivalve
	Inoceramid
	Serpulid
	Dinoflagellate cyst
	Microfossil

Miscellaneous




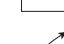

	Erosional boundary
	Sharp boundary
	Gradational boundary
	Trend of the coarsest grain size fraction
	Weak to intense bioturbation

Fig. 8. D: Legend for all sedimentological logs in this paper.



Fig. 9. Type section of the Mågensfjeld Formation, Mågensfjeld hill, Kilen Fjelde. Height of the exposure c. 100 m. View towards the south.

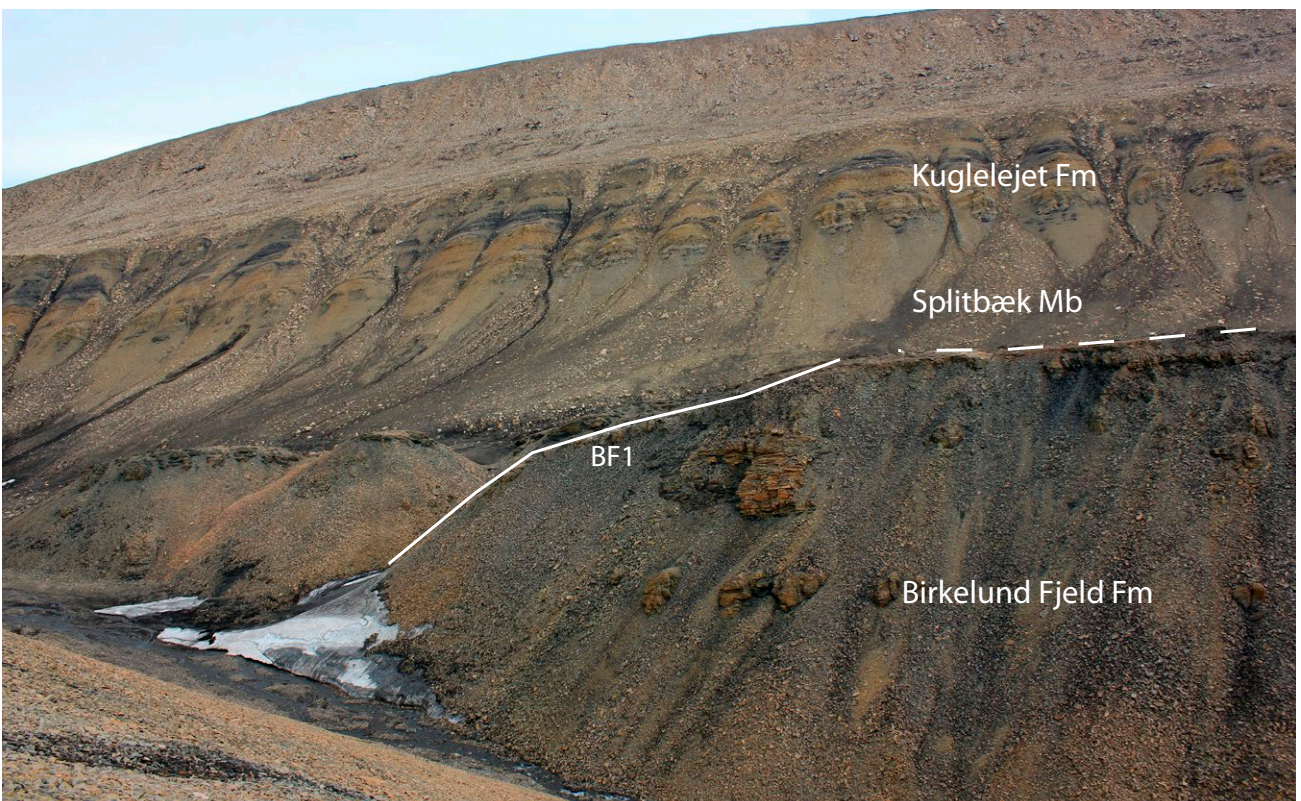


Fig. 10. Type section of the Birkelund Fjeld Formation. Sedimentological log BF1 covers the exposed part of the formation (Fig. 8C); its approximate location is shown. The log trace runs partly behind the ridge. The lower part of the formation is not exposed. The scree slope of the Birkelund Fjeld Formation is c. 50 m high. View towards the west-south-west.

Kuglelejet Formation

Name and history. The unit was mapped by Pedersen (1991) and described by Håkansson *et al.* (1994) and Dypvik *et al.* (2002). It is named after a topographic depression with abundant spherical concretions. The unit is redefined and formalised in the present study, and a new member is erected.

Subdivision. The Splitbæk Member forms the lower part of the formation.

Distribution. The unit crops out in the Dromledome, Lichenryg and Kuglelejet areas, Kilen Fjelde (Fig. 3).

Type section. The Dromledome anticline, where the sedimentological logs K11 and K12 cover the exposed part of the type section (Figs 11–12). The base of the exposure is located at 81°15′05.2″N, 013°55′24.6″W.

Boundaries. The lower boundary is mainly covered by scree, but is placed at the first appearance of black mudstone above bioturbated sandstone of the Birkelund Fjeld Formation (Fig. 10). The upper boundary is partially covered by scree and is placed at the first appearance of black shale (Dromledome Formation; Fig. 14) above bioturbated sandstone.

Thickness. Photogeological mapping suggests that the formation may reach a thickness of ~185 m (Svennevig *et al.* 2016). The exposure is ~80 m thick (Fig. 6).

Fossils and age. The middle Volgian *D. gracilis* Zone was recorded by Håkansson *et al.* (1994), probably derived from material in C. Heinberg's 1980-collection, which contains specimens identified as *D. cf./aff. gracilis* by J.H. Callomon. New ammonite data include upper lower Volgian *Pectinatites groenlandicus*, lower middle Volgian *Pavlovia corona*, middle Volgian *Laugeites cf. greenlandicus* and upper middle Volgian *Epilaugeites vogulicus*. Other fossils include plesiosaurus remains (Håkansson *et al.* 1994; Dypvik *et al.* 2002). The Splitbæk Member interval lacks age diagnostic fossils.

Lithological description. The lower half of the formation comprises an upwards coarsening succession consisting of black sandy mudstone that grades into bioturbated muddy sandstone and further into cross-bedded fine- to medium-grained sandstone. The upper part of the formation is characterised by bioturbated muddy sandstone and bioturbated sandstone. Typical trace fossils include grazing structures, *Thalassinoides* isp. and *Teichichnus* isp. (see also Heinberg & Håkansson 1994; Håkansson *et al.* 1994); cross-bedded intervals show vertical trace fossils such as *Diplocraterion* isp. and *Siphonichnus* isp.

Depositional environment. The deposits lack typical wave-generated sedimentary structures and comprise structures generated by non-oscillatory flows. This together with the trace fossil content and the high bioturbation intensity point to a sheltered setting such as an embayment or a bay.

Splitbæk Member

Name and history. The unit was mapped by Pedersen (1991) and described by Håkansson *et al.* (1994). It is named after a stream in Kilen Fjelde near the type section. The unit is hereby formalised as a member within the Kuglelejet Formation.

Distribution. The formation has a single occurrence in the Dromledome area, Kilen Fjelde (Fig. 3).

Type section. The type section is located on the eastern slope of the Dromledome anticline, Kilen Fjelde (Figs 12A, 13). The exposed part of the section is covered by the log SI-K11. The base of the exposure is located at 81°15′05.2″N, 013°55′24.6″W.

Boundaries. The lower boundary corresponds to that of the formation. It is partly below scree and placed at the first appearance of black mudstone above bioturbated sandstone of the Birkelund Fjeld Formation (Figs 10, 11). The upper boundary is gradational and placed where bioturbated muddy sandstone becomes the dominant facies (undifferentiated Kuglelejet Formation; Fig. 12A).

Thickness. The exposed interval is >20 m thick, but the formation continues below the scree slope. Photogeological mapping suggests that the member reaches a thickness of c. 75 m (Svennevig *et al.* 2016).

Fossils and age. No macrofossils or microfossils have been observed. The late Jurassic age is constrained by the underlying middle Kimmeridgian and the overlying middle Volgian units (Fig. 6B).

Lithological description. An upwards coarsening sandy mudstone succession above the Birkelund Fjeld Formation. The poorly exposed base shows black mudstone rich in framboidal pyrite. The member grades upwards into bioturbated sandstones of the upper part of the Kuglelejet Formation. Common trace fossils include *Phycosiphon* isp. and *Chondrites* isp. at the top of the member.

Depositional environment. The sedimentological characteristics and the trace fossil suite (stressed distal *Cruziana* ichnofacies in the top of the member)

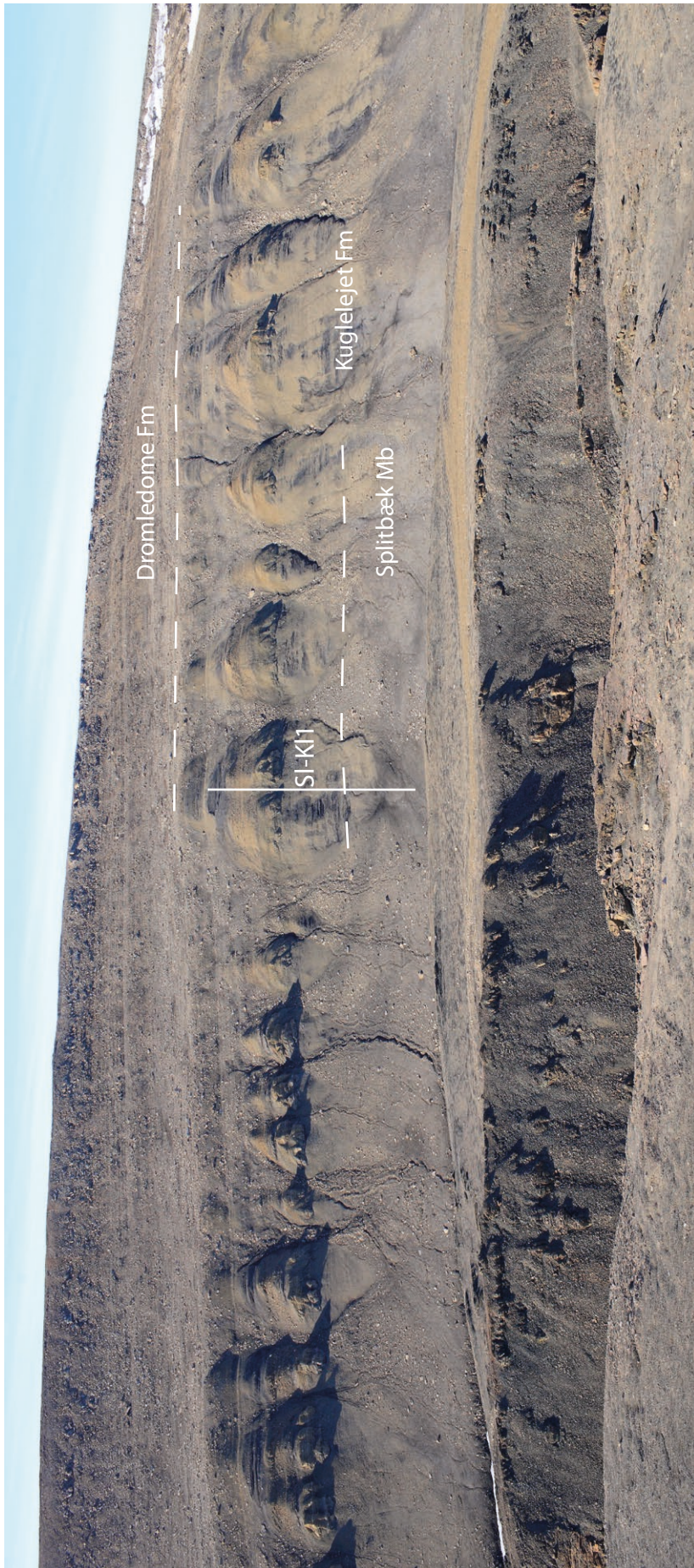


Fig. 11. Type section of the Kuglelejet Formation, Dromledome anticline. Sedimentological log SI-K11 (c. 70 m high, approximate location indicated) represents the lower part of the type section (Fig. 12). See Fig. 14 for location of section KL2. View towards the west.

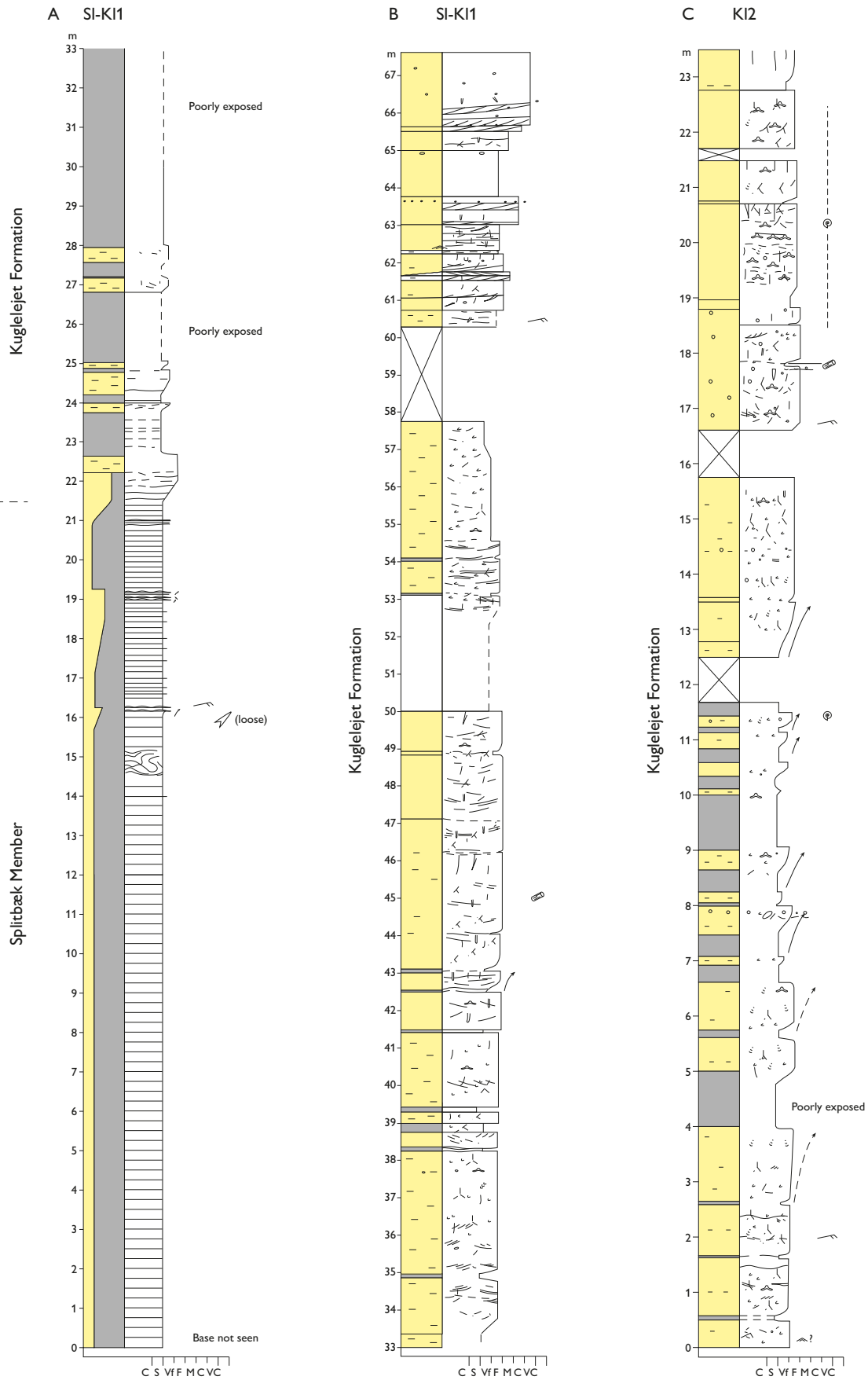


Fig. 12. A and B: Sedimentological log SI-KI1 covering the lower half of the type section of the Kuglelejet Formation, including the Splitbæk Member. A dashed line indicates the approximate position of the upper boundary of the Splitbæk Member. **C:** Sedimentological log KI2 covering the upper part of the type section of the Kuglelejet Formation. For location of the logs see Fig. 3.

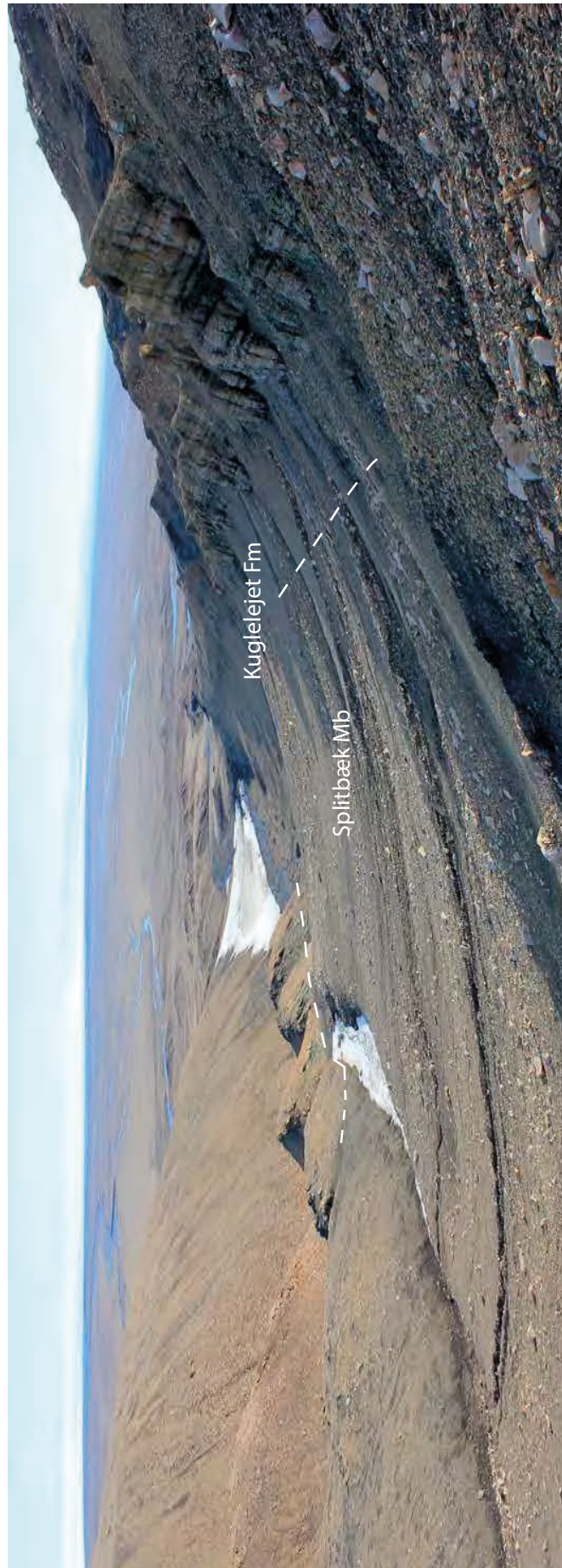


Fig. 13. Type section of the Splitbæk Member of the Kuglelejet Formation, Dromledome anticline. Height of the mudstone dominated slope below the cliff is c.100 m. View towards the south.

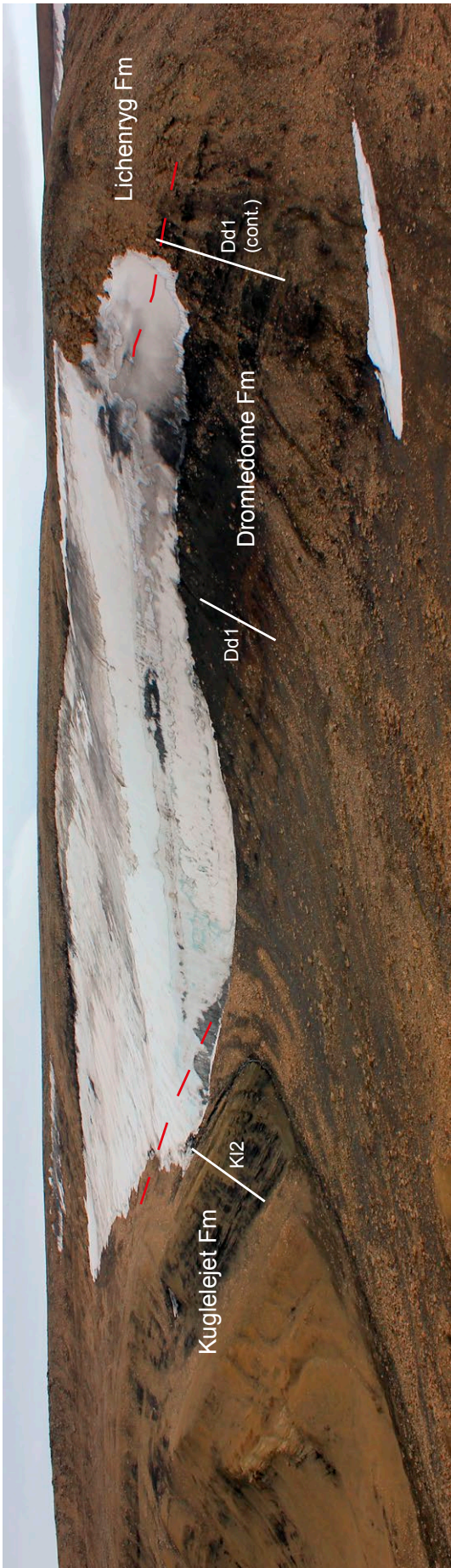


Fig. 14. Type section of the Dromledome Formation, Dromledome anticline. View towards the west. The composite c. 70 m thick log Dd1 (approximate location shown) covers the exposed part of the type section. The location of the section K12 (Fig. 12C) is also indicated

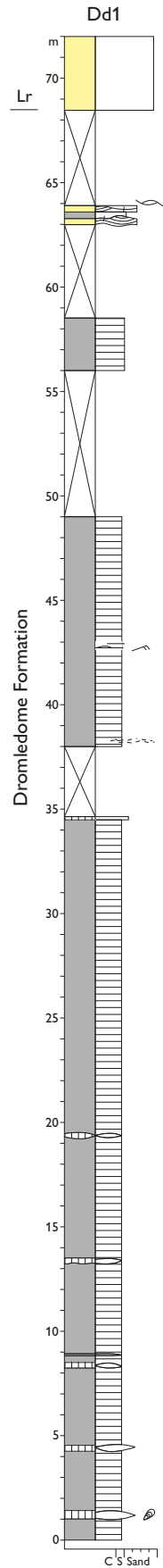


Fig. 15. Sedimentological log Dd1 of the upper part of the type section of the Dromledome Formation and the boundary to the Lichenryg Formation (Lr). For location of the log see Fig. 3.

suggest deposition in an oxygen-restricted offshore environment. The stratigraphic position with a gradational transition to the overlying part of the Kuglelejet Formation (see above) further suggests that the deposition took place in a spatially restricted setting such as an embayment, bay or seaway (see also Heinberg & Håkansson 1994).

Dromledome Formation

Name and history. The unit was mapped by Pedersen (1991) and described by Håkansson *et al.* (1994) and Dypvik *et al.* (2002). It was named after an anticline in the main outcrop area. The unit is formalised here.

Distribution. The formation crops out in the Dromledome and Kuglelejet areas, Kilen Fjelde (Fig. 3).

Type section. The Dromledome area constitutes the type section. The exposed part of the type section is documented in the sedimentological log Dd1 (Figs 14 and 15). The base of the exposure is located at 81°15'39.0"N, 013°57'22.9"W.

Boundaries. The exact lower boundary is covered by scree, but the exposed sediments below and above the scree demonstrate a change in lithology from bioturbated sandstone (Kuglelejet Formation) to black mudstone (Dromledome Formation). The upper boundary is variably exposed but placed at a sharp change in lithology from mudstone with hummocky cross-stratified sandstone layers to conglomerates and coarse-grained sandstone (Lichenryg Formation).

Thickness. The formation is *c.* 70 m thick (Fig. 6).

Fossils and age. The age is late Ryazanian/early Valanginian–Hauterivian based on ammonites, *Buchia* spp. and foraminifera (Fig. 6B). *Buchia* bivalves were reported by Håkansson *et al.* (1981a), and Valanginian polyptychitid ammonites were reported by Birkelund & Håkansson (1983). New data include a diverse ammonite fauna with *Surites* (*Caseyiceras*) *caseyi*, *S. (C.) subanalogus*, *S. cf. simplex*, *Polyptychites* sp., *P. (Euryptychites)* spp., *Nikitinoceras* (*Russanovia*) cf. *diptychum* and possible *N. hoplitoides* and *Dichotomites* (*Dichotomites*) *bidichotomus*, indicating an age range of late Ryazanian to late Valanginian. A specimen of *Sibirskites* (*Milanowskia*) aff. *staffi* in the C. Heinberg and E. Håkansson collection extends the age range into the Hauterivian. New collections of *Buchia sublaevis* and *B. keyserlingi* indicate the late early Valanginian, *B. keyserlingi* Zone based on Surlyk & Zakharov (1982).

The foraminifer fauna includes common *Falsogaudryina praemoesiana* and has a late Valanginian–early late Barremian age.

Lithological description. A black mudstone succession with recurring concretionary intervals in the lower part of the formation (0–20 m in Fig. 15). The top of the formation shows beds with hummocky cross-stratification. Typical trace fossils include *Zoophycos* isp., *Nereites* isp. and *Chondrites* isp. in the lower part of the formation, whereas *Gyrochorte* isp. and *Paleophycus heberti* occur in hummocky-cross-stratified beds.

Depositional environment. The sedimentological characteristics as well as trace fossil and fossil content indicate a shelf to offshore environment.

Lichenryg Formation

Name and history. The unit was mapped by Pedersen (1991) and described by Håkansson *et al.* (1994) and Dypvik *et al.* (2002); see also Røhr *et al.* (2008). It is named after a prominent ridge formed by the formation in the north-western part of Kilen Fjelde. The unit is formalised in the present study.

Distribution. The Kuglelejet, Dromledome and Lichenryg areas, Kilen Fjelde (Fig. 3).

Type section. The Dromledome anticline. The type section is covered by the log Lr1 (Figs 16, 17). The base of the section is located at 81°15'48.1"N, 013°56'55.9"W.

Reference section. Kuglelejet, where the upper part of the formation and the upper boundary are identified (Figs 18 and 19).

Boundaries. The lower boundary is sharp and erosive. It is placed where conglomerates and coarse-grained sandstones overlie the finer-grained Dromledome Formation (Fig. 17). The upper boundary is sharp and demarcated by an abrupt appearance of mudstone of the Galadriel Fjeld Formation above the sandstone of the Lichenryg Formation (Figs 17–19).

Fossils and age. Only plant fragments and moulds of dissolved bivalves have been discovered. The age is confined by the bounding units to the Hauterivian–late Aptian (see above and below; Fig. 6B).

Thickness. The thickness is variable, from *c.* 45 m to *c.* 100 m (Svennevig *et al.* 2016; Fig. 6).

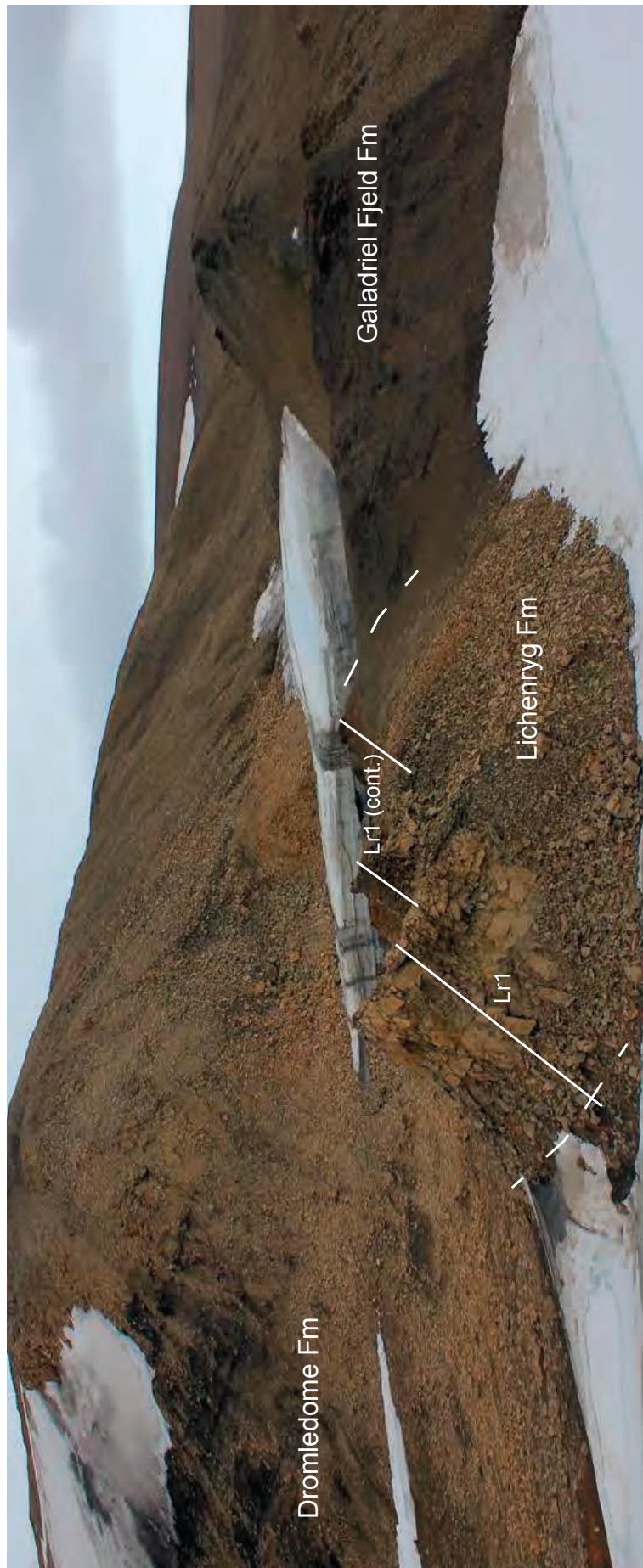


Fig. 16. Type section of the Lichenryg Formation, northern flank of the Dromledome anticline. Approximate location of the log Lr1 is shown. The type section outcrop is c. 45–50 m thick. View towards the west-northwest.

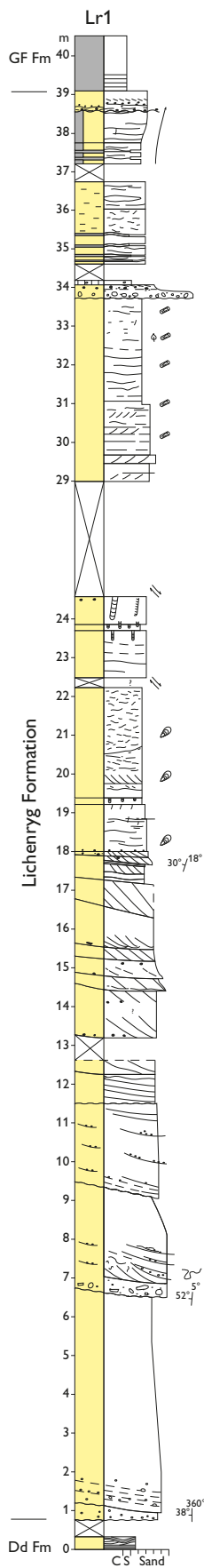


Fig. 17. Sedimentological log Lr1 illustrating the Lichenryg Formation type section. The measured section included a minor repetition which was omitted from this log. Dd Fm: Dromledome Formation. GF Fm: Galadriel Fjeld Formation. For location of the log see Fig. 3.

Lithological description. The lower part of the formation consists of matrix-supported conglomerates and very coarse- to coarse-grained trough and planar cross-bedded sandstones. The upper part of the formation is more heterolithic and shows fine- to medium-grained ripple and dune cross-stratified sandstone, structureless tabular sandstone beds as well as mud-drapes and mudstone interbeds. Erosional surfaces overlain by pebble- or mudclast conglomerates occur locally. Characteristic trace fossils include *Cylindrichnus* isp. and large *Diplocraterion parallelum* in the upper part of the formation (see also Håkansson *et al.* 1994).

Depositional environment. The sedimentological characteristics as well as trace fossil content point to fluvial and estuarine environments.

Galadriel Fjeld Formation

Name and history. The unit was mapped by Pedersen (1991) and described by Håkansson *et al.* (1994) and Dypvik *et al.* (2002). It was named after the hill Galadriel Fjeld in Kilen Fjelde. The formation is here redefined and formalised. Improved biostratigraphic data allow the inclusion of deposits previously referred to five other former formations (Fig. 5). Six new members are erected to cover the lithological variability between the outcrops across Kilen from Iskap and Tågekyst in the south to Saddelfjeld and Dipperne in the north (Figs 3, 4). In addition to the wide geographical distribution, the outcrops represent two thrust sheets that brought originally distant deposits in closer proximity (Svennevig 2017).

Subdivision. The “lower”, “middle”, and “upper” members of the Galadriel Fjeld Formation of Pedersen (1991) and Håkansson *et al.* (1994) are emended. Most of the deposits of the former “lower” and “middle” members are merged into a single new member, the Pil Member (Figs 5, 18). A part of the former “lower member” is exposed east of the major thrust fault (Fig. 3), and these deposits are described as the new Valmue Member. The former “upper member” is described as the new Stenbræk Member, which overlies the Pil Member in the Galadriel Fjeld area (Fig. 18).

The Galadriel Fjeld Formation now includes the sedimentary successions that formerly were referred to five formations, namely the Iver Pynt, Tågekyst, Kangoq Ryg, Hondal, and Dipperne Formations of Pedersen (1991) and Håkansson *et al.* (1994) (Figs 5, 6). The new Tågekyst Member comprises the deposits of the former Tågekyst Formation in central Gåseslette and along the Anduin river (Figs 4–6). The new Kangoq

Ryg Member includes the deposits of the former Iver Pynt and Kangoq Ryg Formations as well as deposits from the Tågekyst area, which formerly were part of the Tågekyst Formation (Figs 4–6). The new Hondal Member comprises the deposits of the former Hondal and Dipperne Formations. A thrust fault separates the new Hondal Member from the Valmue Member (Figs 3, 23A).

Distribution. The Galadriel Fjeld Formation is present in both the Kilen Fjelde and the Gåseslette areas (Figs 3, 4).

Type section. The Kuglelejet area is the type section of the Galadriel Fjeld Formation and of the Pil, Valmue and Stenbræk Members (sections Pi1, Va1 and St1–2, located in Fig. 3, see also Figs 18–22). The remaining members are exposed in various reference sections. The formation is not fully exposed at any single locality.

Reference sections. Sølverbæk river (exposures of the Kangoq Ryg Member), Anduin river (exposures of the Tågekyst Member), Lille Hondal area (exposures of the Valmue Member and the Hondal Member, separated by a thrust), Dipperne (exposures of the Hondal Member), Dromledome (exposures of the Pil Member), see sections Hd1–Hd3, Hd4–Hd5, Tk1 and KR1–KR2, located in Figs 3 and 4; see also Figs 23–31.

Thickness. The formation is *c.* 600 m thick in Kilen Fjelde. Photogeological mapping suggests that the formation may reach a thickness of 1400 m in the Gåseslette area (Svennevig *et al.* 2016; Fig. 5). Some members are coeval lateral equivalents.

Boundaries. The lower boundary is located at the first occurrence of dark grey shale and storm-deposited heteroliths above the sandstone of the Lichenryg Formation (Kuglelejet and Dromledome sections, Figs 17–19). The lower boundary is not exposed in the Gåseslette area. The upper boundary is variably exposed and is placed at the first appearance of a mudstone succession (Sølverbæk Formation) above sandstones, locally bioturbated, of the Hondal and Kangoq Ryg Members (Figs 23A, 29B, 32, 34).

Fossils and age. The formation is late Aptian – early to middle Cenomanian, based on inoceramids, foraminifera, dinocysts, ammonites and belemnites (Fig. 6B). See the discussion below of the ages of the individual members of the Galadriel Fjeld Formation. Scaphopods occasionally occur in large numbers on bedding planes. Other fossils include pectinid-, nucula- and macoma-type bivalves, ophiuroids, asteroids and wood fragments.

Lithological description. The formation is characterised by upwards coarsening successions comprising interbedded mudstone and sandstone. Storm-related deposits such as sandstone with hummocky cross-stratification and wave ripple cross-lamination are typical. The mudstone facies are strongly bioturbated, with trace fossils characteristic of the *Cruziana* ichnofacies.

Depositional environment. The formation is interpreted to represent storm-dominated offshore – shoreface environments (see below).

Pil Member

New member

Name and history. The member is named after the Arctic willow (*Salix arctica*, Arktisk pil in Danish), which grows in Kilen (Håkansson *et al.* 1993, table 1). The Pil Member comprises most of the former lower and middle members of the Galadriel Fjeld Formation (Pedersen 1991; Håkansson *et al.* 1994).

Distribution. The member is present in the Kuglelejet and Dromledome areas, Kilen Fjelde (Fig. 3).

Type section. The Kuglelejet area constitutes the type section (Figs 18, 19). The section is covered by the log Pi1, except for the upper boundary. The base of the section is located at 81°13'18.0"N, 013°53'11.1"W.

Reference section. The Dromledome area forms the reference section.

Boundaries. The lower boundary corresponds to that of the formation and is located at the first occurrence of dark grey shale and storm-generated heteroliths above the sandstones of the Lichenryg Formation. The upper boundary to the Stenbræk Member in the Kuglelejet area is gradational (Fig. 18) and demarcated by the appearance of metre-thick intervals with amalgamated hummocky cross-stratified sandstones which form the base of the Stenbræk Member.

Thickness. The member is *c.* 380 m thick (Fig. 6).

Fossils and age. The member is late Aptian – middle Albian based on foraminifera and inoceramids. The foraminifer fauna includes *Conorboides umiatensis*, *Serovaina loetterlei*, *Quadriformina albertensis* and *Saracenaria* sp. cf. *S. projectura*, which indicate a late Aptian to earliest Albian age in the lower part of the unit. Higher in the succession, inoceramids of the two species *I. cadottensis* and *I. cf. labiatiformis* occur in low



Fig. 18. Type section of the P11 Member (Galadriel Field Formation), Kuglelejet area. View towards the west. The approximate location of the section P11 is shown. The strata dip 40°–50° towards the north. The depositional boundary between the P11 and the Stenbræk Members is indicated (dashed line). The hill in the background is Galadriel Fjeld (c. 200 m high). The outcrops of the Stenbræk Member are located in the lower slope of the Dromledome anticline (Fig. 3).

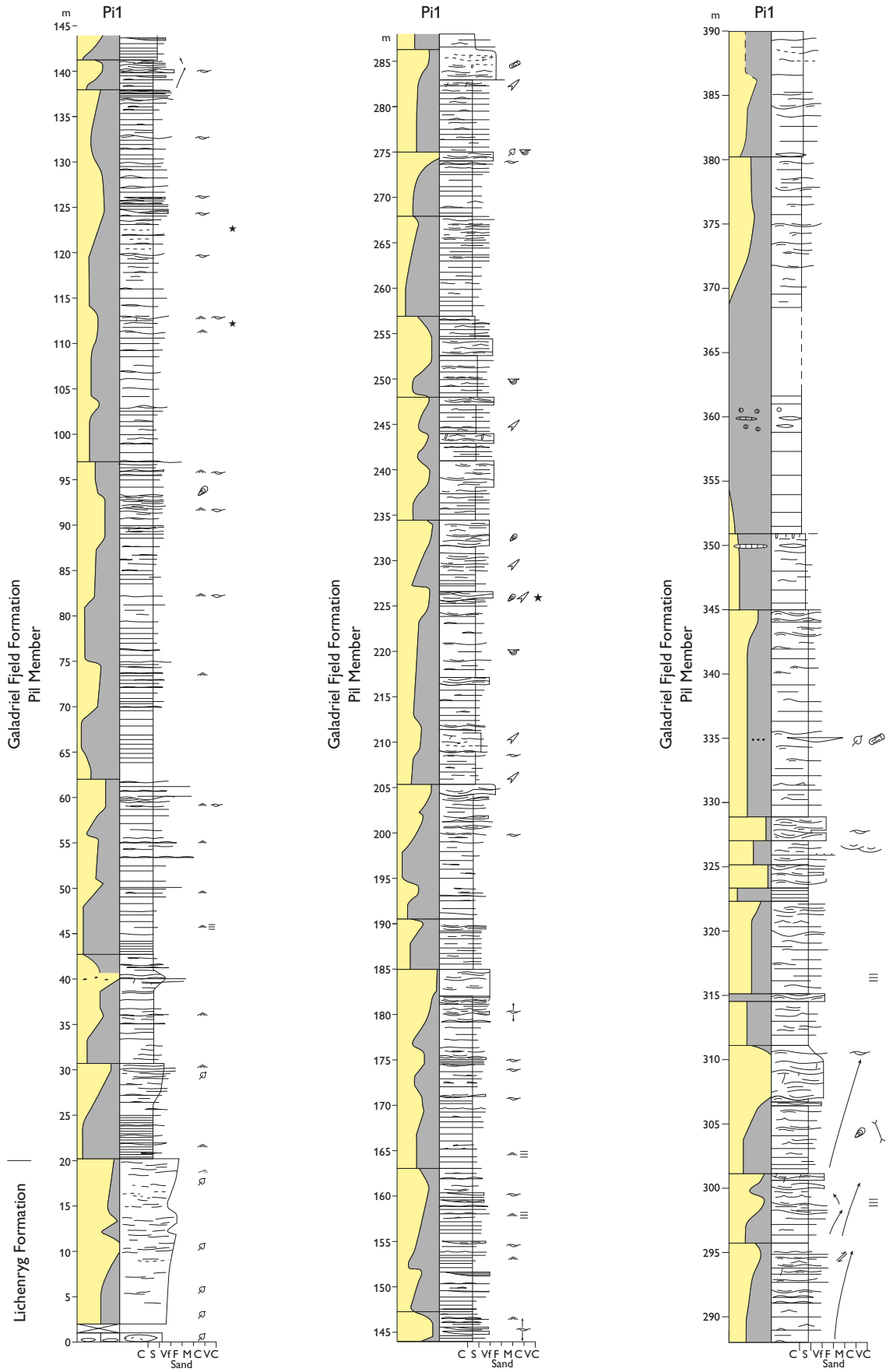


Fig. 19. Sedimentological log Pi1 representing the Pi1 Member type section. For location of the log see Figs 3, 18.

numbers. Both species indicate a middle to late middle Albian age when correlated to Svalbard, North-East Greenland and Arctic Canada (Stolley 1912; Woods 1912; Donovan 1953; Imlay 1961; Jeletzky 1964, 1968; Pchelina 1965; Pergament 1965; Crame 1985). Additional fossils include rare endemic belemnites and one fragment of a heteromorph, crioconic ammonite.

Lithological description. The deposits consist of mudstone-dominated upwards coarsening successions showing very fine- to fine-grained sandstone laminae/beds. The sandstone structures and facies include pinch-and-swell lamination, wave ripples and hummocky cross-stratified beds. Typical trace fossils include *Phycosiphon* isp., *Nereites* isp., *Chondrites* isp. and *Gyrophyllites* isp. (see also Håkansson *et al.* 1993; Heinberg & Håkansson 1994; Håkansson *et al.* 1994; Dypvik *et al.* 2002). The tops of the upwards coarsening successions show a higher trace fossil diversity. Moreover, the deposits are also characterised by glendonites, which occur locally as clusters of radiating pseudomorphs up to *c.* 5 cm in diameter. Glendonites are also reported from the probably time equivalent Invincible Point Member of the Christopher Formation, and in the Valanginian in the older upper Deer Bay Formation in the Sverdrup Basin (Schröder-Adams *et al.* 2014; Grasby *et al.* 2017). Likewise, glendonites occur in the probably equivalent Carolinefjellet Formation, and in the Valanginian in the older Rurikfjellet Formation on Svalbard (Price & Nunn 2010; Mutrux *et al.* 2008; Vickers *et al.* 2016).

Depositional environment. The distribution of storm and fair weather deposits coupled with the trace fossil content indicate deposition in lower offshore – upper offshore environments.

Stenbræk Member

New member

Name and history. The member was previously referred to as the upper member by Pedersen (1991) and Håkansson *et al.* (1994) (Fig. 5). It is named after the Saxifrage plant group (*Saxifraga* in Latin, Stenbræk in Danish), which is represented by seven species that flower at Kilen (Håkansson *et al.* 1993, their table 1). See also Dypvik *et al.* (2002).

Distribution. The member crops out in Kilen Fjelde in the Kuglelejet, Dromledome, and Birkelund Fjeld areas, as well as south of Dromledome (Figs 3, 18, 20).

Type section. The area south of Dromledome forms the type section (Fig. 20). The section illustrates the

lithological characteristics of the member (see logs St1 and St2, Fig. 21), but the boundaries are not visible. The base of section St1 is located at 81°14′27.3″N, 013°50′58.9″W.

Reference sections. The Galadriel Fjeld and Kuglelejet areas constitute the reference sections (Figs 3 and 18). The Kuglelejet area includes the lower boundary of the member.

Boundaries. The lower boundary to the Pil Member is gradational and demarcated by the appearance of several metre thick amalgamated sandstone successions, which form the base of the Stenbræk Member. The upper boundary is not exposed as the member is truncated by the present-day subaerial surface.

Thickness. The exact thickness of the Stenbræk Member is unknown. Photogeological mapping suggests that the unit is more than 200 m thick.

Fossils and age. Fossils include inoceramid- and non-age indicative bivalves such as pectinid-, nucula- and macoma-type bivalves. *Inoceramus cadottensis*, which is also recorded in the Pil Member, indicates the late middle Albian (Woods 1912; Donovan 1953; Pergament 1965; Kauffman 1977; Crame 1985). This age is confirmed by the presence of *Inoceramus* cf. *labiatiformis* and *I. spitzbergensis*, which by correlation to Svalbard and Europe suggests a middle Albian age (Stolley 1912; Woods 1912; Pchelina 1965; Crame 1985).

Lithological description. Sand-dominated, upwards coarsening successions characterised by amalgamated hummocky cross-stratified beds, gutter casts and other channelised storm beds. Typical trace fossils include *Lockeia* isp. and *Gyrochorte* isp. (see also Håkansson *et al.* 1993; Heinberg & Håkansson 1994; Dypvik *et al.* 2002).

Depositional environment. The distribution of storm and fair weather deposits coupled with the trace fossil content indicate deposition in storm-dominated upper offshore – lower and middle shoreface environments. In particular, the trace fossil assemblage of the fair weather deposits, where preserved, records archetypal and proximal *Cruziana* ichnofacies and deposition above fair weather wave base in the top of the upward coarsening successions.

Valmue Member

New member

Name and history. The unit was previously referred to



Fig. 20. Type section of the Valmue and Stenbræk Members (Galadriel Fjeld Formation), to the south of the Dromledome anticline. View towards the north-west. The contact between the members (dashed line) is a fault (Fig. 3). The outcrops of the sandstone-dominated Stenbræk Member form a belt, which is c. 200 m wide in the photo.

as part of the lower member by Pedersen (1991) and Håkansson *et al.* (1994). It is named after the plant Arctic poppy (*Papaver radicum* in Latin or Fjeld-valmue in Danish), which flowers in Kilen (Håkansson *et al.* 1993: their table 1).

Distribution. The Valmue Member is present in the Kuglejet area, Lille Hondal and Mågensfjeld, Kilen Fjelde (Fig 3).

Type section. The Kuglejet area constitutes the type section (Fig. 20). The sedimentological log Va1 illustrates the type section (Figs 3, 22). The base of the section is located at 81°14'18.4"N, 013°50'12.8"W.

Thickness. The exact thickness of the Valmue Member is unknown. Photogeological mapping suggests a thickness of more than 250 m (Svennevig *et al.* 2016; Fig. 6).

Boundaries. The unit is fault-bounded, see Fig. 3.

Fossils and age. The Valmue Member is of late Aptian–early Albian age, based on foraminifera. The foraminifer fauna includes *Conorboides umiatensis*, *Quadriformina albertensis* and *Serovaina loetterlei*, which also characterise the lower part of the Pil Member (see above; Sheldon *et al.* 2017). The member also contains coalified wood.

Lithological description. A black shale/mudstone succession that locally grades into sandy mudstone and heterolithic interlaminated sandstone with pinch-and-swell lamination, wave-ripple cross-lamination and rare thin hummocky cross-stratified sandstone beds. The deposits are also characterised by common large concretions which weather bright yellow. Glendonites and *Teredolites* isp. (bored wood) occur locally. Other typical trace fossils include common *Nereites* isp and

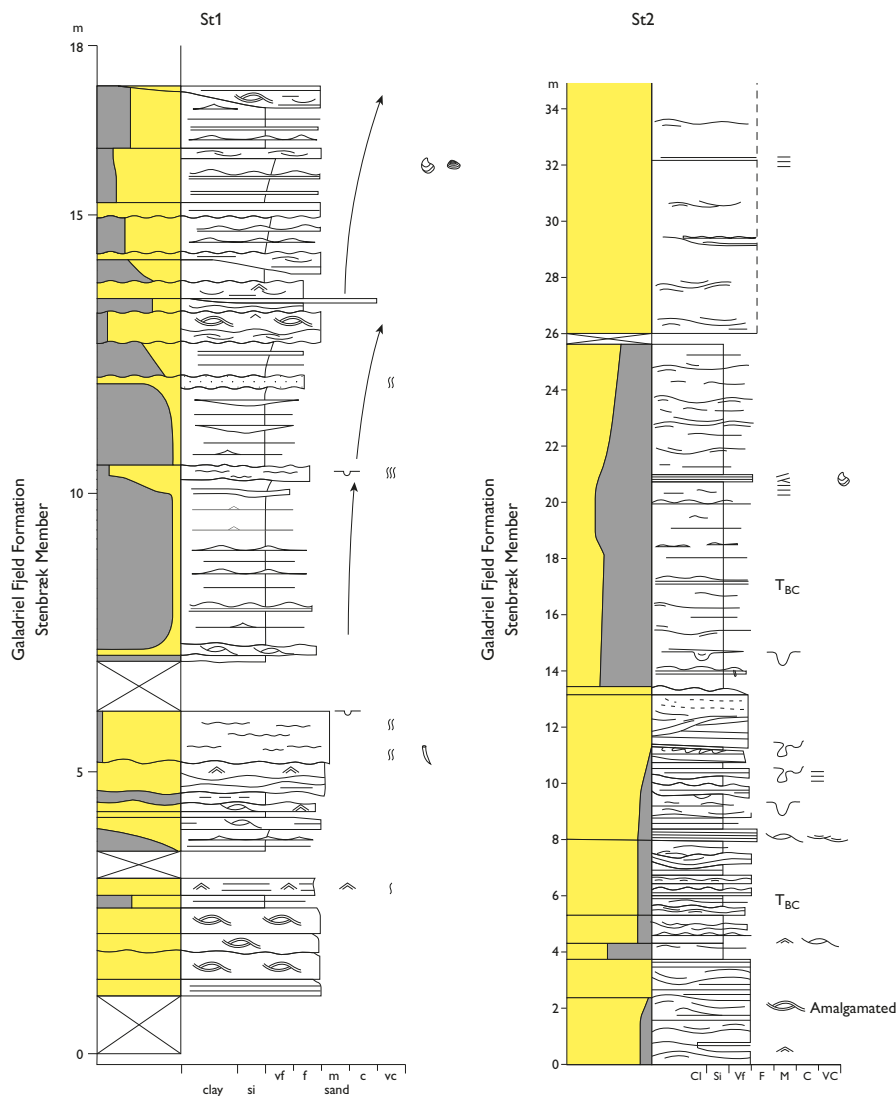
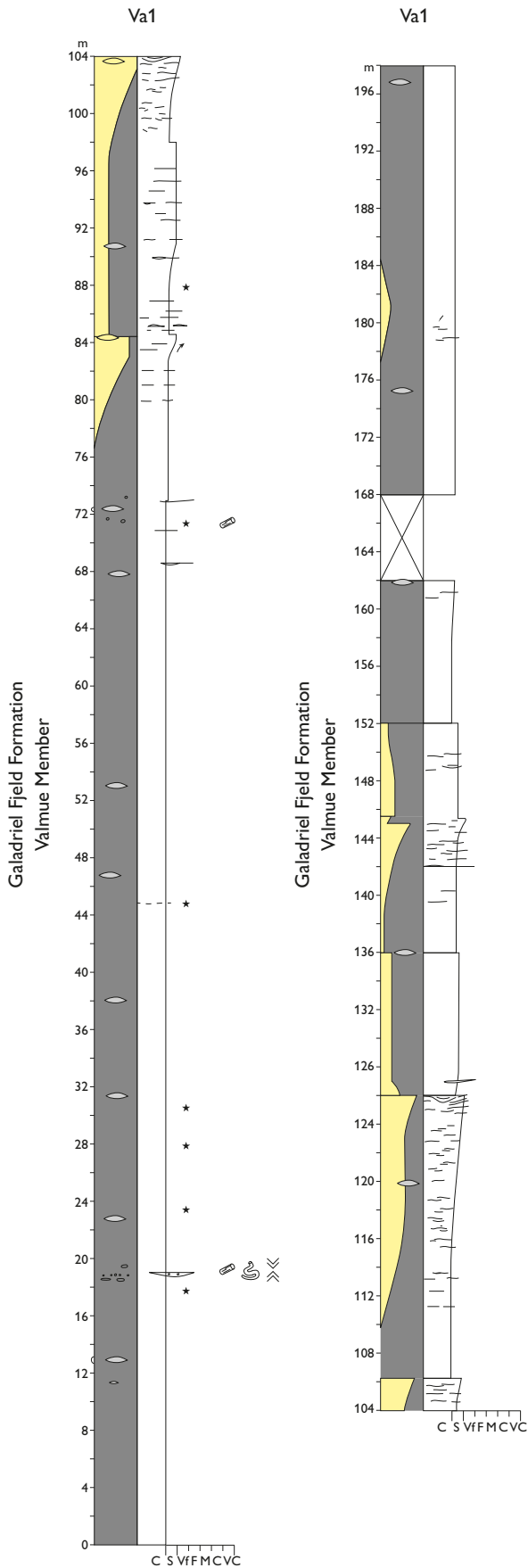


Fig. 21. Sedimentological logs St1 and St2 from the Stenbræk Member type section. The type section is intensively faulted and it is therefore not possible to measure a continuous section through the member. For this reason, the stratigraphic relationship of the measured logs is not clear. For location of the logs see Fig. 3.



Helminthopsis isp. The Valmue Member differs from the coeval Pil Member in grain size (the Valmue Member is more fine-grained) and diagenesis (the characteristic concretions).

Depositional environment. The distribution of storm and fair weather deposits coupled with the trace fossil content indicate deposition in shelf (below maximum storm wave-base) and offshore environments.

Hondal Member

New member

Name and history. The member comprises the successions that were previously described as the Hondal and Dipperne Formations of Håkansson *et al.* (1994). Their distribution was mapped by Pedersen (1991).

Distribution. The Hondal Member crops out in Kilen Fjelde. The member is exposed in Lille Hondal as well as in northernmost Kilen Fjelde at Saddelfjeld and in nunataks in Flade Isblink (Dipperne area) (Fig. 3). The distribution of the Hondal Member was mapped by Svennevig (2018a).

Type section. Lille Hondal (Fig. 23A). Three consecutive sedimentological logs, Hd1–Hd3, represent the type section (Figs 24–25), located in Figs 3 and 23A. The position of the base of Hd1 is 81°16′27.6″N, 013°54′23.13″W.

Reference section. Dipperne (Fig. 23B). The sedimentary logs Hd4 and Hd5 (Fig. 26) cover the lower part of the outcrop area at Dipperne; the top remains unstudied. The stratigraphic relationship between Hd1–Hd3 and Hd4–Hd5 is unclear due to lack of age diagnostic fossils from sections Hd4 and Hd5.

Thickness. A thickness of *c.* 600 m was suggested by Svennevig *et al.* (2016). The measured type section covers 370 m of the Hondal Member, with unexposed sections below and above (Fig. 23A). Håkansson *et al.* (1994) estimated a thickness of 550 m for the Dipperne area.

Boundaries. In Lille Hondal, the lower boundary to the Valmue Member is a thrust fault (Svennevig 2018a; Figs 3, 23A). The upper boundary to the Skalbæk Member of the Sølvbæk Formation is not exposed (Fig. 23A); however, an approximate position of the

Fig. 22. Sedimentological log Va1 illustrating the lithological characteristics of the Valmue Member. Lower part of the type section, for location of the log see Fig. 3.

boundary is indicated by an abrupt change in topography, which suggests a change from dominantly sandstone to mudstone. This upper boundary of the Hondal Member constitutes the upper boundary of the Galadriel Fjeld Formation in the Kilen Fjelde area.

In the northern Kilen Fjelde, the lower boundary is observable in the Saddelfjeld area, where the member directly overlies the Sølverbæk Formation with a thrust fault contact (Svennevig 2018a). The upper boundary is the present-day subaerial erosion surface.

Fossils and age. The Hondal Member is middle to late Albian (Fig. 6), based on inoceramids and ammonites. The Hondal Member is partly coeval with the Stenbræk and the Kangoq Ryg Members of the Galadriel Fjeld Formation on the basis of the faunal assemblages. Age indicative inoceramids include *Gneisoceramus comancheanus* and *Inoceramus anglicus*, which indicate a middle to late Albian age based on correlations to the Western Interior Basin (Walaszczyk & Cobban 2016), East Greenland (Donovan 1953) and Central Europe (Crame 1985). Ammonites include an assemblage of late middle Albian hoplitinids including *Euhoplites lautus*, *Euhoplites truncatus* and *E. aff. sp. subtuberculatus*, and gatrolitid including *Pseudogastrolites draconensis* and *Pseudopulchellia flexicostata*, *P. cf. ballkwilli* (Alsen 2018a). The ammonite fauna also includes slightly younger latest middle Albian *Stelkiceras liardense* and earliest late Albian *Gastrolites cf. cantianus*. Other fossils include *Panopea*-type and pectinid bivalves, brachiopods, ophiuroids, asteroids and scaphopods.

Lithological description. The member is characterised by upwards coarsening successions of interbedded mudstone and sandstone (Figs 24–25). The type section (see logs Hd1–Hd3) demonstrates an overall development from mudstone- to sandstone-dominated facies with trace fossils mainly of the *Cruziana* ichnofacies. Few thin beds of medium- to coarse-grained sandstone occur. Multidirectional trough cross-bedding is locally present in the upper parts of the upward coarsening successions in Dipperne (section Hd5). The Hondal Member differs from the Stenbræk Member by the local presence of medium- to coarse-grained sandstone, trough cross-bedding and the trace fossil *Zoophycos isp.*

Depositional environment. The distribution of storm and fair weather deposits coupled with the trace fossil content indicate deposition in proximal offshore to shoreface environments. The multidirectional trough cross-bedding coupled with occurrences of trace fossil *Macaronichnus* suggest that the environment locally reached the surf zone of the upper shoreface.

Tågekyst Member

New member

Name and history. The member includes some of the sediments that were formerly referred to the Tågekyst Formation (Pedersen 1991; Håkansson *et al.* 1994).

Distribution. The member is mapped from aerial photos across large parts of Gåseslette (Pedersen 1991; Svennevig *et al.* 2015; Svennevig 2018a). It is exposed in low cliffs adjacent to the Anduin river (Fig. 4). The deposits in the Tågekyst area, which were formerly mapped as the Tågekyst Formation (Pedersen 1991), are now referred to the Kangoq Ryg Member.

Type section. The outcrops along the northern part of the Anduin river form the type section (Fig. 27D). A short sedimentological log Tk1 is shown in Fig. 28; this includes neither the lower nor the upper boundary of the member. The position of the base of Tk1 is 81°12'08.2"N, 013°10'51.99"W.

Reference section. The little known outcrops along the southern part of the Anduin river constitute the reference section (Fig. 27D).

Thickness. Photogeological modelling indicates that the member is at least 800 m thick in the type section (Svennevig *et al.* 2016).

Boundaries. The lower boundary is unknown. The upper boundary towards the Kangoq Ryg Member is unknown. Figure 4 shows a fault boundary between the Tågekyst Member and the Sølverbæk Formation at the Anduin river.

Fossils and age. No fossils have yet been found in the Tågekyst Member, and this is considered a significant difference from the Kangoq Ryg Member. Due to the lack of fossils, the age of the Tågekyst Member is unknown. The member is tentatively placed in the lower part of the Galadriel Fjeld Formation, but it is not possible to suggest a correlation with the Pil or Valmue Members.

Lithological description. Sandy, commonly bioturbated mudstones interbedded with fine- to medium-grained sandstone (Fig. 27A). The sandstone may show hummocky cross-stratification and wave-ripples. Coarse-grained sandstone beds occur locally in the area containing the section Tk1 (Figs 27B, C and 28). A diverse trace fossil assemblage represents the *Cruziana* ichnofacies. A strong diagenetic overprint in the Anduin river area is indicated by growth of authigenic minerals along joints.



Fig. 23. A: Type section of the Hondal Member (Galadriel Fjeld Formation) in Lille Hondal (Fig. 3), view towards the west. The type section consists of three consecutive logs, Hd1, Hd2 and Hd3 (Figs 24, 25). The log Hd2 is ~40 m long. The lower boundary to the Valmue Member is tectonic (dashed line). The upper boundary to the Skalbæk Member of the Sølverbæk Formation is not exposed; the approximate location is indicated with a dashed line. **B:** Lower part of the reference section of the Hondal Member at Dipperne (Fig. 3), view towards the north-east. The sedimentological logs Hd4 and Hd5 (Fig. 26) were measured in the lower part of the reference section. Section Hd5 overlies section Hd4. The log Hd5 covers part of the exposure, whereas the log Hd4 represents an underlying exposure not included in the photo. Field of view is c. 100 m.

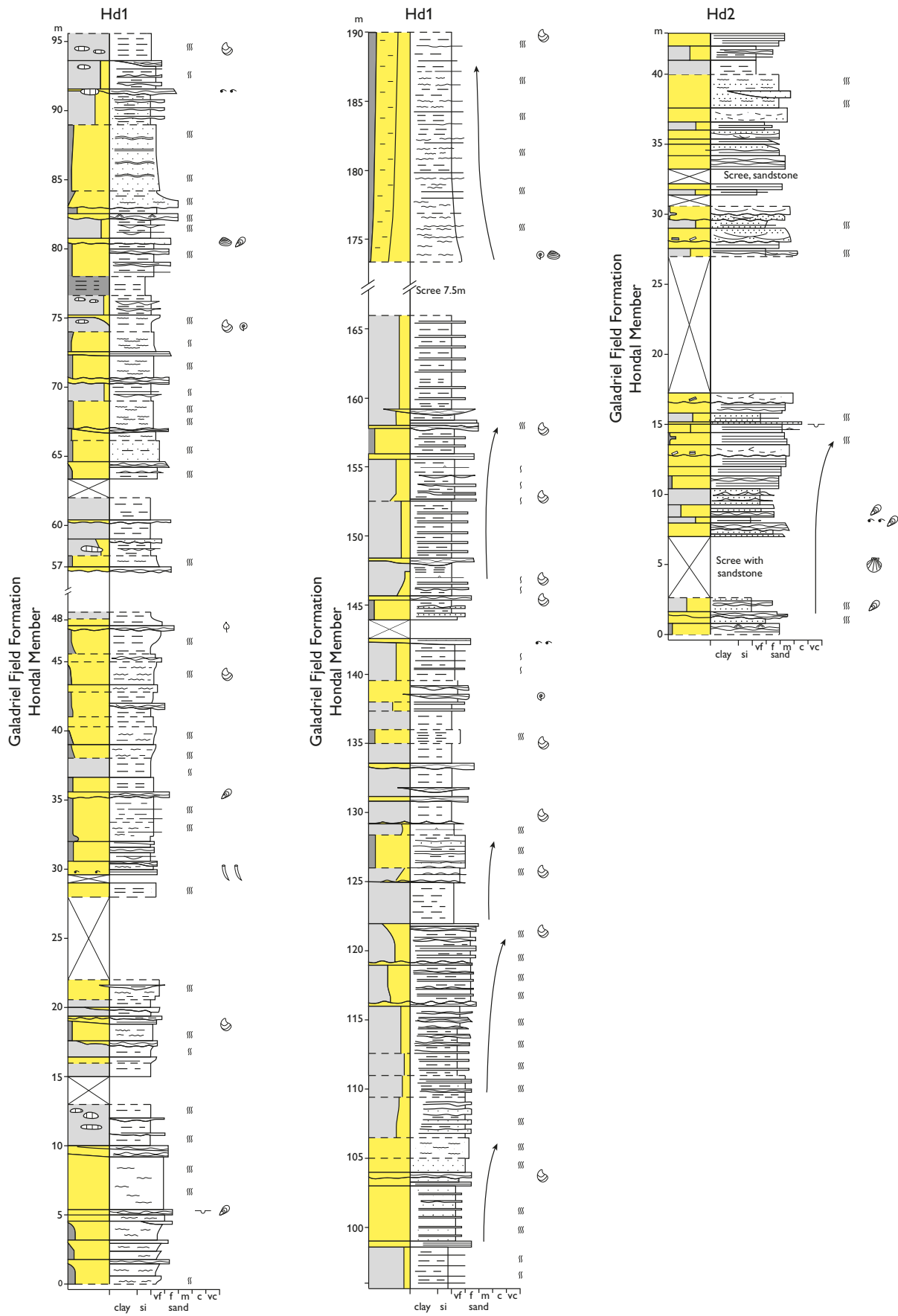


Fig. 24. Lower part of the type section of the middle to upper Albian Hondal Member (Galadriel Fjeld Formation) in Lille Hondal (Fig. 23). Inoceramid bivalves are fairly common in Hd1. For location see Figs 3, 23A.

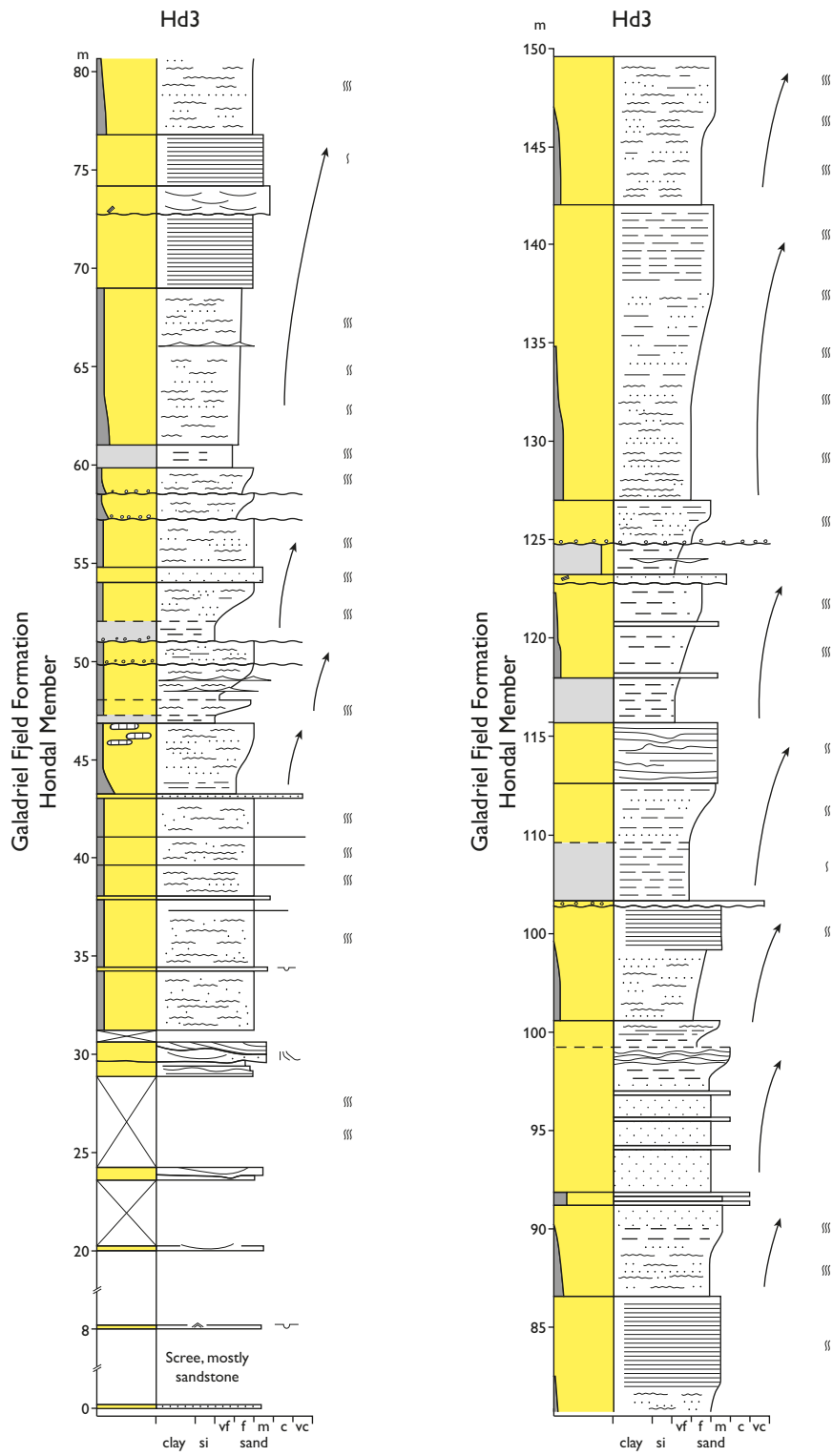


Fig. 25. Upper part of the type section of the middle to upper Albian Hondal Member (Galadriel Fjeld Formation) in Lille Hondal (Fig. 23). For location see Figs 3, 23A.

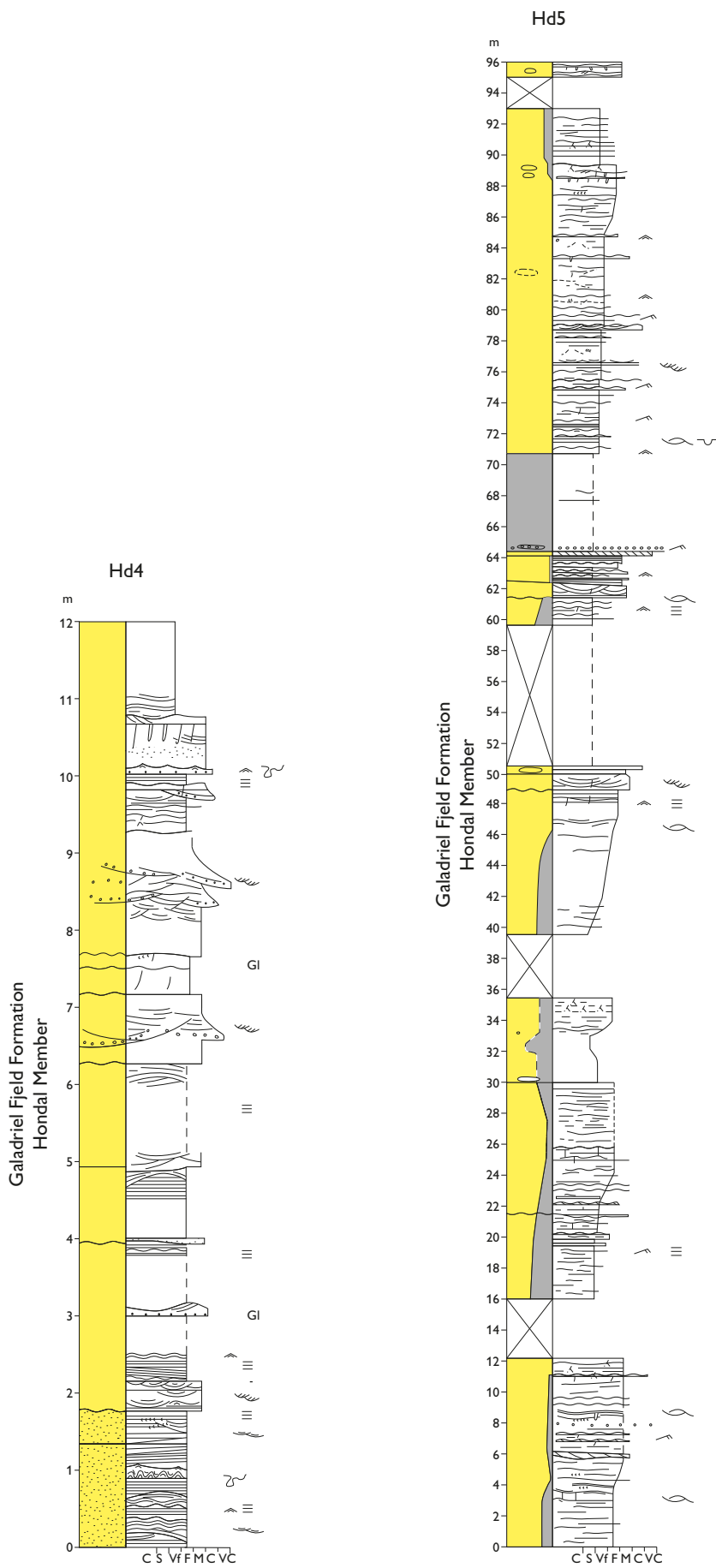


Fig. 26. Sedimentological logs Hd4 and Hd5, illustrating the reference section of the Hondal Member at Dipperne. Hd4 represents the lower part of the member and is stratigraphically overlain by section Hd5. For location see Fig. 3, and text for coordinates.



Fig. 27. Outcrops of the Tågekyst Member of the Galadriel Fjeld Formation close to the Anduin river (Fig. 4). **A:** Steeply dipping, interbedded mudstone and sandstone (see also Fig. 28). **B:** Mudstone overlain by c. 20 cm thick, medium- to coarse-grained sandstone bed with erosive base. Galleries of vertical and horizontal burrows are passively filled by sand. **C:** Short upwards coarsening succession of parallel laminated, medium-grained sandstone overlain by coarse-grained white sandstone with trough cross-bedding. A–C are from the area close to the type section (Fig. 28). **D:** Folded silt- and sandstones, height of exposure 10–15 m, Tågekyst Member along the southern part of the Anduin river.

Depositional environment. The distribution of storm and fair weather deposits coupled with trace fossil content indicate deposition in upper offshore to shoreface environments.

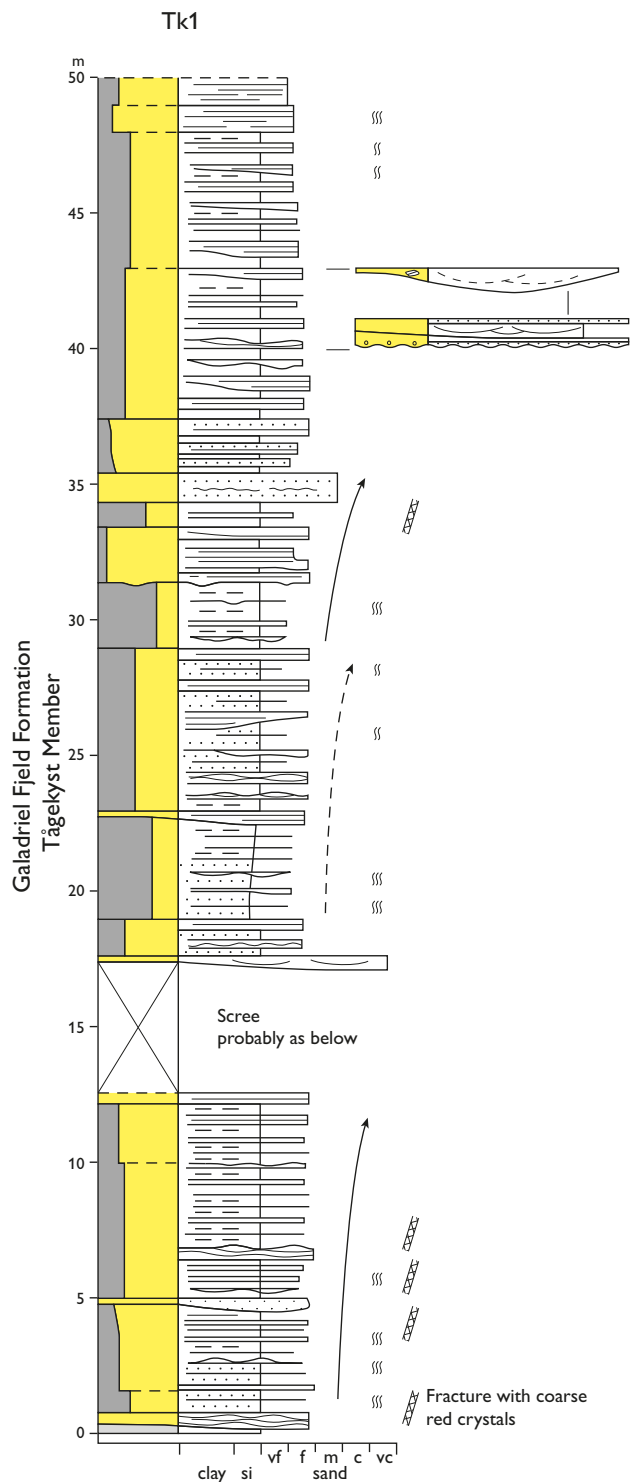


Fig. 28. Sedimentological log Tk1 that illustrates the type section of the Tågekyst Member (Galadriel Fjeld Formation) close to the Anduin river. The section is located in Fig. 4.

Kangoq Ryg Member

New member

Name and history. The member comprises the successions that were previously described as the Iver Pynt, the Tågekyst (in part) and the Kangoq Ryg Formations (Håkansson *et al.* 1994). Their distributions were mapped by Pedersen (1991).

Distribution. The member occurs at Iskap (formerly Iver Pynt), Gåseslette and the southern part of Flagellarisslette (Figs 3, 4). The member is exposed along the Sølverbæk river, in the Tågekyst area, and at Iskap. The distribution of the member in Gåseslette and Flagellarisslette has been mapped on aerial photos (Pedersen 1991; Svennevig *et al.* 2015; Svennevig 2018a).

Type section. Outcrops along the central part of the Sølverbæk river (sections KR1, KR2) constitute the type section (Figs 4, 29A–C, 30, 31). The section KR2 is stratigraphically above KR1; KR2 is based on reconnaissance work. The position of the base of KR1 is 81°09'07.87"N, 013°26'42.96"W.

Reference section. The outcrops along the southern part of the Sølverbæk river constitute the reference section. Only the very top of the member has been logged sedimentologically at this locality (Fig. 32), for location see Fig. 4. The Iskap area has only been visited briefly, and the lithologies are poorly known (Fig. 29D).

Thickness. The strata exposed along the Sølverbæk river are steeply dipping (Fig. 29A) and affected by repeated small-scale thrusting, which makes it difficult to measure the thickness of the Kangoq Ryg Member in outcrop. The structural model based on photogeological mapping suggests a thickness of 650 m (Svennevig *et al.* 2016). The thickness of the Kangoq Ryg Member at Iskap is unknown.

Boundaries. The lower boundary of the Kangoq Ryg Member is not exposed. The upper boundary is recorded as a change from sandstone to a thick mudstone succession (the Sølverbæk Formation) in the reference section (Figs. 29B, 32). The approximate position of the upper boundary is indicated in section KR2 (Fig. 31). The upper boundary of the Kangoq Ryg Member is the best constrained boundary between the Galadriel Fjeld and the Sølverbæk Formations (Fig. 6A, B).

Fossils and age. Ammonites, inoceramids, other bivalves, ophiurids and scaphopods occur in the Kangoq Ryg Member. Dinoflagellate cysts are preserved in

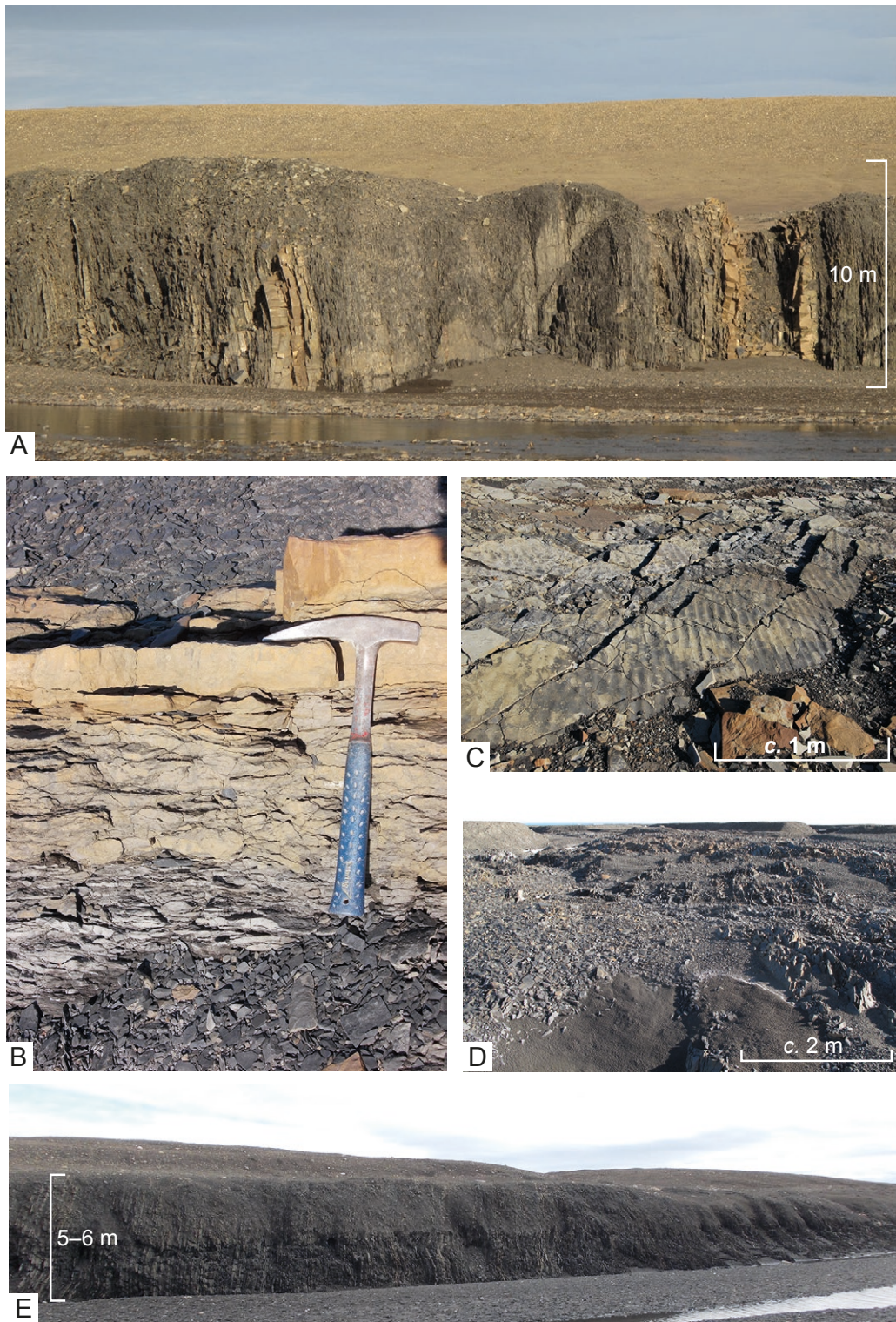


Fig. 29. Type section of the Kangoq Ryg Member (Galadriel Fjeld Formation) and the Sølverbæk Formation in Gåseslette (Fig. 4). **A:** Vertical strata (stratigraphic up to the right) of the Kangoq Ryg Member in cliffs along the Sølverbæk river. The heterolithic sandstones are interbedded with thick yellowish sandstones with hummocky cross-stratification. The photo shows the lower part of the type section KR1 (Fig. 30), located in Fig. 4. **B:** Boundary between the Kangoq Ryg Member and the overlying Sølverbæk Formation, southern Sølverbæk river (Figs 4, 32). **C:** Bedding surface with wave-ripples, Kangoq Ryg Member, southern part of the Sølverbæk river. **D:** The Kangoq Ryg Member at Iskap (formerly Iver Pynt). **E:** Steeply dipping dark grey mudstones. Part of the type section of the Sølverbæk Formation at the Sølverbæk river (SB2–SB4 in Fig. 33).

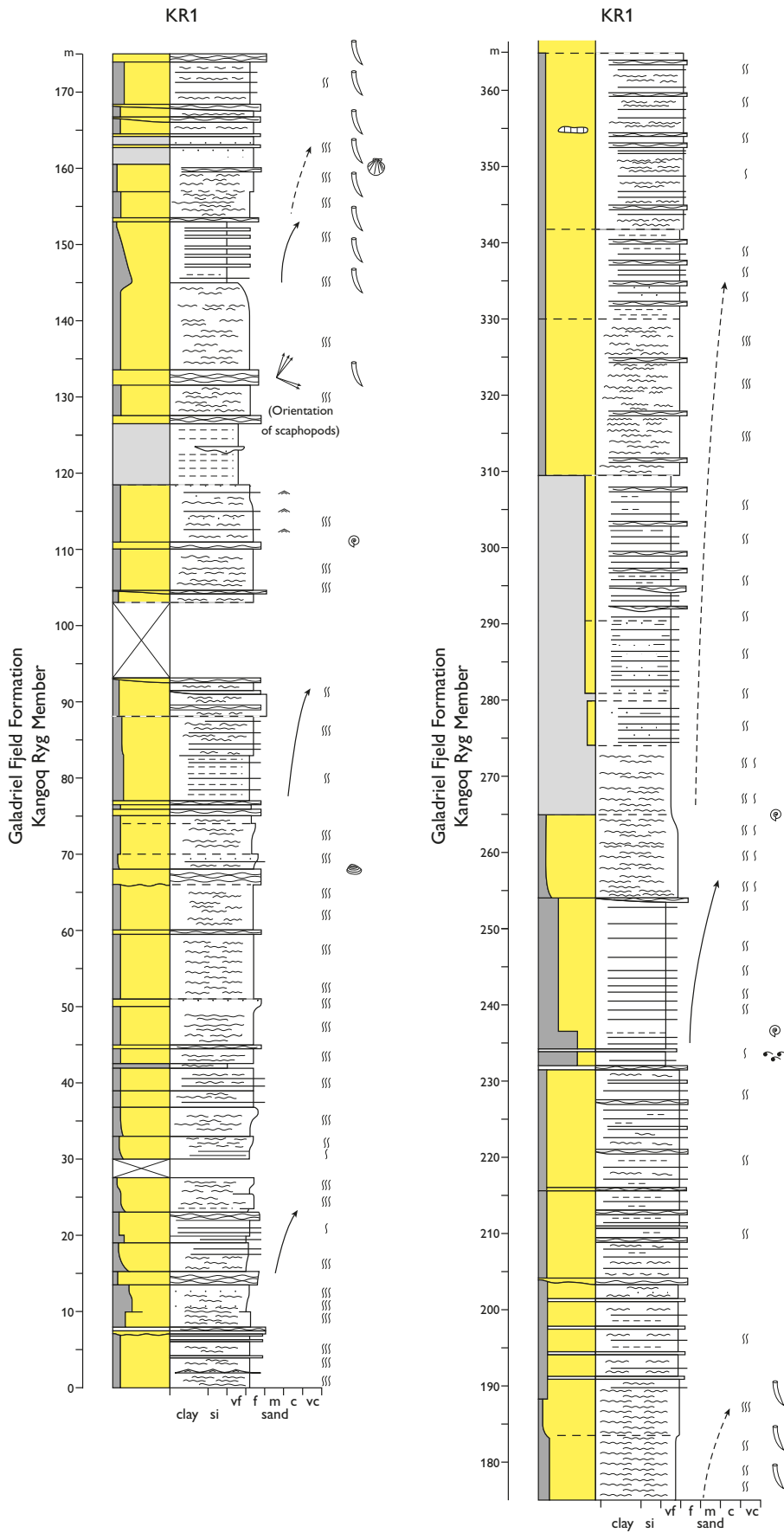


Fig. 30. Sedimentological log KR1, the type section of the Kangoq Ryg Member at the Sølverbæk river (Figs 4, 29A). The section is characterised by interbedded silty mudstones and fine-grained sandstones. The lower boundary of the member is not exposed, the upper boundary is seen in Figs 29B and 32.

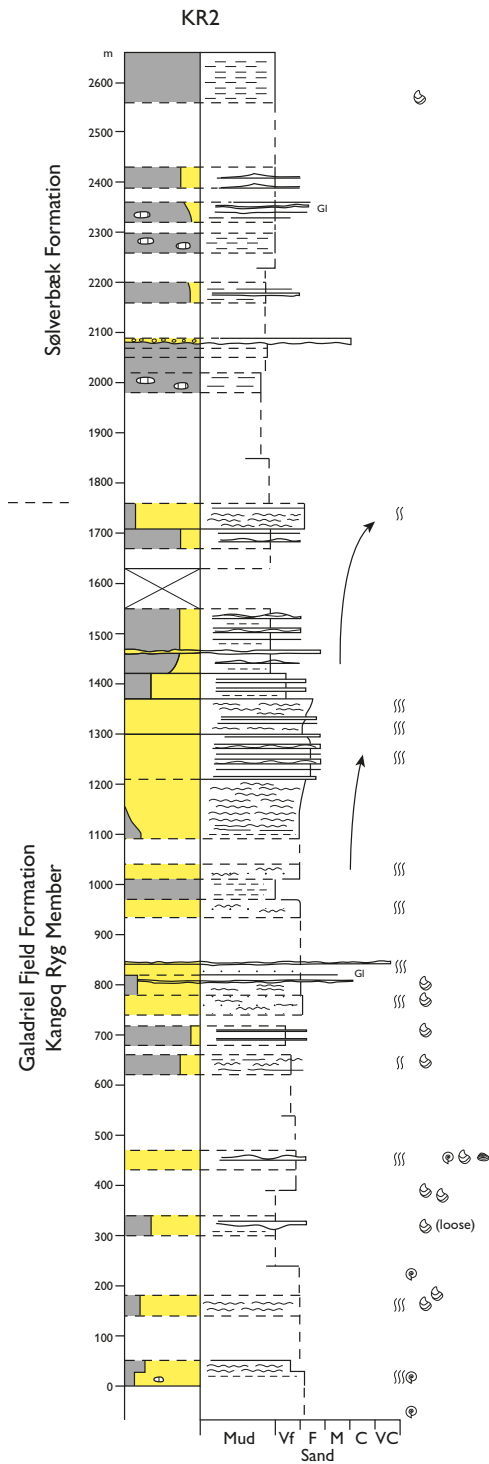


Fig. 31. Sedimentological log KR2 measured during reconnaissance field work at the Sølverbæk river (Fig. 4). The scale indicates horizontal distance instead of bed thicknesses. The strata are steeply dipping, 60–90°. The log covers the upper part of the Kangoq Ryg Member (0–1750 m) and part of the overlying Sølverbæk Formation. Unfortunately the succession 1750–1975 m was inaccessible in the cut bank of the river. The position of the boundary between the Kangoq Ryg Member and the Sølverbæk Formation is therefore uncertain.

samples from the south-eastern part of Gåseslette and provide the most detailed biostratigraphic information (Fig. 6B). The older part of the Kangoq Ryg Member is middle Albian to middle upper Albian based on the presence of *Rhombodella paucispina* and *Chichaouadinium vestitum* (late middle Albian age; Subzone IV2 of Nøhr-Hansen 1993), the presence of *Subtilisphaera kalaalliti* and *Wigginsella grandstandica* (early late Albian age; Subzone V1 of Nøhr-Hansen 1993) and by the presence of *Odontochitina ancala* (middle late Albian age; Subzone V2 of Nøhr-Hansen 1993). The upper Albian succession of the Kangoq Ryg Member seems to be unconformably overlain by an upper lower to possibly middle Cenomanian succession, indicated by the presence of *Endoceratium ludbrookiae*.

The ammonite fauna contains early Albian *Archthoplites* including *A. jachromensis* or *nikitini* and *A. probus* and middle Albian *Beudanticeras glabrum*, *Pseudopulchellia flexicostata*, *Gastrolites* sp., *Stelckiceras* sp. and *Hoplites dentatus*. Scattered inoceramids are represented by *Gnesioceramus comancheanus*, *G. cf. bellvuensis* and *Inoceramus anglicus* of middle to late Albian age (Woods 1911–1912; Pergament 1965; Kauffman 1977; Crame 1985; Walaszczyk & Cobban 2016).

The Kangoq Ryg Member is correlated to the Hondal Member of the Galadriel Fjeld Formation, as both members contain the inoceramid species *G. comancheanus* and *I. anglicus*. An imprint of an ammonite fragment from Iskap (Heinberg & Håkansson collection) represents a middle Albian genus, which supports the assignment of the former Iver Pynt formation to the Kangoq Ryg Member.

Lithological description. Interbedded sand-streaked mudstone and fine-grained sandstone with mud-drapes form upward coarsening successions, 30–50 m thick (Fig. 30). The ratio of mudstone to sandstone is high in the Iskap area (Fig. 29D), nearly equal in other areas, and low in the outcrops in the southern part of the Sølverbæk river (Fig. 29C). Generally the member is strongly bioturbated, and the diverse trace fossil assemblage represents the *Cruziana* ichnofacies. The thick sandstone beds (0.5–1 m) show parallel lamination, hummocky cross-stratification and locally wave-ripple cross-stratification. Locally, large numbers of *Dentalium* shells occur as intraformational clasts in fine- to medium-grained sandstones.

Depositional environment. The distribution of storm and fair weather deposits coupled with the trace fossil content indicate deposition in proximal offshore to lower shoreface environments.

Sølverbæk Formation

Name and history. The formation is named after the Sølverbæk river and was originally mapped by Pedersen (1991) and described by Håkansson *et al.* (1993, 1994). Here the formation is formalised and expanded significantly to comprise most of the Upper Cretaceous of Kilen (Figs 5, 6). In the Gåseslette area, the Sølverbæk Formation has been expanded by a previously unknown succession at the Anduin river. In the Kilen Fjelde area, the Sølverbæk Formation now includes the sediments that formerly were referred to the Anduin, Skalbæk, Røde Bakker, Flagellarisslette, Scaphitesnæse and Sadelbjerg Formations of Håkansson *et al.* (1993, 1994), see Fig. 5. Consequently, all of these former formations are merged into a single formation. The deposits of the former Anduin, Skalbæk and Røde Bakker Formations are now referred to the Skalbæk Member, which includes the Røde Bakker Beds. The deposits of the former Flagellarisslette, Scaphitesnæse and Sadelbjerg Formations are now referred to the Scaphitesnæse Member, which includes the Flagellarisslette mudstone (Figs 5, 6).

Subdivision. In Kilen Fjelde, the Sølverbæk Formation is subdivided into the Skalbæk and Scaphitesnæse Members. The Skalbæk Member contains the Røde Bakker Beds in the Røde Bakker area. The Scaphitesnæse Member contains the informal Flagellarisslette mudstone in the north-eastern Kilen Fjelde area. In the Gåseslette area, the Sølverbæk Formation is not subdivided (Figs 3, 5).

Distribution. The formation occurs at Gåseslette, Flagellarisslette and Kilen Fjelde (Figs 3, 4).

Type section. The outcrops along the Sølverbæk river form the type section (Fig. 29E). The logs are measured in cliffs along c. 1.8 km of the Sølverbæk river (Figs 4, 29E): The stratigraphic thickness is c. 1.4 km including numerous small-scale faults and folds. The sedimentological logs SB3–SB2–SB4–SB5–SB1 constitute a composite type section (Figs 32, 33). In parts of the type section, between the measured logs, the formation is inaccessible in the cut-bank of the river. The position of the base of SB3, just below the lower boundary of the formation, is 81°06'31.54"N, 013°20'07.76"W. The logs SB3–SB5 are nearly continuous. The youngest beds in the type section are encountered between SB5 and SB1. The accessible part of this stretch of the river constitutes section SB8, at 81°07'16.73"N; 013°22'32.03"W. SB8 is located in the axis of the syncline (Fig. 4), and no sedimentological log was measured in this tectonically complex section.

Reference sections. The type sections for the Skalbæk

and Scaphitesnæse Members are reference sections for the Sølverbæk Formation in Kilen Fjelde (Figs 34–39). The outcrops of the formation along the Anduin river constitute a reference section for the youngest part of the Sølverbæk Formation.

Thickness. In the type section the formation is exposed as steeply dipping beds separated by numerous small-scale thrusts (Fig. 29E), which makes it difficult to measure the thickness in outcrops. The modelled minimum thickness of the formation is 600 m in the type section and c. 750 m in Kilen Fjelde (Svennevig *et al.* 2018; Fig. 6).

Boundaries. The lower boundary is placed at a sharp transition from sandstone, at the top of the Hondal and Kangoq Ryg Members, to mudstone. The boundary is exposed in section SB3, indicated in section KR2, and inferred below Sk1 (Figs 31, 32, 34A). The upper boundary is the present-day subaerial erosion surface, locally overlain by a thin cover of recent deposits.

Fossils and age. The fossils include inoceramids, dinoflagellate cysts and ammonites. Dinoflagellate cysts in the lower part of the Sølverbæk Formation date it as early late to late Cenomanian based on the presence of *Isabelidinium magnum* and *Trithyrodinium suspectum* and by the presence of *Cauveridinium membraniphorum*. The middle to upper part of the Sølverbæk Formation is Turonian based on the presence of *Heterosphaeridium difficile* and *Chatangiella* spp., by the presence of *Odon-tochitina* aff. *rhakodes* and by the presence of *Senoniasphaera* aff. *turonica*. The upper part of the Sølverbæk Formation is Coniacian based on the presence of *Xenascus gochtii* and by the presence of *Canningia* aff. *macroreticulata*. The inoceramids are represented by an abundant and diverse fauna of 34 species and 281 specimens. They represent strata from the early Turonian to early Coniacian (e.g. Tröger 1967; Keller 1982; Walaszczyk 1992). Examples are *Inoceramus apicalis* (from early middle Turonian), *Inoceramus lamarcki*, (from middle Turonian), *Mytiloides striaconcentricus* (from late Turonian–early Coniacian) and *Inoceramus lusatie* (from late Turonian–early Coniacian). The four examples listed are found in large numbers at localities both at Gåseslette and Kilen Fjelde.

The youngest deposits (late Santonian to possibly early Campanian) are restricted to outcrops along the Anduin river dated by findings of *Sphenoceramus* species. Ammonites are subordinate for dating this unit. Scaphitids locally occur in high abundances, crushed and fragmented, in hard siderite concretions, both in Kilen Fjelde and in the Gåseslette area. They appear to represent a locally evolved, endemic fauna with affinity to *S. geinitzi* as suggested by Birkelund

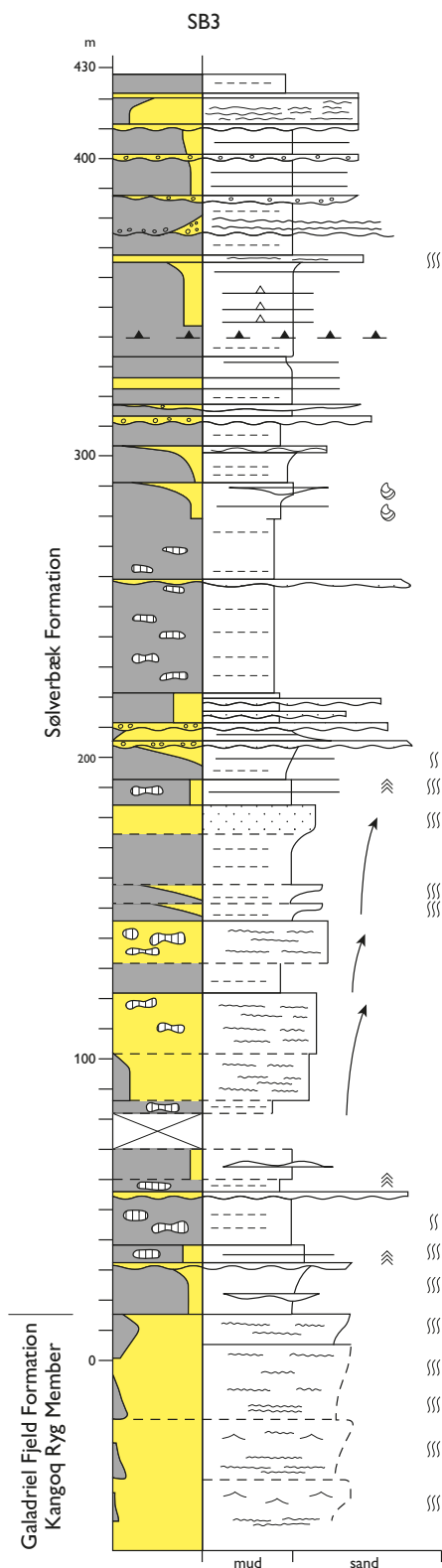


Fig. 32. Lower part of the type section of the Sølverbæk Formation. The section SB3 includes the top of the Kangoq Ryg Member (middle Cenomanian) and the lower boundary of the Sølverbæk Formation. The overlying Sølverbæk Formation is here upper Cenomanian and lower Turonian (Fig. 6). For location of the log see Fig. 4.

& Håkansson (1983). In addition, specimens of long-ranging *Puzosia* (*Mesopuzosia*) are relatively common.

Lithological description. The formation is dominated by mudstone, commonly with streaks of siltstone or very fine-grained sandstone. Siderite concretions are fairly common in the mudstones of the type section. Interbedded mudstones and fine-grained sandstones occur in 10–50 m thick, upwards coarsening successions. The proportion of sandstone is higher in the Skalbæk and Scaphitesnæse Members than in the type section. Siderite-cemented, intraformational conglomerates occur in the sections in Kilen Fjelde and are locally present in the Gåseslette area. The trace fossil assemblages are varied and mainly represent the *Cruziana* ichnofacies. The *Glossifungites* ichnofacies is locally present in association with siderite-cemented conglomerates of the Skalbæk Member.

Depositional environment. Most of the formation represents shelf and offshore environments; nearshore depositional settings occur locally (see below).

Skalbæk Member

New member

Name and History. The member comprises the sediments that were previously mapped and described as the Anduin, Skalbæk, and Røde Bakker Formations by Pedersen (1991) and Håkansson *et al.* (1994). The Skalbæk Member is referred to the Sølverbæk Formation (Figs 5, 6).

Subdivision. The Røde Bakker Beds (formerly the Røde Bakker Formation) are a subunit of the Skalbæk Member in northern Kilen Fjelde (Fig. 3).

Distribution. The Skalbæk Member occurs in the Kilen Fjelde area (Fig. 3).

Type section. The Hondal syncline, west of the Hondal river, Kilen Fjelde (Figs 3 and 34). The sedimentological logs Sk1–Sk3 cover the type section (Figs 35–36). The position of the base of Sk1 is 81°16'47.4"N, 013°55'47.7"W.

Reference section. The Skalbæk and Røde Bakker areas, northern Kilen Fjelde (Fig. 34B). The sedimentological log RB1 illustrates part of the reference section of the Skalbæk Member (Fig. 37).

Thickness. The member is estimated to be up to 565 m thick (Svennevig *et al.* 2016). The exposed part of the type section covered by the logs Sk1–Sk3 is c. 350 m.

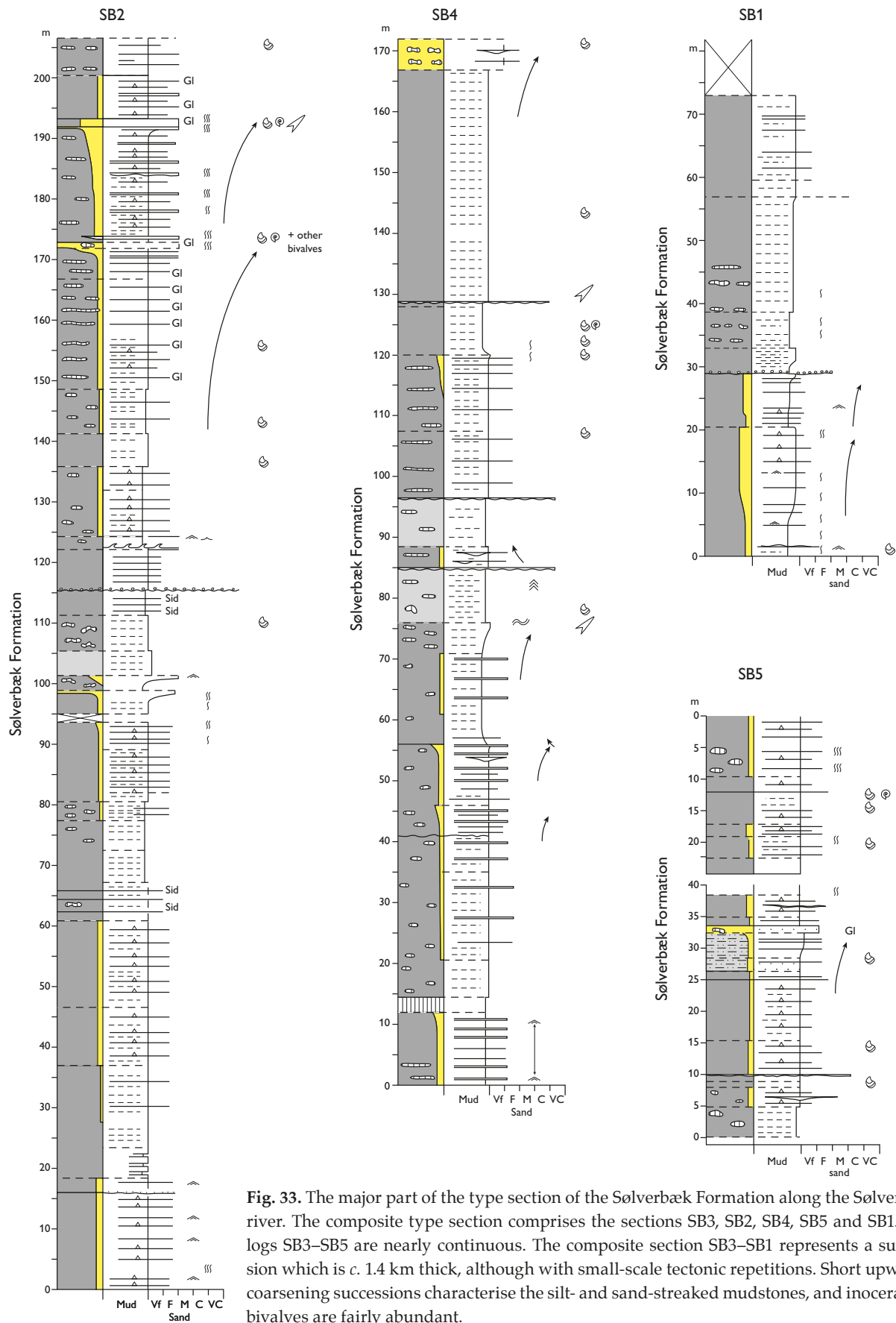


Fig. 33. The major part of the type section of the Sølverbæk Formation along the Sølverbæk river. The composite type section comprises the sections SB3, SB2, SB4, SB5 and SB1. The logs SB3–SB5 are nearly continuous. The composite section SB3–SB1 represents a succession which is c. 1.4 km thick, although with small-scale tectonic repetitions. Short upwards coarsening successions characterise the silt- and sand-streaked mudstones, and inoceramid bivalves are fairly abundant.

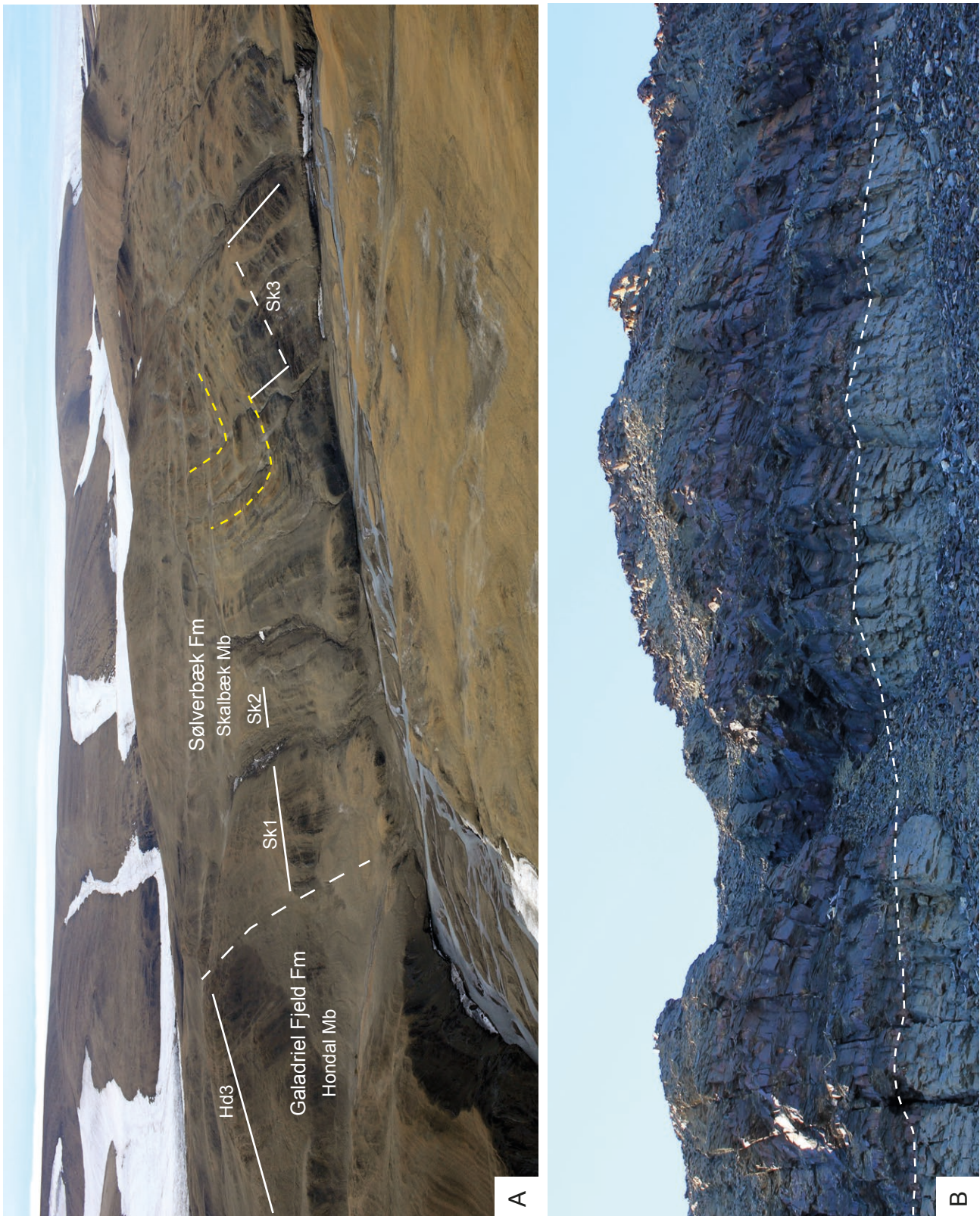


Fig. 34. Type and reference sections of the Skalbæk Member of the Sølverbæk Formation. **A:** Type section of the Skalbæk Member, north of Lille Hondal, view towards the west. The yellow dashed lines outline a distinct syncline. Locations of the sedimentological logs Sk1–Sk3 (Figs 3, 35, 36) are shown; they form a nearly continuous section through the lower part of the Sølverbæk Formation in Kilen Fjelde (Figs 5, 6). Section Sk3 is c. 160 m thick and consists of two parts correlated by a white dashed line. The boundary between the Hondal Member and the Skalbæk Member is also a formation boundary. It is covered by scree, but the approximate position is indicated by a white dashed line. **B:** Type section of the Røde Bakker Beds at Røde Bakker, Kilen Fjelde. The 17 m long sedimentological log RB1 (Fig. 37) covers the exposure. View towards the east-southeast.

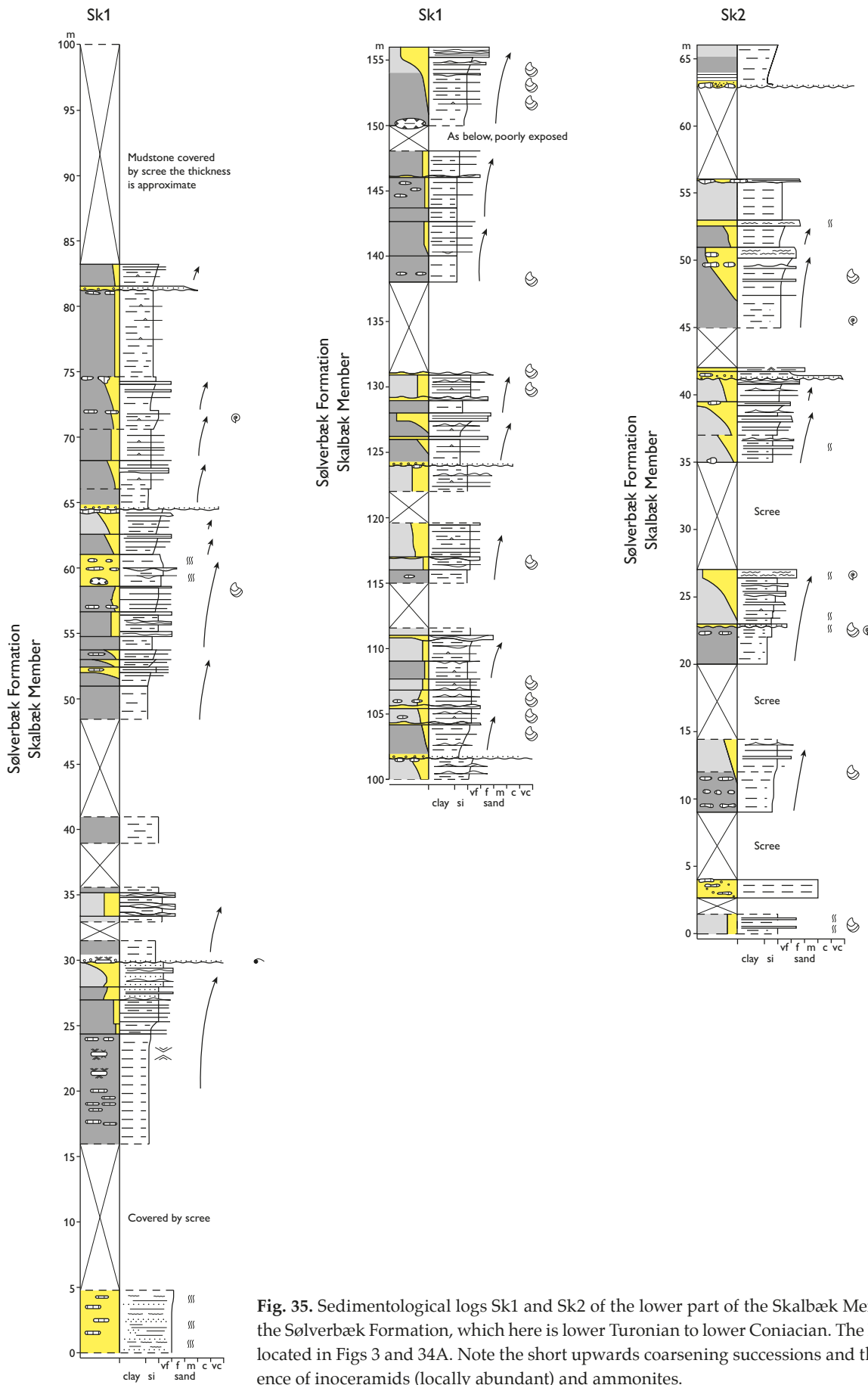
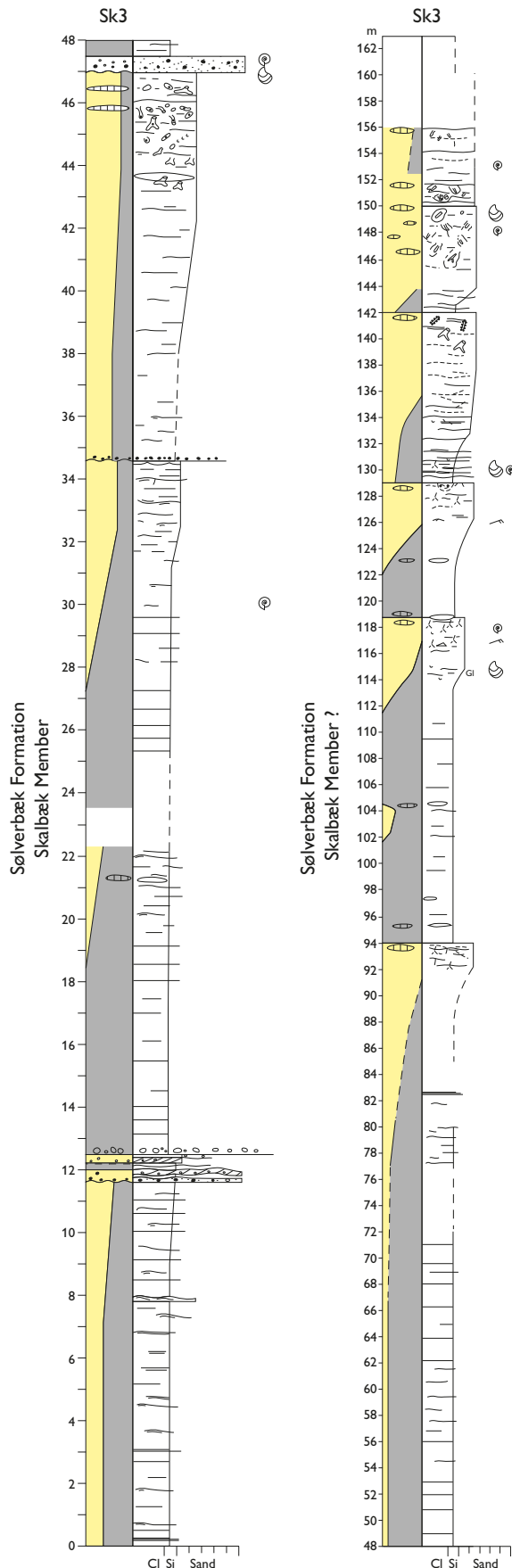


Fig. 35. Sedimentological logs Sk1 and Sk2 of the lower part of the Skalbæk Member of the Sølverbæk Formation, which here is lower Turonian to lower Coniacian. The logs are located in Figs 3 and 34A. Note the short upwards coarsening successions and the presence of inoceramids (locally abundant) and ammonites.



Boundaries. The lower boundary of the Skalbæk Member is also the lower boundary of the Sølverbæk Formation in Kilen Fjelde. The upper boundary is placed at the occurrence of dark mudstone (the Flagellarisslette mudstone) above a prominent siderite-rich sandstone interval (Røde Bakker Beds).

Fossils and age. The member is early Turonian to early Coniacian based on a very rich and diverse inoceramid fauna with 18 species and 99 specimens. Examples of inoceramids encountered are *Inoceramus apicalis* (from early middle Turonian), *Inoceramus lamarcki* (from middle Turonian), *Mytiloides striaconcentricus* (from late Turonian–early Coniacian) and *Inoceramus lusatie* (from late Turonian–early Coniacian) (Tröger & Christensen 1991, Walaszczyk & Wood 1998, Walaszczyk & Cobban 2016, among others). These species are also known from the Sølverbæk Formation at Gåseslette. Examples of common younger species are *Mytiloides africanus* and *Inoceramus annulatus*. These two species are also encountered at Gåseslette. Ammonites including worn specimens possibly of *Scaphites planus* indicate an early to middle Turonian age.

Lithological description. The Skalbæk Member comprises a number of upward coarsening successions, 5–50 m thick, ranging from fissile mudstone with siderite concretions, through sand-streaked mudstone and fine-grained sandstone to siderite-cemented conglomerates with intraformational clasts of mudstone and fragments of fossils (sections Sk1–Sk3, Figs 35, 36). The typical trace fossils represent the *Cruziana* ichnofacies.

Depositional environment. The fine grain size and the distribution of storm- and wave-generated structures, coupled with the fully marine fossils, the high bioturbation intensity and the trace fossil content, point to low wave energy and suggest that most of the Skalbæk Member was deposited in offshore to lower shoreface environments. The succession is overall shallowing-upwards, and the siderite-bearing conglomerates with their distinctive trace fossils indicate deposition in nearshore environments.

Røde Bakker Beds

New unit

Name and history. The Røde Bakker Beds include some of the sediments that were previously referred to the Røde Bakker Formation (Pedersen 1991; Håkansson

Fig. 36. Sedimentological log Sk3 of the upper part of the Skalbæk Member of the Sølverbæk Formation. The upper part of the type section west of the Hondal river. For location see Figs 3 and 34A. Section Sk3 overlies sections Sk1 and Sk2 (Figs 34A, 35).

et al. 1994). New biostratigraphic data suggest that the original formation may have included beds from various stratigraphic levels. Here the unit is revised to include only beds that crop out in the Røde Bakker–Skalbæk area and on the southern flank of the Saddelfjeld hill. The Røde Bakker Beds are included in the Skalbæk Member.

Distribution. The beds occur in Røde Bakker, at Skalbæk and at Saddelfjeld, in the north-eastern part of Kilen Fjelde (Fig. 3). It is possible that the Røde Bakker Beds occur in the Hondal syncline, but the limited exposures do not allow conclusive recognition of characteristic lithologies or stratigraphic trends.

Type section. The sedimentological log RB1 covers the type section at Røde Bakker (Figs 34B and 37). The base of the section is located at 81°18'35.3"N, 013°56'18.7"W.

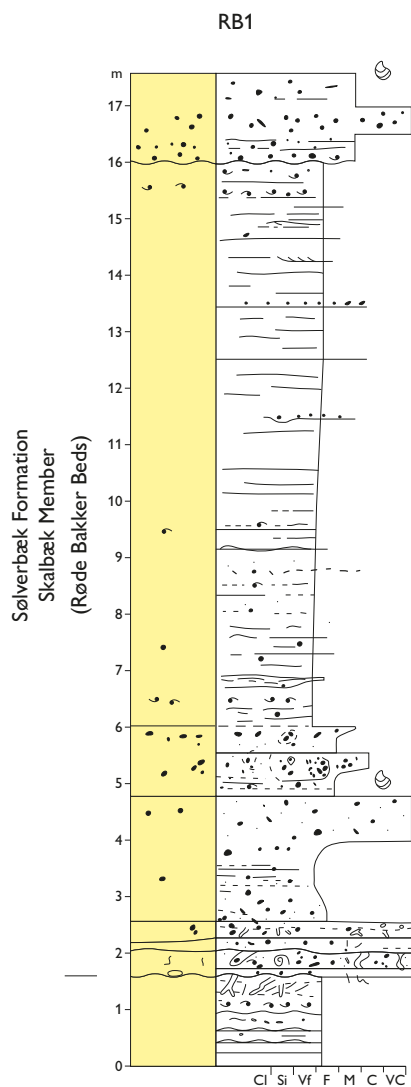


Fig. 37. Sedimentological log RB1 of the Røde Bakker Beds at the type section.

Thickness. The unit is 10–15 m thick.

Boundaries. The lower boundary is placed at the sharp transition from grey sandstone to red, siderite-cemented pebble and conglomerate beds (Fig. 34B). The upper boundary is placed at the first occurrence of black mudstone (the Flagellarisslette mudstone) at the base of the Scaphitesnæse Member.

Fossils and age. Fossils include inoceramids and ammonites. Four species of inoceramids exemplified by *Tethyoceramus wandereri* indicate an early Coniacian age when compared to Tröger & Christensen (1991), Walaszczyk (1992), and Walaszczyk & Wood (1998) (Fig. 6). The ammonite fauna is characterised by very large *Puzosia* specimens (Håkansson *et al.* 1993, their 'Unit 3'), whereas scaphitids are few.

Lithological description. The beds comprise reddish to greyish sandstones, pebbly sandstones and intraformational conglomerates with clasts of mudstone, carbonate and glauconite, and reworked clasts of apatite-cemented, fine-grained sediments (Håkansson *et al.* 1994; R. Weibel, personal communication 2017). A surface containing the *Glossifungites* ichnofacies demarcates the lower boundary of the Røde Bakker Beds.

Depositional environment. The unit is interpreted to represent a nearshore marine environment. The *Glossifungites* ichnofacies and associated intraformational conglomerates point to the formation of a hiatal surface and development of a firm ground surface.

Notes. Correlation of the Røde Bakker Beds from the Røde Bakker area with the type section of the Skalbæk Member in the Hondal area is uncertain at present. The unit may correlate with a siderite-cemented interval in the core of the Hondal syncline and/or an interval on the flank of the syncline (around 47 m in section Sk3, Fig. 36). If either of these occurrences proves to be Røde Bakker Beds in future studies, the lithological character of the Røde Bakker Beds is laterally variable.

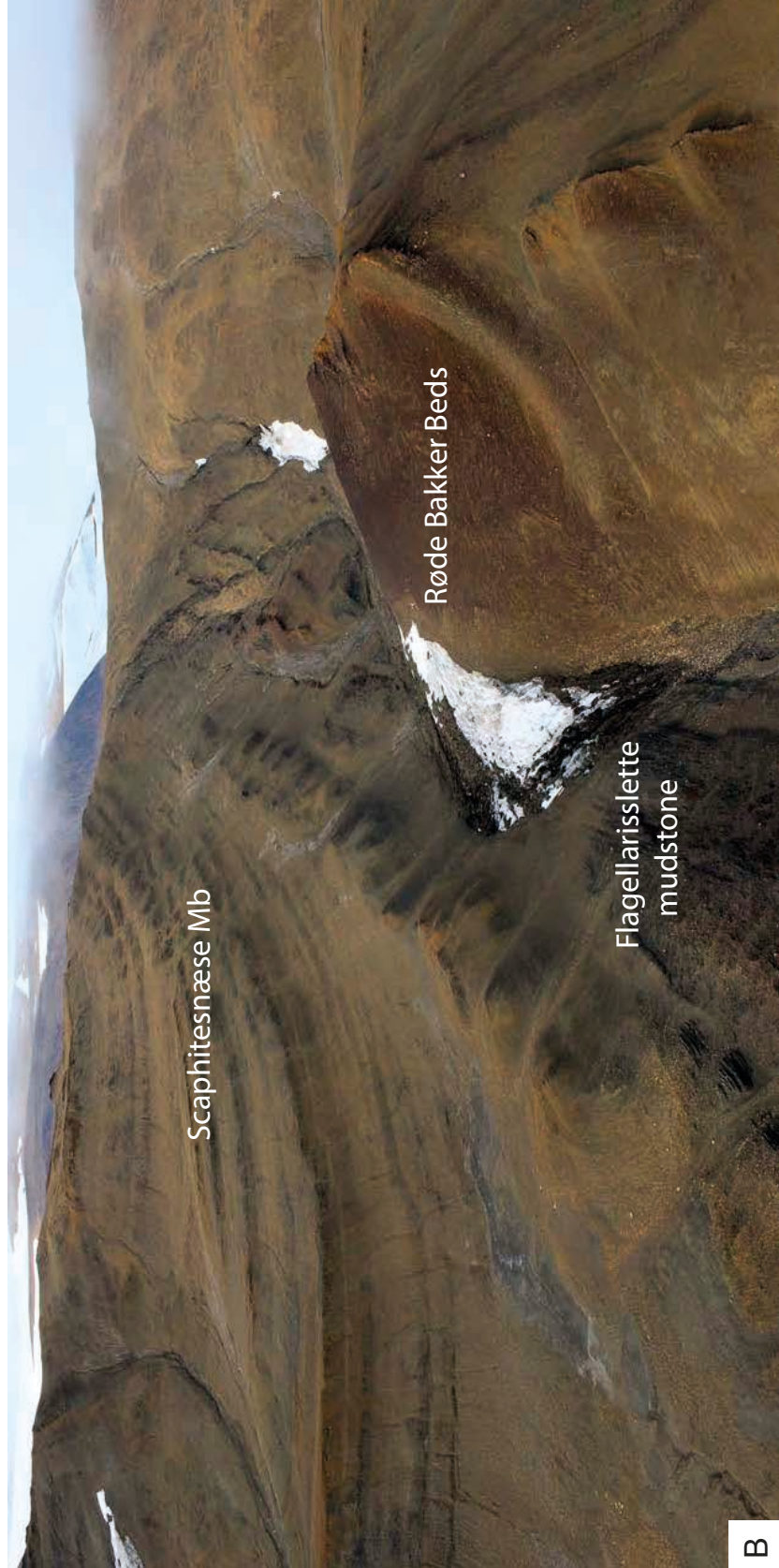
Scaphitesnæse Member

New member

Name and history. The Scaphitesnæse Member includes the sediments that were previously referred to the Flagellarisslette and Scaphitesnæse Formations by Pedersen (1991) and Håkansson *et al.* (1994). The Scaphitesnæse Member is the uppermost member of the Sølverbæk Formation in the Kilen Fjelde area.



A



B

Fig. 38. **A:** Type section of the Scaphitesnæse Member (Sølverbæk Formation), Saddelfjeld area, northernmost part of Kilen. View towards the north. Person (encircled) as a scale. The approximate location of the log Sn1 is shown. **B:** Reference section in the Scaphitesnæse–Saddelfjeld area. View towards the west. The Scaphitesnæse Member (including the Flagellarislette mudstone) is c. 280 m thick.

Subdivision. The Flagellarisslette mudstone constitutes the lower 130 m of the Scaphitesnæse Member in the Kilen Fjelde area.

Distribution. The Scaphitesnæse Member occurs in the north-eastern part of the Kilen Fjelde area (Fig. 3).

Type section. The Saddelfjeld area forms the type section (Fig. 38). The sedimentological log Sn1 illustrates the type section (Fig. 39). The base of the section is located at 81°19'42.6"N, 013°56'31.92"W.

Reference section. The Røde Bakker and Scaphitesnæse areas are the reference sections. The member is stratigraphically more complete here than in the type section but has not been logged.

Thickness. The member is more than 280 m thick (Svennevig *et al.* 2016).

Boundaries. Photogeological mapping shows that the Flagellarisslette mudstone overlies the Røde Bakker Beds of the Skalbæk Member (Svennevig 2018a). The lower boundary is placed at the first appearance of the mudstone succession on the top of siderite cemented conglomerates. The upper boundary is the present subaerial erosion surface.

Fossils and age. Inoceramids and ammonites are present. Håkansson *et al.* (1994) reported rich faunas, dominated by *Scaphites* and inoceramid bivalves, concentrated in the top of the glauconitic sandstones. The present study presents nine inoceramid species, some with relatively long ranges but indicating an early to middle Coniacian age when compared to Walaszczyk (1992). Examples are *Cremnoceramus crassus* (early Coniacian) and *Inoceramus seitzii* (early to middle Coniacian), which are recorded in both the Kilen Fjelde and the Gåseslette areas. The ammonite fauna, which can be rich in some horizons, includes scaphitids of *S. ex. gr. geinitzi* and *Kossmaticeras* (Alsen 2018b).

Lithological description. The member consists of interbedded mudstones and sandstones which form 20–30 m thick, upwards coarsening successions. Glauconite-rich, green sand intervals occur locally (Håkansson *et al.* 1994). The upper part of the member shows wave ripple cross-lamination, hummocky and swaley cross-stratification. The trace fossils represent the *Cruziana* ichnofacies.

Depositional environment. Based on the distribution of storm-generated sediment structures, the fossils as well as trace fossil characteristics, the Scaphitesnæse

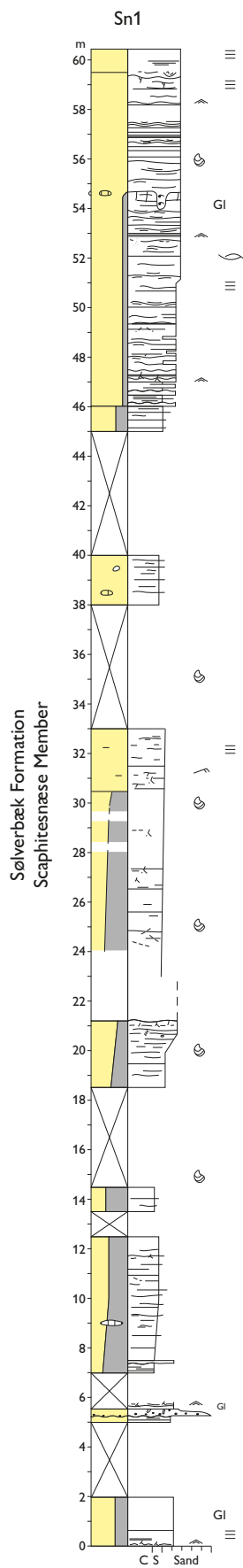


Fig. 39. Sedimentological log Sn1 of the Scaphitesnæse Member illustrating the upper part of the member in the type section at Saddelfjeld. For location of the log see Fig. 3.

Member is interpreted to represent storm-dominated offshore–shoreface environments.

Notes. The lower half of the Scaphitesnæse Member, including the basal fine-grained Flagellarisslette mudstone (see below), was not studied in the type section during the present study. Future work should include detailed documentation of the boundary between the Skalbæk and the Scaphitesnæse Members in the Røde Bakker area in order to gain better understanding of this stratigraphic interval. Furthermore, future work is needed to test whether the lower part of the Scaphitesnæse Member is present in the Hondal syncline (interval ~48–156 m in log Sk3, Fig. 36).

Flagellarisslette mudstone

Name and history. The Flagellarisslette mudstone is an informal lithostratigraphic unit which includes the sediments formerly referred to the Flagellarisslette Formation (Pedersen 1991; Håkansson *et al.* 1994). The name derives from the plant *Saxifraga flagellaris*, which grows on the plain (Håkansson *et al.* 1993, their table 1). The unit constitutes the lower part of the Scaphitesnæse Member. It was not studied during the recent field work and is therefore not formalised.

Distribution. Identical to the distribution of the Scaphitesnæse Member (see Fig. 3).

Type section. The Røde Bakker area.

Thickness. The Flagellarisslette mudstone is 130 m thick (Svennevig *et al.* 2016).

Boundaries. The lower boundary is identical to the lower boundary of the Scaphitesnæse Member. The upper boundary is located at the top of a c. 10 m thick sandstone.

Fossils and age. Inoceramids and ammonites were reported by Håkansson *et al.* (1994). The unit is thought to range from early to middle Coniacian? (Fig. 6).

Lithological description. The lithological description is adapted from Håkansson *et al.* (1994) without changes: “Very uniform upwards coarsening sequence of greyish silty mudstone with storm-sand layers throughout. Topped by c. 10 m thick sandstone.” (Håkansson *et al.* 1994, p. 7).

Depositional environment. The unit is tentatively interpreted to represent a storm-dominated offshore environment due to the distribution of tempestites (Håkansson *et al.*, 1994) and the sedimentary facies

of the overlying part of the Scaphitesnæse Member (see above).

Implications

The Wandel Sea Basin – and Kilen in particular – is a key area for the understanding of the Mesozoic stratigraphy of the Arctic. Together with the biostratigraphic advances, the new lithostratigraphic scheme allows a more straightforward correlation to other arctic areas and forms a robust basis for future sequence stratigraphic and tectonostratigraphic interpretations.

The main changes to the previous lithostratigraphic schemes include a simplification of the ‘mid’ to Upper Cretaceous lithostratigraphy of Kilen (Fig. 5). Previously the strata in Kilen Fjelde were referred to two groups and fifteen formations, while the strata in the Gåseslette area constituted four formations in one group. The new data on lithologies and fossils have allowed a correlation from Kilen Fjelde to Gåseslette, and all the late Aptian to Santonian strata throughout Kilen are now referred to the Galadriel Fjeld and Sølverbæk Formations. Other key changes include the assignment of the Mågensfjeld Formation to the Middle Jurassic instead of the Upper Cretaceous, the recognition of a new Gletscherport Formation below the upper Bajocian interval, and the dating of the Galadriel Fjeld Formation. The redefined Mågensfjeld Formation can be directly correlated with the Pelion Formation in North-East Greenland (e.g. Engkilde & Surlyk 2003), whereas the Galadriel Fjeld Formation correlates closely with the Carolinefjellet Formation on Svalbard (Grundvåg & Olausen 2017) and the Christopher Formation of the Sverdrup Basin (Schröder-Adams *et al.* 2014; Sheldon *et al.* 2017). The redefined Sølverbæk Formation correlates with the Kveite Formation on the Barents shelf, see e.g. Nøtvedt *et al.* (2008).

Finally, there are several significant lithological boundaries that may prove useful in future regional correlations. These include the boundary between the Galadriel Fjeld Formation and the overlying Sølverbæk Formation, where there is a major change in lithology from upper offshore to middle shoreface deposits, dominated by sandstones, to shelf mudstone. Future studies may show faunal changes across this boundary, which would strengthen the value of the Sølverbæk Formation for regional correlation. It is possible that the flooding can be correlated to the extensive late Cenomanian transgression in northern Canada, the Western Interior Seaway and Baffin Bay (Schröder-Adams *et al.* 2014).

Acknowledgements

We are grateful to Andrew Whitham and Lars Stemmerik for constructive reviews that significantly improved the paper, and to the editor Lotte Melchior Larsen for her detailed editorial corrections and the smooth handling of the manuscript. Jette Halskov skillfully prepared all the illustrations. The field work was funded by the Geological Survey of Denmark and Greenland (GEUS), and the paper is published with permission of the director of GEUS. We direct our sincere thanks to all these persons and to GEUS.

References

- Alsen, P. 2018a: A hoplitinid–gastropplitinid ammonite assemblage in North Greenland - linking the upper middle Albian in the Arctic with NW Europe. In: Bengtson, P. (ed.), *Cretaceous Ammonites: A volume in Memory of Richard A. Reyment (1926–2016)*, *Cretaceous Research*, 9 pp, in press. <https://doi.org/10.1016/j.cretres.2017.10.018>.
- Alsen, P. 2018b: *Kossmaticeras* in North Greenland. In: Bengtson, P. (ed.), *Cretaceous Ammonites: A volume in Memory of Richard A. Reyment (1926–2016)*, *Cretaceous Research*, 10 pp, in press. <https://doi.org/10.1016/j.cretres.2017.10.010>.
- Alsen, P., McRoberts, C., Svennevig, K., Bojesen-Koefoed, J., Hovikoski, J. & Piasecki, S. 2017: The Isrand Formation: a Middle Triassic *Daonella*-bearing, black shale unit in Kilen, North Greenland (with a note on the Triassic in Amdrup Land). *Newsletters on Stratigraphy* 50(1), 31–46.
- Bengaard, H.J. & Henriksen, N. 1986: Geological map of Greenland 1:500 000, Sheet 8, Peary Land. Copenhagen: Geological Survey of Greenland.
- Birkelund, T. & Håkansson, E. 1983: The Cretaceous of North Greenland – a stratigraphic and biogeographical analysis. *Zitteliana* 10, 7–25.
- Cohen, K.M., Finney, S.C., Gibbard, P.L. & Fan, J.-X. 2013 (updated 2017): The ICS International Chronostratigraphic Chart. *Episodes* 36, 199–204.
- Crame, J.A. 1985: Lower Cretaceous Inoceramid bivalves from the Antarctic Peninsula region. *Palaeontology* 28, 475–525.
- Dallmann, W.K. *et al.* 1999: Lithostratigraphic Lexicon of Svalbard: Review and Recommendations for Nomenclature Use: Upper Palaeozoic to Quaternary Bedrock. Tromsø: Norsk Polarinstitutt, 318 pp.
- Dawes, P. & Soper, J. 1973: Pre-Quaternary history of North Greenland. In: Pitcher, M.G. (ed.), *Arctic Geology. Memoir of the American Association of Petroleum Geologists* 19, 117–134.
- Donovan, D.T. 1953: The Jurassic and Cretaceous stratigraphy and palaeontology of Traill Ø, East Greenland, *Meddelelser om Grønland* 111, 150 pp.
- Dypvik, H., Håkansson, E. & Heinberg, C. 2002: Jurassic and Cretaceous palaeogeography and stratigraphic comparisons in the North Greenland–Svalbard region. *Polar Research* 21(1), 91–108.
- Engkilde, M. & Surlyk, F. 2003: Shallow marine syn-rift sedimentation: Middle Jurassic Pelion Formation, Jameson Land, East Greenland. In: Ineson, J.R. & Surlyk, F. (eds), *The Jurassic of Denmark and Greenland*. Geological Survey of Denmark and Greenland Bulletin 1, 813–863.
- Grasby, S.E., McCune, G.E., Beauchamp, B. & Galloway, J.M. 2017: Lower Cretaceous cold snaps led to widespread glendonite occurrences in the Sverdrup Basin, Canadian High Arctic. *GSA Bulletin* 129(7/8), 771–787, doi: 10.1130/B31600.1.
- Grundvåg, S.A. & Olausen, S. 2017: Sedimentology of the Lower Cretaceous at Kikutodden and Keilhaufjellet, southern Spitsbergen: implications for an onshore–offshore link. *Polar Research* 36(1), 20 pp. doi: 10.1080/17518369.2017.1302124.
- Håkansson, E. 1979: Carboniferous to Tertiary development of the Wandel Sea Basin, eastern North Greenland. In: Report on the 1978 Geological Expedition to the Peary Land Region, North Greenland. Rapport Grønlands Geologiske Undersøgelse 88, 73–83.
- Håkansson, E. 1994: Scaphitid ammonoids and inoceramids bivalves from Upper Cretaceous strata in North Greenland. In: Håkansson, E. (ed.), *Wandel Sea Basin: Basin analysis*. EFP-91, project No. 0012, Geological Institute, University of Copenhagen, Scientific report 14, 8 pp.
- Håkansson, E. & Pedersen, S.A.S. 1982: Late Paleozoic to Tertiary tectonic evolution of the continental margin in North Greenland. In: Embry, A.F. & Balkwill, H.R. (eds), *Arctic Geology and Geophysics: Proceedings of the Third International Symposium on Arctic Geology*. Canadian Society of Petroleum Geology, Calgary, 331–348.
- Håkansson, E. & Pedersen, S.A.S. 2015: A healed strike-slip plate boundary in North Greenland indicated through associated pull-apart basins. *Geological Society, London, Special Publications* 413, 143–169.
- Håkansson, E. & Stemmerik, L. 1984: Wandel Sea Basin: the North Greenland equivalent to Svalbard and the Barents Shelf. In: Spencer A.M. (ed.), *Petroleum geology of the North European margin*. Proceedings of symposium organised by the Norwegian Petroleum Society, 97–107. London: Graham and Trotman.
- Håkansson, E. & Stemmerik, L. 1989: Wandel Sea basin: A new synthesis of the late Paleozoic to Tertiary accumulation in North Greenland. *Geology* 17, 683–686. doi:10.1130/0091-7613(1989)017<0683>
- Håkansson, E., Birkelund, T., Piasecki, S. & Zakharov, V. 1981a: Jurassic–Cretaceous boundary strata of the extreme arctic (Peary Land, North Greenland). *Bulletin of the Geological Society of Denmark* 30, 11–42.
- Håkansson, E., Heinberg, C. & Stemmerik, L. 1981b: The Wandel Sea basin from Holm Land to Lockwood Ø, eastern North Greenland. In: Report on the 1980 Geological Expedition to the Peary Land Region, North Greenland. Rapport Grønlands Geologiske Undersøgelse 106, 47–63.

- Håkansson, E., Heinberg, C. & Stemmerik, L. 1991: Mesozoic and Cenozoic history of the Wandel Sea Basin area, North Greenland. In: Peel, J. S. & Sønderholm, M. (eds), *Sedimentary Basins of North Greenland*. Bulletin Grønland geologiske Undersøgelse 160, 153–164.
- Håkansson, E., Birkelund, T., Heinberg, C., Hjort, C., Mølgaard, P. & Pedersen, S.A.S. 1993: The Kilen Expedition 1985. Bulletin of the Geological Society of Denmark 40, 9–32.
- Håkansson, E., Heinberg, C. & Pedersen, S.A.S. 1994: Geology of Kilen. In: Håkansson, E. (ed.), *Wandel Sea Basin: Basin analysis*. EFP-91, project No. 0012, Geological Institute, University of Copenhagen, Scientific report 16, 13 pp.
- Heinberg, C. & Håkansson, E. 1994: Late Jurassic – Early Cretaceous stratigraphy and depositional environment. In: Håkansson, E. (ed.), *Wandel Sea Basin: Basin analysis*. EFP-91, project No. 0012, Geological Institute, University of Copenhagen, Scientific report 12, 8 pp.
- Henriksen, N. 2003: Caledonian Orogen, East Greenland 70°–82° N. Geological Map 1:1 000 000. Copenhagen: Geological Survey of Denmark and Greenland.
- Imlay, R.W. 1961: Characteristic Lower Cretaceous megafossils from northern Alaska. U.S. Geological Survey Professional Paper 335, 74 pp.
- Jeletzky, J.A. 1964: Illustrations of Canadian fossils. Lower Cretaceous marine index fossils of the sedimentary basins of western and Arctic Canada. Geological Survey of Canada Papers 64-11, 1–101.
- Jeletzky, J.A. 1968: Macrofossil zones of the marine Cretaceous of the Western Interior of Canada and their correlation with the zones and stages of Europe and the Western Interior of the United States. Geological Survey of Canada Papers 67-72, 1–66.
- Kauffman, E.G. 1977: Illustrated guide to biostratigraphically important Cretaceous macrofossils, Western Interior Basin, USA. *Mountain Geologist* 14, 225–274.
- Keller, S. 1982: Die Oberkreide der Sack-Mulde bei Alfeld (Cenoman – Unt-Coniac), Lithologie, Biostratigraphie und Inoceramen. *Geologisches Jahrbuch*, A64, 3–171.
- Kelly, S.R.A., Whitham, A.G., Koraini, A.M. & Price, S.P. 1998: Lithostratigraphy of the Cretaceous (Barremian–Santonian) Hold with Hope Group, NE Greenland. *Journal of the Geological Society*, London 155, 993–1008.
- Muttrux, J., Maher, H., Shuster, R. & Hays, T. 2008: Iron ooid beds of the Carolinefjellet Formation, Spitsbergen, Norway. *Polar Research* 27, 28–43, doi:10.1111/j.1751-8369.2007.00039.x
- Nielsen, E. 1941: Remarks on the map and the geology of Kronprins Christians Land. *Meddelelser om Grønland* 126(2), 34 pp.
- Nøhr-Hansen, H. 1993: Dinoflagellate cyst stratigraphy of the Barremian to Albian, Lower Cretaceous, North-East Greenland. *Bulletin Grønlands Geologiske Undersøgelse* 166, 171 pp.
- Nøttvedt, A., Johannessen, E.P. & Surlyk, F. 2008: The Mesozoic of Western Scandinavia and East Greenland. *Episodes* 31(1), 59–65.
- Pchelina, T.M. 1965: Mesozoyskiye otlozhchniya rayona Van Kycylcnf'orda (Zapadnyy Shpitsbergen) [Mesozoic deposits around Van Keulenfjorden, Vestspitsbergen]. In: Sokolov, V.N. (ed.), *Muteriuly pogeologii Shpitsbergenu* [Materials on the geology of Spitsbergen]. Nauch. Isslud. Institut Geologii Arktiki, Leningrad.
- Pedersen, S.A.S. 1991 (compiled 1989): Geological map of Kilen, Kronprins Christian Land, North Greenland, 1:100 000 (unpublished). In the archives of the Geological Survey of Denmark and Greenland (GEUS), Copenhagen. http://data.geus.dk/geusmapmore/get_binary_mapdb.jsp?digitalmap_id=4313.
- Pedersen, S.A.S. & Håkansson, E. 2001: Kronprins Christian Land Orogeny, deformational Styles of the End Cretaceous Transpressional Mobile Belt in Eastern North Greenland. *Polarforschung* 69, 117–130.
- Pemberton, S.G., MacEachern, J.A., Dashtgard, S.E., Bann, K.L., Gingras, M.K. & Zonneveld, J.-P. 2012: Shorefaces. *Developments in Sedimentology* 64, 563–603.
- Pergament, M.A. 1965: Inocerams and Cretaceous stratigraphy of the Pacific region. *Trudy Inst. Geol. Nauk. Moskva* 118, 1–102.
- Piasecki, S., Nøhr-Hansen, H. & Dalhoff, F. 2018: Revised stratigraphy of Kap Rigsdagen beds, Wandel Sea Basin, North Greenland. *Newsletters on Stratigraphy*, published online February 2018, doi: 10.1127/nos/2018/0444, 15 pp.
- Piepjoh, K. & von Gosen, W. 2001: Polyphase deformation at the Harder Fjord Fault Zone (North Greenland). *Geological Magazine* 138(4), 407–434.
- Price, G.D. & Nunn, E.V. 2010: Valanginian isotope variation in glendonites and belemnites from Arctic Svalbard: Transient glacial temperatures during the Cretaceous greenhouse. *Geology* 38, 251–254, doi:10.1130/G30593.1.
- Rolle, F. 1981: Hydrocarbon source rock sampling in Peary Land 1980. *Rapport Grønlands Geologiske Undersøgelse* 106, 99–103.
- Røhr, T.S., Andersen, T. & Dypvik, H. 2008: Provenance of Lower Cretaceous sediments in the Wandel Sea Basin, North Greenland. *Journal of the Geological Society*, London 165, 755–767.
- Schröder-Adams, C.J., Herrle, J.O., Embry, A.F., Haggart, J.W., Galloway, J.M., Pugh, A.T. & Harwood, D.M. 2014: Aptian to Santonian foraminiferal biostratigraphy and paleoenvironmental change in the Sverdrup Basin as revealed at Glacier Fiord, Axel Heiberg Island, Canadian Arctic Archipelago. *Palaeogeography, Palaeoclimatology, Palaeoecology* 413, 81–100, doi:10.1016/j.palaeo.2014.03.010.
- Sheldon, E., Lauridsen, B.W. & Alsen, P. 2017: Lower Cretaceous Biostratigraphy of Kilen and Peary Land, Wandel Sea Basin, North Greenland, and its implications for correlation with the Sverdrup Basin, Arctic Canada. Abstract, AAPG 3P (Polar Petroleum Potential) Conference, London, October 15th–18th 2017.
- Soper, N.J., Higgins, A. & Friderichsen, J.D. 1980: The North Greenland fold belt in eastern Johannes V. Jensen Land.

- Rapport Grønlands Geologiske Undersøgelse 99, 89–98.
- Stemmerik, L., Dalhoff, F., Larsen, B.D., Lyck, J., Mathiesen, A. & Nilsson, I. 1998: Wandel Sea Basin, eastern North Greenland. *Geology of Greenland Survey Bulletin* 180, 55–62.
- Stolley, E. 1912: Über die Kreideformation und ihre Fossilien auf Spitzbergen. *Kungliga Svenske Vetenskapsakademien Handlingar* 47(11), Stockholm, 1–29.
- Surlyk, F. & Zakharov, V. 1982: Buchiid bivalves from the Upper Jurassic and Lower Cretaceous of East Greenland. *Palaeontology* 25(4), 727–753.
- Svennevig, K. 2018a: Geological map of Kilen - eastern North Greenland 1:100.000, Kilen 81 Ø.1 Syd. Copenhagen: Geological Survey of Denmark and Greenland, in press.
- Svennevig, K. 2018b: Update of the seamless 1:500 000 scale geological map of Greenland based on recent fieldwork in the Wandel Sea Basin, eastern North Greenland. *Bulletin of the Geological Survey of Denmark and Greenland* 41, 4 pp, in press.
- Svennevig, K., Guarnieri, P. & Stemmerik, L. 2015: From oblique photogrammetry to a 3D model – Structural modeling of Kilen, eastern North Greenland. *Computers & Geosciences* 83, 120–126, doi: 10.1016/j.cageo.2015.07.008.
- Svennevig, K., Guarnieri, P. & Stemmerik, L. 2016: Tectonic inversion in the Wandel Sea Basin: a new structural model of Kilen (eastern North Greenland). *Tectonics* 35, 1–34, doi: 10.1002/2016TC004152.
- Svennevig, K., Guarnieri, P. & Stemmerik, L. 2017: 3D restoration of a Cretaceous rift basin in Kilen, eastern North Greenland. *Norwegian Journal of Geology* 97, 21–32, doi: 10.17850/njg97-1-02.
- Svennevig, K., Alsen, P., Guarnieri, P., Hovikoski, J., Lauridsen, B.W., Pedersen, G.K., Nøhr-Hansen, H. & Sheldon, E. 2018: Descriptive text to the Geological map of Kilen, eastern North Greenland 1:100 000, Kilen 81 Ø.1 Syd. Geological Survey of Denmark and Greenland Map Series 8, in press.
- Tröger, K.-A. 1967: Zur Paläontologie, Biostratigraphie und faziellen Ausbildung der unteren Oberkreide (Cenoman bis Turon). Teil 1. Paläontologie und Biostratigraphie der Inoceramen des Cenomans und Turons Mitteleuropas. *Abhandlung Staatliche Museum Mineralogie und Geologie* 12, 13–207.
- Tröger, K.-A. & Christensen, W.K. 1991: Upper Cretaceous (Cenomanian – Santonian) inoceramid bivalve faunas from the island of Bornholm, Denmark. *Danmarks Geologiske Undersøgelse, Serie A* 28, 1–47.
- Vickers, M.L., Price, G.D., Jerrett, R.M. & Watkinson, M. 2016: Stratigraphic and geochemical expression of Barremian–Aptian global climate change in Arctic Svalbard: *Geosphere* 12(5), 1594–1605, doi:10.1130/GES01344.1.
- Walaszczyk, I. 1992: Turonian through Santonian deposits of the Central Polish Uplands; their facies development, inoceramid palaeontology and stratigraphy. *Acta Geologica Polonica* 42, 122 pp.
- Walaszczyk, I. & Wood, C.J. 1998: Inoceramids and biostratigraphy at the Turonian/Coniacian boundary; based on the Salzgitter-Salder Quarry, Lower Saxony, Germany, and the Słupia Nadbrzezna section, Central Poland. *Acta Geologica Polonica* 48, 395–434.
- Walaszczyk, I. & Cobban, W.A. 2016: Inoceramid bivalves and biostratigraphy of the upper Albian and lower Cenomanian of the United States Western Interior Basin. *Cretaceous Research* 59, 30–69.
- Woods, H. 1911–1912: A monograph of the Cretaceous Lamellibranchia of England, Vol II, parts VII and VIII. Palaeontographical Society, London, 261–284 and 285–340.

A multi-disciplinary macrofossil study of late glacial to early Holocene sediments from Søndre Kobberdam, Hareskovene, Denmark

OLE BENNIKE & MORTEN FISCHER MORTENSEN



Bennike, O. & Mortensen, M.F. 2018. A multi-disciplinary macrofossil study of late glacial to early Holocene sediments from Søndre Kobberdam, Hareskovene, Denmark. © 2018 by Bulletin of the Geological Society of Denmark, Vol. 66, pp. 113–122. ISSN 2245-7070. (www.dgf.dk/publikationer/bulletin).

During the early part of the Allerød period, from c. 13 600 to 13 330 years BP, unstable soils with a tundra-like open, treeless vegetation with *Betula nana* and *Dryas octopetala* were found around Søndre Kobberdam in Hareskovene. Open *Betula pubescens* woodland was not established until the middle Allerød about 13 330 years BP. During the Younger Dryas, *Betula nana* and *Dryas octopetala* spread again, and *Betula pubescens* almost disappeared. From the onset of the Holocene warming an open tundra landscape characterised the area. About 11 300 years BP *Betula pubescens* started to recolonise the region and *Populus tremula* and *Pinus sylvestris* arrived at c. 11 000 years BP, replacing the open landscape by woodland. Along the margin of the lake *Carex paniculata*, *Carex riparia* and *Cladium mariscus* were growing. The lake fauna included a rich and diverse fauna of molluscs that thrived in the carbonate-rich waters. We did not find any evidence for the local presence of *Pinus sylvestris* during the late glacial.

Keywords: Late glacial, vegetation history, fauna history, immigration history, Denmark.

Ole Bennike [ole@geus.dk], Geological Survey of Denmark and Greenland, Øster Voldgade 10, DK-1350 Copenhagen K, Denmark. Morten Fischer Mortensen [morten.fischer.mortensen@natmus.dk], The National Museum of Denmark, I.C. Modewegs Vej, DK-2800 Kongens Lyngby, Denmark.

Corresponding author: Ole Bennike

The study of macrofossils has a long history in Denmark, which is due to the former exploitation of peat and interest in how peat formed. In the beginning of the 1800s there was a great demand for peat in Denmark, particularly in Copenhagen, and huge amounts of peat were cut in bogs north of the city. As much as 70 000 wagonloads of peat were transported by horses to the capital each year (Garboe 1961). This exploitation led to interest in understanding how peat was formed, and in 1816 the Danish Agricultural Society (Landhusholdningsselskabet) offered a prize for a paper on this subject. No one responded, so the price was offered again in 1819, and this time a paper was submitted by Heinrich Dau. Sadly, the high quality of Dau's pioneering work was not recognised, and he did not win the prize, but he published his work as a book (Dau 1823). Dau continued to study peat and published a new book on the results, where he mentioned that he had found remains of *Pinus*, *Betula*, *Quercus* and *Alnus* in bogs on Sjælland, and that these remains showed that the vegetation had changed over time (Dau 1829).

However, soon after he committed suicide (Rørdam 1914; Garboe 1961).

In 1835 the Royal Danish Academy of Sciences offered a new prize for a study of peat formation, and a manuscript was submitted by Japetus Steenstrup who won high honours for the work. Steenstrup established a zonation for Holocene vegetation development in north-eastern Sjælland, with four zones, successively *Populus*, *Pinus*, *Quercus* and *Alnus* (Steenstrup 1842). In 1871 A.G. Nathorst from Sweden found remains of arctic plants in late glacial sediments in north-eastern Sjælland (Nathorst 1892, 1914). Steenstrup's work on plant macrofossils in Danish deposits was continued by Nicolaj Hartz who concentrated on late glacial and interglacial deposits (Hartz & Milthers 1901; Hartz 1902, 1909). Hartz and Milthers found evidence of a warm late glacial period in the Allerød clay pit. Numerous later works on the vegetation history of Denmark have been conducted, mainly based on pollen analysis alone. In recent years, however, the importance of macrofossils has been recognised again

(e.g. Birks 1993; Mortensen *et al.* 2011). Macrofossils have a number of advantages compared with pollen. For example, macrofossils do not spread as far and wide as pollen and may therefore provide a better picture of the local vegetation. The local presence of prolific pollen producers, such as *Betula* and *Pinus*, is particularly difficult to establish from pollen analysis. Another advantage is that macrofossils commonly can be determined to species, whereas pollen grains commonly can be determined to genus or family only. Moreover, it is possible to use samples of macroscopic plant remains for radiocarbon age determinations by accelerator mass spectrometry (AMS). In this way it is possible to directly date remains of key species and provide minimum ages for the timing of their immigration to the study site.

Even though studies of the vegetation history of Denmark go back almost 200 years, and even though many studies have been conducted in past decades, many details of late glacial and Holocene vegetation and environmental changes are still poorly known. The aim of this paper is to describe and interpret the results of macrofossil studies of Søndre Kobberdam, a small lake basin in Hareskovene, north-eastern Sjælland, not far from the classical sites investigated by Steenstrup and Hartz. The study is the first radiocarbon dated macrofossil study of late glacial deposits from north-eastern Sjælland. Data from the site were used in the analysis by Mortensen *et al.* (2014a, supplementary material), but no details were provided. The results are compared with other recent detailed works on late glacial and early Holocene deposits in Denmark (Bennike *et al.* 2004; Mortensen *et al.* 2011, 2014a, b; Fischer *et al.* 2013).

Study area

The studied lake, Søndre Kobberdam, is located in north-eastern Sjælland, approximately 13 km from the centre of Copenhagen and 9.4 km south-south-west of the classical Allerød clay pit locality (Fig. 1; Hartz & Milthers 1901). Søndre Kobberdam is located in the eastern part of Hareskovene. There are three small lakes east of a hill named Højnæsbjerg, which reaches a height of 48 m above sea level. The lakes are named Kobberdammene and Søndre Kobberdam is the southernmost of them (Gladsaxe 2017). Because of its small size it was considered suitable for plant macrofossil analyses. The lake is oval in shape and measures 60 × 40 m; it is located 21 m above sea level and was presumably formed as a kettle hole by melting of a body of stagnant ice. The geographical coordinates of the coring site are 55°46.33'N, 12°26.29'E and the water depth was 450 cm.

The region was glaciated during the last glacial maximum and was deglaciated between 17 000 and 18 000 years BP, according to cosmogenic surface exposure dating of large erratic boulders (Houmark-Nielsen *et al.* 2012). The pre-Quaternary bedrock of the region consists of Lower Tertiary (Danian) limestone, and the area is a moraine landscape that formed during the Weichselian. It is dominated by glaciofluvial sand and gravel and sandy clayey till (Milthers 1922). The glacial and glaciofluvial deposits are carbonate-rich except near the soil surface where they have been leached during the Holocene. The landscape is hilly with numerous kettle holes and the area is unsuitable for agriculture due to its poor nutrient status and because it is hilly. Hence parts of the area have probably been covered by forests during most of the Holocene. The present

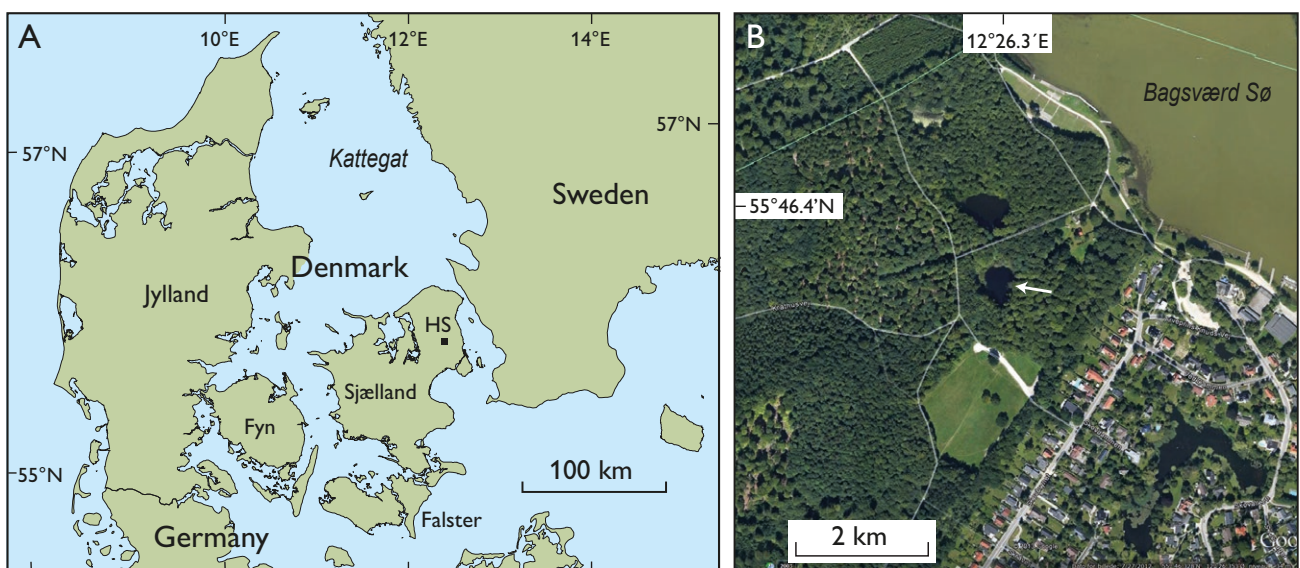


Fig. 1. A. Map of Denmark showing the location of Hareskovene (HS). B. Google Earth satellite image of the study area. The arrow shows Søndre Kobberdam.

day forests in Hareskovene are dominated by *Fagus sylvestris*, with some *Quercus robur* and *Tilia cordata* on well-drained soils. Moist and wet soils are dominated by *Ulmus glabra*, *Fraxinus excelsior*, *Alnus glutinosa*, *Betula pubescens* and *Betula pendula*. *Acer pseudoplatanus* is currently spreading rapidly. The climate is temperate; the mean July temperature was 17.1°C and the mean annual precipitation was 620 mm during the period from 1982 to 2012, according to <https://da.climate-data.org/>.

Methods

Coring was carried out in the central and deepest part of the lake, in winter during a short cold period when the lake was ice-covered. The coring equipment was a Russian peat corer with a chamber length of 100 cm and a diameter of 7.5 cm (Jowsey 1966). We took overlapping cores to ensure that the nose of the corer did not disturb the sediments below. The cores were transferred from the corer to plastic liners, and whole cores were brought to the laboratory where the cores were opened and correlated visually. The cores were carefully cleaned to avoid down-core contamination, and 64 contiguous samples of 2 cm length were taken for macrofossil analysis. The samples were wet sieved

on 0.4 and 0.2 mm sieves and the residues left on the sieves were transferred to petri dishes and investigated using a dissecting microscope. Plant and animal remains were identified using reference material as well as keys and illustrations in books and papers.

Selected identified macrofossils of terrestrial plants from four levels were dried and submitted for accelerator mass spectrometry (AMS) radiocarbon dating. Dating was carried out at the Universities of Cologne (COL) and Lund (LuS). The radiocarbon ages were calibrated to calendar years before present (BP) using the CALIB program (Stuiver *et al.* 2017) which calibrates to calendar years according to the INTCAL13 data. In this paper we only discuss calibrated ages. The widespread occurrence of carbonate-rich glacial deposits in Denmark results in large hard-water effects, and hence it is important to use remains of terrestrial plants for dating.

Results

Sediments, dating and sedimentation rates

The analysed core was 155 cm long (Fig. 2). The lower part of the succession from 630 to 573 cm below lake level consists of layered fine-grained sand and silt, and the upper part from 573 to 475 cm consists of gyttja. Thin clay layers are found at 550–551 cm and at 543–544.5 cm. The gyttja is homogenous up to 507 cm and laminated in the upper part. Above 475 cm a thin layer of greenish, fresh-looking *Fagus sylvatica* leaves was found. This indicates that a major part of the Holocene sediments is missing. As mentioned above, large amounts of peat have been cut in bogs north of Copenhagen, and it is likely that peat digging transformed a former bog into a lake during the 1800s and is the reason for the lack of Holocene sediments.

The late glacial and early Holocene stratigraphy in Søndre Kobberdam differs from other sites in the area. The sediments in the Allerød clay pit consisted of clay, Allerød gyttja, Younger Dryas clay and Holocene peat, and similar successions have been found in other clay pits on Sjælland (Hartz & Milthers 1901; Hartz 1902; Krog 1954). Iversen (1947) listed a number of different late glacial sedimentary successions, but none of them is similar to the succession from Søndre Kobberdam. Hence it may represent a local, rather unusual lithostratigraphy.

Results of the radiocarbon dating of four samples are shown in Table 1. Based on these ages, a tentative age-depth curve can be drawn (Fig. 2). There are too few ages to construct a well constrained age-depth curve, but according to the tentative curve the sedi-

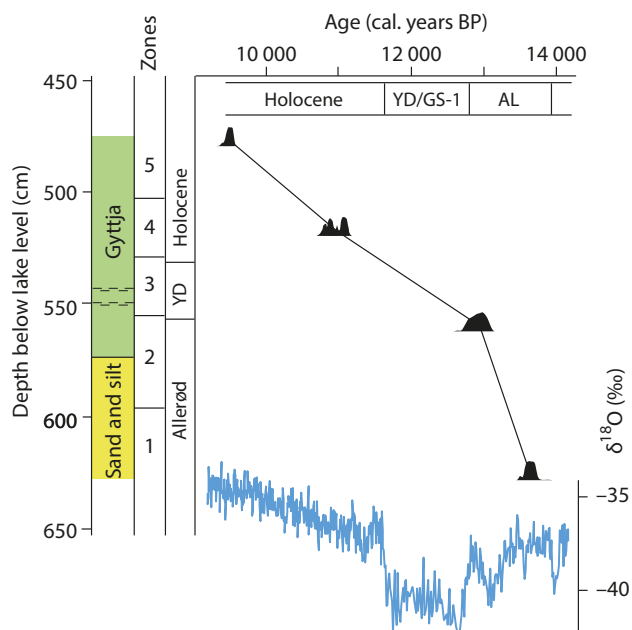


Fig. 2. Age–depth model for the succession in Søndre Kobberdam. Thin clay layers are found at 550–551 cm and 543–544.5 cm. YD = Younger Dryas, AL = Allerød, GS-1: Greenland stadial 1. The lower part of the figure shows oxygen isotope ratios from the GRIP deep ice core from Greenland from Johnsen *et al.* (1992). The ice core chronology is from Rasmussen *et al.* (2014).

mentation rate was *c.* 0.94 mm/year in the lower part of the succession and *c.* 0.24 mm/year in the upper part. The mineral-rich sediments in the lower part indicate that there was a marked in-wash into the lake, which is confirmed by the age-depth model.

Macrofossils

The results of the macrofossil analyses are presented in two macrofossil diagrams (Figs 3, 4). The diagrams

were divided by visual inspection into four local macrofossil assemblage zones that are described in the following.

Zone 1 (13 600–13 330 years BP, 628–596 cm)

Zone 1 is dominated by *Dryas octopetala* and *Betula nana*. Other woody plants are represented by a few leaves of *Salix polaris*, a few endocarps of *Arctostaphylos uva-ursi*. Herbaceous plants are dominated by *Carex* sp., a few of which could be identified as *Carex rostrata*; all may

Table 1. AMS radiocarbon ages from Søndre Kobberdam, Hareskovene, 55°46.33'N, 12°26.29'E

Laboratory number	Depth (cm)	Material	Age (¹⁴ C years BP) ¹	Calibrated age (years BP) ²	Calibrated age (years BP) ³
COL-1059	475–477	<i>Salix</i> sp.	8483 ± 41	9447–9537	9499
LuS-9172	515–517	<i>Pinus sylvestris</i>	9650 ± 65	10 775–11 200	10 992
COL-1060	557–561	<i>Betula pubescens</i>	11 077 ± 45	12 808–13 063	12 944
LuS-9173	624–628	Twigs	11 840 ± 70	13 482–13 780	13 657

¹ Radiocarbon ages are reported in conventional radiocarbon years BP (before present = 1950; Stuiver & Polach 1977). The ¹⁴C ages have been corrected for isotopic fractionation by normalising to a δ¹³C value of -25 ‰. ² Calibration to calendar years BP is according to the INTCAL13 data (Reimer *et al.* 2013). ³ Mean probability ages.

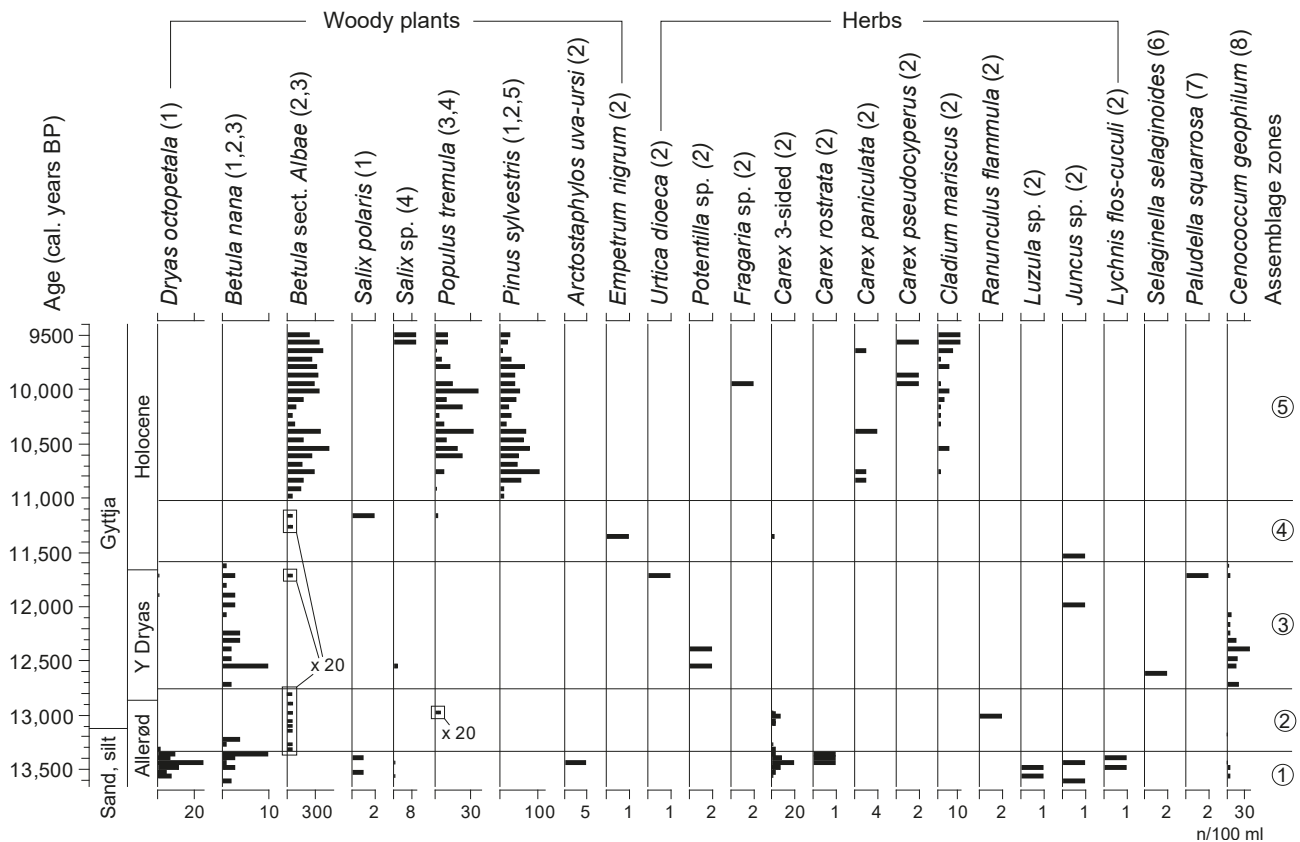


Fig. 3. Simplified macrofossil concentration diagram for Søndre Kobberdam (terrestrial and telmatic species). × 20: the columns are exaggerated 20 times. 1: leaves and leaf fragments, 2: seeds and fruits, 3: female catkin scales, 4: bud scales, 5: bark fragments, 6: megaspores, 7: leafy shoots, 8: sclerotia.

belong to this species which is common in late glacial assemblages from Denmark. *Juncus* sp., *Luzula* sp. and *Lychnis flos-cululi* are represented by few seeds. Only few remains of limnic plants (*Chara* sp. and *Potamogeton filiformis*) and invertebrates were found, including a few *Daphnia* cf. *pulex* type, chironomids (not shown in the diagram), the alder fly *Sialis* sp., trichopterans (not shown) and the bryozoans *Cristatella mucedo* and *Plumatella* sp.

Zone 2 (13 330–12 780 years BP, 596–555 cm)

Zone 2 is characterised by the occurrence of tree birch (*Betula* sect. *Albae*) remains. Remains that could be identified to species came from *Betula pubescens*. In the lower part of Zone 2 *Dryas octopetala* and *Betula nana* also occur. Woody plants are also represented by a single bud scale of *Populus tremula*. *Carex* sp. and two achenes of *Ranunculus flammula* are the only herbaceous telmatic plants in this zone.

At the beginning of zone 2 there are marked peaks of *Chara* sp. and *Potamogeton perfoliatus*; other water plants include *Ranunculus* sect. *Batrachium*, *Hippuris vulgaris*, *Myriophyllum alterniflorum*, *Ceratophyllum de-*

mersum and *Potamogeton filiformis*. Limnic invertebrates include the fish leach *Piscicola geometra*, the tad-pole shrimp *Lepidurus* sp., *Daphnia* cf. *pulex*, chironomids, trichopterans, *Sialis* sp. and *Cristatella mucedo*. In the middle of the zone ostracodes are abundant; they include *Cytherissa lacustris*, *Limnocythere* spp. and *Candona* spp. Scales of the fish *Perca fluviatilis* are also found in part of zone 2.

Zone 3 (12 780–11 600 years BP, 555–529 cm)

Zone 3 is characterised by *Betula nana* remains; in addition there are a few *Dryas octopetala*, *Betula* sect. *Albae* and *Salix* sp. remains. Herbaceous plants include *Urtica dioeca* and *Potentilla* sp.. Sclerotia of *Cenococcum geophilum* are common; in addition two spores of *Selaginella selaginoides* and two shoots with leaves of the bryophyte *Paludella squarrosa* were also found.

Remains of macrolimnophytes are rare in zone 3, only *Ranunculus* sect. *Batrachium*, *Hippuris vulgaris* and *Myriophyllum alterniflorum* were noted. *Ranunculus* sect. *Batrachium* is common in the upper part of the zone. Remains of limnic invertebrates are rare and include *Daphnia* cf. *pulex*, ostracodes, chironomids,

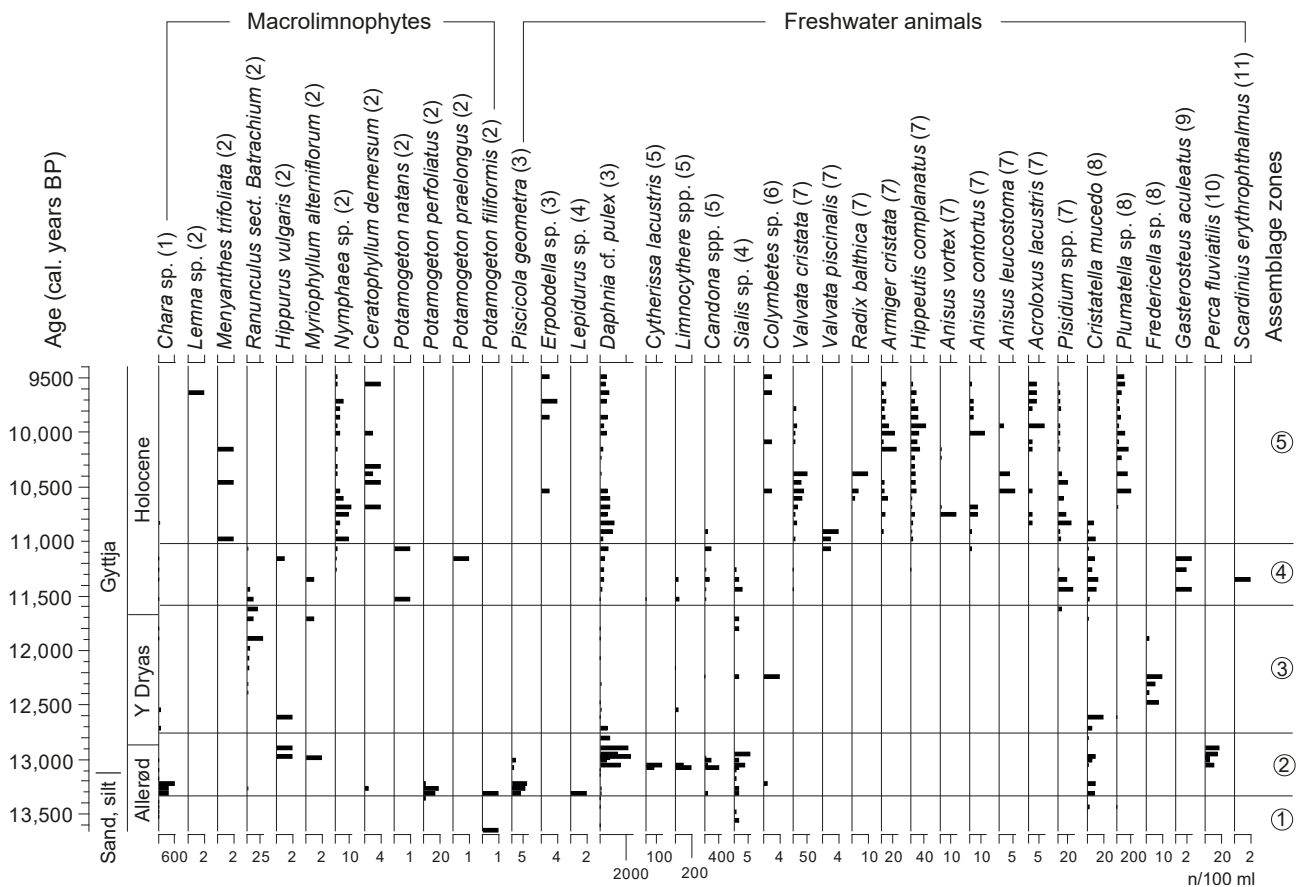


Fig. 4. Simplified macrofossil concentration diagram for Søndre Kobberdam (limnic species). 1: oospores, 2: seeds and fruits, 3: egg cocoons, 4: mandibles, 5: valves, 6: elytra fragments, 7: shells, 8: statoblasts, 9: spines, 10: scales, 11: pharyngeal teeth.

trichopterans, *Sialis* sp., the diving beetle *Colymbetes* sp., *Cristatella mucedo* and *Fredericella* sp.

Zone 4 (11 600–11 000 years BP, 529–503 cm)

In zone 4, only a few remains of terrestrial and telmatic plants are found; they come from *Betula* sect. *Albae*, *Salix polaris*, *Empetrum nigrum*, *Carex* sp. and *Juncus* sp. Water plants include *Ranunculus* sect. *Batrachium* (mainly in the oldest part of the zone) and *Nymphaea* sp. (in the younger part of the zone) in addition to rare occurrences of *Potamogeton natans*, *P. praelongus* and a few other taxa. Freshwater invertebrates include *Daphnia* cf. *pulex*, rare ostracodes, *Sialis* sp., the small bivalve *Pisidium* spp. and *Cristatella mucedo*. Fishes are represented by *Gasterosteus aculeatus* and *Scardinius erythrophthalmus*.

Zone 5 (11 000–9 500 years BP, 503–475 cm)

Zone 5 is characterised by *Betula* sect. *Albae*, *Populus tremula* and *Pinus sylvestris*. Many of the *Betula* sect. *Albae* could be identified to species, and all came from *Betula pubescens*. Herbaceous plants include *Fragaria* sp., *Carex paniculata*, *C. pseudocyperus* and *Cladium mariscus*. Macrolimnophytes include *Nymphaea* sp., *Ceratophyllum demersum*, *Menyanthes trifoliata*. Aquatic invertebrates include the leach *Erpobdella* sp., *Daphnia* cf. *pulex*, diving water beetles (*Colymbetes* sp.) and *Plumatella* sp. Molluscs are represented by a range of gastropod species as well as the bivalves *Pisidium* spp. and *Sphaerium corneum*, the latter represented by a single shell.

Discussion

Zone 1

Zone 1, from c. 13 600 to c. 13 330 years BP correspond to the early and middle part of the Allerød period, or the Greenland Interstadial 1c (GI-1c) event (Björck *et al.* 1998). The vegetation, with *Dryas octopetala*, *Betula nana*, *Salix polaris* and *Arctostaphylos uva-ursi*, is interpreted as an open pioneer, tundra-like vegetation with dwarf-shrub heaths. *Dryas octopetala* leaves are common in deposits from the early late glacial and the Younger Dryas period in the region (Iversen 1954) and the plant must have been an important component of the vegetation. It thrives on sites with calcareous soils. In addition, *Dryas octopetala* has root nodules that house nitrogen-fixing bacteria, which enables it to grow on raw soils with little nutrients. The water plants *Chara* sp. and *Potamogeton filiformis* are common in late glacial sediments; the latter is mainly a northern species. Mandibles and labra of larvae of *Sialis* sp. (alder fly) are common in late Quaternary lake sediments (Frey 1964).

The soils around the lake, especially on the Højnæs-

bjerg hill, were unstable, and sand, silt and clay was washed into the lake. The lake water was probably turbid and therefore only supported a sparse flora and fauna. It is also possible that stagnant ice was still present in the basin, which would have led to low water temperatures.

Studies of beetle remains (Coope *et al.* 1998; Lemdahl *et al.* 2014) and chironomid larvae (Heiri *et al.* 2014) from deposits from north-western Europe indicate that summer temperatures during this time period were fairly high. The lack of tree birch during this period may be due to delayed immigration, perhaps due to unstable soils with stagnant ice still present.

Zone 2

Zone 2, from c. 13 330 to c. 12 780 years BP, corresponds to the middle and late part of the Allerød period and the oldest part of the Younger Dryas, or the GI-1a-b events and the oldest part of the GS-1 event. During zone 2 open woodland with *Betula pubescens* and rare *Populus tremula* developed around the lake. The woodland may have been so dense that the heliophilous dwarf shrubs *Dryas octopetala* and *Betula nana* disappeared from the near vicinity of the lake. The soils around the lake became more stable. The lake housed a rich vegetation of submerged macrolimnophytes, a rich fauna of invertebrates and the fish *Perca fluviatilis*. Remains of *Perca fluviatilis* have previously been reported from Allerød period deposits from Sjælland, Fyn and Jylland (Rosenlund 1976). The flora and fauna indicate that the water in the lake became clearer and warmer. Sedges and *Ranunculus flammula* grew along the shores of the lake. *Ranunculus flammula* remains are extremely rare in Allerød deposits from Denmark.

The Allerød period is commonly considered a period characterised by open forests dominated by *Betula pubescens* in Denmark. However, a recent compilation of the available data by Mortensen *et al.* (2014a) shows that there were marked regional differences in the vegetation in Denmark. Birch forests were restricted to the southern and eastern parts of the country, whereas the north-western parts of Denmark were characterised by shrubs and copses with *Betula nana*. Furthermore, the early part of the Allerød period was characterised by open tundra-like vegetation, and birch forests did not spread until well into the Allerød period. The results from Søndre Kobbendam indicate that also at this site the early part of the Allerød period was characterised by a tundra-like, open, treeless landscape.

During the late part of the Allerød period, *Populus tremula* arrived. There are only a few reports of macrofossils of this species from Allerød layers in Denmark. Hartz (1902) reported a branch from Lundbæk in eastern Jylland and unspecified remains from Skinder-

bygaard Mose on Bornholm, but at both localities the remains may come from early Holocene deposits. A few more recent finds from eastern Jylland, Fyn, Sjælland and Falster are surely of Allerød age (Nielsen & Sørensen 1992; Fischer *et al.* 2013; Mortensen *et al.* 2014a). The scarcity of finds shows that *P. tremula* was rare in Denmark, and it was probably confined to the southern and eastern part.

The other tree birch species which grows in Denmark, *Betula pendula*, has also been reported from several localities in Denmark, including the Allerød clay pit (Hartz 1902; Jensen 1985). However, Iversen (1954) did not include it in his list of plants found in late glacial deposits in Denmark, and the remains were probably confused with *Betula pubescens*, which can be very variable.

Betula sect. *Albae*, *Populus tremula*, *Potamogeton perfoliatus*, *Ceratophyllum demersum*, *Cristatella mucedo* and *Cytherissa lacustris* are fairly warmth demanding and indicate that the mean July temperature was above 10 °C.

Zone 3

Zone 3, from c. 12 780 to c. 11 600 years BP, corresponds to the Younger Dryas cold period or the GS-1 event, which is characterised by a return to colder conditions in the North Atlantic region, as illustrated by the $\delta^{18}\text{O}$ curve from the GRIP ice core from Greenland (Fig. 2). *Betula nana* and rare *Dryas octopetala* returned to the area and the vegetation became tundra-like again, with *B. nana* dominated dwarf-shrub heaths. The rare occurrence of *Betula pubescens* may indicate that tree birch survived but became very rare. A radiocarbon age of a tree birch stem from Birkerød, also in north-eastern Sjælland, of c. 12 350 years BP (K-6151; $10\,490 \pm 155$ ^{14}C years BP) may also indicate that tree birch survived during the Younger Dryas in the region (Mortensen *et al.* 2014a). The find of *Urtica dioeca* is noteworthy because remains of this thermophilous and nutrient-demanding plant are extremely rare in Younger Dryas deposits in Denmark. However, it has been recorded from Younger Dryas layers from southern Sjælland by Fischer *et al.* (2013) and from western Skåne in southern Sweden by Liedberg Jönsson (1988). It requires nitrogen- and phosphorus-rich soil. Maybe there were droppings of reindeer (*Rangifer tarandus*) or other vertebrates near the lake. The common presence in the lower part of the zone of sclerotia of the soil-inhabiting fungus *Cenococcum geophilum* indicates increased soil erosion and unstable soils around the lake (Liedberg Jönsson 1988).

The mean July temperature was probably below 10 °C, and the diversity of limnic organisms decreased strongly, probably due to turbid waters. However, the bryozoan *Fredericella* sp. was fairly common in the middle of the zone; this bryozoan is perhaps the most

cold-adapted fresh-water bryozoan. It is common in lakes in northern Norway (Økland & Økland 2001) and the statoblasts can be common in Holocene lake sediments in south-western Greenland (Wagner & Bennike 2012).

Zone 4

The lower boundary of zone 4 is placed at the last occurrence of *Betula nana*; at the same time an increase in the warmth-demanding *Cristatella mucedo* is seen. Surprisingly, there are almost no remains of woody plants in the earliest Holocene sediments. The only exception is *Empetrum nigrum*, which was common in some regions of Denmark during the late Younger Dryas and earliest Holocene (Iversen 1973; Bennike *et al.* 2004; Mortensen *et al.* 2011). The lack of remains of terrestrial plants could perhaps be caused by low lake levels, as has been documented for other lakes in the region (Digerfeldt 1988). Low lake level in Søndre Kobberdam could potentially lead to poor preservation. However, it is also possible that spreading of trees was delayed by the cold event about 11 400 years BP, the Preboreal oscillation (Björck *et al.* 1997; Rasmussen *et al.* 2014). Similarly, at Hasselø in south-eastern Denmark, no remains of tree birch or other trees were reported from earliest Holocene sediments (Mortensen *et al.* 2014b). It is noteworthy that *Salix polaris* is present as late as 11 200 years BP; its presence indicates an open landscape in the first several hundred years after the onset of the Holocene warming. The find represents the first record of this arctic species from the early Holocene in Denmark. However, other arctic species such as *Dryas octopetala* (Andersen 1923) and *Rangifer tarandus* (Aaris-Sørensen *et al.* 2007) have also been recorded from early Holocene deposits in Denmark.

The first tree to appear in the record is *Betula* sect. *Albae* (at c. 11 300 years BP), but it took several hundred years before tree birch expanded at the site. The delay in the spreading of tree birch is hardly due to migrational delay from glacial refugia because the tree occurred in the region during the Younger Dryas (Liedberg Jönsson 1988; Mortensen *et al.* 2014a). Perhaps its spread and expansion were delayed by a relatively arid and windy continental climate with strong seasonality, late-spring frost and warm dry summers (Birks & Birks 2014).

Zone 5

The arrival of *Betula* sect. *Albae* was followed by *Populus tremula* and then by *Pinus sylvestris* at c. 11 000 years BP, which is one of the earliest *P. sylvestris* ages from Denmark. The area was again forested. The flora at the margin of the lake included the sedges *Carex paniculata*, *C. pseudocyperus* and *Cladium mariscus*; these plants are common in early Holocene deposits in

Denmark. The calciphilous and thermophilous *Cladium mariscus* was a common reed plant in Denmark in the early Holocene, but it has declined due to leaching of the calcareous soils throughout the Holocene and due to decreasing temperatures after the Holocene Temperature Maximum.

The lake supported a species-rich flora and fauna in the early Holocene. *Ranunculus* sect. *Batrachium* was common in the earliest Holocene, and *Potamogeton natans* was also present at an early stage, but soon *Nymphaea* sp. began to dominate, together with *Ceratophyllum demersum*. The early Holocene sediments contain a rich fauna of bivalves and gastropods. *Pisidium* spp. were the first to arrive, soon followed by *Valvata cristata*, *Hippeutis complanatus*, *Valvata piscinalis*, *Anisus contortus*, *Armiger cristata*, *Acroloxus lacustris*, *Anisus vortex*, *Anisus leucostoma* and *Radix balthica* (synonym *Lymnaea peregra*). These species are common in small lakes in Denmark, and the fauna is typical of early Holocene deposits in Denmark (Johansen 1904). However, the record from Hareskovene provides one of the first well dated records of the immigration of these species to Denmark. The early Holocene lake fauna also included *Cristatella mucedo*, *Erpobdella* sp., *Plumatella* sp. and the fishes *Gasterosteus aculeatus* and *Scardinius erythrophthalmus*.

Directly above zone 5, a thin layer of sub-recent leaves of *Fagus sylvatica* was found. We suggest that peat digging transformed a former bog into a lake during the 1800s and estimate that 5000–7000 m³ of peat may have been removed from Søndre Kobberdam.

Immigration history

According to the local deglaciation chronology, the region became free of active glacier ice between 16 000 and 17 000 years ago (Houmark-Nielsen *et al.* 2012). However, the oldest sediments with plant remains are dated to about 13 600 years BP (Table 1). The lack of older plant remains is best explained by assuming that the landscape was characterised by widespread occurrences of stagnant ice, which meant that the landscape was highly unstable and plants had great difficulties to gain a foothold. If the lake basin formed because of melting of a stagnant ice body, this could also explain the lack of older sediments.

It is a common feature of Danish lakes that sedimentation did not begin until several millennia after the last deglaciation. Similarly, the oldest ages obtained for late glacial plant remains from Denmark are several millennia younger than the last deglaciation (e.g. Bennike & Jensen 1995; Korsager *et al.* 2003; Mortensen *et al.* 2011, 2014b) and the oldest age of

reindeer (*Rangifer tarandus*) remains from Sjælland is about 14 000 years BP (Aaris-Sørensen *et al.* 2007). Reindeer was the most common large herbivore during the late glacial in Denmark.

The deglaciated area around Søndre Kobberdam was colonised by pioneer taxa in the early Allerød. The dwarf-shrubs *Dryas octopetala*, *Betula nana* and *Salix polaris* and the herbs *Luzula* sp. and *Juncus* sp. were among the first to arrive. These species are among the first immigrants after the last deglaciation in Denmark (Bennike *et al.* 2004). *Betula pubescens* was the first tree to arrive, with the oldest find dated to c. 13 330 years BP. This is somewhat later than at the few other sites in eastern Denmark where the timing of its arrival has been dated to between 13 700 and 13 600 years BP. Unstable soils around Søndre Kobberdam may have delayed the local spread of tree birch. The dating confirms that tree birch did not arrive until the Middle Allerød, as concluded by Mortensen *et al.* (2014a). *Populus tremula* was present in the late Allerød, but it was extremely rare. During the Younger Dryas woodland was replaced by an open tundra landscape with dwarf-shrub heaths with *Betula nana*, *Dryas octopetala*, *Salix* sp. and *Empetrum nigrum*. This landscape type may have persisted from the onset of the Holocene warming until woodland started to dominate about 11 000 years BP. The next new tree to arrive was *Pinus sylvestris*, with the oldest find dated to c. 11 000 years BP. Pollen grains of *P. sylvestris* are abundant in late glacial sediments in Denmark, but so far there are no records of macrofossil finds, and the pollen is probably long-distance transported from the south or east. However, *Pinus sylvestris* macrofossils have been reported from late glacial lake sediments from Blekinge in south-eastern Sweden (Wohlfarth *et al.* 2017) and it may be speculated that it was easier for *Pinus sylvestris* to spread to the rocky terrain in Blekinge than to the unstable soft sediment terrain of Sjælland.

Among the reed plants, *Carex rostrata* arrived at Søndre Kobberdam in the Allerød, and *Carex paniculata* and *Cladium mariscus* in the early Holocene at c. 10 800 years BP. The water plants *Ranunculus* sect. *Batrachium*, *Potamogeton perfoliatus*, *Potamogeton filiformis*, *Myriophyllum alterniflorum*, *Hippurus vulgaris* and *Ceratophyllum demersum* arrived in the Allerød; the latter species is new to the late glacial flora of Denmark. The early Holocene flora of water plants includes *Potamogeton natans*. Among animals in the Søndre Kobberdam, *Piscicola geometra*, *Cristatella mucedo* and *Perca fluviatilis* arrived in the Allerød, and during the early Holocene a rich fauna of mollusc became established together with the fishes *Gasterosteus aculeatus* and *Scardinius erythrophthalmus*.

Conclusions

After the last deglaciation of north-eastern Denmark, it took several millennia before vegetation spread, probably due to unstable soils and widespread occurrence of stagnant ice. During the late glacial and early Holocene, the landscape around Sønder Kobberdam in Hareskovene in eastern Denmark changed markedly. The early and middle Allerød landscape was tundra-like and treeless, with pioneer vegetation that included the dwarf-shrubs *Dryas octopetala* and *Betula nana*. During the late Allerød period *Betula pubescens* woodlands with rare *Populus tremula* characterised the area, and the lake supported a rich flora. The lake fauna included the fish *Perca fluviatilis*. During the Younger Dryas a tundra-like vegetation returned, which prevailed during the earliest part of the Holocene. The first trees that spread in the early Holocene was *Betula pubescens*, *Populus tremula* and *Pinus sylvestris*. The early Holocene fauna included a rich and diverse fauna of freshwater molluscs that thrived in the carbonate-rich waters. *Cladium mariscus* and *Carex* spp. grew along the lake shore.

Acknowledgements

We are grateful to Peter Rasmussen for help with the field work. The local division of the Danish Nature Agency gave us permission to core the lake. Radiocarbon dating was supervised by Göran Skog, University of Lund, and Janet Rethemeyer, University of Cologne.

References

- Aaris-Sørensen, K., Mühldorff, R. & Petersen, E.B. 2007: The Scandinavian reindeer (*Rangifer tarandus* L.) after the last glacial maximum: time, seasonality and human exploitation. *Journal of Archaeological Science* 34, 914–923.
- Andersen, S.A. 1923: Senglaciale relikter i postglacial Tørv. *Meddelelser fra Dansk Geologisk Forening* 6(3), 1–5.
- Bennike, O. & Jensen, J.B. 1995: Near shore Baltic Ice Lake deposits in Fakse Bugt, southeast Denmark. *Boreas* 24, 185–195.
- Bennike, O., Sarmaja-Korjonen, K. & Seppänen, A. 2004: Re-investigation of the classic late-glacial Bølling Sø sequence, Denmark: chronology, macrofossil, Cladocera and chydorid ephippia. *Journal of Quaternary Science* 19, 465–478.
- Birks, H.H. 1993: The importance of plant macrofossils in late-glacial climatic reconstructions: an example from western Norway. *Quaternary Science Reviews* 12, 719–726.
- Birks, H.H. & Birks, H.J.B. 2014: To what extent did changes in July temperature influence Lateglacial vegetation patterns in NW Europe? *Quaternary Science Reviews* 106, 262–277.
- Björck, S., Rundgren, M., Ingólfsson, O. & Funder, S. 1997: The Preboreal oscillation around the Nordic Seas: terrestrial and lacustrine responses. *Journal of Quaternary Science* 12, 455–465.
- Björck, S., Walker, M.J.C., Cwynar, L.C., Johnsen, S., Knudsen, K.-L., Lowe, J.J., Wohlfarth, B. & INTIMATE Members 1998: An event stratigraphy for the Last Termination in the North Atlantic region based on the Greenland ice-core record: a proposal by the INTIMATE group. *Journal of Quaternary Science* 13, 283–292.
- Coope, G.R., Lemdahl, G., Lowe, J.J. & Walking, A. 1998: Temperature gradients in northern Europe during the last glacial–Holocene transition (14–9 ¹⁴C kyr BP) interpreted from coleopteran assemblages. *Journal of Quaternary Science* 13, 419–433.
- Dau, J.H.C. 1823: Neues Handbuch über den Torf – dessen Natürliche Entstehung und Wiedererzeugung, Nutzen im Allgemeinen und für den Staat, 240 pp. Leipzig: J.C. Hinrichsche Buchhandlung.
- Dau, J.H.C. 1829: Allerunterthänigster Bericht an die Königliche Dänische Rentekammer über die Torfmoore Seelands nach einer im Herbst 1828 unternommenen Reise, 316 pp. Copenhagen: Gyldendahl.
- Digerfeldt, G. 1988: Reconstruction and regional correlation of Holocene lake-level fluctuations in Lake Bysjön, south Sweden. *Boreas* 17, 165–182.
- Fischer, A., Mortensen, M.F., Henriksen, P.S., Mathiassen, D.R. & Olsen, J. 2013: Dating the Trollesgave site and the Bromme culture – chronological fix-points for the Lateglacial settlement of southern Scandinavia. *Journal of Archaeological Science* 40, 4663–4674.
- Frey, D.G. 1964: Remains of animals in Quaternary lake and bog sediments and their interpretation. *Archiv für Hydrobiologie, Beihefte. Ergebnisse der Limnologie* 2, 114 pp.
- Garboe, A. 1961: *Geologiens historie i Danmark*, vol. 2, Forskere og resultater, 522 pp. Copenhagen: Reitzels Forlag.
- Gladsaxe 2017: <http://gladsaxe-ltk.cowi.webhouse.dk/dk/bagsvaerd-soe-og-lyngby-soe-med-omgivelser/delomraader/alderstvile-skov/kobberdammene/kobberdammene.htm>. Accessed 11 December 2017.
- Hartz, N. 1902: Bidrag til Danmarks senglaciale Flora og Fauna. *Danmarks Geologiske Undersøgelse II. Række, Vol. 11*, 80 pp.
- Hartz, N. 1909: Bidrag til Danmarks tertiære og diluviale Flora. *Danmarks Geologiske Undersøgelse II. Række, Vol. 20*, 292 pp.
- Hartz, H. & Milthers, V. 1901: Det senglaciale Ler i Allerød Teglværksgrav. *Meddelelser fra Dansk geologisk Forening* 2(8), 31–60.
- Heiri, O. *et al.* 2014: Validation of climate model-inferred regional temperature change for late-glacial Europe. *Nature communications* 5, no. 4914, 7 pp.
- Houmark-Nielsen, M., Linge, H., Fabel, D., Schnabel, C., Xue, S., Wilcken, K.M. & Binnie, S. 2012: Cosmogenic surface exposure dating the last deglaciation in Denmark: discrepancies with independent age constraints suggest delayed

- periglacial landform stabilisation. *Quaternary Geochronology* 13, 1–17.
- Iversen, J. 1947: Plantevækst, Dyreliv og Klima i det senglaciale Danmark. *Geologiska Föreningens i Stockholm Förhandlingar* 69, 67–78.
- Iversen, J. 1954: The late-glacial flora of Denmark and its relation to climate and soil. *Danmarks Geologiske Undersøgelse II. Række*, Vol. 80, 87–119.
- Iversen, J. 1973: The development of Denmark's nature since the Last Glacial. *Danmarks Geologiske Undersøgelse V. række*, Vol. 7-C, 120 pp.
- Jensen, H.A. 1985: Catalogue of late- and post-glacial macrofossils of Spermatophyta from Denmark, Schleswig, Scania, Halland, and Blekinge dated 13,000 B.P. to 1536 A.D. *Danmarks Geologiske Undersøgelse Serie A*, Vol. 6, 95 pp.
- Johansen, A.C. 1904: Om den fossile Kvartære molluskfauna i Danmark og dens relationer til forandringer i klimaet, land- og ferskvandsmolluskfaunaen, 136 pp. Copenhagen: Gyldendalske Boghandel.
- Johnsen, S., Clausen, C.U., Dansgaard, W., Fuhrer, K., Gundestrup, N., Hammer, C.U., Iversen, P., Jouzel, J., Stauffer, B. & Steffensen, J.P. 1992: Irregular interstadials recorded in a new Greenland ice core. *Nature* 359, 311–313.
- Jowsey, P.C. 1966: An improved peat sampler. *New Phytologist* 65, 245–248.
- Korsager, B., Bennike, O. & Houmark-Nielsen, M. 2003: *Salix polaris* leaves dated at 14.3 ka BP from northern Jylland, Denmark. *Bulletin of the Geological Society of Denmark* 50, 151–155.
- Krog, H. 1954: Pollen analytical investigations of a C¹⁴-dated Allerød-section from Ruds-Vedby. *Danmarks Geologiske Undersøgelse II. Række*, Vol. 80, 120–139.
- Lemdahl, G., Buckland, P.I. & Mortensen, M.F. 2014: Lateglacial insect assemblage from the Palaeolithic site Slotseng: new evidence concerning climate and environment in SW Denmark. *Quaternary International* 341, 172–183.
- Liedberg Jönsson, B. 1988: The Late Weichselian macrofossil flora in western Skåne, southern Sweden. LUNDQUA Thesis 24, 12 pp + 2 appendices.
- Milthers, V. 1922: Nordøstsjælland's Geologi. *Danmarks Geologiske Undersøgelse V. række*, Vol. 3, 192 pp.
- Mortensen, M.F., Birks, H.H., Christensen, C., Holm, J., Noe-Nygaard, N., Odgaard, B.V., Olsen, J. & Rasmussen, K.L. 2011: Late-glacial vegetation development in Denmark – new evidence based on macrofossils and pollen from Slotseng, a small-scale site in southern Jutland. *Quaternary Science Reviews* 30, 2534–2550.
- Mortensen, M.F., Henriksen, P.S. & Bennike, O. 2014a: Living on the good soil: relationships between soils, vegetation and human settlement during the late Allerød time period in Denmark. *Vegetation History and Archaeobotany* 23, 195–205.
- Mortensen, M.F., Henriksen, P.S., Christensen, C., Petersen, P.V. & Olsen, J. 2014b: Vegetation development in south-east Denmark during the Weichselian Late Glacial: palaeoenvironmental studies close to the Palaeolithic site of Hasselø. *Danish Journal of Archaeology* 3, 33–51.
- Nathorst, A.G. 1892: Über den gegenwärtigen Standpunkt unserer Kenntniss von dem Vorkommen fossiler Glacialpflanzen. Bihang till Kungliga Svenska Vetenskaps Akademiens Handlingar 17, III, no. 5, 32 pp.
- Nathorst, A.G. 1914: Minnen från Samarbete med Japetus Steenstrup 1871 och från en därpå följande tjugofemårig Korrespondens. In: Jungersen, H.F.E. & Warming, E. (eds), *Mindeskript i anledning af hundredaaret for Japetus Steenstrups fødsel*, no. 5, 22 pp. Copenhagen: Bianco Lunos Bogtrykkeri.
- Nielsen, H. & Sørensen, I. 1992: Taxonomy and stratigraphy of late-glacial *Pediastrum* taxa from Lysmosen, Denmark – a preliminary study. *Review of Palaeobotany and Palynology* 74, 55–75.
- Økland, K.A. & Økland, J. 2001: Freshwater bryozoans (Bryozoa) of Norway II: distribution and ecology of two species of *Fredericella*. *Hydrobiologia* 459, 103–123.
- Rasmussen, S.O. *et al.* 2014: A stratigraphic framework for abrupt climatic changes during the Last Glacial period based on three synchronized Greenland ice-core records: refining and extending the INTIMATE event stratigraphy. *Quaternary Science Reviews* 106, 14–28.
- Reimer, P.J. *et al.* 2013: IntCal13 and Marine13 radiocarbon age calibration curves 0–50,000 years cal BP. *Radiocarbon* 55, 1869–1887.
- Rørdam, K. 1914: Et hidtil utrykt arbejde vedrørende tørve-moser af Japetus Steenstrup. In: Jungersen, H.F.E. & Warming, E. (eds), *Mindeskript i anledning af hundredaaret for Japetus Steenstrups fødsel*, no. 3, 45 pp. Copenhagen: Bianco Lunos Bogtrykkeri.
- Rosenlund, K. 1976: Catalogue of subfossil Danish vertebrates, fishes, 108 pp. Copenhagen: Zoological Museum.
- Steenstrup, J.F.S. 1842: Geognostisk-geologisk Undersøgelse af Skovmoserne Vidnesdam- og Lillemose i det nordlige Sjælland, ledsaget af sammenlignende Bemærkninger, hentede fra Danmarks Skov- Kjær- og Lyngmoser i almindelighed. *Det Kongelige Danske Videnskabernes Selskabs Skrifter, Naturvidenskabelige og Mathematiske Afdeling* 9, 17–120.
- Stuiver, M. & Polach, H.A. 1977: Discussion of reporting ¹⁴C data. *Radiocarbon* 19, 355–363.
- Stuiver, M., Reimer, P.J., & Reimer, R.W. 2017: CALIB 7.1 [WWW program] at <http://calib.org>. Accessed 11 December 2017.
- Wagner, B. & Bennike, O. 2012: Chronology of the last deglaciation and Holocene environmental change in the Sisimiut area, south-west Greenland based on lacustrine records. *Boreas* 41, 481–493.
- Wohlfarth, B., Muschitiello, F., Greenwood, S.L., Andersson, A., Kylander, M., Smittenberg, R.H., Steinthorsdottir, M., Watson, J. & Whitehouse, N.J. 2017: Hässeldala – a key site for Last Termination climate events in northern Europe. *Boreas* 46, 143–161.

Stratigraphy and geothermal assessment of Mesozoic sandstone reservoirs in the Øresund Basin

– exemplified by well data and seismic profiles

M. ERLSTRÖM, L.O. BOLDREEL, S. LINDSTRÖM, L. KRISTENSEN, A. MATHIESEN, M.S. ANDERSEN, E. KAMLA & L.H. NIELSEN



Erlström, M., Boldreel, L.O., Lindström, S., Kristensen, L., Mathiesen, A., Andersen, M.S., Kamla, E. & Nielsen, L.H. 2018. Stratigraphy and geothermal assessment of Mesozoic sandstone reservoirs in the Øresund Basin – exemplified by well data and seismic profiles. © 2018 by Bulletin of the Geological Society of Denmark, Vol. 66, pp. 123–149. ISSN 2245-7070. (www.2dgf.dk/publikationer/bulletin).

The Øresund Basin in the transnational area between Sweden and Denmark forms a marginal part of the Danish Basin. The structural outline and stratigraphy of the Mesozoic succession is described, and a novel interpretation and description of the subsurface geology and geothermal potential in the North Sjælland Half-graben is presented. The subsurface bedrock in the basin includes several Mesozoic intervals with potential geothermal sandstone reservoirs. Parts of the succession fulfill specific geological requirements with regard to distribution, composition and quality of the sandstones. A characterisation of these is presently of great interest in the attempt to identify geothermal reservoirs suitable for district heating purposes. The results presented in this paper include for the first time a comprehensive description of the stratigraphic intervals as well as the characteristics of the potential Mesozoic geothermal reservoirs in the Øresund region, including their distribution, composition and physical properties. This is illustrated by seismic cross-sections and well sections. In addition, results from analyses and evaluations of porosity, permeability, formation fluids and temperature are presented. Six potential geothermal reservoirs in the Mesozoic succession are described and assessed. Primary focus is placed on the characteristics of the reservoirs in the Lower Triassic and Rhaetian–Lower Jurassic succession. The study shows that the Mesozoic reservoir sandstones vary considerably with respect to porosity and permeability. Values range between 5–25% for the pre-Rhaetian Triassic sandstones and are commonly >25% for the Rhaetian–Lower Jurassic and Lower Cretaceous sandstones. The corresponding permeability rarely reaches 500 mD for the pre-Rhaetian Triassic reservoirs, while it is commonly above one Darcy for the Rhaetian–Lower Jurassic and the Lower Cretaceous sandstones. The interpreted formation temperatures are 45–50°C at 1500 m, 60–70°C at 2000 m and 70–90°C at 2500 m depth. The combined results provide a geological framework for making site-specific predictions regarding appraisal of viable geothermal projects for district heating purposes in the region as well as reducing the risk of unsuccessful wells.

Keywords: Geothermal reservoirs, depth structure maps, formation fluids, porosity, permeability, temperature gradient, geothermal potential.

M. Erlström [mikael.erlstrom@sgu.se; mikael.erlstrom@geol.lu.se], Geological Survey of Sweden, Kiliansgatan 10, SE-223 50 Lund, Sweden; also Department of Geology, Lund University, Sölvegatan 12, SE-223 62 Lund, Sweden. L.O. Boldreel [lob@ign.ku.dk], Department of Geosciences and Natural Resource Management, Geology Section, University of Copenhagen, Øster Voldgade 10, DK-1350 Copenhagen K, Denmark. S. Lindström [sli@geus.dk], L. Kristensen [lk@geus.dk], A. Mathiesen [anm@geus.dk], M.S. Andersen [misa@geus.dk], L.H. Nielsen [lhni@geus.dk], Geological Survey of Denmark and Greenland (GEUS), Øster Voldgade 10, DK-1350 Copenhagen K, Denmark. E. Kamla [eka@geo.dk], GEO, Maglebjergvej 1, DK-2800 Kgs Lyngby, Denmark.

The Øresund region includes the cities of Helsingør, Helsingborg, Landskrona, Malmö, Lund and Copenhagen (Fig. 1) and is the most densely populated region in Scandinavia with c. 3.8 million inhabitants. Despite favourable geological and socio-economical conditions, geothermal energy has not yet been uti-

lised to any great extent. So far only two of the cities, Copenhagen and Lund, have incorporated geothermal energy in their district heating systems, even though geological investigations have indicated significant possibilities for other urban areas and communities in the region (Mahler & Magtengaard 2010).

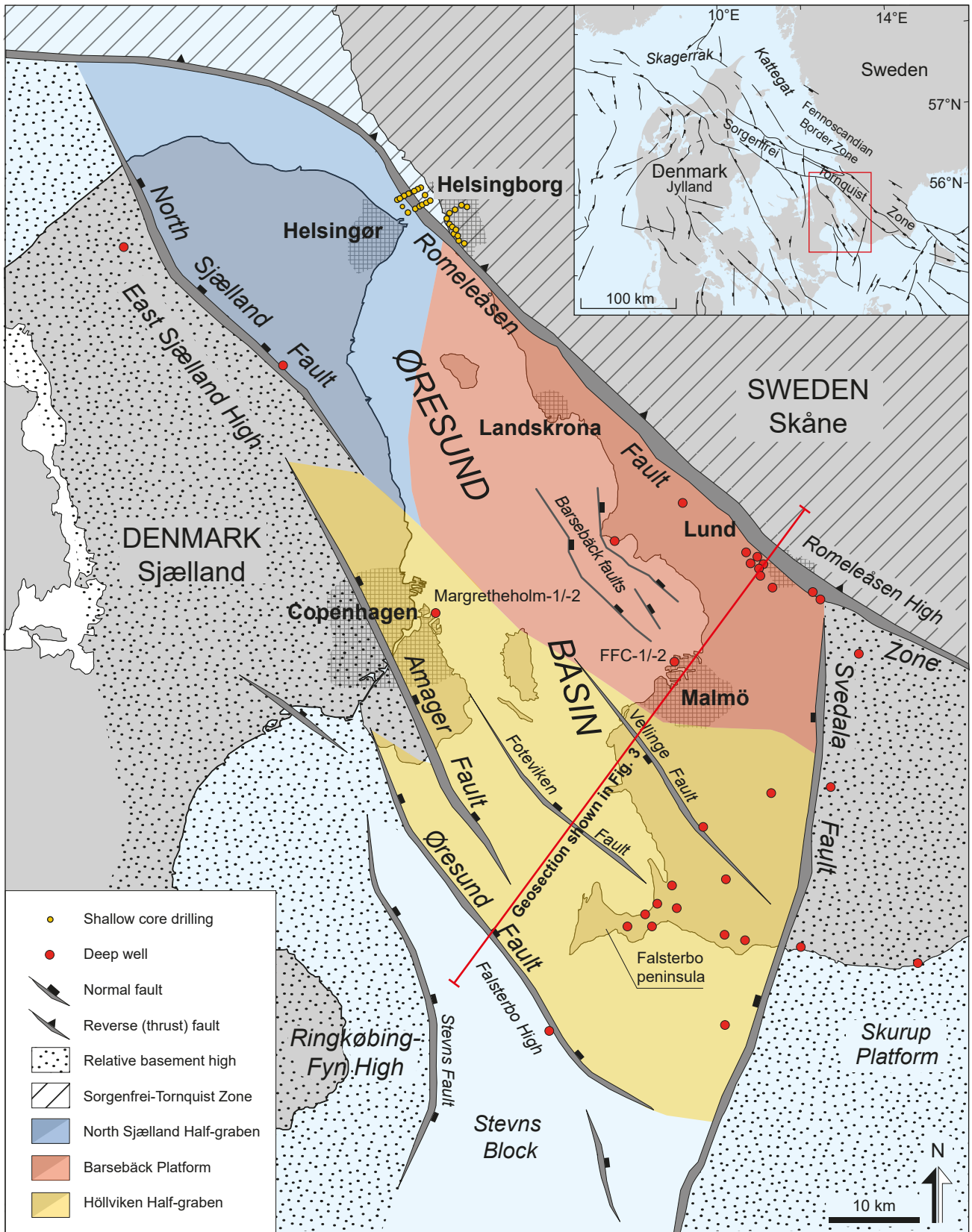


Fig. 1. Schematic structural map showing the location of the main structural elements in the Øresund Basin. Land areas have darker colours, sea-covered areas have lighter colours.

In accordance with the EU Renewable energy sources directive (Directive 2009/28/EC of the European Parliament and the Council), there is presently increasing interest in assessing and exploiting the geothermal resources from deep reservoirs, particularly in Denmark where several areas of geothermal potential have been identified (Nielsen *et al.* 2004; Mathiesen *et al.* 2009). Until now, 12 licenses for geothermal exploration in Denmark have been approved (Danish Energy Agency 2013). One of these license areas covers most of eastern Sjælland, including the urbanised zone between the cities of Copenhagen

and Helsingør along the Danish coastline of the sound Øresund. The geology of this area has been relatively poorly constrained, which has stressed the need for a comprehensive geological description and interpretation of the subsurface geology. Besides being a natural seaway between Denmark and Sweden, the Øresund has acted as a geographical barrier between the two countries. This is also apparent in geology where, traditionally, Swedish geologists have used one nomenclature for the lithostratigraphy of the Mesozoic succession and Danish geologists have used another. This has so far hampered correlation as well

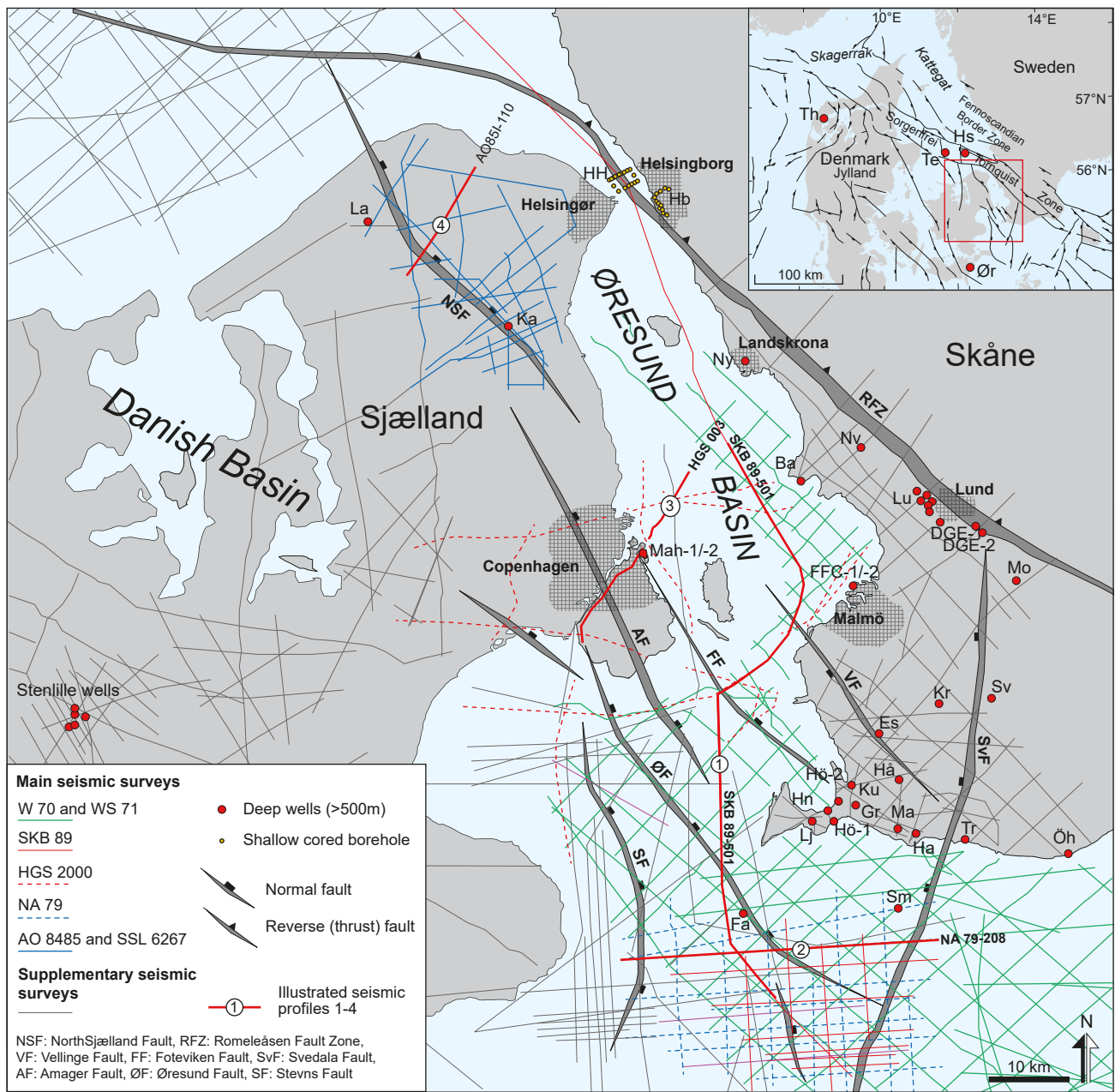


Fig. 2. Overview map showing locations of wells and seismic lines in the studied area. Locations of the profiles illustrated in Fig. 4 are also shown. The well abbreviations are explained in Table 1.

Table 1. Summary of well information including operator, year of drilling, total depth and reached stratigraphic level

Borehole	Abbreviation in Fig. 2	Total depth, metres below mean sea level	Reached stratigraphic level	Operator/year
Barsebäck-1	Ba	2255	Precambrian	OPAB/1972
DGE-1	DGE-1	3673	-“-	Lund Energy AB/2003
DGE-2	DGE-2	1901	-“-	Lund Energy AB/2004
Eskilstorp-1	Es	2463	L. Cambrian	OPAB/1971
Falsterborev-1	Fa	1396	L. Cambrian	OPAB/1973
FFC-1	FFC-1	2100	Precambrian	Sydskraft/EON/2002
FFC-2	FFC-2	2110**	-“-	EON/2003
Granvik-1	Gr	1254*	L. Cretaceous	Nordstjernan/1947
Hans-1	Hs	3028	U. Carboniferous	DUC/1983
Hammarlöv-1	Ha	2369	L. Cambrian	OPAB/1971
Helsingborg	Hb	30–40	Rhaetian–Hettangian	Helsingborg city/2006, 2009
Helsingør-Helsingborg	HH	40–120	Jurassic–Cretaceous	Geoteknisk Institut/1968
Håslöv-1	Hå	2554	L. Cambrian	OPAB/1972
Höllviken-1	Hö-1	1411	U. Jurassic	SGU/1941–43
Höllviken-2	Hö-2	1919	L. Triassic	SGU/1943–47
Höllviksnäs-1	Hn	2605	L. Cambrian	OPAB/1971
Karlebo-1/1A	Ka	2260**	U. Triassic	Tethys Oil/2006
Kungstorp-1	Ku	2066	L. Triassic	OPAB/1971
Lavø-1	La	2413	-“-	DAPCO/1959
Kruseberg	Kr	508	U. Cretaceous	Swedegas AB/1994
Ljunghusen-1	Lj	2276	Silurian	SGU/1954–55
Lund wells	Lu	611–802	Campanian	Lund Energy/1981–85
Margretheholm-1	Mah-1	2677	Precambrian	HGS, DONG/2002
Margretheholm-2	Mah-2	2750**	-“-	HGS, DONG/2003
Maglarp-1	Ma	1938	Silurian	OPAB/1971
Mossheddinge	Mo	1785	Precambrian	OPAB/1973
Norrevång-1	Nv	2127	-“-	OPAB/1971
Nyhem-1	Ny	1068	Santonian	Lund University/1981
Smygehuk-1	Sm	1660	Silurian	OPAB/1973
Svedala-1	Sv	1628	-“-	SGU/1948–51
Terne-1	Te	3361	L. Cambrian	Amoco/1985
Thisted-3	Th	1208	U. Triassic	DONG/1983
Trelleborg-1	Tr	1201	L. Cretaceous	SGU/1947
Ørslev-1	Ør	2537	Carboniferous	DUC/1968
Östratorp hamn	Öh	338	U. Cretaceous	SGU/1948

* Depth from rotary table ** Deviated well, depth converted to true vertical depth

Table 2. General information regarding the main seismic surveys on which the subsurface characterisation of the Øresund Basin has been performed

Seismic survey	Company	Acquisition date	Quality	Format
W 70	OPAB	September 1970	Fair	Scanned jpg
SKB 89	SECAB	May 1989	Good	Scanned jpg
WS 71	OPAB	June–August 1971	Fair	Scanned jpg
NA 79	OPAB	May–July 1979	Good	Scanned jpg
HGS 2000	DONG	2000	Excellent	SEGY
AO 8485	Phillips Petroleum	1984–85	Fair-poor	SEGY
SSL 6267	Mærsk Oil	1962–67	Poor	Scanned jpg

as assessment of potential geothermal reservoirs, but with increasing demands for geothermal energy an evaluation of these reservoirs is warranted (Nielsen *et al.* 2004; Mahler & Magtengaard 2010; Røgen *et al.* 2015). In addition, there is a need for characterising the lateral changes in lithofacies in the Mesozoic succession across the Øresund region, i.e. between the distal and marginal parts of the Danish Basin, and to establish a stratigraphic framework for these deposits.

The aims of this paper are, firstly, to describe the geological setting and geothermal properties of the Mesozoic reservoirs and provide an assessment of the geothermal potential, and secondly to contribute to the geoscientific understanding of the Øresund Basin in order to reduce the geological risks of unsuccessful geothermal wells.

Data and Methodology

By utilising the gearchives at the Geological Survey of Denmark and Greenland (GEUS) and the Geological Survey of Sweden (SGU), a comprehensive database combining Danish and Swedish seismic surveys and well data has been compiled (Fig. 2; Tables 1 and 2). This includes, for the first time, previously unpublished petrophysical and hydraulic properties of the reservoirs. Most of the information comes from well data and seismic surveys acquired between 1960 and 2003. Consequently, the data varies considerably with regard to format, quality and extent.

Seismic data set

The southern and central part of the studied area is covered by a relatively dense grid of seismic surveys, in contrast to the north-eastern part of Sjælland and the area between Helsingør and Landskrona, where seismic lines are few (Fig. 2). Most of the Swedish seismic surveys consist of low resolution data acquired during the 1970s (WS 71 and W 70 surveys). Relatively high quality surveys (NA 79 and SKB 89) exist in the southernmost part of the investigated area (Fig. 2). The SKB 89-501 line is a key line that transects the central part of the Øresund Basin and enables the tracing of marker horizons across the southern, central and northern parts of the Øresund Basin. Older analogue seismic lines have been digitised and integrated with the newer lines in SEG-Y format, a standard format for storing geophysical data established by the Society of Exploration Geophysicists (Hagelund & Levin 2017). The seismic data also include the HGS 2000 survey, which was performed for geothermal purposes around Copenhagen and Malmö and in the

sea between the two cities (Fig. 2). In addition, a set of older survey lines (AO 8485 and SSL 6267) located on northern Sjælland were reprocessed, which increased the quality and usefulness of the data. A compilation of pertinent survey data included in the study is shown in Table 2.

The depth maps presented here were constructed using the combined Danish and Swedish seismic data. Interpretation and seismostratigraphic mapping was performed by tracing marker horizons in wells in the western, eastern and southern parts of the study area, namely the Karlebo-1/1A, Margrethholm-1 and -2, Stenlille-19, Falsterborev-1, Smygehuk-1 and Ørslev-1 wells (Fig. 2).

Well data

A substantial amount of well information is derived from cored boreholes on the Falsterbo peninsula drilled by the Geological Survey of Sweden (SGU), and from hydrocarbon exploration wells in south-west Skåne drilled by the Swedish Oil and Gas Prospecting Company (OPAB) during the 1970s. More recently, comprehensive data obtained from four geothermal project wells drilled in Copenhagen (Margrethholm-1 and -2) and Malmö (FFC-1 and -2) in 2002–2003, a hydrocarbon exploration well (Karlebo-1/1A) drilled in 2006 in northern Sjælland, geothermal wells in the Lund area (1981–1985) and shallow cored boreholes in Helsingborg (2006–2009) have provided additional data (Table 1).

Results from geophysical wire-line logging obtained during the different drilling operations have been valuable, as amounts and quality of available geological material (cores and cuttings), analytical results and descriptions from the boreholes vary greatly.

Bottom hole temperature data primarily come from recordings performed during the wire-line logging operations. Data from two temperature profiles performed in FFC-1 and Ljunghusen-1 were recorded after drilling and reflect normalised temperature conditions.

Porosity and permeability measurements performed on sandstone beds in the cored boreholes (Höllviken-1, -2 and Ljunghusen-1), sidewall cores (FFC-1 well), and from outcrops and cores in the Helsingborg area, have provided actual data on these properties and have also been used for calibration of the geophysical wire-line log data (Springer 1997; Hjuler *et al.* 2014).

Data on formation fluids and gases were gathered from unpublished reports on performed analyses in the geothermal projects in Malmö and Lund (Bjelm & Alm 1995; Laier 2003).

The stratigraphic framework used for the correla-

tion of the different Mesozoic sandstone reservoirs in the Øresund Basin is largely based on palynological data presented in Lindström & Erlström (2011) and Lindström *et al.* (2017).

Geological setting

The Øresund Basin constitutes a local structure within the Danish Basin and is located in the transition zone between the Danish Basin to the west and south-west and the Fennoscandian Shield to the north-east. The subsurface bedrock in this transnational area between Sweden and Denmark is composed of a several kilometres thick succession of Phanerozoic strata overlying the Precambrian crystalline basement. Lower Palaeozoic strata in the area are so far only verified in parts of the Höllviken Half-graben (Figs 3, 4, 5). The Danish Basin formed as a result of Late Carboniferous–Early Permian rifting (Sørensen 1986; Liboriussen *et al.* 1987; Vejrbæk 1997). Due to the Sorgenfrei-Tornquist Zone (STZ) bordering the Øresund Basin to the north-east, Late Palaeozoic to Cenozoic deposits in this area reflect a complex tectonic history including periods of extension as well as compression of the bedrock in this marginal eastern part of the Danish Basin (e.g. Erlström *et al.* 1997; Nielsen 2003). The NW–SE oriented STZ is characterised by extensive block-faulting along the south-western margin of the Fennoscandian Shield (Sorgenfrei & Buch 1964; Rolle *et al.* 1979; Liboriussen *et al.* 1987). The STZ has been repeatedly active since Late Palaeozoic times with the main events occurring during the Mesozoic Era. Several Triassic–Jurassic extensional episodes are recognised (Norling & Bergström 1987), but these and older Palaeozoic events are often obscured due to Late Cretaceous–Palaeogene inversion tectonics (Norling & Bergström 1987; Michelsen & Nielsen 1991, 1993; Mogensen 1994; Michelsen 1997; Erlström *et al.* 1997; Mogensen & Korstgård 2003). The western and south-western margin of the Øresund Basin is outlined by the Øresund, Amager and North Sjælland faults and the East Sjælland High (Fig. 1).

The structural outline of the Øresund Basin is controlled by a set of right-stepping normal extension faults to the west and by the reverse Romeleåsen Fault Zone to the east, which constitutes the boundary to the STZ. The normal faults to the west were initiated during Carboniferous–Permian rifting and reactivated during Triassic E–W tension (Erlström *et al.* 1997; Sivhed *et al.* 1999). Extension and subsidence in the Early and Middle Triassic resulted in localised accommodation space and thickening of the corresponding strata towards the delimiting faults,

especially the Øresund, Amager and North Sjælland faults. The displacements on the faults vary as the individual fault dies out laterally. This is especially seen along the Øresund Fault which dies out to the north-north-west and the North Sjælland Fault where the displacement fades out to the south-south-east. A geo-section illustrating main tectonic events and stratigraphical representation in a SW–NE oriented transect across the southern parts of the Øresund Basin is presented in Fig. 3.

The marginal position of the Øresund Basin, with the Fennoscandian Border Zone and the Sorgenfrei-Tornquist Zone to the north-east, has resulted in the formation of a Mesozoic sedimentary succession that is largely composed of deposits formed in shallow marine to fluvial environments. This has resulted in several sandstone-dominated intervals with potential as geothermal reservoirs.

During Triassic–Jurassic time, erosion of the Fennoscandian Shield delivered material to the thermally controlled, post-rift subsiding Øresund and Danish basins (Liboriussen *et al.* 1987; Vejrbæk 1989; Erlström *et al.* 1997).

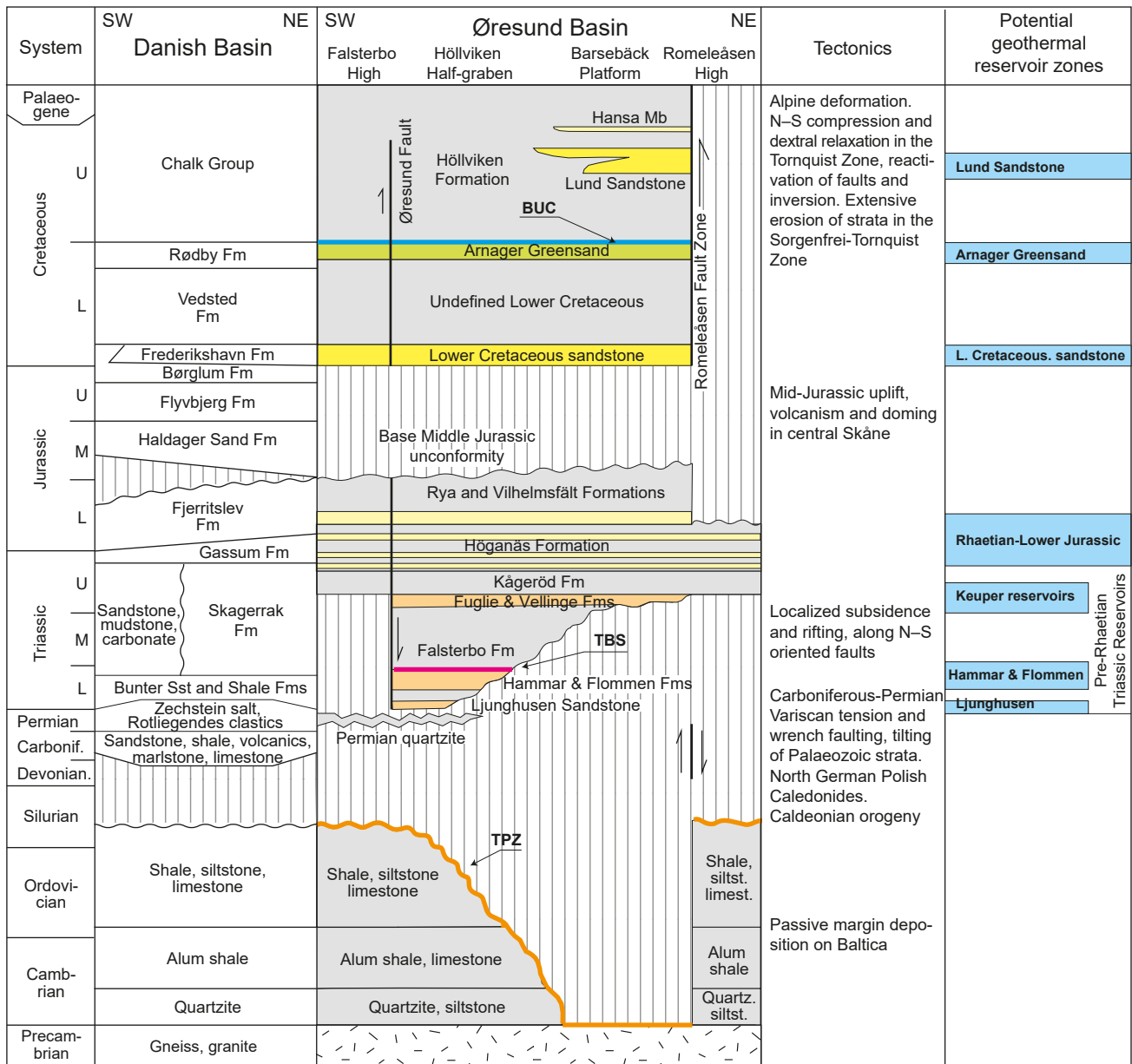
The Øresund Basin is divided into the Höllviken Half-graben, the Barsebäck Platform and the North Sjælland Half-graben (Fig. 1). The Barsebäck Platform constitutes a transfer zone between the North Sjælland and Höllviken half-grabens. The platform is characterised by horizontally bedded strata and a relatively thin Triassic succession overlying the Precambrian basement, in contrast to the Höllviken Half-graben which displays successively increasing thicknesses and representation of strata towards the Øresund, Amager and North Sjælland faults. (Figs 3, 4).

Interpreted key profiles

The general subsurface structure of the Øresund Basin is illustrated by four interpreted seismic key profiles (Fig. 4). Profile 1, oriented N–S through the southern part of the Øresund Basin, displays the lateral variation of thicknesses and stratigraphic representation of the sedimentary succession, as the profile crosses not only the Barsebäck Platform but also the Höllviken Half-graben and the Øresund Fault (Fig. 4). The profile, which corresponds to a large part of the SKB 89-501 line, displays a southward dipping and thickening pre-rift Lower Palaeozoic succession in the Höllviken Half-graben, as well as a syn-rift Triassic succession with increasing thickness towards the Øresund Fault. The data shows that the Triassic–Jurassic succession is relatively thin (c. 350 m) on the Barsebäck Platform, whereas it is up to 700 m thick adjacent to the Øresund

Fault. A corresponding, however less pronounced, lateral increase in thickness of the Jurassic–Lower Cretaceous interval towards the Øresund Fault is also indicated in the interpreted profile (Fig. 4). The

Upper Cretaceous–Palaeogene succession increases in thickness towards the Romeleåsen Fault Zone. This is verified by an up to 1800 m thick Upper Cretaceous–Palaeogene succession in the Barsebäck-1 and



Potential geothermal reservoirs

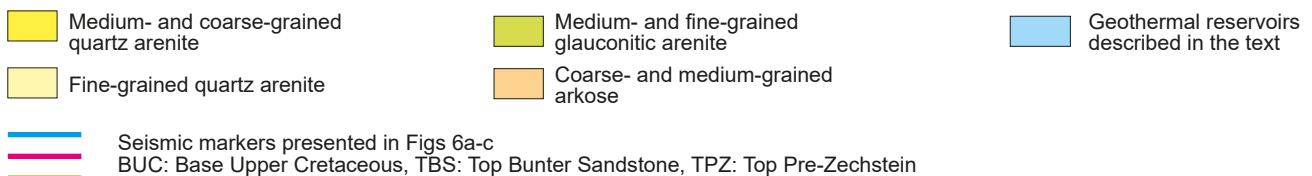


Fig. 3. Geo-section of the Øresund Basin representing a section from the north-east to the south-west, covering the southern parts of the basin. The location is shown in Fig. 1. For comparison, the lithostratigraphic division of the Danish Basin is summarised in a separate column. The right column shows the position of the potential geothermal reservoir intervals which are discussed in the text.

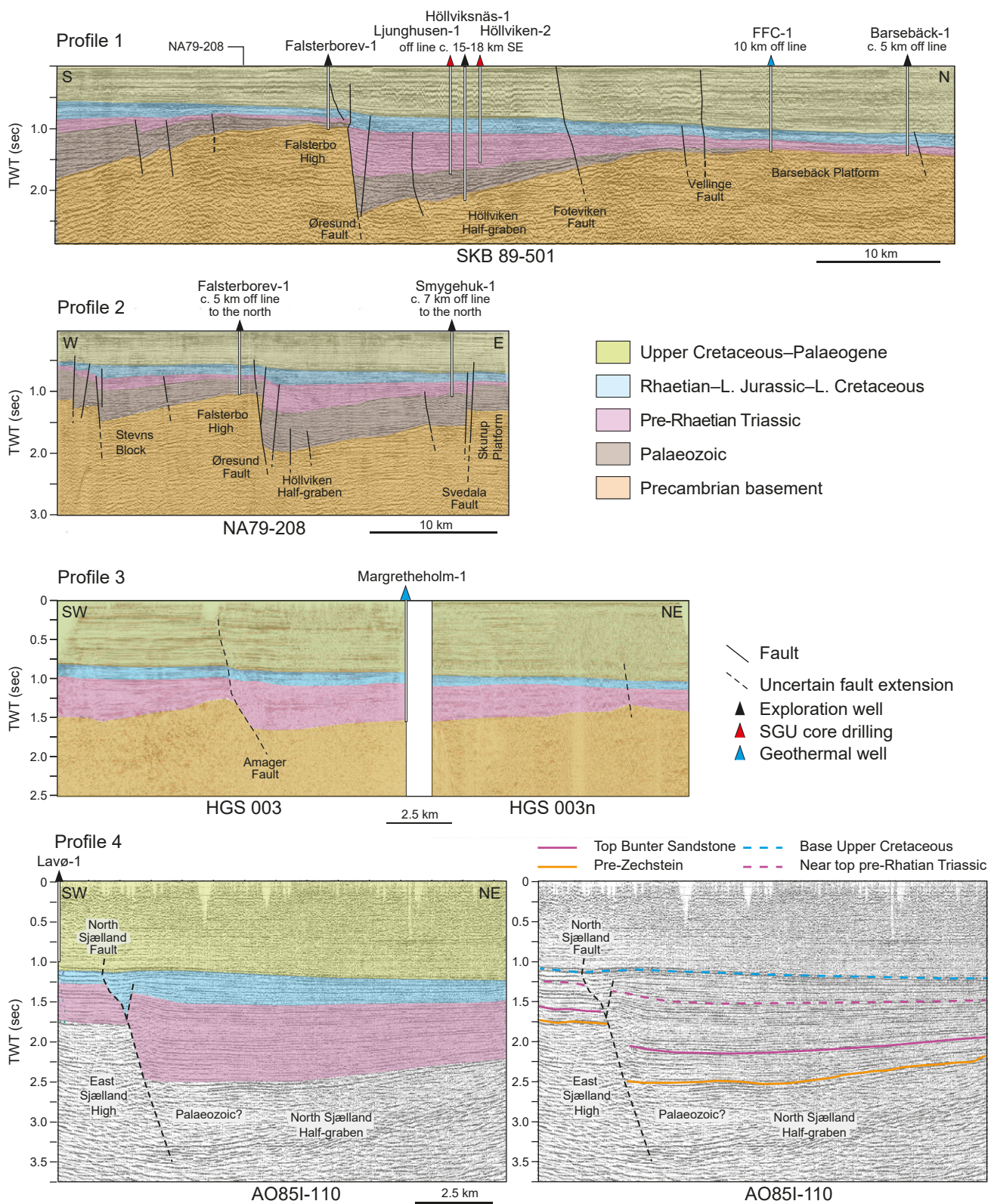


Fig. 4. Interpreted profiles 1–4 based on the seismic lines SKB 89-501, NA79-208, HGS003 and AO851-110. The profile on northern Sjælland is also illustrated with the marker horizons shown. The profile locations are shown in Fig. 2.

Norrevång-1 wells adjacent to the Romeleåsen Fault Zone (Sivhed *et al.* 1999), while the same interval is only c. 900 m thick in the south part of the profile, e.g. in the Falsterbørev-1 well (Fig. 5). This lateral variation is caused by greater subsidence in the eastern parts of the Øresund Basin, linked to Late Cretaceous to Palaeogene inversion of the Sorgenfrei-Tornquist Zone. This has created accommodation space for a several hundred metres thick syn-tectonic Campanian sandstone (the Lund Sandstone) adjacent to the Romeleåsen Fault Zone, and here this sandstone contributes significantly to the total thickness of the Upper Cretaceous (Erlström 1994; Erlström *et al.* 1997).

The Na 79-208 line (Fig. 4, profile 2) crosses the south parts of the Höllviken Half-graben perpendicular to profile 1. The Lower Palaeozoic succession is here clearly visible in the seismic data, as is the increasing thickness of the pre-Rhaetian Triassic succession against the Øresund Fault. A similar lateral increase in thickness is also seen in the gently dipping Stevns Block west of the Falsterbo High towards the Stevns Fault. The seismic data also indicate that the Triassic as well as the Jurassic–Lower Cretaceous succession is <200 m thick on the Skurup Platform. In the Svedala-1 well, the pre-Rhaetian Triassic succession is only 66 m thick (Erlström & Sivhed 2012) and the Jurassic–Lower Cretaceous succession is 86 m thick, including the Cenomanian Arnager Greensand (Sivhed *et al.* 1999).

The interpretation of the HGS 003 line (Fig. 4, profile 3) is largely based on data from the Margretheholm (Mah-1/-2) geothermal wells. The profile shows a similar thickening of the pre-Rhaetian Triassic succession towards the Amager Fault as observed towards the Øresund Fault in profile 1. This is mainly due to increased thickness of the Lower and Middle Triassic strata, which is verified in the Mah-1/-2, Ljunghusen-1, Höllviksnäs-1 and Höllviken-2 wells. Profiles 1 and 3 show a gently dipping half-graben with only minor faulting outside the main delimiting faults. Similar subsurface structures and depths are also indicated in profile 4 in the northern part of the Øresund Basin; this profile extends over parts of the North Sjælland Half-graben and crosses the North Sjælland Fault (Fig. 4). The seismic signature is interpreted to represent a sedimentary succession similar to that in the Höllviken Half-graben. It is significant that the seismic data indicates an even thicker Triassic succession in comparison to the Höllviken Half-graben, reaching perhaps a total thickness in excess of 1000 m. Furthermore, the seismic signature indicates that there may be an up to 6500 m thick sedimentary succession in the deepest parts of the North Sjælland Half-graben. This suggests the presence of thick Palaeozoic deposits underlying the Triassic, similar to the geological setting in the Höllviken Half-graben (Fig. 4, profiles 1 and 2).

Well correlation

The seismic profiles were carefully matched with stratigraphical and geophysical data from several wells, especially the geothermal wells Mah-1/-2 and FFC-1/-2 in Copenhagen and Malmö, but data from Falsterbørev-1, Höllviksnäs-1, Barsebäck-1 and Karlebo-1/1A were also important. A well-log panel for these wells displays the drilled pre-Upper Cretaceous sedimentary succession, which shows a heterogeneous Triassic–Lower Cretaceous succession with several rock types represented (Fig. 5). Significant lateral variation is evident within the pre-Rhaetian Triassic interval, as well as changes in thickness of the Rhaetian–Jurassic interval. In contrast, the Lower Cretaceous strata appear more consistent in thickness, with e.g. the Lower Cretaceous sandstone beds and the Cenomanian Arnager Greensand displaying a more uniform regional distribution than what is observed for the underlying succession.

Individual beds, especially in the Triassic–Lower Jurassic interval, are difficult to correlate between wells due to frequent lateral shifts in lithofacies in the proximal depositional setting. There is, however, an overall greater proportion of geothermally interesting sandstone beds in the pre-Rhaetian succession that can be correlated between wells, *i.e.* the Lower Triassic Ljunghusen Sandstone, the Hammar–Flommen Formations and the Middle Keuper Vellinge Formation (Fig. 3).

Depth structure maps

Three marker horizons (Fig. 3): the Top Pre-Zechstein, the Top Bunter Sandstone Formation (corresponding to the Hammar and Flommen Formations in the Øresund Basin) and the base Chalk/Upper Cretaceous have been mapped and are presented as depth maps in Figs 6a–c. One additional map shows the gross thickness of the Base Chalk/Upper Cretaceous–Top Pre-Zechstein interval (Fig. 6d), the purpose of which is to visualise the gross thickness of the interval in which the various potential geothermal reservoirs described in this paper are found, with the exception of the Upper Cretaceous Lund Sandstone.

Top Pre-Zechstein surface

The Top Pre-Zechstein surface occurs at depths varying from 1100 m to 6500 m (Fig. 6a). Its shallowest levels are in the southern part of the study area approaching the Ringkøbing-Fyn High, and in the central part of the area on the East Sjælland High.

The Top Pre-Zechstein surface is found at its deepest level in the North Sjælland Half-graben adjacent to the North Sjælland Fault and in an area in the south in the Höllviken Half-graben close to the Øresund Fault (Fig. 6a). The outline of the Top Pre-Zechstein surface is intersected by several normal faults (Ste-

vns, Øresund, Amager, North Sjælland, Foteviken, Vellinge and Svedala faults). These faults are oriented NW-SE, however, the Svedala Fault in the easternmost part of the area is oriented more or less N-S. The faults and their interpreted offset on the individual seismic profiles, together with the depth to the Top

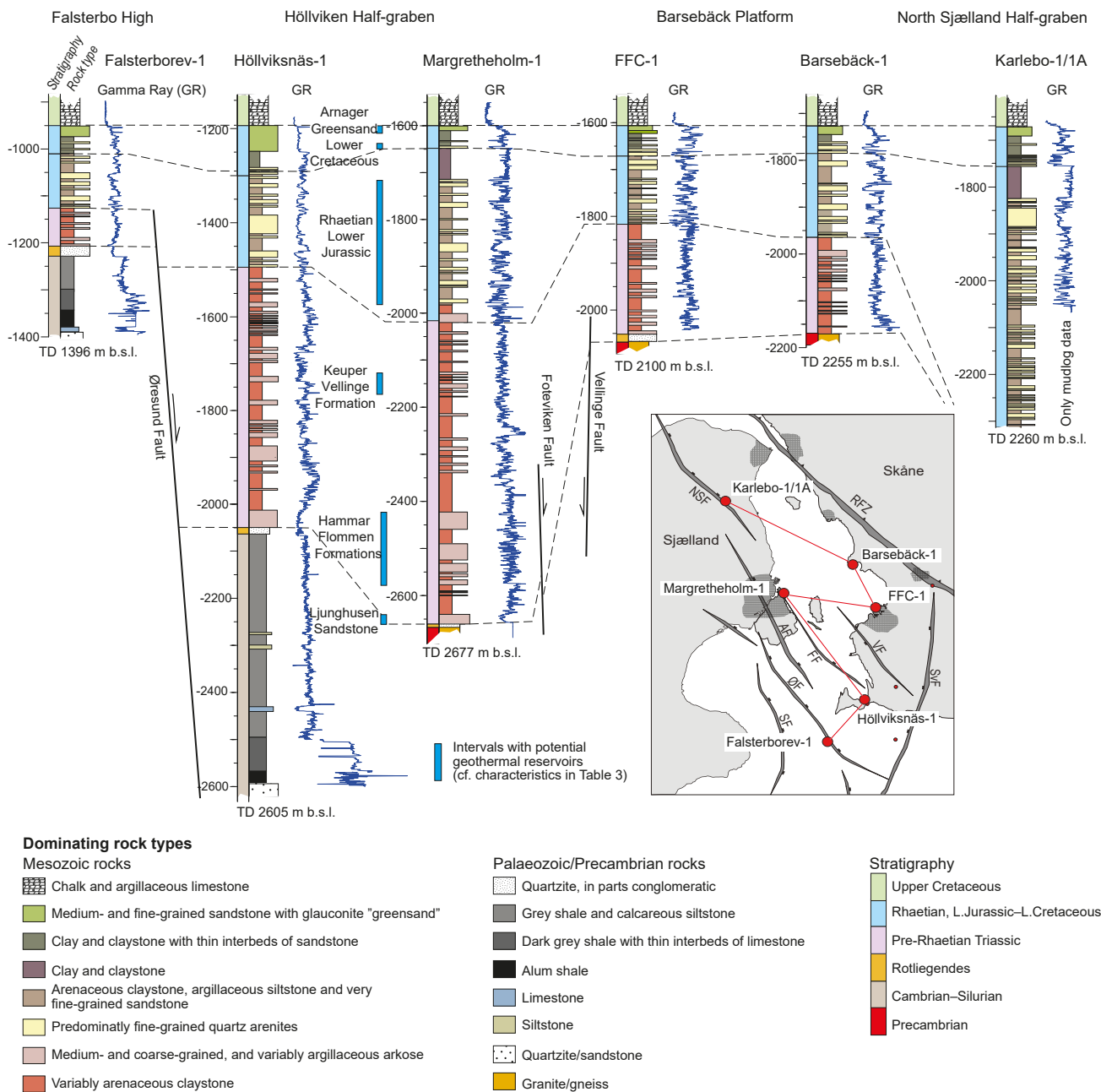


Fig. 5. Illustration showing a stratigraphic well correlation panel including the wells Karlebo-1/1A, Barsebäck-1, FFC-1, Margrethesholm-1, Höllviksnäs-1 and Falsterborev-1. The wells illustrate the sedimentary succession in different parts of the area, *i.e.* the Höllviken Half-graben, the Barsebäck Platform and the North Sjælland Half-graben. The well paths are flattened to the top Arnager Greensand, *i.e.* top Cenomanian. The correlation is based on a combination of data from well site geology reports, geophysical wire line logs and biostratigraphical data (e.g. Lindström & Erlström 2011). The main geothermal reservoir intervals are presented for the Margrethesholm-1 well. Their characteristics are summarised in Table 3.

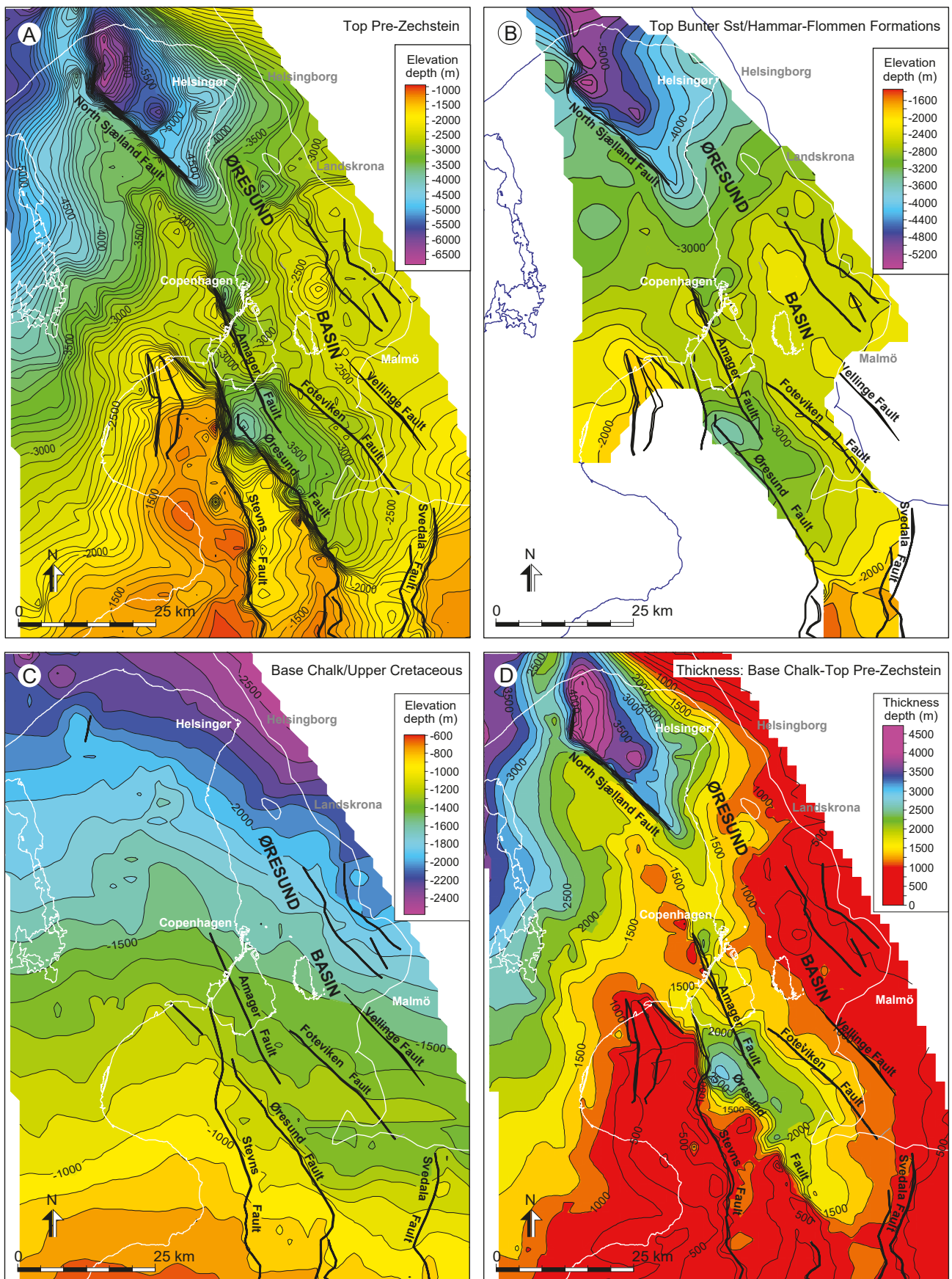


Fig. 6. Depth maps. A: Top Pre-Zechstein. B: Top Bunter. C: Base Chalk/Upper Cretaceous. D: Map illustrating the gross thickness of the interval between the Top Pre-Zechstein and Base Chalk/Upper Cretaceous, in which the assessed potential geothermal reservoirs are found, except for the Upper Cretaceous Lund Sandstone.

Pre-Zechstein, show that most faults are organised in arrays. This influences the depth map by causing an irregular depth pattern of the Top Pre-Zechstein reflector, especially close to the faults. The depth map shows several half-grabens that are generally down-faulted to the west (Fig. 6a). As exemplified by profile 1 in Fig. 4, the lower part of the Triassic exhibits onlap towards the successively elevated Top Pre-Zechstein surface which corresponds to the Top Palaeozoic or the Top Precambrian. Only the uppermost part of the Triassic succession is more uniformly distributed in the Øresund Basin.

Top Bunter Sandstone Formation (Top Hammar–Flommen) surface

In the Danish Basin, the Top Bunter surface corresponds to the top or near top of the Bunter Sandstone Formation. Eastward tracking of this seismic reflector into the Øresund Basin is complicated by a change in acoustic impedance caused by the transition between claystone and sandstone beds near the top of the Hammar and Flommen Formations.

The Top-Bunter surface onlaps the Top Pre-Zechstein surface on the flanks of the Ringkøbing Fyn High and the East Sjælland High (Figs 1, 6b). Consequently, the Bunter Sandstone Formation is thin or absent immediately south-west of the Øresund Fault. Towards the north, the Top-Bunter surface can be traced west and east of the Amager and North Sjælland faults. Its deepest level occurs in a NNW–SSE oriented area delimited to the west by the Øresund, Amager and North Sjælland faults. The surface is located at its deepest level in the deepest parts of the half-grabens outlined by the Top Pre-Zechstein reflector (Fig. 6b).

Base Chalk/Upper Cretaceous surface

In the Øresund Basin, the Base Chalk surface corresponds to the base of the Upper Cretaceous (*i.e.* Höllviken Formation; Sivhed *et al.* 1999). It represents a pronounced reflector occurring at the interface between the Arnager Limestone and the Arnager Greensand and is present throughout the study area. The surface reaches its highest level close to the Ringkøbing-Fyn High and the East Sjælland High (Fig. 1). The Base Chalk/Upper Cretaceous surface exhibits a general dip towards the NE in the Øresund Basin (Fig. 6c). It is intersected by a few faults in the southern part of the study area between the Øresund and Svedala faults, with minor offsets affecting the lower third of the Upper Cretaceous succession (profile 1, Fig. 4). Farther to the north, e.g. around the Amager Fault, the seismic profile indicates subsequent inversion. Faulting appears to have taken place later, as the Chalk

strata only appear affected within approximately 50 m depth below the sea floor.

Gross thickness of the Base Chalk/Upper Cretaceous–Top Pre-Zechstein interval

In the Øresund Basin, this interval commonly ranges between 500 m and 2000 m in thickness. East of the East Sjælland High there are two depocentres where thicknesses exceed 2500 m, namely the North Sjælland Half-graben and the Höllviken Half-graben. These are separated by the Barsebäck Platform which exhibits a much thinner succession (Fig. 6d). The northern depocentre, the North Sjælland Half-graben, is delimited by the North Sjælland Fault and the gross thickness here is interpreted to be as much as 4500 m (Fig. 6d). The Höllviken Half-graben depocentre can be subdivided into three parts. One part is located adjacent to and along the Øresund Fault. The maximum thickness of the Base Chalk/Upper Cretaceous–Top Pre-Zechstein interval is here about 2700 m. The second part of the Höllviken Half-graben depocentre is bounded by the Amager Fault to the west, and the maximum thickness of the Base Chalk/Upper Cretaceous–Top Pre-Zechstein interval is here close to 2300 m. To the north along the Amager Fault a third subarea of the Höllviken depocentre is outlined by the seismic data. Here the maximum thickness is estimated to reach 1800 m, decreasing towards the north-east. The depocentres related to the Amager Fault display different seismic characteristics indicating a somewhat variable geological development, possibly involving a separation of the Amager Fault into two fault segments, at least periodically.

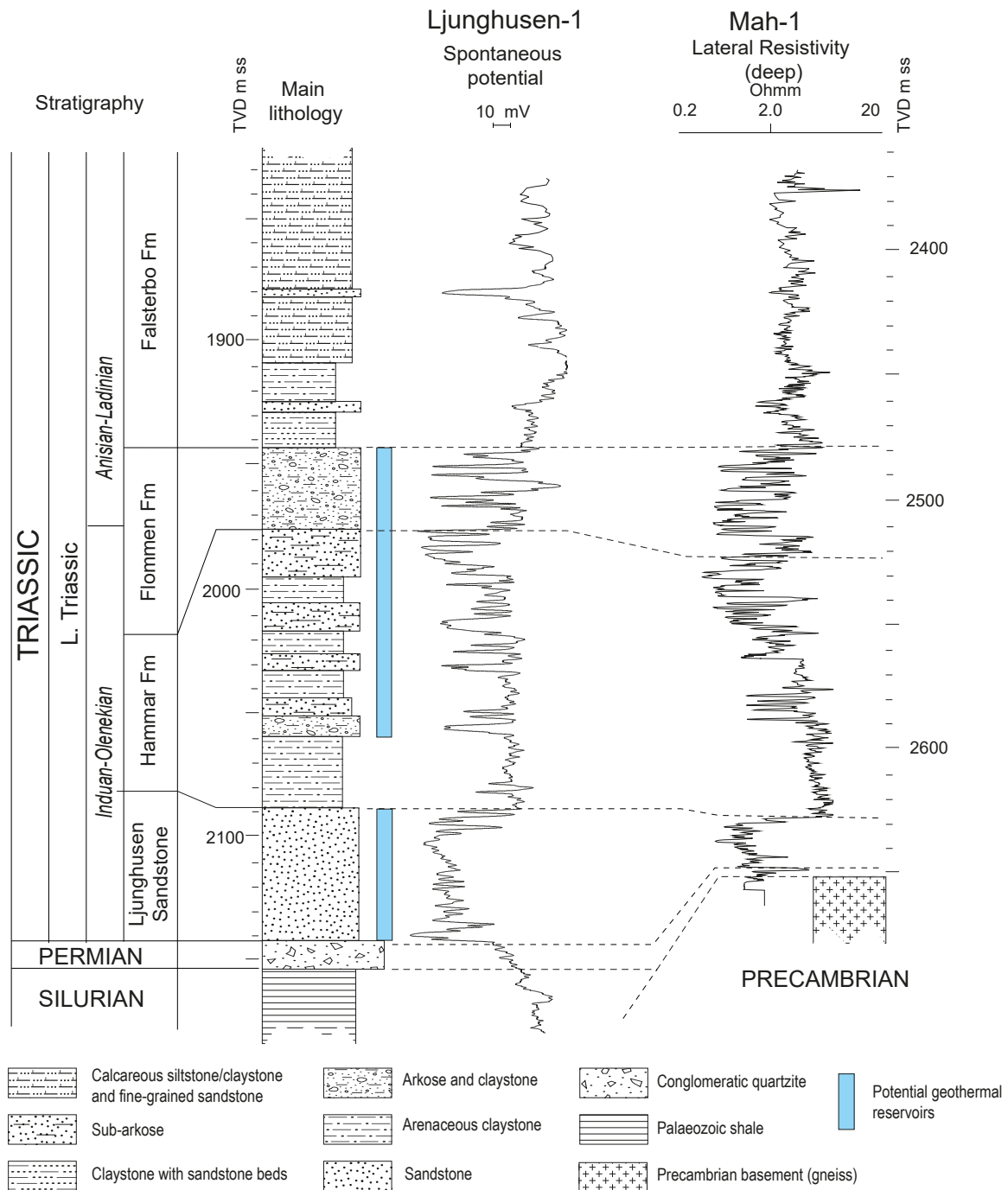
Geothermal reservoirs in the southern and central part of the Øresund Basin

Pre-Rhaetian Triassic reservoirs

The lithostratigraphic subdivision of the Triassic in the Øresund Basin corresponds in many parts to the German-type Facies Province and the Danish Basin (Bertelsen 1980; Beutler & Schüler 1987; Beutler 1998; Michelsen & Clausen 2002; Erlström & Sivhed 2012). However, it is difficult to fully extrapolate the German stratigraphy into the Øresund Basin, mainly due to its predominantly proximal position compared to the North German and Danish basins (Erlström & Sivhed 2012). There is a pronounced lack of biostratigraphically important fossils in the Øresund Basin, which hampers age dating and correlation. However, a few

marker beds in the Höllviken Half-graben have been identified, and these provide correlation of at least parts of the Triassic succession to the German-type Facies Province and stratigraphy (Erlström & Sivhed 2012). One example is the Falsterbo Formation in Skåne and equivalent beds in the Danish Basin and

Danish Central Graben which have been assigned a late Ladinian–early Carnian age based on palynology (Bertelsen 1975; Piasecki 2005; Lindström *et al.* 2009; Lindström *et al.* 2017). In the Höllviken Half-graben these sediments consist of argillaceous, dark grey beds with coal fragments and thin coal layers, which inter-



TVD m ss: True Vertical Depth in metres below sea level

Fig. 7. Composite well log panel of Ljunghusen-1 and Margrethholm-1 (Mah-1), illustrating the main lithology and selected electrical log responses for the Lower–Middle Triassic Ljunghusen Sandstone and Hammar–Flommen reservoirs.

rupt the otherwise reddish argillaceous–arenaceous and poorly sorted pre-Rhaetian Triassic succession (Erlström & Sivhed 2012). The palynofloras enable correlation between the Falsterbo Formation and the Lower Keuper Erfurt Formation, also named Lettenkohle or Lettenkeuper (Beutler & Schüler 1987; Beutler 1998; Piasecki 2005).

The possibly continuous Triassic succession in the Höllviken Half-graben is exemplified by a thick pre-Rhaetian Triassic succession in the wells Ljunghusen-1 (638 m) and Höllviksnäs-1 (569 m) on the Falsterbo peninsula. The Triassic rests on Precambrian crystalline rocks or on the Pre-Zechstein surface represented by an up to 40 m thick conglomeratic quartzite of presumably Permian (Rotliegendes) age on top of truncated Lower Palaeozoic successions of shale, limestone and quartzite (Erlström & Sivhed 2012; Fig. 7). The pre-Rhaetian Triassic succession is shown in a selection of wells in Figs 5 and 7.

Three main geothermal reservoirs are recognised in the pre-Rhaetian Triassic interval in the Höllviken Half-graben, namely the Ljunghusen Sandstone, the Hammar–Flommen Formations and the Keuper reservoir interval, which includes primarily the Vellinge Formation (Figs 5, 7).

The Bunter Sandstone Formation in the Danish Basin is defined as Lower Triassic, predominantly reddish, poorly sorted sub-arkose interbedded with thin beds of claystone (Rhys 1974; Bertelsen 1980). The formation is widely recognised in the North Sea and in North Germany. North of the Ringkøbing-Fyn High, the formation interfingers with the lower part of the Skagerrak Formation (Fig. 3) and displays more varied lithologies and thicknesses in comparison to south of the Ringkøbing-Fyn High in the North German Basin (Bertelsen 1980; Nielsen & Japsen 1991; Michelsen & Clausen 2002; Olivarius & Nielsen 2016). In the Lower Triassic succession in the North German Basin there are four distinct sandstone units separated by thick claystone-dominated intervals and informally named Volprieshausen, Detfurth, Hardeggen and Solling sandstones of the Buntsandstein (Lepper & Röhling 1998; Bachmann 1998; Beutler 1998; Hagdorn *et al.* 1998; Bachmann *et al.* 2005).

Based on correlation of geophysical well-logs, the reservoirs in the Ljunghusen Sandstone and Hammar–Flommen Formations exhibit a relatively uniform lateral continuity with regard to their petrophysical and lithological properties, while the Keuper reservoir interval is more heterogeneous both laterally and vertically. The three pre-Rhaetian Triassic reservoirs are described below, and overall predictions and empirical data on the characteristics of these units are summarised in Table 3.

Ljunghusen reservoir

The Ljunghusen Sandstone occurs at 2088–2150 m in the Ljunghusen-1 well, at 2010–2063 m in the Höllviksnäs-1 well and at 2640–2658 m depth in the Margrethholm-1 well (Table 3). Thin occurrences are found in the Kungstorp-1 well and possibly also in the Eskilstorp-1 well (Erlström & Sivhed 2012). From these observations it is judged that the Ljunghusen reservoir has a wedge-like distribution restricted to the deepest parts of the Höllviken Half-graben, where it thickens towards the bounding Amager and Øresund faults in the west and south-west. It is unclear if it occurs in the North Sjælland Half-graben.

In the Ljunghusen-1, Höllviksnäs-1 and Margrethholm wells, the formation is composed of relatively homogeneous, reddish to pinkish, medium- and coarse-grained, well-sorted sandstone with siltstone layers and traces of carbonate cement. Thin iron coatings are common on the grains. Quartz grains are dominantly smooth and rounded, occasionally also with a frosted grain surface. Accessory minerals are subordinate and mica is lacking. These characteristics indicate an aeolian depositional setting (Nielsen 2001). Even though the corresponding parts of the Bunter Sandstone Formation is dominated by fluvial sandstone and lacustrine claystone deposited in ephemeral river systems and lakes, aeolian deposits are known both from the marginal parts of the Danish Basin and in the North German Basin (Mader & Yardley 1985).

The Ljunghusen reservoir is well-defined by the log response. The spontaneous potential and resistivity logs indicate a porous homogeneous unit, clearly distinguished from the overlying arenaceous claystone (Fig. 7). The basal boundary is defined by a presumed Permian (Rotliegendes) dense, conglomeratic quartzite which occurs beneath the Triassic in most wells in the Höllviken Half-graben (Fig. 7).

The Ljunghusen Sandstone is interpreted to be contemporaneous with the Volprieshausen Sandstone in the lower Middle Buntsandstein in Northern Germany, which constitutes the lowermost of four sandstone units in the Buntsandstein that are recognised in the Netherlands and in North Germany along the south side of the Ringkøbing-Fyn High (Aigner & Bachman 1992; Lepper & Röhling 1998).

To date, no hydraulic well tests or porosity and permeability analyses have been carried out on the Ljunghusen Sandstone interval. Despite this, it is still considered to be a potentially good geothermal reservoir. This is based on petrographic studies on cuttings from Höllviksnäs-1 that indicate a uniform, well-sorted sandstone with only minor cementation and (in contrast to other pre-Rhaetian Triassic intervals) low clay matrix content. Evaluations of wire-line logs give an average effective porosity of 22.5% (Nielsen 2001).

Hammar-Flommen reservoir

Coarse- and medium-grained, sub-arkosic sandstone beds interbedded with variably coloured red-green-brown and purple claystone are found at 2470–2660 m in the Margrethholm-1 well, at 1890–2007 m in the Höllviksnäs-1 well and at 1938–2082 m in the Ljunghusen-1 well (Table 3). The unit has a similar geophysical resistivity log response in the Margrethholm-1 and the Ljunghusen-1 wells (Fig. 7). The serrated geophysical log pattern combined with mud log data illustrate frequent changes in petrophysical properties, as well as rock types, where poorly sorted sub-arkose dominates (Fig. 7). In Skåne, this interval is defined as the Hammar and Flommen Formations, which are tentatively correlated with the Bunter Sandstone Formation in the Danish Basin and the corresponding Solling Formation in North Germany. The sandstone beds are often poorly consolidated and highly permeable (Erlström & Sivhed 2012).

So far the Hammar–Flommen interval is verified only in the southern and south-western parts of the Øresund Basin. To the north it becomes successively thinner and is absent on most parts of the Barsebäck Platform (Erlström & Sivhed 2012). It is unclear if the presumed equivalent, seismostratigraphically mapped, thick Triassic succession in the North Sjælland Half-graben includes strata of the same age and lithological properties as the Hammar–Flommen interval in the Höllviken Half-graben.

The Lower Triassic deposits in north-western Europe were primarily formed in a low relief landscape. Playa lakes (mudflats) and interfingering braided fluvial systems of ephemeral character dominated the depositional environment. Similar conditions prevailed in much of the North German Basin during the Early Triassic (Lepper & Röhling 1998). Similar depositional settings most likely occurred in the Øresund Basin, however, with a more pronounced influx of coarse clastic deposits from the Fennoscandian Shield. This highly variable depositional setting may lead to difficulties in assessing the hydraulic communication and the textural properties of this geothermally interesting interval. The present knowledge of the reservoir properties is mainly based on information from hydrological tests and production data from the Margrethholm-1 and -2 wells. Production data for this interval in Margrethholm-1 give an average permeability of 400 mD for a 92 m long, perforated section at a mid-point depth of 2550 m and 48 m net sand. The 73°C warm formation water from this depth has a chloride content of *c.* 130 g/l (Table 3).

The Keuper reservoir interval

In the Höllviken Half-graben the Keuper reservoir interval consists of the sandstone interval in the Vellinge

Formation and coarse-grained and conglomeratic beds of arkose in the overlying Fuglie and Kågeröd Formations. The Vellinge Formation is a 15–20 m thick sandstone interval overlying Ladinian to lowermost Carnian grey, micaceous, fine-grained beds of the Falsterbo Formation (Lindström *et al.* 2009; Lindström *et al.* 2017). The Vellinge Formation is interpreted as reflecting a change from relatively humid conditions, witnessed by a well-preserved and diverse palynoflora in the Falsterbo Formation, to more arid conditions with continental proximal deposition of variably sorted sandstone with numerous conglomerate beds (Lindström *et al.* 2009; Lindström *et al.* 2017). Part of the succession is composed of stratified fluvial sandstone beds with a grey overprint which indicates that there were still periods of more humid conditions. The sandstone beds of the Vellinge Formation have been tentatively correlated with the Hauptsandstein of the Erfurt Formation in the North German Basin (Erlström & Sivhed 2012).

The frequent presence of loose, permeable and poorly sorted sandstone beds with pedogenic-related features (nodules, dendritic calcite, rhizoliths and calcrete) and conglomerates results in very heterogeneous reservoir properties, with large variations both vertically and laterally within the interval. This renders an overall assessment of the Keuper reservoir interval difficult. Production tests in the FFC-1 well gave a productivity index of 2.9 m³/hr/bar for the Keuper interval. The 110 m of net sand over a 213 m long, perforated section with a mid-point at 1950 m depth gave an average permeability of 53 mD and a production temperature of 62.8°C (DONG 2003). Analyses on cores from individual sandstone beds in the FFC-1 and Höllviken-1 wells gave permeability values below 100 mD (Table 3).

Rhaetian–Lower Jurassic reservoir

In the late Triassic (Rhaetian), the structural pattern changed from local graben development to widespread subsidence of the Danish Basin. Eustatically controlled progressive overstepping of the Øresund Basin by the sea was accompanied by a change from seasonally arid to more humid climate with more widespread deposition (Bertelsen 1978; Norling & Bergström 1987; Ahlberg *et al.* 2003; Nielsen 2003). Thus, the texturally immature detrital sediments of the Carnian–Norian Kågeröd Formation were followed by Rhaetian–Hettangian chemically and texturally mature deposits (Ahlberg 1994). These comprise several repeatedly occurring similar successions of shallow marine and coastal depositional settings, including lagoonal, fluvial, estuarine, shoreline and marine facies associations (Norling *et al.* 1993; Ahlberg *et al.* 2003; Nielsen 2003). Most of the Rhaetian–Lower

Jurassic succession belongs to the 100–300 m thick Rhaetian to lowermost Sinemurian Gassum Formation, corresponding to the Höganäs Formation and the basal part of the Döshult Member in the Rya Formation in Skåne (Ahlberg *et al.* 2003; Nielsen 2003; Lindström *et al.* 2017).

In the Øresund Basin these strata are dominated by fine-grained shallow marine and shore face sandstones alternating with heterolites and clays deposited in coastal environments (Michelsen *et al.* 2003; Nielsen 2003). Six major lithofacies have been recognised, *i.e.* fine-grained quartz arenite, medium-grained arenite, silt- and clay-dominated heterolites, sand-dominated heterolites, claystone and coal (Bou Daher 2012).

In the central parts of the Danish Basin, the Lower Jurassic (Hettangian–lowermost Aalenian, post-Gassum Formation) succession consists predominantly of marine claystone and siltstone of the Fjerritslev Formation (Michelsen *et al.* 2003). The Stenlille-1, Lavø-1, Karlebo-1/1A, Margrethholm-1 and -2 wells in the eastern part of the Danish Basin encountered a 129–170 m thick post-Gassum Lower Jurassic succession with an eastward increasing amount of sandstone, interpreted as distal equivalents to the sandstone intervals in the Lower Jurassic of Skåne (Nielsen 2003; Hjuler *et al.* 2014).

The lower Sinemurian in Skåne is dominated by near-shore mature, coarse-grained arenite, forming the Döshult Member of the Rya Formation (Troedsson 1951; Norling & Bergström 1987; Norling *et al.* 1993; Erlström *et al.* 1999). Additional minor sandstone intervals are found in north-western Skåne in the overlying upper Sinemurian–lower Aalenian Katslösa and Rydebäck members (Sivhed 1984; Norling *et al.* 1993).

All in all, sandstone beds constitute as much as 40–60% of the Rhaetian–Lower Jurassic succession in Skåne. However, most of the sandstone beds are dominated by fine-grained micaceous quartz arenites with poor hydraulic properties. Analyses on cores show a permeability ranging from 50 mD for the fine-grained sandstone beds to 1500 mD for medium-grained varieties (Erlström & Sivhed 1997).

The petrography of the Rhaetian–Sinemurian sandstones is mainly known from studies by Ahlberg (1994), Ahlberg & Ohlsson (2001) and Hjuler *et al.* (2014). The composition and reservoir characteristics of the succession are relatively well constrained by these studies, as well as by hydraulic tests performed in the FFC-1 well. In the Malmö–Copenhagen and Helsingborg areas, the major part of this interval is composed of wavy- and flaser-bedded, fine-grained quartz arenites. The degree of cementation varies considerably. Poorly cemented beds, with interlocking grain-to-grain silica cementation, dominate. Coarser-grained sandstone beds are mainly found in the middle and

upper Rhaetian and uppermost Hettangian, *i.e.* the Bjuv Member, the Boserup beds and the Fleninge beds of the Höganäs Formation (Sivhed 1984). Medium- and coarse-grained units are also found in the Sinemurian Döshult Member of the Rya Formation (Norling *et al.* 1993). The overall dominance of fine-grained texture of the sandstone beds limits the reservoir properties with regard to the transmissivity. Pumping tests specifically targeting the Rhaetian–Lower Jurassic interval have not yet been performed. However, a pumping test in FFC-1 of the interval combined with the Lower Cretaceous interval gave a productivity index of 7.0 m³/hr/bar (Table 3). Nevertheless, judging from flow meter logging, not more than 20% of this was related to the Rhaetian–Lower Jurassic reservoir. Despite the indicated poor production capacity in the southern parts of the Øresund Basin, the general trend of increasing grain-size and amount of net sand to the north and north-east indicates increased potential for geothermal use of the Rhaetian–Lower Jurassic reservoir in this direction (Hjuler *et al.* 2014).

Lower Cretaceous including the Arnager Greensand reservoirs

In the Øresund Basin a 50–125 m thick Lower Cretaceous (Berriasian–Cenomanian) succession (Fig. 5) includes an up to 30 m thick sandstone overlying the base Middle Jurassic unconformity that truncates Lower Jurassic strata (Nielsen 2003; Lindström & Erlström 2011). The sandstone interval is overlain by variegated claystone layers with interbeds of sandstone, followed by the Arnager Greensand (Aptian–Cenomanian). The latter constitutes the top of the Lower Cretaceous mixed clastic succession formed in a marginal-marine and shallow shelf setting (Norling 1981; Gravesen *et al.* 1982; Packer & Hart 1994; Vajda-Santivanez & Solakius 1999; Larsson *et al.* 2000).

The lowermost part of the Lower Cretaceous succession in the FFC-1 well is represented by a 10 m thick bed composed of medium-grained quartz arenite showing excellent reservoir properties and a permeability in the range of several Darcy. Extensive hydraulic tests in FFC-1 have verified a regionally extensive reservoir with a transmissivity of 7.9×10^{-4} m²/s.

In the Margrethholm-1 well this sandstone unit is only represented by a few metres of net sand, while in the Lavø-1 and Karlebo-1/1A wells a 15–30 m thick sandstone-dominated interval has been identified. This indicates a trend of increasing thickness of the Berriasian–Barremian sandstone succession toward the north and north-east, in contrast to the Aptian–Cenomanian Arnager Greensand which thins to the north.

The Arnager Greensand is highly porous and permeable in the southern part of the Øresund Basin,

verified by results from core analyses from wells on the Falsterbo peninsula, where it has a permeability of several Darcy and a porosity of up to 35% (Erlström & Sivhed 1997). Analyses on sidewall cores from the Arnager Greensand in the FFC-1 well indicate significantly poorer reservoir properties. Here the permeability is <100 mD and the porosity in the range of 20%. These relatively low values are caused by a high amount of matrix, a fine-grained texture and carbonate cement, compared to the medium-grained, matrix-poor and uncemented, permeable varieties found in the wells to the south. The Arnager Greensand is up to 60 m thick in the southern part of the Øresund Basin, but thins considerably to the north accompanied by decreasing grain-size as well as poorer reservoir properties.

Lund Sandstone reservoir

This up to several hundred metres thick sandstone reservoir is found between 350 and 1100 m depth in

wells located along the Romeleåsen Fault Zone, e.g. in the Lund geothermal wells. Peak inversion and uplift of the STZ during the Santonian–Campanian resulted in formation of thick deltaic sand deposits at the north-eastern margin of the Øresund Basin, along the Romeleåsen Fault Zone (Erlström *et al.* 1997). Further basinward the sandstone is only a few metres thick and has significantly poorer reservoir properties (Erlström 1990). The sandstone unit shows good to excellent geothermal properties close to the Romeleåsen Fault Zone where it has a net sand thickness exceeding 100 m within a 7–15 km wide, undulating zone. Even though the formation temperature is low in comparison to the other potential reservoirs, the Lund Sandstone may be considered as a possible geothermal resource and aquifer for thermal energy storage. The permeability of the sandstone is commonly >1 Darcy and the porosity is 27–32% (Table 3). These geological conditions enable a production rate of up to 150 l/s of 21°C warm formation water in the Lund geothermal

Table 3. Summary of the main characteristics of the potential geothermal reservoirs in the Øresund Basin.

	Ljunghusen Sandstone	Hammar and Flommen Formations "Bunter Sandstone"	Keuper reservoir interval Vellinge, Fuglie and Kågeröd Formations	Rhaetian–Lower Jurassic reservoir Gassum, Höganäs and Rya Formations	Arnager Greensand and Lower Cretaceous	Lund Sandstone
Reservoir rock type	Medium- and coarse-grained, sandstone	Medium- and coarse-grained sub-arkose with interbeds of arenaceous claystone	Coarse-grained arkose and conglomerate	Fine- and medium-grained quartz arenite	Fine- and medium-grained glauconitic quartz arenite	Medium- and coarse-grained quartz arenite
Depositional setting	Arid, terrestrial, eolian	Arid–semi arid, ephemeral floodplain and playa-like	Arid red beds, alluvial fans, fluvial	Deltaic–marginal marine	Marginal marine–shallow shelf	Deltaic
Age	Early Triassic (Induan–Olenekian)	Early Triassic (Olenekian–Anisian)	Ladinian–Norian	Rhaetian–Pliensbachian	Berriasian–Cenomanian	Campanian
Net sand	20–60 m ¹⁾	80–120 m	20–50 m	60–100 m	20–50 m	200–350m
Depth below mean sea level	2010–2063 m ¹⁾ 2640–2658 m ²⁾ 2088–2150 m ⁵⁾	1890–2007 m ¹⁾ 2470–2660 m ²⁾ 1940–2088 m ³⁾	1498–1678 m ¹⁾ 2016–2230 m ²⁾ 1860–2075 m ³⁾	1288–1498 m ¹⁾ 1638–1965 m ²⁾ 1672–1820 m ³⁾	1190–1288 m ¹⁾ 1591–1638 m ²⁾ 1605–1672 m ³⁾	350–1100 ⁸⁾
Permeability	(High?)	400 mD ²⁾	<50 mD ⁴⁾ <100 mD ³⁾	50–1500 mD ^{3,6,7)}	10–4000 mD ^{1,3)}	>1 D ⁸⁾
Porosity	20–28% (logs) ¹⁾	23–25% (logs) ^{1,5)}	2–16% ⁴⁾	18–34% ^{1,3)}		27–32% ⁸⁾
Temperature	56–57° ¹⁾ 77° ²⁾	53–55° ¹⁾ 73° ²⁾	46–47° ¹⁾	36–38° ¹⁾ 52–54° ³⁾	36–38° ¹⁾ 44–45° ³⁾	20–25° ⁸⁾
Cl⁻ content	--	130 g/l ²⁾	120–190 g/l ^{1,3)}			100 g/l ⁸⁾
Productivity index	--	5.6 m ³ /hr/bar ²⁾	2.9 m ³ /hr/bar ³⁾	7.0 m ³ /hr/bar ¹⁾		>10 m ³ /hr/bar ⁸⁾

¹⁾Höllviksnäs-1. ²⁾Margretheholm-1. ³⁾FFC-1. ⁴⁾Höllviken-2. ⁵⁾Ljunghusen-1. ⁶⁾Höllviken-1. ⁷⁾Svedala-1. ⁸⁾Lund wells.

wells, completed with up to 150 m long gravel-packed slotted screens. The maximum heat capacity of the Lund Geothermal system was 47 MW when it started in 1984 (Ottosson 2005). The effect has, however, after more than 30 years of operation decreased somewhat due to gradually lower temperatures in the production wells caused by influence from the 'colder' injection wells.

Discussion

Possible geothermal reservoirs in the North Sjælland Half-graben

In comparison to the southern parts of the Øresund Basin there is a greater uncertainty regarding occurrence and characteristics of the potential geothermal reservoirs in the North Sjælland Half-graben. Lower and Middle Triassic geothermal reservoirs are so far only verified in the Höllviken Half-graben. However, the interpreted seismic lines in the North Sjælland Half-graben indicate a similar Triassic succession (Fig. 4), which could be even thicker than that in the Höllviken Half-graben.

Seismic markers corresponding to the base of the Upper Cretaceous and the top pre-Rhaetian Triassic can be traced throughout the Øresund Basin and provide a reliable prediction on the presence of Rhaetian–Lower Jurassic and Lower Cretaceous geothermal reservoirs. The Rhaetian–Lower Jurassic reservoir is well known from the adjacent Helsingborg area in the eastern margin of the half-graben (Norling *et al.* 1993; Ahlberg *et al.* 2003; Bou Daher 2012; Hjuler *et al.* 2014). Uncertainty regarding the Gassum Formation is much reduced because of the comprehensive data set from Helsingborg, which clearly demonstrates the presence of laterally equivalent Rhaetian–Hettangian–lower Sinemurian strata, *i.e.* the Höganäs Formation and the Döshult Member of the Rya Formation (Fig. 3). Thus, a similar reservoir succession is expected to be present in North Sjælland. The interpreted larger overall grain-size and net sand content of the Rhaetian–Lower Jurassic in North Sjælland suggests somewhat better geothermal properties than for the southern parts of the Øresund Basin. Further, the interpreted seismic data suggest a relatively uniform thickness of about 100–170 msec TWT (Two Way Travel time) of the Gassum Formation, corresponding to 175–300 m assuming an interval velocity of 3500 m/s. The low end of this thickness span is in correspondence with the thickness of the Helsingborg composite succession, while the upper end corresponds well to the thickness of the Gassum Formation in the wells Hans-1 and Terne-1 located in the Kattegat sea area north of

Sjælland (Fig. 2; Michelsen & Nielsen 1991; Nielsen & Japsen 1991; Hjuler *et al.* 2014).

The interpretation of the seismic line presented in Fig. 4, profile 4, suggests a thickness of *c.* 400 m from the base Gassum Formation to the base Upper Cretaceous succession using velocity data from Margrethholm-1 well. The estimated thickness of 400 m is very small compared to the thickness of *c.* 1000 m estimated for the tilted Jurassic strata in the wells in the Øresund area, located in the flexure zone to the Romeleåsen Fault Zone (Larsen *et al.* 1968). However, the tilted strata between Helsingør and Helsingborg also include Middle Jurassic deposits. In north-western Skåne, the Middle Jurassic Vilhelmsfält Formation includes one potential geothermal reservoir, the Bathonian Glass Sand Member, which reflects high energy proximal coast environments such as delta front sands and beach–foreshore settings (Rolle *et al.* 1979). In the Danish Basin, the Middle Jurassic is represented by the Haldager Sand Formation which is primarily known from north Jylland, within the STZ, and in the Skagerrak and Kattegat areas (Fig. 2). It is uncertain whether any Middle Jurassic deposits and geothermal reservoirs occur in the northernmost parts of the Øresund Basin. However, on the basis on the observations between Helsingør and Helsingborg, it is possible that strata equivalent to the Vilhelmsfält Formation may be present (Larsen *et al.* 1968).

A Lower Cretaceous succession of claystone and sandstone beds was encountered in the Lavø-1, Karlebo-1/1A, Margrethholm-1 and Stenlille-1 wells. In the Lavø-1 and Karlebo-1/1A wells, the lower part of the Lower Cretaceous succession comprises a 15–30 m thick sandstone-dominated interval of similar composition as in south-west Skåne. The sandstone interval is a few metres thick in Stenlille-1 and Margrethholm-1, indicating a distinct trend of increasing thickness toward the north and north-east. An unpublished formation evaluation shows 21 m of net sand in the Karlebo-1/1A well, while the net sand value cannot be determined in Lavø-1 due to an incomplete log-suite. However, assuming a similar ratio between gross and net sand in the two wells, a net sand value of 10.5 m is estimated in Lavø-1. As hydraulic tests of the corresponding sandstone unit in FFC-1 have provided extremely good values (Table 3), it is expected that the Lower Cretaceous sandstone is also a potential geothermal reservoir in the North Sjælland Half-graben.

Formation fluids

In the Øresund Basin the formation fluids in the geothermal reservoirs are composed of brine formation water with only a few percent of dissolved gases. No hydrocarbons have been encountered. The chloride

content in the formation fluids in the described reservoirs varies between 100 and 190 g/l, mainly related to the depth of the reservoir (Table 3). These data indicate that the salinity increases almost linearly with depth, approaching saturation with respect to halite at 3000 m. This is interpreted to be caused by diffusion of salt from the extensive deposits of Permian–Triassic evaporites in the Danish Basin and entrapped residual brines in the formations (Laiier 2003). A few chloride concentrations in formation waters from various wells and reservoirs are presented in Table 3.

Compared to other geological formation waters, there are no explicit anomalies in those analysed from the FFC-1 well that could lead to problems with precipitates during geothermal heat production (Laiier 2003). However, an iron content of 40–70 mg/l will lead to significant precipitation of iron-oxyhydroxides under oxygenated conditions. Therefore, a closed and pressurised geothermal system without access to oxygen is required.

Gases are dominated by nitrogen and minor amounts of methane and noble gases such as he-

lium and argon. Analyses of two Keuper samples, from 1840 and 1860 m depth in the FFC-1 well, gave a solute gas content of 86 cm³ per litre of formation fluid, consisting of nitrogen with small admixtures of hydrocarbons (<2%), carbon dioxide (0.52%) and a relatively high share of helium (5.7%). Similar results were also obtained in the Lund geothermal field, where the 21°C warm formation water from the Lund Sandstone reservoir contains 2.5 litre of gas per 100 litre, composed primarily of nitrogen (92%), methane (3%) and helium (3%). The fluid has a pH of 6.8 and a salinity of *c.* 6‰. The content of total dissolved solids is *c.* 6 000 ppm (Bjelm & Alm 1995).

Porosities and permeabilities

Figure 8 illustrates a regional porosity–permeability trend for the Bunter and Gassum sandstones, based on porosity and permeability data for core samples from various wells in the Danish Basin (Mathiesen *et al.* 2009; Kristensen *et al.* 2016). This shows that the porosity of the Bunter sandstone in general varies between 5

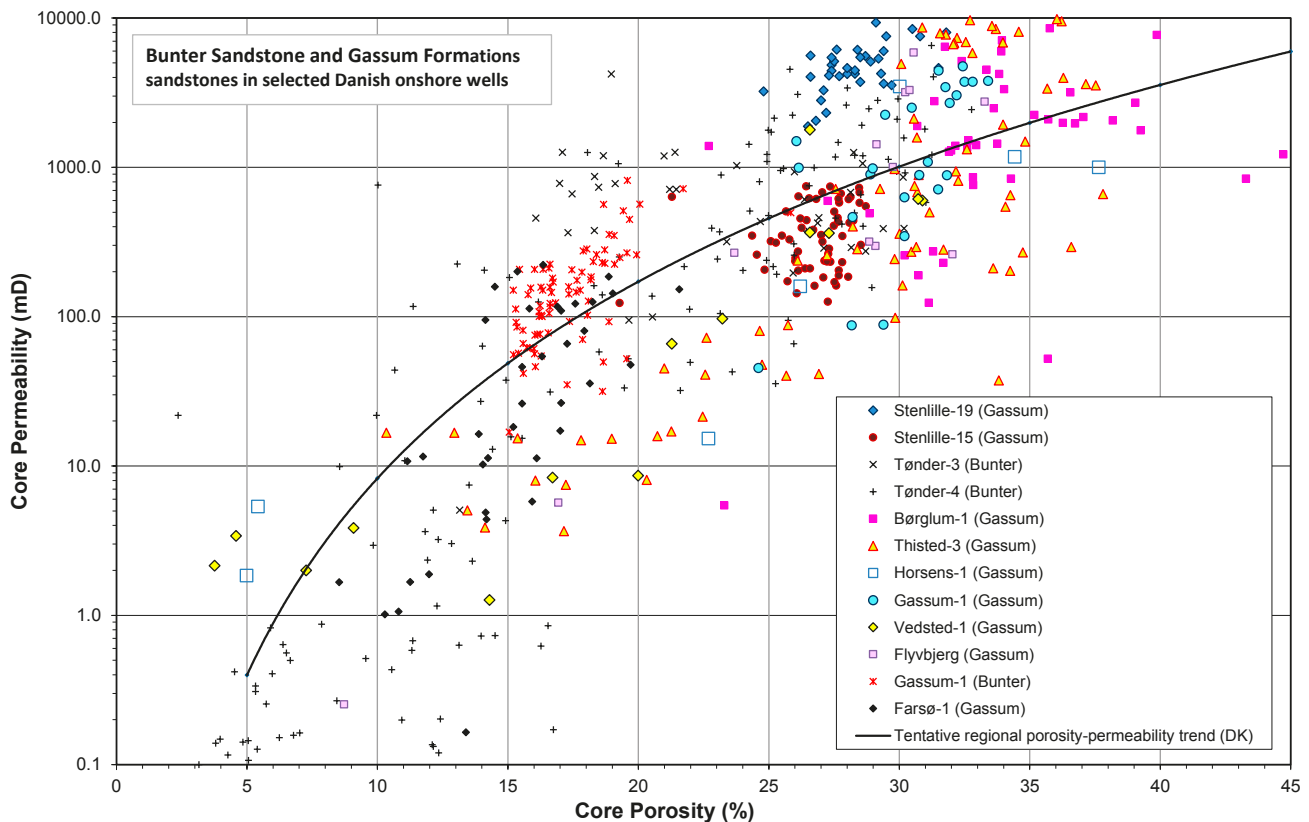


Fig. 8. Plot displaying the regional porosity–permeability relationship for the Bunter Sandstone and Gassum Formations in the Danish Basin onshore Denmark (Mathiesen *et al.* 2009). This compiled data set originates from core analysis reports provided by various core analysis laboratories during a period of *c.* 50 years (1950–2000). The core analysis reports are either company reports or in-house DGU and GEUS reports, and all reports are available from the GEUS Subsurface Archive. Data are fitted to a power function and the black line is a non-linear regression line.

and 25% while the Gassum sandstones show values that are commonly higher than 25%. There is also a corresponding decrease in permeability in the Bunter samples which rarely exhibit values above 500 mD, while the Gassum samples often show results above one Darcy. The plotted core data in Fig. 8 represent two geological formations and a wide range of depositional environments, resulting in a fairly scattered data set. Data from the two formations have been used in order to strengthen the definition of a regional correlation line. Analyses performed on cored intervals in wells from south-west Skåne have provided a less extensive data set on porosity and permeability values for the reservoirs in the Øresund Basin (Fig. 9; Erlström 1990; Springer 1997) In addition, a relatively new data set exists from analyses performed on cores of the Höganäs Formation in the Helsingborg area (Hjuler *et al.* 2014). The Helsingborg data are plotted in Fig. 8 which shows that these data fit into the various distributions of the porosity and permeability as presented in Fig. 9.

The porosity and permeability distributions for the Keuper as well as for the Lower Jurassic sandstones

in the Øresund Basin are more or less equivalent with the trend and ranges of values for the Bunter and Gassum sandstones in the Danish Basin shown in Fig. 8. Figure 10 shows a porosity–permeability plot solely of the Gassum and Höganäs sandstones, comprising data from selected Danish onshore wells as well as data from shallow wells drilled in the Helsingborg area (Hjuler *et al.* 2014). The Helsingborg dataset fits into the distributions of the porosity and permeability for the various geothermal reservoirs as presented in Fig. 9 and, moreover, the data contribute to establishing a tentative ‘North Sjælland–Helsingborg’ trend line (Fig. 10). Further drilling and coring in the North Sjælland area is needed in order to confirm (or reject) this relationship.

In Fig. 10, most of the Gassum Formation data from Thisted-3 and Stenlille-19 (location and well data in Fig. 2 and Table 1) are considered to signify elevated (or higher) permeability relative to the Gassum Formation sandstones found in the Øresund Basin, due to e.g. sedimentological differences, differences in grain size and different depositional environments. Figure

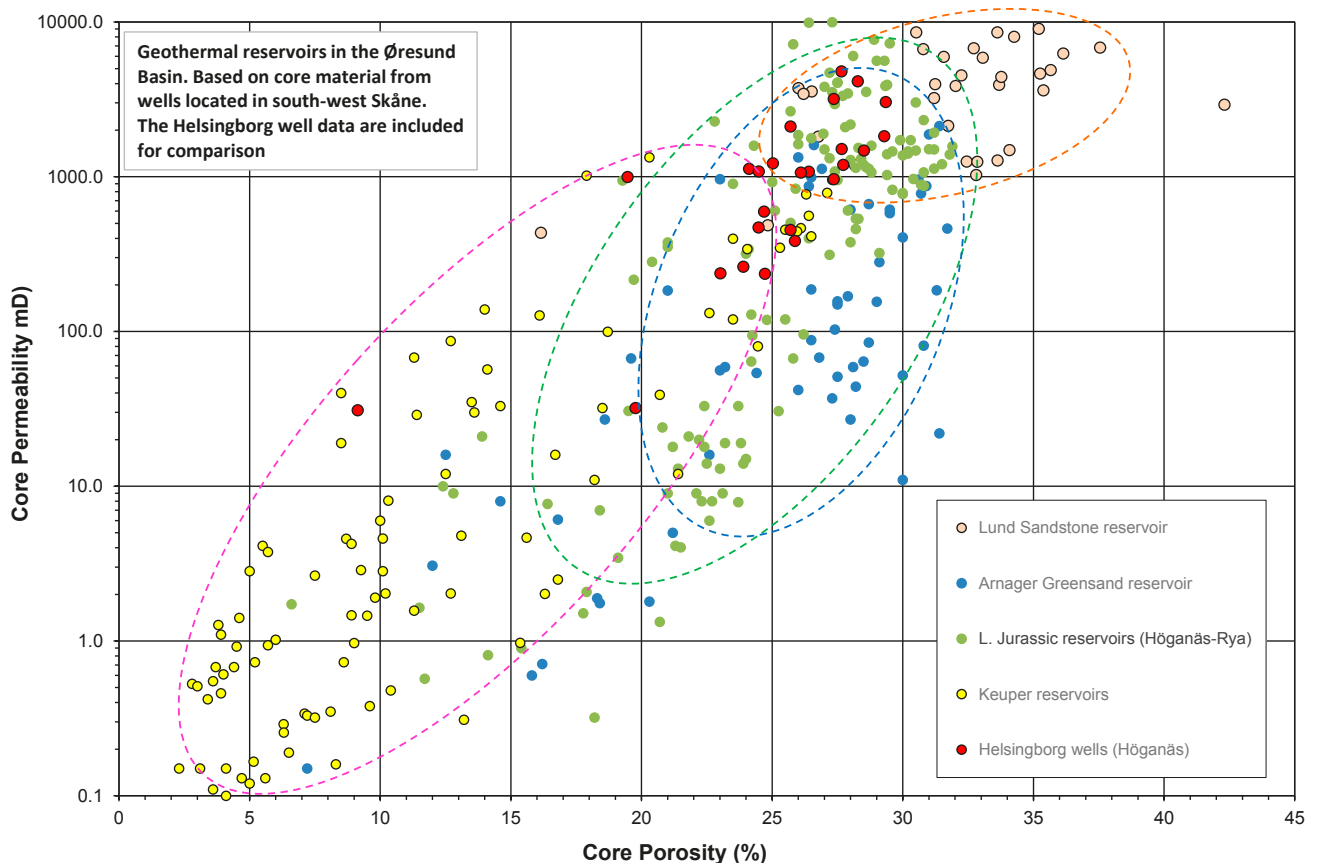


Fig. 9. Plot of the porosity–permeability relationship for different geothermal reservoirs in the Øresund Basin. The values are derived from analyses on core material from wells in south-west Skåne (Erlström 1990; Springer 1997). The dashed ellipses represent the assessed main distribution of the porosity and permeability of the various reservoirs. Porosity–permeability data from shallow wells drilled in the Helsingborg area are plotted for comparison (these data represent sandstones of the Höganäs Formation).

10 also includes data from the Gassum Formation in the Stenlille-15 well, and it is noteworthy that the data from the two Stenlille wells do not fit the suggested porosity–permeability trend line, which is based primarily on core analysis data from selected wells located in Jylland. Core analysis data from Jylland are largely measured on plug samples of medium-grained sandstones, while the Stenlille-15 samples primarily consist of fine-grained sandstones, suggesting that the depositional environment and the sandstone provenance are different. Conversely, the Stenlille-19 samples primarily consist mostly of coarse-grained and almost clay-free sandstones, resulting in elevated permeabilities. Hence, the Stenlille-15 and -19 data plot below and above the trend line, respectively.

The overall data set shows that the Triassic reservoir sandstones vary considerably with respect to porosity and permeability, reflecting their heterogeneous composition and texture. Well sorted, matrix-poor beds and beds with no or limited amounts of cement are subordinate in the Triassic succession. The highest permeability values are found in the Bunter Sandstone

Formation interval, where permeabilities between 100 and 1000 mD are recorded. The corresponding values for the Keuper interval are considerably lower (Table 3). There are unfortunately no core analyses or hydraulic test data for the lowermost Triassic Ljunghusen reservoir. However, the log response indicates a permeable, porous and up to 50 m thick homogeneous sandstone at the base of the Triassic succession.

Interpretation of log data from the reservoir sandstones in the pre-Rhaetian Triassic interval in the FFC-1 well, i.e. predominantly Keuper strata, gives an average porosity of 24–25% and a volume of shale matrix in the range of 20–22%. The corresponding interpretation of the Rhaetian–Lower Jurassic and Lower Cretaceous interval gives an average porosity of 21–23%, however with a significantly lower matrix content of 10–12%. The porosity and permeability values for the Lower Jurassic reservoirs are more consistent, reflecting the more homogeneous petrophysical properties compared to the Triassic reservoirs. However, the predominance of fine-grained sandstone beds generally results in poor permeability. In the FFC-1 well, an approximately 10

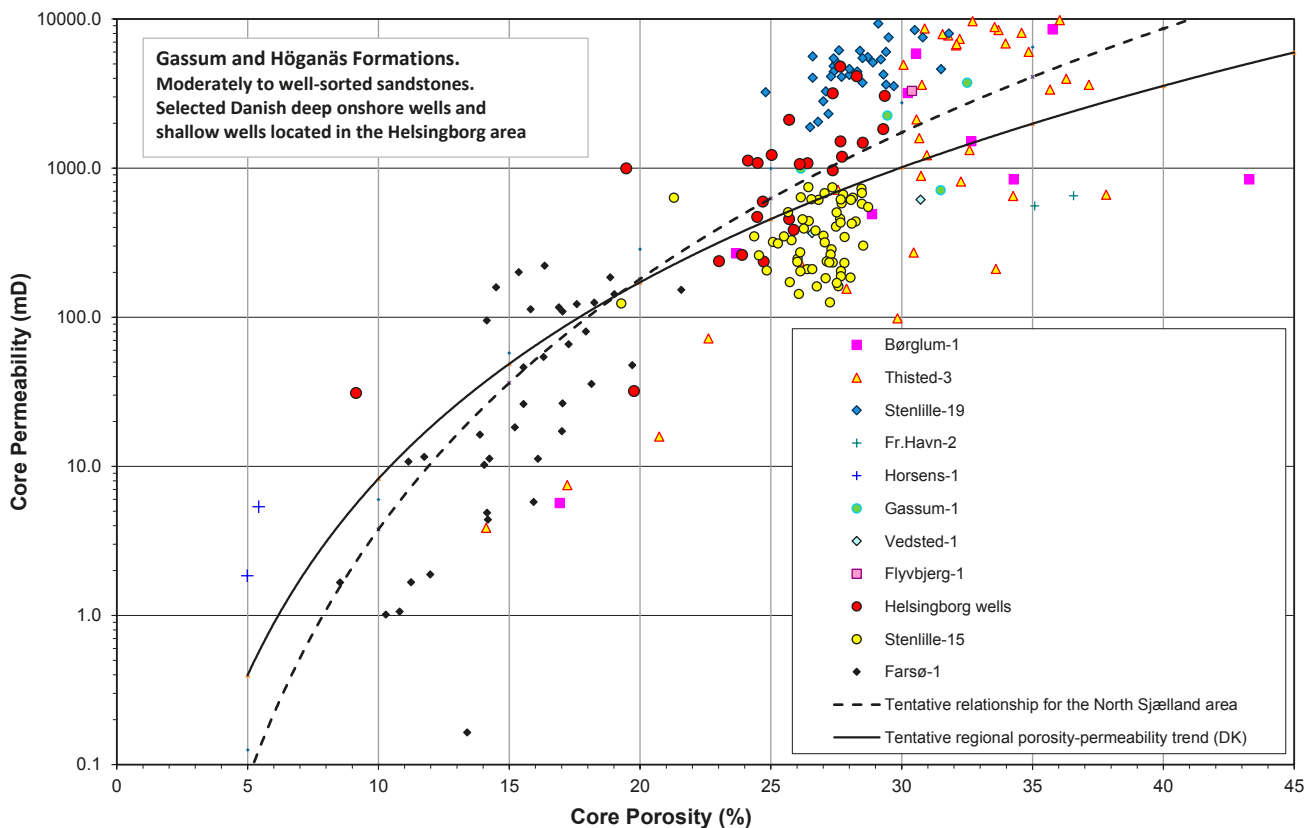


Fig. 10. Plot of the porosity–permeability relationship for moderately to well sorted sandstones in the Lower Jurassic Gassum and Höganäs Formations, from selected onshore wells in Denmark and shallow wells from Helsingborg (data from Hjuler *et al.* 2014). The regional porosity–permeability relationship for the Danish area (Fig. 8) is plotted for comparison. A tentative trend line for the North Sjælland and Helsingborg areas is suggested (dashed line).

m thick bed of medium-grained and highly permeable sandstone, i.e. the Lower Cretaceous sandstone on top of the Middle Jurassic unconformity, was found to contribute to as much as 80% of the water flow. The remaining 20% originate from an approximately 200 m thick Rhaetian–Lower Jurassic and Lower Cretaceous section between 1605 and 1818 m with a net sand thickness of 110 m. This signifies the important effect of grain-size on the permeability. The permeability of the fine-grained sandstone beds is generally less than 200 mD in the Höllviken Half-graben. The results from analyses on cores from the Lower Jurassic succession in Helsingborg indicate overall significantly higher permeabilities, commonly as high as 1–2 Darcy (Fig. 10). These high values are coupled to a predominance of medium-grained and highly porous sandstone. The high permeability values in the Helsingborg area could be speculated to be caused by Late Cretaceous uplift and pressure release, triggering chemical dissolution or mechanical disintegration of pre-existing cements in the rock, leading to elevated secondary porosities. However, no such processes have been verified (Ahlberg 1994; Hjuler et al. 2014). Based on the limited data set, it is assumed that the grain-size of the sandstones in the Rhaetian–Hettangian succession, i.e. the Gassum and Höganäs Formations, increases towards the north and north-west, which is also indicated from the Helsingborg area (Hjuler et al. 2014). The Lower Cretaceous reservoirs appear to show the same trend, as indicated by well data from the southern part of the Øresund Basin and the Karlebo-1/1A and Lavø-1 wells located on northern Sjælland.

Prediction models

Regarding prediction of the permeability and porosity of a potential geothermal reservoir in an area with poor data coverage, depth models for both the Gassum Formation and the Bunter Sandstone Formation in the Danish Basin were presented by Kristensen et al. (2016) and Weibel et al. (2017). A ‘best practice’ technique for predicting average porosity and permeability for these reservoirs was also presented by Kristensen et al. (2016), using primarily core analysis data and well-logs. The model by Weibel et al. (2017) also includes assessments of grain-size, detrital clay content and grain shape as well as diagenetic alterations, and shows that the porosity–permeability properties of the sandstone reservoirs in the Gassum Formation follow a steeper depth gradient than the Bunter Sandstone Formation due to higher degrees of mechanical compaction and diagenetic alterations. Further, there is a depth-related decrease in porosity for the Gassum Formation of 5%/1000 m in the Danish Basin. A similar situation may be assumed for the Øresund Basin, however with the consideration that the sandstone beds are likely to be

slightly more coarse-grained towards the Fennoscandian Border Zone to the north-east.

Temperature gradients

The available temperature data for the Øresund Basin are illustrated in Fig. 11. Most of the recorded temperatures are bottom hole temperatures (BHT) monitored during wire-line logging operations. The readings are likely to be affected by drilling operations, e.g. circulation of mud in the borehole before logging, which lead to relatively low measured temperatures. The temperature logging data for the FFC-1 and Ljunghusen-1 wells are corrected for the drilling operation and its effect on the recorded temperatures, but the BHT data from Skåne are not. Consequently, the scattered BHT values plot slightly to the left of the temperature profiles for FFC-1 and Ljunghusen-1 (Fig. 11).

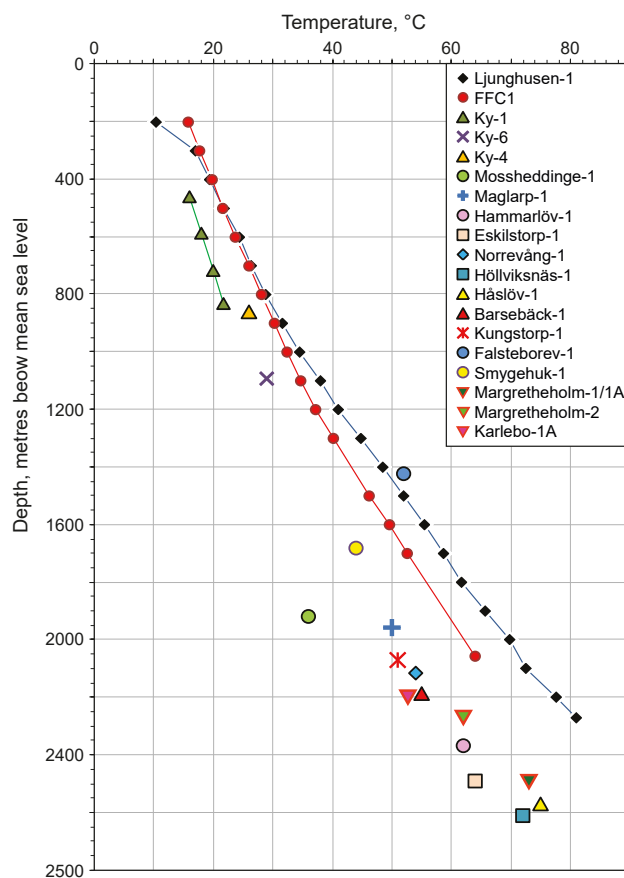


Fig. 11. Temperature data from deep wells in south-west Skåne and on Sjælland registered immediately after drilling, i.e. most of the data are bottom hole temperatures (BHT) values. The temperature profile in the FFC-1 and Ljunghusen-1 wells represent normalised conditions. The three Danish data represent updated estimates of equilibrium temperatures (Margretheholm-1/1A and -2) and BTH values (Karlebo-1). Danish values are from Poulsen *et al.* 2013).

The temperature gradient varies in the Ljunghusen-1 well between 27°C and 35°C/1000 m and is 29.5 °C in FFC-1, considering an average temperature of 10°C in the upper 200 m of the bedrock. Based on the data in Fig. 11 a formation temperature of 45–50°C at 1500 m, 60–70°C at 2000 m and 70–90°C at 2500 m depth may be expected for the reservoirs in the Øresund Basin.

Summarised assessment of the geothermal potential

The distribution, depth and petrophysical characteristics of the described geothermal reservoirs provide very variable geological conditions for utilising

geothermal energy in different parts of the Øresund Basin. A composite prognosis map regarding the geothermal potential in the Øresund Basin (Fig. 12) shows that the best conditions prevail along the western part of the basin in the Höllviken and North Sjælland half-grabens. There, multiple alternative reservoirs, in the Bunter Sandstone, Rhaetian–Lower Jurassic and Lower Cretaceous intervals, are interpreted to exist at depths ranging between 1500 and 4500 m. The corresponding reservoir temperatures for the same intervals are assessed to range between 45° and 85°C. In addition, the gross thickness of the Triassic to Lower Cretaceous interval with geothermal potential is at least 1000 m in those areas where the likelihood of finding Lower Triassic reservoirs with temperatures above 60°C is the greatest.

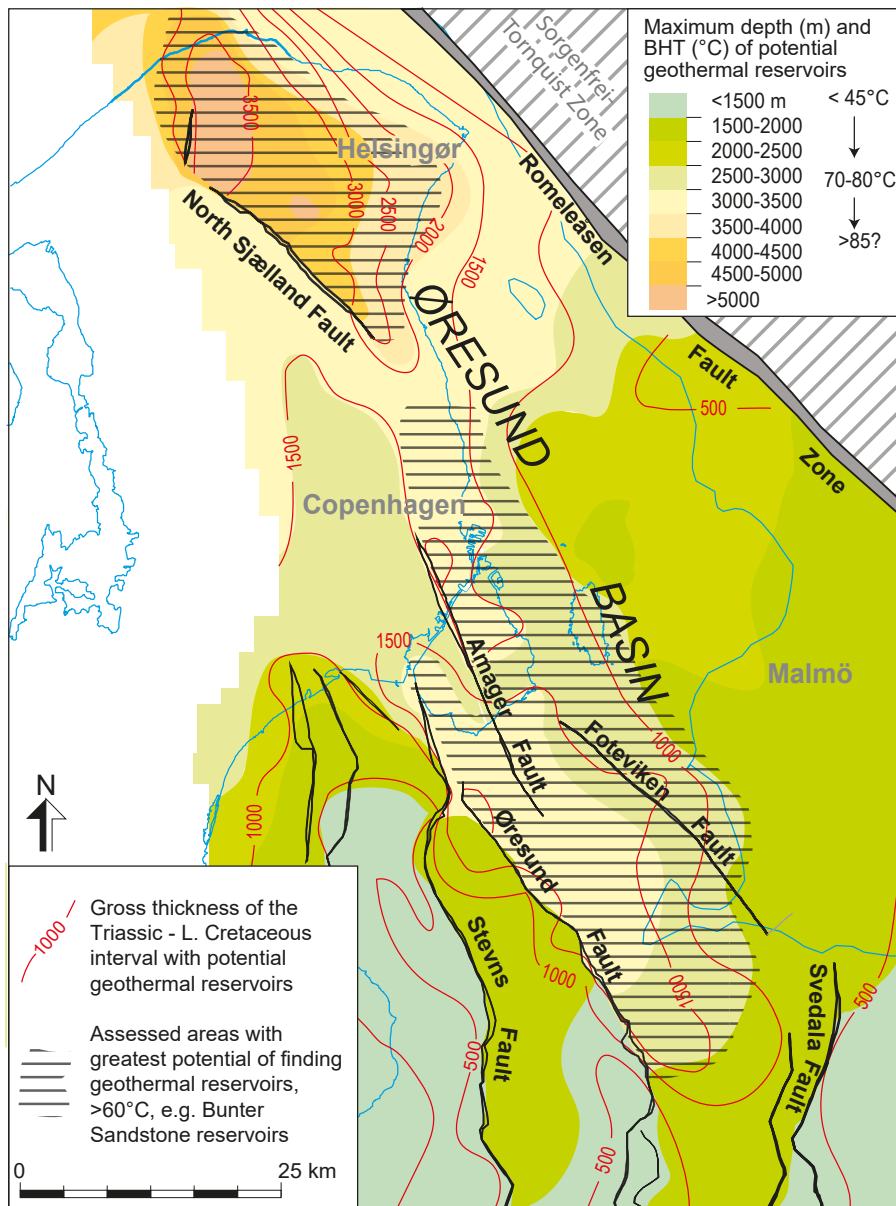


Fig. 12. Schematic prognosis map illustrating the maximum depth, gross thickness and the estimated corresponding maximum formation temperatures of the assessed, pre-Rhaetian Triassic, Rhaetian–Lower Jurassic and Lower Cretaceous geothermal reservoirs in the Øresund Basin. Areas of judged greatest potential for suitable geothermal reservoirs with a temperature >60°C are shown, mainly related to the occurrence of Bunter Sandstone reservoirs.

Pre-Rhaetian Triassic

The deepest reservoirs, i.e. the Bunter sandstones including the Ljunghusen Sandstone, and the Flommen and Hammar Formations, are located at 2200–2600 m depth adjacent to the Øresund and Amager faults. A similar succession with geothermal potential within the Triassic is indicated in the North Sjælland Half-graben. There, the depth of the Lower Triassic sandstone reservoirs is interpreted to be even greater than in the Höllviken Half-graben, which would result in higher temperatures. However, the porosity and permeability could suffer because of the greater burial depth.

In the Margrethholm-1 well, the temperature of the Lower–Middle Triassic succession is between 60° and 73°C. A productivity index of 5.6 m³/hr/bar is reached in a 75 m long perforated well section of the Flommen–Hammar interval. The reservoir has been in production since 2005. However, decreasing flow rates have been registered recently, possibly caused by migration of fine particles or precipitation of inorganic compounds, i.e. scales. Scales are formed by precipitation in geothermal water and may coat perforations, casing, valves, pumps and other technical equipment, thereby significantly reducing the production capacity of a well. Despite this, the Lower–Middle Triassic succession is still judged to have a considerable potential as geothermal reservoir, as it displays favourable formation temperatures and transmissivities, provided that there are technical solutions mitigating fines production from the commonly poorly sorted and argillaceous reservoir, and precipitation of scales. The heterogeneous reservoirs in the Keuper interval that exhibit smaller thicknesses and lower permeability are not considered suitable as geothermal reservoirs. However, they could be part of, and contribute to, a composite production interval in the Triassic, provided that mixing of formation fluids from different intervals does not cause scaling or give rise to precipitates (Laier 2003).

Rhaetian–Lower Jurassic

A succession encompassing the Rhaetian–Lower Jurassic sandstone reservoirs is present in all parts of the Øresund Basin. The succession is consequently evaluated to have the greatest geothermal potential, even if the individual reservoir properties vary within the basin. For instance, the Rhaetian–Hettangian reservoir sandstones are predominantly fine-grained and have a relatively low transmissivity in the south, whereas grain-size, net sand and transmissivity of the interval are interpreted to increase in the northern parts of the Øresund Basin. The medium-grained sandstone beds in the succession are highly permeable. However, it is difficult to map the distribution of these beds prior

to drilling of exploration wells. Detailed pre-drilling modelling and prediction of the geothermal potential of this interval is therefore uncertain for a specific site.

Cretaceous

The highly permeable Lower Cretaceous sandstone unit overlying the Middle Jurassic unconformity is distributed throughout the Øresund Basin. It is considered an alternative geothermal reservoir to the Bunter Sandstone and Rhaetian–Lower Jurassic reservoirs. The progressively increasing depth of the Lower Cretaceous reservoirs towards the Romeleåsen Fault Zone gives slightly higher relative temperatures of this interval in the north-east. In the Øresund Basin the top of this interval is found at depths between 1200 and 1700 m, corresponding to a temperature of 35–55°C.

The Lund Sandstone has the best overall reservoir properties, but has a limited geographical distribution and low formation temperatures between 20° and 25°C. This requires technical solutions involving compression heat pumps with input of preferably renewable electricity as the driving energy.

Acknowledgements

We especially acknowledge the Danish Agency for Science, Technology and Innovation who funded the project “The geothermal energy potential in Denmark - reservoir properties, temperature distribution and models for utilisation” (DSF-No. 2104-09-0082); and also the Innovation Fund Denmark which funded the project “GEOTHERM – Geothermal energy from sedimentary reservoirs – Removing obstacles for large scale utilisation (6154-00011B); the two grants facilitated the Danish-Swedish cooperation and establishment of a common database. We also thank Katrine Juul Andresen for valuable comments on the manuscript and Stefan Sølberg (GEUS) who improved the artwork considerably.

References

- Aigner, T. & Bachmann, G.H. 1992: Sequence-stratigraphic framework of the German Triassic. *Sedimentary Geology* 80, 115–135.
- Ahlberg, A. 1994: Deposition and diagenesis of the Rhaetian–Hettangian succession (Triassic–Jurassic) in southern Sweden. A synthesis. *Lund Publications in Geology* 123, 1–16.
- Ahlberg, A. & Ohlsson, I. 2001: Petroleum assessment of the Mesozoic succession in the Höllviken Graben and on the

- Skurup Platform, southern Sweden. GFF 123, 85–95.
- Ahlberg, A., Sivhed, U. & Erlström, M. 2003: The Jurassic of Scania, southern Sweden. In: Ineson, J.R. & Surlyk, F. (eds), *The Jurassic of Denmark and Greenland*. Geological Survey of Denmark and Greenland Bulletin 1, 527–541.
- Bachmann, G.H. 1998: The Germanic Triassic. General. In: Eigenfeld, F. (ed.), *International Symposium on the Epicontinental Triassic*. Halle Saale. Hallesches Jahrbuch für Geowissenschaften B5, 19–22.
- Bachmann, G.H., Beutler, M., Szurlies, M., Barnasch, J. & Franz, M. 2005: Field Guide for the International Field Workshop on the Triassic of Germany and surrounding countries. Martin-Luther-Universität Halle-Wittenberg institut für Geologischen Wissenschaften, 75 pp.
- Bertelsen, F. 1975: Triassic palynology and stratigraphy of some Danish North Sea boreholes. *Danmarks Geologiske Undersøgelse årbog* 1974, 17–32.
- Bertelsen, F. 1978: The Upper Triassic–Lower Jurassic Vinding and Gassum Formations of the Norwegian-Danish Basin. *Danmarks Geologiske Undersøgelse Serie B* 3, 1–26.
- Bertelsen, F. 1980: Lithostratigraphy and depositional history of the Danish Triassic. *Danmarks Geologiske Undersøgelse Serie B* 4, 1–59.
- Beutler, G. 1998: The Keuper of Germany. An overview. Results from the German Keuper Working Group. In: Eigenfeld, F. (ed.), *International Symposium on the Epicontinental Triassic*. Halle Saale. Hallesches Jahrbuch für Geowissenschaften B5, 45–60.
- Beutler, G. & Schüler, F. 1987: Probleme und Ergebnisse der lithostratigraphischen Korrelation der Trias am Nordrand der Mitteleuropäischen Senke. *Zeitschrift der geologischen Wissenschaften Berlin* 15, 421–436.
- Bjelm, L. & Alm, P.G. 1995: Geothermal Energy in Scania. A summary of research activities and results within the national program for geothermal energy in sedimentary rocks, 1977–1994. NUTEK project 656 090-3. Lund Institute of Technology Report, 80 pp.
- Bou Daher, S. 2012: Lithofacies analysis and heterogeneity study of the subsurface Rhaetian–Pliensbachian sequence in SW Scania and Denmark. Dissertation, Department of Geology, Lund University 296, 52 pp.
- Danish Energy Agency 2013: Geothermal heat and other use of the subsoil. In: *Oil and Gas production in Denmark 2013 – and Subsoil use*, 100–103. https://ens.dk/sites/ens.dk/files/OlieGas/oil_and_gas_in_denmark_2013.pdf
- Directive 2009/28/EC of the European Parliament and of the Council of 23 April 2009 on the promotion of the use of energy from renewable sources and amending and subsequently repealing Directives 2001/77/EC and 2003/30/EC. *Official Journal of the European Union* 5.6, 62 pp. <http://eur-lex.europa.eu/legal-content/EN/TXT/PDF/?uri=CELEX:32009L0028&from=EN>
- DONG 2003: Final Testing Report – FFC-1. DONG Energy, Report No. 16005, 134 pp.
- Erlström, M. 1990: Petrology and deposition of the Lund Sandstone, Upper Cretaceous, south-western Scania. *Sveriges Geologiska Undersökning Serie Ca* 74, 91 pp.
- Erlström, M. 1994: Evolution of Cretaceous sedimentation in Scania. *Lund Publications in Geology* 122, 37 pp.
- Erlström, M. & Sivhed, U. 1997: Förstudie angående geotermisk potential i Köpenhamnsområdet. *Sammanställning av geologiska basdata från Sydvästskåne*. Sveriges Geologiska Undersökning Rapport, Diarienummer 08-973/97, 83 pp.
- Erlström, M. & Sivhed, U. 2012: Pre-Rhaetian Triassic strata in Scania and adjacent offshore areas – stratigraphy, petrology and subsurface characteristics. *Geological Survey of Sweden, Rapporter och Meddelanden* 132, 74 pp.
- Erlström, M., Thomas, S.A., Deeks, N. & Sivhed, U. 1997: Structure and tectonic evolution of the Tornquist Zone and adjacent sedimentary basins in Scania and the southern Baltic Sea area. *Tectonophysics* 271, 191–215.
- Erlström, M., Sivhed, U. & Surlyk, F. 1999: A backstepping, fluviatile–paralic–marine succession (Sinemurian, Lower Jurassic), Örby, Scania, Sweden. *Bulletin of the Geological Society of Denmark* 46, 1–12.
- Gravesen, P., Rolle, F. & Surlyk, F. 1982: Lithostratigraphy and sedimentary evolution of the Triassic, Jurassic and Lower Cretaceous of Bornholm, Denmark. *Danmarks Geologiske Undersøgelse Serie B* 7, 51 pp.
- Hagdorn, H., Horn, M. & Simon, T. 1998: Muschelkalk. In: Eigenfeld F. (ed.), *International Symposium on the Epicontinental Triassic*. Halle Saale. Hallesches Jahrbuch für Geowissenschaften B5, 35–44.
- Hagelund, R. & Levin, S.A. 2017: SEG-Y_r2.0: SEG-Y revision 2.0 Data Exchange Format. SEG Technical Standard Committee, 147 pp. Society of Exploration Geophysicists. Tulsa Oklahoma.
- Hjuler, M.L., Erlström, M., Lindström, S., Nielsen, L.H., Kristensen, L., Mathiesen, A. & Bidstrup, T. 2014: Extended evaluation of possible geothermal reservoirs in the Helsingør area including geological data from Helsingborg and Helsingør. Contribution to an evaluation of the geothermal potential. *Danmarks og Grønlands Geologiske Undersøgelse Rapport* 2014/29, 110 pp.
- Kristensen, L., Hjuler, M.L., Frykman, P., Olivarius, M., Weibel, R., Nielsen, L.H. & Mathiesen, A. 2016: Pre-drilling assessments of average porosity and permeability in the geothermal reservoirs of the Danish area. *Geothermal Energy* 4:6, Doi 10.1186/s40517-016-0048-6, 27 pp.
- Laier, T. 2003: Prediction of scaling problems likely to occur during geothermal heat production using the FFC-01 well. *Danmarks og Grønlands Geologiske Undersøgelse Rapport* 2003/14, 29 pp.
- Larsen, G., Christensen, O.B., Bang, I. & Buch, A. 1968: Øresund. Helsingør–Hälsingborg Linien. *Geologisk rapport*. Danmarks Geologiske Undersøgelse Rapport 1, 90 pp. + table volume (summary in English).
- Larsson, K., Solakius, N. & Vajda, V. 2000: Foraminifera and palynomorphs from the greensand-limestone sequences (Aptian–Coniacian) in southwestern Sweden. *Neues Jahrbuch für Geologie und Paläontologie* 231, 1–12.

- rbuch für Geologie und Paläontologie Abhandlungen 216, 277–312.
- Lepper, J. & Röhling, H.G. 1998: Buntsandstein. In: Eigenfeld, F. (ed.), International Symposium on the Epicontinental Triassic. Halle Saale. Hallesches Jahrbuch für Geowissenschaften B5, 27–34.
- Liboriussen, J., Ashton, P. & Tygesen, T. 1987: The tectonic evolution of the Fennoscandian Border Zone. *Tectonophysics* 137, 21–29.
- Lindström, S. & Erlström, M. 2011: Basin analysis of the uppermost Triassic to Lower Cretaceous, Danish Basin. *Biostratigraphy and log correlation. Danmarks og Grønlands Geologiske Undersøgelse Rapport 2011/82*, 55 pp.
- Lindström, S., Vosgerau, J.H., Piasecki, S., Nielsen, L.H., Dybkjær, K. & Erlström, M. 2009: Ladinian palynofloras in the Norwegian-Danish Basin: a regional marker reflecting a climate change. In: Bennike, O., Garde, A.A. & Watt, W.S. (eds), Review of Survey Activities 2008. Geological Survey of Denmark and Greenland Bulletin 17, 21–24.
- Lindström, S., Erlström, M., Piasecki, S., Kristensen, L. & Springer, N. 2017: Middle Triassic to Early Jurassic terrestrial ecosystem change in the Danish Basin. *Review of Palaeobotany and Palynology* 244, 65–95.
- Mader, D. & Yardley, J. 1985: Migration, modification and merging in aeolian systems and the significance of the depositional mechanism in Permian and Triassic dune sands of Europe and North America. *Sedimentary Geology* 45, 85–218.
- Mahler, A. & Magtengaard, J. 2010: Country update report for Denmark. In: Proceedings from the World Geothermal Congress 2010, Bali, Indonesia, April 25–29, 9 pp.
- Mathiesen, A., Kristensen, L., Bidstrup, T. & Nielsen, L.H. 2009: Vurdering af det geotermiske potentiale i Danmark. *Danmarks og Grønlands Geologiske Undersøgelse Rapport 2009/59*, 30 pp.
- Michelsen, O. 1997: Mesozoic and Cenozoic stratigraphy and structural development of the Sorgenfrei-Tornquist Zone. *Zeitschrift Deutsches Geologische Gesellschaft* 148, 33–50.
- Michelsen, O. & Clausen, O.R. 2002: Detailed stratigraphic subdivision and regional correlation of the southern Danish Triassic succession. *Marine and Petroleum Geology* 19, 563–587.
- Michelsen, O. & Nielsen, L.H. 1991: Well records on the Phanerozoic stratigraphy in the Fennoscandian Border Zone, Denmark. *Danmarks Geologiske Undersøgelse Serie A* 29, 37 pp.
- Michelsen, O. & Nielsen, L.H. 1993: Structural development of the Fennoscandian Border Zone, offshore Denmark. *Marine and Petroleum Geology* 10, 124–134.
- Michelsen, O., Nielsen, L.H., Johannessen, P., Andsbjerg, J. & Surlyk, F. 2003: Jurassic lithostratigraphy and stratigraphic development onshore and offshore Denmark. In: Ineson, J.R. & Surlyk, F. (eds), The Jurassic of Denmark and Greenland. Geological Survey of Denmark and Greenland Bulletin 1, 147–216.
- Mogensen, T.E. 1994: Palaeozoic structural development along the Tornquist Zone, Kattegat, Denmark. *Tectonophysics* 240, 191–214.
- Mogensen, T.E. & Korstgård, J.A. 2003: Triassic and Jurassic transtension along part of the Sorgenfrei-Tornquist Zone in the Danish Kattegat. In: Ineson, J.R. & Surlyk, F. (eds), The Jurassic of Denmark and Greenland. Geological Survey of Denmark and Greenland Bulletin 1, 439–458.
- Nielsen, L.H. 2001: Vurdering af reservoirkvaliteten af Ljunghusen Formationen i Höllviken Graven. En petrografisk-sedimentologisk analyse af borespåner og petrofysiske borehulslogs fra Höllviksnäs-1 boringen, Skåne. *Danmarks og Grønlands Geologiske Undersøgelse Rapport 2001/107*, 44 pp.
- Nielsen, L.H. 2003: Late Triassic – Jurassic development of the Danish Basin and Fennoscandian Border Zone, Southern Scandinavia. In: Ineson, J.R. & Surlyk, F. (eds), The Jurassic of Denmark and Greenland. Geological Survey of Denmark and Greenland Bulletin 1, 459–526.
- Nielsen, L.H. & Japsen, P. 1991: Deep wells in Denmark 1935–1990. Lithostratigraphic subdivision. *Danmarks Geologiske Undersøgelse Serie A* 31, 179 pp.
- Nielsen, L.H., Mathiesen, A. & Bidstrup, T. 2004: Geothermal energy in Denmark. In: Sønderholm, M. & Higgins, A.K. (eds), Review of survey activities 2003. Geological Survey of Denmark and Greenland Bulletin 4, 17–20.
- Norling, E. 1981: Upper Jurassic and Lower Cretaceous geology of Sweden. *Geologiska Föreningens i Stockholm Förhandlingar* 103, 253–269.
- Norling, E. & Bergström, J. 1987: Mesozoic and Cenozoic tectonic evolution of Scania, southern Sweden. *Tectonophysics* 137, 7–19.
- Norling, E., Ahlberg, A., Erlström, M. & Sivhed, U. 1993: Guide to the Upper Triassic and Jurassic geology of Sweden. *Sveriges Geologiska Undersökning Serie Ca* 82, 71 pp.
- Olivarius, M. & Nielsen, L.H. 2016: Triassic palaeogeography of the greater eastern Norwegian-Danish Basin: Constraints from provenance analysis of the Skagerrak Formation. *Marine and Petroleum Geology* 69, 168–182.
- Ottosson, P. 2005: District Heating Production With Heat Pumps Based On Geothermal Energy. In: Proceedings from the World Geothermal Congress 2005, Antalya, Turkey, 24–29 April, 8 pp.
- Packer, S.R. & Hart, M.B. 1994: Evidence for sea level change from the Cretaceous of Bornholm, Denmark. *GFF* 116, 167–173.
- Piasecki, S. 2005: A new Ladinian palynoflora in the Triassic of Sweden. Palynological analysis of the Triassic succession in the FFC-1 and -2 wells at Malmö, Sweden. *Danmarks og Grønlands Geologiske Undersøgelse Rapport 2005/41*, 36 pp.
- Poulsen, S.E., Balling, N. & Nielsen, S.B. 2013: Analysis of bottom hole temperatures on- and nearshore Denmark, Scientific technical report, Department of Geoscience, Aarhus University, Denmark, 23 pp.
- Rhys, G.H. 1974: A proposed standard lithostratigraphic

- nomenclature for the southern North Sea and an outline structural nomenclature for the whole of the (UK) North Sea. Institute of Geological Sciences Report 8, 14 pp.
- Rolle, F., Koch, J.-O., Frandsen, N. & Surlyk, F. 1979: Jurassic environments in the Fenno-scandian Border Zone. In: Symposium on 'Sédimentation jurassique W. européen', Association Sédimentologues Français Publication Spéciale 1, 15–31.
- Røgen, B., Ditlefsen, C., Vangkilde-Pedersen, T., Nielsen, L.H. & Mahler, A. 2015: Geothermal Energy Use. 2015 Country Update for Denmark. Proceedings World Geothermal Congress 2015. Melbourne, Australia, 19–25 April 2015, 7 pp.
- Sivhed, U. 1984: Litho- and biostratigraphy of the Upper Triassic–Middle Jurassic in Scania, southern Sweden. Sveriges Geologiska Undersökning Serie C 806, 31 pp.
- Sivhed, U., Wikman, H. & Erlström, M. 1999: Beskrivning till berggrundskartorna 1C Trelleborg NV och NO samt 2C Malmö SV, SO, NV och NO. Sveriges Geologiska Undersökning Af 191–194, 196 och 198, 143 pp.
- Sorgenfrei, T. & Buch, A. 1964: Deep tests in Denmark, 1935–1959. Danmarks Geologiske Undersøgelse III Række 36, 146 pp.
- Springer, N. 1997: Kerneanalyse for Energistyrelsen. Geotermisk potentiale i Københavnsområdet. Del 1. Daglokaliteter i Scania. Del 2. Dybe borer i Scania. Danmarks og Grønlands Geologiske Undersøgelse Rapport 1997/6, 36 pp.
- Sørensen, K. 1986: Danish Basin Subsidence by Triassic rifting on a lithosphere cooling background. *Nature* 319, 550–663.
- Troedsson, G. 1951: On the Höganäs series of Sweden (Rhaetolias). *Lunds Universitets Årsskrift* 2, 269 pp.
- Vajda-Santivanez, V. & Solakius, N. 1999: Palynomorphs, foraminifera, and calcispheres from the greensand–limestone transition at Arnager, Bornholm: Evidence of transgression during the late Cenomanian to early Coniacian. *GFF* 121, 252–256.
- Vejbæk, O.V. 1989: Effects of asthenospheric heat flow in basin modelling exemplified with the Danish Basin. *Earth and Planetary Science Letters* 95, 97–114.
- Vejbæk, O.V. 1997: Dybe strukturer i danske sedimentære bassiner. *Geologisk Tidsskrift* 4, 1–34.
- Weibel, R., Olivarius, M., Kristensen, L., Friis, H., Hjuler, M.L., Kjøller, C., Mathiesen, A. & Nielsen, L.H. 2017: Predicting permeability of low enthalpy geothermal reservoirs: examples from the Upper Triassic–Lower Jurassic Gassum Formation, Norwegian–Danish Basin. *Geothermics* 65, 135–157.

Interpretational challenges related to studies of chalk particle surfaces in scanning and transmission electron microscopy

MORTEN LETH HJULER, VIDAR FOLKE HANSEN & IDA LYKKE FABRICIUS



Hjuler, M.L., Hansen, V.F. & Fabricius, I.L. 2018. Interpretational challenges related to studies of chalk particle surfaces in scanning and transmission electron microscopy. © 2018 by Bulletin of the Geological Society of Denmark, Vol. 66, pp. 151–165. ISSN 2245-7070. (www.2dgf.dk/publikationer/bulletin).

Received 1 December 2017
Accepted in revised form
1 April 2018
Published online
31 August 2018

Scanning and transmission electron microscopy (SEM and TEM) are capable of characterising the morphology and structure of sub-micron size substances attached to chalk particle surfaces. Some characteristics, however, may originate from sample preparation or reflect interaction between sample and the electron beam. Misinterpretation of surface features may lead to wrong conclusions regarding grain surface properties and cementation level and thus to erroneous characterisation of hydrocarbon reservoirs with respect to e.g. wettability, mechanical strength and maximum burial depth. In SEM, conductive coatings may mask surface details or generate artificial ornamentations, and carbon adhesive discs may cause the chalk surface to be covered with a thin carbon film. Electron beam acceleration voltage controls the degree of detail revealed by the electron beam, but in SEM a high electron beam acceleration voltage may provoke bending or curling of ultrathin particles. Recent organic filaments may be confused with clay flakes, and authigenic non-carbonate minerals may have formed in the pore fluid and settled during fluid removal. In TEM, the high acceleration voltage may cause beam damage to calcite and transform the outermost atomic layers into Ca oxide. Thin graphite membranes observed by TEM may be contamination from the carbon film supporting the sample, and overlapping chalk particles in samples formed by drying of a suspension may give the impression of being cemented together. In TEM residual adhesive from the ion-milling process can be confused with cementation features.

Keywords: Scanning electron microscopy, transmission electron microscopy, chalk, surface coating, surface ornamentation, image interpretation.

Morten Leth Hjuler, Geological Survey of Denmark and Greenland (GEUS), Øster Voldgade 10, DK-1350 Copenhagen K, Denmark [present e-mail: coccoleth@hotmail.com]. Vidar Folke Hansen [vidar.hansen@uis.no], Department of Mechanical and Structural Engineering and Materials Science, University of Stavanger, N-4036 Stavanger, Norway. Ida Lykke Fabricius [ilfa@byg.dtu.dk], Department of Civil Engineering, Technical University of Denmark, Nordøvej, Building 119, DK-2800 Kgs. Lyngby, Denmark.

Oil recovery from chalk reservoirs in the North Sea is governed by the low permeability of the chalk matrix where significant amounts of oil are retained within the micrometre- or nanometre-sized pores. Oil recovery is further controlled by the properties of the particle surface in terms of its affinity towards various pore fluids. The chalk surface may vary from completely oil-wet over mixed-wet to completely water-wet depending on factors such as type of pore fluid and its affinity towards calcite or e.g. clay minerals covering the calcite surface. Further, the surface area available for wetting may be controlled by the amount, type and distribution of clay and silica minerals (Røgen & Fabricius 2002) and by the degree of diagenesis, which in turn is controlled by maximum burial depth

and timing of oil invasion (Hjuler & Fabricius 2009). In order to improve recovery efficiency, various improved oil recovery (IOR) and enhanced oil recovery (EOR) techniques are being tested and employed. In this context, understanding the properties of chalk particle surfaces is crucial and reliable characterisations are necessary.

Chalk is a granular material which seems rather homogenous to the naked eye, but on closer scrutiny visual traces of e.g. bioturbation, hardgrounds and diagenetic alterations are revealed. Microscopically, the heterogeneous appearance of chalk is further increased. Microfossils, remains of larger fossils and clasts of non-carbonates are unevenly distributed in a matrix of partly or completely disintegrated nanno-

fossils, mainly coccoliths (Fabricius 2007). Diagenetic alterations are seen as recrystallised calcite particles, calcite-cemented fossil cavities and fractures, moulds after siliceous fossils, authigenic silica and clay, as well as stylolites transecting the chalk matrix.

Research into reservoir chalk properties addresses the interaction between chalk particles and pore fluids in order to understand and control how mechanical and chemical mechanisms affect reservoir stiffness and strength (Risnes & Flaageng 1999; Heggheim et al. 2005; Katika et al. 2015; Generosi et al. 2017; Nermoen et al. 2018) as well as oil recovery (Austad & Standnes 2003; Strand et al. 2007; Katika et al. 2018). The relation between the calcite surface and other non-carbonate minerals or other substances plays a central role in this discussion, and it is thus of interest to reveal any presence of ultrathin organic films or clay coatings covering the calcite surface.

Several petrographic investigation techniques have been employed to improve our understanding of chalk behaviour including scanning electron microscopy (SEM) and transmission electron microscopy (TEM) (e.g. Hjuler & Fabricius 2009) and atomic force microscopy (AFM) (e.g. Generosi et al. 2017), as well as various spectroscopy techniques including energy dispersive X-ray spectroscopy (EDS) and electron energy loss spectroscopy. This article focuses on SEM and TEM.

SEM and TEM investigations of chalk performed at high magnifications present the microscopist with numerous interpretational challenges. Contamination from various sources must be identified and excluded from interpretation. Sample interaction with the electron beam may alter the sample morphologically and structurally. Removal of pore fluids may cause suspended material to settle at the surface of particles, thus changing the spatial distribution of pore space constituents. Similarly, pore fluid removal may force

dissolved ions to combine, precipitate and settle on the particle surfaces. The application of a conductive surface coating, e.g. gold, may mask surface details and in addition generate secondary ornamentation.

Although the above mentioned sources of error cannot always be identified or described satisfactorily, it is important to be aware of their existence during investigation and interpretation in high magnification studies. This study presents a number of cases where morphological information (SEM) and structural information stored in diffraction patterns (TEM) is prone to misinterpretation. For a fundamental introduction to electron microscopy, see e.g. Goodhew et al. (2001). For in-depth information on the SEM and TEM techniques, respectively, see e.g. Goldstein et al. (2003) and Williams & Carter (2009).

Methods

Sample material

The chalk samples used in this study were collected from outcrops in various countries in the North Sea area and sampled from well cores from the Central Graben in the North Sea; a single Greensand sample was included. More sample information is presented in Table 1.

SEM investigations

Small pieces of chalk were placed on a carbon adhesive disc mounted on an aluminium stub and coated with gold or gold-palladium by an Emitech K550 sputter coater. The sample chamber was evacuated and filled with argon at a pressure of 10^{-1} mbar, and the coating applied with a current of 17 mA. Coating was applied

Table 1. Sample localities

Onshore location	Locality	Outcrop	Age
France	Hardivillers	Hardivillers quarry	Late Santonian
Germany	Lägerdorf	Schinkel	Santonian–Campanian
		Heidestrasse	Campanian
		Saturn	Campanian–Maastrichtian
Denmark	Stevns	Sigerslev quarry	Maastrichtian
	Ellidshøj	Ellidshøj quarry	Maastrichtian
	Vokslev	Vokslev quarry	Maastrichtian
	Aalborg	Rørdal quarry	Maastrichtian
	Taasinge	Quarry at Bjerreby	Palaeogene*
Offshore location	Field	Depth	Age
North Sea, Central Graben	Ekofisk	3200–3600 m	Maastrichtian
North Sea, Central Graben	Valhall	3200–3300 m	Maastrichtian

Onshore data from Hjuler & Fabricius (2009). Offshore data from Røgen *et al.* (1999).

*Greensand

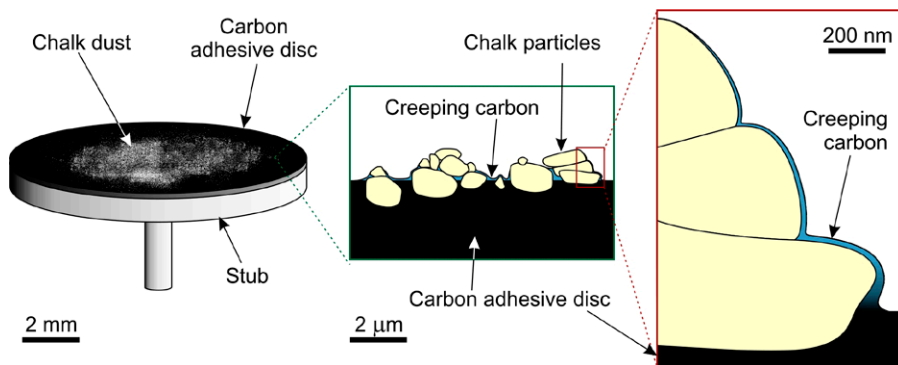


Fig. 1. Aluminium stub mounted with a double-sided carbon adhesive disc. Chalk pieces and dust distributed on the surface may sink partly or completely into the carbon substrate. Carbon from the disc may migrate onto and cover chalk particles with thin, barely visible films.

to the samples for 30 seconds or 2 minutes at a sputter rate of 18 nm/min, resulting in estimated thicknesses of 9 and 36 nm, respectively. Investigations were carried out in high vacuum mode in a Zeiss Supra 35VP field emission microscope using the secondary electron (SE) detector for imaging and the energy dispersive spectrometer (EDS) for mineral identification.

TEM investigations

TEM investigations were carried out in a Jeol JEM-200CX and a Jeol 2000FX transmission electron microscope, both equipped with an EDS detector and operated at 200 kV. Two types of samples were prepared:

Suspension samples. Gently crushed chalk was suspended in ethanol and a droplet of the mixture pipetted onto a carbon film supported by a copper grid, leaving a fine layer of chalk dust behind after drying. This preparation technique allows the study of isolated particles and provides diffraction data with minimum interference from neighbouring particles.

Ion-milled samples. A slice of chalk was impregnated with epoxy, ground into a thin section and polished,

then impregnated with a soluble adhesive and ion-milled. Subsequently, the adhesive was removed. The objective of using this technique was to study the contact points between calcite particles. One disadvantage of this method is the risk of altering the structure of the sample surface as the sample integrity may be affected during the ion-milling process.

Interpreting SEM images of chalk

Artificial surface coatings produced by carbon adhesive

Apart from adhesive qualities, the carbon adhesive disc conducts electricity and may prevent or reduce charging problems. However, chalk particles and small aggregates may sink into the carbon disc and become completely buried (Fig. 1). From the carbon disc, carbon may climb partly embedded particles and small aggregates, covering their surfaces and smudging surface details (Figs 1, 2A). Carbon may also spread to the lower parts of larger chalk aggregates, covering particle surfaces with a thin film (Figs 1, 2B). The film gradually thins toward the upper parts

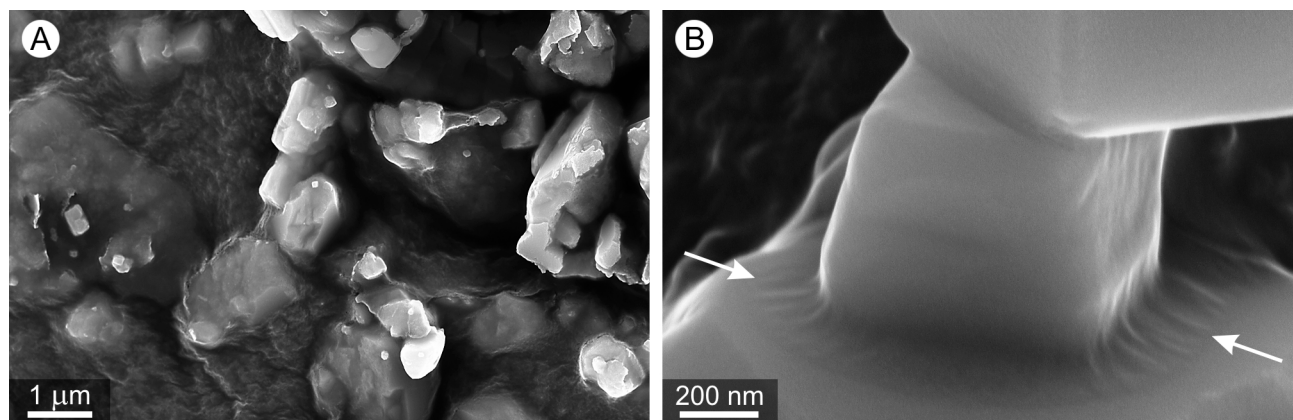


Fig. 2. Carbon spreading from the carbon disc. A: Chalk particles completely or partly embedded in carbon of a carbon adhesive disc; towards the right the presence and effect of carbon is harder to estimate. Chalk from Vokslev, Denmark. B: Ultrathin carbon film visible at the contact points between calcite particles (arrows). Chalk from Lägerdorf, Germany.

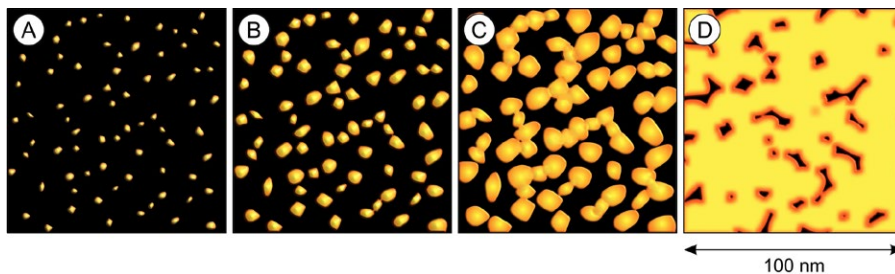


Fig. 3. Film growth during sputter coating. Initially, atoms settle on the sample surface forming tiny islands (A), which grow as more atoms arrive (B), then coalesce (C) to finally produce a conductive coating (D).

of the aggregate where it may disappear or become unobservable. The carbon artefacts should not be mistaken for original organic coatings, clay or any other natural coating. The observation that carbon is capable of climbing and covering calcite particles and aggregates indicates a strong carbon affinity towards calcite. Whenever carbon coatings may cause interpretational difficulties it is advisable to avoid studying single particles or parts of aggregates in direct contact with or close to the carbon disc.

Masking of surface detail by conductive coatings

Chalk is composed of electrically non-conductive calcite, and as an uncoated chalk sample is bombarded with electrons it builds up charge that interferes with the incident electron beam, causing flares and sample drift. In order to avoid these unwanted side effects, chalk samples should be kept small and excess electrons should be guided away by a thin coating of a conductive material such as carbon, gold or gold-palladium. For most chalk investigations the conductivity of carbon is insufficient and the more conductive metal coatings are preferred. Thus, carbon coatings will not be discussed further here.

A sputter coater is commonly used to apply a 10–40 nm thick layer of metal to the chalk sample. The mode of operation involves the initial release of atoms from a coating source; released atoms are directed towards the sample where they bind to the sample surface and each other, forming tiny ‘islands’ (Fig. 3A). As more atoms arrive, these islands grow laterally (Fig. 3B) and finally coalesce (Fig. 3C) to produce a continuous film on top of the sample surface (Fig. 3D) (Goldstein et al. 2003). A 40 nm thick coating is acceptable for standard investigations of chalk at relatively low magnifications. At high magnification, examination demands a much thinner coating to avoid masking of delicate details (e.g. Folk & Lynch 2001; Henriksen et al. 2004). A thinner coating causes increased risk of charging, but we find that a 10 nm thick layer is a reasonable compromise as charging is small and masking effects are limited. This is illustrated by high magnification images of the delicate blades of opal-CT lepispheres (Fig. 4). A 36 nm thick gold coating increases the blade thickness and gives them a robust appearance, and fine structural details remain hidden below the coating or may be confused with topographical features of the thicker coating (Fig. 4A). With a 10 nm thick coating, a more correct representation of the thinness and fragility of the blades is produced and the tiny crystals

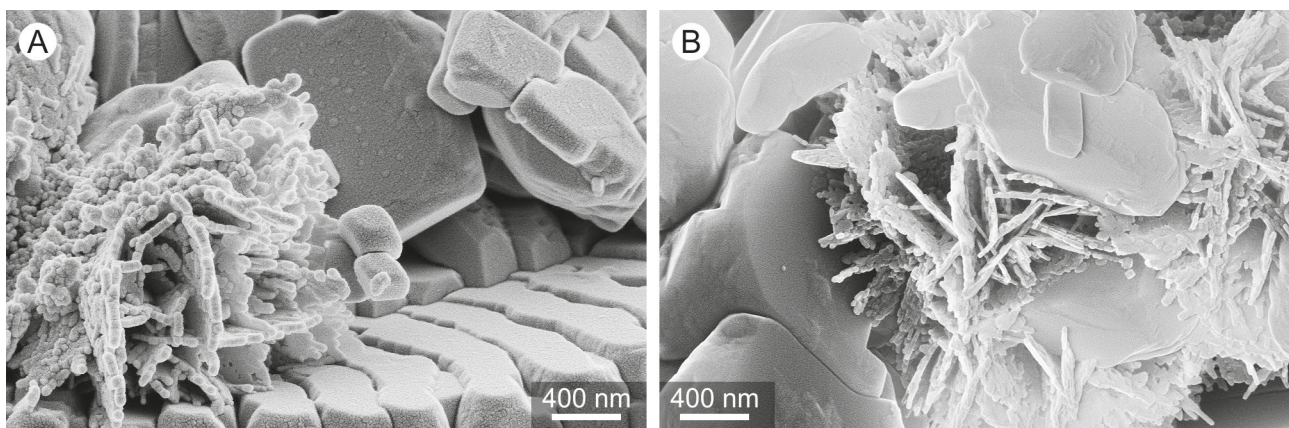


Fig. 4. Masking and distortion of details caused by coating thickness. A: Blades of opal-CT lepisphere covered with c. 36 nm of gold which more than doubles the blade thickness. B: Reducing coating thickness to c. 10 nm reveals blade delicacy and the tiny blade-building crystals. Chalk from Aalborg (A) and Ellidshøj (B), Denmark.

building each lepisphere blade are revealed (Fig. 4B).

The chemisorbed water film covering the surface of chalk grains, often referred to as the irreducible water layer, is estimated to be c. 5 nm thick (Larsen & Fabricius 2004) and thus 2–8 times thinner than the 10–40 nm thick coating. This implies that original topographical features may be masked by the coating and thus that the surface area defining the amount of chemisorbed water may be significantly changed, most likely reduced as the coating tends to smooth the surface topography. Therefore, attempts to assess surface area and the amount of chemisorbed water should be approached with caution.

Artificial surface textures created by conductive coatings

The complex interaction between sample and sputter coater settings may result in coatings which at high magnifications display ornamentations. At small coating thicknesses (10 nm) ornamentations are hardly visible (Fig. 5A), but thicker coatings of 40 nm or

more may display significant ornamentations such as reticulate crack-like patterns (Fig. 5B) or grainy surfaces (Fig. 5C). At high magnification, the single grains/drops of the coating material become clearly visible and may dominate the ornamentation of the sample surface (Fig. 5D).

Affinity between coating and sample

Whereas carbon has high affinity to the calcite surface (Fig. 2), the opposite is observed for metal coating (Fig. 6). In this extreme case, the gold atoms probably aggregated before settling due to insufficient vacuum in the sputter coater and failed to spread out on the calcite surface. The reason for this difference is that calcite is a covalently and ionically bonded mineral (Skinner et al. 1994) with a monolayer of hydrolysed water so strongly chemisorbed to the surface that it is preserved even in ultra-high vacuum (Stipp 1999). Gold and gold-palladium are noble metals that cannot bond to the water layer, whereas graphite coal has the possibility to share electrons covalently. Gold and

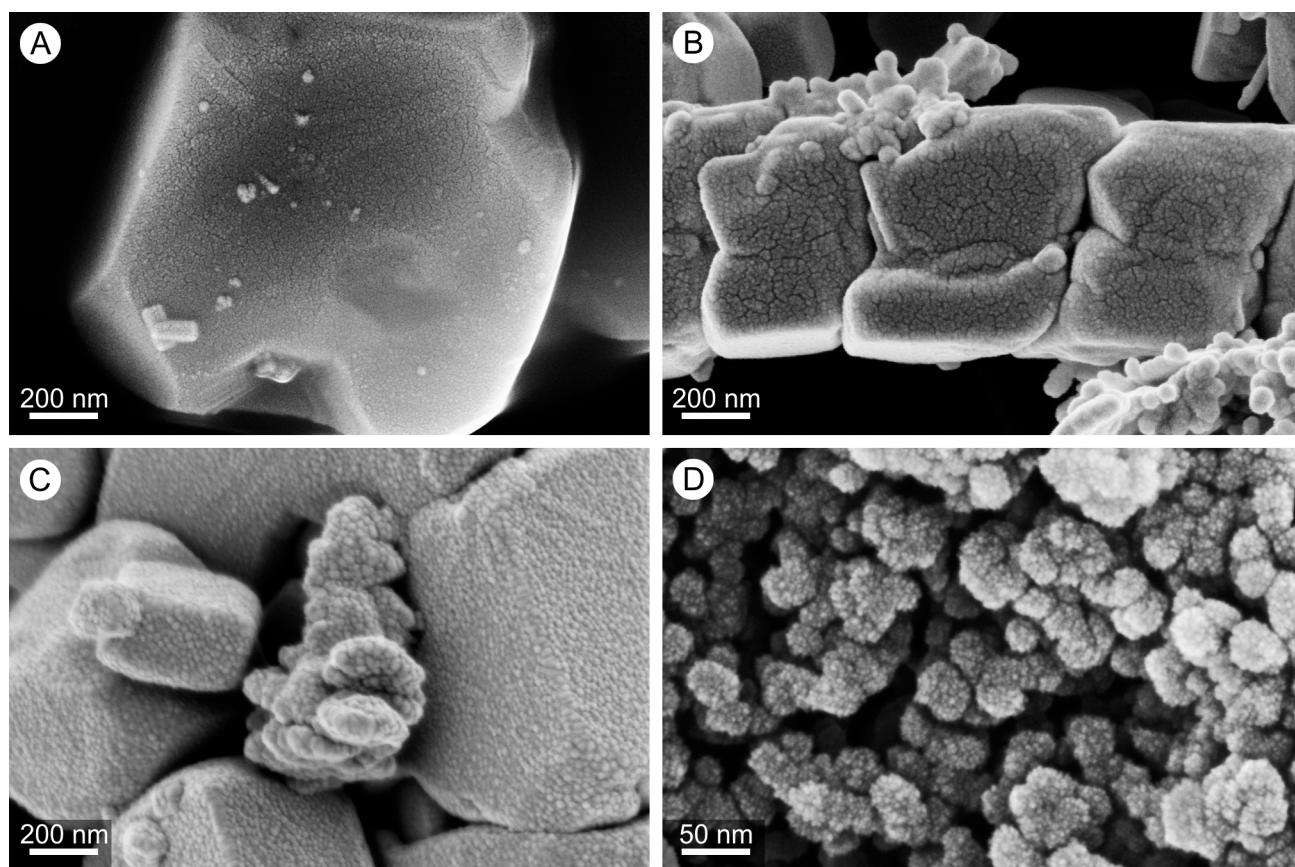


Fig. 5. Surface textures produced by coatings. A: Barely visible, 10 nm thick gold-palladium film; sample details smaller than 50 nm are clearly visible. Chalk from Valhall field, North Sea. B: Approximately 36 nm thick film with a pronounced crackled appearance; sample details smaller than 50 nm are hard to discern from the coating. Chalk from Aalborg, Denmark. C: coating 36 nm thick, showing grainy texture. Chalk from Stevns, Denmark. D: 20–30 nm-sized opal-CT crystallites covered with gold grains less than 5 nm in diameter. Greensand from Taasinge, Denmark.

gold-palladium coatings with crack-like appearance were accordingly also observed at surfaces of other water-wet minerals such as quartz, opal-CT, clinoptilolite, various clays and apatite.

That metal coatings may not be strongly attached to the surface of the investigated minerals was observed on several occasions during EDS spot analysis at high

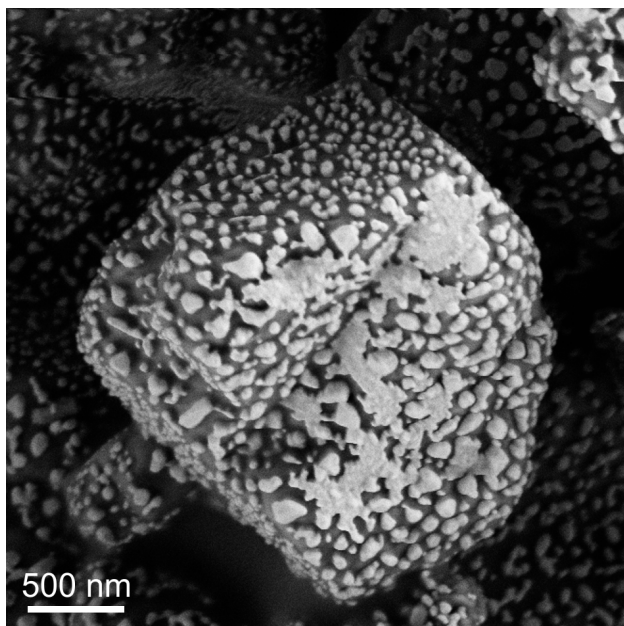


Fig. 6. Gold coating concentrated in isolated droplets due to a malfunctioning sputter coater; charging is not prevented. Chalk from Lägerdorf, Germany.

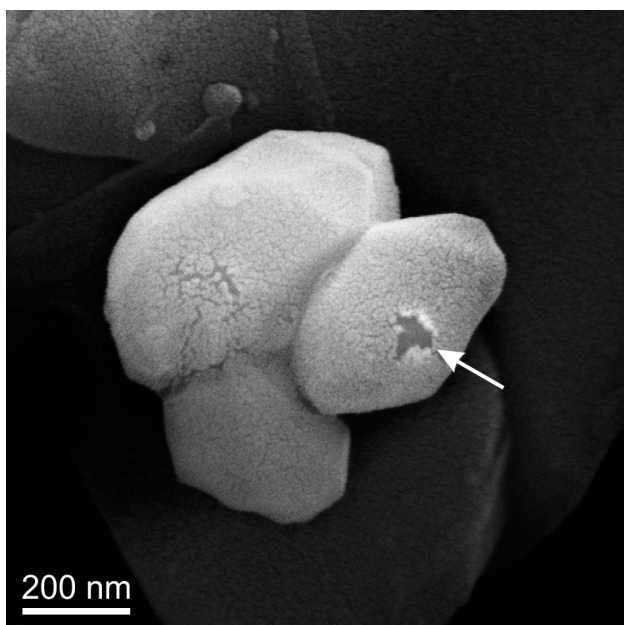


Fig. 7. Electron bombardment during EDS analysis has locally removed the gold-palladium coating from the surface of a quartz particle (arrow). Chalk from the Ekofisk field, North Sea.

magnification (Fig. 7). The continuous electron bombardment of a restricted area over time has removed the coating from the sample surface.

Acceleration voltage and surface detail

The acceleration voltage determines the energy of beam electrons and is thus a major control of electron capability to penetrate into the sample. At high acceleration voltages (15–30 kV) the beam electrons penetrate beneath the sample surface to produce electron signals mostly carrying information of the sample interior (Goldstein et al. 2003) (Fig. 8). Thus relatively few of the secondary electrons are generated at or near the surface and little surface information is obtained, so that surface ornamentation is weakly depicted in the final SEM image (Figs 9A and C). By reducing the acceleration voltage to 5 kV or less the penetration depth of the beam electrons is confined to near-surface regions (Fig. 8C). Accordingly, the resulting electron signal will carry surface related information from which a SEM image rich in surface detail is provided (Figs 9B and D). Enhancing surface detail also increases the relative contribution from surface coatings.

One negative consequence of lowering the acceleration voltage is reduced production of secondary electrons per time unit (signal) and thus reduced image quality. One way to overcome this problem is to reduce scan speed. Unfortunately, this action also increases the possibility of charging effects and sample drift. Charging may be avoided without loss of image quality by producing an average image from a number of identical high speed scans; this method, however, is time-consuming and may prove useless due to beam drift, especially at high magnifications.

Electron-induced sample alteration

Tiny substances within chalk may be morphologically modified during interaction with the electron beam. Among such substances are clay flakes extending for less than 1 μm and attaining thicknesses below 50 nm (including coating). Clay flakes often protrude into the pore space and are likely to bend when hit by the focused electron beam at high magnification. The clay mineral illite frequently occurs as filaments which will curl into spirals when hit by electrons (Fig. 10). The sample sensitivity to electron beam interaction may be reduced by lowering the acceleration voltage.

Sample contamination by recent organic material

Characteristic thin filaments (hyphae of fungi?) are

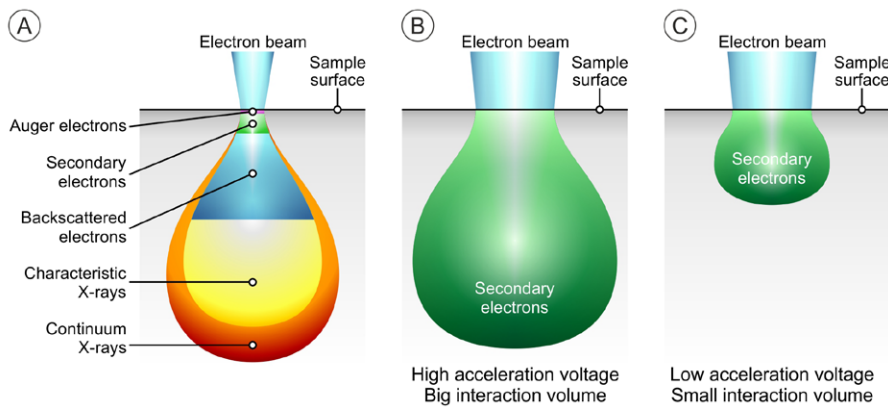


Fig. 8. Electron–sample interaction. A: Interaction depth and volumes of various SEM signals. Penetration depth of secondary electrons is limited but may be controlled by adjusting the acceleration voltage. B: High acceleration voltage: significant electron penetration depth and limited surface information. C: Low acceleration voltage: shallow electron penetration and increased surface information.

frequently observed in outcrop chalk. These recent, cobweb- or spaghetti-like occurrences may cover large areas or volumes (Fig. 11A) and presumably develop within chalk fractures in situ or at chalk surfaces during sample preparation. The filaments are easily discernible from calcite and non-carbonate particles, however, the filament terminations may form flattened attachments on the surfaces of chalk particles which resemble clay flakes (Fig. 11B).

Suspended or appended growth of authigenic non-carbonates

During diagenesis, some non-carbonate minerals such as kaolinite and opal-CT grow in the pore water, but as pore water is removed during sample preparation, these minerals will settle on calcite particles. Thus, SEM images do not necessarily reflect the original position of non-carbonate minerals relative to chalk

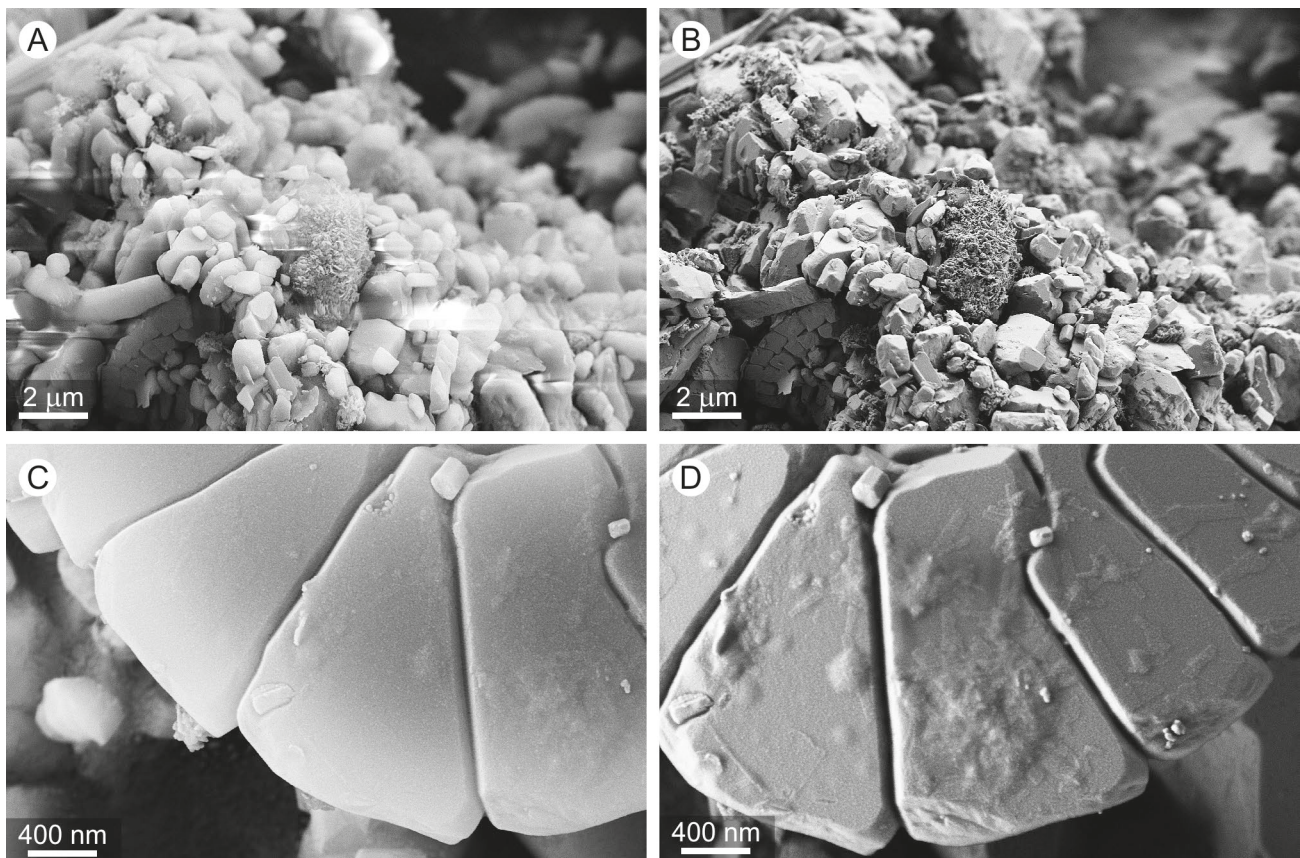


Fig. 9. The effect of high and low acceleration voltages. The amount of surface details is significantly increased when the acceleration voltage is reduced from 10 kV (A, C) to 2 kV (B, D). A and B: Chalk from Lägerdorf, Germany; C and D: Chalk from Hardivillers, France.

particles. The diagenetic fabric of chalk may reveal whether or not a mineral occupies its original position.

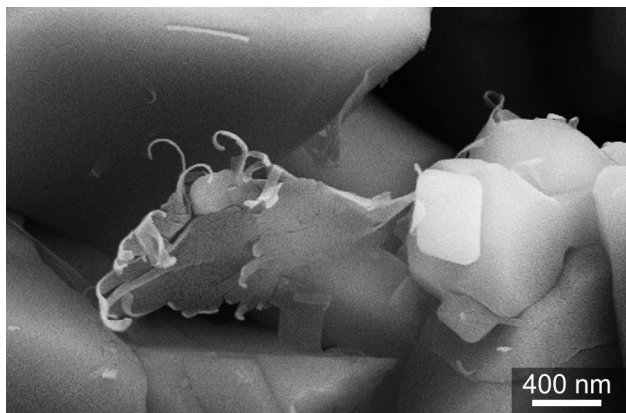


Fig. 10. Tiny filaments at the rim of a clay flake curl in response to the electron beam. Chalk from the Ekofisk field, North Sea.

During recrystallisation and cementation of chalk, the expanding surfaces (overgrowths) of calcite particles may grow around and embed another mineral attached to the surface (Fig. 12A); or the non-carbonate mineral may grow around a calcite particle (Fig. 12B). In these cases it is evident that the minerals occupy their original positions. Where clay flakes are positioned on top of calcite particles, it cannot be decided whether their position is original or whether they settled from suspension during sample preparation (Fig. 12C).

Mineral precipitation during evaporation of pore water

If chalk samples are not cleaned for salt and hydrocarbons before SEM investigation, various salts and possibly clay flakes few nanometres thick will precipitate during drying of the sample (Fig. 13).

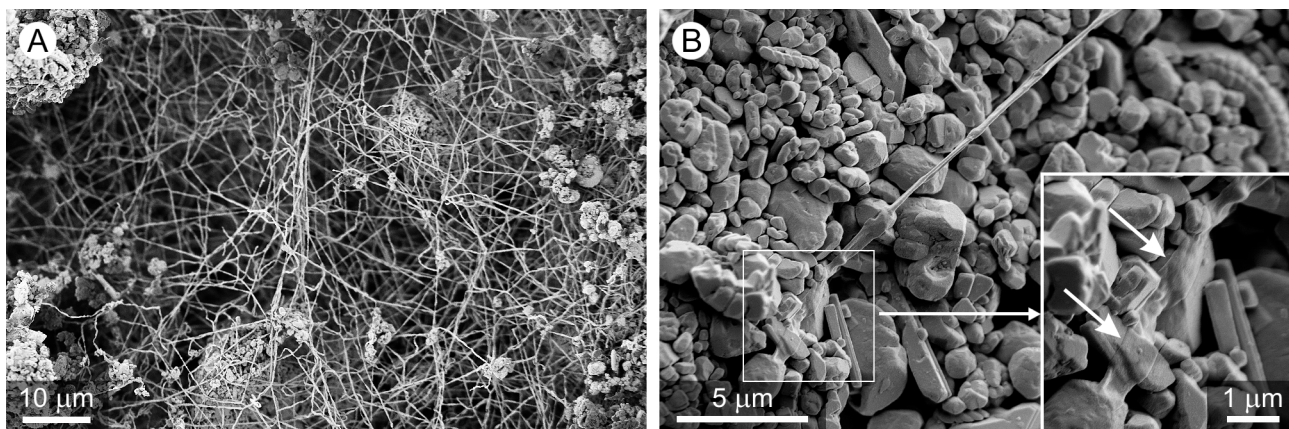


Fig. 11. Contamination by recent organic material. A: A web of organic filaments spans a crevice in chalk. Chalk from Aalborg, Denmark. B: Flattened filament terminations (arrows) form thin attachments similar to clay flakes. Chalk from Stevns, Denmark.

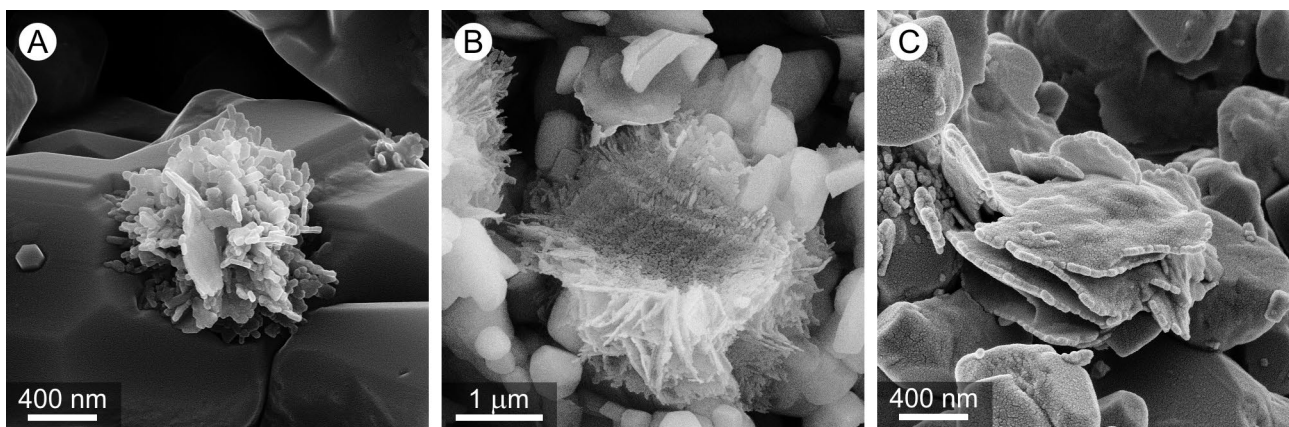


Fig. 12. Growth of non-carbonate minerals in chalk. A: Appended growth: opal-CT lepisphere partly embedded in overgrown calcite crystal. B: Appended growth: opal-CT lepisphere once growing around a now disappeared coccolith, as witnessed by the impression left. C: Appended or suspended growth (?): clay flakes positioned on top of chalk particles. A: Chalk from Lägerdorf, Germany; B and C: Chalk from Aalborg, Denmark.

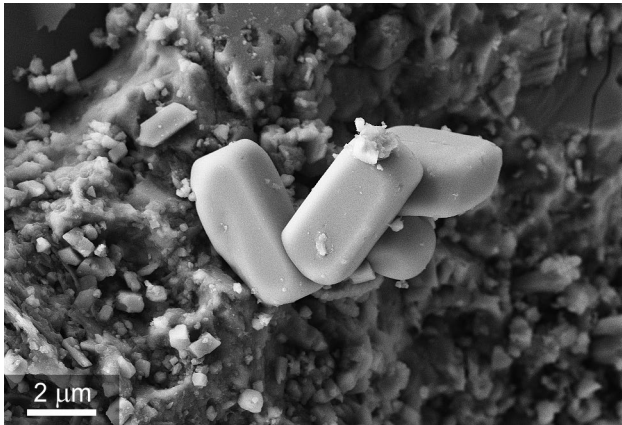


Fig. 13. Halite crystals presumably precipitated from brine in the pore space. Chalk from the Ekofisk field, North Sea.

Interpreting TEM images of chalk

Destruction of the atomic structure of calcite

In order to perform analytical studies in the TEM, beam electrons are accelerated to energies high enough to allow sample transmittance. However, high electron energy also produces the undesirable side effect of beam damage, by which the atomic arrangements of the sample are altered irreversibly either by displacement of atoms (knock-on damage) or by breakage of chemical bonds (radiolysis) (Williams & Carter 2009). An electron beam fixed in one spot for some time may cause the atomic structure to change from crystalline into amorphous, a process directly observable in the TEM as the diffraction pattern becomes more diffuse. Different materials respond differently to the impact of electrons and display vary-

ing degrees of susceptibility to beam damage. Beam damage probably always occurs to some degree, but may not be noticeable.

Formation of new mineral coatings on calcite

Based on TEM investigations of Cretaceous and Palaeogene chalk, Bürki et al. (1982) and Glasser & Smith (1986) reported siliceous coatings covering the surfaces of coccoliths and proposed that these coatings were formed from an organic membrane produced by the living organism. Attempting to observe these reported coatings in situ on fossil coccoliths should be done with beam damage in mind. Beam damage may be restricted to the sample surface, causing displacement of surface atoms and possibly altering surface chemistry (Williams & Carter 2009). This may explain observations in this work of ultrathin polycrystalline coatings covering the surface of calcite particles (Fig. 14A). The coating is evidenced by barely visible diffraction rings superposed onto the diffraction pattern of the calcite crystal (Fig. 14B). By calibrating these

Table 2. Interplanar spacings (d) of observed surface coatings of calcite and CaO

Observed coatings d spacing (Å)	CaO d spacing (Å)	CaO Relative intensity (X-ray?)	hkl
2.8	2.7799	38	111
2.4	2.4075	100	002
1.7	1.7024	59	022
	1.4518	16	113
1.4	1.3900	18	222
	1.2038	8	004
	1.1046	7	133

Diffraction data for CaO based on information from Fiquet *et al.* (1999).

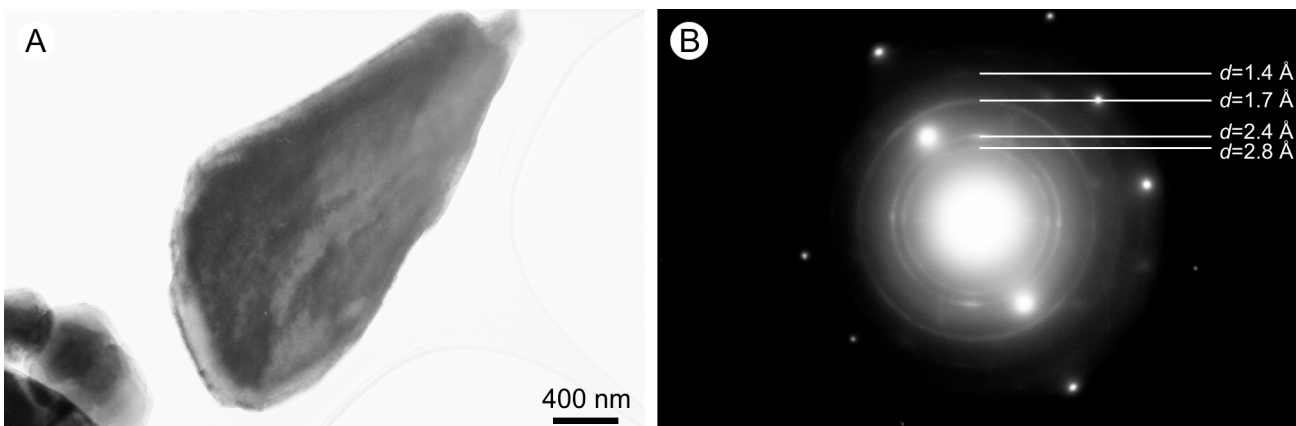


Fig. 14. Beam damage. A: Bright field image of particle identified as calcite based on its diffraction patterns. B: Diffraction pattern representing the $[\bar{1} \bar{7} 6]$ projection of the calcite particle with superposed diffraction rings belonging to polycrystalline CaO. Chalk from Aalborg, Denmark.

diffraction rings towards the interplanar spacing in a calcite diffraction pattern of known crystallographic orientation, the coating was identified as CaO (lime) (Table 2). Presumably, the surface layers of calcite were chemically altered into polycrystalline CaO during interaction with the electron beam.

The well-defined diffraction rings prove the CaO layer to be polycrystalline rather than amorphous, and diffuse higher-intensity areas on the rings indicate a minor degree of preferential orientation. To

observe these diffraction rings, long exposure time is needed and thus the rings are easily overlooked. Consequently, estimating the prevalence of this type of beam damage is difficult.

Carbon contamination

The siliceous coatings described by Bürki et al. (1982) and Glasser & Smith (1986) are depicted as ultrathin, low contrast membranes often reflecting the structure

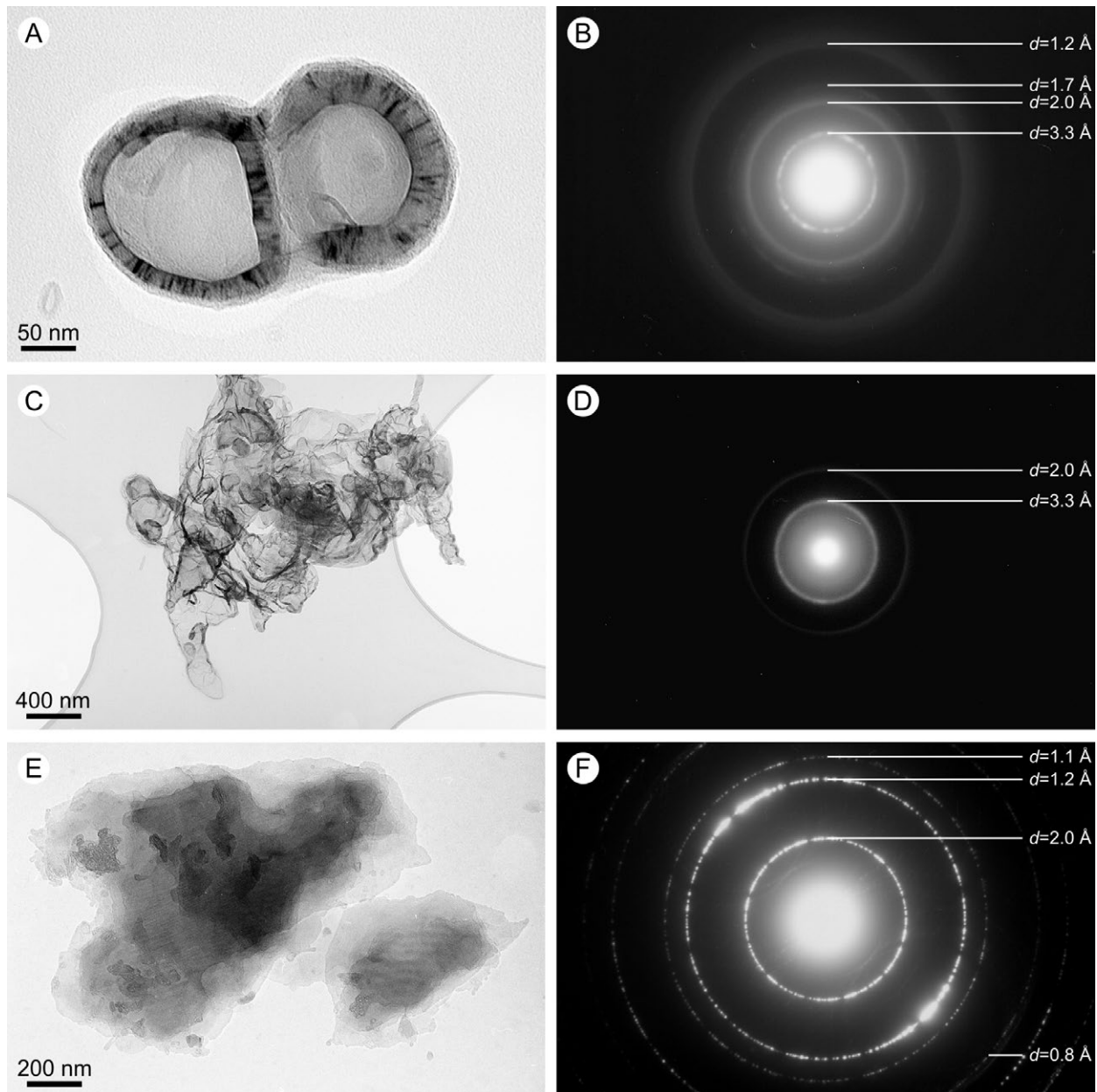


Fig. 15. Graphite particles. A and C: Bright field images showing membrane-like structures. B and D: Diffraction patterns of A and C showing relatively well-defined diffraction rings indicating polycrystallinity; interplanar spacings (d) are indicated. E: Bright field image of graphite viewed along the [001] projection. F: Diffraction pattern of E, polycrystallinity is clearly visible. In order to better observe details in the bright field images, the contrast has been significantly increased. A–F: Chalk from Aalborg, Denmark.

of coccoliths (Glasser & Smith 1986, figs 11.2, 11.4a). In the present study, similar membrane-like structures were frequently observed scattered on TEM carbon films. These membranes are ultrathin, probably just a few nanometres, and irregularly shaped with sizes ranging from less than 100 nm to more than 5 μm (Fig. 15A and C). Size and shape of the membranes are difficult to determine due to their crumpled appearance, and none of the observed examples reflect coccolith morphology. The membranes produce fairly well-defined diffraction rings suggesting the coatings to be polycrystalline rather than amorphous (Fig. 15B and D). The diffraction planes with a d spacing of 3.6 Å and 1.8 Å, respectively, normally show some degree of preferential orientation (Fig. 15B and D). Initially, we thought that these membranes were siliceous coatings as described by Bürki *et al.* (1982) and Glasser & Smith (1986). The interplanar spacing of diffraction planes observed in Fig. 15B and D, however, did not correspond to those of silica. Ultimately the membranes were found to consist of graphite, as evidenced from comparison of observed diffraction data with graphite diffraction data (Table 3). It is thus possible that the membranes of this study and the coatings of Bürki *et al.* (1982) and Glasser & Smith (1986) are separate phenomena.

Occasionally more crystallographically mature versions of membranes are found (Fig. 15E) with diffraction patterns corresponding to the [001] projection of graphite (Fig. 15F). Possibly, this graphite originates from the carbon film supporting the chalk sample.

Apparent cohesion between calcite particles

In order to understand and describe the mechanical strength of chalk, the cementation features related to particle contacts were investigated in TEM, but interpretation of contact points between calcite particles should be approached cautiously. Fig. 16A shows two calcite particles from a suspension sample; the particles are apparently grown together along a line bounded by meniscus-like cement (Fig. 16B). These

Table 3. Interplanar spacings (d) of observed membranes and graphite

Observed membranes d spacing (Å)	Graphite d spacing (Å)	Graphite Relative intensity	hkl
3.3	3.3553	100.0	002
	2.1319	3.5	100
2.0	2.0318	16.7	101
	1.7994	3.0	102
	1.6777	5.4	004
1.7	1.5433	4.5	103
	1.3184	0.7	104
	1.2309	5.0	110
	1.1556	7.3	112
1.2	1.1358	1.0	105
	1.1184	0.7	006
	1.0659	0.1	200
	1.0527	1.0	201
	1.0159	0.3	202
	0.9924	4.1	114
1.1	0.9904	2.0	106
	0.9623	0.8	203
	0.8997	0.2	204
	0.8743	0.4	107
	0.8388	0.3	008
	0.8347	0.6	205
	0.8277	2.7	116
	0.8058	0.3	210
0.8	0.8000	1.5	211
	0.7835	0.5	212

Diffraction data for graphite are cited from Howe *et al.* (2003).

observations fit well with the dissolution-precipitation theory presented by Heggheim *et al.* (2005) and discussed further by Strand *et al.* (2007).

However, during tilting of the stage it became clear that this cementation phenomenon was an optical illusion created by one particle partly covering another (Fig. 17A). As coverage was increased during tilting of the stage, the apparent line of coalescence grew longer and the meniscus-like cement was pushed outwards

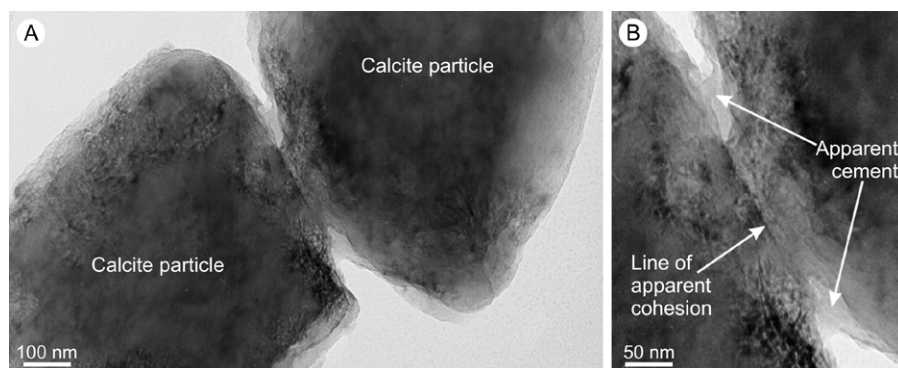


Fig. 16. Apparent cohesion. A: Two calcite particles apparently in contact with each other. B: Close-up of the contact area. The particles seem to have grown together along a line flanked with meniscus-like cement.

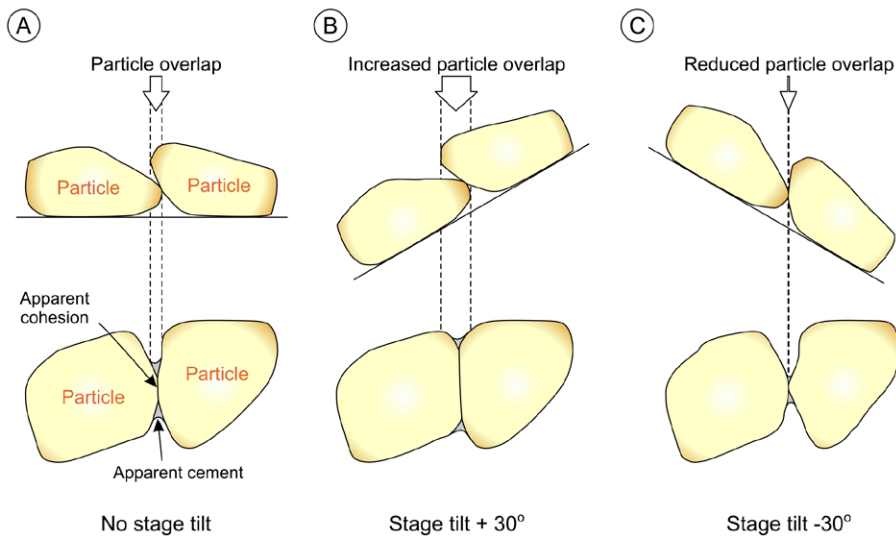


Fig. 17. Apparent cohesion. The upper row of drawings represents lateral views of the particles; the lower row shows the particles as observed in the microscope, i.e. from above. A: Slight overlap, the particles seem to have grown together. B: Tilting the sample $+30^\circ$ increases the overlap; the particles seem intimately intergrown. C: Tilting the sample -30° decreases the overlap; the particles appear to be loosely connected.

(Fig. 17B). Reversing the tilt angle reduced the contact area between the two particles correspondingly (Fig. 17C), and ultimately it became probable that what we saw was two separate particles settled next to each other during sample preparation.

By tilting the stage it may be possible to visually separate two calcite particles apparently in contact. However, revealing truly intergrown calcite particles visually poses significant difficulties; irregularly shaped interfingering particles may not have been

in contact originally but this fact may remain hidden during stage tilting as the particles will seem to be in contact visually at all times.

Residual adhesive in ion-milled samples

Highly porous and weakly consolidated chalk is a challenging material when it comes to preparing samples of limited thickness, e.g. ion-milled samples. Thinning of such chalk by ion-milling requires stabilisation of the chalk structure by saturating the pore space with a soluble adhesive. After finishing the thinning process, the slice of chalk is cleaned by adding a solvent removing the adhesive. However, traces of adhesive will probably always be left behind, and to avoid charging, a thin carbon film is applied to the chalk sample. This can lead to a false interpretation of two calcite particles being cemented together (Fig. 18).

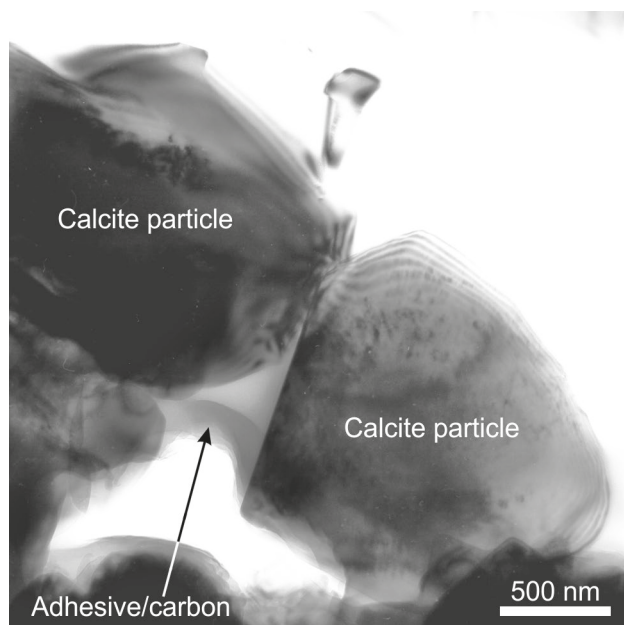


Fig. 18. Ion-milled chalk sample. The meniscus-like structure situated between two calcite particles may be interpreted as cementation but is more likely constituted by residual adhesive from the thinning process or carbon from the conductive carbon film.

Consequences of misinterpretations

Erroneous characterisation of particle surface chemistry may result in wrong assessment of wettability and how wettability may be modified to increase oil recovery. Thus, correct detection of coatings and other substances a few nanometres thick attached to particle surfaces, and determining the extent of such matters, are important tasks in attempts to increase oil recovery. This study has pointed out several cases where sample preparation and instrument settings of SEM and TEM are responsible for creating, hiding, altering or preventing identification of structures related to chalk particle surfaces and particle contacts.

Artificial surface coatings

SEM. Carbon from the carbon adhesive disc may spread to and cover calcite particles with a uniform, few nanometres thick coating (Figs 1–2) that should not be confused with any original organic coatings and seen as an indicator of oil wettability. Conductive metal coatings applied to the chalk particle surface may change the appearance of the surface texture depending on type and thickness of the coating (Figs 3–5).

TEM. Ultrathin graphite membranes (Fig. 15), possibly originating from the sample holder, should not be mistaken for organic coatings originally covering the particles with the implication this would have for chalk surface properties.

Artificial surface substances and appearances

SEM. Electron-induced sample alteration may have implications for illite filaments, which will curl into tiny spirals when hit by electrons (Fig. 10). As illite commonly is associated with smectite in mixed-layer structures (e.g. Lindgreen *et al.* 2002), the erroneous conclusion may be drawn that the curling phenomenon is due to smectite losing water and transforming into illite. This, however, requires that a sufficient amount of potassium ions is available for the illite structure from the pore fluid, which necessarily has to be water as oil is incapable of transporting ions. The transformation from smectite to illite is used as an indicator of maximum burial depth, and wrong determination of the smectite–illite transition may lead to wrong assessments of maximum burial depth.

Recent organic filaments in chalk (Fig. 11) are easily identified, but the clay-like flattened terminations of the filaments may deceive as they often cover large parts of the chalk particle surfaces and thus give the impression that clay plays a major role in the particle surface–pore fluid interaction.

Whether authigenic non-carbonates, typically clays or submicron-sized quartz, were originally suspended in the pore fluid or attached to or covering the chalk particle surface is difficult to affirm. If the non-carbonates originally stuck to the particle surfaces, they would determine the interaction between particle and pore fluid. In order to investigate original positions of non-carbonates in chalk, a cryo (freezing) SEM should be employed. Original pore fluids must remain in place during and after sampling and sample preparation. In the frozen sample, suspended constituents remain suspended and fixed in the pore fluid and may be observed *in situ*.

Normally, chalk is cleaned for salt and drilling mud before it is subjected to various analyses. However, sometimes evaporating pore water leaves some salt behind in the chalk, which may affect the outcome of e.g. X-ray diffraction analysis (XRD) and conventional core analysis (porosity and permeability).

TEM. Beam damage (Fig. 14, Table 2) may not only change the mineralogy of the particle surface layers, but possibly also the particle properties. This may have an effect on wettability.

Hidden surfaces

SEM. The thin carbon coatings derived from the carbon adhesive disc (Figs 1–2), and also the applied conductive metal coatings (Figs 3–6), may mask the true nature of the particle surfaces, depending on the type and thickness of the coating. Important information regarding surface mineralogy may remain undetected and result in erroneous characterisation of the surface properties of the particle.

Undetected substances adhering to the particle surface

SEM. The effect of high acceleration voltage is loss of surface detail (Fig. 9A, C) and thus loss of information on ultrathin substances adhering to the particle surface, as seen in Fig. 9B, D. That ultrathin flakes adhering to calcite may be clay was proposed by Skovbjerg *et al.* (2012), who also demonstrated intermediate wettability of the flakes. This finding suggests that barely detectable clay particles may play a major wettability-controlling role and thus emphasises the importance of careful analysis of particle surfaces. However, it still remains unresolved whether these flakes before removal of the pore fluids were adhering to the particle surface or were suspended in the pore fluids.

Apparent contact cement between chalk particles

SEM. When conductive metal coatings are applied to chalk in thicknesses of 40 nm or more, submicron-sized details become blurred and indistinct and attain a false robustness (Fig. 5). The contact cementation between chalk particles may appear more well-developed than it really is, which may lead to overestimation of chalk consolidation and mechanical strength.

TEM. The visual challenges related to identification of particle contacts in TEM (Figs 16–17) as well as identification of residual adhesive (Fig. 18) may

result in overestimation of the degree of cementation between particles and the mechanical strength of the chalk.

Conclusions

SEM and TEM investigation of chalk at high magnification provides detailed information on the morphology, size and mineralogy of chalk particles, and structural features including cementation and spatial distribution of non-carbonate minerals can be visualised. However, the ability to resolve fine details also exposes morphological and structural changes caused by sample preparation and interaction between sample and electron beam. Misinterpretation of features as described in this study may lead to inaccurate characterisation of the surfaces of chalk particles and untenable conclusions with regard to their properties. As a possible consequence, wettability, mechanical strength and maximum burial depth of a chalk reservoir may be evaluated wrongly.

For SEM investigations of chalk, microscopists are encouraged to pay attention to the following phenomena.

1. Conductive coatings may produce artificial surface textures and artificial ornaments, which may mask genuine surface details. To minimise these effects, coating application time should be kept at a minimum.
2. Chalk particles and small chalk aggregates mounted on carbon adhesive discs may submerge into the carbon substrate, or their surfaces may be covered by an ultrathin film of creeping carbon.
3. Acceleration voltage determines the probing depth of the electron beam and thus the amount of observable detail. By lowering the acceleration voltage, an apparently smooth surface may reveal significant ornamentation.
4. High-energy electrons hitting delicate particles may cause the particle shape to change. For example, submicron-sized thin clay flakes tend to bend or curl when hit by electrons.
5. Flattened terminations of organic filaments attached to calcite particle surfaces mimic clay flakes.
6. Authigenic non-carbonate minerals attached to the calcite surface may have resided suspended in pore fluids and settled when the fluids were removed during sampling or sample preparation.
7. Removal of pore fluids by drying may cause suspended ions to concentrate and precipitate. The occurrence of salt crystals indicates the original presence of brine.

During TEM investigations of chalk, attention should be paid to the following phenomena:

1. The high acceleration voltage necessary to transmit electrons through calcite particles may damage the crystal structure and cause gradual amorphisation. A thin CaO coating is interpreted as a mineralogical change from CaCO_3 to CaO (lime) caused by beam damage restricted to the calcite surface.
2. Ultrathin membranes sharing similarities with siliceous coatings described in earlier literature may be graphite, possibly derived from the carbon film supporting the chalk sample.
3. Calcite particles overlapping each other in suspension samples may seem to be cemented together but may in fact be separate particles settled next to each other during sample preparation.
4. Residual adhesive from the ion milling process or applied conductive carbon film should not be confused with cementation.

Acknowledgements

The Research Council of Norway and BP Norway are gratefully acknowledged for financial support. Several persons have directly or indirectly been involved in this study via discussions and technical assistance and we want to thank them all. From the University of Oslo, we especially want to thank Professor Johan Taftø for beneficial discussions and assistance in interpreting polycrystalline and amorphous material observed in TEM. Ingunn Cecilie Oddsen and Ola Risvik from the University of Stavanger are thanked for technical assistance during SEM investigations. Jørgen Bilde-Sørensen from Risø National Laboratory is acknowledged for technical and interpretational assistance related to TEM investigations. Emil Makovicky from the University of Copenhagen is acknowledged for providing important insight into some of the problems described. Finally, the manuscript was improved by the constructive comments of the referees.

References

- Austad, T. & Standnes, D.C. 2003: Spontaneous imbibition of water into oil-wet carbonates. *Journal of Petroleum Science and Engineering* 39, 363–376.
- Bürki, P.M., Glasser, L.S.D. & Smith, D.N. 1982: Surface coatings on ancient coccoliths. *Nature* 297, 145–147.
- Fabricius, I.L. 2007: Chalk: composition, diagenesis and physical properties. *Bulletin of the Geological Society of Denmark* 55, 97–128.

- Fiquet, G., Richet, P. & Montagnac, G. 1999: High-temperature thermal expansion of lime, periclase, corundum and spinel. *Physics and Chemistry of Minerals* 27, 103–111.
- Folk, R.L. & Lynch, F.L. 2001: Organic matter, putative nanobacteria and the formation of ooids and hardgrounds. *Sedimentology* 48, 215–229.
- Generosi, J., Ceccato, M., Andersson, M.P., Hassenkam, T., Dobberschütz, S., Bovet, N.E. & Stipp, S.L.S. 2017: Calcite wettability in the presence of dissolved Mg^{2+} and SO_4^{2-} . *Energy & Fuels* 31(1), 1005–1014.
- Glasser, L.S.D. & Smith, D.N. 1986: Siliceous coatings on fossil coccoliths – how did they arise? In: Sieveking, G.D.G. & Hart, M.B. (eds), *The Scientific Study of Flint and Chert. Proceedings of the Fourth International Flint Symposium held at Brighton Polytechnic 10–15 April 1983*, 105–109. Cambridge: Cambridge University Press.
- Goldstein, J., Newbury, D., Joy, D., Lyman, C., Echlin, P., Lifshin, E., Sawyer, L. & Michael, J. 2003: *Scanning Electron Microscopy and X-Ray Microanalysis*. Kluwer Academic/Plenum Publishers, New York, 689 pp.
- Goodhew, P.J., Humphreys, J. & Beanland, R. 2001: *Electron microscopy and analysis*. Taylor & Francis, London, 251 pp.
- Heggheim, T., Madland, M.V., Risnes, R. & Austad, T. 2005: A chemical induced enhanced weakening of chalk by seawater. *Journal of Petroleum Science and Engineering* 46, 171–184.
- Henriksen, K., Young, J.R., Bown, P.R. & Stipp, S.L.S. 2004: Coccolith biomineralisation studied with atomic force microscopy. *Palaeontology* 47(3), 725–743.
- Hjuler, M.L. & Fabricius, I.L. 2009: Engineering properties of chalk related to diagenetic variations of Upper Cretaceous onshore and offshore chalk in the North Sea area. *Journal of Petroleum Science and Engineering* 68, 151–170.
- Howe, J.Y., Rawn, C.J., Jones, L.E. & Ow, H. 2003: Improved crystallographic data for graphite. *Powder Diffraction* 18(2), 150–154.
- Katika, K., Addassi, M., Alam, M.M. & Fabricius, I.L. 2015: The effect of divalent ions on the elasticity and pore collapse of chalk evaluated from compressional wave velocity and low-field Nuclear Magnetic Resonance (NMR). *Petroleum Science and Engineering* 136, 88–99.
- Katika, K., Alam, M.M., Alexeev, A., Chakravarty, K.H., Fosbøl, P.L., Revil, A., Stenby, E., Xiarchos, I., Yousefi, A. & Fabricius, I.L. 2018: Elasticity and electrical resistivity of chalk and greensand during water flooding with selective ions. *Petroleum Science and Engineering* 161, 204–218.
- Larsen, J.K. & Fabricius, I.L. 2004: Interpretation of water saturation above the transitional zone in chalk reservoirs. *SPE Reservoir Evaluation and Engineering* 7, 155–163.
- Lindgreen, H., Drits, V.A., Sakharov, B.A., Jakobsen, H.J., Salyn, A.L., Dainyak, L.G. & Krøyer, H. 2002: The structure and diagenetic transformation of illite-smectite and chlorite-smectite from North Sea Cretaceous–Tertiary chalk. *Clay Minerals* 37, 429–450.
- Nermoen, A., Korsnes, R.I., Storm, E.V., Stødle, T., Madland, M.V. & Fabricius, I.L. 2018: Incorporating electrostatic effects into the effective stress relation – insights from chalk experiments. *Geophysics* 83, 1–62.
- Risnes, R. & Flaageng, O. 1999: Mechanical Properties of Chalk with Emphasis on Chalk-Fluid Interactions and Micromechanical Aspects. *Oil & Gas Science and Technology – Revue de l’Institut Français du Pétrole* 54(6), 751–758.
- Røgen, B. & Fabricius, I.L. 2002: Influence of clay and silica on permeability and capillary entry pressure of chalk reservoirs in the North Sea. *Petroleum Geoscience* 8, 287–293.
- Røgen, B., Fabricius, I.L. & Gommessen, L. 1999: *Chalk Rock Catalogue: Joint Chalk Research Phase V, Project 4* (text vol.+Appendix). Technical University of Denmark, Copenhagen, 94+130 pp.
- Skinner, A.J., LaFemina, J.P. & Jansen, H.J.F. 1994: Structure and bonding of calcite: A theoretical study. *American Mineralogist* 79, 205–214.
- Skovbjerg, L., Hassenkam, T., Makovicky, E., Hem, C.P., Yang, M., Bovet, N.E. & Stipp, S.L.S. 2012: Nano sized clay detected on chalk particle surfaces. *Geochimica et Cosmochimica Acta* 99, 57–70.
- Stipp, S.L.S. 1999: Toward a conceptual model of the calcite surface: Hydration, hydrolysis, and surface potential. *Geochimica et Cosmochimica Acta* 63, 3121–3131.
- Strand, S., Hjuler, M.L., Torsvik, R., Pedersen, J.I., Madland, M.V. & Austad, T. 2007: Wettability of chalk: Impact of silica, clay content, and mechanical properties. *Petroleum Geoscience* 13, 69–80.
- Williams, D.B. & Carter, C.B. 2009: *Transmission Electron Microscopy: A Textbook for Materials Science*. 760 pp., 2nd. edition. Springer, New York.

Beach-ridge architecture constrained by beach topography and ground-penetrating radar, Itilleq (Laksebugt), south-west Disko, Greenland – implications for sea-level reconstructions

PRISCILA E. SOUZA, AART KROON & LARS NIELSEN



Souza, P.E., Kroon, A. & Nielsen, L. 2018. Beach-ridge architecture constrained by beach topography and ground-penetrating radar, Itilleq (Laksebugt), south-west Disko, Greenland – implications for sea-level reconstructions. © 2018 by Bulletin of the Geological Society of Denmark, Vol. 66, pp. 167–179. ISSN 2245-7070. (www.2dgf.dk/publikationer/bulletin).

Detailed topographic data and high-resolution ground-penetrating radar (GPR) reflection data are presented from the present-day beach and across successive raised beach ridges at Itilleq, south-west Disko, West Greenland. In the western part of the study area, the present low-tide level is well defined by an abrupt change in sediment grain size between the sandy foreshore and the upper shoreface that is characterised by frequently occurring large clasts. The main parts of both fine and large clasts appear to be locally derived. Seaward-dipping reflections form downlap points, which are clearly identified in all beach-ridge GPR profiles. Most of them are located at the boundary between a unit with reflection characteristics representing palaeo-foreshore deposits and a deeper and more complex radar unit characterised by diffractions; the deeper unit is not penetrated to large depths by the GPR signals. Based on observations of the active shoreface regime, large clasts are interpreted to give rise to scattering observed near the top of the deeper radar unit. We regard the downlap points located at this radar boundary as markers of palaeo-low-tide levels. In some places, scattering hyperbolas are more pronounced and frequent than in others, suggesting differences in the occurrence of large boulders.

Keywords: Downlap points, sea level, berm evolution, beach ridges, Arctic coasts.

Priscila E. Souza [pes@ign.ku.dk], Aart Kroon [ak@ign.ku.dk], Lars Nielsen [ln@ign.ku.dk], Department of Geosciences and Natural Resource Management, Faculty of Science, University of Copenhagen, Øster Voldgade 10, DK-1350 Copenhagen, Denmark.

Corresponding author: Priscila E. Souza.

After the deglaciation of the coastal area of Disko between 9.25 ka and 9 ka before present, the sea transgressed to the Holocene marine limit (Ingólfsson *et al.* 1990). The elevation of marine limits increased from *c.* 50 m to *c.* 90 m in a south-east direction across Disko, indicating that the western areas experienced lower rates of land rise than the eastern ones (Ingólfsson *et al.* 1990). Marine terraces and successive beach ridges were formed below the marine limit during the emergence of coasts (Donner 1978; Rasch & Nielsen 1995).

Most beach ridges are relict berms. They originate in the intertidal and supratidal zones by wave-related processes, mainly swash, backwash and percolation, and are preserved as the shoreline progrades (Otvos 2000). Understanding how berms are formed and

evolve in time and space on the current active beach is a helpful tool to assess and interpret the internal structure of beach ridges and to point out reliable past sea-level markers (Bendixen *et al.* 2013). Moreover, beach-ridge deposits have been used as sea-level indicators in numerous studies in temperate as well as Arctic and Antarctic coastal regions (Rodriguez & Meyer 2006; Nielsen & Clemmensen 2009; Simms *et al.* 2011; Pedersen *et al.* 2011; Lindhorst & Shutter 2014; Billy *et al.* 2015; Nielsen *et al.* 2017). However, their present surface morphology in Arctic regions may not accurately correspond to past sea level, because of subsequent surface erosion, solifluction processes and/or sediment redeposition (e.g. Nielsen *et al.* 2017). Such processes may have altered the surface significantly.

On the other hand, the internal structure of beach ridges is often well preserved and can be depicted from ground-penetrating radar (GPR) data. The GPR reflections, which are observations in the recorded data, reveal the bed morphology and thus constitute a potentially important key for reconstruction of past sea levels as seen from GPR investigations at different localities (Tamura *et al.* 2008; Nielsen & Clemmensen 2009; Clemmensen & Nielsen 2010; Hede *et al.* 2013), including Disko and southern Greenland (Nielsen *et al.* 2017).

Nielsen *et al.* (2017) document characteristics of numerous fossil raised beach ridges from the south-east coast of Disko and two localities in South Greenland. They identified several downlap points in the internal structure of these fossil ridges. Downlap points were interpreted to represent levels correlated to sea level at the time of deposition, most likely close to low-tide levels. The specific depth with respect to sea level is dependent on factors such as local wave conditions and tidal ranges.

In this paper, we document the internal architecture of modern and fossil beach ridges at Itilleq

(Laksebugt), south-west Disko. We use observations of well-developed modern analogues to constrain our interpretation of the fossil, raised systems. We identify several downlap points in the internal sedimentary structure of fossil raised beach ridges at Itilleq. The downlap points are interpreted in relation to past sea level at the time of deposition and a model for berm formation with respect to the sea level at the time of deposition is presented. This model is based on investigation of a well-developed modern analogue in the area. Our work provides a basis for later reconstruction of a detailed relative sea-level (RSL) curve for Itilleq, provided that the past sea-level markers are dated.

Study area

Itilleq is an embayment on the south-western coast of Disko, central West Greenland (Fig. 1). Disko is mainly covered by Tertiary plateau basalts (Pedersen *et al.* 2000), but sedimentary deposits characterise the

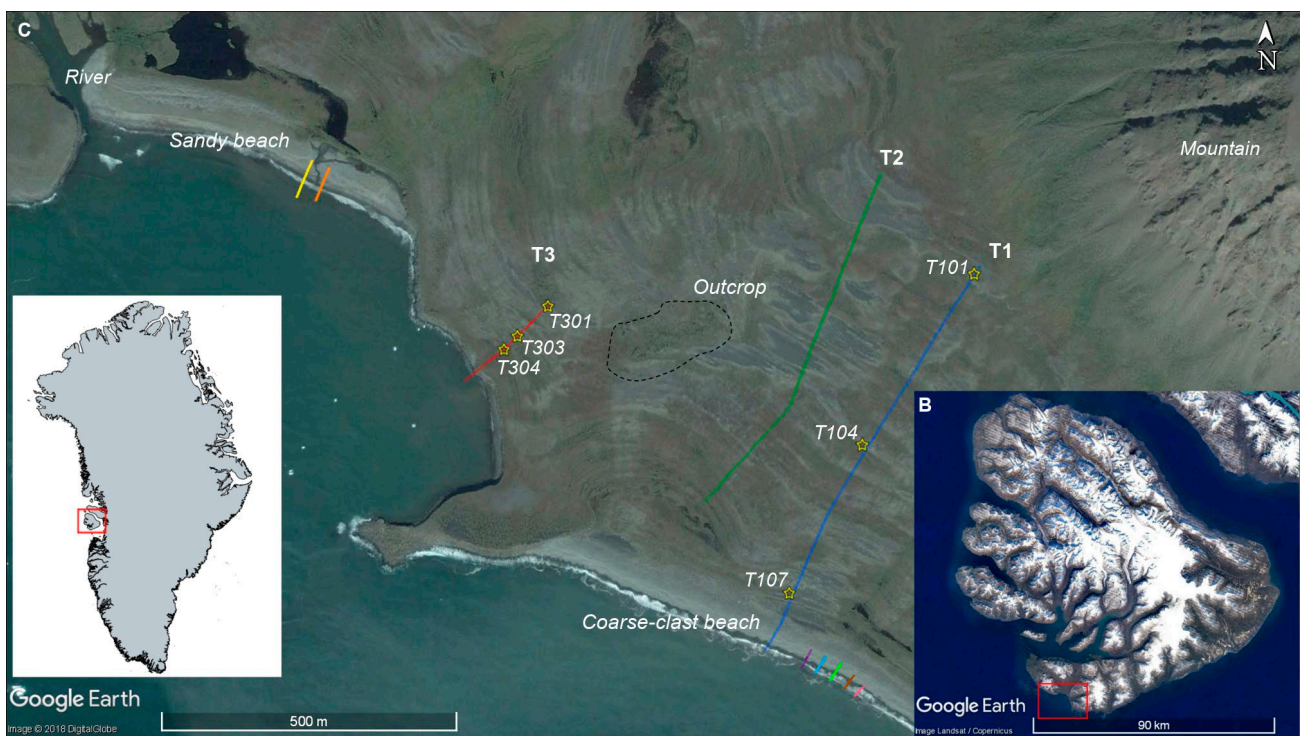


Fig. 1. Study area. **A:** Overview map of Greenland showing the location of Disko island on the west coast (red box). **B:** Satellite image of Disko showing the location of Itilleq (red box). **C:** Satellite image of Itilleq showing the location of both sandy and coarse-clast present-day beaches. Coloured lines: GPR transect lines. Yellow stars: the location and code of holes dug along the transects. The local sediment sources are river, outcrop and mountain. Differently coloured GPR transects across recent beaches represent: Line 26 (purple), Line 27 (blue), Line 28 (green), Line 29 (brown) and Line 30 (pink) on the coarse-clast beach, and Line 32 (orange) and Line 33 (yellow) on the sandy beach. The three GPR transects across beach ridges are labelled T1 to T3. Satellite images in B and C are generated by Google Earth (provided, respectively, by Landsat/Copernicus in December 2016, and by DigitalGlobe on August 23, 2004).

Itilleq coastal area, where relatively wide stretches of beach deposits as well as coastal cliffs occur. Alluvial fans and a marine terrace extend from the base of the steep mountain slopes, more than 40 m above the lowest astronomical tide, down to either the present shoreline or to the top of coastal cliffs located about 8 m above the lowest astronomical tide.

Successive beach ridges are present on the lower slopes of the talus of the mountains and the marine terrace. They are mainly NW–SE oriented but change orientation at their western end, becoming N–S oriented (Fig. 1C). The beach ridges are mainly covered by lichen-covered, round boulders. Swales between the ridges are also characterised by coarse-grained material but more remarkably by an uneven hummocky terrain, ‘patterned ground’, a characteristic feature generated by freezing and thawing processes (French 1996).

Two beaches occur in the area: a western, sandy beach and an eastern, coarse-clast beach with a mixture of sand and gravel. The shorelines of both beach types are aligned nearly NW–SE but differ in their exposure to incoming waves. The beach types are separated by a cusped foreland which projects from the western end of the coarse-clast beach and therefore shields the sandy beach from wind waves coming from the east (Fig. 1C).

The sandy beach is approximately 500 m long; it is cut by a river at its northern end and bordered by the N–S oriented coastal cliff at the cusped foreland at its southern end (Fig. 1C). The western half of this beach

is up to 100 m wide. Here, there is a clear berm with a gradually dipping backshore ending in a lagoon. The eastern half of the sandy beach is narrower (10 to 60 m wide) and steeper. Its easternmost part is backed by an 8 m high cliff that separates the present-day beach system from the inland alluvial fans and marine terraces. The coarse-clast beach is twice as long as the sandy beach and not separated by any cliffs from the marine terrace. Towards the east, the shoreline orientation turns to N–S and is interrupted by a river (not shown in Fig. 1C). Cobble- and boulder-size sediments prevail all over the beach stretch.

The climate in the area is polar maritime with an annual mean temperature of -4°C (Ingólfsson *et al.* 1990). Easterly winds are the most frequent all year around (Fig. 2). However, they do not contribute significantly to wave generation because Itilleq is an embayment on the coast facing south-west (Fig. 1B), sheltered at its east side by land. An ice-free period generally occurs from late May to November (Danish Meteorological Institute, DMI 2015). The coastal area experiences a semidiurnal meso-tidal regime. The average tidal range is 1.34 m at Qeqertarsuaq town 15 km east of Itilleq, with maximum spring tidal levels of 2.5 m above mean low water.

Methods

Ground-penetrating radar (GPR) data and topographic profiles were measured during a field campaign in August 2015. Elevations, presented as metres above sea level (m a.s.l.), are relative to the chart datum which is the lowest astronomical tide.

Cross-shore profile collection and processing

GPR data were acquired along transects approximately perpendicular to the beach ridges and the present-day beach using shielded 250 MHz transmitter and receiver antennae from Sensors & Software. The antenna configuration and recording settings were similar to those used by e.g. Hede *et al.* (2013) and Nielsen *et al.* (2017). Transmitter and receiver were mounted on a hand-pulled skid plate in contact with the ground. The antennae were placed with a separation of 0.38 m between the antenna centres and in connection with an odometer wheel. We used a recording time window of 450 ns and a trace spacing of 0.05 m; at each recording location eight recordings were stacked into a single trace in order to strengthen the signal-to-noise ratio. Three transects were made across successive beach ridges that lie significantly above present mean sea level, T1,

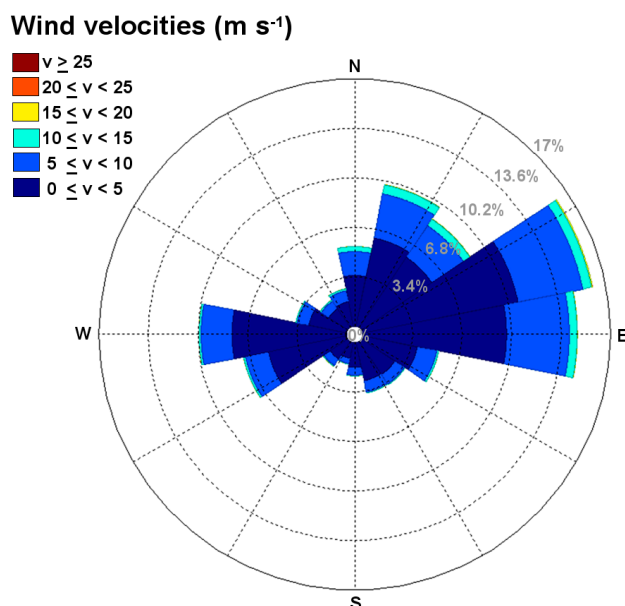


Fig. 2. Wind rose for Qeqertarsuaq from 1995 to 2011 during ice-free months (late May to November; data from the Danish Meteorological Institute 2015).

T2 and T3; seven other transects were obtained close to the present-day beach, two on the sandy beach stretch and five on the coarse-clast beach (Fig. 1C).

The GPR data were processed using the Ekko_Project software package provided by Sensors & Software. The main processing steps were somewhat similar to the ones used by Nielsen & Clemmensen (2009), Hede *et al.* (2013) and Nielsen *et al.* (2017): (1) repositioning of traces, (2) automated 'dewow'-filtering, (3) gain correction using an automatic gain control algorithm with a maximum scaling factor of 200 and window width of 0.5, (4) migration (in some cases) and (5) time-depth conversion and topography correction. Repositioning of traces and topography correction were both based on DGPS measurements acquired with a RTK-Trimble R8 with an accuracy of 0.02 m. These topographic measurements were carried out on the same day as the GPR data collection.

Migration and time-depth conversion are dependent on the radar wave velocity, which is a function of the mean physical material characteristics, water content, and porosity (e.g. Neal 2004). We estimated radar wave velocities based on analysis of diffraction hyperbolas in the recorded un-migrated GPR data. Small variations were observed in both horizontal and vertical directions. Horizontally, wave velocities varied from 0.085 m ns⁻¹ below the beach ridges to 0.079 m ns⁻¹ below intervening swales. Vertically, wave velocities were higher in the upper parts of the profiles. Hede *et al.* (2013) observed the same, and this velocity decrease with depth is most likely due to increasing water content with depth (Reynolds 1997). For migration and time-depth conversion we used a constant velocity of 0.082 m ns⁻¹, which is the average velocity calculated from vertical and horizontal variations.

The peak frequency of the reflected signals is between 150 and 200 MHz. The vertical resolution is about one fourth of the dominant wavelength (e.g. Jol 1995), which is about 0.1 m in our case. Radar vertical resolution, errors in topographic measurements and interpolation, uncertainties in estimated velocities for time-depth conversion, and possible filtering artefacts account for a total uncertainty of 0.25–0.27 m on the reading of depths based on the GPR data (Nielsen & Clemmensen 2009).

Estimation of significant wave height and wind setup

The significant wave heights (H_s) were estimated using the wind conditions and fetch lengths (Coastal Engineering Research Center 1984). This method only estimates the sea waves whereas swell waves are not included. Wind velocity data from Disko were obtained from the Danish Meteorological Institute (DMI) for the years 1962–1980 and 2000–2014 (DMI 2015). We

only used onshore winds from south, south-west and west directions during the ice-free periods.

The maximum potential significant wave heights were verified by an inverse approach using the height of the beach berms (H_b). The run-up level related to H_b is given by the run-up relative to the still-water level (R_{sw}) plus a high-tide water level. Thus, by measuring the height of beach berms and knowing possible high-tide water levels, we could calculate R_{sw} values. The deep-water significant wave height (H_s) was then estimated using the relationship by Guza & Thornton (1982):

$$R_{sw} = 0.7 H_s \quad (\text{Equation 1})$$

The wind setup in the embayment was estimated using a simple balance equation (Equation 2) between the force of the wind stress and the pressure gradients that opposed it (Pugh 2004). It assumes steady-state wind conditions, a constant depth of the embayment, and uses a maximum fetch that can generate the highest possible stress (Pugh 2004):

$$S = (C_D \rho_A W^2) / (g \rho D) \quad (\text{Equation 2})$$

Where S is the wind setup, C_D is a drag coefficient (c. 0.0029), ρ_A is the density of air, W is the wind velocity, g is gravity acceleration, ρ is the density of seawater, and D is water depth.

Results

Only 30% of the winds are from directions favourable for inducing onshore waves during ice-free months at Itilleq. In general, significant wave heights (H_s) are small because the mean wind speed is about 3 m s⁻¹. Winds of 6 m s⁻¹, which is the average speed occurring 21% of the time, should blow for 4 hours over an unlimited fetch to generate a H_s of 0.5 m and a period of 3.3 s and for 10 hours to generate a H_s of 1 m and a period of 5.8 s. Wind speeds above 8.5 m s⁻¹ rarely occur, and only one third of such strong winds exceed the average 10.4 m s⁻¹ (Fig. 2). Therefore, sea waves are mostly subordinate to tidal water level changes and not dominant at Itilleq. However, swell waves can sometimes occur in Disko Bay.

Table 1 shows the role of the waves for berm formation. Here, we estimated H_s from the heights of berm crests as a function of different tide heights. The estimated H_s are quite high, up to 3.67 m, considering the prevailing mild weather conditions presented above. This means that the berms we observed were built under conditions much more energetic than usual if

tides and waves are the only processes that account for local water level oscillations. However, the wind setup can also play a role. Winds of 10 m s^{-1} over an embayment with a constant depth of 50 m and a maximum fetch length of 100 km give a wind setup of 0.07 m at the beach in our case. However, this contribution does not significantly reduce the estimated H_s value.

Table 1. Significant wave heights (H_s) estimated from run-up heights on sandy beaches at high tide for different berm crest heights and tidal stages. All values in metres.

Profile	BCH	NHT: 1.63 H_s	MHT: 1.81 H_s	SHT: 2.01 H_s
L32	4.20	3.67	3.41	3.13
	3.00	1.96	1.70	1.41
	2.40	1.10	0.84	0.56
L33	4.10	3.53	3.27	2.99
	2.90	1.81	1.56	1.27
	2.00	0.53	0.27	-0.01

BCH: berm crest height. NHT: neap high tide.
MHT: mean high tide. SHT: spring high tide.

Active modern beach geomorphology

Topographic profiles measured along the cross-shore transects on the active sandy beach are about 85 m long and similar in shape, with two distinct berms and a gentle step seaward (Fig. 3A). The gentle steps

are at 2 and 2.40 m a.s.l. Berm crests are at 3 and 4 m a.s.l., which is a height much above the spring high-tide level. The foreshore gradient is 3° .

Cross-shore transects on the coarse-clast beach are shorter, about 35 m long, and the topographic profiles are slightly different from the sandy ones (Fig. 3B). We did not make a systematic analysis of the grain size distribution; however we noted that the size of the clasts on the coarse-clast beach ranged from cobbles (64 to 256 mm in diameter) to boulders (> 256 mm in diameter). Differences in grain size might have caused the moderate differences in the topography between the fine- and coarse-grained beaches. The coarse-clast beach profiles have a step around spring high-tide level and distinct berm crests farther ashore at levels around 3 and 4 m a.s.l. These observations are similar to what is observed for the sandy beach profiles. However, the gradient of the foreshore is steeper, about 7° . Likewise, the step at around 2 m a.s.l. is more prominent here than for the sandy profiles.

The mean low-tide level is well marked at the modern sandy beach by an abrupt change in sediment size. The foreshore is sandy, while the upper shoreface is characterised by the presence of cobbles and boulders (Fig. 4). Both sediment sizes are expected to be present on the beach and nearshore zone due to the contribution of different local sources (within tens to

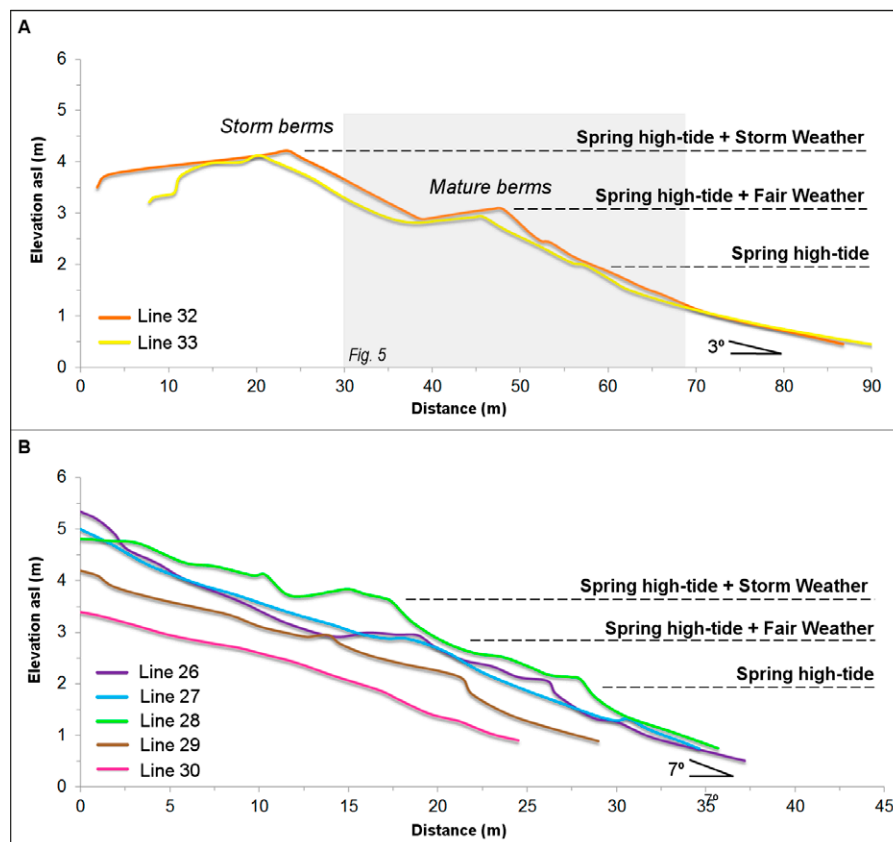


Fig. 3. Active beach topographic profiles. **A:** Profile lines 32 and 33 obtained on the sandy beach. **B:** Profile lines 26 to 30 obtained on the coarse-clast beach. Horizontal dashed lines indicate water levels at various conditions, as labelled. The grey box corresponds to the section shown in Fig. 5. Elevation is related to the chart datum, which is the lowest astronomical tide. Note that the horizontal axes are not at the same scale: profiles in A are twice as long as profiles in B.



Fig. 4. Modern sandy beach at Itilleq. The mean low-tide level is clearly marked by an abrupt change in sediment size: the upper shoreface is characterised by pebbles, cobbles and boulders, while the foreshore is sandy. The red dotted line indicates this sharp transition. The distance between the photographer and the boat was approximately 300 m. Photo August 2015.

hundreds of metres). Fine sediments are likely to be supplied by, for example, the river at the western end of the sandy beach (Fig. 1C). Large clasts are likely to be produced from mountains adjacent to the beach, to be eroded from outcrops by waves during high water levels, and/or to be dragged to the beach by small icebergs and growlers (Nichols 1961).

We interpret the sharp transition around mean low-tide level to be a response to local prevailing fair-weather conditions, when tide oscillation is the process that accounts most for water-level variation. While fine sediment can easily be transported and deposited farther inland to the fore/backshore by swash processes, the larger materials may not. They are unlikely to be remobilised beyond the low water

level due to their size and the local prevailing low wave energy. Coastal progradation, however, is an ongoing process and, as it continues, finer material is deposited above the larger clasts, covering the former upper shoreface. The boundary between upper shoreface and foreshore, which corresponds to former mean low-tide levels, is likely to be preserved in the subsurface of the beach deposits (Figs 5 and 6).

Internal sedimentary structures of modern beach deposits

GPR data collected along the beach transects are limited in depth penetration due to salt-water intrusion (Fig. 5). On the sandy beach, we could only image the internal

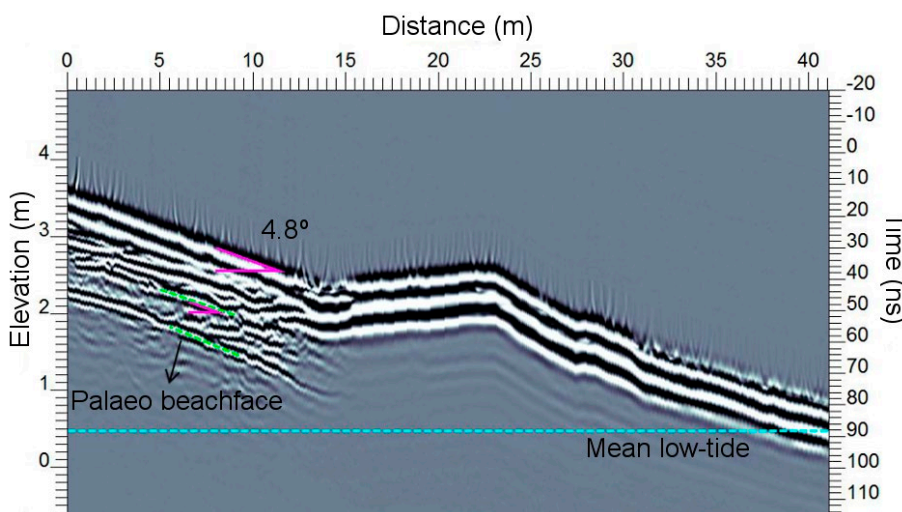


Fig. 5. Migrated GPR reflections from the modern sandy beach (line 32). Green dashed lines exemplify topography-induced radar reflections, interpreted to correspond to palaeo beachface surfaces. Magenta solid lines indicate average slope (4.8°). Low-tide downlap points could not be identified here; they must be at or just below the mean low-tide level (dashed cyan line). Note poor signal penetration presumably due to the conductivity of the salt water in the pores. This profile corresponds to the grey box area in Fig. 3A. Elevation is related to the chart datum, which is the lowest astronomical tide.

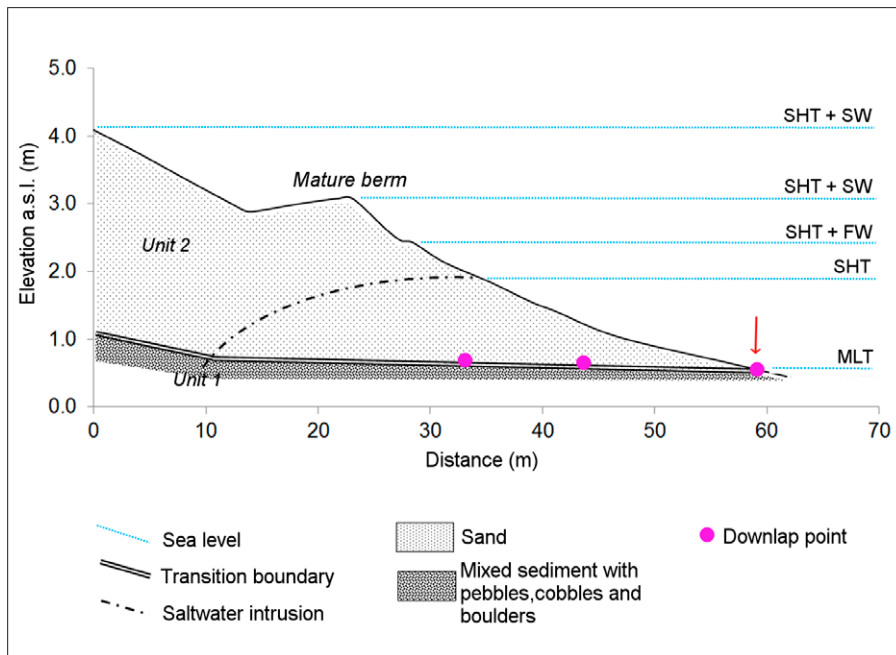


Fig. 6. Observational model of the modern beach at Itilleq based on radar, topographic and visual observations. Horizontal blue lines indicate sea levels determined by: spring high-tide and storm weather with excessive Hs (SHT + SW); spring high-tide and fair weather with low but accountable Hs (SHT + FW); spring high-tide (SHT) and mean low-tide (MLT). Red arrow represents the red dotted line around mean low-tide level in Fig. 4. The model depicts the two sedimentary units we have interpreted, based on GPR data, to correspond to upper shoreface (Unit 1) and foreshore deposits (Unit 2). Unit 1 is characterised by mixed sediment with pebbles, cobbles and boulders, while Unit 2 is sandy. Downlap points (magenta filled circles) occur at the transition

boundary, which corresponds to mean low-tide levels. The height of the berm, which eventually becomes a beach ridge, is related to higher sea-water levels. Elevation is related to the chart datum, which is the lowest astronomical tide.

structure of the seaward-dipping flank of the highest berm. All depicted radar reflections lie above mean low-tide level and, similarly to the modern topography, with an average seaward slope of 4.8° (Fig. 5). We therefore interpret these topography-concordant reflections to correspond to palaeo-beachface surfaces. It is expected that these palaeo-beachface reflections are followed downwards by less steep reflections, corresponding to palaeo-shoreface surfaces (Fig. 6). However, since the radar depth penetration was limited to above the mean low-tide level at the modern beach (Fig. 5, dashed blue line), we could not image the upper shoreface regime with GPR at the modern beach. Accordingly, we could not identify downlap points marking the transition between upper shoreface and beachface, but they would presumably be located at or below the mean low-tide level.

Geomorphology of raised, fossil beach ridges

The topography profiles along the GPR transects T1 to T3 show beach ridges and intervening swales (Fig. 7). T1 and T2 both extend from around 40 m a.s.l. near the base of the mountain talus to the coarse-clast beach (Fig. 1C). T1 is 723.80 m long and terminates at the present-day coarse beach. Four zones with different slopes are identified along T1: 6.4° for distances of 0–80 m, 3° for distances of 80–460 m, 1.6° for distances of 460–690 m and 6.3° for distances from 690 m to the end of the transect (Fig. 7A). The slope along T2 varies less, decreasing from $c. 4.5^\circ$ at 0–140 m distance to $c. 3.5^\circ$ along

the remaining profile. Yet there is a noticeable change in the terrain surface of T2 at around 350 m distance because the upper part is quite uneven, with mounds and depressions, whereas the lower part is much more even (Fig. 7B). T3 is shorter and does not cover the oldest successive raised beach ridges (Fig. 1C). The slope is not steep ($c. 4^\circ$), yet it becomes $c. 2^\circ$ flatter from 100 to 180 m distance (Fig. 7C).

In general, the observed changes in the terrain slope along transects T1 and T3 follow changes in the sedimentary structure of the beach ridges from 0 to $c. 1$ m below the surface: the slope is less steep where fine-grained sediments are more abundant (Figs 7, 8A–B and 8D–F). An exception is observed in T1 for profile distances 638–738 m (Fig. 7A), where coarse clasts (>64 mm in diameter) are dominant over fine sediment, yet the slope is not steep (Fig. 8C).

Internal sedimentary structures of fossil beach deposits

The applied radar antennae and the characteristics of the sediment allowed us to image the raised beaches to depths of about 3 m below the surface (Fig. 9). The very top part was affected by arrival of the direct air wave. Below this arrival, we identified two radar units separated by a clear boundary at about 1.5 m below the surface and approximately parallel to the overall topography (Fig. 10A). From here on, this boundary will be referred to as the transition boundary. In general, caution must be taken regarding interpretation of

arrivals from below this transition boundary. Reflections below the transition boundary are weak and may be affected by multiple arrivals from shallower levels. Marked diffractions (observed as hyperbolas in unmigrated GPR sections) originating from the transition boundary characterise several intervals of the GPR sections (Fig. 10A). The unit above the transition boundary (Unit 2) is characterised by subparallel,

continuous reflections dipping seaward by 0.5° to 2° (Fig. 10A). This pattern is present along most of the profiles, but exceptions occur, mainly beneath swales, where the transition boundary is not as evident due to fuzzier reflections. Here, the diffractions from the top of the lower unit (Unit 1) appear relatively stronger in comparison to those observed beneath the ridges (Fig. 10A, for example).

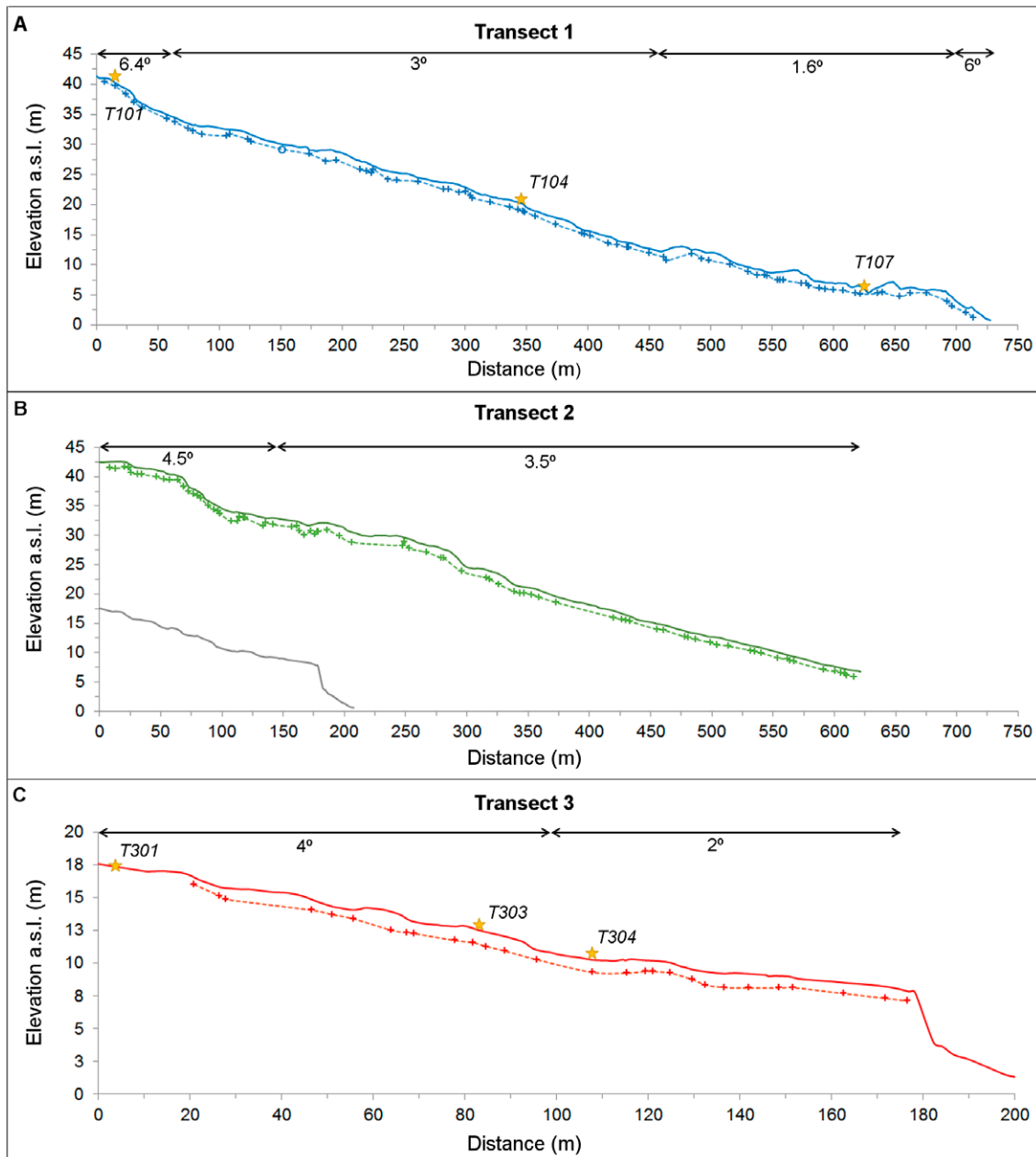


Fig. 7. Transect profiles across successive raised beach ridges. Continuous lines correspond to differential GPS measurements; dashed lines are constructed from the elevation of individual downlap points (crosses along the dashed line) identified in the GPR images; yellow stars show the location of holes; horizontal arrows indicate the extent of stretches of similar topographic slopes. Note that the vertical and horizontal scales in C are different from those in A and B because Transect 3 is considerably smaller than the other two transects. For comparison, Transect 3 is plotted in grey below Transect 2 in B. Elevation is related to the chart datum, which is the lowest astronomical tide.

Two types of seaward-dipping sets of downlap points were identified: one occurring within Unit 2 at shallow levels between 0.5–1.5 m below the surface (Fig. 10B, green circles) and one at a slightly deeper level. We only identified a few of the shallow downlap points. We interpret these shallow downlap points to correspond to the transition between foreshore and upper shoreface at higher sea levels at the time of deposition of storm berms.

A set of deeper downlap points marks the transition boundary (Fig. 10B, magenta circles). They are frequently present along all profiles. We interpret the deeper downlap points as corresponding to the mean low-tide level at the time of deposition, consistent with Nielsen *et al.* (2017). The points mark the transition to a deep layer with strong signal scattering (Fig. 10), which most likely was produced by an abrupt change in sediment properties such as a clast-size increase downwards. This sharp lithological boundary resembles what we have observed around mean low-tide level (Fig. 4) during fair weather conditions on the present active sandy beach (Fig. 1C).

The locations of these GPR markers of palaeo mean low-tide level are shown in Fig. 7 (crosses along dashed lines). The highest downlap points identified along T1 and T2 indicate a relative sea level of about 40 m above the present sea level (Fig. 7A).

Discussion

Mature berms under calmer conditions are often correlated to high-tide levels or to mean water levels in case of non-tidal environments (Bendixen *et al.* 2013). Itilleq represents a micro- to meso-tidal environment and the mature modern berm height at 3 m a.s.l. is well above the high-tide levels (Fig. 3A). This suggests that other processes, besides the prevailing high-tide levels, must have contributed to produce the higher sea levels at which berm crests were deposited. Therefore, berm crest height cannot be directly related to mean sea level at the time of deposition at Itilleq.

The upper shoreface and foreshore deposits on

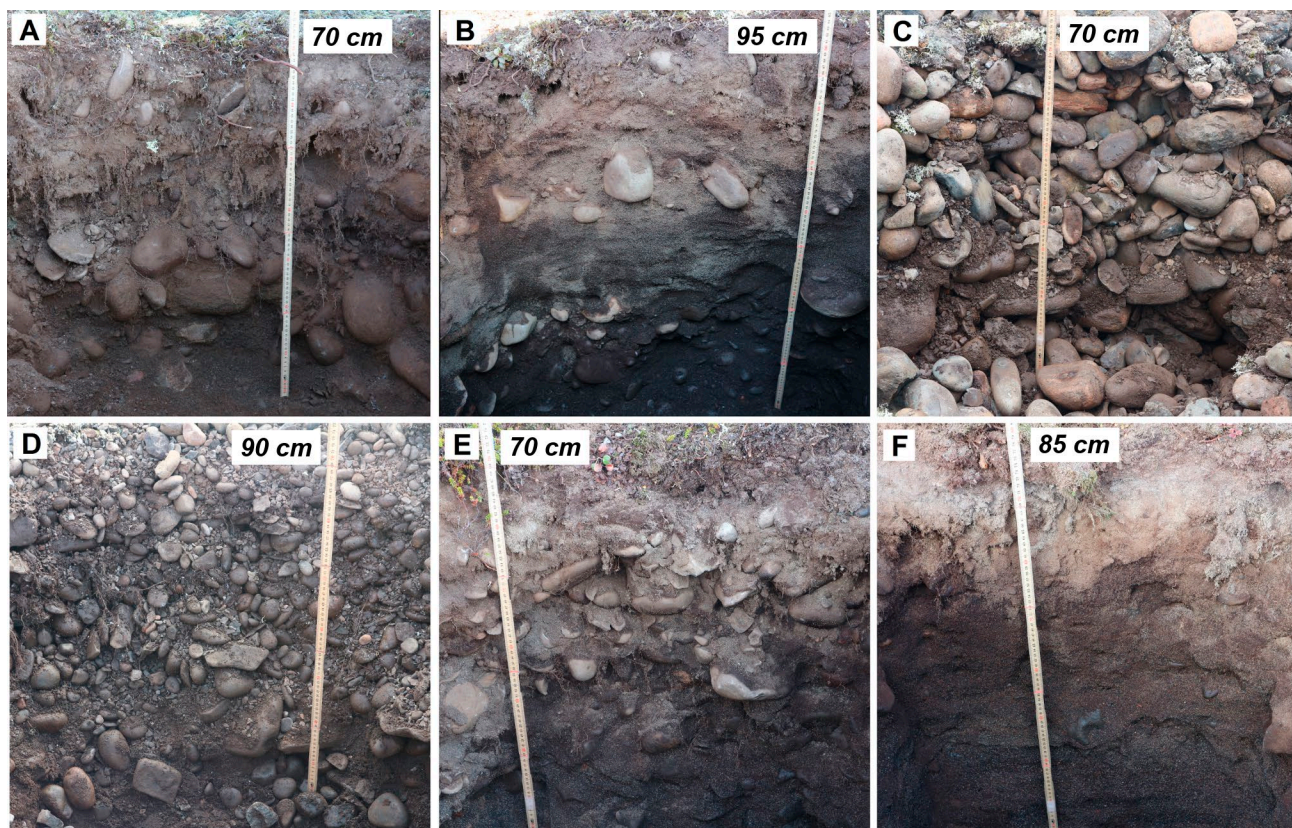


Fig. 8. Photographs of holes dug along transects T1 (A, B and C) and T3 (D, E and F). **A:** Hole T101 was 70 cm deep and located on the oldest beach ridge covered by GPR measurements (c. 40 m a.s.l.). **B:** Hole T104 was 95 cm deep and located in the central part of T1 (c. 20 m a.s.l.). **C:** Hole T107 was 70 cm deep and located at the end of T1 (c. 6 m a.s.l.), close to the present-day coarse-clast beach. **D:** Hole T301 was 90 cm deep and located at the oldest beach ridge of T3 (c. 16 m a.s.l.). **E:** Hole T303 was 70 cm deep and located in the central part of T3 (c. 12 m a.s.l.). **F:** Hole T304 was 85 cm deep and located about 30 m from T303, at c. 10 m a.s.l..

the present-day beach, however, are well defined, as seen for several other prograding beach deposits (e.g. Tamura *et al.* 2008; Nielsen & Clemmensen 2009; Clemmensen & Nielsen 2010; Billy *et al.* 2015; Nielsen *et al.* 2017). At Itilleq the boundary between them is observed as an abrupt change in sediment grain size and appears to coincide approximately with the mean low-tide level (Fig. 4). This boundary is likely to be preserved and delineated by downlap points in the internal sedimentary architecture of raised beach deposits (Fig. 6). Similarly, Tamura *et al.* (2008) have shown that the boundary between upper shoreface and foreshore facies on a beach plain in Japan corresponds to about 1 m below mean sea level, which is the local spring low-tide level. Nielsen & Clemmensen (2009) have shown that the downlap points identified on GPR reflections from a modern beach of the micro-tidal regime in the Kattegat Sea correspond to the mean sea-level at the time of deposition.

The transition between foreshore and upper shoreface deposits is often observed by a marked change

in the bed morphology on radar profiles. Foreshore deposit reflections are moderately continuous, gently seaward-dipping, and followed vertically downwards by more complex reflections, which characterise upper shoreface deposits (Tamura *et al.* 2008; Nielsen & Clemmensen 2009; Clemmensen & Nielsen 2010; Nielsen *et al.* 2017). In this study, while foreshore reflections are noticeable and of characteristic bed shape along the T1, T2 and T3 transects, typical upper shoreface cross-bedding reflections cannot be clearly identified due to diffractions and a relatively weak signal-to-noise ratio (Fig. 9). Nevertheless, GPR signal scattering is consistent with the abrupt change of sediment grain size observed around mean low-tide level on the modern beach. Such consistency supports the interpretation that the lower GPR unit corresponds to palaeo upper shoreface deposits.

Permafrost is known to cause reflectivity in GPR data sections (e.g. Jørgensen & Andreassen 2006). We cannot rule out that permafrost may contribute to some of the reflectivity observed in our GPR reflection sec-

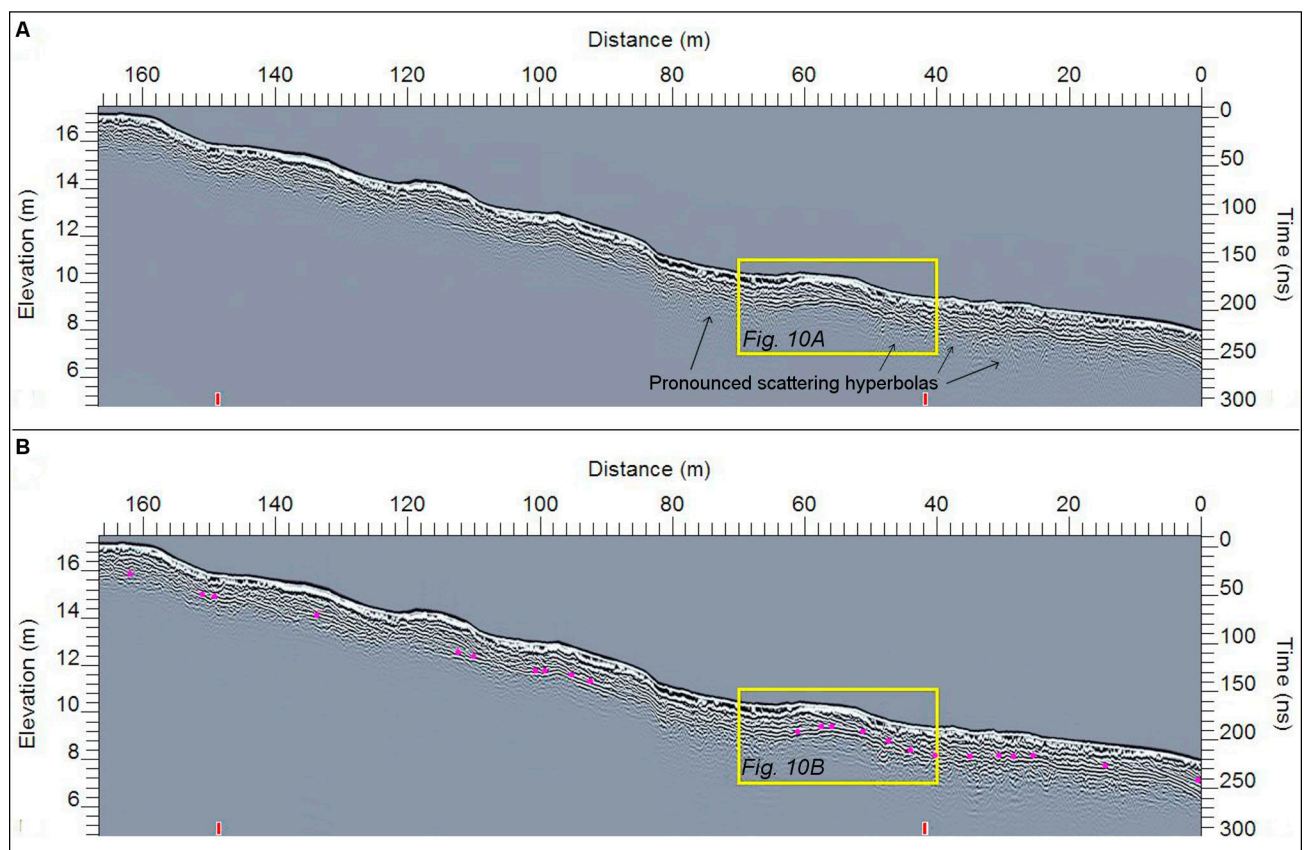


Fig. 9. GPR reflections from Transect T3. **A:** Non-migrated data: scattering hyperbolas are present around 1.5 m below terrain surface all over the radar profile, but they are stronger and more frequent in some places (indicated by arrows). **B:** Migrated data: pink dots show some downlap points identified along T3, which are the same as plotted along the dashed line in Fig. 7C. Yellow boxes in both A and B correspond to the section shown in greater detail in Figs 10A and B. Note that the horizontal axis is in reverse direction compared to Fig. 9; this is because the GPR data of Transect 3 was collected from the youngest (and lowest) towards the oldest beach ridges. Elevation is related to the chart datum, which is the lowest astronomical tide.

tion, e.g. where the transition from the upper unit to the lower unit appears as a relatively strong reflection. However, permafrost was not encountered in any of the holes up to c. 1 m deep that were dug for our study. Besides, we would expect to find permafrost below the swales due to ice grown in soils with high water content, and not below the beach ridges.

Gravelly beach ridges are expected to be formed under energetic wave conditions (Otvos 2000). However, if the local source of coarse-grained sediment is very close, the shoreline consists of gravelly berms, and consequently gravelly beach ridges. Sources of large clasts (mountain and eroding outcrop, see Fig. 1C) are within only tens to hundreds of metres from the beach at Itilleq, and swash and backwash processes can easily build the beach ridges. Growlers (fragmented ice) could also contribute by dragging clasts of various sizes, including large boulders (Nichols 1961). Large cobbles and boulders, however, are likely to be restricted to the upper shoreface because they cannot be easily reworked by swash processes once they settle on the beach.

Changes in the sedimentary structure of successive beach ridges suggest different local sediment sources. From T101 to T104 (Fig. 8A and B), for example, large clasts become less abundant and more diverse (with regard to mineralogy) in the sedimentary matrix as the beach ridges are situated farther from the inland mountain (see Fig. 1C for location). Clasts in T101 are likely to be derived from the adjacent basaltic mountain, while clasts in T104 could be delivered from the mountain but also from other sources, i.e. they could be non-basaltic ice-transported material (see light-coloured rocks in Fig. 8B). Besides, fine sediment is abundant in the sedimentary matrix of T104, which implies that another source besides the mountain has become important. Another change in the main sediment source has probably taken place between T104 and T107. Unlike T104, the sedimentary matrix of T107 is coarse-grained and supports clasts larger than 10 cm in diameter, and almost devoid of sand (Fig. 8C). In fact, it resembles the present-day coarse-clast beach, which is c. 200 m distant (Fig. 1C). It may be

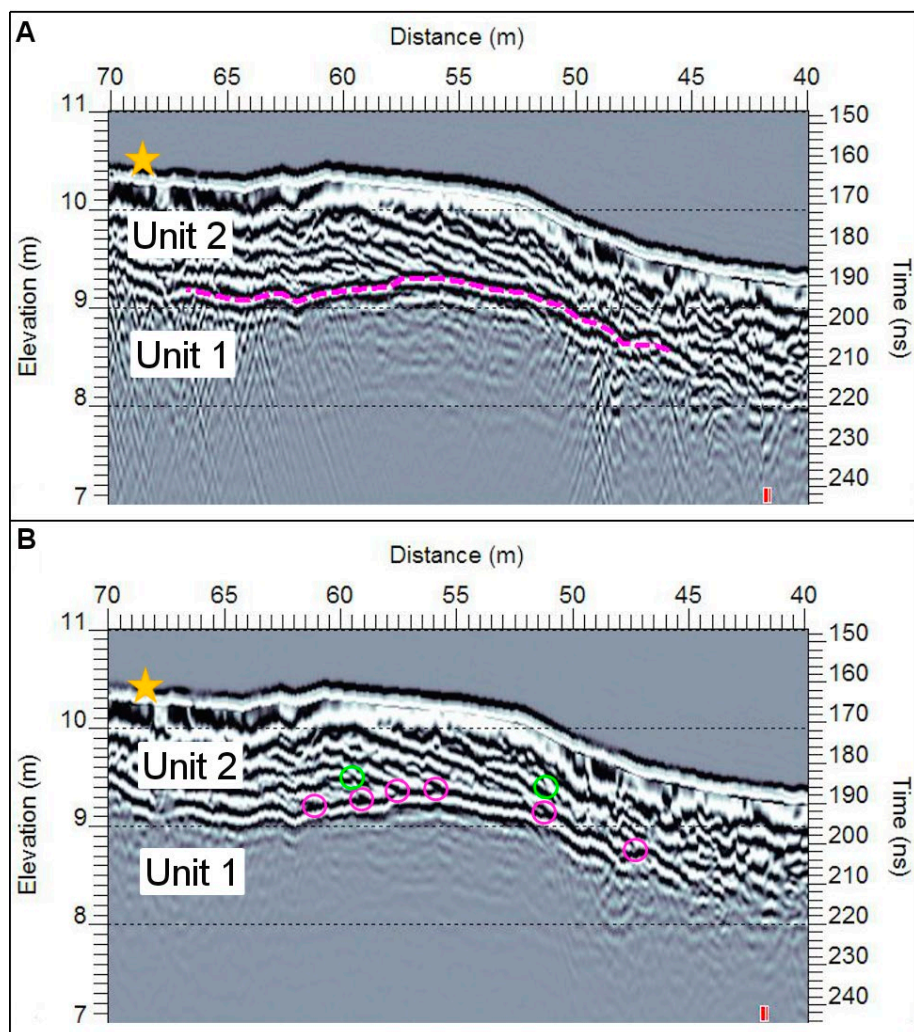


Fig. 10. Section of GPR reflections from Transect T3 at distances 70 to 40 m (yellow boxes in Fig. 9). **A:** Non-migrated radar image showing the transition boundary (dashed magenta line) between units 1 and 2. **B:** Migrated radar image showing some downlap points identified at the transition boundary (magenta circles) or just above it (green circles), within Unit 2. See text for interpretation. Yellow star shows the location of Hole T304. Elevation is related to the chart datum, which is the lowest astronomical tide.

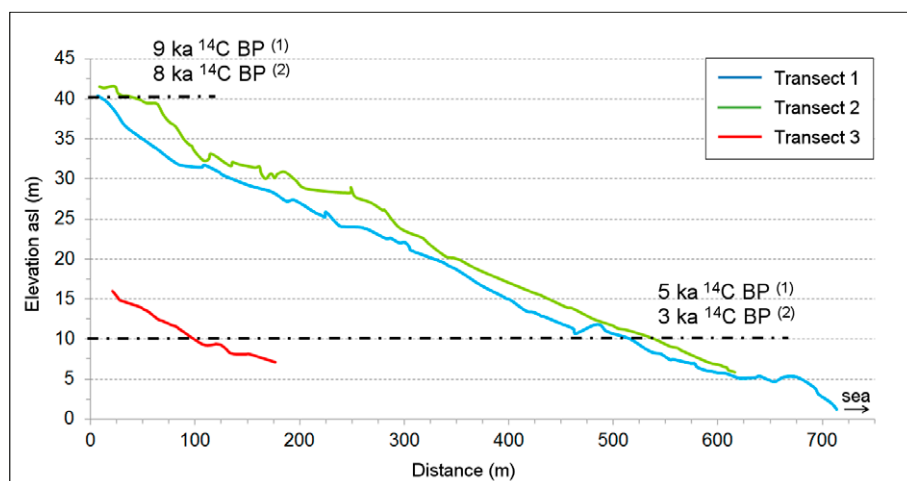


Fig. 11. First order age model for palaeo-sea levels at Itilleq. Transect profiles are based on the elevation of downlap points, which represent palaeo mean low-tide levels. Dash-dotted black lines show the elevation of palaeo-sea levels radiocarbon dated by Ingólfsson *et al.* 1990 (1) and Rasch & Nielsen 1995 (2) at 40 and 10 m a.s.l. Elevation is related to the chart datum, which is the lowest astronomical tide.

that the same sediment source has contributed to their formation.

The sedimentary matrix of the beach ridges also varies along T3, showing a decrease in sediment grain size from the higher to the lower parts of the transect (Fig. 8D-F). T301 resembles T107, with clasts of various sizes and apparently of different mineralogy (see clasts of various colours in Fig. 8D). As in T107, the clasts here could have originated from eroding outcrops. At T303 finer sediments (sand) are as abundant as large clasts (Fig. 8E), and at T304 the sedimentary matrix is mainly sandy and almost devoid of large clasts (Fig. 8F). Again, we can infer a change in the role of local sediment sources over time. Here, the river at the western end of the sandy beach is likely to be the major source of sand (Fig. 1C).

We have observed changes in the sedimentary matrix down to 70 to 95 cm depth (Fig. 8). In some parts of the profiles we observe relatively strong GPR scattering hyperbolas at the level (c. 1.5 m below the surface) which we interpret to represent the top of the upper shoreface palaeo deposits (for example, Fig. 10A at distances 67–70 m and 51–40 m). We assume that the strong diffractions indicate the existence of relatively large clasts. The fact that they do not occur at this level all through the profiles suggests, again, changes in the role of the main sediment source.

Optically Stimulated Luminescence (OSL) dating is commonly used for dating sedimentary deposits without material suitable for ^{14}C -dating (Murray & Olley 2002; Pedersen *et al.* 2011). However, it is difficult to apply standard OSL techniques at our field site because of the very limited amount of sand fraction material in the matrix. Therefore, we used existing curves based on radiocarbon dates from the broader Disko Bay area to provide a first order age model for the late Holocene at Itilleq. Datings made by Ingólfsson *et al.* (1990) suggest ages of 9 ka ^{14}C BP and 5 ka ^{14}C BP for palaeo-sea levels at 40 and 10 m a.s.l., respectively (Fig. 11). Datings by

Rasch & Nielsen (1995) suggest slightly younger ages for the same palaeo-sea levels: 8 ka ^{14}C BP at 40 m a.s.l. and 3 ka ^{14}C BP at 10 m a.s.l. (Fig. 11). Roughly, these intervals represent an overall relative sea-level fall rate of 0.6–0.7 cm a $^{-1}$ from 9 ka ago to present day.

Conclusions

At Itilleq, berms are deposited above the sea level reached during high tides. They are most likely deposited under sporadically occurring high-energy conditions, and their height does not reflect mean sea level.

On the sandy beach, the mean low-tide level is well defined by an abrupt change in sediment grain-size: the foreshore is characterised by sand, whereas the upper shoreface is characterised by coarse clasts. As beach progradation continues, upper shoreface coarse deposits are overlain by foreshore sediment, and the boundary between them is preserved in the fossil beach deposits.

Sources of both fine and coarse sediments are likely to be both local and ice-transported. However, differences in grain size and mineralogy of sedimentary structures along the transects suggest that different sources have played variable roles over time.

We identified several seaward-dipping downlap points in the GPR reflection data collected over the raised beach ridges at Itilleq. Most of these downlap points are located at the transition boundary between two radar units with different reflection patterns. Diffractions characterise the transition from upper shoreface to foreshore deposits in many places. Based on our observations on the modern active beach, we interpret the diffractions to be caused by an abrupt change (increase) in sediment size. Consequently, the downlap points located at the transition boundary can be used as proxies for past mean low-tide levels.

Acknowledgements

We acknowledge funding by Geocenter Denmark, the Brazilian Government's program Science Without Borders (CNPq), and Independent Research Fund Denmark. We thank Sigurd Bohr, Asger Meldgaard and Bruno Bainy for their contributions during field work in 2016. Further, we thank Ingelise Møller Balling, Gunver Krarup Pedersen, Michael Houmark-Nielsen, and Lotte Melchior Larsen for their comments on an earlier version of this manuscript, which greatly helped improve the manuscript.

References

- Bendixen, M., Clemmensen, L. & Kroon, A. 2013: Sandy berm and beach-ridge formation in relation to extreme sea-levels: a Danish example in a micro-tidal environment. *Marine Geology* 344, 53–64.
- Billy, J., Robin, N., Hein, C.J., Certain, R. & FitzGerald, D.M. 2015: Insight into the late Holocene sea-level changes in the NW Atlantic from a paraglacial beach-ridge plain south of Newfoundland. *Geomorphology* 248, 134–146.
- Coastal Engineering Research Center (CERC) 1984: Shore protection manual (4th edition), Chapter 3: Wave and water level predictions, 143 pp. Vicksburg: Coastal Engineering Research Center.
- Clemmensen, L.B. & Nielsen, L. 2010: Internal architecture of a raised beach system (Anholt, Denmark) resolved by ground-penetrating radar investigations. *Sedimentary Geology* 223, 281–290.
- Danish Meteorological Institute (DMI) 2015: <http://www.dmi.dk/en/groenland/> [29 September 2015].
- Donner, J. 1978: Holocene history of the west coast of Disko, Central West Greenland. *Geografiska Annaler* 60, 63–72.
- French, H. 1996: The periglacial environment, 341 pp. Harlow: Longman.
- Guza, R. & Thornton, E. 1982: Swash oscillations on a natural beach. *Journal of Geophysical Research* 87, 483–491.
- Hede, M.U., Bendixen, M., Clemmensen, L.B., Kroon, A. & Nielsen, L. 2013: Joint interpretation of beach-ridge architecture and coastal topography show the validity of sea-level markers observed in ground-penetrating radar data. *The Holocene* 23(9), 1238–1246.
- Ingólfsson, Ó., Povi, F., Funder, S. & Humlum, O. 1990: Palaeoclimatic implications of an early Holocene glacier advance on Disko Island, West Greenland. *Boreas* 19, 297–311.
- Jol, H.M. 1995: Ground penetrating antennae frequencies and transmitter powers compared for penetration depth, resolution and reflection continuity. *Geophysical Prospecting* 43, 693–709.
- Jørgensen, A.S. & Andreassen, F. 2007: Mapping of permafrost surface using ground-penetrating radar at Kangerlussuaq Airport, western Greenland. *Cold Regions Science and Technology* 48, 64–72.
- Lindhorst, S. & Shutter, I. 2014: Polar gravel beach-ridge systems: Sedimentary architecture, genesis, and implications for climate reconstructions (South Shetland Islands/Western Antarctic Peninsula). *Geomorphology* 221, 187–203.
- Murray, A.S. & Olley, J.M. 2002: Precision and accuracy in the optically stimulated luminescence dating of sedimentary quartz: a status review. *Geochronometria* 21, 1–16.
- Neal, A. 2004: Ground-penetrating radar and its use in sedimentology: principles, problems and progress. *Earth-Science Reviews* 66, 261–330.
- Nichols, R.L. 1961: Characteristics of beaches formed in polar climates. *American Journal of Science* 259, 694–708.
- Nielsen, L. & Clemmensen, L.B. 2009: Sea-level markers identified in ground-penetrating radar data collected across a modern beach ridge system in a microtidal regime. *Terra Nova* 21, 474–479.
- Nielsen, L., Bendixen, M., Kroon, A., Hede, M., Clemmensen, L., Weßling, R. & Elberling, B. 2017: Sea-level proxies in Holocene raised beach ridge deposits (Greenland) revealed by ground-penetrating radar. *Scientific Reports* 7, Article number 46460. doi:10.1038/srep46460.
- Otvos, E.G. 2000: Beach ridges - definition and significance. *Geomorphology* 32, 83–108.
- Pedersen, A.K., Ulf-Møller, F., Larsen, L.M., Pedersen, G.K. & Dueholm, K.S. 2000: Geological Map of Greenland, 1:100 000, Uiffaq 69 V.1 Syd. Copenhagen: Geological Survey of Denmark and Greenland.
- Pedersen, J.B.T., Kroon, A. & Jakobsen, B.H. 2011: Holocene sea-level reconstruction in the Young Sound region, Northeast Greenland. *Journal of Quaternary Science* 26, 219–226.
- Pugh, D. 2004: Changing Sea-levels: Effects of Tides, Weather and Climate, 265 pp. Cambridge: Cambridge University Press.
- Rasch, M. & Nielsen, N. 1995: Coastal morpho-stratigraphy and Holocene relative sea-level changes at Tuapaat, southeastern Disko Island, central West Greenland. *Polar Research* 14, 277–289.
- Reynolds, J. 1997: An Introduction to Applied Environmental Geophysics, 806 pp. Chichester: Wiley.
- Rodriguez, A. & Meyer, C. 2006: Sea-level variation during the Holocene deduced from the morphologic and stratigraphic evolution of Morgan Peninsula, Alabama, U.S.A.. *Journal of Sedimentary Research* 76, 257–269.
- Simms, A.R., DeWitt, R., Kouremenos, P. & Drewry, A. 2011: A new approach to reconstructing sea levels in Antarctica using optically stimulated luminescence of cobble surfaces. *Quaternary Geochronology* 6, 50–60.
- Tamura, T., Murakami, F., Nanayama, F., Watanabe, K. & Saito, Y. 2008: Ground-penetrating radar profiles of Holocene raised-beach deposits in the Kujukuri strand plain, Pacific coast of eastern Japan. *Marine Geology* 248, 11–27.

A crocodylian coprolite from the lower Oligocene Viborg Formation of Sofienlund Lergrav, Denmark

JESPER MILÀN, ERIK SKOVBJERG RASMUSSEN & KAREN DYBKJÆR



Milàn, J., Rasmussen, E.S. & Dybkjær, K. 2018. A crocodylian coprolite from the lower Oligocene Viborg Formation of Sofienlund Lergrav, Denmark. © 2018 by Bulletin of the Geological Society of Denmark, vol. 66, pp. 181–187. ISSN 2245-7070. (www.2dgf.dk/publikationer/bulletin).

A large, well-preserved vertebrate coprolite found in the clay pit Sofienlund Lergrav, Jylland, is identified as crocodylian due to its size and morphology. The coprolite consists of several concentric layers wrapped around a more homogeneous core. Weak constriction marks are present on the surface. Dinoflagellate cyst contents of the coprolite indicate a mid-Lutetian to earliest Rupelian (middle Eocene to earliest Oligocene) age, which at Sofienlund Lergrav places it within the lower Oligocene Viborg Formation. The coprolite can thus be dated as approximately 33–34 Ma old. The Viborg Formation in Denmark represents a period with deposition of hemipelagic marine clay and formation of glaucony. The nearest shoreline was located c. 200 km north of the location of the present day Sofienlund Lergrav, and the climate was humid, warm-temperate to sub-tropical. The presence of a crocodylian coprolite is an important addition to the sparse Oligocene vertebrate fauna of Denmark, which previously only consisted of sharks and cetaceans.

Keywords: Coprolite, Palaeogene, Oligocene, vertebrate fauna, Denmark, Crocodylian.

Jesper Milàn [jesperm@oesm.dk], Geomuseum Faxe, Østsjælland Museum, Østervej 2, DK-4640 Faxe, Denmark; also Natural History Museum of Denmark, Øster Voldgade 5-7, DK-1465 Copenhagen K, Denmark. Erik Skovbjerg Rasmussen [esr@geus.dk] and Karen Dybkjær [kd@geus.dk], Geological Survey of Denmark and Greenland, Øster Voldgade 10, DK-1350 Copenhagen K, Denmark.

Corresponding author: Jesper Milàn.

Received 29 August 2017
Accepted in revised form
26 May 2018
Published online
11 September 2018

Coprolites are important palaeoecological indicators and are with increasing frequency included in palaeoecological analyses, as they can provide important additional information about extinct animals and their diet, in form of preserved inclusions of undigested prey remains (e.g. Thulborn 1991; Hunt *et al.* 1994; Northwood 2005; Prasad *et al.* 2005; Chin 2007; Souto 2008; Eriksson *et al.* 2011; Milàn *et al.* 2012a,b; Hansen *et al.* 2016). Coprolites are regarded as ichnofossils and were first recognised as fossil feces by William Buckland (1835) who coined the term coprolite. Today vertebrate coprolites are known from the Silurian to the present (Hunt *et al.* 2012). The Danish fossil record of coprolites is sparse, with only a few specimens known from the Lower Cretaceous of Bornholm (Milàn *et al.* 2012b), the Upper Cretaceous of Stevns Klint (Milàn *et al.* 2015), the Lower Paleocene (lower Danian) of Hammelev Kalkbrud (Milàn & Hunt 2016), the middle Danian of Faxe Kalkbrud (Milàn 2010) and Bed L2 of the Eocene Lillebælt Clay Formation (Heilmann-Clausen *et al.* 1985). A new specimen originating from the lower Oligocene Viborg Formation of Sofienlund

Lergrav (Fig. 1) is thus the hitherto youngest coprolite from Denmark. The aim of this study is to describe the new-found specimen, identify its producer, and discuss its palaeoecological context.

Geological Setting

During the Palaeogene and Neogene, the North Sea Basin formed an epicontinental basin (Ziegler 1990). The carbonate deposition that dominated during the Late Cretaceous continued into the earliest part of the Palaeogene (early Paleocene). It was succeeded by deposition of deep marine clays during most of the Paleocene and Eocene (Nielsen *et al.* 2015 and references therein). Volcanic activity in the North Atlantic became extensive at the Paleocene–Eocene transition and resulted in sedimentation of ash-rich layers throughout the North Sea Basin and diatomites locally in parts of the eastern North Sea area (Pedersen & Surlyk 1983). During the Oligocene, the first



Fig. 1. Pre-Quaternary map of Denmark indicating the location of the clay-pit Sofienlund Lergrav in the Oligocene–Miocene deposits at the small town of Ulstrup (56° 23.4002'N, 09° 48.3961' E). Modified from Håkansson & Pedersen (1992).

prograding fluvio-deltaic systems were established south of the Fennoscandian Shield (Schjøler *et al.* 2007; Jarsve *et al.* 2014). These systems were restricted to a narrow rim around present-day Norway (Śliwińska *et al.* 2014). A branch of delta lobes that prograded deeper into the North Sea Basin are found south-west of present-day Norway (Jarsve *et al.* 2014). The eastern part of the North Sea Basin, however, remained fully marine, with a water depth at a minimum of 300 m and dominated by deposition of glaucony-rich mud. Late Oligocene – early Miocene inversion in the Central Graben and probably in the Norwegian-Danish

Basin resulted in relatively shallow water in the eastern North Sea Basin (Rasmussen 2009). A coincident uplift of Norway during the Miocene (Japsen *et al.* 2010; Rasmussen & Utescher 2016) initiated major progradation of delta systems into the eastern North Sea Basin, and parts of the area covered by present-day Denmark became dry land.

The landscape was characterised by a coastal lowland with a few major wave-dominated delta systems (Rasmussen *et al.* 2010; Śliwińska *et al.* 2014). The fluvial systems that conveyed sediments to the sea were mainly the meandering type, but braided systems developed in the earliest early Miocene, associated with the inversion tectonism. Spit systems and barrier-lagoonal complexes formed in between the major delta lobes. The coastline was dominated by mangrove swamp, and on elevated areas in the hinterland sequoia and oaks vegetated the landscape.

During most of the Palaeogene and Neogene, the climate was warm temperate to subtropical. The annual precipitation was most of the time in the order of 1000–1500 mm (Utescher *et al.* 2009; Larsson *et al.* 2011). Temporal climatic deterioration occurred during the early and middle Oligocene and at the end of the Miocene.

Christensen & Ulleberg (1973) subdivided the succession in the clay-pit Sofienlund Lergrav into the Viborg Formation, the Ulstrup Clay, the Sofienlund Clay and the Sofienlund Sand. However, the regional study of Rasmussen *et al.* (2010) abandoned the upper three units and included the Ulstrup Clay in the Brejning Formation, which is late Oligocene in age, and included the Sofienlund Clay and Sand in the lower Miocene Vejle Fjord Formation. The Viborg Formation was deposited in a relatively deep marine environment (> 300 m of water) at a minimum of 150 km from the shoreline. A major hiatus separates the Viborg Formation from the Brejning Formation (Fig. 2). The hiatus was probably formed by deep marine currents (e.g. Hansen *et al.* 2004). Even though the Brejning Forma-

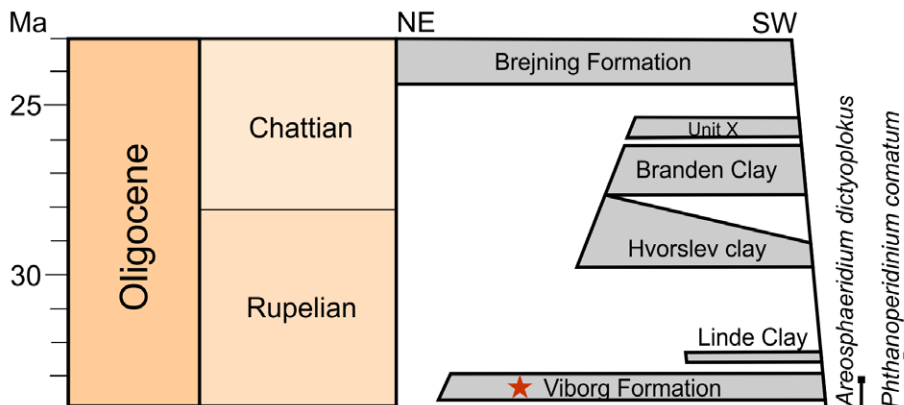


Fig. 2. Chronostratigraphy of the Oligocene sediments in a NE–SW transect through Jylland, Denmark. At Sofienlund Lergrav only the Brejning Formation and the Viborg Formation are present, separated by a major hiatus. The range of the dinoflagellate cysts retrieved from the coprolite places it within the Viborg Formation, indicated by an asterisk. Modified from Śliwińska *et al.* (2012, fig. 13).

tion was deposited in slightly shallower water, the shoreline was displaced farther north due to relatively high sea level during the late Oligocene. The shallowing of the water depth was a result of inversion of the Norwegian-Danish Basin. During the early Miocene the shoreline migrated from present-day Norway into the Danish area, and the Vejle Fjord Formation represents sediments deposited in a prodelta environment in front of the fluvio-deltaic Billund Formation.

Material and methods

A well-preserved coprolite was found in the collection of the Natural History Museum of Denmark (NHMD-227230), with the only information being that it was found in Sofienlund Lergrav but without any reference to a specific formation, or date of collecting. To determine the stratigraphic age, a small sample was extracted from the outer coil of the coprolite and analysed for dinoflagellate cysts. The sample was processed using HCl to dissolve calcareous matter and HF to dissolve silicates. The acid treatment was followed by neutralisation with water. The residue was filtered on a 6µm nylon mesh and mounted on a glass slide using glycerine gel. The organic particles, including the dinoflagellate cysts, were studied using a normal light microscope.

Description of specimen

The specimen is 66 mm long and 31 mm in widest diameter, tapering towards the ends (Fig. 3A). One end appears complete while other end is broken. Just prior to the break, the specimen has a circumferential constriction mark, which coincides with a bend at an angle of approximately 150° (Fig. 3B).

The colour of the specimen is light brown, and the outer surface is smooth but covered with small pits, grooves and irregularities. Parts of the outer surface layer are missing, exposing a perfectly smooth layer underneath (Fig. 3A). The internal architecture of the specimen is visible at both ends which show a massive, apparently structureless core of the specimen, measuring 11 mm in diameter at the rounded termination and 19 mm at the broken, incomplete end. Around the structureless core, several thin, concentric layers are deposited successively. Each layer is between 0.5 and 2 mm in thickness, and the thickness is unevenly distributed around the specimen (Fig. 3C). The texture of the individual layers is homogenous with no apparent inclusions of any kind.

Microfossil dating

A small sample extracted from a loose part of the outer coil of the coprolite was analysed for its dinoflagellate cyst content in order to provide a dating. The sample comprised a very sparse dinoflagellate cyst assemblage including the following taxa: *Areosphaeridium dictyoplokus*, *Phthanoperidinium comatum* and *Areosphaeridium michoudii*. The co-occurrence of these taxa indicates a mid-Lutetian to earliest Rupelian (middle Eocene to earliest Oligocene) age. As the coprolite was found at Sofienlund Lergrav where the Viborg Formation of earliest Oligocene age is the oldest deposits outcropping, it must be assumed that the coprolite came from that unit. The occurrence of *A. michoudii*, which has a last occurrence in the Eocene, indicates that the single occurrence of this taxa is due to reworking. Reworking of Eocene deposits into the Viborg Formation is a well-known phenomenon (Śliwińska *et al.* 2012).

Discussion

Origin of the feces

Identifying the exact producer of a coprolite is a challenging task with many possible uncertainties, as feces from many unrelated animal groups can appear to be very similar, due to diet and mode of egestion. To further complicate the picture, feces from the same animal can show a wide morphological variation as well (e.g. McAllister 1985; Chin 2002; Chame 2003; Milàn 2012).

The known Oligocene vertebrate fauna of Denmark is limited to small cetaceans (Ravn 1926; Hoch 2000; Bonde *et al.* 2008) and sharks, where one find of a tooth from *Carcharocles angustidens* suggests a length of the shark of up to 10 m (Bonde *et al.* 2008). Marine mammals including cetaceans usually have very liquid feces with a water content of up to 90 percent, which would be classified as diarrhea (Lewin 1999) and thus unable to be preserved as coprolites. This makes a cetacean origin of the coprolite unlikely. Coprolites from sharks and other actinopterygians are very common in the fossil record and are distinct in being spiral-coiled, reflecting the spirally valvular intestines of actinopterygians, and giving the coprolites the superficial appearance of a coiled pinecone (Williams 1972; McAllister 1985; Hunt & Lucas 2012). While the size of the Sofienlund coprolite is in agreement with a large shark, the morphology excludes a shark as a producer. The best morphological match for the Sofienlund coprolite is a crocodilian. Crocodilian coprolites are generally sausage shaped and circular

in cross section, with few structures visible on their outer surface except for occasional striations or traces from coprophageous organisms (Souto 2010; Milàn 2012). A study of the morphological variation within fresh feces from 10 species of extant crocodilians demonstrated that a commonly occurring feature of crocodilian feces is circumferal constriction marks and a bend between 120° and 150°; their internal structure is composed of concentric layers of various thickness around a central core of a more homogenous mass (Milàn 2012; Milàn & Hedegaard 2010) (Fig. 3D, E). Crocodilian feces are devoid of any bone or shell remains as the digestive system of crocodilians effec-

tively dissolves any bone or shell remains of their prey (Fischer 1981), leaving only hair and feathers behind (Milàn 2012). The total body length of a crocodile can be estimated from the diameter of the feces (Milàn 2012). In this case a diameter of 31 mm corresponds to a crocodile with a body length of around 260 cm (Milàn 2012).

Palaeoenvironment

The Viborg Formation containing the coprolite was deposited during the early Oligocene. The Norwegian-Danish Basin was generally sediment starved, as indi-

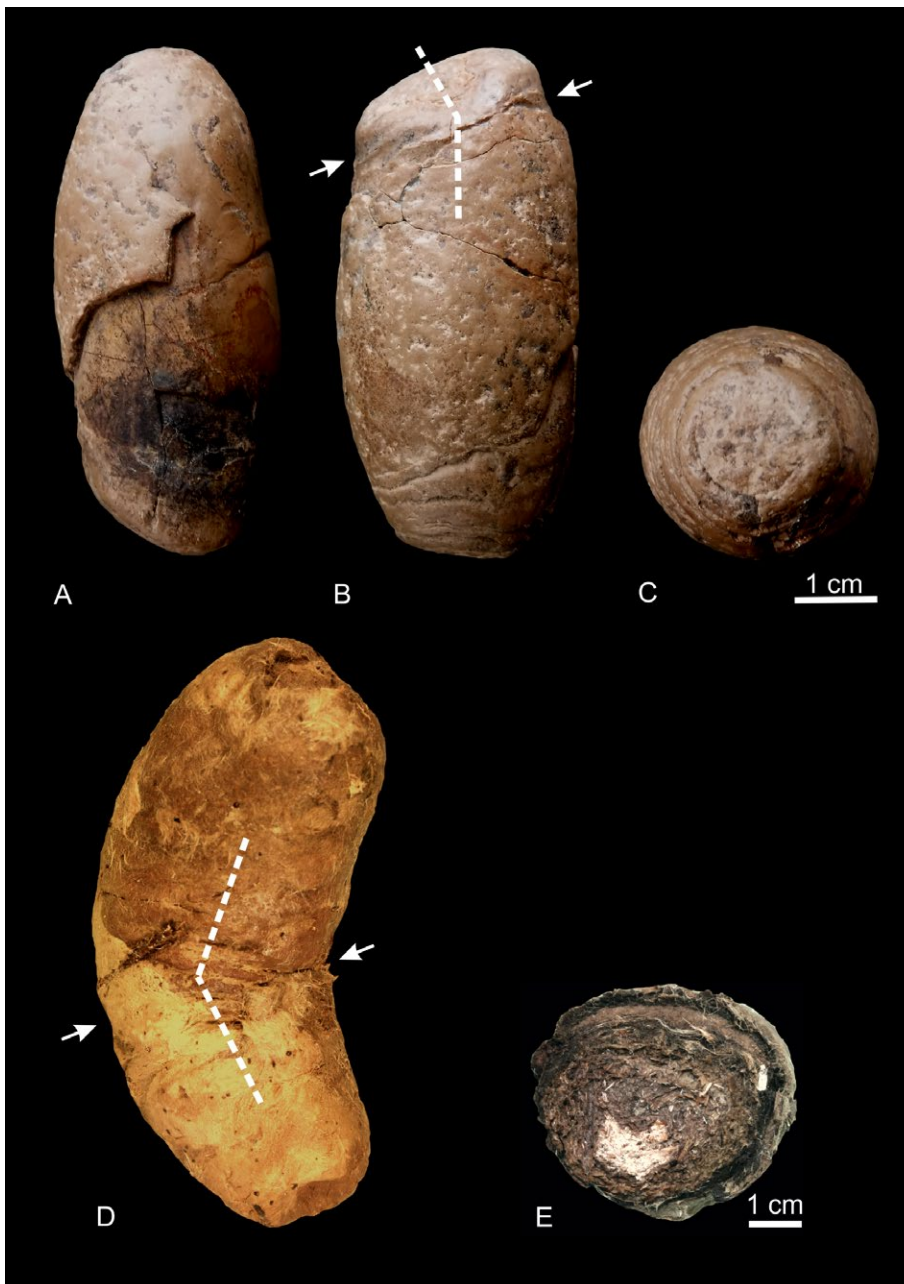


Fig. 3. The Sofienlund coprolite NHMD 227230 shown in three views, with comparisons. **A:** Lateral view where parts of the outer layer is broken off, revealing the inner, smooth surface. **B:** Lateral view showing the circumferal zone of constriction, indicated by arrows, and the 150° bending of the specimen at the zone. **C:** Axial view, showing the architecture of a dense featureless core wrapped in several millimetre-thick concentric layers. **D:** Fresh feces from a dwarf crocodile, *Osteolemus tetraspis*, showing a smooth surface and weak zone of circumferal constriction initiating a bend of 135°. **E:** Cross section of fresh feces from a dwarf crocodile, showing the typical layered internal architecture of crocodilian feces.

cated by the presence of glaucony, but progradation of a delta shoreline occurred south of the Fennoscandian Shield during the early Oligocene (Schiøler *et al.* 2007; Jasve *et al.* 2014). The shoreline was probably located 200 km to the north of the present-day Sofienlund Lergrav and the estimated depth of the water in front of the delta was more than 300 m based on the height of the clinoformal package around the Inez-1 well (Schiøler *et al.* 2007). Recent crocodiles are able to swim for considerable distances. A GPS-tagged saltwater crocodile (*Crocodylus porosus*) is reported to have swum 590 km in 25 days without going ashore (Campbell *et al.* 2010), and a juvenile saltwater crocodile has been observed to survive 4 months without feeding in fully marine conditions (Taplin & Grigg 1989). Lower Paleocene (Danian) records of crocodilian body fossils from Denmark and southern Sweden are also from sedimentary environments which represent deposition in excess of 100 km from the nearest shoreline (Troedsson 1924; Schwarz-Wings *et al.* 2014; Adolfssen *et al.* 2017), and presumed crocodilian coprolites are found in the middle Danian Faxe Formation of Faxe Kalkbrud (Milàn 2010). Therefore, it is not unlikely to find a crocodile coprolite at Sofienlund Lergrav despite its relatively long distance from the palaeo-shoreline. An alternative explanation is that the coprolite was produced onshore and subsequently transported by currents to its final resting place, or it could have been rafted by a floating root net and dropped to the sea bottom. A gneiss clast 25 cm in diameter and several pebbles have been found in the basal layer of the Sydklint Member, Brejning Formation at Siltstrup in northern Jylland (Heilmann-Clausen 1997). Land material transported by root nets and deposited as dropstones are thus well known in marine sedimentary environments (Bennett *et al.* 1996).

The sedimentological context of the specimen in the Viborg Formation, together with the morphology showing a featureless surface, a homogenous inner core wrapped in thin concentric layers, no prey remains, and a zone of constriction which initiates a 150° bend, strongly suggest a crocodilian origin of the coprolite, even though no skeletal remains exist to support it. The presence of crocodilians indicates that the climate during the deposition of the Viborg Formation was at minimum warm-temperate to subtropical.

Conclusions

A well-preserved coprolite from Sofienlund Lergrav in Jylland, Denmark, is identified as crocodilian in origin, based on its size and morphology. Dinoflagellate cysts extracted from the coprolite date it to the early

Oligocene, which in Sofienlund Lergrav corresponds to the Viborg Formation, giving the coprolite an age of 33–34 Ma.

This is the first record of crocodilians in the Oligocene vertebrate fauna of Denmark, which previously only consisted of sharks and cetaceans.

The find indicates that the climate during deposition of the Viborg Formation was warm-temperate to subtropical.

Acknowledgements

We are grateful to Sten Lennart Jakobsen for bringing the specimen to our attention. Kai Ingemann Schnetler is thanked for helpful discussions on the Oligocene fauna of Denmark and help with references to old literature. Rene Hedegaard from KrokodilleZoo in Denmark is thanked for his cooperativeness and help to secure fresh specimens for comparative study. Adrian P. Hunt and Claus Heilmann-Clausen are thanked for their critical and constructive reviews.

References

- Adolfssen, J.S., Milàn, J. & Friedman, M. 2017: Review of the Danian vertebrate fauna of southern Scandinavia. *Bulletin of the Geological Society of Denmark* 65, 1–23.
- Bonde, N., Andersen, S., Hald, N. & Jakobsen, S.L. 2008: Danekræ – Danmarks bedste fossiler, 224 pp. Gyldendal, Copenhagen.
- Bennett, M.R., Doyle, P. & Mather, A.E. 1996: Dropstones: Their origin and significance. *Palaeogeography, Palaeoclimatology, Palaeoecology* 121, 331–339.
- Buckland, W. 1835: On the discovery of coprolites, or fossil faeces, in the Lias at Lyme Regis, and in other formations. *Transactions of the Geological Society of London* 3, 223–238.
- Campbell, H.A., Watts, E.M., Sullivan, S., Read, M.A., Choukroun, S., Irwin, S.R. & Franklin, C.E. 2010: Eustarine crocodiles ride surface currents to facilitate long-distance travel. *Journal of Animal Ecology* 79, 955–964.
- Chame, M. 2003: Terrestrial mammal feces: a morphometric summary and description. *Memoirs Instituto Oswaldo Cruz, Rio de Janeiro* 98 (Supplement I), 71–94.
- Chin, K. 2002: Analyses of coprolites produced by carnivorous vertebrates. *Paleontological Society Papers* 8, 43–50.
- Chin, K. 2007: The paleobiological implications of herbivorous dinosaur coprolites from the Upper Cretaceous Two Medicine Formation of Montana: Why eat wood? *Palaios* 22, 554–566.
- Christensen, L. & Ulleberg, K. 1973: Sedimentology and micro-palaeontology of the Middle Oligocene sequence at

- Sofienlund. *Bulletin of the Geological Society of Denmark* 22, 283–305.
- Eriksson, M.E., Lindgren, J., Chin, K. & Månsby, U. 2011: Coprolite morphotypes from the Upper Cretaceous of Sweden: novel views on an ancient ecosystem and its implications for coprolite taphonomy. *Lethaia* 44, 455–468.
- Fischer, D.F. 1981: Crocodylian scatology, microvertebrate concentrations, and enamel-less teeth. *Paleobiology* 7, 262–275.
- Hansen, J.P.V., Clausen, O.R. & Huuse, M. 2004: 3D Seismic Analysis Reveals the Origin of Ambiguous Erosional Features at a Major Sequence Boundary in the Eastern North Sea: near Top Oligocene. Geological Society, London, *Memiors* 29, 83–90.
- Hansen, B.B., Milàn, J., Clemmensen, L.B., Adolfssen, J.S., Estrup, E.J., Klein, N., Mateus, O. & Wings, O. 2016: Coprolites from the Late Triassic Kap Stewart Formation, Jameson Land, East Greenland: Morphology, classification and prey inclusions. *Geological Society of London Special Publications* 434, 49–69.
- Heilmann-Clausen, C. 1997: How one diatomite led to the development of another diatomite – the Oligocene section at Silstrup, NW Denmark. *Tertiary Research* 18, 31–34.
- Heilmann-Clausen, C., Nielsen, O.B. & Gersner, F. 1985: Lithostratigraphy and depositional environments in the Upper Paleocene and Eocene of Denmark. *Bulletin of the Geological Society of Denmark* 33, 287–323.
- Hoch, E. 2000: Olfaction in whales: evidence from a young odontocete from the Late Oligocene North Sea. *Historical Biology* 14, 67–89.
- Hunt, A.P., Chin, K. & Lockley, M.G. 1994: The paleobiology of vertebrate coprolites. In: Donovan, S. (ed.), *The Palaeobiology of Trace Fossils*, 221–240. John Wiley & Sons, London.
- Hunt, A.P. & Lucas, S.G. 2012: Classification of vertebrate coprolites and related trace fossils. *New Mexico Museum of Natural History and Science Bulletin* 57, 137–146.
- Hunt, A.P., Lucas, S.G., Milàn, J. & Spielmann, J.A. 2012: Vertebrate coprolites: status and prospectus: New Mexico Museum of Natural History and Science, *Bulletin* 57, 5–24.
- Håkansson, E. & Pedersen, S.S. 1992: Geologisk kort over den danske undergrund. VARV Special publication. København: Tidsskriftet VARV.
- Japsen, P., Green, P.F., Bonow, J.M., Rasmussen, E.S., Chalmers, J.A. & Kjennerud, T. 2010: Episodic uplift and exhumation along North Atlantic passive margins: implications for hydrocarbon prospectivity. In: Vining, B.A. & Pickering, S.C. (eds), *Petroleum Geology: From Mature Basins to New Frontiers*. Proceedings of the 7th Petroleum Geology Conference, 979–1004. Geological Society, London.
- Jarsve, E.M., Faleide, J.I., Gabrielsen, R.H. & Nystuen, J.P. 2014: Mesozoic and Cenozoic basin configurations in the North Sea. In: Martinus, A.W., Ravnås, R., Howell, J.A., Steel, R.J. & Wonham, J.P. (eds), *From depositional systems to sedimentary succession on the Norwegian continental margin*. Special Publication of the International Association of Sedimentologist 46, 417–452.
- Larsson, L.M., Dybkjær, K., Rasmussen, E.S., Piasecki, S., Utescher, T. & Vajda, V. 2011: Miocene climate evolution of northern Europe: A palynological investigation from Denmark. *Palaeogeography, Palaeoclimatology, Palaeoecology* 309, 161–175.
- Lewin, R.A. 1999: *Merde, Excursions into scientific, cultural and socio-historical coprology*. 164 pp. Aurum Press, London.
- McAllister, J.A. 1985: Reevaluation of the formation of spiral coprolites. *University of Kansas, Paleontological Contributions* 144, 1–12.
- Milàn, J. 2010: Coprolites from the Danian limestone (Lower Paleocene) of Faxe Quarry, Denmark. *New Mexico Museum of Natural History and Science Bulletin* 51, 215–218.
- Milàn, J. 2012: Crocodylian scatology – a look into morphology, internal architecture, inter- and intraspecific variation and prey remains in extant crocodylian feces. *New Mexico Museum of Natural History and Science Bulletin* 57, 65–71.
- Milàn, J. & Hedegaard, R. 2010: Interspecific variation in tracks and trackways from extant crocodylians. *New Mexico Museum of Natural History and Science Bulletin* 51, 15–29.
- Milàn, J. & Hunt, A.P. 2016: *Daniacopros hofstedtae*, ichnogen. et ichnosp. nov., a new vertebrate coprolite ichnotaxon from the Lower Danian Stevns Klint Formation of the Hammelev limestone quarry, Denmark. *New Mexico Museum of Natural History and Science Bulletin* 74, 159–161.
- Milàn, J., Rasmussen, B.W. & Lynnerup, N. 2012a: A coprolite in the MDCT-scanner – internal architecture and bone contents revealed. *New Mexico Museum of Natural History and Science Bulletin* 57, 99–103.
- Milàn, J., Rasmussen, B.W. & Bonde, N. 2012b: Coprolites with prey remains and traces from coprophagous organisms from the Lower Cretaceous (Late Berriasian) Jydegaard Formation of Bornholm, Denmark. *New Mexico Museum of Natural History and Science Bulletin* 57, 235–240.
- Milàn, J., Hunt, A.P., Adolfssen, J.S., Rasmussen, B.W. & Bjerager, M. 2015: First record of a vertebrate coprolite from the Upper Cretaceous (Maastrichtian) chalk of Stevns Klint, Denmark. *New Mexico Museum of Natural History and Science Bulletin* 67, 227–229.
- Nielsen, O.B., Rasmussen, E.S. & Thyberg, B. 2015: Distribution of clay minerals in the northern North Sea Basin during the Paleogene and Neogene: a result of source-area geology and sorting processes. *Journal of Sedimentary Research* 85, 562–581.
- Northwood, C. 2005: Early Triassic coprolites from Australia and their palaeobiological significance. *Palaeontology* 48, 49–68.
- Pedersen, G.K. & Surlyk, F. 1983: The Fur Formation, a late Paleocene ash-bearing diatomite from northern Denmark. *Bulletin of the Geological Society of Denmark* 32, 43–65.
- Prasad, V., Caroline A. E. Stromberg, C. A. E., Alimohammadian, H. & Sahni, A. 2005: Dinosaur coprolites and the early evolution of grasses and grazers. *Science* 310, 1177–1180.
- Rasmussen, E.S. 2009: Neogene inversion of the north-eastern North Sea. *Tectonophysics* 465, 84–97.

- Rasmussen, E.S. & Utescher, T. 2016: Early Miocene tectonism: an important event in the evolution of southern Norway. Onshore – Offshore relationships on the North Atlantic Margins, Trondheim 18th-19th October 2016, Abstracts 70–71.
- Rasmussen, E.S., Dybkjær, K. & Piasecki, S. 2010: Lithostratigraphy of the Upper Oligocene – Miocene succession of Denmark. *Bulletin of the Geological Survey of Denmark and Greenland* 22, 92 pp.
- Ravn, J.P.J. 1926: On a Cetacean, *Squalodon (Microzeuglodon?) wingei* n. sp., from the Oligocene of Jutland. *Meddelelser fra Dansk Geologisk Forening* 7, 45–54.
- Schiøler, P., Andsbjerg, J., Clausen, O.R., Dam, G., Dybkjær, K., Hamberg, L., Heilmann-Clausen, C., Johannessen, E.P., Kristensen, L.E., Prince, I. & Rasmussen, J.A. 2007: Lithostratigraphy of the Palaeogene–Lower Neogene sediments (Rogaland to Westray Groups) in the Danish sector of the North Sea. *Geological Survey of Denmark and Greenland Bulletin* 12, 1–77.
- Schwarz-Wings, D., Milàn, J. & Gravesen, P. 2014: A new eusuchian (Crocodylia) tooth from the Early or Middle Paleocene, with a description of the Early Middle Paleocene boundary succession at Gemmas Allé, Copenhagen, Denmark. *Bulletin of the Geological Society of Denmark* 62, 17–26.
- Śliwińska, K.K., Abrahamsen, N., Beyer, C., Brünings-Hansen, T., Thomsen, E., Ulleberg, K. & Heilmann-Clausen, C. 2012: Bio- and magnetostratigraphy of Rupelian–mid Chattian deposits from the Danish land area. *Review of Palaeobotany and Palynology* 172, 48–69.
- Śliwińska, K.K., Dybkjær, K., Schoon, P.L., Beyer, C., King, C., Schouten, S. & Nielsen, O.B. 2014: Paleoclimatic and paleoenvironmental records of the Oligocene–Miocene transition, central Jylland, Denmark. *Marine Geology* 350, 1–15.
- Souto, P.R.F. 2008: *Coprolitos do Brasil – Principais ocorrências e studio*, 93 pp. Publitt: Rio de Janeiro.
- Souto, P.R.F. 2010: Crocodylomorph coprolites from the Bauru basin, Upper Cretaceous, Brazil. *New Mexico Museum of Natural History and Science Bulletin* 51, 201–208.
- Taplin, L.E. & Grigg, G.C. 1989: Historical zoogeography of the eusuchian crocodylians. *American Zoologist* 29, 885–901.
- Thulborn, R.A. 1991: Morphology, preservation and palaeobiological significance of dinosaur coprolites. *Palaeogeography, Palaeoclimatology, Palaeoecology* 83, 341–366.
- Troedsson, G.T. 1924: On Crocodylian Remains from the Danian of Sweden. *Lunds Universitets Årsskrift, Ny följd. Avdeling* 2, 20, 1–75.
- Utescher, T., Mosbrugger, V., Ivanov, D. & Dilcher, D.L. 2009: Present-day climatic equivalents of European Cenozoic climates. *Earth and Planetary Science Letters* 284, 544–552.
- Williams, M.E. 1972: The origin of spiral coprolites. *University of Kansas Palaeontological Contributions* 59, 1–19.
- Ziegler, P.A. 1990: *Geological atlas of Western and Central Europe*, 239 pp. Geological Society Publication, Bath, UK.

Meandering river deposits in sediment cores, the Middle Jurassic Alma Field, Southern Danish Central Graben

ASLAUG C. GLAD, MADSE. WILLUMSEN, LARS O. BOLDREEL & LARS B. CLEMMENSEN



Glad, A.C., Willumsen, M.E., Boldreel, L. O. & Clemmensen, L.B., 2018. Meandering river deposits in sediment cores, the Middle Jurassic Alma Field, Southern Danish Central Graben. © 2018 by Bulletin of the Geological Society of Denmark, Vol. 66, pp. 189–209. ISSN 2245-7070. (www.2dgf.dk/publikationer/bulletin).

Received 26 September 2017
Accepted in revised form
28 April 2018
Published online
26 September 2018

Fluvial deposits are amongst the most important terrestrial hydrocarbon reservoirs, but the complex nature of these deposits is challenging in subsurface reservoir characterisation. This study is the first detailed facies analysis of the meandering river deposits of the Middle Jurassic Alma Field situated in the southern Danish North Sea. The fluvial sandstones and their associated deposits are described and interpreted based on studies from two core sites (Alma-1X and Alma-2X). The facies analysis of the cores demonstrates the presence of three meandering river facies associations: Channel deposits, channel margin deposits and floodplain deposits. The channel deposits comprise channel thalweg and point bar sediments, the channel margin deposits include crevasse channel and crevasse splay sediments, while the floodplain deposits comprise overbank and backswamp sediments. The point bar deposits are composed of fine- to medium-grained sandstones but can contain intervals of finer grained sediments, particularly in their upper parts where they can grade into muddy sandstones or true heterolithic deposits. Preserved sand body thicknesses (channel thalweg and point bar deposits) in both Alma cores have a mean value of 2.6 m and a maximum value of 4.35 m (Alma-1X) and 6.55 m (Alma-2X). Using maximum values of channel deposit thicknesses, and assuming the preservation conditions are met, the width of the largest ancient channel belt in Alma-1X would be between 90 m and 200 m or around 900 m, depending on whether the fluvial system is mud-rich or sand-rich. The same method applied to Alma-2X gives a width of the largest channel belt between 130 m and 330 m or around 1300 m.

Fluvial sediments of the Middle Jurassic Scalby Formation (north-east England) were deposited in a sandy meandering river with sedimentary characteristics corresponding to those observed in the Alma cores. Outcrop analogue investigations of this formation were carried out to examine the architecture of the fluvial facies in a two-dimensional section with emphasis on channel thalweg and point bar deposits.

Combined evidence from core analysis and outcrop analogue studies suggests that the fluvial deposits in the Alma Field represent a mixed-load meandering river system with sandy point bars. The meandering river system developed on a coastal plain with overbank fines and organic-rich backswamp deposits. The mud-rich or heterolithic deposits in the upper part of the point bar facies intervals are noteworthy and could indicate markedly fluctuating discharge in a mixed-load river.

Keywords: Meandering river deposits, Middle Jurassic, Alma Field, core studies, facies analysis, analogue outcrop study, fluvial reservoirs.

Aslaug C. Glad [gukke.glad@gmail.com; presently also Acglad@dtu.dk], *Lars Ole Boldreel* [Lob@ign.ku.dk] and *Lars B. Clemmensen* [Larsc@ign.ku.dk], Department of Geosciences and Natural Resource Management, University of Copenhagen, Øster Voldgade 10, DK-1350 Copenhagen K, Denmark. *Mads E. Willumsen* [mew@geus.dk], Geological Survey of Denmark and Greenland (GEUS), Øster Voldgade 10, DK-1350 Copenhagen K, Denmark.

Corresponding author: Aslaug C. Glad.

Meandering river deposits constitute a prominent depositional type among the non-marine environments, and their presence in various past environmental and tectonic settings makes them valuable archives of past fluvial system evolution and climatic

conditions (e.g. Allen 1965, 1978; Leeder 1978; Bridge & Leeder 1979; Miall 1996, 2014). Mineral and petroleum deposits associated with fluvial environments have resulted in numerous studies of meandering river sediments and facies architecture, including analysis

of depositional scales, fluvial style, and subsurface characteristics (e.g. Tyler & Finley 1991; Miall 1996, 2014; Bridge 2001). Fluvial sandstones are important, but highly heterogeneous reservoirs and account for more than 20% of the world's remaining hydrocarbon reserves (Keogh *et al.* 2007). The heterogeneity is expressed at many scales from vertical stratigraphic variations, channel body stacking, channel shape, interconnectivity and channel sediment variability (Keogh *et al.* 2007). Identification and characterization of fluvial facies in subsurface settings is challenging and highly dependent on several datasets, including core material. Facies description and interpretation of core material benefit greatly from outcrop analogue studies by illustrating the large-scale two-dimensional facies relationships (e.g. Owen *et al.* 2017).

Middle Jurassic fluvial sandstones constitute petro-

leum reservoirs in the Danish North Sea (Andsbjerg *et al.* 2001; Andsbjerg 2003; Schwarzer *et al.* 2007). The Alma structure is an antiform located in the southern part of the Danish Central Graben (Fig. 1); the structure was originally investigated by Maersk Oil during the early 1990s. This potential oil field of Middle Jurassic age is composed of presumed meandering river deposits with channel and channel-margin deposits of moderate to high reservoir quality (Schwarzer *et al.* 2007). The Middle Jurassic sections of Alma-1X and Alma-2X have been cored.

The purpose of this study is to present a facies analysis of the two Alma cores, with interpretations supported by an analogue study of world-class exposures of Middle Jurassic meandering river deposits of the Scalby Formation, north-east England (fig. 1; Ielpi & Ghinassi 2014).

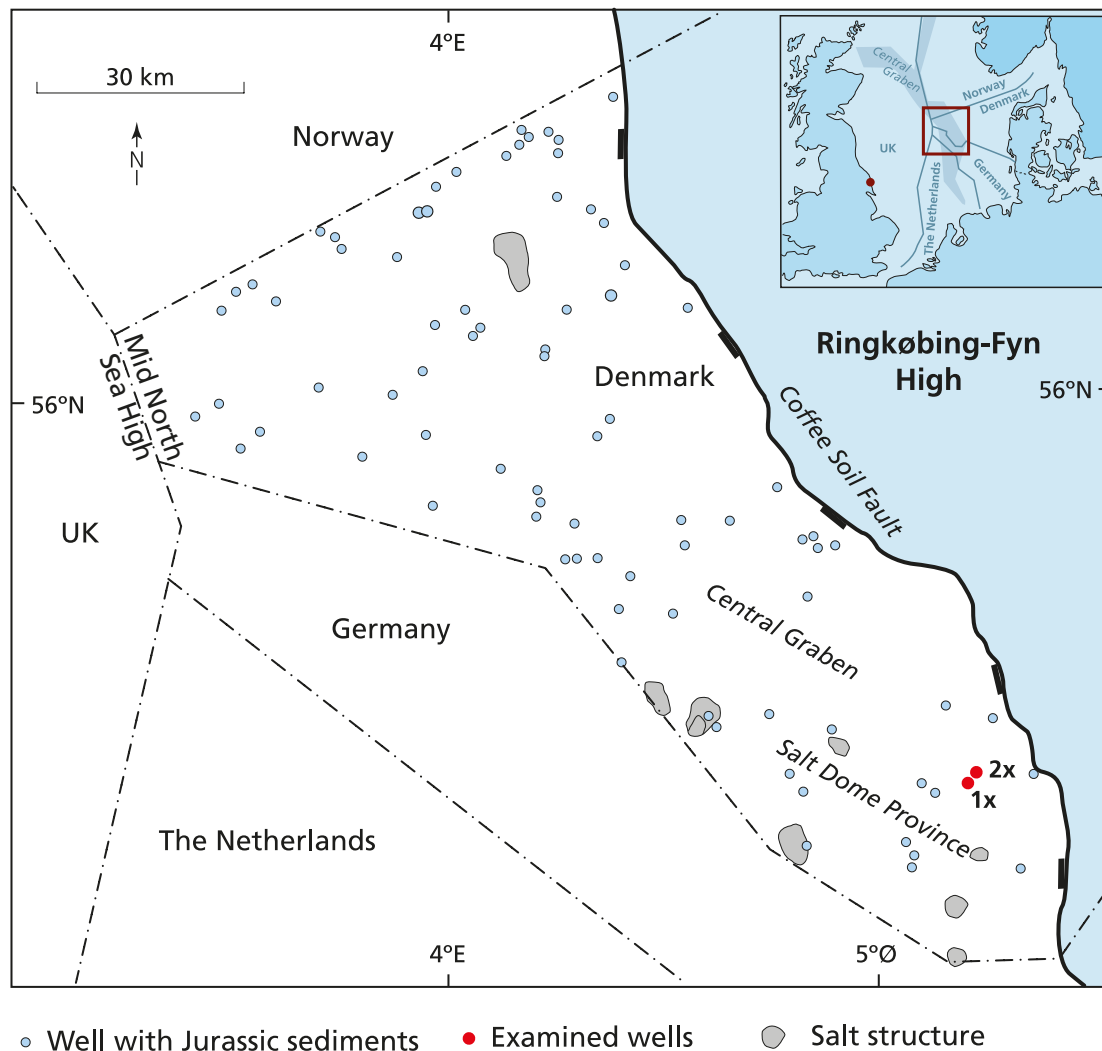


Fig. 1. Map of the Danish Central Graben with Jurassic deposits west of the Coffee Soil Fault. The studied wells of the Alma Field are situated in the south-eastern part of the Danish Central Graben and are marked by 1X and 2X with red dots. Dashed lines mark the territorial boundaries of Norway, Denmark, Germany, the Netherlands and the UK. The Scalby Formation in the eastern UK is shown by a red dot on the overview map. (Modified from Thomsen *et al.* 2013).

The Alma Field

Geological setting

The Alma Field is located in the southern part of the Danish Central Graben (Fig. 1). The Alma Field has a mapped closure of 16.8 km² and a relief of 300 ft (~100 m) and is situated on a faulted salt dome structure (Maersk Oil 1993a). The central part of the salt structure is severely faulted by generally N-S trending normal faults; both eastward and westward inclined faults appear to have developed antithetically (Maersk Oil 1993a; Fig. 2).

The Danish Central Graben, bounded by the Coffee Soil Fault to the east and the Mid North Sea High to the west, is part of the Central Graben which covers a large area in the central and southern North Sea (Ziegler 1990). The Danish Central Graben is made up of a series of NNW-SSE trending half-grabens and forms the southern rift arm of a failed Jurassic rift system (Møller & Rasmussen 2003). The Alma Field is situated in the Salt Dome Province, characterised by salt structures formed by Permian evaporites deposited in the North German Basin (Japsen *et al.* 2003). During the Late Triassic, regional thermal subsidence was

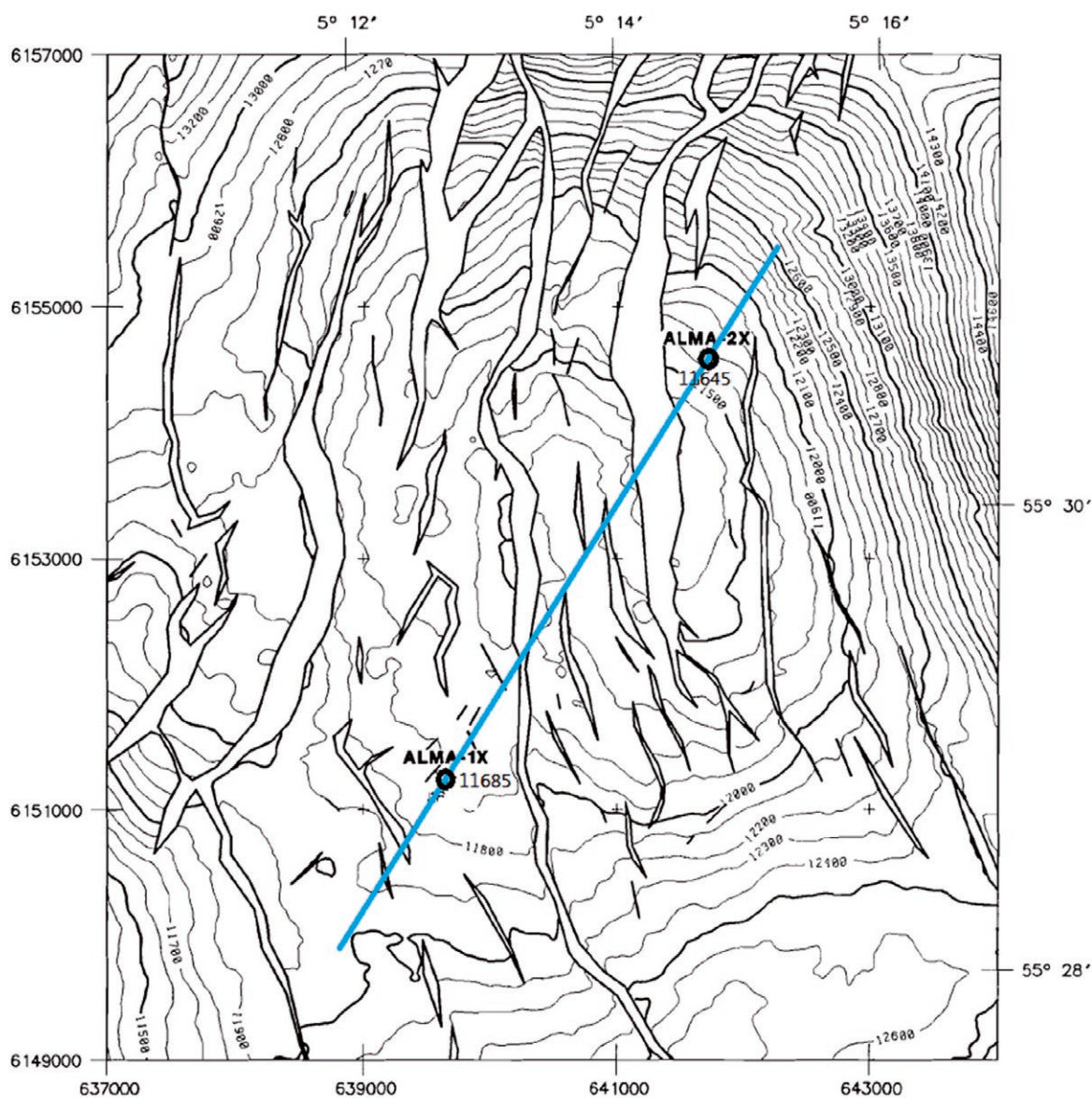


Fig. 2. Structural map of the Alma Field. The Alma Field is situated on a faulted antiform with a mapped closure of 16.8 km² and a relief of 300 ft (~100 m). The central part of the structure is dissected by dominantly N-S trending normal faults. The positions of the two wells are shown. The blue line is the seismic line in Fig. 4. The contour lines record the depth (in feet) of the top surface of the Lower Graben Sand Formation, equivalent to the Bryne Formation. Modified from Maersk (1993a). The length of the blue line is approximately 6 km.

initiated in the Central Graben and lasted until the beginning of the Middle Jurassic (Møller 1986). The period from the Middle Jurassic to the Early Cretaceous was characterised by an interplay of rifting, sea-level variations and halokinesis, resulting in a complex structural evolution and sediment deposition in the Central Graben (Ziegler 1990; Andsbjerg 2003; Andsbjerg & Dybkjær 2003; Michelsen *et al.* 2003). Prior to the Middle Jurassic–Early Cretaceous rifting, large areas of the North Sea Basin experienced thermal uplift resulting in the formation of the Central North Sea Rift Dome (Ziegler 1990; Japsen *et al.* 2003), which caused the Late Aalenian unconformity that influenced large parts of the North Sea including the Danish Central Graben (Andsbjerg *et al.* 2001). Following the thermal uplift, active faulting created accommodation space for deposition of Late Aalenian–Callovian sediments, which initially were continental coastal plain deposits and eventually became marine during a transgression of the Danish Central Graben in the Callovian (Andsbjerg *et al.* 2001; Husmo *et al.* 2002).

Stratigraphy

The Middle Jurassic fluvial deposits of the southern Danish Central Graben were originally referred to as the Central Graben Group by Jensen *et al.* (1986) but were included in the Bryne Formation by Michelsen *et al.* (2003) and Andsbjerg (2003). The Middle Jurassic deposits unconformably overlie Triassic and Lower Jurassic deposits. Palynostratigraphic analysis of the fluvial sediments in the Alma-1X and Alma-2X cores indicates a Middle Jurassic (Bathonian) age (DGU 1991, 1993; Maersk Oil 1991a, 1993a, 1999), thus placing the sediments in the middle part of the Bryne Formation (Fig. 3). The Bryne Formation is overlain by the Callovian shallow marine Lulu Formation in the Søgne Basin and by the estuarine(?) Middle Graben Formation in the Salt Dome Province (Fig. 3). These formations are overlain by marine mudstones of the Lola Formation of Oxfordian to Kimmeridgian age (Andsbjerg 2003).

Palaeogeography

The northern part of the Danish Central Graben was characterised by an extensive coastal plain and shallow marine environments during deposition of the lower and middle part of the Bryne Formation in the Aalenian – Late Bathonian (Andsbjerg 2003). During periods of low base level, laterally migrating meandering rivers dominated sediment deposition, whereas periods of high base level resulted in distal floodplain, lake and lacustrine delta sedimentation with occasional marine influence (Andsbjerg 2003; Husmo *et al.* 2002). During deposition of the upper Bryne Formation in the late Bathonian – earliest Callovian, estuarine and tidally influenced river sediments were deposited in major incised valleys (Andsbjerg 2003). Schwartz *et al.* (2007) showed the existence in the Danish Central Graben of meandering rivers separated by large overbank areas with coal formation during deposition of Middle Jurassic sediments (Bryne Formation?). The meandering rivers were running in southerly directions, but unfortunately Schwartz *et al.* (2007) did not propose in which part of the Central Graben river deposition took place. Andsbjerg (2003) found that rivers in the northern part of the Central Graben were running in easterly and northerly directions.

The palaeogeography of the southern part of the Danish Central Graben is less well known, however, Michelsen *et al.* (2003) found that the lower part of the Middle Jurassic succession (Bryne Formation) is characterised by thick sandy deposits interbedded with silt- and claystones and occasional coal beds. Sedimentation took place on a coastal plain during strong fluvial influence.

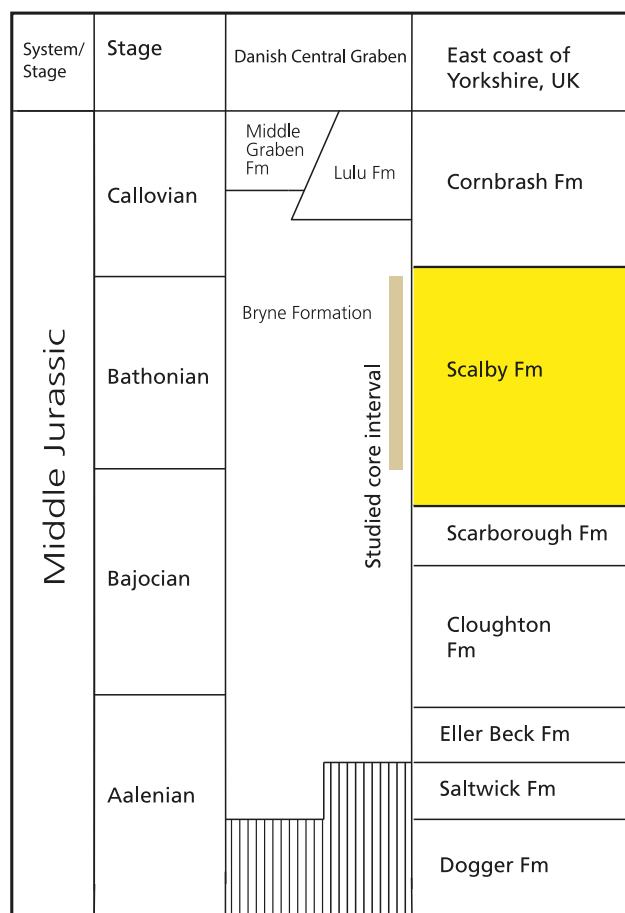


Fig. 3. Middle Jurassic stratigraphy of the Danish Central Graben (Andsbjerg 2003). For comparison, the stratigraphy of the Middle Jurassic deposits on the east coast of Yorkshire (UK) is also shown. After Ielpi & Ghinassi (2014).

Climate model experiments by Sellwood & Valdes (2006) and geological studies in the Yorkshire Basin by Morgans *et al.* (1999) indicate that the North Sea Region had a temperate, winter-wet climate during the Middle Jurassic. The presence of coal in the Middle Jurassic fluvial successions of the North Sea, including the deposits in the investigated cores, indicates mire formation under a relatively high and permanent water table (Petersen *et al.* 1998).

Data set and methodology

Internal reports and geophysical data

Maersk Oil and the Geological Survey of Denmark and Greenland (GEUS) prepared a suite of internal reports on the Alma Field that were made available for this study. The used reports are Final Well Reports Alma-1X (Maersk Oil 1991a) and Final Well Report Alma-2X (Maersk Oil 1993a), Core photos Alma-1X (Maersk Oil 1991b) and Core photos Alma-2X (Maersk Oil 1993b), Alma-1X Central Trough palynofacies (DGU 1991) and Alma-2X Central Trough palynofacies (DGU 1993) and Palynostratigraphy of the Jurassic Intervals from wells Alma-1X and Alma-2X, Danish North Sea (Maersk Oil 1999).

Maersk Oil provided a 3D seismic cube covering the Alma Field in Petrel version 2013.5. The Petrel dataset also contained petrophysical data in the form of wireline logs from the two Alma wells (Fig. 4). In this study the geophysical data is used to illustrate the structural setting of the Alma Field. Detailed interpretation of the seismic data and wireline logs are not included.

Core data

The Middle Jurassic cored intervals of Alma-1X have a core diameter of 5 cm. This core was drilled at a nearly vertical angle, with a to 1–2° offset from vertical (Fig. 4). The structural dip at the Alma-1X core site is around 1° in the same direction as the offset of the well; as a result the dip of horizontally deposited strata in the core can be neglected. The Alma-2X core sections were drilled with a diameter of 9.5 cm, and the well was oblique with a vertical offset angle of 33°–35° (Fig. 4). The structural dip at this site is around 20°, and horizontally deposited strata in the core would have a dip around 36°. This is in agreement with core observations, see later.

The Bryne Formation is represented by an interval of 117 m in the Alma-1X well (11816 to 12202 feet measured depth) and an interval of 219 m in the Alma-2X well (13657 to 14377 feet measured depth). In Alma-1X, 73.9 m (measured) of the formation was covered by

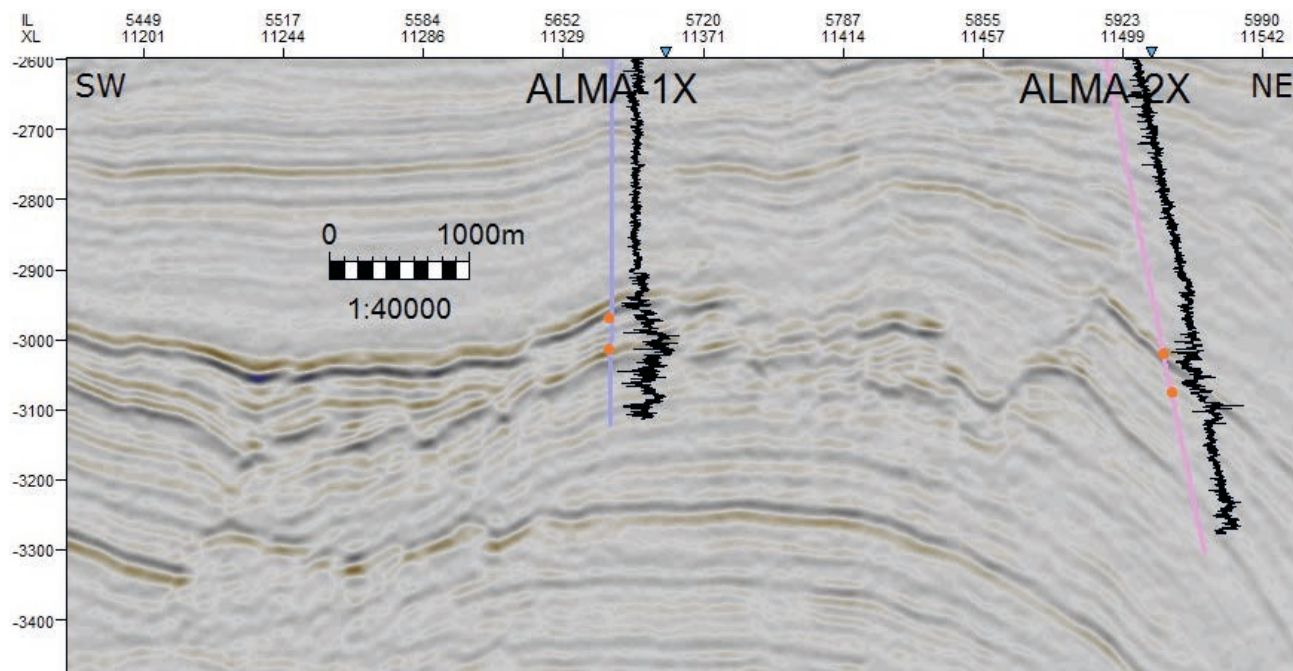


Fig. 4. Seismic overview of the two Alma wells. The studied interval in the Middle Jurassic section is delimited by the orange dots at the top and bottom of the interval. The vertical seismic resolution in the Middle Jurassic interval is calculated to be 12.5–30 m. Alma-1X is drilled vertically in an area where the Jurassic strata dip weakly SW, while the deviated Alma-2X penetrates Jurassic strata which dip relatively steeply NE. Along the wells their respective gamma ray tracks are shown. 3D seismic data set provided by Maersk Oil.

four core sections with a combined thickness of 35.4 m, and in Alma-2X 109.9 m (measured) of the formation was covered by eight core sections with a combined thickness of 60.8 m. Detailed sedimentological logs, at scale 1:10, were measured in the cored intervals of the Bryne Formation in the two wells. The narrow width of the Alma-1X core and the frequent occurrence of broken-up sections (rubble) caused some difficulties with regard to facies description and interpretation. The wider and more coherent core sections of Alma-2X made facies description and interpretation easier to carry out (Fig. 5). The logs were checked against the cores three months after the first visit to control that all details were shown correctly.

Field data

To supplement the sedimentological observations of

the Alma cores and to obtain perspective on the architecture and relations of the fluvial facies elements, an analogue outcrop study was undertaken in northern Yorkshire, England. Field investigations focused on the Middle Jurassic Long Nab Member of the Scalby Formation, which is well exposed in cliff sections and contains a succession of meandering river channel, channel margin and floodplain deposits (Ielpi & Ghinassi 2014). The collected field data was used to evaluate the facies model developed for the Alma Field and to illustrate some of the challenges related to facies description and interpretation on core material. Results from the field study are briefly presented after the description of the Alma cores. However, observations from the field study are used as comparative data in the interpretation of the sedimentary facies in the Alma cores.



Fig. 5. Overview of representative core parts. Left: Alma-1X. Right: Alma-2X. The core quality of Alma-1X is considered moderate to good while the general quality of Alma-2X is considered to vary from good to very good due to the larger core diameter and more coherent cores. Alma-2X is not vertical, which results in the steep apparent dip of the strata (Fig. 4). Photographs by Maersk Oil. Scale in feet. Core parts shown are for Alma-1X: 11900'00''–11979'04'' (core 2), and for Alma-2X: 13830'02''–13841'07'' (core 2).

Facies description and interpretation

The genetic facies classification scheme used here builds on the widely used classifications by Reineck & Singh (1973) and Miall (1996) as well as on the descriptions of fluvial meandering river deposits by Ghinassi & Ielpi (2015). Three meandering river facies associations are recognised: *channel deposits* include channel thalweg and point bar facies, *channel margin deposits* include crevasse channel and crevasse splay facies, and *floodplain deposits* include overbank and backswamp facies.

The recognised facies are given as occurrence, percentage and thickness for each core (Fig. 6). The deposits, and in particular the sandstones, are tightly cemented, rarely calcareous, occasionally micromicaceous. Grains are subangular, sorting is moderate and visible porosity is poor to very poor (Maersk Oil 1991a; 1993a).

Channel deposits

Channel thalweg deposits

Description. This facies represents the most coarse-grained deposits in the two Alma cores. The sediment is composed of sand, granules and pebbles and is either a clast-rich sandstone or a conglomerate, commonly with intraformational coal and clay clasts and more rarely extraformational clasts (Fig. 7). The intraformational clasts are angular and range from a few millimetres to a few centimetres in length, while the extraformational clasts are relatively well rounded, typically of quartz, and of granule to pebble size. The channel thalweg conglomerate matrix is fine- and medium-grained sand with a light grey colour, while the intraformational clasts are dark grey and black. The sediments exhibit low-angle stratification in some cases, but are generally structureless with a random orientation of the intraformational clasts. The channel

thalweg facies has an erosive and sometimes down-cutting base to the underlying sediments.

In Alma-1X the channel thalweg facies is represented by six intervals ranging between 0.05 and 0.25 m in thickness and comprises 2% of all facies. In Alma-2X the facies is represented by 16 intervals with thicknesses between 0.03 and 1.60 m (the thicker deposits are gradational into overlying point-bar deposits with numerous intraformational clasts) and constitutes 11% of all facies in this core (Fig. 6).

Interpretation. The channel thalweg deposits of the Alma cores closely resemble the intraformational conglomerate facies of Andsbjerg (2003); these sediments formed at the base of meandering river channel fills in the Bryne Formation in the northern part of the Danish Central Graben. They also share many characteristics with intraformational conglomerates seen at the base of point bar elements in the Scalby Formation (Ielpi & Ghinasi 2014 and own observations, see later). The lack of extraformational clasts in most conglomerates indicates limited supply from distant sites (hinterland), and the lithology of the intraformational clasts shows erosion of channel margin and floodplain deposits (Bridge & Jarvis 1982; Miall 1996).

Point bar deposits

Description. The lower and main parts of the sediments of this facies are primarily composed of fine- and medium-grained sandstones of brown, yellow or grey colour, but in their upper intervals the sandstones may grade into muddy sandstones or true heterolithic deposits (Figs 8, 9). The facies shows a variety of structures, including planar lamination, small-scale (ripple) cross-lamination, irregular lamination, root structures, deformation structures, microbrecciation and coal fragments or flakes. In the heterolithic intervals wavy lamination is present with some of the laminations being outlined by coal flakes. In some of the upper point bar units, mottling, iron staining

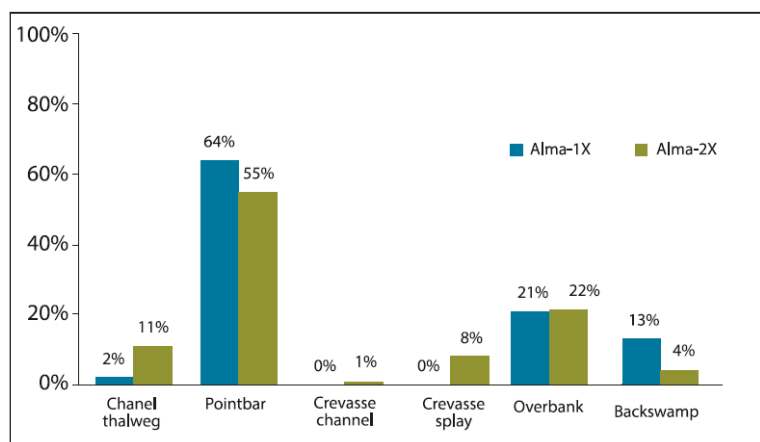


Fig. 6. Distribution in percentages of the sedimentary facies in the two sediment cores Alma-1X and Alma-2X. The percentages represent the accumulated thickness of each facies in the cored Middle Jurassic sections.

and rootlets are observed. The deposits are typically underlain by channel thalweg and overlain by flood-plain deposits.

In Alma-1X such sandstones are represented by six intervals ranging in thickness from 0.4 to 3.85 m and constituting 64 % of the sediments. In Alma-2X there are 21 intervals with point bar deposits, which are 0.10–6.05 m thick and comprise 55 % of all facies. The facies forms part of channel units, which are usually initiated by channel thalweg deposits. In some cases, the sandstones are amalgamated and individual sandstone units may be as thin as 0.1 m.

Point bar strata in Alma-1X have dips between 0° and 20° with the majority around 10°–15°, while the point bar strata in Alma-2X dip between 10° and 60° with the majority around 20° and 45°.

Interpretation. The point bar deposits in the Alma cores can be compared with point bar deposits of the Scalby Formation (Ielpi & Ghinassi 2014 and own observations, see later). Point bar deposits typically display both large-scale and small-scale cross-stratification (Miall 1985, 1996, 2014). Such structures are also observed in the Scalby Formation (Ielpi & Ghinassi

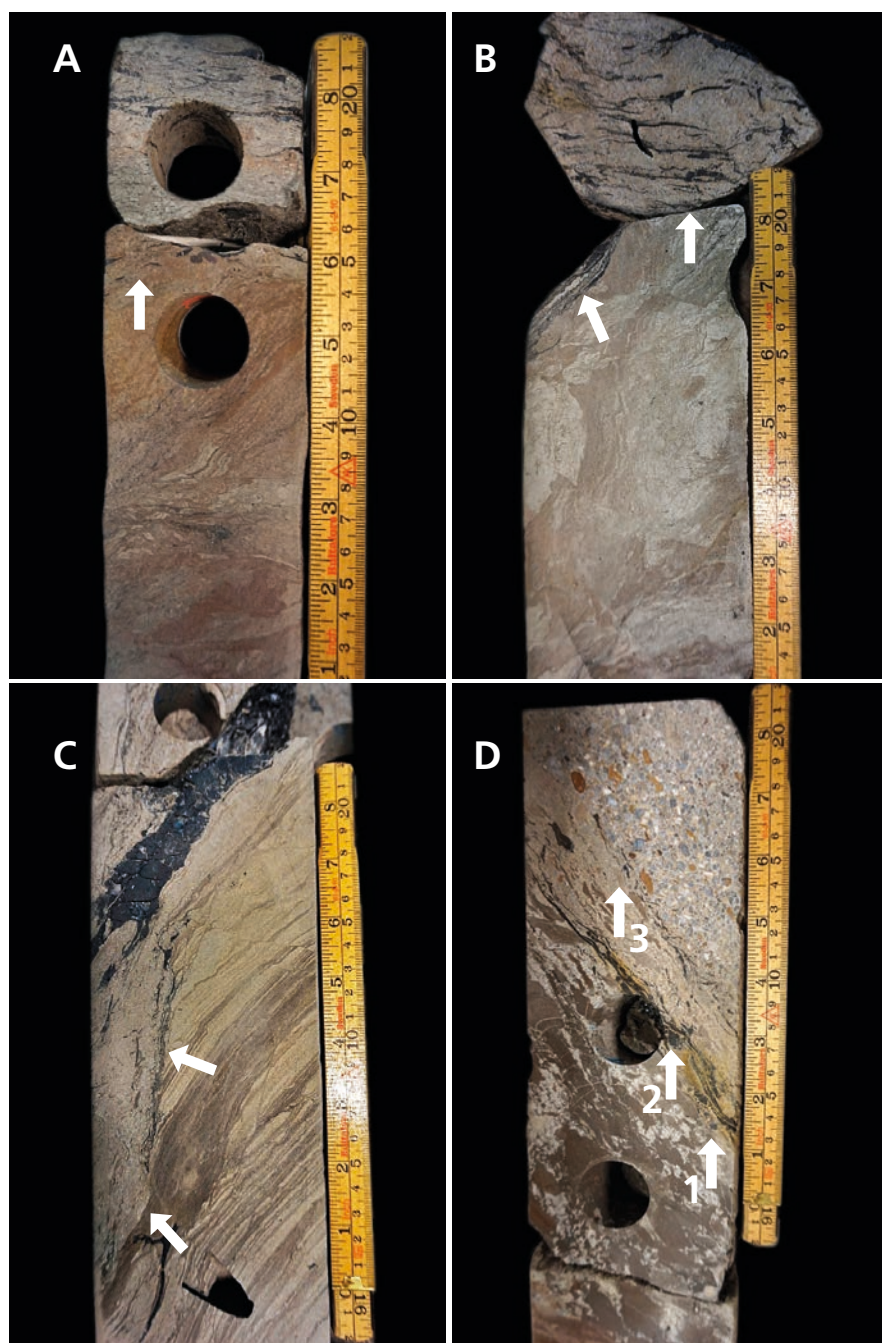


Fig. 7. Channel thalweg facies of the Alma cores. The arrows indicate the lower boundary of the channel thalweg deposit. **A:** Alma-1X, core 2/5, box 1. The channel thalweg deposit is composed of medium-grained sand with intraformational mud and coal clasts. The channel thalweg sediment overlies deformed point bar deposits with a sharp boundary. **B:** Alma-2X, core 2/9, box 15. The channel thalweg deposit is composed of medium-grained sand with intraformational coal and mud clasts. The channel base has an undulatory and sharp boundary to the underlying point bar deposits that are severely deformed. **C:** Alma-2X, core 2/9, box 2. The channel base is outlined by a down-cutting boundary to underlying point bar sands. The channel thalweg deposit is composed of medium-grained sand with small mud and coal clasts as well as one large coal clast. The point bar strata dip 40°, which is a sum of an oblique angle of the core (30–35°) and a morphological dip of the point bar of 5–10°. **D:** Alma-2X, core 7/9, box 10. The channel thalweg facies is developed as a composite deposit. An early phase of erosion (arrow 1) is overlain by medium-grained sand with extraformational clasts of granule size. Phase 2 (indicated by arrow 2) is composed of medium-grained sand with intraformational mud and coal clasts, while phase 3 (indicated by arrow 3) is composed of medium-grained sand with extraformational clasts of granule and pebble size. The composite channel thalweg deposits overlie dipping point bar strata. The ruler shows both centimetres and inches.

2014). The apparent lack of large-scale cross-bedding in the Alma point bar deposits is therefore surprising, as is the scarcity of small-scale cross-lamination. However, due to the limited dimension of the cores, large-scale cross-bedding may be hard to identify and therefore may actually be present in the Alma point bar deposits.

Fining-upward patterns occur (two examples in Alma-1X and seven in Alma-2X), as expected (Miall 1996). However, less systematic grain-size patterns are also observed and could be related to sections on upstream parts of the point bar where the flow

is not fully developed (Jackson 1976). Deposits from upstream parts of the point bar elements in the Scalby Formation also display poor fining-upward trends (Ielpi & Ghinassi 2014). Some of the thinnest sandstones may represent either point bar or crevasse sediments, which are similar in lithology and structures. The sequential setting of the sandstones is used here to interpret their depositional environment. Amalgamation of the point bar deposits could indicate channel migration (or avulsion) and later reoccupation of the site by a new river course. However, observations in the Scalby Formation (see later)



Fig. 8. Point bar facies from Alma-2X. The apparent opposite dips of the cores depend on which half of the core is seen. **A:** core 1/9, box 4. Fine-grained sand with scattered small coal flakes. The apparent dip of 15° is less than expected but could be related to a point bar surface dipping in the opposite direction of the 30–35° dip of the core. **B:** core 2/9, box 3. Fine-grained point bar sandstone with a large fragment of coalified wood. The sediment has an apparent dip of 45° which may correspond to a morphological dip of ~10°. **C:** core 6/9, box 7. Point bar deposit of fine-grained sandstone with darker streaks of silt. Microbrecciation including microfaults occur in the lower part of the core (arrows). The sediment has a low apparent dip. **D:** core 2/9, box 7. Point bar deposit of fine-grained sand with drapes of silty material. The core interval has an apparent dip of ~40°, slightly more than the dip of the core.

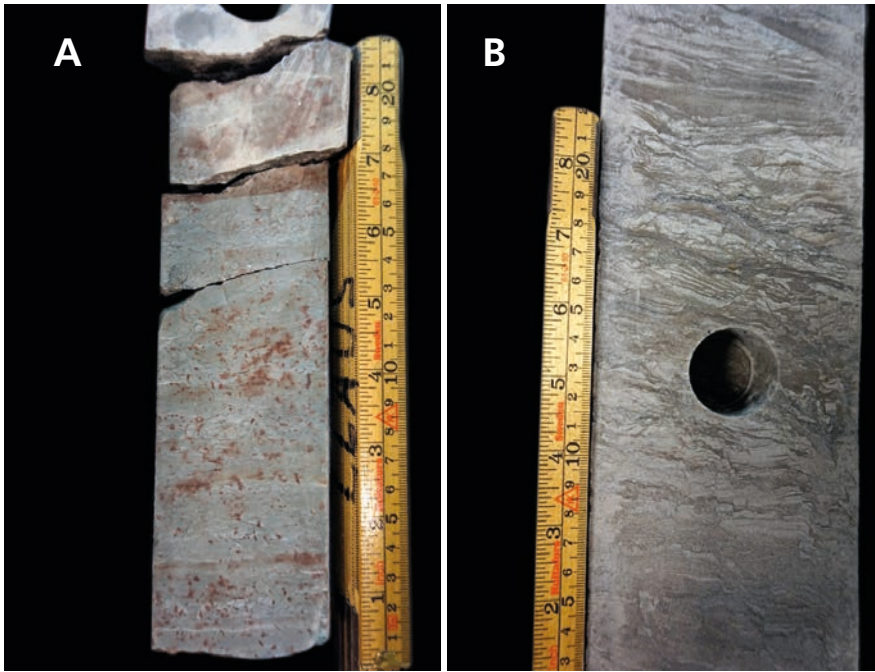


Fig. 9. Upper point bar deposits. **A:** Alma-1X, core 4/5, box 7. Upper point bar deposit composed of muddy and fine-grained sand with small dark root structures and red-brown spots of iron-enriched material. The apparent dip of the strata is 3° which is close to the morphological dip. **B:** Alma-2X, Core 6/9, box 7. Heterolithic upper point bar deposit with even and wavy lamination overprinted by mottling and microbrecciation. The measured dip of the strata is around 10° .

suggest the deposition could have taken place in only one channel during dynamic interfingering of point bar and channel thalweg deposits due to variations in flow strength and channel width with time.

Point bar sandstones in the cores (particularly Alma-2X) are not always recognised as clean sandstones but can contain various amounts of clay or silt, making them muddy sandstones, siltstones or true (inclined) heterolithic strata (Thomas *et al.* 1987). These deposits typically occur at the top of the point bar units but are also locally preserved as thin intervals in the lower or middle parts of the point bar deposits. A possible cause for the heterolithic nature of the upper point bars could be tidal influence (Pearson & Gingras 2006). However, the somewhat unsystematic nature of the heterolithic strata and the scarcity of bioturbation seem to indicate that there is another cause for the heterolithic strata. This could be fluctuating discharge of a mixed and suspension-rich river, causing alternating deposition of sand and mud on the upper point bar (Thomas *et al.* 1987), or the heterolithic sediments could represent 'swale' deposits formed between scroll bars in the transition zone between the point bar and the channel margin, as observed in the Scalby Formation (Ielpi & Ghinassi 2014 and own observations, see later). However, sandy scroll bar deposits have not been identified with certainty in the Alma cores. The mud-rich to heterolithic intervals observed in some point bar deposits may also represent counter point bar deposits, i.e. sediments formed on the distal-most part of the point bar; such sediments are typically dominated by silt and can form

inclined heterolithic strata (Smith *et al.* 2009). From the available core data we cannot evaluate which of the mentioned interpretations is the most likely, and therefore classify all sediments here as upper point bar deposits for the sake of simplicity.

The limited lateral extent of the cores makes it impossible to identify lateral accretion structures. In the Alma-1X core, floodplain deposits typically have dips between 0° and 5° , while presumed point bar deposits dip between 0° and 20° . In the Alma-2X core, floodplain deposits have dips between 30° and 35° , while presumed point bar deposits may dip as much as 60° or as little as 10° , although the majority of these sediment have less extreme dips centered either around 20° or around 45° . The additional dip shown by the point bar deposits probably represents a natural dip formed by deposition on a point bar slope. As we do not know how the cores were slabbled with respect to the original bedding, we cannot calculate exact dips of the Alma point bar deposits, although it seems that most had dips between 5° and 10° . In the Scalby Formation, point bar deposits typically have dips between 5° and 15° and can occasionally reach 20° (Ielpi & Ghinassi 2014 and own observations, see later).

Channel margin deposits

Crevasse channel deposits

Description. These deposits are composed of fine to medium-grained sandstone with intraformational clay and coal clasts near the base. There is a clear ero-

sive lower boundary and a fining-upward trend. The deposits display small-scale (ripple) cross-lamination at the base, are structureless/mottled, and show a large-scale deformation structure at the top. The facies only occurs once in Alma-2X where the deposit is 0.4 m thick and comprises 1% of all facies (Fig. 6). The channel deposit is both over- and underlain by overbank deposits.

Interpretation. Deposits similar to this facies are recognised as crevasse channel deposits in the Scalby Formation (Mjøs *et al.* 1993; Ielpi & Ghinassi 2014 and own observations, see later). Intraformational clasts, however, seem to be rare or absent at the base of the deposits, but mudstone clasts and coal fragments are common features of other Middle Jurassic crevasse deposits (Andsbjerg 2003). The crevasse channel deposits in the Alma field probably formed as the flood water broke through a levee during peak discharge. The erosive base and presence of intraformational clasts indicate relatively strong currents during deposition of the crevasse channel sediments (Miall 1996).

Crevasse splay deposits

Description. Deposits of this facies are also composed of fine- and medium grained sandstone; they are distinguished from point bar deposits and crevasse channel deposits by their lack of basal conglomerates and close association with floodplain sediments. The sediment has an irregular lamination and is frequently mottled and microbrecciated and may also contain root structures. The deposits have an even and sharp boundary to underlying sediments and a sharp to gradational upper boundary except where overlain erosively by thalweg deposits. They are typically interbedded with overbank deposits.

In Alma-2X this facies is represented by eight intervals ranging in thickness from 0.3 to 0.9 m and comprising 8% of all facies in Alma-2X; thicker units may be amalgamated. In Alma-1X there are no observed crevasse splay deposits (Fig 6).

Interpretation. These deposits of the Alma-2X core closely resemble crevasse splay deposits of the Scalby Formation (Mjøs *et al.* 1993; Ielpi & Ghinassi 2014 and own observations, see later). The crevasse splay sandstones in the Alma-2X core were probably deposited at the edge of crevasse channels as lobes and sheets under relatively high energy that could transport fine- to medium- grained sand across a mud-rich floodplain. Root structures and mottling indicate a break in sedimentation after the formation of the crevasse splay and that the surface of the sand was colonised by vegetation (Mjøs *et al.* 1993; Miall 1996; Ielpi & Ghinassi 2014).

Floodplain deposits

Overbank deposits

Description. This facies is defined to comprise all non-organic claystones, siltstones and some heterolithic deposits. The claystones are structureless and frequently show mottling, while the siltstones and heteroliths are structureless, laminated and wavy-bedded. Microbrecciation, root structures and deformation structures are common in all overbank deposits. The deposits occasionally contain millimetre-sized coal flakes. The colours are grey, yellow, brown and dark grey. Black carbonaceous mudstones are treated in the paragraph on backswamp deposits. The overbank deposits are found over- and underlying both channel margin and channel deposits.

Overbank sediments occur in five intervals in Alma-1X and 15 intervals in Alma-2X. The units are 0.1 to 2.60 m thick in Alma-1X and 0.05 to 2.70 m thick in Alma-2X. The facies constitutes 22 % of the succession in Alma-2X and 21% in Alma-1X (Fig. 6).

Interpretation. Deposits of this facies closely resemble the floodplain fines and lake fills of the Scalby Formation (Ielpi & Ghinassi 2014 and own observations, see later). The deposits also share similarities with the disturbed silty mudstones of the vegetated floodplain facies association in the Middle Jurassic Bryne Formation in the Danish North Sea (Andsbjerg 2003). The geometry of the overbank facies cannot be assessed in the sedimentary cores, and thus the facies could represent abandoned meander channels (oxbow lakes). Deposition took place during periods of overbank flooding from slowly streaming or nearly stagnant water. Mottling may indicate periods of higher biological activity.

Backswamp deposits

Description. This facies of the Alma cores comprises dark grey carbonaceous mudstones and coherent black coal beds, with a gradational transition into dark-grey overbank mudstones. The mudstone is structureless but locally contains scattered root structures and millimetre-sized coal flakes. In Alma-2X these deposits are overlain by point bar deposits and crevasse splay and channel sandstones, while they overlie point bar heteroliths, overbank sediments and point bar sandstones. The transitions are characterised by sharp and even boundaries except in one case where a crevasse channel cuts erosively down into the carbonaceous mudstone. In Alma-1X the deposits are over- and underlain by point bar sandstones and heteroliths all characterised by sharp transitions.

The backswamp deposits occur in five intervals in Alma-2X where they are 0.1 to 1.10 m thick. In Alma-1X

there are two intervals 1.20 and 1.50 m thick. In Alma-1X backswamp deposits comprise a total of 13% while they constitute 4% of the total facies in Alma-2X (Fig 6).

Interpretation. This facies shows many similarities to the organic-rich floodplain fines and lake fills of the Scalby Formation (Ielpi & Ghinasi 2014 and own observations, see later), and also shares many characteristics with the organic-rich laminated mudstones of the vegetated floodplain facies association of the Middle Jurassic Bryne Formation in the Danish North Sea (Andsbjerg 2003). Backswamp sediments in the Alma cores were deposited in the floodplain area from organic and terrigenous material. The majority of the backswamp areas probably developed as lake swamp environments with possible algae blooms, while others were increasingly vegetated and eventually became overgrown, resulting in peat/coal formation. Palynological studies of eight samples of floodplain

sediments in Alma-1X revealed that they primarily formed in lake and swamp environments without marine influence. A few samples from Alma-2X contain broken/rare dinoflagellate cysts (DGU 1991, 1993). These marine dinoflagellate cysts could indicate sporadic connection to the sea or rare episodes of marine inundation during storm floods (Goslin & Clemmensen 2017).

Shoreline sandstones

Overlying the fluvial deposits (after a long non-cored section) of Alma-1X is an 8 m thick, fine- to medium-grained, light grey and yellow, structureless sandstone. This is difficult to interpret due to a complete lack of sedimentary structures; it is tentatively interpreted to represent a beach and/or shoreface environment that may record a general transgression of the area in the Callovian (Andsbjerg 2003).

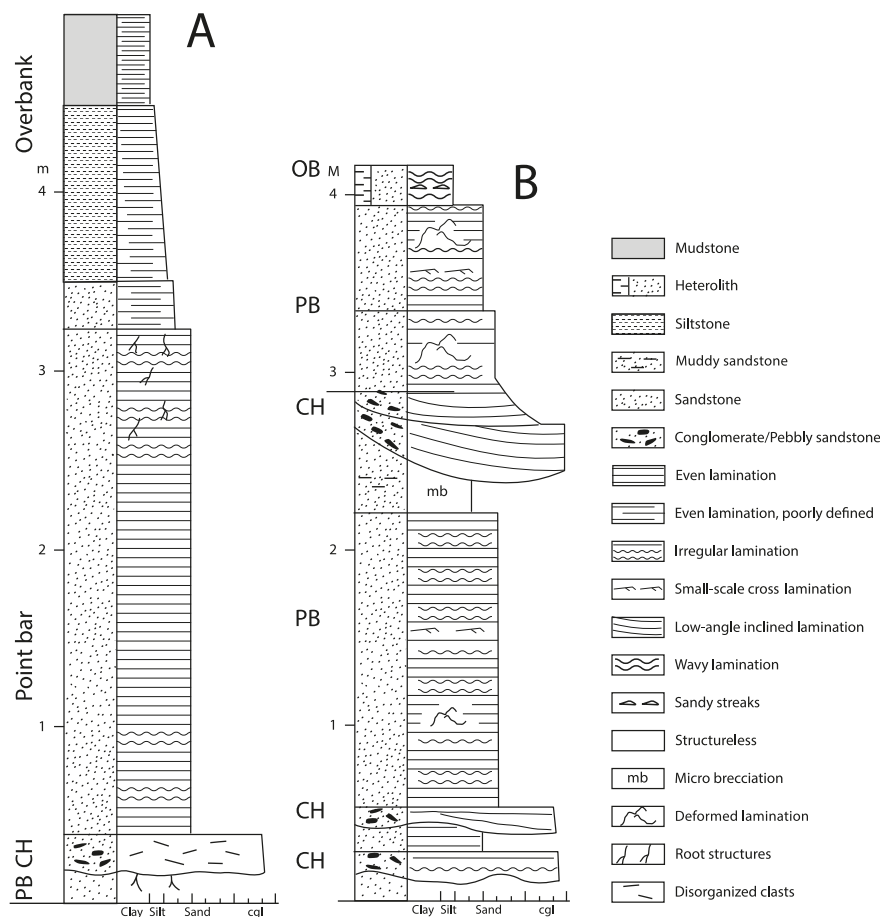


Fig. 10. A: Sedimentological log of a fully developed channel succession overlain by floodplain (overbank and backswamp) deposits. The contact between point bar sandstone and overbank fines is placed at the base of the siltstone. Note the dominance of even and irregular lamination in the point bar sandstones, and the apparent lack of large- and small-scale cross stratification. The apparent dip of the point bar deposits is between 0° and 10° (not shown on log). The log is based on core material from Alma-1X, core 3/5 in box 7–12. **B:** Sedimentological log of two channel successions. The lowermost channel succession (0–2.5 m) is characterised by a double channel thalweg conglomerate overlain by point bar sandstones. The repeated occurrence of channel thalweg conglomerates at the base of the succession may indicate two episodes of channel expansion separated by a period of channel contraction in line with observations from the Scalby Formation (Fig. 14). The overlying channel succession has one basal channel conglomerate overlain by point bar sandstones. Note the fining-upward pattern of both successions, the existence of ripple cross lamination in both successions, and low-angle large-scale cross bedding in the channel conglomerate of the upper succession. The apparent dip of the point bar deposits is between 30° and 40°. The log is based on core material from Alma-2X, core 2/9 in box 1–6.

successions, the existence of ripple cross lamination in both successions, and low-angle large-scale cross bedding in the channel conglomerate of the upper succession. The apparent dip of the point bar deposits is between 30° and 40°. The log is based on core material from Alma-2X, core 2/9 in box 1–6.

Alma-1X

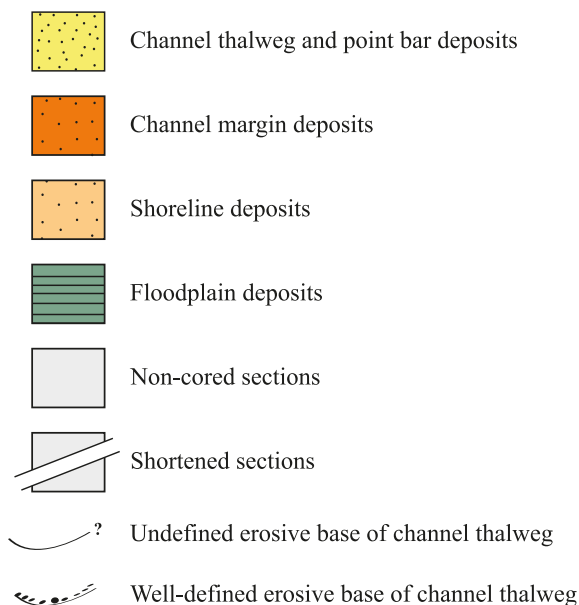
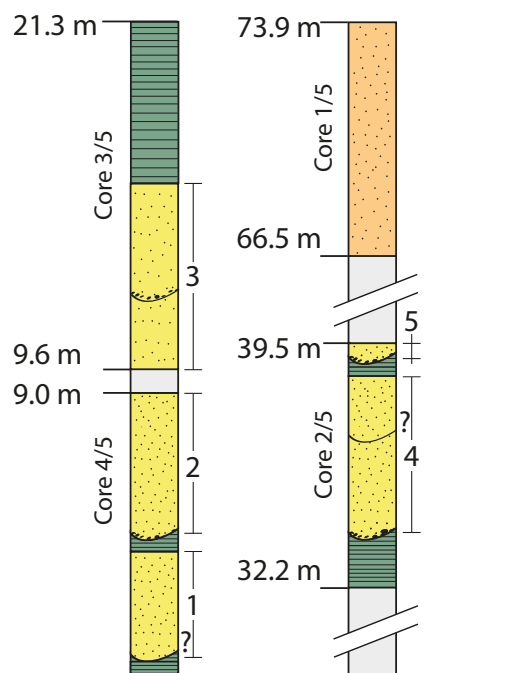


Fig. 11. Simplified sedimentological log of the investigated interval of the Alma-1X core, compiled from the original 1:10 logs. The log provides an overview of the facies with a focus on the channel deposits (channel thalweg and overlying point bar facies). Amalgamated channel deposits are grouped into sand units 1–5 which are considered to be the major reservoir units. Metres shown on the logs are measured from the base of the investigated interval upwards. Core sections are given as e.g. core 3/5. There is probably a stratigraphic break between the fluvial deposits (Bathonian) and the overlying shoreline sandstones (Upper Callovian).

Fluvial facies successions and depositional model

Channel deposits (channel thalweg and point bar sediments) form erosively bounded successions of sand-rich intervals. The channel successions are typically overlain by overbank deposits of varying thickness. Seven channel successions ranging in thickness from 0.25 to 4.35 m are recognised in Alma-1X, and fifteen individual channel successions are defined in Alma-2X ranging in thickness from 0.6 to 6.55 m. Two of the channel successions in Alma-1X and seven in Alma-2X show a well-defined fining-upward pattern (Fig. 10), while the remaining successions do not display any systematic grain-size trend. Based on the facies description and interpretation, and characteristics of the facies successions, a depositional model for the sediments in both cores is proposed.

Alma-2X

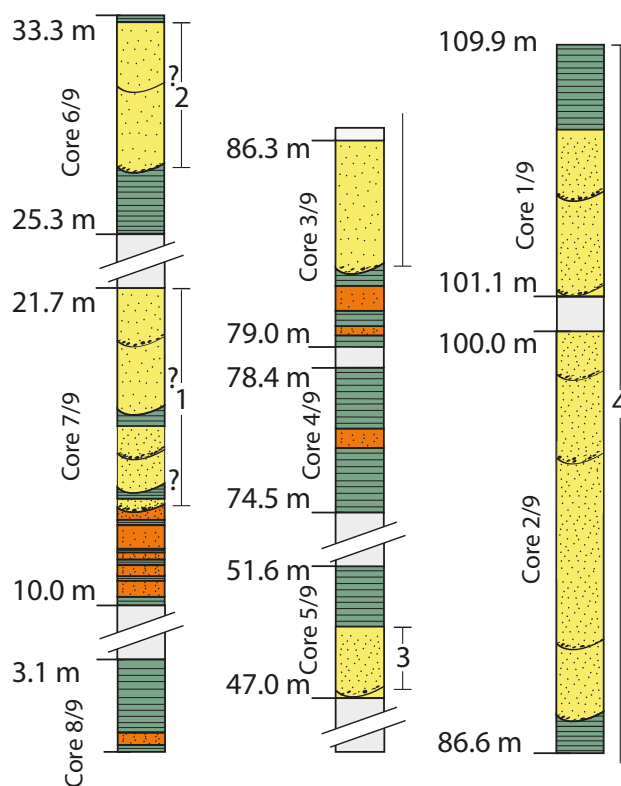


Fig. 12. Simplified sedimentological log of the investigated interval of the Alma-2X core, compiled from the original 1:10 logs. The log provides an overview of the facies with a focus on the channel deposits (channel thalweg and overlying point bar facies). Amalgamated channel deposits are grouped into sand units 1–4 which are thought to represent major reservoir units. Metres shown on the logs are measured from the base of the investigated interval upwards. Core sections are given.

The repeated presence of eroded surfaces overlain by channel thalweg, point bar, channel margin and/or floodplain deposits, in some cases observed with a fining-upward pattern, strongly suggests deposition in a meandering stream environment by autogenic processes, in agreement with the classical model for such deposits first proposed by Bernard *et al.* (1962) and Allen (1963). An alternative interpretation of deposition in a braided river system is considered less likely because of the close association with common, relatively thick floodplain facies. Compared to idealised fluvial successions from meandering streams, the observed sequences most likely formed by deposition in a sand-rich, mixed-load meandering river, corresponding to model 6 of Miall (1985). The presence of mud-rich intervals in some point bar units is intriguing but may simply indicate markedly fluctuating discharge in a mixed-load river (Thomas *et al.* 1987). The relatively frequent occurrence of floodplain and channel margin (crevasse sand) sediments suggests either relatively high rates of subsidence or frequent avulsion (Miall 1996, 2014). The balance between mud-rich floodplain deposits and more sand-rich channel deposits fluctuates over time, indicating changing avulsion rate, changing rates of subsidence, changing sediment supply or a variation of all three elements over time (Bridge & Leeder 1979).

Long-term stacking patterns

Based on the facies and facies associations recognised in the Alma-1X and Alma-2X cores, the long-term stacking pattern of the deposits is shown in Figs 11 and 12. In Alma-1X, core 4/5 is dominated by channel deposits interbedded with thin overbank units. Core 3/5 has a general fining-upward trend changing abruptly from channel deposits into floodplain deposits. Core 2/5 shows a coarsening-upward trend from floodplain into dominantly channel deposits. Finally, core 1/5 is exclusively composed of presumed shoreline deposits that were only briefly considered for this study.

In Alma-2X, core 8/9 has one thin channel margin unit at the base and is otherwise composed of floodplain sediments. Core 7/9 shows a transition from floodplain and channel margin deposits into channel deposits with subordinate floodplain interbeds. Core 6/9 shows a well-developed coarsening-upward trend from floodplain into channel deposits. Core 5/9 illustrates a change from channel to floodplain deposits. Core 4/9 is composed of floodplain deposits with a single channel margin unit. Core 3/9 has a coarsening-upward pattern with floodplain and channel margin deposits at the base, overlain by channel deposits. Core 2/9 is an alternation between floodplain and channel deposits. Finally, core 1/9 is composed of interbedded

channel sands and floodplain deposits with a single channel margin unit.

Due to the near-amalgamated nature of some of the channel successions, they have been divided into five channel groups (sand units) in Alma-1X and four channel groups (sand units) in Alma-2X (Figs 11, 12). This division has been made in order to define suitable reservoir units.

The Scalby Formation: an analogue outcrop study

The Middle Jurassic (Bathonian) Scalby Formation is situated in the Cleveland Basin, North Yorkshire. The Scalby Formation is a fining-upward succession that unconformably overlies the marine Scarborough Formation and can be subdivided into the lower Moor Grit Member of fluvial (meandering river) channel and point bar sandstones and the upper Long Nab Member of floodplain–paralic mudrocks and subordinate fluvial sandstones. The untilted fluvial deposits occur along an outcrop belt (vertical coastal cliffs and horizontal tidal platforms) for approximately 4 km which makes the study of the ancient point-bar deposits and the overall fluvial geomorphological architecture particularly favourable (Ghinassi & Ielpi 2015).

The facies classification developed for the Alma cores is also used to describe the meandering river deposits observed in the Long Nab Member of the Scalby Formation. The Long Nab Member comprises the same three facies associations as the Alma cores: *channel deposits* including channel thalweg and point bar facies, and in addition chute bar, scroll bar and oxbow lake facies; *channel margin deposits* including crevasse channel, crevasse splay and levee facies; and *floodplain deposits* including overbank and backswamp facies.

As point bar and associated channel thalweg deposits are considered the most characteristic facies of ancient meandering river deposits (Miall 1985, 1996, 2014), we only describe these two facies from the Scalby Formation. Additional facies comprising channel margin and floodplain deposits are described briefly. We investigated primarily the cliff exposures of the Long Nab Member, while Ielpi & Ghinassi (2014) made most of their observations in the tidal platform exposures of the Mor Grit Member.

Channel thalweg deposits

This facies is typically an intraformational conglomerate or a sandstone with scattered intraformational clasts including mud and coal fragments of overbank and backswamp origin. The conglomerates show all

transitions between clast-supported and matrix-supported deposits. The clasts are angular to subrounded, lie in a fine- to medium-grained sandstone matrix and have typical sizes between 0.01 and 0.05 m, but can be up to 0.1 m. The clasts are disorganised and display no size sorting. The contact to underlying sediments can be relatively sharp with an irregular outline. Observed from a distance the facies forms the base of the fluvial sandstone bodies. The thalweg facies deposits are typically overlain by point bar sandstones with accretion strata dipping at low angles. Laterally, channel thalweg deposits show intricate contacts with point bar sandstone varying from small-scale step-wise contacts to large-scale interfingering (see later). The deposits are 0.1 to 2.40 m thick, most frequently between 0.2 and 1 m.

Point bar deposits

The point bar deposits are composed of fine-grained or medium-grained sandstones with low-angle dipping lateral accretion surfaces; internally the sandstones show even lamination, small-scale cross lamination sometimes developed into climbing ripples, and less common large-scale cross-bedding. The point bar deposits may show fining-upward trends or be without clear change in grain size. The lateral accretion surfaces that define the point bar unit deposits have in most examples a dip of 5–15°. Measured point bar successions are between 0.3 and 3 m thick and typically have sharp and erosive or interfingering contacts with channel conglomerate at the base (see later). They are typically overlain by (or interfinger with) mud-rich floodplain deposits (see later).

Ielpi & Ghinassi (2014) found that point bar deposits comprise up to 45% of their planform exposures. They are formed of inclined bedsets with typical dips between 5° and 15° and occasionally reaching 20°. In vertical sections they appear as fining-upward sandstone units overlying a basal intraformational conglomerate. The sandstones are fine- to coarse-grained with scattered mud clasts or coal fragments; they are dominated in their central parts by interbedded ripple cross-laminated and wavy plane-parallel-laminated sediments associated with massive mudstones. Point bar top deposits are enriched in iron oxide and siderite (Ielpi & Ghinassi 2014).

Crevasse channel deposits

Crevasse channel deposits are composed of fine- to medium-grained sandstone with erosive bases, and there is an apparent lack of a basal conglomerate. The sandstone is structureless to evenly laminated. Observed from a distance the deposits possess an extensive sheet-like geometry with pinch and swell geometry. They are interbedded with floodplain de-

posits and are typically between 0.3 and 0.5 m thick; the thicker and truly channel-shaped parts of these sandstone bodies are around 5–10 m wide.

Crevasse splay deposits

Crevasse splay deposits are composed of fine-grained sandstone that is structureless or evenly laminated. The deposits have thicknesses between 0.1 and 0.3 m and are traceable for over 100 m; viewed from a distance they form sheet-like sandstone bodies. They are over- and underlain by dark grey floodplain deposits; their contacts to the underlying sediments are typically sharp.

Overbank deposits

These deposits are composed of siltstone, silty claystone and claystone with a varying amount of organic material and thereby colours from pale to dark grey. The mudrocks are 0.3 to 3 m thick and may stretch laterally for several hundreds of metres. Viewed from a distance they have a sheet-like geometry and alternate with the crevasse splay and crevasse channel sandstones. The overbank deposits are generally structureless but may exhibit signs of mottling and pedogenic overprints. There is a gradational transition from the overbank to the backswamp facies.

Backswamp deposits

The backswamp deposits include all organic-rich claystones and siltstones as well as carbonaceous mud and coalified wood. The high content of organic material gives the fine sediment particles of this facies a dark grey to black colour. *In situ* deposits of coal are not recognised in this facies although coal fragments, including large tree stumps, occur within other facies. The backswamp sediments are 0.05 to 0.5 m thick and may extend laterally for several hundreds of metres. The backswamp sediments are generally structureless but have some indication of pedogenic overprinting and mottling.

Facies geometry

The geometries of the channel thalweg and point bar facies (channel deposits) of The Long Nab Member are illustrated in some detail at two sites. At the first site the channel deposits form a 4–6 m thick sand sheet which can be traced laterally for at least 85 m. The central part of the sand sheet is cut by a lens-shaped unit composed of basal thalweg conglomerates overlain by point bar sandstones with lateral accretion surfaces (Fig. 13). Thus, the sand sheet is an amalgamated deposit formed by two or more episodes of channel construction (and migration) within the ancient meandering river channel belt. The lens-shaped sand unit

records the final phase of meandering river deposition at this site.

Another site demonstrates that one side of a channel system is well exposed, while the other side is poorly defined. The exposed side of the channel body is clearly lens-shaped and the channel fill displays an intricate interfingering of point bar sandstones and channel thalweg conglomerates (Fig. 14). The width of these interfingering channel deposits is around 15 m, and the deposits have a cumulative thickness of more than 3 m. This sedimentary architecture would

probably indicate alternating periods of expansion and contraction of the channel thalweg induced by discharge variations.

Some of the exposed channel deposits in the Scalby Formation grade laterally and upwards into floodplain deposits, and one mud-rich tongue is seen to split individual point bar sandstones (Fig. 14A). Such an architecture could explain the unexpected occurrence of some fine-grained intervals in the lower and middle part of some Alma point bar deposits.



Fig. 13. **A:** Overview and **B:** close-up of a channel unit in the Scalby Formation. The channel deposits form a sheet-like body of sandstone containing in its central part (with the person) a clear channel-shaped body. This locality thereby demonstrates the different size and morphology of a channel body and a channel belt body. Darker coloured floodplain deposits overlie the channel deposits. Note the gently dipping lateral accretion surfaces in the central channel body indicating channel and point bar migration to the north, and the cut bank just to the right of the person.

Discussion

Facies characterisation

Facies description and recognition in sedimentary cores is limited by core width and quality, and field investigations of the architecture and contacts of the fluvial facies of the Scalby Formation were important for the interpretation of the sedimentary cores. Particularly the observation of the interfingering nature of channel thalweg conglomerates and point bar sandstones is valuable, as it illustrates a vertical repetition of these two facies (Fig. 14B). Thus, the occurrence of channel thalweg deposits only separated by thin point bar deposits as illustrated in Fig. 10 could reflect deposition within the same channel system and thereby not represent erosion by a later channel system. The observed pattern is therefore interpreted to be caused by a dynamic interfingering of point bar and channel thalweg deposits due to variations in flow strength and channel width.

Channel and channel belt dimensions

Lateral migration of meandering rivers over time create channel belts (Fig. 15; Milliken *et al.* 2012). A major concern in the reconstruction of fluvial architecture in the subsurface is the size and width of the channel fill, as well as that of the channel belt sandstones. Gibling (2006) studied scaling relationships in ancient fluvial deposits, but more precise data on these relationships can be obtained from modern fluvial systems. Milliken *et al.* (2012) found statistical relationships between channel thickness, channel width and channel belt width in modern systems (Fig. 15). They divided meandering river systems into Low-Net End Members (mud-rich systems with highly aggradational stacking) and High-Net End Members (sand-rich systems with low aggradational stacking). These studies found that in the Low-Net End Member systems the channel belts are 20–50 times wider than the channel sandstone thickness, while in the High-Net End Member systems the channel belts are about

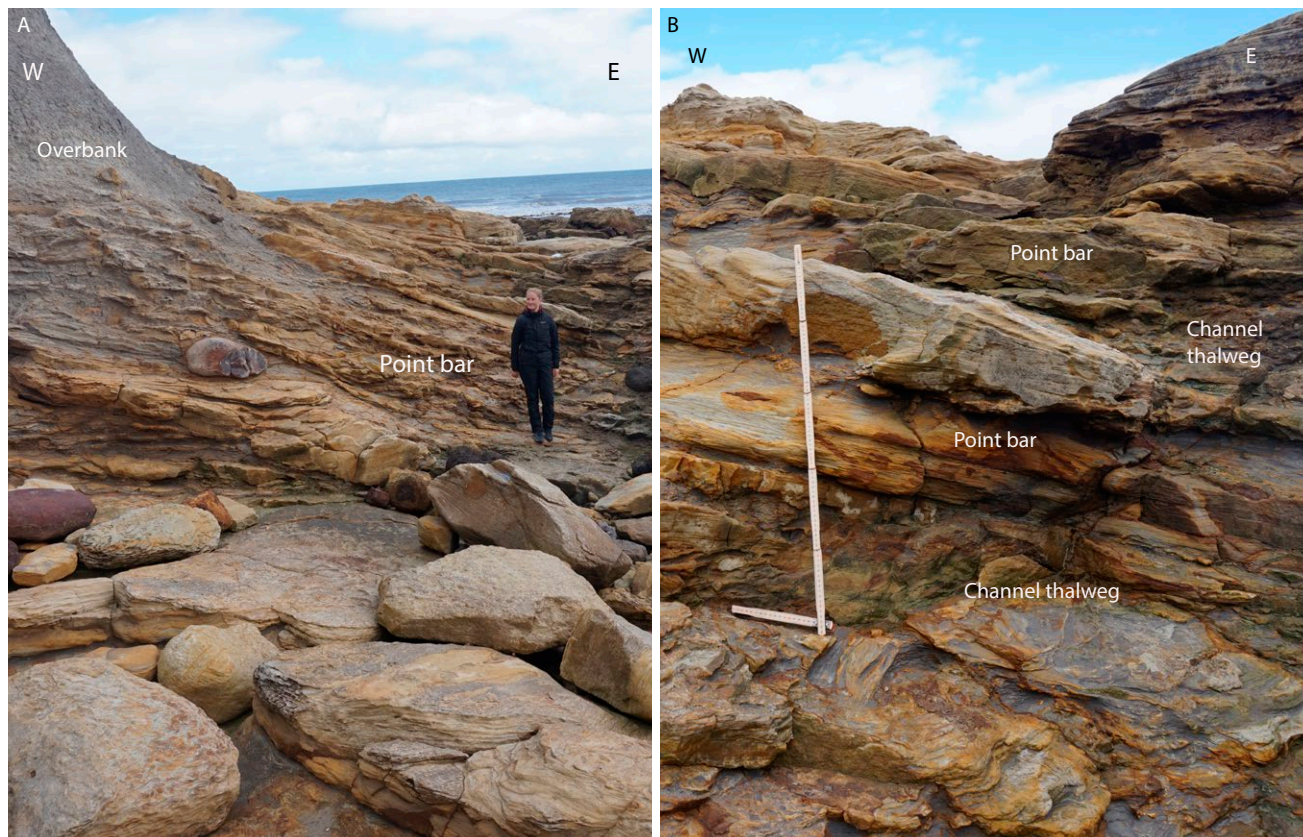


Fig. 14. Cross-section of meandering river deposits in the Scalby Formation. **A:** The western margin of the exposure shows light yellow point bar deposits that interfinger laterally with dark grey overbank mudstones (only partly seen on the photo). The whole succession is overlain by dark grey overbank mudstone. This section illustrates the presence of tongues of fine-grained material between sandstone lenses of upper point and scroll bar origin. **B:** The central part of the exposure with eastward-dipping point bar sandstones interfingering with channel thalweg conglomerates. Vertical length of ruler *c.* 1 m.

200 times wider than the thickness of the individual channel deposits. This relation requires preservation of the complete succession.

Channel thalweg and point bar successions (channel deposits) in the Alma-1X core have a mean thickness of 2.60 m with a minimum thickness of 0.25 m, and a maximum thickness of 4.35 m. In Alma-2X the corresponding values are a mean thickness of 2.60 m, a minimum thickness of 0.6 m and a maximum

thickness of 6.55 m. Using maximum values of channel thicknesses and assuming the preservation conditions are met, the width of the largest ancient channel belt in Alma-1X would be between 90 and 200 m (Low-Net End Member) or around 900 m (High-Net End Member). In Alma-2X the width of the largest channel belt would be between 130 and 330 m (Low-Net End Member) of around 1300 m (High-Net End Member). The predicted channel belt dimensions in the Alma

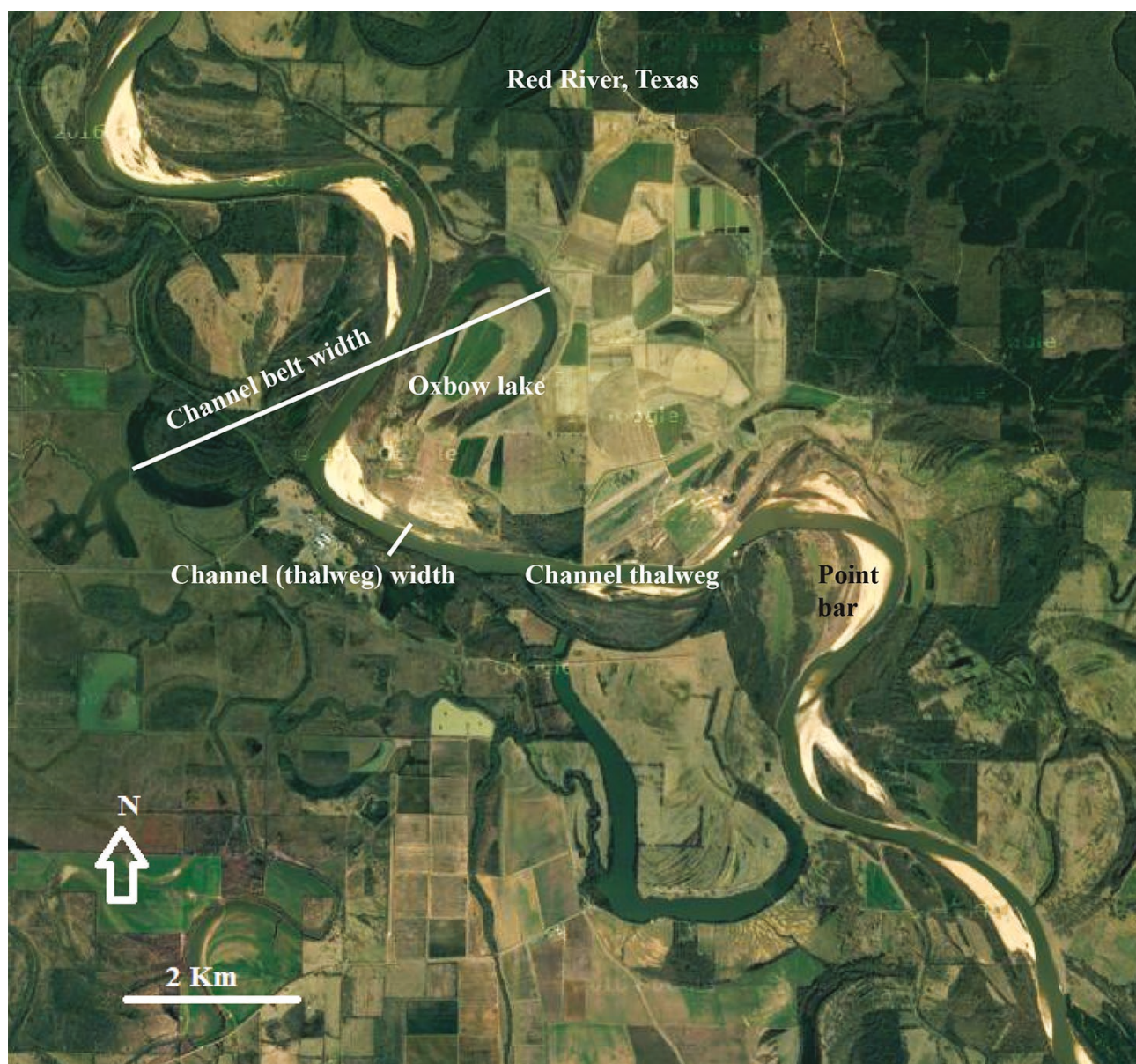


Fig. 15. Satellite image of the Red River, Texas. The photo illustrates two of the channel environments and related facies recognised in the Alma cores: channel thalweg and point bar deposits. The sandy point bars flank the meandering channel (thalweg). The distance between the outermost abandoned or active bends of the most recent river system defines the channel belt width, which is considerably larger than the width of the channel (the thalweg). The channel belt width of the Red River is of the same order as the channel belt width of the rivers in the Alma cores. The Red River in this image is situated inland, while the rivers in the Alma cores probably were situated close to the coast, with wide overbank areas in which mud was deposited and coal formation was favoured. Photo from Google Maps.

fluvial system would characterise these fluvial-channel bodies as medium in the Low-Net End Member scenario but as wide in the High-Net End Member case (Gibling 2006). The preservation of floodplain fines in the present study would indicate that at least parts of the Alma systems were formed in the Low-Net End Member scenario. According to Milliken *et al.* (2012) such systems are typical in meandering river systems close to the coast, dominated by avulsion processes.

Coastal vs. inland setting

The lack of any marine indicators in Alma-1X suggests that the fluvial system developed here was situated somewhat inland and possibly formed part of a wide coastal plain. The presence of very rare dinoflagellate cysts in Alma-2X (particularly near the top of the studied interval) suggests fluvial deposition in a coastal setting with possible rare marine inundations during storm events (Goslin & Clemmensen 2017). The formation and preservation of heterolithic and mud-rich uppermost point bar as well as common floodplain deposits, including coals from backswamps in both cores, would be in line with a coastal setting with subsidence and a high preservation potential.

Autogenic vs allogenic control

The stacking pattern of facies in the two Alma cores can be used to extract information on the avulsion rate of the fluvial system (autogenic control) or changes in base level (allogenic control). Base level is controlled by either subsidence or rising sea level (Miall 2014). Fine-grained floodplain sediments are the dominant sediments deposited (and preserved) during periods of rising sea level, while channel and channel margin sands constitutes the dominant sediments deposited and preserved during stable or slowly rising base level (Miall 2014). Another factor controlling the architecture of the fluvial system is avulsion. Avulsion is the process by which a meandering river shifts its primary course abruptly, and frequent avulsion leaves less time for lateral migration of the river, causing the formation of narrow channel sands (Miall 2014). Milliken *et al.* (2012) also state that narrow channel sandstones (ribbon sandstones) form in a Low-Net End Member system dominated by avulsion processes.

This study found that floodplain deposits comprise about 34% of the core material in Alma-1X and about 26% in Alma-2X (Figs 11, 12). This is interpreted to reflect an overall high preservation rate due to a rising sea level on a coastal plain with relatively frequent avulsion. However, several intervals in the cores contain amalgamated channel sandstones (channel unit 3 and 4 in Alma-1X, and channel unit 2 and

the main part of channel unit 4 in Alma-2X). These intervals may therefore represent times with a slowly rising or stagnant sea level or, perhaps more likely, periods of less frequent avulsion. These intervals may therefore also be characterised by the widest channel belt sandstones.

Conclusions

Studies of sedimentary cores of the Middle Jurassic Alma Field indicate that deposition took place in mixed-load meandering river systems. Channel successions are typically initiated by channel thalweg conglomerates overlain by point bar sandstones. The point bar sand cores are relatively well sorted with most sand being fine- to medium-grained. In some channel successions the point bar units show a fining-upward of grain size and many units are overlain by mud-rich floodbasin deposits. The occurrence of muddy and heterolithic upper point bar deposits is striking and suggest a high preservation potential of the point bar sediments and markedly fluctuating discharge in a mixed-load river.

The stacking pattern of the fluvial facies suggests that the fluvial system switched from a mud-rich Low-Net End Member system with high aggradational rates and frequent avulsion to a sand-rich High-Net End Member system with low aggradational rates and less frequent avulsion. The width of the largest ancient channel belt in Alma-1X would be between 90 and 200 m (Low-Net End Member) or around 900 m (High-Net End Member). In Alma-2X the width of the largest channel belt would be between 130 and 330 m (Low-Net End Member) or around 1300 m (High-Net End Member). The predicted channel belt dimensions in the Alma fluvial system would characterise these fluvial-channel bodies as medium in the Low-Net End Member scenario but as wide in the High-Net End Member case.

The study of the Scalby Formation broadly supports the mixed-load meandering river model proposed from the core studies and adds significantly to the understanding of scaling, geometry and internal contacts between the facies. In particular, the channel thalweg and point bar deposits often have a repetitive interfingering contact, and thus the channel thicknesses in the core studies could be misinterpreted and thought to represent numerous minor channel events rather than one. The observations revealed marked lateral variations across the cliff profiles. The geometrical outline of the facies elements, such as channel deposits, show changes in thickness and shape, and thus the facies given in a well could be

very different some tens of metres away. On a larger scale (hundreds to thousands of metres), the Long Nab Member in the Scalby Formation illustrates that the channel sand bodies occur sporadically and are separated by wide intervals of channel margin and floodplain deposits.

These observations indicate that there are some difficulties related to defining subsurface channel sand bodies from single wells. Such a well may be located in an interchannel area and thereby yield an underrepresentation of channel sandstones; if it is located in an area with a concentration of fluvial channel sandstones there is a risk of overestimating the amount of such sandstones.

Acknowledgements

This research has received funding from the University of Copenhagen and from the Geological Society of Denmark (DGF). We are thankful to the scientific editor Henrik Tirsgaard and the reviewers Henrik Olsen and Gunver Krarup Pedersen who provided detailed and constructive reviews. Lotte Melchior Larsen is thanked for her thorough and constructive corrections to the manuscript. The Danish Underground Consortium (DUC) is thanked for granting permission to publish the paper, Maersk Oil is thanked for assisting with acquiring data and core studying facilities, and Schlumberger is thanked for issuing a University grant to University of Copenhagen (Petrel).

References

- Allen, J.R.L. 1963: The classification of cross-stratified units. With notes on their origin. *Sedimentology* 2, 93–114.
- Allen, J.R.L. 1965: A review of the origin and characteristics of recent alluvial sediments. *Sedimentology* 5, 89–191.
- Allen, J.R.L. 1978: Studies in fluvial sedimentation: an exploratory quantitative model for the architecture of avulsion-controlled suites. *Sedimentary Geology* 21, 129–147.
- Andsbjerg, J. 2003: Sedimentology and sequence stratigraphy of the Bryne and Lulu Formations, Middle Jurassic, northern Danish Central Graben. In: Ineson, J.R. & Surlyk, F. (eds), *The Jurassic of Denmark and Greenland*. Geological Survey of Denmark and Greenland Bulletin 1, 301–347.
- Andsbjerg, J. & Dybkjær, K. 2003: Sequence stratigraphy of the Jurassic of the Danish Central Graben. In: Ineson, J.R. & Surlyk, F. (eds), *The Jurassic of Denmark and Greenland*. Geological Survey of Denmark and Greenland Bulletin 1, 265–300.
- Andsbjerg, J., Nielsen, L.H., Johannesen, P.N. & Dybkjær, K. 2001: Divergent development of two neighbouring basins following the Jurassic North Sea doming event: the Danish Central Graben and the Norwegian-Danish Basin. In: Martinsen, O.J. & Dreyer, T. (eds), *Sedimentary environments offshore Norway – Palaeozoic to Recent*. Norwegian Petroleum Society (NPF) Special Publication 10, 175–197.
- Bernhard, H.A., LeBlanc, R.J. & Major, C.F. 1962: Recent and Pleistocene geology of southeast Texas. *Geol. Gulf Coast and central Texas and guidebook of excursion*. Houston Geological Society, 175–224.
- Bridge, J.S. 2001: Characterization of fluvial hydrocarbon reservoirs and aquifers: problems and solutions. *AAS Revista* 8, 87–114.
- Bridge, J.S. & Jarvis, J. 1982: The dynamics of a river bend: a study in flow and sedimentary processes. *Sedimentology* 29, 499–541.
- Bridge, J.S. & Leeder, M.R. 1979: A simulation model of alluvial stratigraphy. *Sedimentology* 26, 61–74.
- DGU 1991: Service Report: Alma-1X Central Trough palynofacies, 20 pp.
- DGU 1993: Service Report: Alma-2X Central Trough palynofacies, 17 pp.
- Ghinassi, M. & Ielpi, A. 2015: Stratal Architecture and Morphodynamics of Downstream-Migrating Fluvial Point Bars (Jurassic Scalby Formation, U.K.). *Journal of Sedimentary Research* 85, 1123–1137.
- Gibling, M.R. 2006: Width and thickness of fluvial channel bodies and valley fills in the geological record: a literature compilation and classification. *Journal of Sedimentary Research* 76, 731–770.
- Goslin, J. & Clemmensen, L.B. 2017: Proxy records of storm events in coastal barrier systems: Storm-wave induced markers. *Quaternary Science Reviews* 174, 80–119.
- Husmo, T., Hamar, G., Høiland, O., Johannessen, E.P., Rømuld, A., Spencer, A. & Titterton, R. 2002: Middle Jurassic. In: Evans, D., Graham, C., Armour, A. & Bathurst, P. (eds), *The Millennium Atlas. Petroleum Geology of the Central and Northern North Sea*. The Geological Society, London, 128–155.
- Ielpi, A. & Ghinassi, M. 2014: Planform architecture, stratigraphic signature and morphodynamics of an exhumed Jurassic meander plain (Scalby Formation, Yorkshire, UK). *Sedimentology* 61, 1923–1960.
- Jackson, R.G. 1976: Depositional model of point bars in the Lower Wabash River. *Journal of Sedimentary Petrology* 46, 579–594.
- Japsen, P., Britze, P. & Andersen, C. 2003: Upper Jurassic – Lower Cretaceous of the Danish Central Graben: structural framework and nomenclature. In: Ineson, J.R. & Surlyk, F. (eds), *The Jurassic of Denmark and Greenland*. Geological Survey of Denmark and Greenland Bulletin 1, 233–246.
- Jensen, T.F., Holm, L., Frandsen, N. & Michelsen, O. 1986: Jurassic – Lower Cretaceous lithostratigraphic nomenclature for the Danish Central Trough. *Danmarks Geologiske Undersøgelse Serie A* 12, 65 pp.
- Keogh, K.J., Martinius, A.W. & Osland, R. 2007: The develop-

- ment of fluvial stochastic modelling in the Norwegian oil industry: A historical review, subsurface implementation and future directions. *Sedimentary Geology* 202, 249–268.
- Leeder, M.R. 1978: A quantitative stratigraphic model for alluvium with special reference to channel deposit density and interconnectedness. In: Miall, A. (ed.), *Fluvial Sedimentology*. Canadian Society of Petroleum Geologists Memoir 5, 587–596.
- Maersk Oil 1991a: Final well report Alma-1X, 85 pp.
- Maersk Oil 1991b: Alma-1X Core photos, 33 pp.
- Maersk Oil 1993a: Final well report Alma-2X, 140 pp.
- Maersk Oil 1993b: Alma-2X Core photos, 51 pp.
- Maersk Oil 1999: Palynostratigraphy of the Jurassic Intervals from wells Alma-1X and Alma-2X, Danish North Sea, 19 pp.
- Miall, A. 1985: Architectural-Element Analysis: A new method of facies analysis applied to fluvial deposits. *Earth Science Reviews* 22, 261–308.
- Miall, A. 1996: *The geology of fluvial deposits*, 582 pp. Springer Verlag, Berlin.
- Miall, A. 2014: *Fluvial depositional systems*, 316 pp. Springer Verlag, Berlin.
- Michelsen, O., Nielsen, L.H., Johannesen, P.N., Andsbjerg, J. & Surlyk, F. 2003: Jurassic lithostratigraphy and stratigraphic development onshore and offshore Denmark. In: Ineson, J.R. & Surlyk, F. (eds), *The Jurassic of Denmark and Greenland*. Geological Survey of Denmark and Greenland Bulletin 1, 147–216.
- Milliken, K. Blum, M. & Martin, J. 2012: Scaling relationships in fluvial depositional systems. *AAPG Abstract, Search and Discovery Article* 30245.
- Mjøs, R., Walderhaug, O. & Prestholm, E. 1993: Crevasse splay sandstone geometries in the Middle Jurassic Ravenscar Group of Yorkshire, UK. In: Marzo, M. & Puigdefabregas, C. (eds), *Alluvial Sedimentation*. Special Publications of the International Association of Sedimentologists 17, 167–184.
- Møller, J.J. 1986: Seismic structural mapping of the Middle and Upper Jurassic in the Danish Central Trough. *Danmarks Geologiske Undersøgelse Serie A* 13, 37 pp.
- Møller, J.J. & Rasmussen, E.S. 2003: Middle Jurassic – Early Cretaceous rifting of the Danish Central Graben. In: Ineson, J.R. & Surlyk, F. (eds), *The Jurassic of Denmark and Greenland*. Geological Survey of Denmark and Greenland Bulletin 1, 247–264.
- Morgans, H.S., Hesselbo, S.P. & Spicar, R.A. 1999: The seasonal climate of the Early-Middle Jurassic Cleveland Basin, England. *Palaios* 14, 261–272.
- Owen, A., Ebinghaus, A., Hartley, A.J., Santos, M.G.M. & Weissmann, G.S. 2017: Multi-scale classification of fluvial architecture: An example from the Palaeocene–Eocene Bighorn Basin, Wyoming. *Sedimentology* 64, 1572–1596.
- Pearson, N.J. & Gingras, M.K. 2006: An ichnological and sedimentological facies model for muddy point-bar deposits. *Journal of sedimentary research* 76, 771–782.
- Petersen, H.I., Andsbjerg, J., Bojsen-Kofoed, J.A., Nytoft, H.P. & Rosenberg, P. 1998: Petroleum potential and depositional environments of Middle Jurassic coals and non-marine deposits, Danish Central Graben, with special reference to the Søgne Basin. *Geology of Denmark Survey Bulletin* 36, 78 pp.
- Reineck, H. & Singh, I.B. 1973: *Depositional sedimentary environments*, 439 pp. Springer Verlag, Berlin.
- Schwarzer, D., Fronval, T., Clausen, L.F. & Ensley, R. 2007: Mellem Jura ‘Play Analysis’ i den danske Centralgrav – et integreret multidisciplinært studie for den 6. udbudsrunder. *Geologisk Tidsskrift* 2007, 3–5.
- Sellwood, B.W. & Valdes, P.J. 2006: Mesozoic climates: General circulation models and the rock record. *Sedimentary Geology* 190, 269–287.
- Smith, D.G., Hubbard, S.M., Leckie, D.A. & Fustic, M. 2009: Counter point bar deposits: lithofacies and reservoir significance in the meandering modern Peace River and ancient McMurray Formation, Alberta, Canada. *Sedimentology* 56, 1655–1669.
- Thomas, R.G., Smith, D.G., Wood, J.M., Visser, J., Calverley-Range, E.A. & Koster, E.H. 1987: Inclined heterolithic stratification – Terminology, description, interpretation and significance. *Sedimentary Geology* 53, 123–179.
- Thomsen, E., Dybkjær, K. & Johannesen, P. 2013: Jurassiske sandstensreservoirer – Hvad kan det betyde for Danmarks fremtidige energiforsyning. In: *Olie og gas i Dansk undergrund*. *Geoviden* 2013(1), 7–9.
- Tyler, N. & Finley, R.J. 1991: Architectural controls on the recovery of hydrocarbons from sandstone reservoirs: Concepts in *Sedimentology and Paleontology* 3, 1–5.
- Ziegler, P.A. 1990: Tectonic and palaeogeographic development of the North Sea rift system. In: Blundell, D.J. & Gibbs, A.D. (eds), *Tectonic evolution of the North Sea rifts*, 1–36. Oxford, Clarendon Press.

Two new finds of turtle remains from the Danian and Selandian (Paleocene) deposits of Denmark with evidence of predation by crocodylians and sharks

KRISTINE STEIGARDOTTER MYRVOLD, JESPER MILÀN & JAN AUDUN RASMUSSEN



Myrvold, K.S., Milàn, J. & Rasmussen, J.A. 2018. Two new finds of turtle remains from the Danian and Selandian (Paleocene) deposits of Denmark with evidence of predation by crocodylians and sharks. © 2018 by Bulletin of the Geological Society of Denmark, Vol. 66, pp. 211–218. ISSN 2245-7070. (www.2dgf.dk/publikationer/bulletin).

Two new fragments of a turtle carapace and a turtle plastron (hypoplastron) have been recovered from glacially transported boulders of Danian and Selandian age. The hypoplastron is identified as *Ctenochelys* cf. *stenoporus*, while the carapace fragment can only be assigned to the family Cheloniidae indet. Both specimens show evidence of predation by crocodylians in the form of rows of circular pits in the bones, and one specimen has rows of elongated scrape traces interpreted as scavenging by sharks. Together with the other, rare finds from the middle Danian of the Faxe Quarry and from late Danian deposits in the Copenhagen area, these new finds add important new knowledge to the sparse fossil record of turtles in Scandinavia, as well as evidence that the genus *Ctenochelys* survived across the K/Pg Boundary.

Received 31 October 2017
Accepted in revised form
27 May 2018
Published online
4 October 2018

Kristine Steigardotter Myrvold [hld388@alumni.ku.dk], Natural History Museum of Denmark, Øster Voldgade 5–7, DK-1350 Copenhagen K, Denmark. Jesper Milàn [jesperm@oesm.dk], Geomuseum Faxe/Østsjælland Museum, Østervej 2, DK-4640 Faxe, Denmark; also Natural History Museum of Denmark, Øster Voldgade 5–7, DK-1350 Copenhagen K, Denmark. Jan Audun Rasmussen [jan.rasmussen@museummors.dk], Fossil and Moclays Museum/Museum Mors, Skarrehagevej 8, DK-7900 Nykøbing Mors, Denmark.

Corresponding author: Jesper Milàn.

Turtle remains are very rare in the Cretaceous and Paleocene chalk, limestone and marl deposits in Denmark and southern Scandinavia, and are restricted to a few incomplete finds which are hard to identify to higher taxonomic levels. Historically, turtles are known from a collection of carapace fragments from the upper Danian København Limestone Formation and the Selandian Lellinge Greensand Formation found in excavations in Copenhagen (Dames 1897; Rosenkrantz 1920, 1921, 1923). A recent revision of this material identified parts of it as *Rafetoides henrici* (Owen & Bell 1849), while the rest belongs to the order Testudines gen. et sp. indet. (Karl & Lindow 2012). Additional material has been found in the middle Danian Faxe Formation of the Faxe quarry and consists of two carapace fragments assignable to Chelonioida indet. (Milàn *et al.* 2011; Adolfsson *et al.* 2017). Three peripheral elements from the carapace of a marine turtle of the family Cheloniidae are known from the upper Maastrichtian limestone of the Møns Klint Formation (Surlyk *et al.* 2013) at Stevns Klint (Karl &

Lindow 2009). This study describes two new finds of turtle fragments in glacially transported boulders from respectively Jyske Rev (the Jutland Bank) and the Gundstrup gravel pit (Fig. 1), identifies them to the highest possible taxonomic level and discusses their taphonomic history.

Material and Methods

The oldest specimen studied consists of a turtle carapace fragment embedded in typical light grey, Danian bryozoan limestone. The specimen was found at the harbour of Esbjerg in a rock pile, which was extracted from the seafloor at Jyske Rev of the North Sea (approximately 57.0°N, 07.7°E; Fig. 1). It is assumed that it was transported from nearby Danian deposits during the last glaciation (Leth 1996; Larsen *et al.* 2009; Jensen *et al.* 2010). The second and youngest specimen consists of an almost complete hypoplastron fragment and a

caudal vertebra, which were found in a boulder (32×16 cm) of Selandian Kerteminde Marl retrieved from glacial deposits in the Gundstrup gravel pit, northern Fyn at 55.56°N, 10.35°E. The Kerteminde Marl Formation is exposed at the nearby coastal cliffs south of Kerteminde on eastern Fyn (Fig. 1). Both specimens are declared Danekræ, national fossil trove (DK-794 and DK-779, respectively) and are stored in the collection of the Natural History Museum of Denmark (NHMD 227324 and 227325).

The plastron fragment NHMD 227325 was compared visually with Late Cretaceous and Paleocene turtles to find overall morphological matches. Subsequently, diagnostic morphological characters used to discriminate between different testudine families and genera were studied (see e.g. Hirayama 1997 and Lehman & Tomlinson 2004). Finally, a simple morphometric analysis was generated to compare selected, critical ratios in the studied plastron with published species.

Three morphometric distances (L1, L2 and L3) were measured (Fig. 2) and compared with values obtained from measurements of specimens in the literature, measured directly on the published illustrations when measurements were not stated (Table 1). The



Fig. 1. Map of Denmark with the locations of the specimens indicated. NHMD 227324 was found at Esbjerg Harbour (blue star) in a pile of rocks extracted from Jyske Rev (blue square). NHMD 227325 was found at Gundstrup gravel pit in northern Fyn (red star) and originates from the Kerteminde Marl Formation exposed in the coastal cliffs south of the town Kerteminde (red square).

two morphological ratios $R1 = L1/L3$ and $R2 = L2/L3$ were then plotted against each other. A high $R1$ value indicates a relatively wide and narrow hypoplastron, while a high $R2$ value suggests that the suture line that connected the right hypoplastron with the left hypoplastron is relatively short. In contrast to individual distance measures, ratios reflect morphological differences directly. All values were measured at their maximum values as indicated on Fig. 2.

Table 1. Length measurements and morphological ratios of late Cretaceous and Paleocene turtle hypoplastrons

	L1 (cm)	L2 (cm)	L3 (cm)	R1	R2
NHMD 227325	10.5	5.7	13.0	0.8	0.4
<i>L. natatrix</i>	4.0	3.0	5.5	0.7	0.5
<i>C. tenuitesta</i>	5.0	2.9	6.0	0.8	0.5
<i>C. stenoporus</i>	4.4	2.3	5.2	0.8	0.4
<i>C. stenopora</i>	3.5	2.0	4.0	0.9	0.5
<i>G. suykerbuycki</i>	3.8	4.1	6.5	0.6	0.6
<i>T. latiremis</i>	2.9	1.1	3.0	1.0	0.4
<i>L. niobrarae</i>	2.1	1.3	2.5	0.8	0.5
<i>O. emarginatus</i>	1.0	0.3	0.7	1.4	0.4
<i>D. casieri</i>	0.6	0.25	0.6	1.0	0.4

For L1, L2 and L3, see Fig. 2.

$R1 = L1/L3$; $R2 = L2/L3$.

Sources of the measurements are given in Fig. 5.

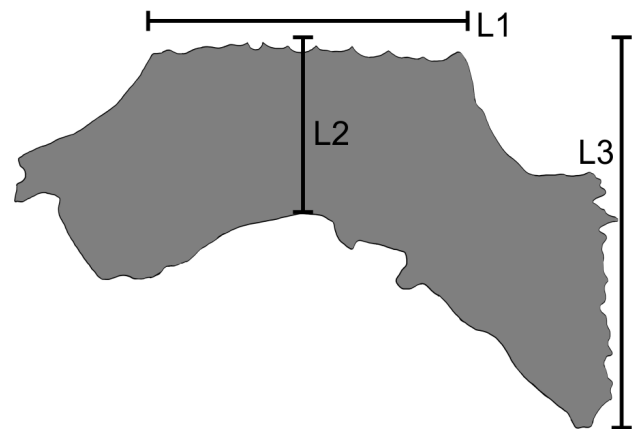


Fig. 2. Sketch of hypoplastron showing the three distances used in the analysis (L1, L2, L3).

Brief notes on the geological framework

The two turtle specimens described were found in erratic Danian and Selandian sedimentary boulders that have been eroded and transported by one or more ice sheets during the Pleistocene and subsequently mixed with Quaternary sediments.

The Danian strata of the Danish Basin are characterised by a variety of limestone types, predominantly bryozoan limestone, coccolith chalk and, in the upper part, relatively coarse skeletal packstones and grainstones. A major regression took place at the end of the Danian at about 61.6 Ma (Vandenberghé *et al.* 2012), resulting in a widespread unconformity (e.g. Thomsen & Heilmann-Clausen 1985; Clemmensen & Thomsen 2005). The succeeding Selandian transgression resulted in a very different sedimentary regime characterised by a considerably higher supply of siliciclastic material. The reasons for this are not clear, but it has been suggested that a tectonic uplift of the Scotland-Shetland Platform played a major role (Clemmensen and Thomsen 2005). Moreover, the significant drop in calcium carbonate sedimentation in the basal Selandian may be explained by the narrowing or closure of the connections to the warmer oceans towards the south, which would have caused less favourable living conditions for the organisms whose skeletons were the main source of calcium carbonate to the sediments (Clemmensen & Thomsen 2005; Heilmann-Clausen 2010).

The Danian limestones were deposited in a subtidal shelf palaeoenvironment up to a few hundred metres deep, while the overlying Selandian Kerteminde Marl Formation characterised an offshore, but shallower, inner shelf environment.

Systematic Palaeontology

The taxonomical interpretation of the superfamily Chelonioidea is still debated. Lehman & Tomlinson (2004) regarded the family Cheloniidae as the only family in the superfamily Chelonioidea, whereas Zangerl (1953) subdivided Chelonioidea into Toxochelyidae and Cheloniidae. Karl & Nyhuis (2012) followed the interpretation of Zangerl (1953). Hirayama (1997), on the other hand, subdivided Chelonioidea into the families Cheloniidae and Protostegidae. However, it was recently argued that it is highly implausible that the protostegids are crown chelonoids (Joyce *et al.* 2013). In addition, the position of the various subfamilies within the superfamily Chelonioidea is highly debated. Zangerl (1953) placed Toxochelyinae, Lophochelyinae and Osteopyginae within the family Toxochelyidea, whereas Weems (1988) placed Toxochelyinae and Lophochelyinae within Toxochelyidea, and Osteopyginae within Cheloniidae.

With regard to the overall suprageneric classification, the Converted Clade Names (CCN) suggested by Joyce *et al.* (2004) are used below.

Order Testudines Batch 1788

Suborder Cryptodira Cope 1868

Superfamily Chelonioidea Baur 1893

The superfamily Chelonioidea is the only cryptodiran group that is highly adapted to the marine environment. The fossil record of chelonoids can be traced back into the Early Cretaceous, roughly at 110 Ma. Modern chelonoids form a relatively small group comprising six genera and seven species within two families, Cheloniidae and Dermochelyidae (Hirayama 1997).

Family Cheloniidae Bonaparte 1832

Remarks. The oldest known cheloniid genera, *Toxochelys* and *Ctenochelys*, are documented from Late Cretaceous deposits of North America (Hirayama 1997).

Family Cheloniidae indet.

Figure 3A–F

Material. One specimen, NHMD 227324.

Description. The specimen is a partial pleural plate from a turtle carapace and is approximately 19 cm long and 8 cm wide (Fig. 3). The specimen is broken into four pieces that are held together in an almost anatomically correct position by the sediment (Fig. 3A, C). On the dorsal side of the bone, a shallow groove from the connection between the overlying horny scutes is visible along the midline of the plate and splits into two towards the margin of the plate (Fig. 3C, D). An unidentified flat piece of bone fused to the ventral side of the specimen probably represents a part of the appendicular skeleton.

Remarks. The incomplete specimen NHMD 227324 does not possess morphological characters that allow a more precise determination than Chelonioidea indet.

Occurrence and stratigraphical age. The specimen is from an erratic limestone boulder collected at Jyske Rev off the west coast of Jylland some 40 km west of the town Hanstholm (approximately 57.0°N, 07.7°E). Due to substantial silicification we did not observe identifiable calcareous nannoplankton specimens in the matrix, but the texture and overall nature of the bryozoan limestone demonstrate that it is Danian rather than Maastrichtian in age. Hence, the fossiliferous bryozoan limestone originates either from one of the Danian outcrops situated in the belt extending from the town of Hanstholm on the northern west coast

of Jylland across northern and central-east Jylland to eastern Sjælland (e.g. Thomsen 1995), or alternatively from Danian deposits that are exposed on the seafloor near the Jyske Rev area (Leth 1996, 2003).

Genus *Ctenochelys* Zangerl 1953

Remarks. Zangerl (1953) remarked that *Ctenochelys* and *Lophochelys* are difficult to distinguish from each other. Hirayama (1997) went one step further and was of the opinion that the species of the genus *Lophochelys* erected by Zangerl (1953), including the original type

species *Lophochelys natatrix* Zangerl, were based on poorly preserved juvenile specimens of *Ctenochelys* or *Toxochelys*, indicating that the identification of *Lophochelys* is dubious.

Ctenochelys cf. *stenoporus* (Hay 1905)

Figure 4

Material. One hypoplastron and one caudal vertebra, NHMD 227325.

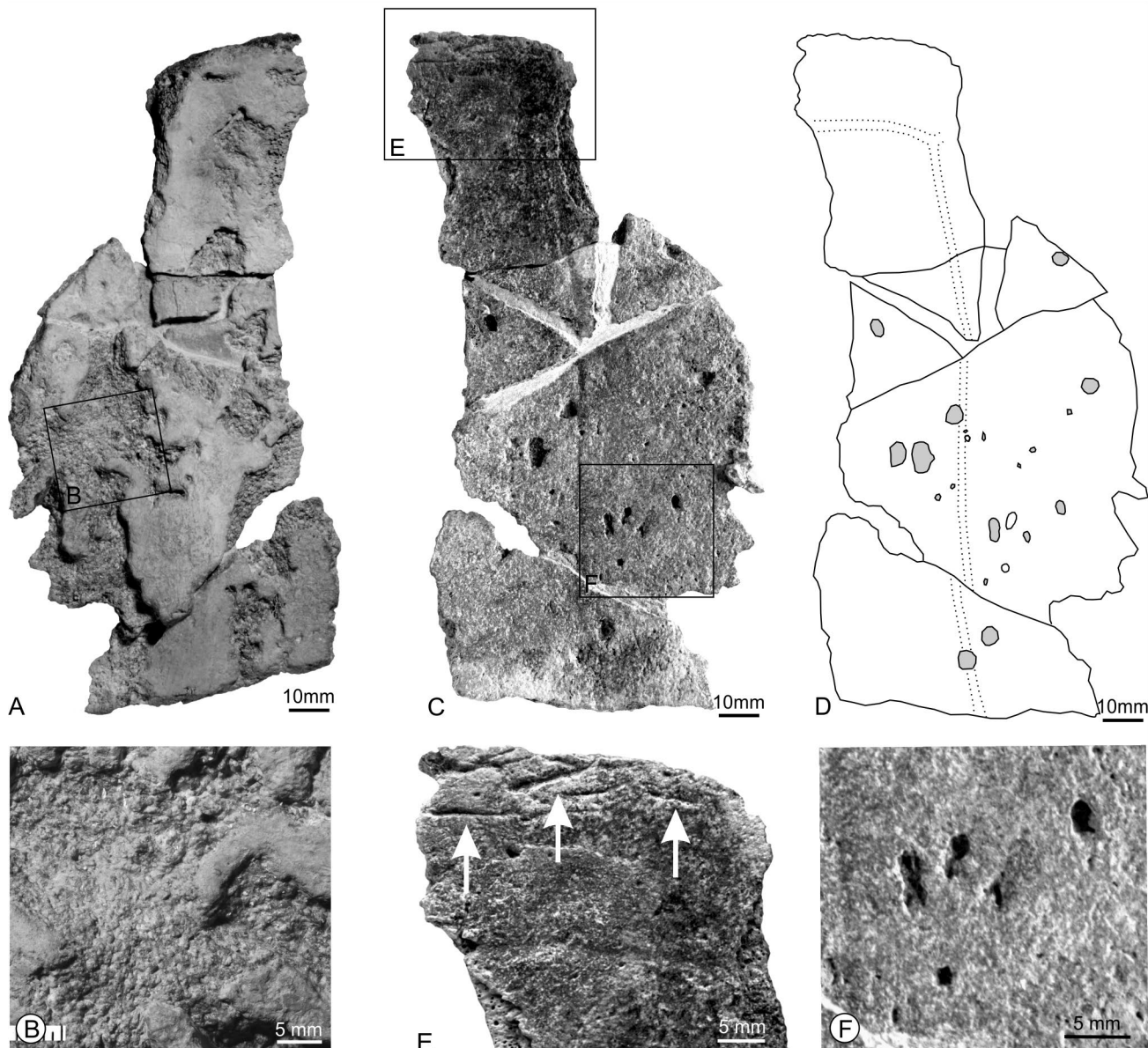


Fig. 3. Carapace fragment (NHMD 227324) with traces of bites. **A:** Ventral surface of the fragment, showing areas of bioerosion and pathologies. **B:** Close-up of the exposed parts of the spongy bone in the eroded areas. **C:** Dorsal side of the six fragments held together by sediment. **D:** Sketch of the dorsal surface showing rows of circular bite traces. The shallow groove from the contact between the overlying horny scutes is indicated. **E:** Close-up of elongated scratch traces interpreted as scavenging by sharks. **F:** Close-up of circular bite traces interpreted as predation by crocodilians.

Synonymy.

cf. 1875 *Toxochelys serrifer* n. sp. - Cope, p. 299, (Hay 1905, p. 178, figs. 1–3).

cf. 1905 *Ctenochelys stenoporus* n. sp. - Hay, pp. 180–181, figs. 8–11.

cf. 1905 *Toxochelys procax* Cope - Hay, pp. 181–182, figs. 13–14.

cf. 1908 *Toxochelys elkader* Hay - Hay, pp. 174–176, figs. 221–223.

cf. 1953 *Lophochelys natatrix* n. sp. - Zangerl, pp. 218–220, figs. 91–93.

cf. 1953 *Lophochelys venatrix* n. sp. - Zangerl, pp. 224–226, figs. 95–97.

cf. 1953 *Ctenochelys tenuitesta* n. sp. - Zangerl, pp. 227–237, figs. 99–106.

cf. 1997 *Ctenochelys stenoporus* (Hay) - Hirayama, pp. 226–227, fig. 1 (includes synonymy).

Description. The specimen is a hypoplastron preserved in a boulder of marl. Associated with the hypoplastron is a single caudal vertebra (Fig. 4). The hypoplastron is 19 cm long and roughly 6 cm wide throughout, making it much longer than wide. The suture that connected the hypoplastron to the hyoplastron is

serrated, as is the medial edge. The lateral edge is missing. The morphology of the specimen shows that this possessed a large fontanelle in the midline of the plastron (Fig. 4B).

Discussion. Because of the incomplete nature of many of the holotypes of previously erected *Ctenochelys* species, all known *Ctenochelys* species were synonymised by Hirayama (1997), resulting in a single species, *C. stenoporus*. Moreover, Hirayama (1997) regarded *Lophochelys natatrix* as a synonym of *Ctenochelys stenoporus* and *Lophochelys niobrarae* as a synonym of *Toxochelys latiremis*. This interpretation is followed here.

In the morphometric plot (Fig. 5), NHMD 227325 is situated very close to *Ctenochelys stenoporus* (including its junior synonyms *C. tenuitesta* and *Lophochelys natatrix*) and *L. niobrarae*, which indicates that these four taxa have a similar shape of the hypoplastron. This is in support of the taxonomical interpretation by Hirayama (1997) and suggests that NHMD 227325 belongs to *Ctenochelys stenoporus* or a closely related descendant of this species. Because of the incomplete material and the ensuing uncertainty, however, we have chosen to use open nomenclature, and specimen

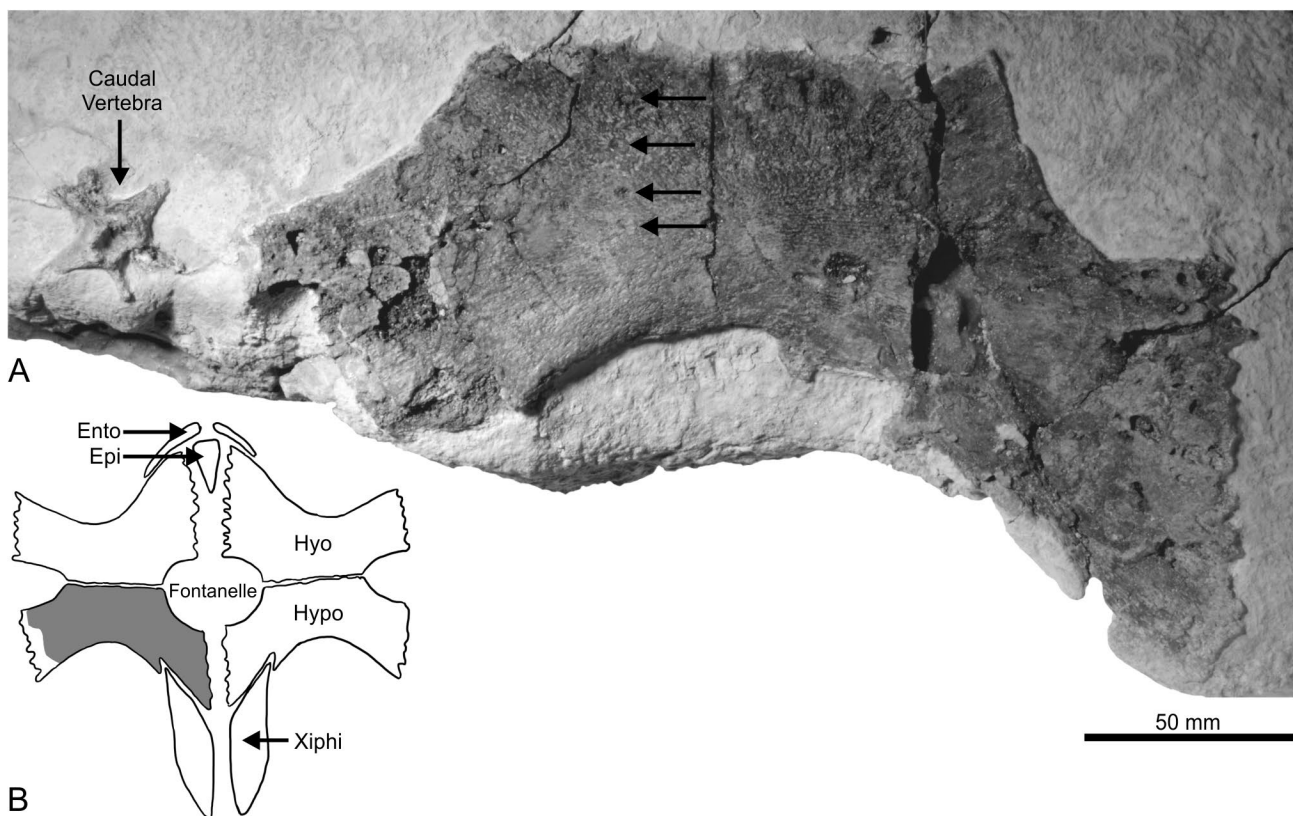


Fig. 4. A: Hypoplastron (NHMD 227325) partly embedded in Kerteminde Marl. A row of four circular bite traces is indicated by arrows. B: Sketch of turtle plastron with names of the individual skeletal elements indicated. Ento: entoplastron, Epi: Epiplastron, Hyo: Hyoplastron, Hypo: Hypoplastron, Xiphi: Xiphiplastron. The central fontanelle is formed by recession of the margins of the paired Hyo- and Hypoplastrons.

NHMD 227325 is referred to *Ctenochelys cf. stenoporus*. Weems (2014, fig. 12) described a Danian cheloniid specimen which was interpreted as *?Lophochelys* sp. Superficially, it resembles NHMD 227325, but the R2 ratio is much larger in *?Lophochelys* than in the studied specimen (1.16 versus 0.4).

Occurrence and stratigraphical age. The specimen was found in an erratic boulder of the Kerteminde Marl Formation retrieved from the Gundstrup gravel pit, Fyn, Denmark (approximately 55.56°N, 10.35°E). The presence of the calcareous nannofossils *Neochiastoygus perfectus*, common *Prinsius dimorphosus* and rare reworked Cretaceous nannofossils (Schnetler & Nielsen 2018) in the marly matrix reveal a basal Selandian age of the turtle specimen (Thomsen 1995, Clemmensen & Thomsen 2005, Schnetler & Nielsen 2018).

Discussion

Identification of the specimens

Fossil turtle remains from the Late Paleocene are relatively rare, and the general lack of described material from this period has resulted in a scant and incomplete phylogeny of the family Cheloniidae (Weems 1988). Most fossils belonging to Cheloniidae have been found in North America. However, considering the relative proximity of North America and Europe during the

Paleocene, it is not unlikely that the range extended further east than previously assumed.

With very few exceptions, the cheloniids discussed here, including *Ctenochelys stenoporus*, have been recorded from the Cretaceous only (Zangerl 1953; Hirayama 1997). This leads to three obvious interpretations with regard to the specimen NHMD 227325 (*Ctenochelys cf. stenoporus*): 1) *Ctenochelys* existed through a longer time interval than previously assumed and survived the Cretaceous/Paleogene boundary; 2) the specimen is not a *Ctenochelys* but belongs to a closely related descendant not previously described, and 3) the specimen is reworked from the Cretaceous. The last interpretation, however, seems unlikely because all other macrofossils documented from the marl blocks at Gundstrup - including several Danekræ - are of lower middle Paleocene (lower Selandian) age.

Predation traces

Both specimens studied display predation traces consisting of circular pits arranged in rows. NHMD 227324 has several rounded pits with diameters between 3–6 mm present on the surface, some arranged in smaller groups or rows. The pits are u-shaped in cross section (Fig. 3D, F). In addition to the circular pits, one end of the carapace plate bears groups of elongated scratch traces up to 11 mm in length, 2 mm in width and 1 mm deep. The traces are V-shaped in cross section (Fig. 3E). NHMD 227325 has a row of small, 3–4 mm wide, circular pits with a U-shaped

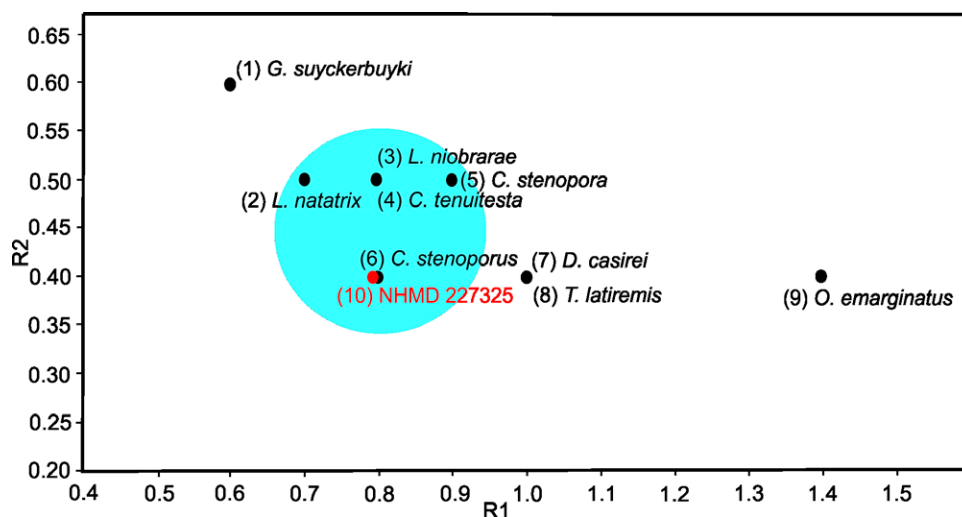


Fig. 5. Graphical representation of the calculated morphological ratios ($R1 = L1/L3$, $R2 = L2/L3$, see Methods). The specimens are named by their original species designations. (1) *Glyptochelone suyckerbuyki* (Lehman & Tomlinson 2004, fig. 6, bottom left); (2) *Lophochelys natatrix* (Zangerl 1980, fig. 3e); (3) *Lophochelys niobrarae* (Zangerl 1953, fig. 94); (4) *Ctenochelys tenuitesta* (Zangerl 1980, fig. 3f); (5) *Ctenochelys stenopora* (Zangerl 1953, fig. 111); (6) *Ctenochelys stenoporus* (Hirayama 1997, fig. 1B); (7) *Dollochelys casirei* (Zangerl 1980, fig. 3d); (8) *Toxochelys latiremis* (Zangerl 1953, fig. 73); (9) *Osteopygis emarginatus* (Zangerl 1980, fig. 3a). The light blue shaded area indicates the field of *C. stenoporus sensu stricto*.

cross section present in the middle part of the plastron (Fig. 4A). The distance between the pits is 9–11 mm.

In both specimens, the uniform arrangement of the pits, as well as the uniformity of their size and shape, suggest that they are bite traces. Identical traces are present in a turtle specimen found in the middle Danian limestone of the Faxe quarry (Milàn *et al.* 2011), which were interpreted as crocodylian bite traces. The uniformity of the pits suggests they are from a predator with more or less homodont uniform dentition such as a crocodylian, which frequently preys on turtles (Milàn *et al.* 2010); this also fits well with the geological age of the specimens. Crocodylians are known from several isolated finds from both the Cretaceous and Paleocene chalk and limestones, and in the Danian at least two crocodylomorphs co-existed, the longirostrine *Thoracosaurus* (Troedsson 1924; Adolfssen *et al.* 2017) and a more robust, possible alligatorid (Schwarz-Wings *et al.* 2014). Furthermore, specimen NHMD 227324 (Fig. 3) has preserved elongated scrapes which are fairly similar to scrapes seen in the specimens described from the Faxe quarry (Milàn *et al.* 2011). These are interpreted as traces from scavenging by sharks which were abundant during the Paleocene (Adolfssen & Ward 2015). Bite traces on the fossil bone surface indicate a factual interaction between animals, whether antagonistic, scavenging or predator–prey interaction, which can provide direct evidence of the feeding behaviour of extinct carnivores, as well as information on the trophic structure of the palaeocommunity (Botfalvai *et al.* 2014). In this case it demonstrates that the Paleocene turtles in Denmark coexisted with crocodylian predators that either actively hunted turtles, or at least scavenged them.

Dissolution pits

The dissolved areas on the ventral surface of NHMD 227324 are very similar to dissolution pits described by Botfalvai *et al.* (2014) in carapace fragments of Cretaceous turtles. The pits on NHMD 227324 are interpreted as pathologies, although post-mortem bioerosion by invertebrates or microbial activity cannot be fully excluded.

Conclusions

The two new turtle fragments add important new information about the Paleocene turtle fauna of Denmark. Despite the very limited material, a hypoplastron and a carapace fragment, the morphological and morphometrical analysis allows us to identify the hypoplastron NHMD 227325 as *Ctenochelys* cf. *stenop-*

rus. This is the first evidence of the genus *Ctenochelys* surviving the K/Pg boundary mass extinction event. The carapace fragment NHMD 227324 can be assigned to the family Cheloniidae indet. only. Both specimens show evidence of crocodylian predation or scavenging, and the carapace fragment further show evidence of scavenging by sharks.

Acknowledgements

The present study is partly based on a B.Sc. project by the first author at the Natural History Museum of Denmark, supervised by the two co-authors. We are grateful to Mette A.G. Hofstedt, Peter Mortensen and Mogens S. Nielsen, who discovered the specimens and brought them to our attention. Mette A.G. Hofstedt provided excellent preparation work of the specimens. Sten L. Jakobsen kindly provided photos and practical help. Peter Mortensen is also thanked for fruitful discussions on fossils from the Gundstrup gravel pit. Erik Thomsen and Bent Lindow are thanked for their critical and constructive reviews of the manuscript.

References

- Adolfssen, J.S., Milàn, J. & Friedman, M. 2017: Review of the Danian vertebrate fauna of southern Scandinavia. *Bulletin of the Geological Society of Denmark* 65, 1–23.
- Adolfssen, J.S. & Ward, D.J. 2015: Neoselachians from the Danian (Early Palaeocene) of Denmark. *Acta Palaeontologica Polonica* 60, 313–338.
- Botfalvai, G., Prondvai, E., & Ösi, A. 2014: Inferred bite marks on a Late Cretaceous (Santonian) bothremydid turtle and a hylaeochampsid crocodylian from Hungary. *Cretaceous Research* 50, 304–317.
- Clemmensen, A. & Thomsen, E. 2005: Palaeoenvironmental changes across the Danian–Selandian boundary in the North Sea Basin. *Palaeogeography, Palaeoclimatology, Palaeoecology* 219, 351–394.
- Dames, W. 1897: Ueber Meeresschildkröten aus der oberen Kreide von Kopenhagen. *Meddelelser fra Dansk Geologisk Forening* 1, 73–74.
- Hay, O.P. 1905: A revision of the species of the family of fossil turtles called Toxochelyidae, with descriptions of two new species of *Toxochelys* and a new species of *Portochelys*. *Bulletin of the American Museum of Natural History* 21, 177–185.
- Heilmann-Clausen, C. 2010: Palaeogen – Fra drivhus til kølehus. *Geoviden* 2010/3, 2–11.
- Hirayama, R. 1997: Distribution and diversity of Cretaceous chelonoids. In: Callaway, J.M. & Nicholls, E.L. (eds), *Ancient marine reptiles*, 225–243. San Diego: Academic Press.

- Jensen, J.B., Leth, J.O., Borre, S. & Nørgaard-Pedersen, N. 2010: Model for potentielle sand- og grusforekomster for de danske farvande. Delområdet Jyske Rev – Lille Fisker Banke. Danmarks og Grønlands Geologiske Undersøgelse Rapport 2010/23, 52 pp.
- Joyce, W.G., Parham, J.F. & Gauthier, J.A. 2004: Developing a protocol for the conversion of rank-based taxon names to phylogenetically defined clade names, as exemplified by turtles. *Journal of Paleontology* 78, 989–1013.
- Joyce, W.G., Parham, J.F., Lyson, T.R., Warnock, R.C.M. & Donoghue, P.C.J. 2013: A divergence dating analysis of turtles using fossil calibrations: an example of best practises. *Journal of Paleontology* 87, 612–634.
- Karl, H.-V. & Lindow, B.E.K. 2009: First evidence of a Late Cretaceous marine turtle (Testudines: Chelonioida) from Denmark. *Studia Geologica Salmanticensia* 45, 175–180.
- Karl, H.-V. & Lindow, B.E.K. 2012: Revision of the Paleocene turtles of Denmark. *Studia Geologica Salmanticensia* 9, 175–192.
- Karl, H.-V. & Nyhuis, C.J. 2012: *Ctenochelys stenoporus* (Hay, 1905) (Testudines: Toxochelyidae) and *Clidastes* sp. (Squamata: Mosasauridae) from the Upper Cretaceous of NW-Germany. *Studia Palaeochelonologica* IV, 129–142.
- Larsen, N.K., Knudsen, K.L., Krohn, C.F., Kronborg, C., Murray, A.S. & Nielsen, O.B. 2009: Late Quaternary ice sheet, lake and sea history in southwest Scandinavia – a synthesis. *Boreas* 38, 732–761.
- Lehman, T.M. & Tomlinson, S.L. 2004: *Terlinguachelys fishbecki*, a new genus and species of sea turtle (Chelonioida: Protostegidae) from the Upper Cretaceous of Texas. *Journal of Paleontology* 78, 1163–1178.
- Leth, J.O. 1996: Late Quaternary geological development of the Jutland Bank and the initiation of the Jutland Current, NE North Sea. *Norges Geologiske Undersøgelse Bulletin* 430, 25–34.
- Leth, J.O. 2003: Nordsøen efter istiden – udforskningen af Jyske Rev. *Geologi – Nyt fra GEUS* 2003/3, 12 pp.
- Milàn, J., Kofoed, J., & Bromley, R.G. 2010: Crocodylian-chelonian carnivory: bite traces of dwarf caiman, *Paleosuchus palpebrosus*, in red-eared slider, *Trachemys scripta*, carapaces. *New Mexico Museum of Natural History and Science Bulletin* 51, 195–200.
- Milàn, J., Lindow, B.E.K., & Lauridsen, B.W. 2011: Bite traces in a turtle carapace fragment from the middle Danian (Lower Paleocene) bryozoan limestone, Faxø, Denmark. *Bulletin of the Geological Society of Denmark* 59, 61–67.
- Owen R. & Bell T. 1849: Chelonia. Supplement to the Eocene Chelonia. In: *Palaeontological Society of London* (ed.), *Monograph on the fossil Reptilia of the London Clay*, Part I, 1–79.
- Rosenkrantz, A. 1920: Craniakalk fra Kjøbenhavns Sydhavn. *Danmarks Geologiske Undersøgelse*, II række 36, 1–79.
- Rosenkrantz, A. 1921: Meddelelse om tertiære Skildpadder fra Danmark. In: *Oversigt over Dansk geologisk Forenings Møder og Ekskursioner fra Januar til December 1921*. *Meddelelser fra Dansk Geologisk Forening* 6, 2–3.
- Rosenkrantz, A. 1923: En Trionyx fra Craniakalk-blokke i København. *Meddelelser fra Dansk Geologisk Forening* 6, 3–14.
- Schnetler, K.I. & Nielsen, M.S. 2018: A Palaeocene (Selandian) molluscan fauna from boulders of Kerteminde Marl in the gravel-pit at Gundstrup, Fyn, Denmark. *Cainozoic Research* 18, 3–81.
- Schwarz-Wings, D., Milàn, J., & Gravesen, P. 2014: A new eusuchian (Crocodylia) tooth from the Early or Middle Paleocene, with a description of the Early Middle Paleocene boundary succession at Gemmas Allé, Copenhagen, Denmark. *Bulletin of the Geological Society of Denmark* 62, 17–26.
- Surlyk, F., Rasmussen, S.L., Boussaha, M., Schiøler, P., Shovsbo, N.H., Sheldon, E., Stemmerik, L. & Thibault, N. 2013: Upper Campanian–Maastrichtian holostratigraphy of the eastern Danish Basin. *Cretaceous Research* 46, 232–256.
- Thomsen, E. 1995: Kalk og kridt i den danske undergrund. In: Nielsen, O.B. (ed.), *Danmarks geologi fra Kridt til i dag*. *Århus Geokompender* 1, 31–68. Århus University.
- Thomsen, E. & Heilmann-Clausen, C. 1985: The Danian-Selandian boundary at Svejstrup with remarks on the biostratigraphy of the boundary in western Denmark. *Bulletin of the Geological Society of Denmark* 33, 341–362.
- Troedsson, G.T. 1924: On Crocodylian Remains from the Danian of Sweden. *Lunds Universitets Årsskrift, Ny följd, Avdelning* 2, 20, 1–75.
- Vandenbergh, N., Hilgen, F.J. & Speijer, R.J. 2012: The Paleogene Period. In: Gradstein, F.M., *et al.* (eds), *The Geologic Time Scale 2012*, 855–921. Amsterdam: Elsevier.
- Weems, R.E. 1988: Paleocene turtles from the Aquia and Brightseat Formations, with a discussion of their bearing on sea turtle evolution and phylogeny. *Proceedings of the Biological Society of Washington* 101, 109–145.
- Weems, R.E. 2014: Paleogene chelonians from Maryland and Virginia. *PaleoBios* 31, 1–32.
- Zangerl, R. 1953: The vertebrate fauna of the Selma Formation of Alabama. Part IV. The turtles of the family Toxochelyidae. *Fieldiana: Geology Memoirs* 3, 137–277.
- Zangerl, R. 1980: Patterns of Phylogenetic Differentiation in the Toxochelyid and Cheloniid Sea Turtles. *American Zoologist* 20, 585–596.



Book Review: Oceans of Archaeology

OLE BENNIKE

Received 19 July 2018
Accepted in revised form
5 September 2018
Published online
26 October 2018

Bennike, O. 2018. Book review: *Oceans of Archaeology*. ©2018 by Bulletin of the Geological Society of Denmark, Vol. 66, pp. 219–221. ISSN 2245-7070. (www.2dgf.dk/publikationer/bulletin).

Ole Bennike [obe@geus.dk], Geological Survey of Denmark and Greenland, Øster Voldgade 10, DK-1350 Copenhagen K, Denmark.

Fischer, A. & Pedersen, L. (eds) 2018: *Oceans of Archaeology*. Jysk Arkæologisk Selskabs Skrifter vol. 101, 237 pp. ISBN 978-87-93423-18-3. Aarhus: Aarhus Universitetsforlag.

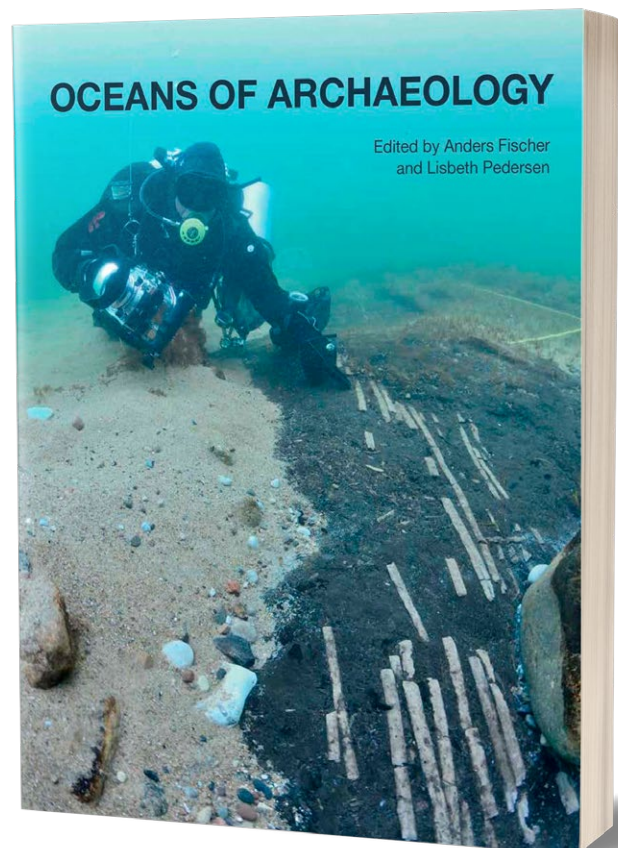
This book describes flooded Stone Age settlements in Europe and puts them into a temporal and spatial context. During the last ice age, the global sea level was *c.* 130 m lower than at present. About 20 000 years ago, the sea level began to rise and vast shallow-water areas with settlements were flooded. In many parts of the world, high energy levels and large waves mean that traces of former archaeological sites were erased when the coastal shelf was inundated. However, at places that have been sheltered from large waves, the submarine archaeological sites may be far better preserved than sites on land. This book presents numerous examples of such well-preserved sea floor sites from all over Europe, with a strong representation of sites from the sheltered inner Danish waters.

The last decades have seen a marked rise in exploitation of the sea floor around the world. At the same time, there has been tremendous technological advances in high-resolution submarine surveys. Also scuba diving has developed, allowing researchers and amateur archaeologists to explore the sea floor much more efficiently than before. Another technological development concerns chemical analyses of lipids found as food crusts on pottery, an aspect briefly touched on in one chapter. Finally, radiocarbon dating by accelerator mass spectrometry has led to a revolution in age determination of small samples.

Oceans of Archaeology developed out of an EU network. Two books have appeared as a result of the network's effort: one on the geology of submerged prehistoric landscapes and the present volume dealing with archaeology.

Although *Oceans of Archaeology* mainly deals with archaeology, the volume also includes a wealth of data and interpretations that are highly relevant to

geologists. Perhaps the most important issues relate to relative sea-level changes and the palaeogeographical evolution after the last deglaciation. These subjects have been debated for many years. In 1840, J.G. Forchhammer noted that raised marine and littoral deposits in Denmark are found only in the north-eastern part of the country, and he suggested that this part of the



land was rising whereas areas to the south-east were subsiding. His so-called tilt line dividing these areas is included in a map on page 68; however modern GPS measurements and high-precision levelling now indicate that land is rising all over Denmark, even in the south-west.

Several curves showing sea-level changes are included in the book. One shows global eustatic changes over the past 450 000 years, another curve provides a more detailed picture of changes over the last 35 000 years, and a curve shows relative sea-level changes in Øresund. Unfortunately, it is difficult to evaluate the latter curve because no details are provided on the samples that were used to construct the curve or how differences in land uplift were accounted for. Hopefully, details will be published elsewhere. Anyway, there is a large potential for cooperation between geologists and archaeologists when it comes to study relative shore-level changes in southern Scandinavia. The book also states: "it would clearly be advantageous to develop partnerships with the geological and technical research disciplines engaged in studying submerged landscapes" (page 198).

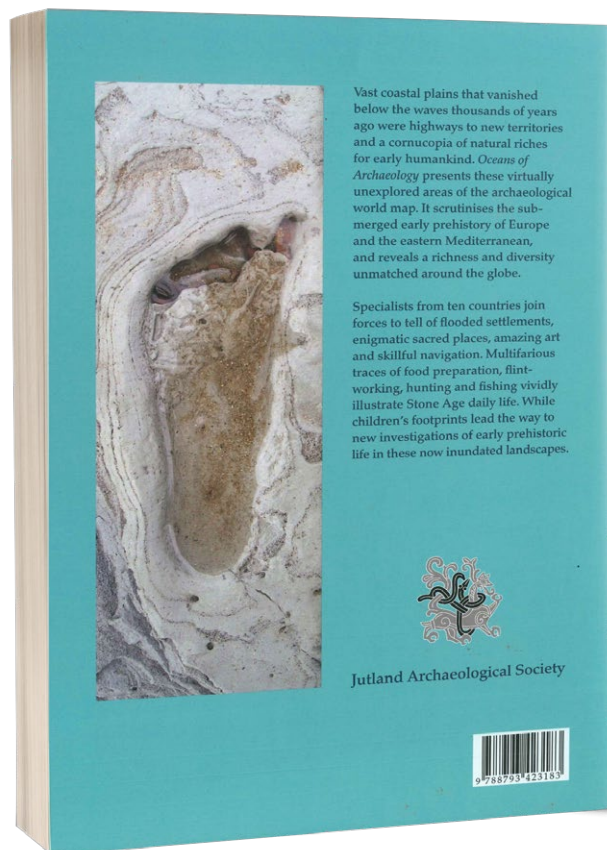
A few maps show the distribution of submerged sites across Europe. The high concentration of sites in Danish waters is remarkable. A series of six maps illustrate the palaeogeographical evolution of southern Scandinavia from 14 000 to 6500 years BP; these maps are based on publications by Danish, Swedish and Polish geologists. The book also contains numerous photographs, all of a high quality, showing divers in action, tree stumps on the sea floor and 6000 years old, still green leaves, but the majority of the photos shows artefacts, many of them made of wood. There are also many drawings, the most remarkable are perhaps those showing paddle blades from Tybrind Vig in Denmark. The blades show detailed patterns that are interpreted as human faces.

Some of the photographs show remains of mammals dredged from the sea floor. From a site in Køge Bugt come reindeer remains that have been modified by humans, and from the North Sea comes a red deer antler also modified by humans. From the southern North Sea is a skull of a mammoth, several molars of mammoth and a canine of a walrus found on a beach in Belgium. The latter was originally identified as a horn of the woolly rhinoceros, but according to the figure caption, it is now identified as an upper canine of the extant walrus (*Odobenus rosmarus*). However, the dark colour of the specimen may indicate that it comes from the Pliocene walrus *Ontocetus*. The inclusion of these non-archaeological finds helps to widen the scope of the book.

The book comprises 33 chapters that are grouped into six parts. Part 1 is an introduction, part 2 deals

with land-based sites, part 3 explores inundated sites and provides national overviews, part 4 describes methods, management and preservation of flooded sites, part 5 provides a synthesis and discusses strategies for the future, and part 6 includes a long list of radiocarbon dates. The list includes laboratory numbers and radiocarbon ages. This means that the reader will be able to re-calibrate ages when the calibration curves are modified in the future. Many older archaeological articles only give calibrated ages and no laboratory numbers, which means that the reader is unable to re-calibrate the ages. Hence, it is a great help that these details are provided in the book. It is also a great help to geologists that the book uses years BP throughout; archaeologists often use years BC/AD, which can hamper discussions between geologists and archaeologists. Each chapter is followed by a list of references, which is a great help to the reader, instead of having all references listed at the very end of the book.

Because the book developed from an EU network, most chapters deal with Europe, but some notes on Israel and Turkey are also included. Denmark is strongly represented both in terms of chapters and in terms of contributors. This reflects the fact that Denmark has by far the largest dataset, with several sites studied in detail.



One of the chapters discusses how far prehistoric people travelled over the sea. Already about 50 000 years ago, people crossed over from south-east Asia to Australia, a journey at least 70 km long. In Denmark, Stone Age people travelled 25 km from Sjælland to Hesselø for hunting, and travelled on the Kattegat during winter to hunt sea birds that came from breeding grounds in the north. Early prehistoric seafarers also crossed Skagerrak, travelled along the coast of Norway and from the Orkney Islands to the Shetland Islands – but not to the Faroe Islands or Iceland.

During the reading, I discovered very few errors, reflecting thorough editorial handling and work by the reviewers – two reviewers evaluated each chapter. However, I was surprised to learn on page 185 that European Neanderthals hunted penguins during the last interglacial. I assume it should be great auk (*Pinguinus impennis*, gejrfugl). The name penguin was originally applied to the great auk – but later used for a similar-looking, flight-less bird in the south.

A total of 35 authors from ten countries have contributed to the book, and an additional c. 70 persons

have acted as reviewers, provided photos or helped in other ways. From these numbers it is clear that it has taken a tremendous effort to put the book together. Many of the chapters are authored or co-authored by Anders Fischer, and he has also taken many of the photographs of divers in action. The book is well written and easy to read, well organised and very well illustrated. In addition, the numerous references make it easy for the reader to pursue special interests. The price is 348 DKK ex. VAT for the hard-cover book + e-book; 240 DKK ex. VAT for the e-book.

Several books and numerous papers have appeared during the last decades dealing with submerged Stone Age settlements and drowned landscapes. One may ask if we need another book. However, *Oceans of Archaeology* is the first book to cover the whole European continent. The reviewer was impressed by all the topics covered in this book. I can happily recommend it not only to archaeologists but also to geoscientists, in particular to those interested in the coastal zone, in the huge areas covered by the sea, in Quaternary science and in geoarchaeology.

Anopolenus henrici Salter, a middle Cambrian (Drumian) centroleurid trilobite from the Alum Shale Formation of Scandinavia

THOMAS WEIDNER & JAN OVE R. EBBESTAD



Weidner, T. & Ebbestad, J.O.R. 2018. *Anopolenus henrici* Salter, a middle Cambrian (Drumian) centroleurid trilobite from the Alum Shale Formation of Scandinavia. © 2018 by Bulletin of the Geological Society of Denmark, Vol. 66, pp. 223–228. ISSN 2245-7070. (www.2dgf.dk/publikationer/bulletin).

Centroleurid trilobites include five genera of which *Centroleura* Angelin, *Anopolenus* Salter, *Clarella* Howell and *Luhops* Šnajdr are known from eight species in the traditional middle Cambrian (Miaolingian Series, Drumian Stage) of Sweden and Denmark (Bornholm). *Beishanella* Xiang & Zhang has not been recorded in Scandinavia so far, and no centroleurids have been reported from Norway. Of these taxa, only *Centroleura* is common in Scandinavia. Two pygidia previously identified as *Centroleura* sp. and *Anopolenus* sp. from erratics in Germany and Bornholm, respectively, as well as a new pygidium from Scania in Sweden are here identified as *Anopolenus henrici* Salter. Elsewhere, the species is known from Wales, Avalonian Canada, Siberia, Alaska, and Sardinia, occurring in the *A. atavus* and *P. punctuosus* zones (the former in Siberia only). The presence of this species increases the known diversity of Centroleuridae in Scandinavia and is important for correlation between Baltica and Avalonia.

Keywords: Centroleurid trilobite, Miaolingian, Drumian, Alum Shale Formation, Bornholm, Scania, Scandinavia.

Thomas Weidner [to.we@paradis.dk], Ravnholtvej 23, Rårup, DK-7130 Juelsminde, Denmark. Jan Ove R. Ebbestad [jan-ove.ebbestad@em.uu.se], Museum of Evolution, Uppsala University, Norbyvägen 22, SE-752 36 Uppsala, Sweden.

Corresponding author: Jan Ove R. Ebbestad.

New specimens of *Anopolenus henrici* Salter from Scandinavia (Fig. 1) give fresh insight into the morphology and distribution of centroleurid trilobites. The Miaolingian family Centroleuridae Angelin 1854 includes *Centroleura* Angelin 1854, *Beishanella* Xiang & Zhang 1985, *Anopolenus* Salter 1864, *Clarella* Howell 1933 and *Luhops* Šnajdr 1957 (Dean & Rushton 1997; Fortey & Rushton 2007) (Fig. 2). In Scandinavia, only *Centroleura* is common; *Anopolenus*, *Clarella* and *Luhops* are known from rare findings, while *Beishanella* has not been encountered.

Centroleura is represented in Scandinavia by three species: *C. lovéni* (Angelin 1851) (Sweden and Bornholm, Denmark) and *C. angelini* Westergård 1950 (Sweden), both from the lower part of the *Lejopyge laevigata* Zone (formerly *Solenopleura brachymetopa* Zone) and *C. angustata* Westergård 1950 (Sweden), probably originating from the *Ptychagnostus punctuosus* Zone (Westergård 1950). *Anopolenus* is known from one pygidium in the upper part of the *Acidusus atavus* Zone on Bornholm (Weidner & Nielsen 2014), where

also *Clarella impar* (Hicks 1872) occurs frequently in the uppermost part of the same zone (Weidner & Nielsen 2014). Additional species of *Clarella* on Bornholm are *C. groenwalli* Howell & Poulsen 1933 (? = *Luhops expectans*, see below) known from one cranidium in the *P. punctuosus* Zone, and *C. steenstrupi* (Angelin 1878) known from the lower part of the *L. laevigata* Zone. Westergård (1950) reported a single cranidium of *Clarella* cf. *impar* from the *P. punctuosus* Zone at Andrarum, Scania, Sweden. *Luhops expectans* (Barrande 1852) is known from one fragmentary pygidium reported from the upper part of the *A. atavus* Zone on Bornholm (Weidner & Nielsen 2014), but it is noted that Rushton (2011) questionably reassigned *C. groenwalli* to *L. expectans*. Centroleurid trilobites have not been described from Norway so far, but one damaged pygidium of *Luhops* has been found in the *A. atavus* Zone of the Oslo Region in Norway (M. Høyberget, personal communication 2018). For world-wide distribution of the Centroleuridae, we refer to Dean & Rushton (1997) and Rushton (2011).

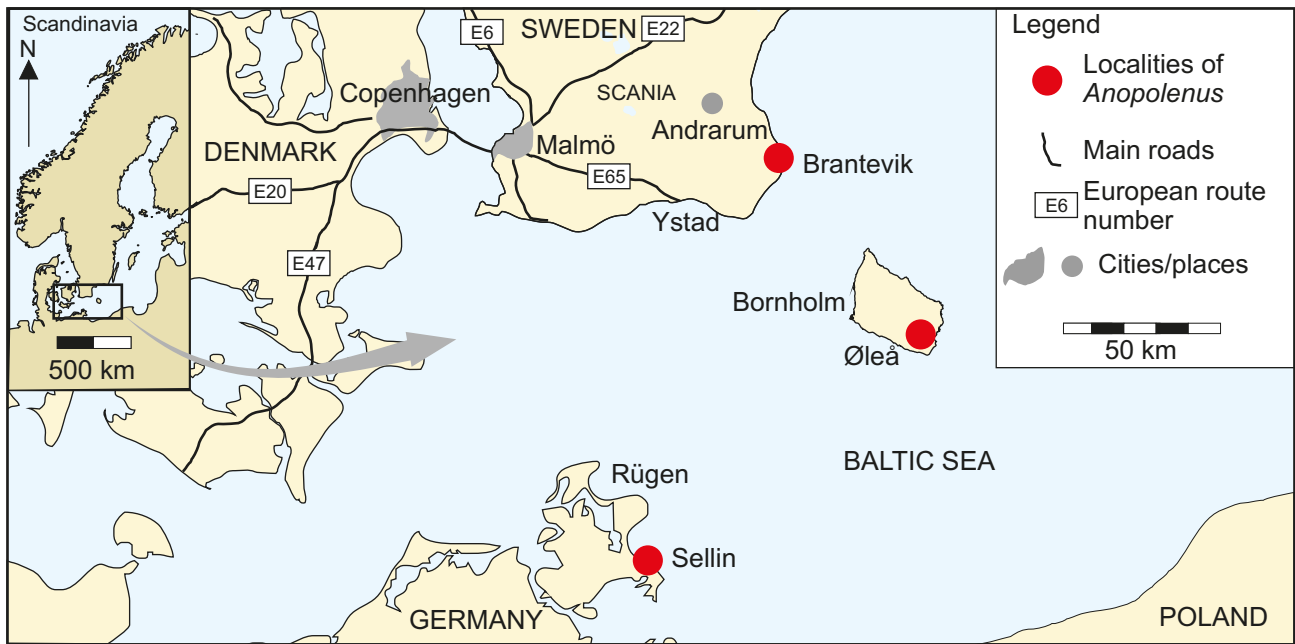


Fig. 1. Map of southern Sweden and northern Germany showing the localities mentioned for the material described herein.

Chronostratigraphy				Trilobite biostratigraphy			Ranges of Centropleuridae in Scandinavia		
System	Series	Global Stage	Local Stage	Superzones	Polymerid Zonation	Agnostoid zonation			
Cambrian	Miaolingian	Guzhangian	Not defined	<i>Paradoxides forchhammeri</i>	<i>Simulolenus alpha</i>	<i>Agnostus pisiformis</i>	SB	S	
					Not defined	<i>Lejopyge laevigata</i>			
					<i>Solenopleura? brachymetopa</i>				
		Drumian	Not defined	<i>Paradoxides paradoxissimus</i>	Not defined	<i>Paradoxides davidis</i>	<i>Goniagnostus nathorsti</i>	S	SB
					<i>Baillia ornata</i>	<i>Ptychagnostus punctuosus</i>			
		Wuliuan	Almbackenian	Bödan	<i>Acadoparadoxides oelandicus</i>	<i>Ctenocephalus exsulans</i>	<i>Triplagnostus gibbus</i>	B	S
	<i>Acadoparadoxides pinus</i>					<i>Pentagnostus praecurrens</i>			
					<i>Eccaparadoxides insularis</i>	Not defined			

Fig. 2. Biozonation of the Miaolingian Series with ranges and occurrences of Centropleuridae in Scandinavia. Occurrences are given with S = Sweden, B = Bornholm. The ranges of the different taxa are colour coded for clarity. Revised zonation according to Weidner & Nielsen (2015); regional stages according to Nielsen & Schovsbo (2015).

Howell (1933) used the curvature of the palpebral lobes to differentiate the genera and this approach was adopted by Dean & Rushton (1997). Westergård (1950) observed the same difference between *Centropleura* and *Anopolenus* but pointed out that it was less marked in juvenile specimens. Most of the illustrations of *A. henrici* show cranidia. Complete specimens have been figured as well (Egorova *et al.* 1982; Levi-Setti 1993),

while other complete specimens are displayed on private homepages, but illustrated pygidia are scarce and the photos are generally of low standard and quality.

Two pygidia previously referred to *Centropleura* sp. (Buchholz 1991; Rudolph 1994) and *Anopolenus* sp. (Weidner & Nielsen 2014) and an additional new specimen are now identified as *Anopolenus henrici* and described herein. The presence of this species

increases the known diversity of Centroleuridae in Scandinavia and is important for the correlation between Baltica and Avalonia.

Illustrated and cited material is housed in the collections at the Natural History Museum, University of Copenhagen (MGUH), the Palaeontological collections, Museum of Evolution, Uppsala University, Sweden (PMU), the collection of Buchholz, Stralsund (SB-MK), and the Sedgwick Museum of Earth Sciences, Cambridge, England (SM).

Systematic palaeontology

Family Centroleuridae Angelin 1854

Genus *Anopolenus* Salter 1864

Type species (by monotypy). *Anopolenus henrici* Salter 1864; Menevian Beds (*Hypagnostus parvifrons* and *Ptychagnostus punctuosus* agnostoid zones), St. David's, Wales.

Diagnosis. See Lake (1934) and Dean & Rushton (1997).

Anopolenus henrici Salter 1864

Figure 3A1–C4

1864 *Anopolenus henrici* n.sp. – Salter, p. 236, pl. 13, figs 4–5.

1865 *Anopolenus henrici* Salter – Salter, pp. 476–477, 480–482, figs 2–3.

1865 *Anopolenus salteri* n.sp. – Hicks, pp. 477–480, fig. 1.

1934 *Centroleura henrici* (Salter) – Lake, pp. 189–192, pl. 24, figs 1–12.

1962 *Anopolenus henrici* Salter – Hutchinson, p. 112, pl. 17, figs 12–18.

1982 *Anopolenus henrici* Salter – Egorova *et al.*, p. 78, pl. 6, figs 8–9; pl. 10, figs 1–2; pl. 12, fig. 14; pl. 13, figs 1–3; pl. 14, fig. 4; pl. 15, figs 6–7; pl. 17, figs 9–11; pl. 56, fig. 9; pl. 61, fig. 8.

1991 *Centroleura* sp. – Buchholz, p. 220, pl. 2, fig. 9.

1993 *Anopolenus henrici* Salter – Levi-Setti, pl. 95.

1994 *Centroleura* sp. 1 – Rudolph, p. 176, pl. 18, fig. 14.

cf. 1995 *Anopolenus* cf. *Henrici* – Loi *et al.*, pl. 4, fig. 21.

1995 *Anopolenus henrici* Salter – St. John & Babcock, fig. 7J.

1997 *Anopolenus henrici* Salter – Dean & Rushton, pp. 478–479, fig. 309:2a–c.

2014 *Anopolenus henrici* Salter – Rees *et al.*, figs 1.11a, 1.12c, f.

2014 *Anopolenus* sp. – Weidner & Nielsen, p. 70, fig. 42L.

2016 *Anopolenus henrici* Salter – Bushuev & Makarova, p. 21, pl. 2, fig. 4.

Lectotype (designated by Morris 1988). Latex cast of external mould of a cephalon, SM A5367, from the *Ptychagnostus punctuosus* Zone at Porth-y-rhaw, Wales. It was originally figured by Lake (1934, pl. 24, fig. 1).

Occurrence. *Anopolenus henrici* is previously reported from Wales (Lake 1934; Rees *et al.* 2014), Avalonian Canada (Hutchinson 1962; Levi-Setti 1993) and Siberia (Egorova *et al.* 1982; Bushuev & Makarova 2016). It is very rare in Alaska (St. John & Babcock 1995) and on Sardinia, Italy (Loi *et al.* 1995). In Siberia, the species occurs in the lower and upper part of the *A. atavus* Zone; in the other areas in the *P. punctuosus* Zone or equivalent strata.

Material. Three pygidia are available (Fig. 3). One is from the upper part of the *Acidusus atavus* Zone at Øleå, Bornholm, Denmark (Fig. 3A₁–A₄, 0.62 cm long) (MGUH 30155, figured by Weidner & Nielsen 2014, fig. 42L as *Anopolenus* sp.). The second is from an ice-rafted limestone block found at Sellin on the island of Rügen, Germany, with provenance from the Bornholm area (figured by Buchholz 1991, pl. 2, fig. 9, SB-MK 143.53, and Rudolph 1994, pl. 18, fig. 14 as *Centroleura* sp.; a cast is kept at the Museum of Evolution, PMU 31754). It derives from the *P. punctuosus* Zone (Fig. 3B₁–B₄, 0.93 cm long). The third specimen is from a boulder of the *P. punctuosus* Zone found at the shore near Brantevik, Scania, Sweden (Fig. 3C₁–C₄, 1.44 cm long) (PMU 31755). Measurements of the three specimens are listed in Table 1.

Table 1. Measurements of the available specimens of *Anopolenus henrici* Salter 1864

Specimen	Width (cm)	Length (cm)	Width axis (cm)	Length axis (cm)
Fig. 3A, MGUH 30155	1.10	0.62	0.40	0.47
Fig. 3B, SB-MK 143.53 (PMU 31754, cast)	1.43	0.93	0.46	0.64
Fig. 3C, PMU 31755	2.50	1.44	0.88	1.06

Length measurements do not include the articulating half ring.

Description. Since Lake (1934), no new descriptions of *A. henrici* have been published. Lake's meticulous description of the pygidium is repeated here with some modifications using modern terminology (Lake 1934, pp. 190–191):

- rather wide, without any definite antero-lateral angle, anterior border arching backwards at the sides and passing into the lateral border.

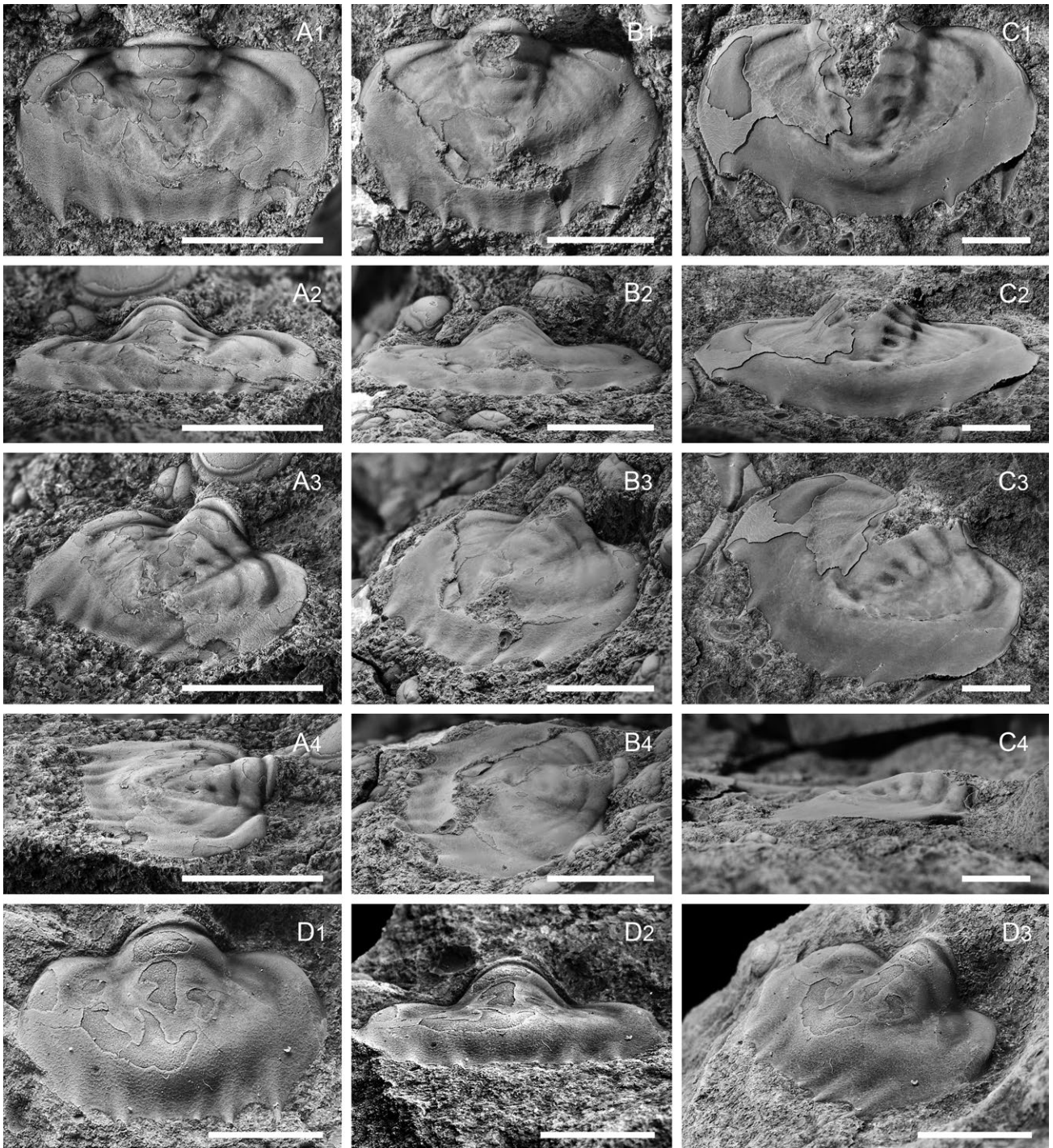


Fig. 3. **A₁–C₄**: pygidia of *Anopolenus henrici* Salter 1864 in dorsal, posterior, oblique and lateral views. **A₁–A₄**: MGUH 30155, *Acidusus atavus* Zone, Øleå, Bornholm, Denmark. This was previously figured by Weidner & Nielsen (2014). **B₁–B₄**: SB-MK 143.53, *Ptychagnostus punctuosus* Zone, Sellin, island of Rügen, Germany; cast PMU 31754 kept at the Museum of Evolution, Uppsala. This was previously figured by Buchholz (1991) and Rudolph (1994). **C₁–C₄**: PMU 31755, *P. punctuosus* Zone, Brantevik, Scania, Sweden, collected by H.-J. Schmütz. **D₁–D₃**: MGUH 30153, pygidium of *Clarella impar* (Hicks 1872) for comparison in dorsal, posterior and oblique views. *Acidusus atavus* Zone at Øleå, Bornholm, Denmark. This was figured previously by Weidner & Nielsen (2014). Scale bars represent 5 mm.

- the posterior border nearly straight, but with at least three projecting points on each side (i.e. three pairs of spines), of which the one at the postero-lateral angle is most prominent.
- there is a broad and slightly concave margin with a raised interior edge, the doublure of the margin carries terrace lines.
- axis prominent, conical, occupying about a third of the total width at the anterior margin, not quite reaching the concave margin, consisting of four rings in addition to the terminal piece.
- the lateral lobes show indications of several pleurae of which the anterior is well defined, broadens outwards and curves backwards; the next two are recognizable, the rest are obscure; all are totally effaced on the external surface of the concave margin.
- on the internal cast they are represented by ridges crossing the doublure and ending in points on the posterior border.
- on each side three of these ridges and points are usually visible and correspond with the first three pleurae, but there are several less distinct ridges interior to these (Fig. 3B₁) which may have ended in smaller points.

The pygidia figured here agree with the description provided by Lake (1934). As indicated by him, all specimens have in addition to three distinct pairs of spines an inner pair of incipient spines. In the largest pygidium (Fig. 3C), the pleurae on the posterior border are less pronounced than in the other two specimens. Lake (1934) stated that the posterior margin is almost straight, however, in all well-preserved pygidia the margin is somewhat rounded (Lake 1934, pl. 24, fig. 10–12; Levi-Setti 1993, pl. 95; Dean & Rushton 1997, fig. 309:2c). Weidner & Nielsen (2014) discussed the three specimens we describe here and tentatively suggested that they could represent different species.

On Bornholm, *Clarella impar* (Hicks 1872) may occur associated with *Anopolenus henrici*. It differs from *A. henrici* in having a longer axis, obscured axial furrows, less pronounced segmentation of the axis and especially of the pleural fields, the lack of a border, and by having a straight posterior margin (Fig. 3D₁–D₃; Weidner & Nielsen 2014, fig. 42E–G, I).

Only one pygidium tentatively assigned to *Centroleura lovéni* (Angelin 1851) has been illustrated (Westergård 1950). The specimen is from the Andrarum Limestone Bed of the lower part of the *L. laevigata* Zone in Scania and is distinguished from *A. henrici* by having three axial rings plus the terminal piece, two distinct pleurae that terminate in posterior border spines and one fainter pleura that ends in a small point at the posterior margin. A border is not developed.

Conclusion

Anopolenus and *Clarella* are typical members of the Avalonian faunas of England, Wales, and eastern Newfoundland (Howell 1933). *Luhops* was originally described from Bohemia, Czech Republic (Snajdr 1957) and subsequently also reported from England (Rushton 2011). The occurrence of *Anopolenus*, *Clarella*, and *Luhops* on Bornholm confirms the close biogeographic relationship between faunas from the middle Miaolingian of Bornholm and Avalonia (Weidner & Nielsen 2014). The relationship between Bornholm and the remainder of Scandinavia is less pronounced.

Acknowledgements

We are grateful to Dr Alfred Buchholz, Stralsund, for lending us the specimen in his collection and permitting a cast to be made and stored at the PMU. Hans-Jürgen Schmütz, Laboe, is thanked for kindly donating his specimen from southern Sweden to the PMU collection. Magne Høyberget, Mandal, kindly provided information on Norwegian occurrences of centroleurids. Comments from Per Ahlberg, Lund, and Arne Thorshøj Nielsen, Copenhagen, greatly improved the manuscript.

References

- Angelin, N.P. 1851: Palæontologia Svecica 1. Iconographia Crustaceorum Formationis Transitionis, Part 1. Weigel, Leipzig, Bergeling, Lund, 24 pp.
- Angelin, N.P. 1854: Palæontologia Scandinavica 1. Iconographia Crustaceorum Formationis Transitionis, Part 2. Weigel, Leipzig, Bergeling, Lund, i–x, 21–92.
- Angelin, N.P. 1878: Palæontologia Scandinavica 1. Crustacea Formationis Transitionis, Parts 1–2. Edited by G. Lindström. Samson & Wallin, Stockholm, x + 96 pp.
- Barrande, J. 1852: Système silurien du centre de la Bohême. Ière partie: Recherches paleontologiques. I. Crustacés. Trilobites. Prague, xxx + 935 pp.
- Buchholz, A. 1991: Mittelkambrische Geschiebe vom Bornholm-Typ (Hyalithenkalk) mit *Opsidiscus rugiensis* n. sp. und einer reichen Begleitfauna. Archiv für Geschiebekunde 1, 217–224.
- Bushuev, E.V. & Makarova, A.L. 2016: Middle Cambrian polymerid trilobites of the Chaya Formation from Ust-Mayskaya 366 well (southeastern Siberian Platform). Geology and mineral resources of Siberia, DOI 10.20403/2078-0575, 3, 2016, 11.
- Dean W.T. & Rushton, A.W.A. 1997: Systematic Description of the Superfamily Paradoxidoidea, 470–481. In: Kaesler,

- R.L. (ed.), *Treatise on Invertebrate Paleontology. Part O. Arthropoda 1, Trilobita*, revised. Volume 1. Geological Society of America, Boulder, Colorado & Lawrence, Kansas.
- Egorova, L.I., Shabanov, Yu.Ya., Pegel, T.V., Savitsky, V.E., Suvchov, S.S. & Chernysheva, N.E. 1982: [Maya Stage of Type Locality (Middle Cambrian of Siberian platform)]. *Academy of Sciences of the USSR, Ministry of Geology of the USSR, Transactions* 8, 146 pp. [In Russian].
- Fortey, R.A. & Rushton, A.W.A. 2007: The mid-Cambrian trilobite *Beishanella* and the limits of convergent evolution. *Memoirs of the Association of Australasian Palaeontologists* 34, 391–399.
- Hicks, H. 1865: Note on the genus *Anopolenus*. *Quarterly Journal of the Geological Society of London* 21, 478–480.
- Hicks, H. 1872: On some undescribed fossils from the Menevian Group. *Quarterly Journal of the Geological Society of London* 28, 173–185.
- Howell, B.F. 1933: The classification of the trilobite subfamily, *Centropleurinae*. *Meddelelser fra Dansk Geologisk Forening* 8, 215–219.
- Howell, B.F. & Poulsen, C. 1933: A new Cambrian trilobite, *Clarella grönwalli*, from Bornholm. *Meddelelser fra Dansk Geologisk Forening* 8, 220–223.
- Hutchinson, R.D. 1962: Cambrian stratigraphy and trilobite faunas of southeastern Newfoundland. *Geological Survey of Canada, Bulletin* 88, 1–156.
- Lake, P. 1934: A Monograph of the British Cambrian Trilobites. Part 8. *Monograph of the Palaeontographical Society*, London 86 (391), 189–192.
- Levi-Setti, R. 1993: *Trilobites*, 342 pp. The University of Chicago Press. Chicago and London.
- Loi, A., Pillola, G.L. & Leone, F. 1995: The Cambrian and Early Ordovician of south-western Sardinia. In: Cherchi, A. (ed.), *Sardinia 95, 6th Paleobenthos International Symposium, Guide-book. Rendiconti del Seminario della Facoltà di Scienze dell'Università di Cagliari, supplement* 65, 63–81.
- Morris, S.F. 1988: A review of British trilobites, including a synoptic revision of Salter's monograph. *Monograph of the Palaeontographical Society*, London 140 (574), 1–316.
- Nielsen, A.T. & Schovsbo, N.H. 2015: The regressive Early–Mid Cambrian 'Hawke Bay Event' in Baltoscandia: Epeirogenic uplift in concert with eustasy. *Earth-Science Reviews* 151, 288–350.
- Rees, A.J., Thomas, A.T., Lewis, M., Hughes, H.E., & Turner, P. 2014: The Cambrian of SW Wales: towards a united Avalonian stratigraphy. *Geological Society Memoir* 42, 1–139.
- Rudolph, F. 1994: *Die Trilobiten der mittelmambrischen Gesschiebe*. Verlag Frank Rudolph, Wankendorf, 309 pp.
- Rushton, A.W.A. 2011: The mid-Cambrian (Drumian) centropleurid trilobite *Luhops* and its relatives from the Abbey Shale Formation near Nuneaton, central England. *Memoirs of the Association of Australasian Palaeontologists* 42, 93–104.
- Salter, J.W. 1864: On some new fossils from the Lingula-flags of Wales. *Quarterly Journal of the Geological Society of London* 20, 233–241.
- Salter, J.W. 1865: On some additional fossils from the Lingula-flags (With a Note on the Genus *Anopolenus* by H. Hicks). *Quarterly Journal of the Geological Society of London* 21, 476–482.
- Šnajdr, M. 1957: O nových trilobitech z českého Kambria [On new trilobites of the Cambrian of Bohemia]. *Věstník Ústředního Ústavu Geologického* 32, 235–244. [In Czech].
- St. John, J.M. & Babcock, L.E. 1997: Late Middle Cambrian trilobites of Siberian aspect from the Farewell Terrane, southwestern Alaska. In: Dumoulin, J.A. & Gray, J.E. (eds), *Geologic studies in Alaska by the U.S. Geological Survey, 1995: U.S. Geological Survey Professional Paper* 1574, 269–281.
- Weidner, T. & Nielsen, A.T. 2014: A highly diverse trilobite fauna with Avalonian affinities from the Middle Cambrian *Acidusus atavus* Zone (Drumian Stage) of Bornholm, Denmark. *Journal of Systematic Palaeontology* 12, 23–92.
- Weidner, T. & Nielsen, A.T. 2015: *Agraulos longicephalus* and *Proampyx? depressus* (Trilobita) from the Middle Cambrian of Bornholm, Denmark. *Bulletin of the Geological Society of Denmark* 63, 1–11.
- Westergård, A.H. 1950: Non-agnostidean trilobites of the Middle Cambrian of Sweden. II. *Sveriges Geologiska Undersökning Serie C* 511, 1–56.
- Xiang, L.W. & Zhang, T.R. 1985: Description of the trilobites. In: Wang, J. *et al.*, *Stratigraphy and trilobite faunas of the Cambrian in the western part of the Northern Tianshan, Xinjiang*. Ministry of Geology and Mineral Resources, *Geological Memoirs, Series 2, Stratigraphy and Palaeontology* 4, 64–165. [in Chinese with English summary].

First record of *Epicymatoceras vaelsense* (Nautilida) from the Maastrichtian white chalk of northern Denmark

OKSANA MALCHYK & MARCIN MACHALSKI



Malchyk, O. & Machalski, M. 2018. First record of *Epicymatoceras vaelsense* (Nautilida) from the Maastrichtian white chalk of northern Denmark. © 2018 by Bulletin of the Geological Society of Denmark, Vol. 66, pp. 229–235. ISSN 2245-7070. (www.2dgf.dk/publikationer/bulletin).

The atypical Late Cretaceous nautilid *Epicymatoceras vaelsense* (Binkhorst van den Binkhorst, 1862) is described and illustrated on the basis of three specimens from the Maastrichtian white chalk of Denmark. One of these is probably from the lower/upper Maastrichtian boundary interval at Frejlev, while the other two originate from the uppermost Maastrichtian chalk as exposed in the Dania quarry; both localities are in Jylland, northern Denmark. These are first reports of *E. vaelsense* from Denmark; the species has previously been recorded from the uppermost Campanian and lower Maastrichtian of the Netherlands, Belgium, northern Germany and Poland. The presence of *E. vaelsense* in the topmost Maastrichtian white chalk in the Dania quarry is considered the youngest record of *Epicymatoceras* known to date, suggesting the persistence of the genus until the end of the Cretaceous. The diameter of the embryonic conch of the Danish *E. vaelsense* may be estimated at c. 30 mm, based on an individual from the Dania quarry, confirming earlier observations that the species possessed one of the largest embryonic conchs amongst Late Cretaceous nautilids.

Keywords: Upper Cretaceous, Cephalopoda, *Epicymatoceras*, Denmark, embryonic conch, K–Pg mass extinction.

Oksana Malchyk [omalcz@twarda.pan.pl], Marcin Machalski [mach@twarda.pan.pl], Institute of Paleobiology, Polish Academy of Sciences, Twarda 51/55, 00-818 Warszawa, Poland.

Received 27 May 2018
Accepted in revised form
31 October 2018
Published online
22 November 2018

Fossil nautilids are uncommon in Maastrichtian and Danian deposits of Denmark. In addition, they are still rather poorly presented in the literature (e.g. Ravn 1902; Rosenkrantz 1944, 1960; Gravesen 2001). The following species have been described from the Maastrichtian and Danian of Denmark: *Eutrephoceras darupense* (Schlüter, 1876), *E. bellerophon* (Lundgren, 1867), *Cymatoceras? patens* (Kner, 1848), *Hercoglossa danica* (von Schlotheim, 1820) and *Danathuroidea fricator* (Beck, in Lyell 1835). Of these, *E. darupense* has been recorded from the lower/upper Maastrichtian interval at Frejlev (Jylland), *C.? patens* from the same interval and locality as well as from the lower Maastrichtian of Møns Klint, south-eastern Denmark, while *E. bellerophon*, *H. danica*, and *D. fricator* are on record from the middle Danian at Faxø and the upper Danian at Saltholm, both in Sjælland, eastern Denmark (Ravn 1902). Rosenkrantz (1944) reported on the presence of *Eutrephoceras* and *Hercoglossa* in the Maastrichtian chalk of Stevns Klint, south-eastern Sjælland. In addition, several specimens assigned to *Eutrephoceras*, *Cimomia*(?), *Cymatoceras* or “*Nautilus*”(?) have been recorded from Maastrichtian strata exposed at Møns Klint, Gedser Odde in south-eastern Denmark and in Jylland, northern Denmark (Gravesen & Jakobsen 2013), see Fig. 1A.

The aim of the present note is to describe and illustrate the first records of the nautilid *Epicymatoceras vaelsense* (Binkhorst van den Binkhorst, 1862) from the Maastrichtian white chalk of Denmark. This material, three specimens in total, comes from two Maastrichtian sites in Jylland, northern Denmark (Fig. 1B). The specimens studied are stored in the collections of the Natural History Museum of Denmark, Copenhagen (registration numbers MGUH 33073, 33074 and 33075); they were briefly mentioned by Malchyk *et al.* (2017, p. 3). These new specimens contribute to a better understanding of regional and global patterns of nautilid turnover during the Late Cretaceous and early Paleogene interval, which is significant in the context of the ongoing debate on the nature of the Cretaceous–Paleogene (K–Pg) mass extinction (e.g. Goolaerts *et al.* 2014; Landman *et al.* 2014; Goolaerts 2018; Malchyk 2018).

Stratigraphy and localities

Traditionally, the upper Campanian to Maastrichtian chalk in Denmark has been subdivided into ten

microbrachiopod zones (Surlyk 1970, 1984). These were correlated with the conventional European belemnite zonal scheme, according to which the base of the Maastrichtian was defined by the first occurrence (FO) of *Belemnella lanceolata* (e.g. Birkelund 1957; Schulz & Schmid 1983; Christensen 1996, 1997). However, in recent years, the definition of the Campanian–Maastrichtian boundary has changed. The Global Stratotype Section and Point (GSSP) for the base of the Maastrichtian Stage is placed at the 115.2 m level at Tercis near Dax, south-west France (Odin 2001; Odin & Lamaurelle 2001). According to the Tercis definition, the base of the Maastrichtian

Stage is significantly higher than the level of the FO of *Belemnella lanceolata* (e.g. Walaszczyk 2004; Remin 2012; see also Machalski 2012). Therefore, the Campanian–Maastrichtian boundary as defined at Tercis is placed in Denmark within the *Rugia spinosa*–*Terebratulina subtilis* Zone of Surlyk (1970, 1984) (Fig. 1C).

The precise geographical provenance of one of the specimens studied (MGUH 33074) is unknown. However, as stated on the original label, it is most likely from Frejlev, northern Denmark (Fig. 1B). The Frejlev section spans the lower–upper Maastrichtian interval boundary, the *Rugia tenuicostata*–*Meonia semiglobularis* Zone to the *Meonia semiglobularis*–*Rue-*

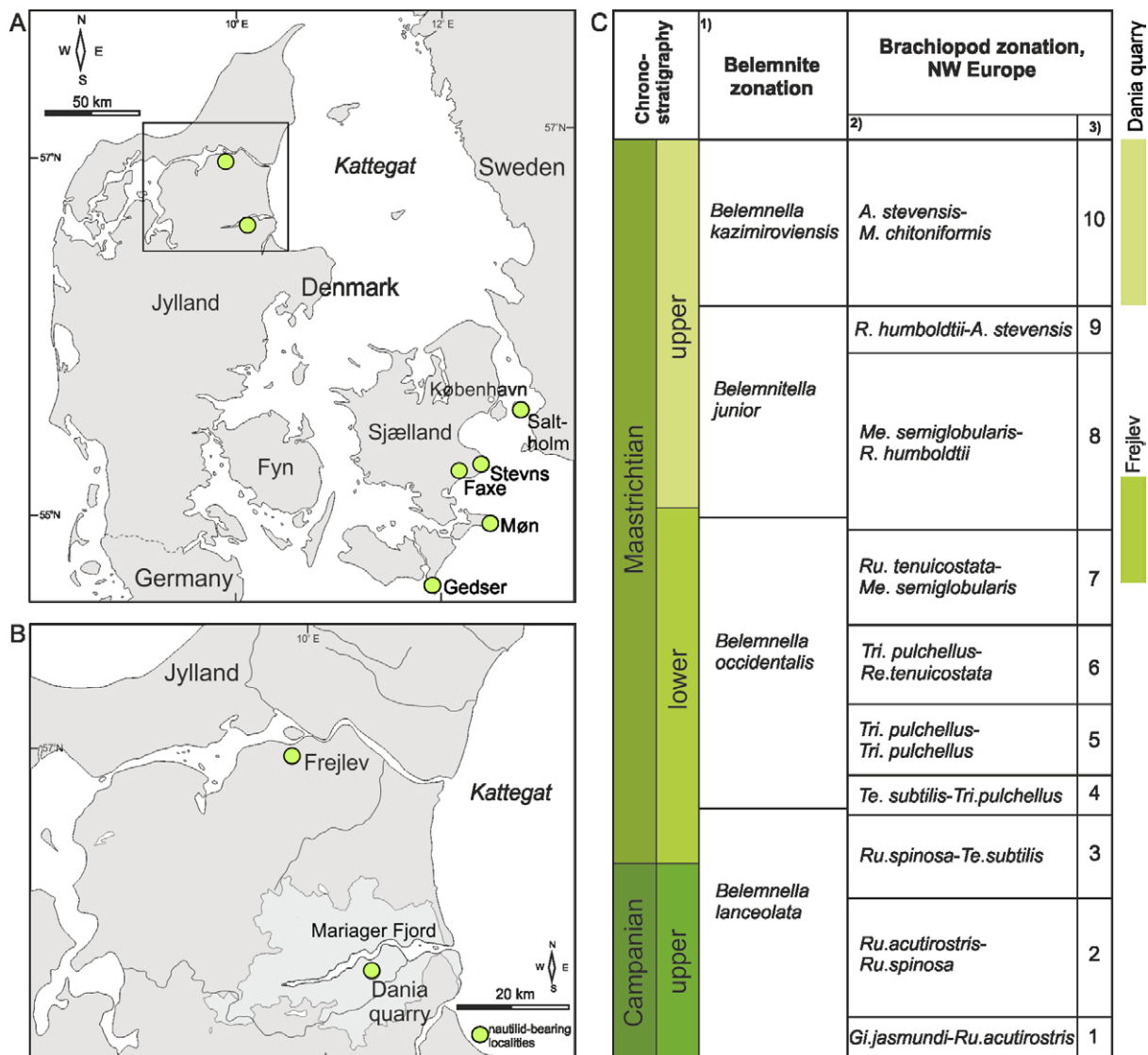


Fig. 1. A: Map of Denmark with localities mentioned in the text. B: Location of the two sections that yielded the nautilid *Epicymatoceras vaelsense* in northern Denmark. C: Stratigraphy of upper Campanian and Maastrichtian strata in north-western Europe. Sources: 1) Birkelund (1957); 2) Surlyk (1984); 3) Surlyk (1970). Abbreviations: A.: *Argyrotheca*; Gi.: *Gisilina*; M.: *Magas*; Me.: *Meonia*; Rue.: *Ruegenella*; Ru.: *Rugia*; Te.: *Terebratulina*; Tri.: *Trigonosemus*. Chronostratigraphy modified according to the new definition of the base of the Maastrichtian Stage and subsequent correlations (Odin 2001; Odin & Lamaurelle 2001; Walaszczyk 2004; Remin 2012).

genella humboldtii Zone of Surlyk (1984) (Fig. 1C). In terms of belemnite zonation, this stratigraphic interval belongs to the lower part of the *Belemnitella junior* Zone and the upper part of the *Belemnella fastigata* Zone (Schulz 1979; Schulz & Schmid 1983). Therefore, MGUH 33074 is probably from either the uppermost lower Maastrichtian *Ru. tenuicostata*–*Me. semiglobularis* Zone, or from the lowermost upper Maastrichtian *Me. semiglobularis*–*Rue. humboldtii* Zone.

Specimens MGUH 33073 and MGUH 33075 are from the Dania limestone quarry. This is an abandoned chalk pit, currently overgrown by vegetation (S.L. Jakobsen, personal communication 2018), situated on the south side of Mariager Fjord (Fig. 1A). A Maastrichtian–Danian boundary succession of carbonate deposits, c. 30 m thick, was formerly available at this quarry (Håkansson & Hansen 1979). The Maastrichtian part of the Dania quarry succession corresponds to the *Argyrotheca stevensis*–*Magas chitoniformis* brachiopod Zone (Fig. 1C), which is the equivalent of the *Belemnella kazimiroviensis* Zone (Schulz 1979; Schulz & Schmid 1983; Surlyk 1984; Birkelund 1993) and can be correlated with the *Palynodinium grallator* dinoflagellate Zone of Hansen (1977). It should also be noted that the Maastrichtian part of the Dania succession yielded the topmost Maastrichtian zonal coccolith species *Micula prinsii* (Håkansson & Hansen 1979). The precise position of both nautilid specimens within the Dania section is unknown. However, they are safely assigned a latest Maastrichtian age, based on the data presented above. Specimen MGUH 33073 was collected by Mogens Steentoft Nielsen at the beginning of the 21st century and subsequently transferred to the collections of the Natural History Museum of Denmark (Copenhagen), having been declared Danekræ (catalogue number 886, see <http://www.danicafossils.dk/>).

Systematic palaeontology

Order Nautilida Agassiz, 1847

Superfamily Nautiloidea de Blainville, 1825

Family Cymatoceratidae *sensu* Chirat and Bucher, 2006

Genus *Epicymatoceras* Kummel, 1956

Type species. *Nautilus vaelsensis* Binkhorst van den Binkhorst, 1862. p. 15, pl. 5, fig. 2.

Diagnosis. “Widely evolute, greatly compressed; whorl section subquadrate, nearly twice as high as wide; ventral shoulders angular, venter narrow and flattened; flanks only slightly inflated; umbilical shoulders broadly arched; suture with shallow ventral lobe and shallow lateral lobe; position of siphuncle unknown; surface bearing fine sinuous ribs that curve backward toward ventral shoulders and form slight sinus on venter” (Kummel 1964, p. K454).

Epicymatoceras vaelsense (Binkhorst van den Binkhorst, 1862).

1862 *Nautilus vaelsensis* Binkhorst van den Binkhorst, p. 15, pl. 5, fig. 2a–c.

1876 *Nautilus vaelsensis* Binkhorst van den Binkhorst – Schlüter, p. 177, pl. 51, fig. 3.

1887 *Nautilus vaelsensis* Binkhorst van den Binkhorst – Holzapfel, p. 68, pl. 4, fig. 4.

1956 *Epicymatoceras vaelsense* (Binkhorst van den Binkhorst) – Kummel, p. 439, pl. 23, figs. 1–2.

2012 *Epicymatoceras vaelsense* (Binkhorst van den Binkhorst) – Jagt, p. 141, pl. 30, figs G–H.

2017 *Epicymatoceras vaelsense* (Binkhorst van den Binkhorst) – Malchuk *et al.*, p. 5, fig. 3.

Material. Three specimens in mould preservation (MGUH 33073, 33074 and 33075). Specimen MGUH 33074 probably originates from the lower/upper Maastrichtian boundary at Frejlev; specimens MGUH 33073 and 33075 come from the topmost Maastrichtian succession in the Dania limestone quarry.

Description. Specimen MGUH 33073 (Fig. 2A) from the Dania quarry is an internal mould comprising the larger part of the phragmocone, measuring approximately 73 mm in maximum preserved diameter. The whorl section is compressed and subquadrate. Coiling is relatively evolute. The umbilicus is wide, c. 25 per cent of the diameter, with steeply inclined umbilical wall and broadly rounded umbilical shoulder. The flanks are flat. The ventrolateral shoulder of this specimen is angular in the early part of conch and seems to be more rounded in the latest stage, as preserved. The venter is generally flat; however, it seems to be slightly convex on the outermost part of the last preserved whorl of the phragmocone. The position of the siphuncle is uncertain. The ornamentation of MGUH 33073 consists of coarse radial ribs, up to 3 mm in maximum width and separated by narrow and deep grooves (> 1 mm). Ribs arise at the umbilical seam, broadening across the flank with a sigmoidal curve and suddenly curving backwards at the ventrolateral shoulder, forming a narrow ventral sinus. They are poorly expressed and almost

effaced on the higher flank and the early stages of the phragmocone, but are stronger and more convex at mid-flank and ventrolateral shoulder on the later part of the phragmocone.

A nepionic constriction delimiting pre- and post-hatchling stages is well recognised as a narrow depression on the innermost whorl (Fig. 2A). The embryonic conch is characterised by a poorly expressed reticulate pattern dominated by longitudinal lirae and measures about 15 mm in visible diameter. Based on the assumption that in the early whorl stages in *Epicymatoceras* the height of every next whorl is half covered by the next one (see Malchyk *et al.* 2017), the total embryonic diameter is estimated to have been approximately 30 mm, thus matching the hatching diameter reported for specimens of *E. vaelsense* from the Upper Cretaceous of Poland.

MGUH 33074 (Fig. 2B) from Frejlev(?) is probably the most complete specimen of *E. vaelsense* ever to

have been recorded. It is an internal mould of the phragmocone and a large portion of the body chamber, extending to the aperture with a maximum preserved conch diameter of c. 128 mm. A partially preserved apertural margin is recognised on the right side of the specimen studied as a slightly curved outline (Fig. 2C). Unfortunately, the shape of the hyponomic and ocular sinuses could not be determined due to the fragmentary preservation of the specimen. One may note that the ribs tend to become weaker and less pronounced in the adapertural part of the shell, when compared to the main body of the individual (Fig. 2C). Conch shape is relatively evolute, gradually becoming more evolute towards the later whorl stages. The whorl section is compressed with generally flattened flanks. The umbilicus is large and comprises about 27 per cent of the diameter, the umbilical wall is inclined and the umbilical shoulder is broadly rounded. The ventrolateral shoulder is an-

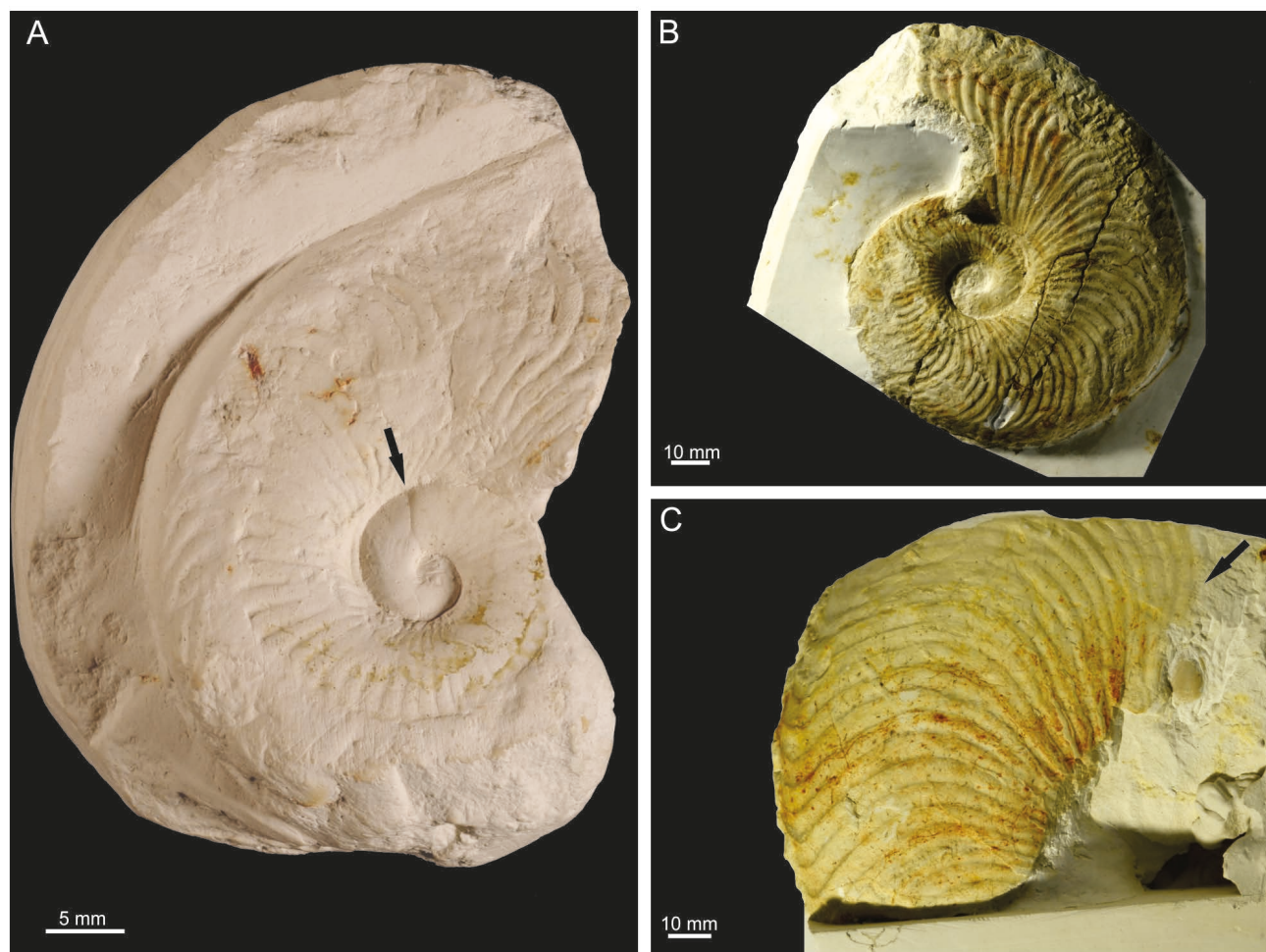


Fig. 2. The cymatoceratid *Epicymatoceras vaelsense* from the Maastrichtian of northern Denmark (Jylland). **A:** Specimen MGUH 33073 from the Dania quarry. The arrow indicates the nepionic constriction between embryonic and post-embryonic parts of the shell. **B** and **C:** Specimen MGUH 33074, probably from Frejlev. **B:** Left view. **C:** Right view of a partially broken body chamber displaying the apertural margin (arrow).

gular, the venter is flat. The surface of MGUH 33074 is ornamented by very prominent ribbing. Ribs are about 1 mm in width at the umbilicus and become up to 4–5 mm wide towards the aperture, showing some bifurcation at mid-flank. Ribs are strongly expressed on the phragmocone and become less conspicuous on the adapertural part of the body chamber. The embryonic conch is not visible in this particular specimen.

MGUH 33075 from Dania is a fragmentary internal mould consisting of three fragments, not illustrated here. The largest piece comprises a portion of the umbilicus and flank and measures about 50 mm in length. One of the other remaining fragments is preserved as an external impression, probably of part of the lower and middle flank, and another one is the internal mould of a portion of the lower flank.

Comparison. *Epicymatoceras* Kummel, 1956 is an atypical Late Cretaceous nautilid genus that belongs to the family Cymatoceratidae Spath, 1927 (*sensu* Chirat & Bucher 2006; for a detailed discussion of the systematic position of *Epicymatoceras*, see Malchyk *et al.* 2017). Its relatively evolute conch coiling and prominent radial ribbing of the shell surface makes it easily recognisable (e.g. Kummel 1956; Goolaerts & Frank 2014; Malchyk *et al.* 2017). At present, it comprises only two species, namely *Epicymatoceras vaelsense* (Binkhorst van den Binkhorst, 1862) and *E. monstrum* Shimansky, 1975. The former has been recorded from the Netherlands, Belgium, Germany and Poland in Europe, with a stratigraphic range from the upper Campanian to the lower Maastrichtian (Binkhorst van den Binkhorst 1862; Schlüter 1876; Holzapfel 1887; Jagt *et al.* 1998; Jagt 2012; Goolaerts & Frank 2014; Malchyk *et al.* 2017). In the original description of Binkhorst van den Binkhorst (1862, p. 15), *Nautilus vaelsensis* is diagnosed as follows: “Testâ compressâ, discoïdali, striis numerosis, proximantibus, arcualis, ornatâ. Aperturâ subquadrilaterâ. Septis paululúm arcuatis”. The second species, *E. monstrum*, is known exclusively from the upper Maastrichtian of Mangyshlak, Kazakhstan (Shimansky 1975).

The morphological features of the present material allow it to be identified as *Epicymatoceras vaelsense*. However, the Danish specimens differ from the type material of *E. vaelsense* from the lower Maastrichtian of Vaals, province of Limburg, the Netherlands (Binkhorst van den Binkhorst 1862, pl. 5, fig. 2a–c), in having a slightly more convex venter and more strongly impressed ribbing. The specimens studied here are most closely similar to conspecific material from the upper Campanian and lower Maastrichtian of Poland (Malchyk *et al.* 2017, fig. 3A–B), but the Danish specimens show more rounded ventrolateral shoulders. These differences are most probably the

result of intraspecific variability of *E. vaelsense*.

Epicymatoceras monstrum, as described and figured by Shimansky (1975, p. 122, pl. 27, fig. 3), from the upper Maastrichtian of Mangyshlak is a generally similar form; however, it differs from the Danish specimens in having a much wider umbilicus (U ~ 30 per cent), more rounded umbilical and ventrolateral shoulders and more convex venter.

Occurrence. *Epicymatoceras vaelsense* is known from the upper Campanian to Maastrichtian of Belgium and the Netherlands (Binkhorst van den Binkhorst 1862; Jagt *et al.* 1998; Jagt 2012; Goolaerts & Frank 2014), Germany (Schlüter 1876; Holzapfel 1887), Poland (Malchyk *et al.* 2017) and Denmark (this work).

Discussion and conclusions

The first record of the genus *Epicymatoceras* from the Upper Cretaceous white chalk deposits of northern Denmark (Jylland) is presented. The Danish occurrences include three specimens of *Epicymatoceras vaelsense*, one from the lower/upper Maastrichtian boundary interval, the other two from the top of the Maastrichtian. Previous data on the stratigraphic range of *E. vaelsense* across Europe extended from the upper Campanian to the lower Maastrichtian (see above). On the basis of these data, the specimens described from the Dania quarry represent the youngest known records of *Epicymatoceras* to date, indicating that the genus extended into the latest Maastrichtian. Nevertheless, despite the persistence of *Epicymatoceras* until the end of the Cretaceous, all ribbed Cretaceous nautilids within the family Cymatoceratidae became extinct prior to, or at, the Cretaceous–Paleogene boundary (e.g. Ward *et al.* 2016; Malchyk *et al.* 2017).

It is possible to recognise the adapertural margin of *Epicymatoceras* for the first time; it was observed as a slightly curved outline on the preserved portion of the body chamber in specimen MGUH 33074, probably from Frejlev.

The cast of the embryonic conch of *Epicymatoceras vaelsense* is observable in specimen MGUH 33073 from the Dania quarry; its diameter is estimated to have been *c.* 30 mm. These new data on *E. vaelsense* from Denmark and the previously recorded hatchling diameter of *Epicymatoceras* from the upper Campanian from Poland confirm that the hatching size in this genus is near the maximum known range recorded for Cretaceous, Cenozoic and Recent nautilids (Landman *et al.* 1983; Matsumoto *et al.* 1984; Arnold *et al.* 1987; Landman 1988; Saunders *et al.* 1996; Cichowolski

2003; Cichowolski *et al.* 2005; Wani and Ayyasami 2009; Wani *et al.* 2011; Malchyk *et al.* 2017; Landman *et al.* 2018).

Acknowledgements

Sten Lennart Jakobsen (Copenhagen) is thanked for providing access to the nautilid collections under his care. John W.M Jagt (Maastricht) is thanked for linguistic correction of the text. Neil Landman (New York) and Jan Audun Rasmussen (Nykøbing Mors, Denmark) are acknowledged for their helpful reviews and comments.

References

- Agassiz, L. 1847: An introduction to the study of natural history, in a series of lectures delivered in the hall of the College of Physicians and Surgeons, 58 pp. Greeley & Mc-Grath, New York.
- Arnold, J.M., Landman, N.H. & Mutvei, H. 1987: Development of the embryonic shell of *Nautilus*. In: Saunders, W.B. & Landman, N.H. (eds), *Nautilus: the biology and paleobiology of a living fossil*, 373–400. Plenum Press, New York.
- Beck, H.H. (in Lyell, C. 1835–1837): Notes on the geology of Denmark. *Proceedings of the Geological Society of London* 2(43), 217–220.
- Binkhorst van den Binkhorst, J.T. 1862: Monographie des gastéropodes et des céphalopodes de la Craie supérieure du Limbourg, suivie d'une description de quelques espèces de crustacés du même depot crétacé, avec dix-huit planches dessinées et lithographiées par C. Hohe, de Bonn, 44 pp. Muquardt, Brussels; Muller Frères, Maastricht.
- Birkelund, T. 1957: Upper Cretaceous belemnites from Denmark. *Det Kongelige Danske Videnskabernes Selskab, Biologiske Skrifter* 9, 1–69.
- Birkelund, T. 1993: Ammonites from the Maastrichtian White Chalk of Denmark. *Bulletin of the Geological Society of Denmark* 40, 33–81.
- Blainville, H.M.D. de 1825–27: *Manuel de malacologie et de conchyliologie*, 664 pp. Levraut, Paris and Strasbourg.
- Chirat, R. & Bucher, H. 2006: Shell microstructure and morphogenesis of the ornamentation in *Cymatoceras* Hyatt, 1883, Cretaceous Nautilida. *Systematic implications*. *Lethaia* 39, 54–64.
- Cichowolski, M. 2003: The nautiloid genus *Cymatoceras* from the Cretaceous of the Neuquén and Austral basins, Argentina. *Cretaceous Research* 24, 375–390.
- Cichowolski, M., Ambrosio, A. & Concheyro, A. 2005: Nautilids from the Upper Cretaceous of the James Ross Basin, Antarctic Peninsula. *Antarctic Science* 17, 267–280.
- Christensen, W.K. 1996: A review of the Upper Campanian and Maastrichtian belemnite biostratigraphy of Europe. *Cretaceous Research* 17, 751–766.
- Christensen, W.K. 1997: The Late Cretaceous belemnite family Belemnitellidae: taxonomy and evolutionary history. *Bulletin of the Geological Society of Denmark* 44, 59–88.
- Danicafossils: <http://www.danicafossils.dk/>
- Goolaerts, S. 2018: Nautiloid turnover across the Cretaceous/Paleogene Boundary: Chicxulub impact, Deccan volcanism and Europe as key? In: El Hassani, A., Becker, R.T., Hartenfels, S. & Lüddecke, F. (eds), 10th International Symposium Cephalopods – Present and Past, Fes, Morocco, 2018. *Münstersche Forschungen zur Geologie und Paläontologie* 110, 30 only.
- Goolaerts, S. & Frank, J. 2014: *Epicymatoceras*: an exotic evolute nautilid from the European latest Cretaceous that does it all different. In: Klug, C. & Fuchs, D. (eds), *International Symposium Cephalopods – Present and Past, in combination with the 5th International Symposium Coleoid Cephalopods through Time*, Zürich 2014, 42 only.
- Goolaerts, S., Jagt, J.W.M., Jagt-Yazykova, E.A., Landman, N.H., Machalski, M. & Yacobucci, M. 2014: What about nautilids at the Cretaceous/Paleogene boundary? In: Klug, C. & Fuchs, D. (eds), *International Symposium Cephalopods – Present and Past, in combination with the 5th International Symposium Coleoid Cephalopods through Time*, Zürich 2014, 41 only.
- Gravesen, P. 2001: Den geologiske udforskning af Fakse Kalkbrud fra midten af 1700-tallet til nu. *Geologisk Tidsskrift* 2, 1–40.
- Gravesen, P. & Jakobsen, S.L. 2013: *Skrivekridtets Fossiler*, 2. udgave, 170 pp. Gyldendal, København.
- Håkansson, E. & Hansen, J.M. 1979: Guide to Maastrichtian and Danian boundary strata in Jylland. In: Birkelund, T. & Bromley, R.G. (eds), *Cretaceous–Tertiary Boundary Events Symposium I*, 171–188. University of Copenhagen, Copenhagen.
- Hansen, J.M. 1977: Dinoflagellate stratigraphy and echinoid distribution in Upper Maastrichtian and Danian deposits from Denmark. *Bulletin of the Geological Society of Denmark* 26, 1–26.
- Holzappel, E. 1887: Die Mollusken der Aachener Kreide. *Palaeontographica* 34, 29–72.
- Jagt, J.W.M. 2012: Nautiloïden, plesioteuthididen en sepiïden uit het Laat-Krijt en Vroeg-Paleogeen van Limburg. *Staringia* 13, 138–153.
- Jagt, J.W.M., Felder, W.M. & Janssens, H.J. 1998: Opmerkelijke Luiks-Limburgse Krijtfossielen. Deel 3. Een 'design' inktvis met een zekere gidswaarde? *Natuurhistorisch Maandblad* 87, 41–46.
- Kner, R. 1848: Versteinerungen des Kreidemergels von Lemberg und seiner Umgebung. *Naturwissenschaftliche Abhandlungen Haidinger* 3(2), 1–42.
- Kummel, B. 1956: Post-Triassic nautiloid genera. *Bulletin of the Museum of Comparative Zoology* 114, 324–494.

- Landman, N.H. 1988: Early ontogeny of Mesozoic ammonites and nautilids. In: Wiedmann, J. & Kullmann, J. (eds), *Cephalopods – Present and Past*, 215–228. Schweizerbart, Stuttgart.
- Landman, N.H., Rye, D.M. & Shelton, K.L. 1983: Early ontogeny of *Eutrephoceras* compared to Recent *Nautilus* and Mesozoic ammonites: evidence from shell morphology and light stable isotopes. *Paleobiology* 9, 269–279.
- Landman, N.H., Goolaerts, S., Jagt, J.W.M., Jagt-Yazykova, E.A. & Machalski, M. 2014: Ammonite extinction and nautilid survival at the end of the Cretaceous. *Geology* 42, 707–710.
- Landman, N.H., Grier, J.W., Cochran, J.K., Grier, J.C., Petersen, G. & Towbin, W.H. 2018: Nautilid nurseries: hatchlings and juveniles of *Eutrephoceras dekeyi* from the lower Maastrichtian (Upper Cretaceous) Pierre Shale of east-central Montana. *Lethaia* 51, 48–74.
- Lundgren, B. 1867: Palaeontologiska Iakttagelser öfver Faxekalken på Limhamn. I. – Lunds Universitets Års-Skrift 3, 1–31.
- Machalski, M. 2012: Stratigraphically important ammonites from the Campanian-Maastrichtian boundary interval of the Middle Vistula River section, central Poland. *Acta Geologica Polonica* 61(1), 91–116.
- Malchyk, O. 2018: Late Cretaceous and early Paleogene nautilids from Poland and western Ukraine. In: El Hassani, A., Becker, R.T., Hartenfels, S. & Lüddecke, F. (eds), 10th International Symposium Cephalopods–Present and Past, Fes, Morocco, 2018. Münstersche Forschungen zur Geologie und Paläontologie 110, 79–80.
- Malchyk, O., Machalski, M., Waksmundzki, B. & Duda, M. 2017: Shell ornament, systematic position and hatching size of *Epicymatoceras vaelsense* (Nautilida): new insights based on specimens in mould preservation from the Upper Cretaceous of Poland. *Cretaceous Research* 80, 1–12.
- Matsumoto, T., Takahashi, T., Obata, I. & Futakami, M. 1984: Cretaceous nautiloids from Hokkaido. *Transactions and Proceedings of the Palaeontological Society of Japan, New Series* 139, 288–299.
- Odin, G.S. 2001: The Campanian-Maastrichtian Boundary: definition at Tercis (Landes, SW France), principle, procedure, and proposal. In: Odin, G.S. (ed.), *The Campanian-Maastrichtian Stage Boundary: Characterization at Tercis les Bains (France) and Correlation with Europe and Other Continents*, 820–833. [Developments in Palaeontology and Stratigraphy Series 19]. Elsevier, Amsterdam.
- Odin, G.S. & Lamaurelle, M.A. 2001: The Global Campanian-Maastrichtian stage boundary at Tercis les Bains, Landes, SW France. *Episodes* 4, 229–237.
- Ravn, J.P.J. 1902: Molluskerne i Danmarks Kridtaflejringer. II. Scaphopoder, Gastropoder og Cephalopoder. *Det Kongelige Danske Videnskabernes Selskabs Skrifter*, 6. Række, Naturvidenskabelig og Matematisk Afdeling 11(4), 205–270 +5 plates.
- Remin, Z. 2012. The *Belemnella* stratigraphy of the Campanian–Maastrichtian boundary; a new methodological and taxonomic approach. *Acta Geologica Polonica* 62(4), 495–533.
- Rosenkrantz, A. 1944: Smaa bidrag til Danmarks Geologi. Meddelelser fra Dansk Geologisk Forening 10, 436–459.
- Rosenkrantz, A. 1960: Danian Mollusca from Denmark. International Geological Congress, XXI Session, Norden, Part V, The Cretaceous–Tertiary Boundary, 193–198.
- Saunders, W.B., Shimansky, V.N. & Amitrov, O. 1996: Clarification of *Nautilus praepompilius* Shimansky from the late Eocene of Kazakhstan. *Journal of Paleontology* 70, 609–611.
- Schlotheim, E.F. von 1820: Die Petrefactenkunde auf ihrem jetzigen Standpunkte durch die Beschreibung seiner Sammlung versteinerner und fossiler Überreste des Thier- und Pflanzenreichs der Vorwelt erläutert. 437 + 114 pp. + 52 plates. Becker'sche Buchhandlung, Gotha.
- Schlüter, C. 1876: Cephalopoden der oberen deutschen Kreide, 2. Abtheilung. *Palaeontographica* 24, 123–255.
- Schulz, M.-G. 1979: Morphometrisch-variationsstatistische Untersuchungen zur Phylogenie der Belemniten-Gattung *Belemnella* im Untermaastricht NW-Europas. *Geologisches Jahrbuch A47*, 3–157.
- Schulz, M.-G. & Schmid, F. 1983: Das Ober-Maastricht von Hemmoor (N-Deutschland): Faunenzonen-Gliederung und Korrelation mit dem Ober-Maastricht von Dänemark und Limburg. *Newletters on Stratigraphy* 13, 21–39.
- Shimansky, N.V. 1975: Melovyie nautiloidei [Cretaceous nautiloids]. *Trudy Paleontologicheskogo Instituta Akademii Nauk SSSR* 150, 1–208. [In Russian].
- Spath, L.F. 1927: Revision of the Jurassic Cephalopod fauna of Kachh (Cutch). *Memoirs of the Geological Survey of India. Palaeontologica India* 9, 1–84.
- Surlyk, F. 1970: Die Stratigraphie des Maastricht von Dänemark und Norddeutschland aufgrund von Brachiopoden. *Newletters on Stratigraphy* 1, 7–16.
- Surlyk, F. 1984: The Maastrichtian Stage in NW Europe, and its brachiopod zonation. *Bulletin of the Geological Society of Denmark* 33, 217–223.
- Walaszczyk, I. 2004. Inoceramids and inoceramid biostratigraphy of the Upper Campanian to basal Maastrichtian of the Middle Vistula River section, central Poland. *Acta Geologica Polonica* 54, 95–168.
- Wani, R. & Ayyasami, K. 2009: Ontogenetic change and intraspecific variation of shell morphology in the Cretaceous nautiloid (Cephalopoda, Mollusca) *Eutrephoceras clementinum* (d'Orbigny, 1840) from the Ariyalur area, southern India. *Journal of Paleontology* 83, 365–378.
- Wani, R., Kurihara, K. & Ayyasami, K. 2011: Large hatchling size in Cretaceous nautiloids persists across the end-Cretaceous mass extinction: new data of Hercoglossidae hatchlings. *Cretaceous Research* 32, 618–622.
- Ward, P., Dooley, F. & Barord, G.J. 2016: *Nautilus*: biology, systematics, and paleobiology as viewed from 2015. *Swiss Journal of Palaeontology* 135, 169–185.

Gamma-ray log correlation and stratigraphic architecture of the Cambro-Ordovician Alum Shale Formation on Bornholm, Denmark: Evidence for differential syndepositional isostasy

ARNE THORSHØJ NIELSEN, NIELS HEMMINGSEN SCHOVSBO, KURT KLITTEN, DAVID WOOLLHEAD & CHRISTIAN MAC ØRUM RASMUSSEN



Nielsen, A.T., Schovsbo, N.H., Klitten, K., Woollhead, D. & Rasmussen, C.M.Ø. 2018. Gamma-ray log correlation and stratigraphic architecture of the Cambro-Ordovician Alum Shale Formation on Bornholm, Denmark: Evidence for differential syndepositional isostasy. © 2018 by Bulletin of the Geological Society of Denmark, Vol. 66, pp. 237–273. ISSN 2245-7070. (www.2dgf.dk/publikationer/bulletin).

Received 19 January 2018
Accepted in revised form
13 August 2018
Published online
19 December 2018

The Cambro–Ordovician Alum Shale Formation on Bornholm, Denmark, is in total 26.7 to ≥ 34.9 m thick in nine boreholes, but may be up to ~ 39 m thick. The well sections are correlated using gamma-ray logs supplemented in some boreholes with resistivity and sonic logs. The gamma radiation of the ‘hot’ Alum Shale Formation primarily reflects the uranium content, which is moderately high in the Miaolingian (\approx middle Cambrian) and Tremadocian (Lower Ordovician), and very high in the Furongian (\approx upper Cambrian). The log pattern is calibrated with the detailed biozonation established in the Gislövshammar-1 and -2 wells in south-eastern Skåne, Sweden. Except for the *Eccaparadoxides oelandicus* Superzone, all superzones known from the Alum Shale in Scandinavia are also developed on Bornholm, but not all zones.

On Bornholm, the Miaolingian interval is 7.2–11.9 m thick, the Furongian is 16.4–22.8 m thick and the Tremadocian is 2.5–4.0 m thick. The Miaolingian strata exhibit no systematic thickness variations across southern Bornholm, whereas the Furongian *Parabolina*, *Peltura* and *Acerocarina* Superzones and, less pronounced, the Tremadocian, show increased condensation towards the south-east. In comparison with Skåne, the Alum Shale Formation is overall strongly condensed on Bornholm, but different stratigraphic levels show variable developments. The Miaolingian *Paradoxides paradoxissimus* Superzone is thus extremely condensed and incomplete, whereas the *Paradoxides forchhammeri* Superzone has almost the same thickness as in Skåne, and locally is even thicker. The Furongian *Olenus* and *Parabolina* Superzones are slightly thinner than in Skåne while the *Protopeltura*, *Peltura* and *Acerocarina* Superzones are half as thick or less. The Tremadocian is also much thinner on Bornholm. The Furongian *Olenus scanicus*–*O. rotundatus* and *Parabolina brevispina* Zones seem to be developed on Bornholm, and a thin ‘*Leptoplastus neglectus*’ Zone is also possibly present. The ‘*Parabolina megalops*’ Zone in the upper part of the *Peltura* Superzone appears to be absent. It is impossible to distinguish the individual thin zones in the lower part of the *Acerocarina* Superzone using wireline logs. A thin veneer of the Lower Ordovician Tøyen Formation, hitherto considered absent on Bornholm, is described from the Billegrav-2 core. It may also be present in the uncored Sømarken-3 and -4 wells. The Middle Ordovician Komstad Limestone Formation thins from c. 4.0–4.7 m in the Læså area to 0.1– c. 2.5 m in the Øleå area.

The general decrease in thickness of Cambro–Ordovician strata from Skåne to Bornholm and also within Bornholm from the Læså to the Øleå area is inferred to reflect isostatic uplift of the southern margin of Baltica commencing with the terminal ‘early’ Cambrian Hawke Bay Event and lasting until the Late Ordovician. In detail, several uplift and subsidence phases can be discerned. The isostatic adjustments are surmised to reflect stress changes related to ongoing plate tectonic processes in the adjacent closing Tornquist Sea.

Keywords: Cambrian, Ordovician, Alum Shale Formation, wireline log correlation, uranium, biostratigraphy, isostasy, Scandinavia, Bornholm.

Arne Thorshøj Nielsen [arnet@ign.ku.dk], Department of Geosciences and Natural Resource Management, University of Copenhagen, Øster Voldgade 10, DK-1350 Copenhagen K, Denmark. Niels Hemmingsen Schovsbo [nsc@geus.dk], Kurt Klitten [kk@geus.dk], Geological Survey of Denmark and Greenland, Øster Voldgade 10, DK-1350 Copenhagen K, Denmark. David Woollhead [dwoollhead@gmail.dk], Toftegårds Allé 7, lejl. 2a, DK-2500 Valby, Denmark. Christian Mac Ørum Rasmussen [christian@snm.ku.dk], Natural History Museum of Denmark, University of Copenhagen, Øster Voldgade 5–7, DK-1350 Copenhagen K, Denmark.

Corresponding author: Arne Thorshøj Nielsen.

The Scandinavian Alum Shale Formation was deposited from the 'mid' Cambrian (Miaolingian) to the Early Ordovician in the offshore deeper parts of a widespread epicontinental sea that covered western Baltica (Fig. 1). The formation comprises blackish, finely laminated, organic- and pyrite-rich mudstone, deposited under dys- and anoxic, maybe occasionally even euxinic conditions (Schovsbo 2000, 2001; Nielsen & Schovsbo 2007, 2015; Hints *et al.* 2014; Egenhoff *et al.* 2015). The mud was deposited extremely slowly; compacted accumulation rates were mostly only 1–2 mm/1000 years on average with a maximum of 4–5 mm/1000 years in southern Scandinavia (e.g. Lindström 1971; Schovsbo 2003). On Bornholm the average Furongian ('late' Cambrian) accumulation rate was ≤ 2.0 mm/1000 years but only *c.* 1 mm/1000 years for the Alum Shale Formation as a whole (compacted values). The low depositional rates in combination with the prevailing low-oxygen conditions near the

seafloor (and euxinia within the sediment) caused a strong enrichment of many trace elements in the shale, including Mo, V and U (Armands 1972; Andersson *et al.* 1985; Buchardt *et al.* 1997; Schovsbo 2001, 2002a). The high uranium content gives the 'hot' Alum Shale Formation a unique gamma-ray log pattern in wells (Pedersen & Klitten 1990; Schovsbo *et al.* 2011, 2015a,b, 2018; Ericsson 2012).

No detailed sea-level reconstructions have been published for the Alum Shale interval. During sea-level lowstands the storm wave base was lowered, causing erosion of the inboard parts of the unit (Nielsen & Schovsbo 2015), which created numerous regional hiatus in the mid-shelf succession (see Martinsson 1974, fig 5). At the same time the offshore successions in Skåne and the Oslo area became expanded due to outboard transport of reworked Alum Shale mud. By combining these data, a rough interpretation of general sea-level changes can be pieced together, which forms the basis

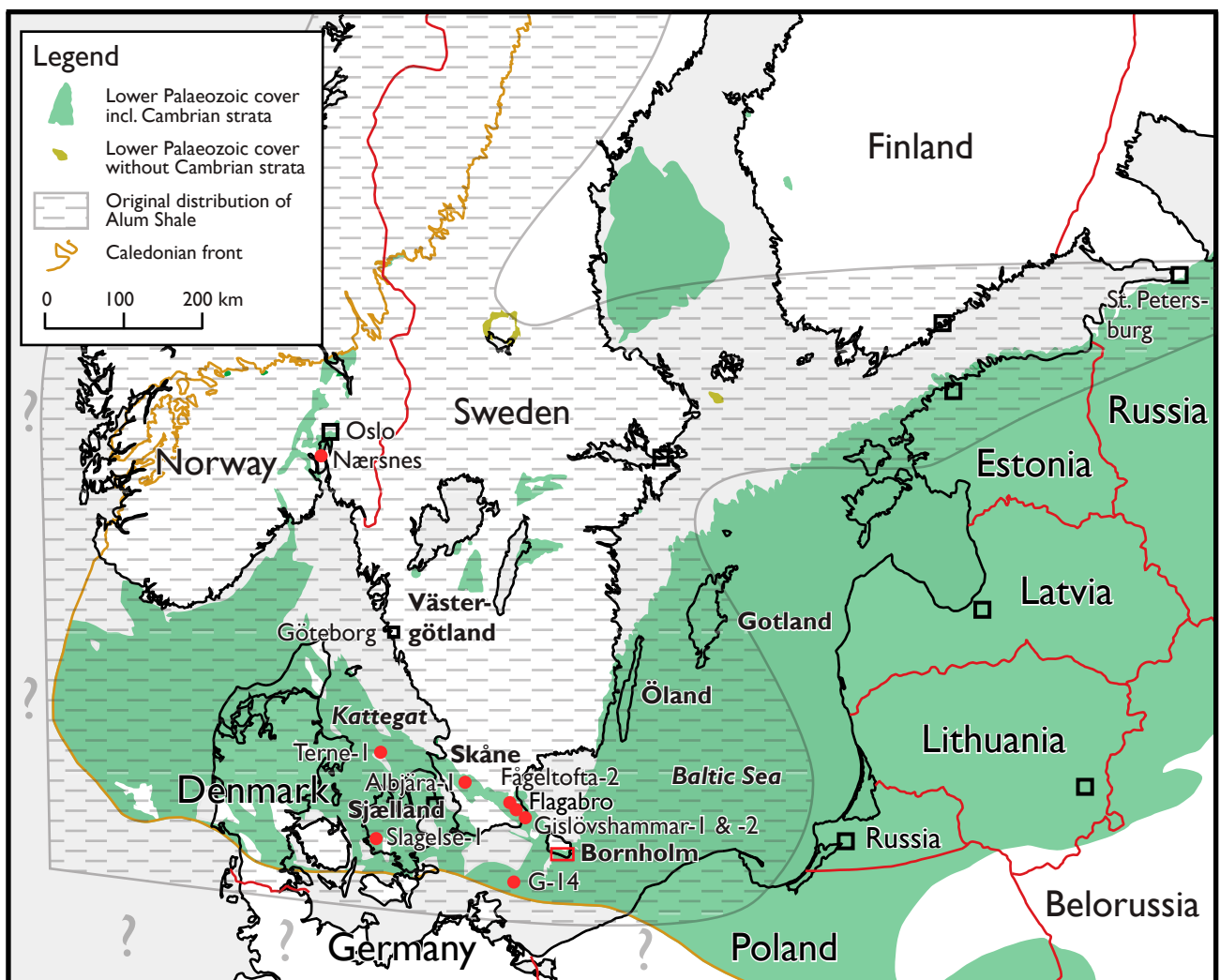


Fig. 1. Location map showing localities and areas referred to in this study. A detailed map of southern Bornholm (red quadrangle) is shown in Fig. 2. The approximate original distribution of the Alum Shale Formation in southern Scandinavia is also shown.

for references to sea-level changes made in this paper.

Despite the prevailing low-oxygen conditions during deposition, the Cambrian Alum Shale contains a low-diverse, but highly abundant trilobite fauna adapted to cope with the harsh living conditions on the seafloor (e.g. Henningsmoen 1957; Clarkson & Taylor 1995; Schovsbo 2000, 2001; Lauridsen & Nielsen 2005; Clarkson 2011). Agnostoids and various ‘normal’ trilobites known from better ventilated facies are common in the Miaolingian interval, while the Furongian is strongly dominated by olenid trilobites (e.g. Westergård 1922, 1946, 1947, 1948, 1950, 1953; Henningsmoen 1957; Terfelt 2006; Høyberget & Bruton 2012). The Tremadocian (Lower Ordovician) Alum Shale contains common graptolites and phosphatic brachiopods (e.g. Tjernvik 1958), whereas trilobites are mostly rare or absent, which is probably a taphonomic artefact caused by dissolution (Schovsbo 2001). Sparse trilobites have, however, been described from Skåne and the Oslo area (Moberg 1898, Henningsmoen 1957, Bruton *et al.* 1988, Terfelt *et al.* 2014). The abundant fauna in the Alum Shale Formation has facilitated definition of a high-resolution bio- and chronostratigraphy comprising three Miaolingian superzones

with seven zones, six Furongian superzones with 22 zones and up to nine Tremadocian zones (see summary of stratigraphy below).

The present study focusses on the Alum Shale Formation of Bornholm, which has for long been known from discontinuous outcrops in the Læså and Øleå stream sections (Fig. 2) (Grönwall 1902, 1916; Poulsen 1922, 1923; Hansen 1945; Berg-Madsen 1985a,b, 1986). The Alum Shale is also intermittently exposed in the Risebæk stream (Fig. 2), but these outcrops have never been studied in any degree of detail.

The Alum Shale Formation of Bornholm has been penetrated in its entirety by eight wells, both cored and uncored (Pedersen 1989; Pedersen & Klitten 1990; Schovsbo *et al.* 2011, 2015b; this study). Seven of these wells plus a well missing only the Ordovician part of the formation are correlated in this study using gamma-ray logs supplemented in some wells with resistivity and sonic logs (for location of the wells, see Fig. 2). The primary aim of this paper is to calibrate the log patterns with the established biozonation via comparison with the intensively studied, fully cored Gislövshammar-1 and Gislövshammar-2 wells in south-eastern Skåne, Sweden.

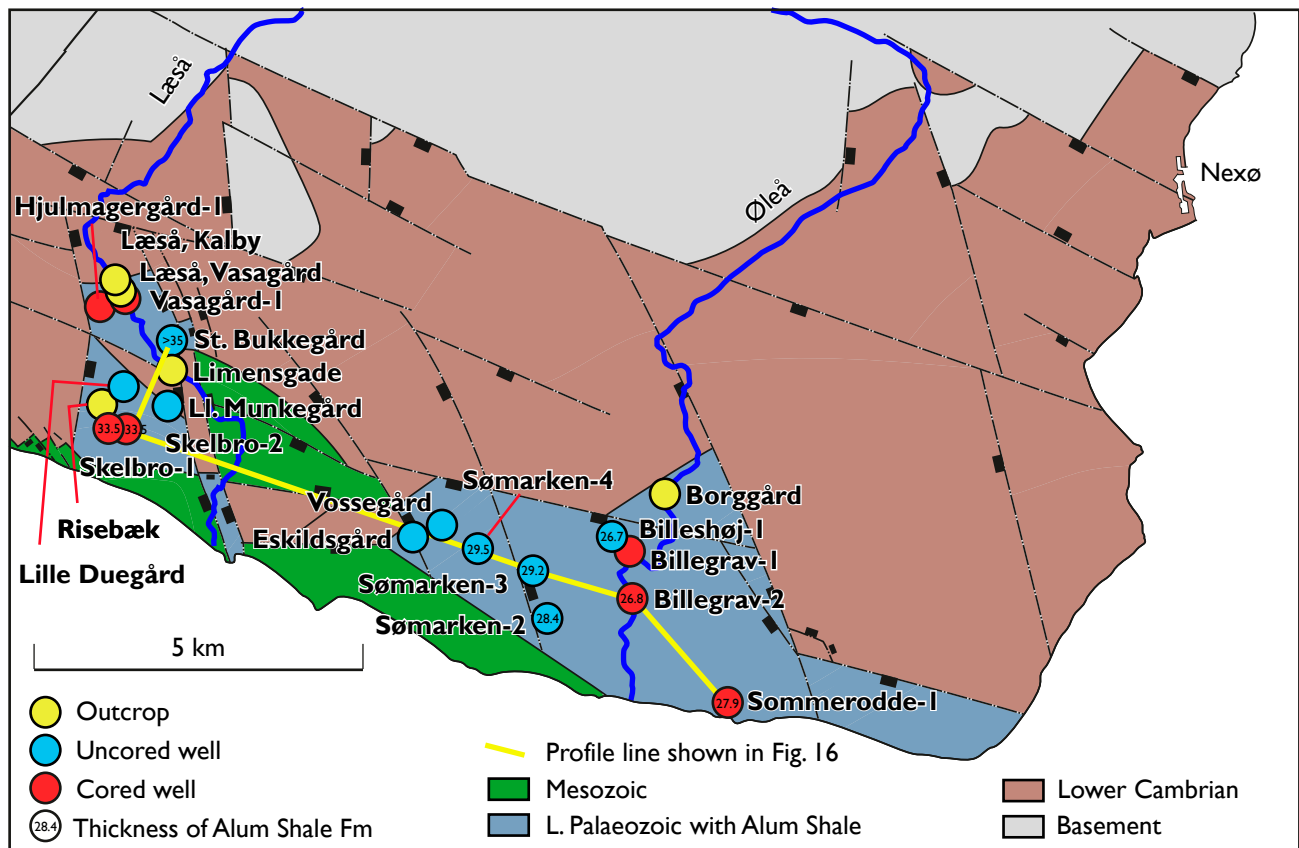


Fig. 2. Location map showing location of the wells and localities referred to in the text. The distribution of the Alum Shale Formation in fault blocks on southern Bornholm is also shown. Geological map modified from Graversen (2009). Thickness data are shown for wells penetrating the entire formation. In the St. Bukkegård well the Ordovician section is missing (see text).

On Bornholm, the Alum Shale Formation is unconformably overlain by the Middle Ordovician Komstad Limestone Formation (Nielsen 1995 and references therein), except in the Billegrav-2 well where a thin veneer of the Lower Ordovician Tøyen Formation is preserved (described below). It is also possible that a thin Tøyen Formation is present in the uncored Sømarken-3 and -4 wells. In south-eastern Skåne the ≤ 1 m thick Bjørkåsholmen Formation and the up to 19 m thick Tøyen Formation are in most places developed between the Alum Shale and the Komstad Limestone Formations.

Stratigraphy of the Alum Shale Formation

Lithostratigraphy

The Alum Shale Formation is 15–25 m thick across large parts of south central Sweden, increasing to 80–100 m in Skåne, southernmost Sweden, and it reaches a maximum thickness of almost 180 m in the Terne-1 well in Kattégat, offshore Denmark (Fig. 1; Michelsen & Nielsen 1991; Buchardt *et al.* 1997; Nielsen & Schovsbo 2007; Schovsbo *et al.* 2016). The formation tapers out in the Baltic Sea east of mainland Sweden, but a tongue of Tremadocian Alum Shale extends into Estonia and the St. Petersburg area (Fig. 1). The Alum Shale Formation also thins southwards of Skåne towards Bornholm and into northern Poland, where it pinches out (Buchardt *et al.* 1997, fig. 7).

In Skåne, the Miaolingian Alum Shale Formation includes four thin bioclastic limestones, 0.1–0.8 m thick, that form easily recognisable marker beds, viz. the Forsemölla, Exsulans, Hyolithes and Andrarum Limestone Beds (Nielsen & Schovsbo 2007 and references therein). On Bornholm, the Forsemölla and Exsulans Limestones are amalgamated to form one thin bed (≤ 0.25 m thick) that unconformably overlies the lower Cambrian Rispebjerg Member of the Læså Formation and marks the lower boundary of the Alum Shale Formation. Higher up, the Hyolithes and Andrarum Limestone Beds are also amalgamated (in total ≤ 1 m thick). Lenticular bituminous limestone concretions, up to 1 m thick and 2.5 m in diameter and traditionally called anthraconite or orsten, occur scattered throughout the Alum Shale Formation, although some stratigraphic levels contain more common limestone than others. Early precipitation of calcite took place immediately below the seafloor, conceivably due to bacterial degradation of organic material that produced bicarbonate (Buchardt &

Nielsen 1985). Bituminous limestone beds also formed by winnowing of trilobite carapaces from the muddy sediment, likely associated with storm reworking. The latter bituminous bioclastic limestone is common in the mid-shelf facies in south central Sweden, whereas the offshore facies in Skåne and Bornholm is primarily characterised by diagenetic limestone concretions. Anthraconitic limestone beds and lenses are comparatively uncommon in the Alum Shale Formation of Bornholm and overall constitute less than 5 % of the formational thickness.

On Bornholm, the Alum Shale Formation has traditionally been subdivided into the 'Lower Alum Shale', including the thin succession between the lower Cambrian Læså Formation and the amalgamated Hyolithes and Andrarum Limestone Beds, and the 'Upper Alum Shale', comprising the shale above the Andrarum Limestone (Johnstrup 1874; Berg-Madsen 1985a,b, 1986; Pedersen 1989). However, these informal member designations are no longer used. Historically, the shale has also been divided into the Paradoxides Shale or Series (Miaolingian up to and including the *Lejopyge laevigata* Zone), the Olenid Shale or Series (the Furongian + the *Agnostus pisiformis* Zone) and the Dictyograptus or Dictyonema Shale (comprising the Ordovician section of the Alum Shale Formation) (Grönwall 1916; C. Poulsen 1922, 1923; V. Poulsen 1966). These chronostratigraphic designations are also abandoned (Nielsen & Schovsbo 2007). The lithostratigraphic classification of the Forsemölla, Exsulans, Hyolithes and Andrarum Limestone Beds has varied through time (see Nielsen & Schovsbo 2007); they are here ranked as formal marker beds of the Alum Shale Formation. A bioclastic limestone in the *Acidusus atavus* Zone is informally referred to as the 'Atavus limestone bed'. It is developed as a distinct bed in Västergötland, south central Sweden (Fig. 1), but on Bornholm it occurs only as scattered pockets immediately on top of the Exsulans Limestone Bed (Weidner & Nielsen 2014).

Regional bio- and chronostratigraphy

Trilobites are common in the Cambrian part of the Alum Shale Formation in Scandinavia, and a detailed zonation has been established (Fig. 3). The Tremadocian zonation is based on graptolites. This paper focusses on correlation of superzones but individual zones are also addressed where possible.

Miaolingian

The Miaolingian (new term, see Yuanlong *et al.* submitted) comprises the traditional 'Middle' Cambrian plus the *Agnostus pisiformis* Zone. It is highly trilobitic in Scandinavia and a robust zonation was outlined by

ma	Chronostratigraphy			Superzones	Scandinavian zonation		Bornholm	Thickness		GR markers	
	Lower	Tremadocian	(not defined)		Polymerid trilobites	Graptolites/ Agnostoids		Læså area	Øleå area		
480	Ordovician	Lower	Tremadocian	(not defined)	<i>Ceratopyge forficula</i>	<i>Kiaerograptus</i> & <i>B. kjerulfii</i>	[uncertain which zones are developed]	3.4 - 4.0 m [4 m at Limensgade]	2.5 - 3.2 m	Tr-I	
					<i>Peltocare incipiens</i>						<i>A. tenellus</i>
					<i>Jujuaspis</i> & <i>Boeckaspis mobergi</i>	<i>R. f. flabelliformis</i>					
					<i>Boeckaspis hirsuta</i>	<i>R. f. socialis</i> & <i>R. f. parabola</i>					
						<i>R. praeparabola</i>				Ac-I	
	Cambrian	Furongian	Stage 10	Acerocarina	<i>Acerocare ecorne</i>	<i>T. holmi</i>	(uncertain which zones are developed)	2.7 - ≥3.8 m	2.0 - 2.5 m	Pe-4	
					<i>Westergaardia scanica</i>						Pe-3
					<i>P. costata</i>						
				<i>A. granulata</i>	Pe-2						
				' <i>Parabolina megalops</i> '							
				<i>Parabolina lobata</i>	PGS						
				<i>C. linnarssoni</i> ' <i>P. scarabaeoides</i> '							
				<i>C. bisulcata</i>	Pr-I						
				<i>Ctenopyge tumida</i>							
				<i>C. spectabilis</i> ' <i>S. angustus</i> '	Pa-I to Pa-3						
			<i>C. similis</i>								
490					Jiangshanian	Protopeltura	<i>Sphaerophthalmus flagellifer</i>	<i>L. americanus</i>	1.1 - 1.2 m	1.0 - 1.2 m	
							<i>C. postcurrrens</i> ' <i>L. neglectus</i> '				
					Paibian	Olenus	<i>Leptoplastus stenotus</i>	<i>P. cyclopyge</i>	0.5 - 0.6 m	0.4 - 0.5 m	
							<i>Leptoplastus crassicornis</i> - <i>Leptoplastus angustatus</i>				
							<i>Leptoplastus raphidophorus</i>				
							<i>Leptoplastus pausisegmentatus</i>				
							<i>Parabolina spinulosa</i> <i>Parabolina brevispina</i>				
			Paibian	Olenus	<i>O. scanicus</i> - <i>O. rotundatus</i>	<i>H. obesus</i> - <i>G. reticulatus</i>	4.1 - 4.5 m	2.0 - 2.9 m	OTGS		
					<i>Olenus dentatus</i>						
					<i>Olenus attenuatus</i>						
					<i>Olenus wahlenbergi</i>						
					<i>Olenus truncatus</i>						
					<i>Olenus gibbosus</i>						
			Guzhangian	<i>Paradoxides forchhammeri</i>	<i>Simulolenus alpha</i>	<i>A. pisiformis</i>	4.9 - 7.8 m	4.6 - 4.8 m	Ag-1 to Ag-3		
					(not defined)						
					<i>Solenopleura? brachymetopa</i>						
			Miaolingian	Drumian	(not defined)	<i>G. nathorsti</i>	1.1 - 1.7 m	0.8 - 2.5 m	AGL		
						<i>P. punctuosus</i>					
						<i>A. atavus</i>					
						<i>Ctenocephalus exsulans</i>					
			Wuliuan	<i>Acadoparadoxides oelandicus</i>	<i>Acadoparadoxides pinus</i>	<i>P. praecurrens</i>	0 m	0 m			
					<i>Eccadoparadoxides insularis</i>						
					(not defined)						

Fig. 3. Biozonation of the Miaolingian to Tremadocian Alum Shale Formation in Scandinavia and on Bornholm. Based on data from Grönwall (1902), Poulsen (1923), von Jansson (1979), Nikolaisen & Henningsmoen (1985), Bruton *et al.* (1988), Axheimer *et al.* (2006), Terfelt *et al.* (2008), Ahlberg & Terfelt (2012), Høyberget & Bruton (2012), Weidner & Nielsen (2013, 2014), Nielsen *et al.* (2014), B.W. Rasmussen *et al.* (2015, 2016, 2017), and this study. The zones listed in inverted commas are used in the sense of Westergård (1944, 1947). This simpler zonation is more workable for the Skåne–Bornholm Alum Shale succession than the elaborate zonation outlined by Henningsmoen (1957). The tentative time scale is adopted from Peng *et al.* (2012). Light grey shading in the Bornholm column indicates unexposed intervals known only from drillings. Correlation with GR (gamma ray) markers is shown in the right-hand column; regional markers defined by Schovsbo *et al.* (2018) are red. The exact correlation of the Ol-1 and Pe-2 markers in relation to the biozonal boundaries is uncertain. Abbreviations: l: lower, u: upper. For remarks on this informal subdivision of the *Olenus* Superzone, see text.

Westergård (1946); for a recent update, see Weidner & Nielsen (2014). Three superzones are now recognised (Fig. 3). Traditionally, the *A. pisiformis* Zone has been assigned to the 'Upper Cambrian' (e.g. Westergård 1922; Henningsmoen 1957), but as the first appearance datum (henceforth FAD) of *Glyptagnostus reticulatus* defines the base of the Furongian Series (Peng *et al.* 2004), the underlying *A. pisiformis* Zone is, accordingly, assigned to the Miaolingian (Fig. 3). Nielsen *et al.* (2014) proposed including the *A. pisiformis* Zone in the *Paradoxides forchhammeri* Superzone.

The Miaolingian on Bornholm represents the *Paradoxides paradoxissimus* and *P. forchhammeri* Superzones. The lower part below the Andrarum Limestone Bed is highly condensed and stratigraphically incomplete.

Furongian

A distinct faunal change marks the base of the Furongian, with sudden appearance of olenid trilobites, and shortly afterwards agnostoids become rare. A detailed Furongian zonation for Scandinavia was outlined by Westergård (1947). Ten years later Henningsmoen (1957) emended this scheme and introduced an exceptionally detailed zonation, where the 'upper' Cambrian above the *A. pisiformis* Zone was subdivided into seven zones holding 31 subzones. Terfelt *et al.* (2008) elevated these subzones to zonal rank and abandoned the longer ranging zones. However, Weidner & Nielsen (2013) and Nielsen *et al.* (2014) proposed with minor amendments to resurrect the old zones as superzones and this approach is followed here. A simplification of the Furongian stratigraphy is planned (Nielsen & Høyberget unpublished), but here we provisionally use some of Westergård's (1947) original zones (referred to using inverted commas, Fig. 3) as they are more readily recognisable in Skåne and Bornholm than the zones defined by Henningsmoen (1957). In this study we also informally refer to the fossil-rich lower part of the *Olenus* Superzone simply as the 'lower part', and to the upper fossil-poor interval as the 'upper part'. The boundary is drawn at the last appearance datum of *Olenus dentatus*.

Lower Ordovician (Tremadocian)

In Scandinavia, the FAD of the graptolite *Rhabdinopora* (= *Dictyonema* or *Dictyograptus* in older literature) has traditionally been taken to indicate the base of the Ordovician. This level is almost certainly located marginally above the formal base of the Ordovician as defined by the FAD of the conodont *Iapetognathus fluctivagus*, but that taxon does not occur in Scandinavia (for remarks on the global boundary, see Terfelt *et al.* 2011). For a comprehensive review of graptolite zones in the Tremadocian, see Cooper (1999). The local Scandinavian zonation has been discussed e.g.

by Westergård (1909), Bulman (1954), Tjernvik (1958), Spjeldnæs (1963, 1985), Bruton *et al.* (1982, 1988), Maletz & Erdtmann (1987) and Maletz *et al.* (2010). In the Nærnes section in Norway, probably the most complete described from Scandinavia, the FAD of *Rhabdinopora socialis* is located just above a thin basal Ordovician interval characterised by *Rhabdinopora preparabola*, leaving no room for a separate *Rhabdinopora parabola* Zone, as recognised in some schemes. In the Flagabro core, south-east Skåne, *R. parabola* and *R. socialis* also appear immediately above the boundary, defined by the FAD of *Rhabdinopora desmograptoides* (see Tjernvik 1958). At Limensgade on Bornholm, *R. socialis* has its FAD 0.2 m above limestone nodules with *Parabolina acanthura*, taken to indicate the Furongian *Acerocare ecorne* Zone (Poulsen 1922; von Jansson 1979). Whether the 0.2 m thick unfossiliferous shale in between is of Ordovician or Cambrian age is unknown. The Tremadocian is treated as one unit ('superzone') in the current study; the zonation is shown in Fig. 3.

Alum Shale geochemistry and chemostratigraphy on Bornholm

The Alum Shale Formation is famous for its high TOC (total organic carbon) content and syngenetic enrichment of chalcophile elements (As, Cd, Cu, Pb, Ni, Zn) and redox-sensitive elements (U, V, Mo). There has been major focus on the latter group due to its economic potential (Armands 1972; Hessland & Armands 1978; Andersson *et al.* 1985; Leventhal 1991;

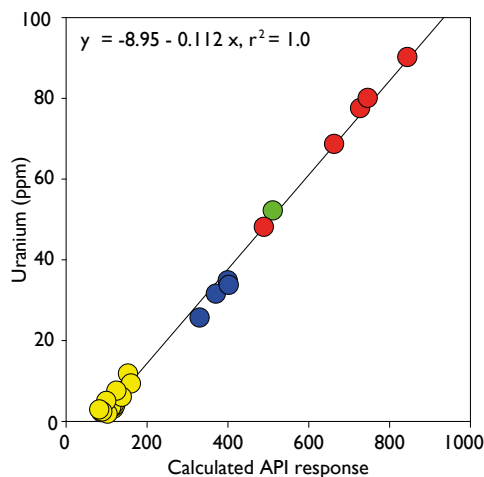
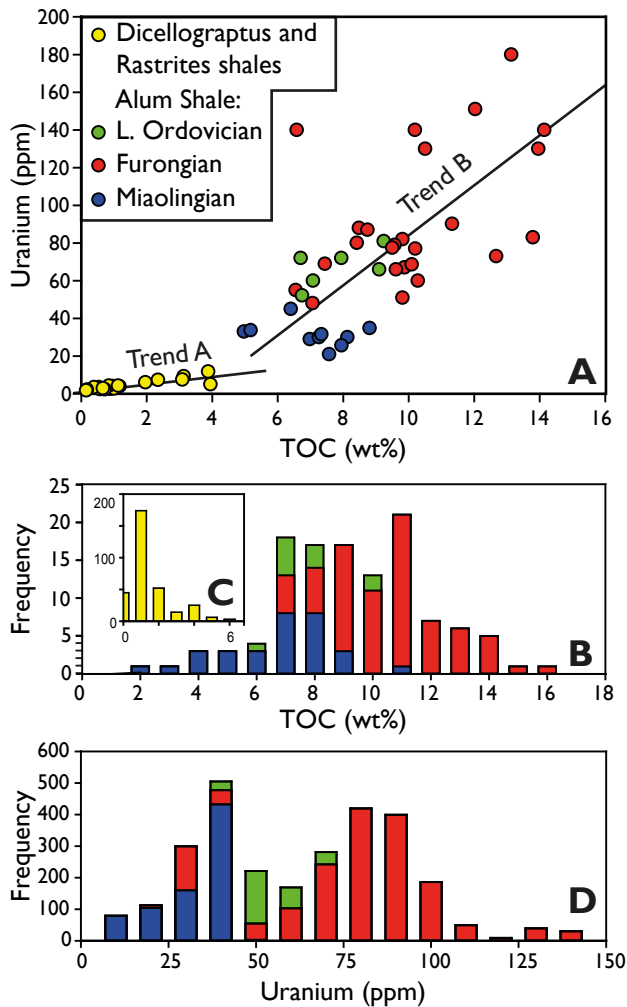


Fig. 4. Uranium concentration versus modelled API (American Petroleum Institute unit) response from measured U, K and Th in the Billegrav-2 well. API response calculated as $4 \times \text{Th (ppm)} + 8 \times \text{U (ppm)} + 16 \times \text{K (wt\%)}$, following Ellis & Singer (2007). Legend as in Fig. 5. Data are presented in Table 2.

Buchardt *et al.* 1997; Lecomte *et al.* 2017) as well as its bearing on the depositional environment (Schovsbo 2000, 2001, 2002a; Gill *et al.* 2011). Of the enriched elements, uranium has a huge impact on the gamma-ray (hereafter GR) log due to its high radiation. Correlations of the Alum Shale based on the GR log thus essentially represent a uranium chemostratigraphy (Fig. 4). As guidance for the correlation we have



numbered several, usually readily traceable intra-superzone GR excursions. The labelled fluctuations are mostly maxima, as GR lows caused by limestone nodules occur semi-randomly in the formation and, hence, may mislead correlation.

Schovsbo (2002a) published average uranium contents for the *Agnostus pisiformis* Zone (38 ppm), the lower and upper parts of the *Olenus* Superzone (average 43 ppm and 92 ppm, respectively), the combined *Protopeltura* and *Peltura* Superzones (113 ppm) and the Lower Ordovician (average 73 ppm) on Bornholm, but no formation average was provided. Based on the calibrated spectral GR log of the Billegrav-2 core the average uranium content of the formation is estimated at 58 ppm with an average content of 27 ppm in the Miaolingian, 74 ppm in the Furongian and 49 ppm in the Lower Ordovician strata (Table 1). The strong stratigraphical control on the enrichment is particularly evident when plotting the U-log readings in a histogram since the Miaolingian and Furongian sample populations are almost mutually exclusive, apart from the relatively low uranium content in Furongian carbonate concretions and the lower part of the *Olenus* Superzone (Fig. 5D).

Fig. 5. Geochemical data from lower Palaeozoic black shales on Bornholm. **A:** TOC versus uranium content for Alum, Dicellograptus and Rastrites Shales on Bornholm. Trends A and B illustrate the different proportionality between organic material and U content in the Dicellograptus and Rastrites Shales vs the Alum Shale. **B:** Histogram of TOC contents in the Alum Shale, Bornholm, divided into its main stratigraphic units (shale facies only). **C:** Histogram of TOC contents in the Dicellograptus and Rastrites Shales. **D:** Histogram of U contents calculated from spectral gamma-ray scanning of the Alum Shale in the Billegrav-2 core, Bornholm, divided into main stratigraphic units. Maturity of the shales (measured on graptolite and vitrinite-like particles, Petersen *et al.* 2013) is 2.3 % Ro (Buchardt *et al.* 1986). Data from Warming *et al.* (1994) and Schovsbo (2012), combined with unpublished reports for the Billegrav-2, Skelbro-2 and Sommerodde-1 wells.

Table 1. Total organic carbon and uranium content in lower Palaeozoic shales on Bornholm

Stratigraphy	Total organic carbon (wt%) ¹					N1	Uranium content (ppm) ²					N2
	Mean	Median	Std. dev.	Min	Max		Mean	Median	Std. dev.	Min	Max	
Rastrites shale	1.1	0.8	0.9	0.0	4.9	180	4.9	4.3	2.5	0.5	18	6138
Lindegård Formation	0.2	0.1	0.2	0.0	0.8	50	2.8	2.7	1.1	0.1	6.8	1445
Dicellograptus Shale	1.2	0.3	1.6	0.0	5.2	89	4.4	4.1	2.2	0.7	16	2145
Alum Shale Fm, total	8.8	8.7	2.6	1.3	15.1	118	58	61	28	2.5	136	2797
L. Ordovician	7.3	6.6	1.3	5.5	9.9	31	49	46	8	38	68	299
Furongian	10.0	10.1	2.0	6.4	15.1	76	74	77	23	18	136	1720
Miaolingian	6.2	6.9	1.9	1.3	10.3	11	27	31	10	2.5	41	778

¹Based on TOC data from Skelbro-1, Skelbro-2, Billegrav-2 and Sommerodde-1.

²Based on calibrated GR spectral log from the Billegrav-2 core.

N1: Number of analysed samples

N2: Number of measurements.

The uranium level in the Alum Shale on Bornholm is comparable to that in Skåne (Schovsbo 2002a) and southern Norway (Schovsbo *et al.* 2018), but is much lower than in the Furongian of south central Sweden and Öland (Hessland & Armands 1978; Andersson *et al.* 1985; Schovsbo 2002a). The strong geographical control on the uranium enrichment is possibly related to water column dynamics in the Alum Shale sea. Schovsbo (2002a) thus showed that the uranium concentration in the '*Peltura scarabaeoides*' Zone is inversely correlated to its thickness (see also Andersson *et al.* 1985) and U enrichments seemingly reflect condensed intervals. Such horizons are suspected to represent flooding events (i.e. abrupt sea-level rises accompanied by reduced sedimentary influx).

No strong trace-element enrichment is seen in the Dicellograptus and Rastrites Shales in the Billegrav-2 well. In these formations, the uranium content averages 2.8–4.9 ppm (Table 1) and the concentrations are

closely related to the TOC content (Trend A in Fig. 5A). In the Alum Shale, the enrichment of uranium exhibits a more general correlation with the TOC level (trend B in Fig. 5A), and is not as closely related to the TOC content as in the Dicellograptus and Rastrites Shales.

The Scandinavian Alum Shale has an average organic carbon content of 9 wt%, with local TOC concentrations reaching 25 wt% in the Furongian strata of south central Sweden (Schovsbo 2002a; Gautier *et al.* 2014). On Bornholm, the highest measured content is 15.2 wt% and the average TOC content of the entire formation is 8.8 wt% (Fig. 5B, Table 1). The Miaolingian, Furongian and Tremadocian intervals exhibit average TOC contents of 6.2 wt%, 10.0 wt% and 7.3 wt%, respectively. The average TOC content in the other lower Palaeozoic shales on Bornholm are much lower and only a few samples reach values > 4 wt% (Table 1).

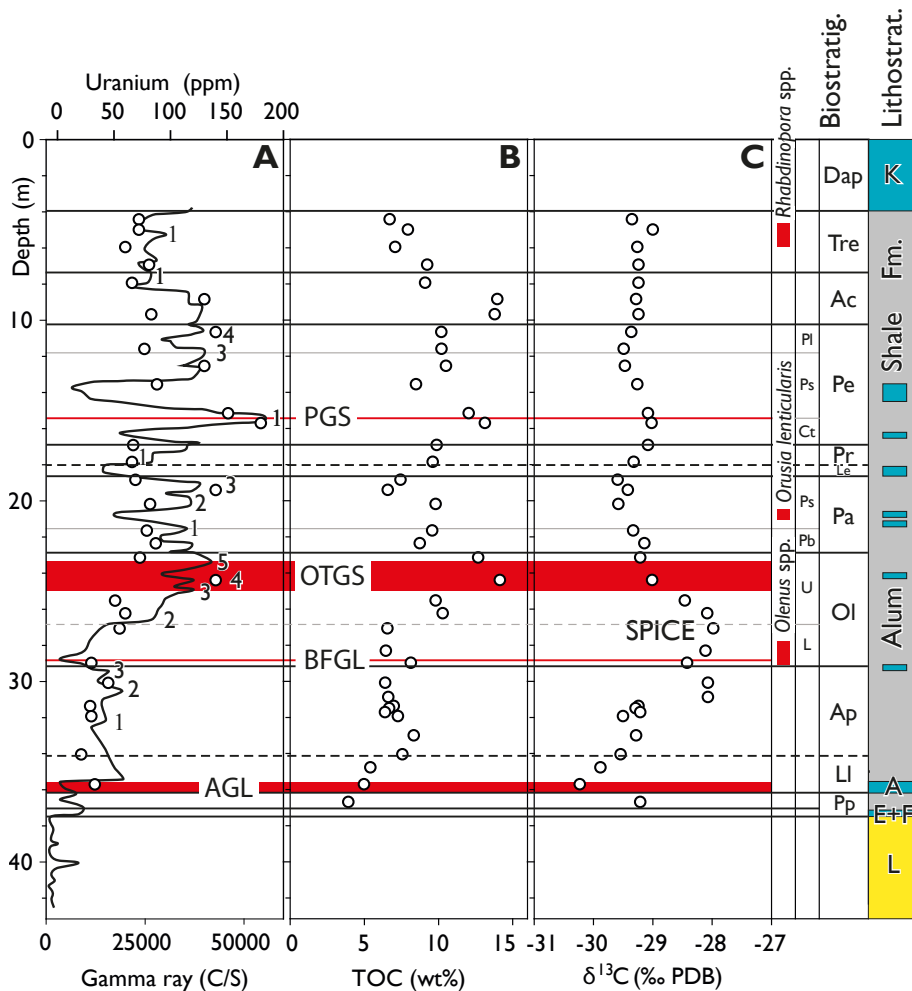


Fig. 6. Simplified lithology and biozonation of the Skelbro-1 well. Identification of the superzone boundaries is based on GR wire-line log correlation with the Gi-2 well in south-eastern Skåne, see text. Vertical red bars to the right indicate findings of fossils in the core (Pedersen 1989, fig. 2). The small numbers 1 and up to 5 in A indicate correlatable minor gamma spikes (see Fig. 16). A: Gamma-ray wireline log (digitised from Pedersen & Klitten 1990) and core U measurements (Warming *et al.* 1994). B: TOC contents (Buchardt *et al.* 1986). C: $\delta^{13}\text{C}$ isotope composition of organic carbon (Buchardt *et al.* 1986); for remarks on the SPICE event, see text. The position of the gamma-ray log markers PGS (*Peltura* Gamma Spike), OTGS (*Olenus* Triple Gamma spike), BFGL (Base Furongian Gamma Low) and AGL (Andrarum Gamma Low) are shown with horizontal red lines. Other abbreviations: L, Læså Formation.; E, Exsulans Limestone Bed; F, Forsemölla Limestone Bed; A, Amalgamated Hyolithes + Andrarum Limestone beds; K, Komstad Limestone Formation;

Pp, *Paradoxides paradoxissimus* Superzone; LI, *Lejopyge laevigata* Zone; Ap, *Agnostus pisiformis* Zone; Ol, *Olenus* Superzone; Pa, *Parabolina* Superzone; Le, *Leptoplastus* Superzone; Pr, *Protopeltura* Superzone; Pe, *Peltura* Superzone; Ac, *Acerocarina* Superzone; Tre, Tremadocian; Dap, Dapingian. See Fig. 14 for explanation of abbreviated zonal designations. Location of the well is shown in Fig. 2.

In Skåne, the TOC content in the Alum Shale increases in a stepwise manner up through the formation (Schovsbo 2001). A prominent upward increase in TOC content can also be seen on Bornholm, especially from the base of the *A. pisiformis* Zone culminating in the *Olenus* Triple Gamma Spike in the upper part of the *Olenus* Superzone, and again from the basal part of the *Parabolina* Superzone culminating in the *Peltura* Gamma Spike within the lowermost part of the *Peltura* Superzone (Fig. 6, see also Fig. 8 below).

Distinctive perturbations in the $\delta^{13}\text{C}$ record have been used as a tool for global correlation in the Cambrian. During Alum Shale deposition the most prominent event is the +2‰ Steptoean positive carbon isotope excursion (SPICE) (Saltzman *et al.* 1998) that occurs in the lower to middle part of the *Olenus* Superzone (Schovsbo 2002b; Ahlberg *et al.* 2009; Hammer & Svensen 2017). Carbon isotope data from Bornholm were presented already by Buchardt *et al.* (1986) from the Skelbro-1 core (Fig. 6); these data in fact outline

the SPICE which at that time was not recognised as a global event. The analysed samples exhibit a gradual shift towards more positive $\delta^{13}\text{C}$ values from the Andrarum Limestone Bed and to the middle of the *Olenus* Superzone (Fig. 6). Two samples indicating -28.07 ‰ $\delta^{13}\text{C}$ in the *A. pisiformis* Zone appear inconsistent with the $\delta^{13}\text{C}$ curve for the Alum Shale established elsewhere (Ahlberg *et al.* 2009; Hammer & Svensen 2017) and we suspect that samples have been mislabelled. Future re-investigation of sections on Bornholm will have to verify whether this suspicion is correct.

Analytical methods

Spectral gamma-ray and bulk density scanings of the Skelbro-2 and Billegrav-2 cores were made in the Core Analysis Laboratory at the Geological Survey of Denmark and Greenland (GEUS), using a density scanner equipped with a Cs source for determining the bulk density. The scanning was performed at a

Table 2. Geochemistry of shale samples from the Billegrav-2 core

Lab. No.	Sample	Formation	Series	Depth m	TOC wt%	TIC wt%	Th ¹ ppm	U ¹ ppm	K ² (wt%)	GR API ³
20025	1	Rastrites shale	Llandovery	5.28	1.0	0.1	9.7	4.1	2.8	116
20026	2	"	"	10.70	0.5	0.1	11.3	3.1	3.0	117
20027	3	"	"	14.97	0.5	0.0	11.0	3.5	2.7	116
20028	4	"	"	19.95	3.9	0.1	7.1	11.8	1.9	153
20029	5	"	"	23.18	2.3	0.1	8.5	7.4	2.4	131
20030	6	"	"	24.90	3.1	0.3	10.5	9.3	2.7	160
20031	7	"	"	29.99	1.2	0.0	11.0	4.0	2.8	121
20032	8	"	"	35.10	0.6	2.6	8.4	2.4	2.1	87
20033	9	"	"	41.15	0.9	2.5	9.0	2.6	2.1	91
20034	10	"	"	42.74	1.0	2.2	9.5	2.8	2.2	96
20035	11	"	"	45.00	0.8	0.0	10.1	4.3	2.8	119
20036	12	"	"	50.90	1.1	0.1	9.3	4.3	2.6	113
20037	13	"	"	56.60	0.4	1.3	10.2	3.5	2.7	112
20038	14	Rastrites shale	Llandovery	61.37	0.2	3.1	8.2	2.2	2.3	87
20039	15	Lindegård Mudst.	U. Ordovician	69.53	0.2	1.2	10.7	1.9	2.8	103
20040	16	Dicellogr. Shale	"	74.99	2.0	0.3	9.6	6.0	3.2	138
20041	17	"	"	76.89	3.1	0.3	6.6	7.6	2.3	124
20042	18	"	"	80.47	3.9	0.4	6.6	5.0	2.0	99
20043	19	"	"	86.68	0.7	0.6	7.2	2.4	2.6	89
20044	20	Dicellogr. Shale	U. Ordovician	93.47	0.7	0.3	8.2	2.9	1.6	82
20045	21	Alum Shale	L. Ordovician	96.76	6.7	0.4	11.6	52.2	2.9	511
20046	22	"	Furongian	98.90	7.1	0.4	12.1	48.1	3.5	489
20047	23	"	"	101.57	9.5	0.4	12.4	77.5	3.6	727
20048	24	"	"	102.93	11.3	0.6	15.5	90.2	3.8	844
20049	25	"	"	105.90	10.1	0.8	12.3	68.7	4.0	663
20050	26	"	"	110.98	8.4	0.6	11.9	80.0	3.6	746
20051	27	"	Furongian	113.35	7.9	0.1	14.0	25.7	4.3	330
20052	28	"	Miaolingian	115.75	8.8	0.6	14.0	34.9	4.0	400
20053	29	"	"	116.86	7.3	0.2	13.6	31.6	4.0	370
20054	30	Alum Shale	Miaolingian	119.90	5.2	0.1	14.5	33.8	4.6	402

¹ICP-MS REE method. ²ICP-MS TotalQuant. ³Calculated as $4 \times \text{Th (ppm)} + 8 \times \text{U (ppm)} + 16 \times \text{K (wt\%)}$, see Ellis & Singer (2007).

TOC: Total organic carbon. TIC: Total inorganic carbon (=total carbon-TOC).

speed of 1 cm/min and the vertical resolution is 1 cm. Calibration of the scanner was made by running in-house standards with known densities. The density scanning is very sensitive to imperfections such as cracks, fractures and drilling damages, and also to poor alignment of the core within the scanner. Generally, the cores were in very good condition and extra care was taken to align them directly under the sensor and to fit broken core pieces together to minimise measuring errors. However, filtration of the density data was made to remove low readings caused by cracks and poor core alignment following the filtering procedure described by Bjerager *et al.* (in press).









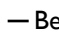

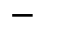

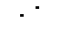






Thirty samples from the Billegrav-2 core were analysed using an Inductively Coupled Plasma Mass Spectrometer (Elan 6100 ICP-MS) at GEUS to provide calibration data for the spectral gamma-ray log. Crushed samples were dissolved in HF and HNO₃ acid for two days at 130°C. Element concentrations were determined using the Perkin Elmer TotalQuant software that provides semi-quantitative concentrations for 66 elements and a GEUS in-house REE method that provides quantitative concentrations for 24 elements (Schovsbo *et al.* 2018). Calibration data used for the spectral core scanner are shown in Table 2.

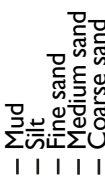
Total organic carbon (TOC), total carbon (TC) and total sulphur (TS) contents were measured on acid-pre-treated samples in a LECO CS-200 carbon/sulphur analyser at GEUS. Dissolution of carbonate was done by treating 0.05 g dried sample with 2M HCl solution at 65°C for 2 hours. The powdered samples were placed together with iron accelerator material in an oven and heated to 1300°C, and the evolved gases were measured by infrared absorption.

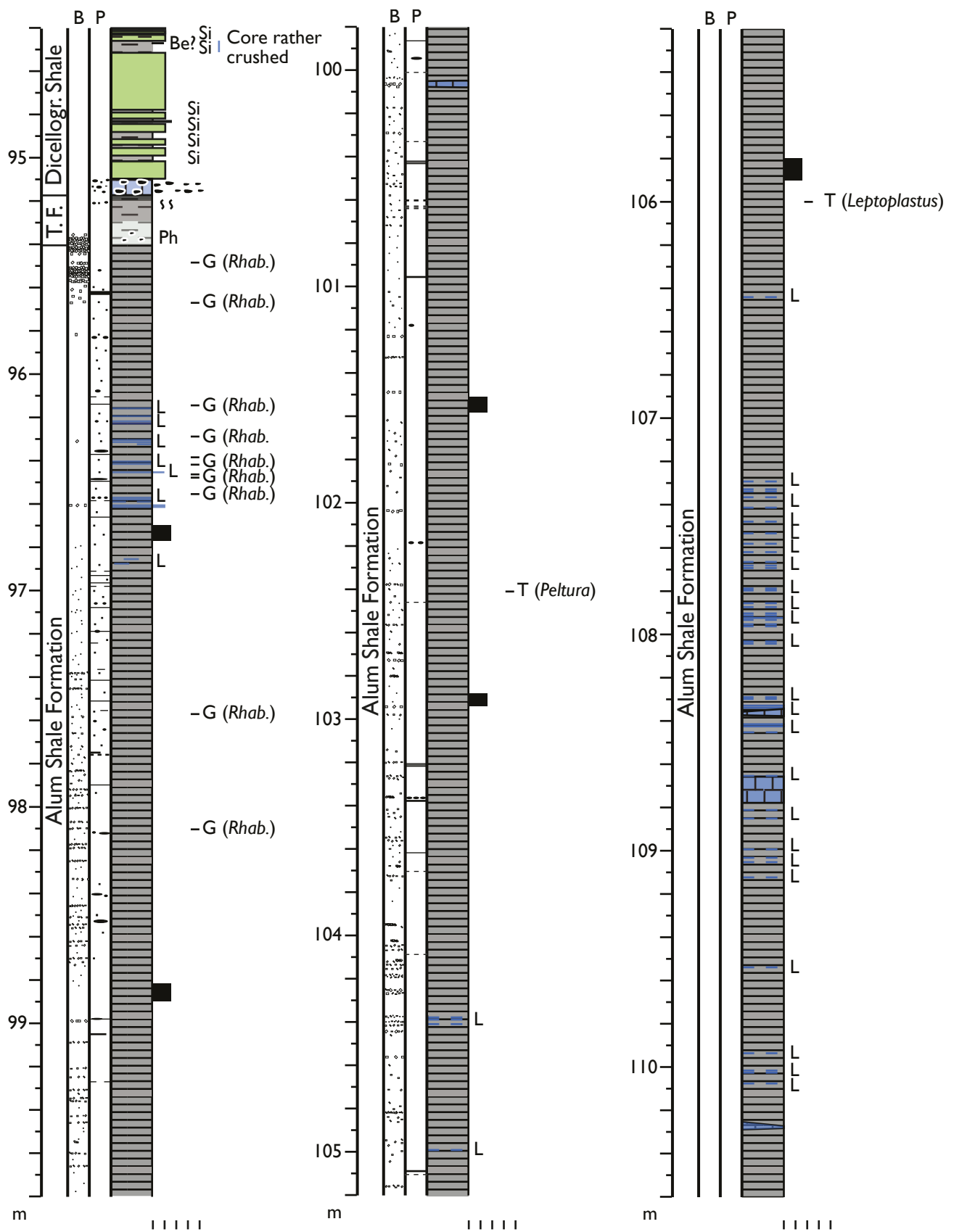
Apart from the Sommerodde-1 and Skelbro-1 wells, all other wireline logs presented in this paper were recorded by GEUS. Logging in the Sommerodde well was conducted by the consulting company Rambøll, and the GR log shown from Skelbro-1 (Fig. 6) is an old analog log made by the Institute for Technical Geology at the Technical University of Denmark and later digitised by GEUS. All boreholes were open wells, i.e. without well screens, but the wells did have a casing pipe in the Quaternary section; in the St. Bukkegård well this casing extends down into the Alum Shale (see below).

►▼ Fig. 7. Lithological log of the core interval 94.4–125.9 m in the Billegrav-2 well, comprising the lowermost part of the Dicollograptus Shale, the Komstad Limestone, the Tøyen Formation (abbreviated T.F.), the Alum Shale Formation and the uppermost part of the Læså Formation. The core is 55 mm in diameter. The section is shown as two consecutive logs on pp 247–248. Location of the well is shown in Fig. 2 and correlation is shown in Fig. 8.

Legend for sedimentological logs

-  Black limestone
-  Grey to dark grey limestone
-  Dark grey to blackish distinctly laminated shale
-  Grey to darker grey mudstone, laminated
-  Light grey mudstone, indistinctly laminated
-  Siltstone
-  Sandstone, quartzose
-  Bentonite > 5 mm thick
-  — Be Thin bentonite 1-5 mm
-  • • • • Conglomerate
-  — Silt lamina
- Ph Phosphorite
- L Limy
- Gl Glauconite
- Si Silicified
-  Barite (incl. pseudomorphs)
- P Pyrite
- B Baryte (incl. pseudomorphs)
-  . . Tiny pyrite, possibly burrow-fill
-  - Pyrite nodule
-  - - Pyrite lamina, not continuous
-  — Pyrite lamina ≤ 1 mm thick
-  — Pyrite lamina/band > 1 mm thick
-  Burrows
-  Core sample (crushed)
- G Graptolite
- T Trilobite
- Br Brachiopod

Grain size: 



Results

The Alum Shale and Tøyen Formations in the Billegrav-2 well

The Billegrav-1 well, drilled in 1984 and described by Pedersen (1989), did not reach the Alum Shale Formation. The fully cored Billegrav-2 well (DGU 248.61), drilled in 2010 to a depth of 129.5 m, was located c. 700 m further south (Fig. 2) and penetrated to the lower Cambrian Norretorp Member of the Læså Formation (Schovsbo *et al.* 2011). The Alum Shale Formation was encountered between 95.4 and 122.2 m and the total thickness is thus 26.8 m (Fig. 7). Gamma-ray, sonic velocity, formation resistivity, density and optical televiewer wireline logs were obtained in the drill

hole (Fig. 8; see also Schovsbo *et al.* 2015b), and spectral gamma-ray and density scanings have been made of the core. The Billegrav-2 well is henceforth referred to as Bi-2; the core has hitherto remained undescribed.

The thin lower Miaolingian interval (120.2–122.2 m) below the traditional *Lejopyge laevigata* Zone comprises the Andrarum (120.41–121.33 m) and Hyolithes (121.35–121.53 m) Limestone Beds, underlain by shale (121.53–122.03 m) and the amalgamated Exsulans (122.03–122.09 m) and Forsemölla (122.09–122.17 m) Limestone Beds, in turn resting unconformably on the 'lower' Cambrian Læså Formation. Fossils have not been encountered in this part of the core (no systematic splitting has been undertaken). The core interval c. 98.1–120.4 m comprises the upper part of the Miaolingian (traditional *L. laevigata* + *A. pisiformis*

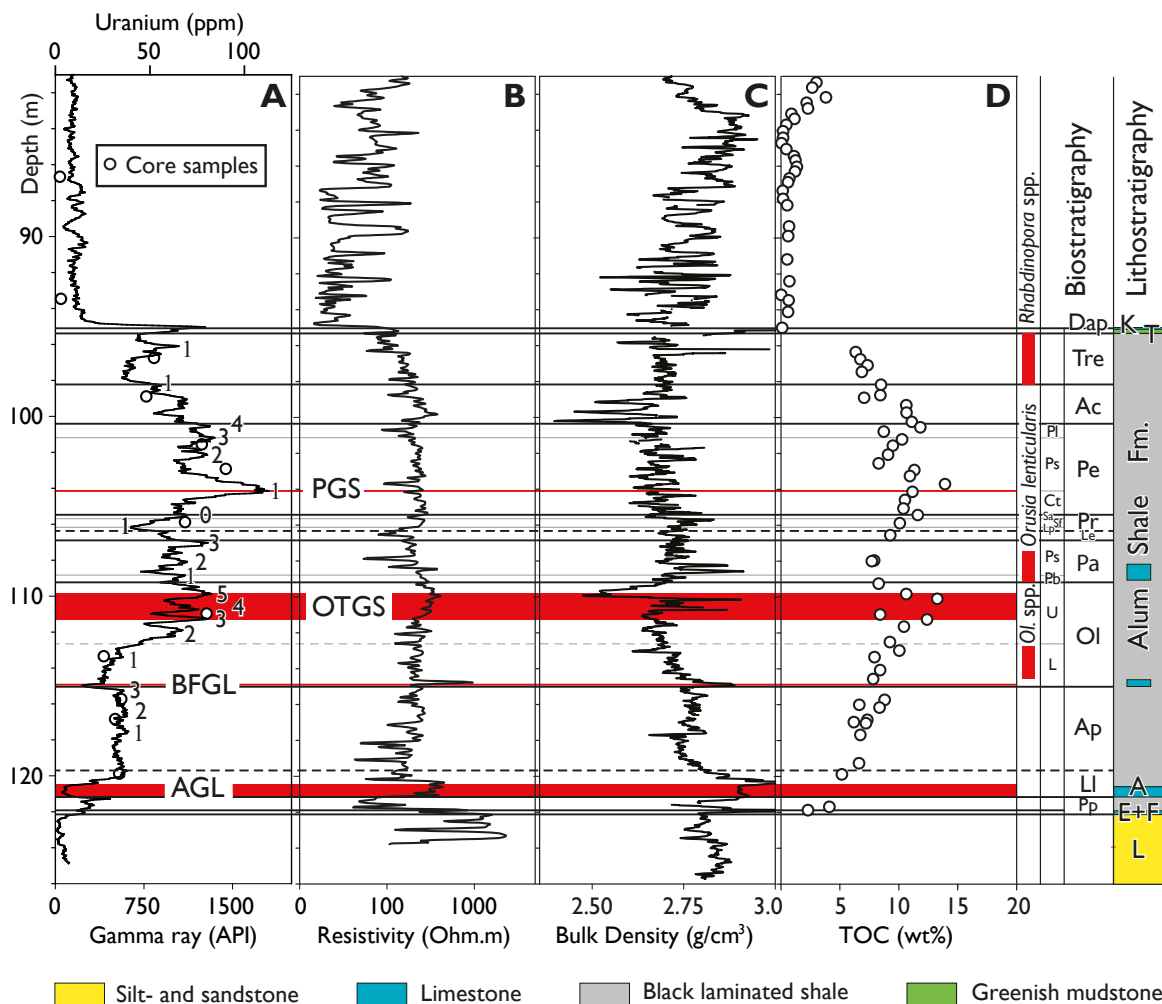
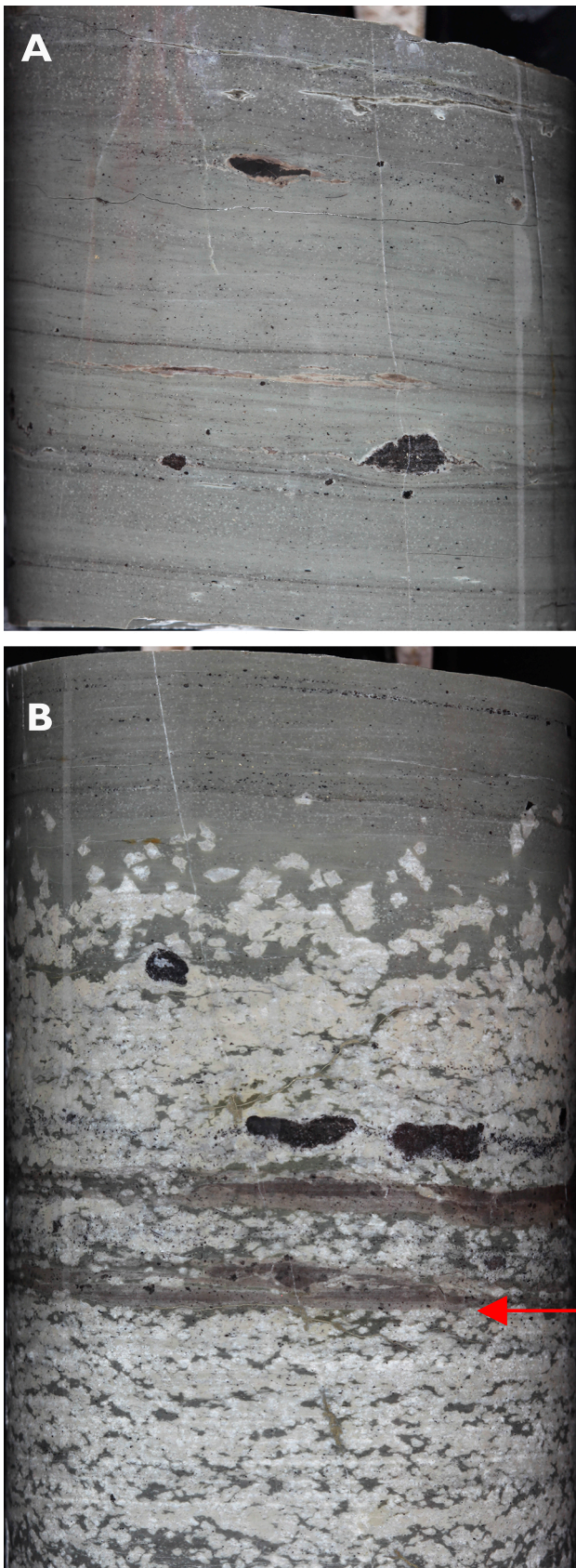


Fig. 8. Simplified lithology and biozonation between 81.0 and 125.9 m in the Billegrav-2 well, covering the interval from the Komstad Limestone to the bottom of the well. The biozonation is based on GR wireline log correlation with the Gi-2 well in south-eastern Skåne, see text. **A:** GR wireline log and core U measurements. The small numbers 1 and up to 5 indicate correlatable minor gamma spikes. **B:** Wireline resistivity log. **C:** Core scanning of bulk density, **D:** TOC content. Legend and abbreviations as in Fig. 6; abbreviated zonal designations as in Fig. 14; T, Tøyen Formation. Wireline log, core scanning and core measurements are from Schovsbo (2011, 2012) and Schovsbo *et al.* (2011). For location of the well, see Fig. 2.



Zones) and the Furongian. Common *Olenus* spp. and a few *Homagnostus obesus* occur between 112.9 and 114.7 m (Fig. 7), proving that this interval represents the lower part of the *Olenus* Superzone. GR log correlation shows that the Miaolingian/Furongian boundary is located at 115.0 m in the well (Fig. 8) and the limestone between 115.0–115.2 m probably corresponds to the unfossiliferous limestone seen just below the base of the Furongian in the Læså section (see Poulsen 1923, locality 2).

The Furongian shale contains very few limestone concretions and the registered fossil content is low. The core interval 107.4–109.2 m yielded abundant brachiopods (*Orusia lenticularis*) characteristic of the *Parabolina* Superzone (Fig. 7). The *Leptoplastus* Superzone is located around 106.0 m as suggested by findings of several *Leptoplastus* cranidia at this level. They resemble *L. neglectus*, characteristic of the eponymous zone in the basal *Protopeltura* Superzone (Fig. 3), but the determination must be regarded as preliminary. A cranidium of a pelturid trilobite from 102.41 m indicates that this level (probably) represents the *Peltura* or (less likely) the *Acerocarina* Superzone; *Peltura* cranidia cannot be safely assigned to species.

Graptolites (*Rhabdinopora* spp.) are common in the Ordovician part of the core (Fig. 7) with a lowermost occurrence noted at 98.1 m. The Cambro–Ordovician boundary is located at 98.2 m according to the GR log correlation (Fig. 8). *Rhabdinopora* ranges to the very top of the Alum Shale Formation in the Bi-2 core, and the *Adelograptus tenellus* and *Bryograptus kjerulfi* Zones known from Limensgade (Poulsen 1922) seem to be absent.

On Bornholm, the Alum Shale Formation unconformably overlies the Komstad Limestone Formation in all sections described so far (e.g. Pedersen & Klitten 1990; Nielsen 1995), but in the Bi-2 core a light grey to greenish mudstone, 0.22 m thick (95.17–95.39 m), is interspersed between these units. The mudstone contains scattered, small, black phosphorite nodules (Fig. 9A–B) showing that the thin unit does not represent bleached Alum Shale. The lithology is identical to the lower part of the Tøyen Formation in Skåne and Oslo of Floian age (Hunnebergian regional Stage) and the thin unit is taken to represent an erosional remnant of that formation. The lower boundary is obscure due

Fig. 9. Photos of the Tøyen Formation and its boundary to the Alum Shale in the Billegrav-2 core. Diameter of the core is 55 mm. **A:** Core interval 95.29–95.39 m, slightly glauconitic greenish mudstone with scattered phosphorite nodules. **B:** Core interval 95.33–95.44 m. Basal part of the unit, showing the indistinct lower boundary against the Alum Shale Formation (at arrow). The whitish lithology is baryte (or pseudomorphs after this mineral, see Callisen 1914) precipitated during diagenesis.

to common baryte, but is likely located just above a bed of amalgamated baryte crystals (Fig. 9B). Despite being indistinct, the boundary must represent a significant unconformity; at this level the upper part of the Ordovician Alum Shale and the Bjørkåsholmen Formation are missing (as well as equivalents of the lowermost parts of the Tøyen Formation in Skåne). The Tøyen Formation is in turn unconformably overlain by the Komstad Limestone Formation of which only the basal conglomerate is preserved in the Bi-2 well (95.10–95.17 m). It is unconformably overlain by the Upper Ordovician Dicellograptus Shale.

The Tøyen Formation (Owen *et al.* 1990) is well known from Skåne and the Oslo area where it is several tens of metres thick, even exceeding 100 m in north-western Skåne (fig. 41 in Nielsen 1995 and references therein). The Tøyen Formation comprises a lower, generally greenish to light greyish part, often with occasional sandstone stringers (Oslo) or limestone beds and nodules (Skåne), and an upper dark grey to blackish part. In the Oslo area these lower and upper subunits are formally separated as members (Owen *et al.* 1990). In the Bi-2 well, the thin Tøyen Formation cannot be discerned on the GR wireline log (Fig. 8), but see remarks on the Sømarken-3 and Sømarken-4 wells below.

Other fully cored wells on Bornholm

The Alum Shale Formation of Bornholm has been penetrated by four fully cored wells (Skelbro-1, Skelbro-2, Billegrav-2 and Sommerodde-1) that have all been investigated by geophysical wireline logging; for location, see Fig. 2. A fifth cored well, Hjulmagergård-1, spudded in 2012, proved to be located in a fault zone and had to be abandoned shortly after entering the Alum Shale Formation (Schovsbo *et al.* 2015b). A sixth cored well, Vasagård-1, was drilled in 1982 on the meadow northwest of Vasagård, Læså, in order to test newly developed drilling equipment. The drilling penetrated the upper part of the Alum Shale Formation (10.0–19.6 m) but the recovered short core has never been investigated and wireline logging was not performed. The Komstad Limestone is 4.7 m thick in this well.

The Skelbro-1 well (DGU 246.749), abbreviated Sk-1, was drilled in 1984 and described by Pedersen (1989). It was spudded on top of the Komstad Limestone within the abandoned limestone quarry at Skelbro (Fig. 2) and penetrated to a depth of 43 m with TD in the uppermost part of the Læså Formation (Norretorp Member). It was the first fully cored well that penetrated the Alum Shale Formation on Bornholm in its entirety;

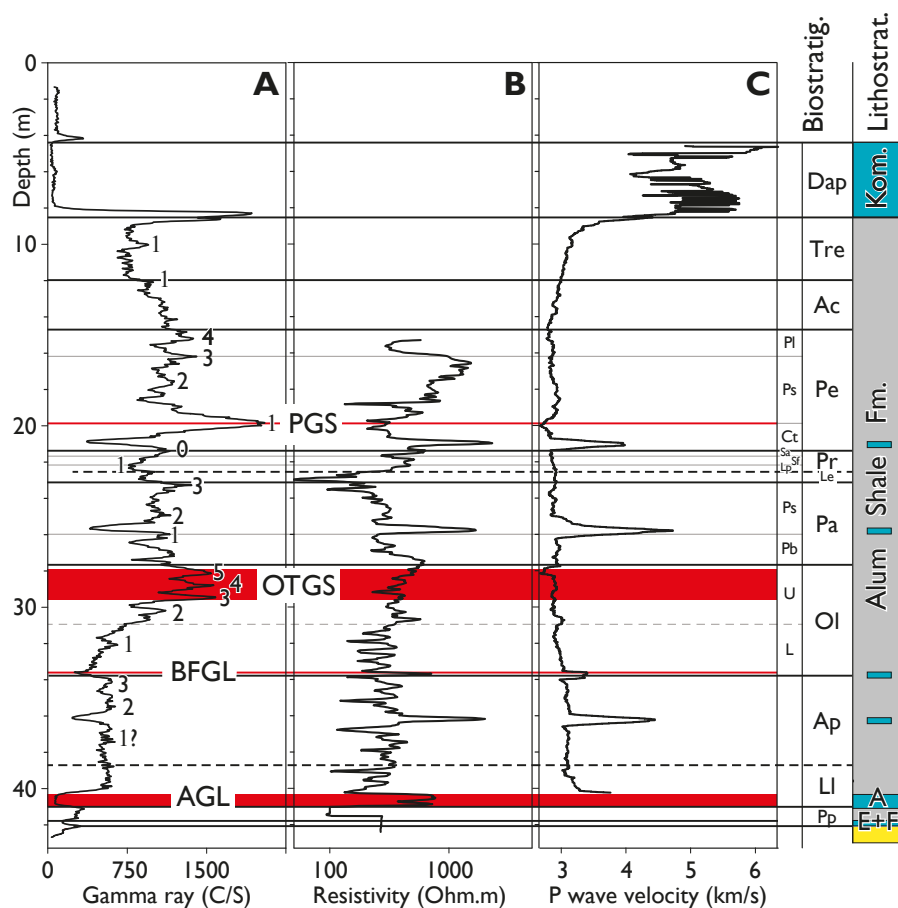


Fig. 10. Simplified lithology and biozonation of the Skelbro-2 well. The biozonation is based on GR wireline log correlation with the Gi-2 well in south-eastern Skåne, see text. **A:** Gamma-ray wireline log. The small numbers 1 and up to 5 indicate correlatable minor gamma spikes. The basal 0.5 m of the GR log is based on spectral gamma scanning of the core. **B:** Resistivity wireline log. The used type of logging tool does not provide reliable readings until 11 m below water table (at 4 m depth in this well). **C:** P-wave velocity from sonic wireline log. Legend and abbreviations as in Fig. 6; abbreviated zonal designations explained in Fig. 14. Wireline log and core measurements are from Baumann-Wilke *et al.* (2012). For location of the well, see Fig. 2.

a GR log was published by Pedersen & Klitten (1990) (here re-illustrated in Fig. 6). The total thickness of the formation in this well is 33.5 m. The diameter of the core is only 1 inch (2.5 cm) and no search for fossils was undertaken. However, the base of the Furongian is undoubtedly located close to 29 m, as indicated by the high abundance of trilobites, likely *Olenus*, at 28–29 m in the core (Fig. 6). The core interval rich in brachiopods at 20.5–21 m represents the *Parabolina* Superzone. The horizon with graptolites at 6 m is indicative of the Tremadocian.

The Skelbro-2 well (DGU 246.817), abbreviated Sk-2, was drilled in 2010 immediately adjacent to the abandoned Duegård Komstad Limestone quarry some 275 m east of the Sk-1 well (Fig. 2). Spectral gamma and density scanning of the core have been made (not shown) in combination with GR, sonic velocity and formation resistivity wireline logging of the drill hole (Fig. 10); see also Schovsbo *et al.* (2011) and Baumann-Wilke

et al. (2012). The Komstad Limestone is 4.1 m thick with the top encountered at 4.4 m below ground level immediately below Quaternary deposits. It is underlain by a 33.5 m thick Alum Shale Formation, corresponding to the thickness encountered in the Sk-1 well. At 42.9 m the well was terminated in the Rispebjerg Member of the Læså Formation.

The Sommerodde-1 well (DGU 248.62), abbreviated So-1, was drilled in 2012. A comprehensive suite of wireline logs was obtained in the drill hole, including GR, sonic velocity, formation resistivity and optical televiewer logs (Fig. 11; see also Schovsbo *et al.* 2015b). The top of the 0.6 m thick Komstad Limestone was encountered at 217.3 m (cored depth). The underlying Alum Shale Formation is 279 m thick with the base located at 245.7 m. The well terminated in the Norretorp Member of the Læså Formation at 250.3 m. The Alum Shale interval of the core has not been studied in detail. A few specimens of *Olenus* were observed on bedding

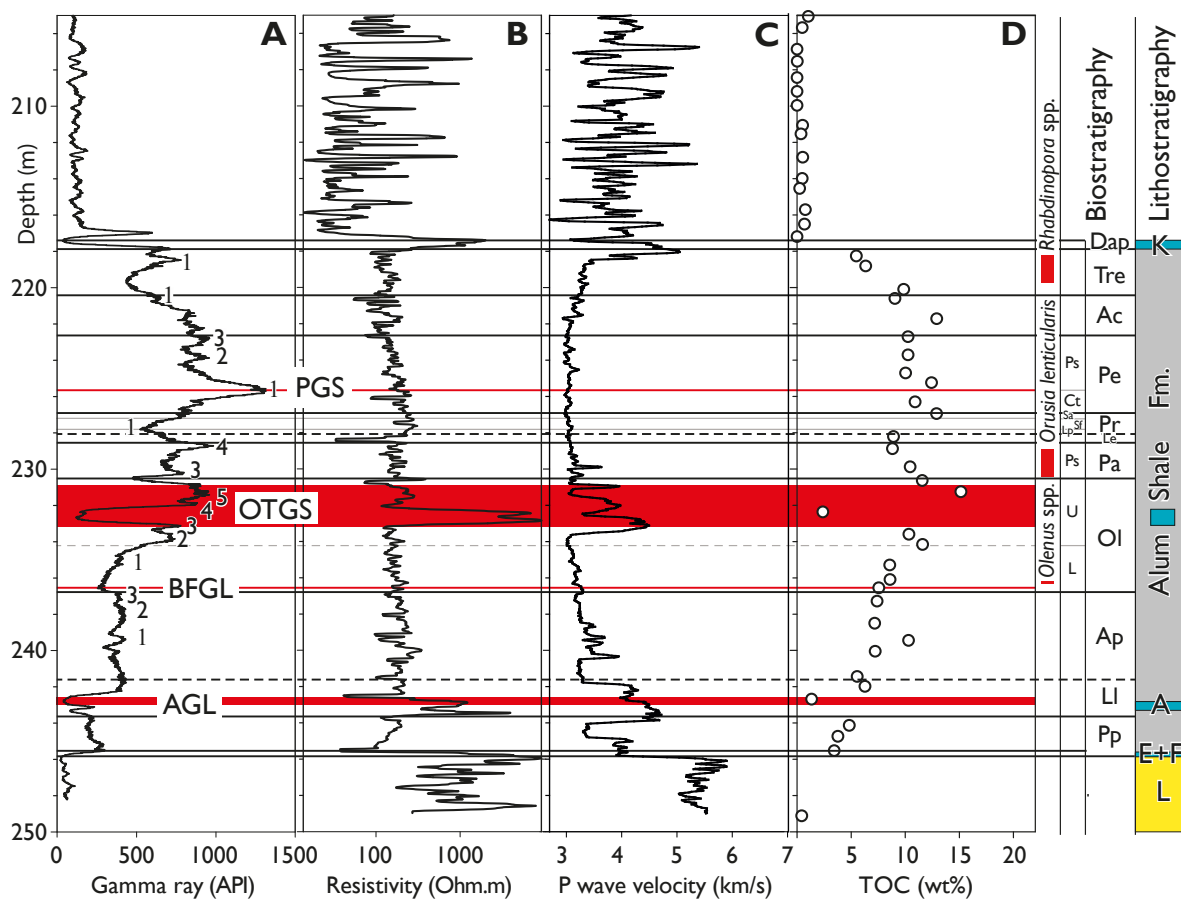


Fig. 11. Simplified lithology and biozonation in the lower part of the Sommerodde-1 well from the Komstad Limestone to the bottom of the well. The biozonation is based on GR wireline log correlation with the Gi-2 well in south-eastern Skåne, see text. **A:** Gamma-ray wireline log. The small numbers 1 and up to 5 indicate correlatable minor gamma spikes. **B:** Resistivity wireline log. **C:** P-wave velocity from sonic wireline log. **D:** TOC content in the core. The double peak on the P-wave velocity log at the two significant limestone beds just below the OTGS and the AGL is a flawed response often seen at such beds when a single transmitter sonic probe is applied. Legend and abbreviations as in Fig. 6; abbreviated zonal designations explained in Fig. 14. For location of the well, see Fig. 2.

planes at 236.2–236.3 m (Fig. 11); the brachiopod *Orusia lenticularis* is common at 228.9–230.4 m and *Rhabdinopora* occurs at 218.2–219.7 m. The Forsemölla Limestone Bed is 9 cm thick and the Exsulans Limestone Bed *s.str.* is 11 cm thick. The base of the Hyolithes Limestone Bed is located at 243.55 m and the top at 243.20 m, which is the base of the 74 cm thick Andrarum Limestone Bed.

Non-cored water wells with wireline logging data

Five non-cored water wells penetrate the Alum Shale Formation (or nearly so). Wireline logs have previously been obtained in Billeshøj-1, Sømarken-2, Sømarken-3, and Sømarken-4 (see Pedersen & Klitten 1990; Schovsbo *et al.* 2015b) and the fifth well, St. Bukkegård-1, was logged in connection with this study.

The St. Bukkegård well (DGU 246.594), henceforth referred to as the Bu-1 well, is located just north of Limensgade in the Læså area (Fig. 2). It was drilled in 1972 and penetrated Alum Shale from *c.* 3.1 m (directly below the Quaternary) to a depth of 37.8 m (Fig. 12). Hence, the Alum Shale Formation seems to be at least 34.7 m thick in the well, which is the maximum thick-

ness recorded on Bornholm. The well was terminated at 48 m within the Læså Formation. A GR log and an induction conductivity log were obtained by GEUS in November 2017. Note that an iron casing affects the log signals in the uppermost 4 m of the well (Fig. 12). The site was visited by ATN at a time when a large silo was under construction just 15 m west of the well site and here the base of the overlying Komstad Limestone was exposed in a shallow excavation. Nonetheless, Ordovician Alum Shale seems to be missing in the well trace (Fig. 12).

The Billeshøj-1 well (DGU 247.510) was drilled in 1984. A GR log was published by Pedersen & Klitten (1990) and shows that the top of the Komstad Limestone is located at *c.* 49.3 m and the unit is *c.* 1.6 m thick. The underlying Alum Shale Formation is *c.* 26.7 m thick. The Sømarken-2 well (DGU 248.36) was drilled in 1969. A GR log of comparatively low resolution was published by Pedersen & Klitten (1990). It shows that the top of the Komstad Limestone is located at *c.* 108.7 m and that the unit is *c.* 2.5 m thick. The underlying Alum Shale Formation is *c.* 28.4 m thick. Modern digital wireline logging has not been made in these two wells and they are not discussed further.

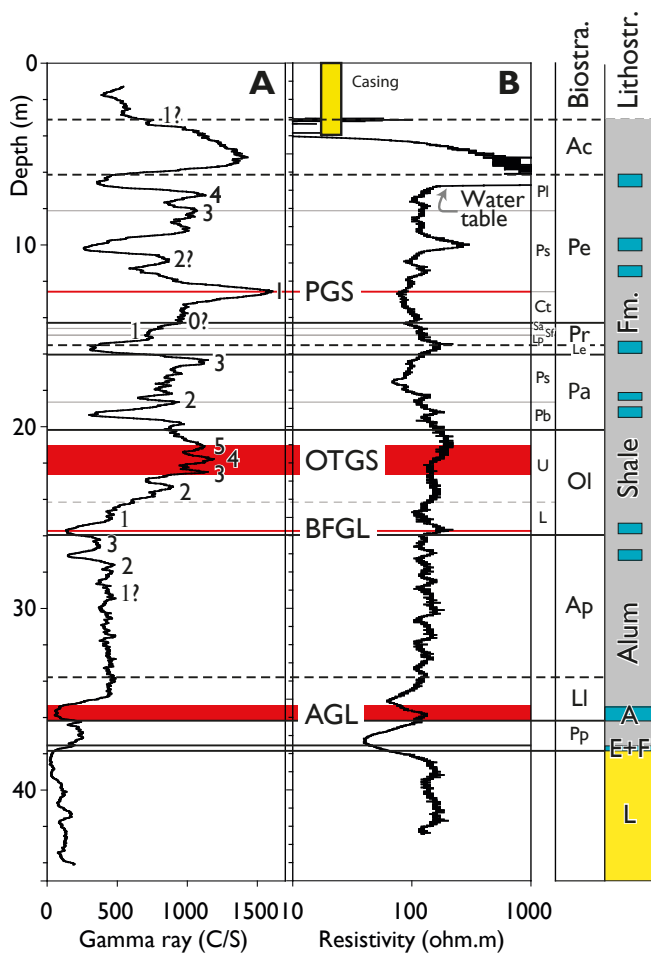


Fig. 12. Simplified lithology and biozonation of the Alum Shale in the uncored well at St. Bukkegård (Bu-1). The biozonation is inferred based on GR wireline log correlation with other wells on southern Bornholm and the Gislövshammar wells in Skåne (Fig. 16). For remarks on the boundary between the *Peltura* and *Acerocarina* Superzones, see the text section on the latter superzone. The resistivity log is calculated from an induction conductivity log, and the very high resistivity in the uppermost part of the well is caused by the dry shale above the water table at 6.8 m depth. The Ordovician Alum Shale Formation seems to be absent at the drill site, and the Furongian strata are directly overlain by Quaternary deposits. The latter exhibit very high radiation levels, likely due to a content of Alum Shale, and it is unclear precisely where the boundary between the Alum Shale and the Quaternary is located, also due to the iron casing in the upper 4 m of the well. **A:** Gamma-ray wireline log. The small numbers 1 and up to 5 indicate correlatable minor gamma spikes. **B:** Resistivity wireline log. Legend and abbreviations as in Fig. 6; abbreviated zonal designations explained in Fig. 14. For location of the well, see Fig. 2.

The Sømarken-3 (DGU 248.39) and Sømarken-4 (DGU 247.312) water wells were both drilled in 1974. They are henceforth referred to as Sø-3 and Sø-4, respectively. GR logs were published by Pedersen & Klitten (1990), but much improved modern digital wireline logging has recently been made in both wells (Fig. 13 and Schovsbo *et al.* 2015b). The top of the Komstad Limestone is located at 68.2 m in Sø-3 and at 50.2 m in Sø-4. The unit is 1.3 m and 1.5 m thick, respectively, in these wells. The underlying Alum Shale Formation is 29.2 m thick in Sø-3 and 29.5 m thick in Sø-4. The very thin Tøyen Formation present

in the Bi-2 core cannot be identified on the wireline logs from that well (Fig. 8), but in the GR logs from the Sø-3 and especially the Sø-4 well a minor low is seen immediately below the Komstad Limestone, which theoretically could be due to the presence of a thin Tøyen Formation (≤ 30 cm) (compare low GR readings in this formation in the Gi-2 well, Fig. 14). In Sø-3, a marked low in the resistivity log is evident at the same level, which is another indication that a thin Tøyen Formation may be present; no lows of the same magnitude are observed in the underlying Alum Shale. However, without cores the interpretation of

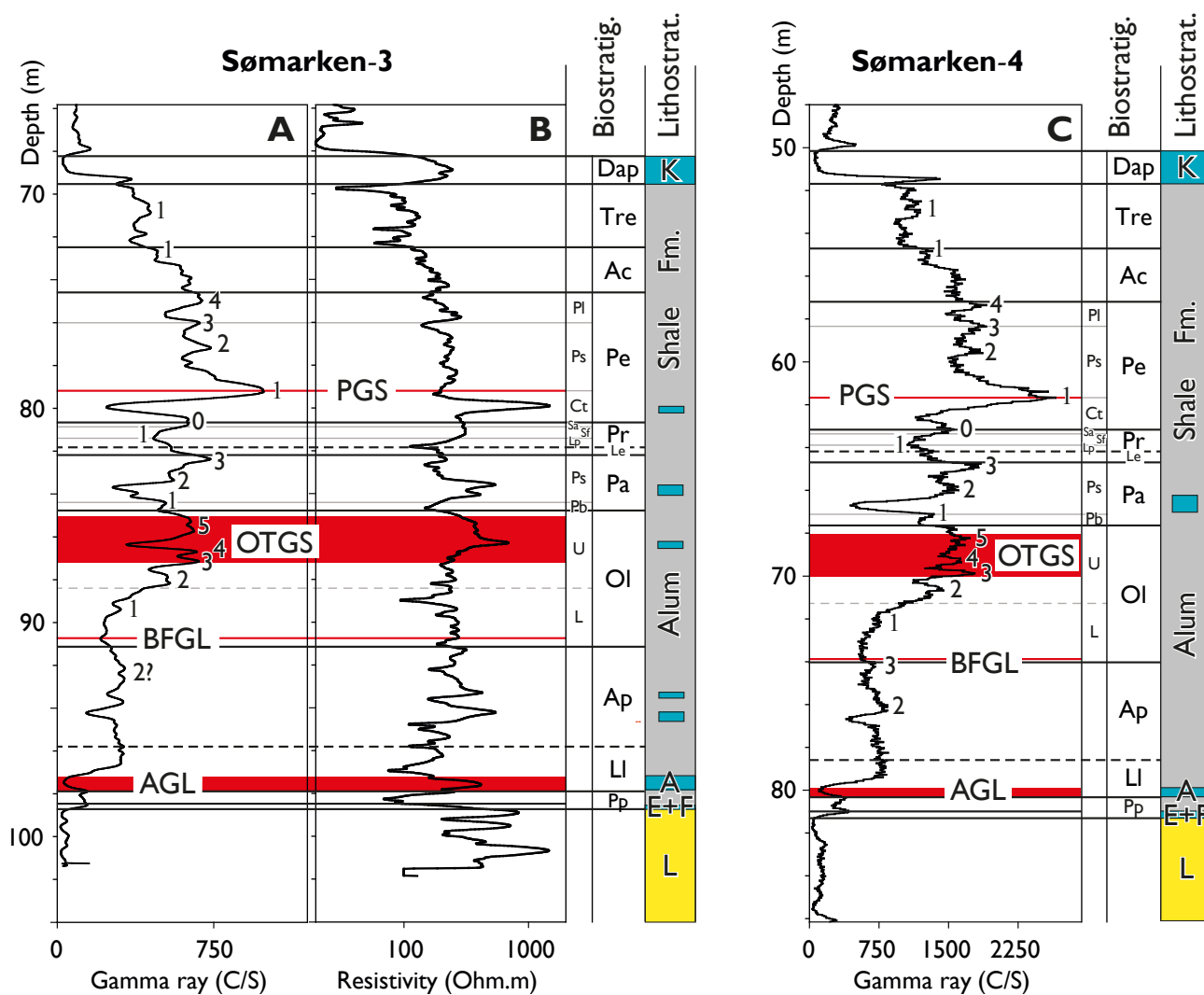


Fig. 13. Simplified lithology and biozonation of the Alum Shale interval in the uncored Sømarken-3 and Sømarken-4 wells. The biozonation is based on GR wireline log correlation with other wells on southern Bornholm (Fig. 16), see text. A: Gamma-ray wireline log from the Sø-3 well. The small numbers 1 and up to 5 indicate correlatable minor gamma spikes. B: Resistivity wireline log from the Sø-3 well. C: Gamma-ray wireline log from the Sø-4 well. It is possible that a thin Tøyen Formation is present in these wells, see text. Legend and abbreviations as in Fig. 6; abbreviated zonal designations explained in Fig. 14. Gamma-ray logs from these wells were first shown by Pedersen & Klitten (1990). The shown wireline logs were measured by GEUS in the Sø-3 and Sø-4 boreholes in 2003 and 1997, respectively. The different magnitude of the gamma radiation in the two wells is caused by differences in detector size. For location of the wells, see Fig. 2.

such a thin unit remains inconclusive; if present, the Alum Shale Formation is slightly thinner than stated. The Sø-3 well was referred to as the Bavnegård well by Poulsen (1978) who briefly summarised the drilled succession.

Other water wells

The Alum Shale Formation has been encountered in a few additional water wells on southern Bornholm, none of which have been wireline logged. The formation is recorded as > 39 m thick in a well at Lille Munkegård (DGU 246.544), but this drill site is located immediately adjacent to a fault and the thickness is regarded as unreliable. The Alum Shale Formation is > 30 m thick in the water well at Lille Duegård (DGU 246.476). This site may also be located adjacent to a fault, but further considerations are meaningless without wireline logs. Near Sø-4, water wells at Eskildsgård (DGU 248.101b) and Vossegård (DGU 247.148) penetrate the lower 14.5 m and upper 6 m of the Alum Shale Formation, respectively.

Gislövshammar-1 and -2, Sweden

The fully cored Gislövshammar-2 (Gi-2) well in southeastern Skåne, Sweden, c. 8 km south of Simrishamn, constitutes the type section of the Alum Shale Formation (Buchardt *et al.* 1997; Schovsbo 2001, 2002a; Nielsen & Schovsbo 2007). The well, drilled in 1991, is located approximately 125 m due south of the older Gislövshammar-1 well site drilled in 1941–42 (Westergård 1942, 1944). In that borehole, the Alum Shale above the Andrarum Limestone Bed is 61.3 m thick. The equivalent interval is 64.0 m in Gi-2, suggesting that one or more undetected minor faults are present in Gi-1. According to the description, minor portions of the Gi-1 core were badly crushed (18–21 m, 22.6–23.6 m, 29.7–32.7, 90.9–91.1 and 98.9–93.2 m), with a core loss of up to 50% (Westergård 1942, 1944). At a depth of 25–26 m the Alum Shale dipped 25–30° and contained narrow fissures filled with calcite. Similar fissure fillings were observed at other levels but apparently not associated with faults, according to Westergård.

The Gi-2 well is 105.9 m deep and penetrated Middle Ordovician to lower Cambrian strata. Here a 19.2 m thick Tøyen Formation is intercalated between the Komstad Limestone and the Alum Shale formations. The thin bed in the Gi-1 well identified as ‘Ceratomyge Limestone’ by Westergård (1942) belongs in our interpretation to the Tøyen Formation and there seems to be no Bjørkåsholmen Formation developed at Gislövshammar.

In Gi-2, the top of the Alum Shale Formation was

encountered at 23.2 m and the base at 103.1 m. The well terminated in the Norretorp Member of the Læså Formation at 105.9 m. A wireline GR log was run in the hole when the drilling had reached a depth of 91.2 m; below this depth a GR log has been constructed based on measurements of the uranium content in the core (Fig. 14; see also Schovsbo 2002a).

For description of the detailed biozonation of the Gi-1 core, see Westergård (1942, 1944); the zones are listed in Table 3. A crude biozonation was sketched for the Gi-2 core by Nielsen & Buchardt (1994), based on fossils incidentally exposed on the bedding planes. A few additional fossil levels were added by Schovsbo (2001). However, the core has not been systematically split in the search for fossils like the older Gi-1 core (ranges of fossils in the core are indicated in Fig. 14). Nonetheless, as can be seen in Fig. 14, the zonal thicknesses established in the Gi-2 core match in detail the comprehensive biozonation established for the Gi-1 core by Westergård (1942, 1944). No particular zone is significantly thicker in the Gi-2 well compared with the Gi-1 well (Table 3), suggesting that the minor difference in thickness of the upper part of the Alum Shale referred to above is not due to a single fault. We further note that the strata dip only c. 5° at the Gi-1 drill site and maybe as much as 11° at the Gi-2 drill site (Nielsen 1995, p. 10), so the real thickness difference may be slightly less than 2 m.

Comparison has also been made with the GR log pattern and crude biozonation established in the cored Fågeltofta-2 and Albjåra-1 wells in Skåne in order to further strengthen the biostratigraphic calibration of the GR log pattern. The latter unpublished data will be presented in a separate paper on the Alum Shale Formation of Skåne.

Wireline log correlation of wells on Bornholm

Previous work

The Alum Shale Formation in Billesløj-1, Sø-2, Sø-3, Sø-4 and Sk-1 was correlated based on GR wireline logs by Pedersen & Klitten (1990). The thin Alum Shale below the Andrarum Limestone Bed with rather low GR intensity was separated as unit B1. The Alum Shale between the Andrarum Limestone Bed and the horizon here referred to as the Ol-2 spike (for explanation, see below) has a higher radiation and was separated as unit B2. Then follows Alum Shale with very high radiation, referred to as unit B3, with an upper boundary corresponding to the highest

radiation levels in the basal part of the *Acerocarina* Superzone. The uppermost part of the Alum Shale Formation has a lower radiation – although not as low as B2 – and was separated as unit B4. Schovsbo *et al.* (2011, 2015b) recognised the same units in the Bi-2 and So-1 wells. The log stratigraphical scheme was further elaborated by Schovsbo *et al.* (2018), discussing correlation with Skåne and southern Norway.

Gamma radiation characterisation of the superzones

Four prominent GR maxima and minima were named by Schovsbo *et al.* (2018), viz. the AGL, BFGL, OTGS and PGS (see below), but in addition to these major fluctuations, many less conspicuous GR spikes can also consistently be recognised in the investigated

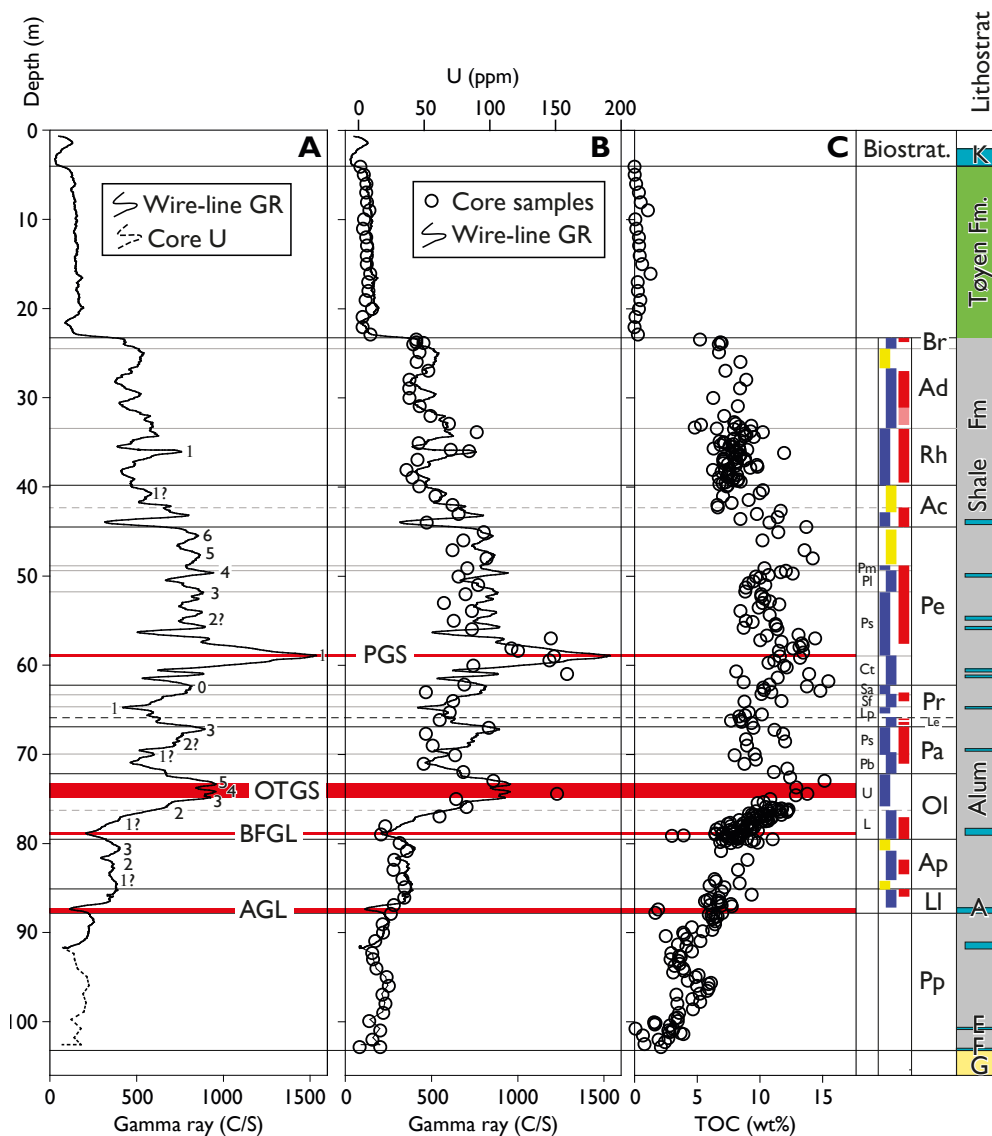


Fig. 14. Simplified lithology and biozonation of the Gislövshammar-2 well in south-eastern Skåne. Identification of the biozone boundaries (listed in Table 3) are guided by comparison with the detailed biozonation established in the adjacent Gislövshammar-1 well (Westergård 1942, 1944). Vertical red bars to the right indicate findings of biostratigraphically diagnostic fossils in the Gi-2 core (Nielsen & Buchardt 1994; Schovsbo 2001); light red bars indicate the presence of fossils tentatively but not safely suggesting zonal assignment. The adjacent blue and yellow bars indicate biozonation and barren intervals, respectively, in the nearby Gi-1 well (Westergård 1942, 1944); the zig-zag pattern reveals the zones discerned by Westergård (see Table 3 for details; zones in the basal *Acerocarina* Superzone are not differentiated). The Gi-1 data are fitted to the depths of the Gi-2 well via comparison with the fossils

found in the latter well and thicknesses of zones. Note that the lower boundary of the *A. pisiformis* Zone is defined by the LAD of *L. laevigata* (Axheimer *et al.* 2006) and thus deviates from the boundary used by Westergård (1942, 1944). A: Wireline gamma-ray log. A running average of U measurements has been used to reconstruct the GR curve below 92 m (shown with dashed line). The small numbers 1 and up to 6 indicate correlatable minor gamma spikes. B: Wireline gamma-ray log and U core measurements. C: TOC content in the Gislövshammar-2 core. Legend and abbreviations as in Fig. 6. Other abbreviations: G: Gislöv Formation; Rh: *Rhabdinopora*; Ad: *Adelograptus*; Br: *Bryograptus*; L: Lower; U: Upper; Pb: *Parabolina brevifrons*; Ps: *Parabolina spinulosa*; Lp: '*Leptoplastus postcurrens*'; Sf: '*Sphaerophthalmus flagellifer*'; Sa: '*Sphaerophthalmus angustus*'; Ct: *Ctenopyge tumida*; Ps: '*Peltura scarabaeoides*'; Pl: *Parabolina lobata*; Pm: '*Parabolina megalops*'. Wireline log and core measurements are from Schovsbo (2001, 2002a); the GR log was made in 1991 using analog recording and has lower resolution than the modern digital logs available from Bornholm. For location of the well, see Fig. 1.

Table 3. Thicknesses (metres) of zones in the Alum Shale Formation in the Gislövshammar-1 and -2 wells, Sweden.

Interval	Gislövshammar-1		Gislövshammar-2	
	Thickness	Depth interval	Thickness ¹	Depth interval ¹
Komstad Limestone	–	–	[9.5] ²	2.0 – 4.0
Tøyen Formation	>12.3	7.2 – 19.5	19.2	4.0 – 23.2
Alum Shale Formation:				
<i>Bryograptus kjerulfi</i> Zone	1.2	19.5 – 20.7	0.8 (1.3)	23.2 – 24.0 (24.5)
Graptolites absent	2.2	20.7 – 22.9	3.0 (2.2)	24.0 – 27.0
<i>Adelograptus tenellus</i> Zone	6.7	22.9 – 29.6	6.5 (6.8)	27.0 (26.7) – 33.5
<i>Rhabdinopora</i> spp. zones	6.4	29.6 – 36.0	6.3	33.5 – 39.8
Tremadocian total	16.5	19.5 – 36.0	16.6	23.2 – 39.8
Trilobite barren interval	3.0	36.0 – 39.0	2.6	39.8 – 42.4
<i>Acerocare ecorne</i> Zone	–	(not found)	–	(not found)
<i>Westergardia scanica</i> Zone	0.5	39.0 – 39.5	} 2.1	} 42.4 – 44.5
<i>Peltura costata</i> Zone	0.5	39.5 – 40.0		
<i>Acerocarina granulata</i> Zone	0.6	40.0 – 40.6		
<i>Acerocarina</i> Superzone total	4.6	36.0 – 40.6	4.7	39.8 – 44.5
Trilobite barren interval	3.9	40.6 – 44.5	4.4	44.5 – 48.9
' <i>Parabolina megalops</i> ' Zone	0.5	44.5 – 45.0	(0.5)	48.9 – (49.4)
<i>Parabolina lobata</i> Zone	2.4	45.0 – 47.4	(2.4)	(49.4) – (51.8)
' <i>Peltura scarabaeoides</i> ' Zone	7.1	47.4 – 54.5	(7.2)	(51.8) – (59.0)
<i>Ctenopyge tumida</i> Zone	3.3	54.5 – 57.8	(3.3)	(59.0) – (62.3)
<i>Peltura</i> Superzone total	17.2	40.6 – 57.8	17.8	44.5 – 62.3
' <i>Sphaerophthalmus angustus</i> ' Zone	1.0	57.8 – 58.8	(0.8)	(62.3) – 63.1
<i>Sphaerophthalmus flagellifer</i> Zone	1.5	58.8 – 60.3	1.0 (1.7)	63.1 – 64.1(64.8)
' <i>Leptoplastus neglectus</i> ' Zone	0.7	60.3 – 61.0	1.8 (1.1)	64.1(64.8) – 65.9
<i>Protopeltura</i> Superzone total	4.3	57.8 – 61.0	3.6	62.3 – 65.9
<i>Leptoplastus</i> Superzone total	1.1	61.0 – 62.1	1.0	65.9 – 66.9
<i>Parabolina spinulosa</i> Zone	3.1	62.1 – 65.2	(3.2)	66.9 – (70.1)
<i>Parabolina brevispina</i> Zone	2.4	65.2 – 67.6	(2.1)	(70.1) – (72.2)
<i>Parabolina</i> Superzone total	5.5	62.1 – 67.6	5.3	66.9 – 72.2
Upper <i>Olenus</i> Superzone	5.4	67.6 – 73.0	(4.1)	(72.2) – (76.3)
Lower <i>Olenus</i> Superzone	1.4	73.0 – 74.4	(3.3)	(76.3) – 79.6
<i>Olenus</i> Superzone total	6.8	67.6 – 74.4	7.4	72.2 – 79.6
Trilobite barren interval	1.0	74.4 – 75.4	1.7 (1.2)	79.6 – 81.3 (80.8)
<i>Agnostus pisiformis</i> Zone	2.9	75.4 – 78.3	2.9 (3.4)	81.3 (80.8) – (84.2)
Trilobite barren interval	0.8	78.3 – 79.1	0.9	(84.2) – 85.1
<i>Agnostus pisiformis</i> Zone	4.7	74.4 – 79.1	5.5	79.6 – 85.1
<i>Lejopyge laevigata</i> Zone	2.5	79.1 – 80.8	2.2	85.1 – 87.3
Andrarum Limestone	0.8	80.8 – 81.6	0.6	87.3 – 87.9
<i>Paradoxides paradoxissimus</i> Superzone	15.3	81.6 – 96.9	15.3	87.9 – 103.1
Total Alum Shale Fm: Logged thickness	–	–	79.9	23.3 – 103.1
Total Alum Shale Fm: Cored thickness	77.4	19.5 – 96.9	79.8	23.3 – 103.1

¹Numbers in brackets are thicknesses and levels deduced from comparison with the Gi-1 well

²Thickness in exposure at Gislövshammar (Nielsen 1995)

wells. For convenience, we refer to these minor peaks as e.g. the Ol-2 or the Pa-2 spike, referring to the abbreviated superzone name and spike number as shown in the respective GR logs (see e.g. Fig. 10). It should be kept in mind that limestone concretions introduce distinct lows in the GR logs. Despite being eye-catching, these lows should be ignored when correlating the GR log pattern as the concretions occur semi-randomly in the succession. For this reason, the GR log interpretation is most reliably done by combining the GR curve with a lithologically sensitive log tool such as the sonic velocity log, the formation resistivity log or

the density log, as a way to detect whether or not GR lows reflect limestone nodules or not. This is obviously only a problem in non-cored wells.

The following features in the GR logs have been used for tracing the superzonal boundaries on Bornholm, guided by correlation with the well-constrained biozonation of the Gi-2 succession in Skåne (Figs 14, 15).

- The base of the Alum Shale Formation is characterised by a small GR peak that likely reflects the phosphorite and glauconite content of the basal conglomerate. The amalgamated Forsemölla and Exsulans limestone beds at the base of the

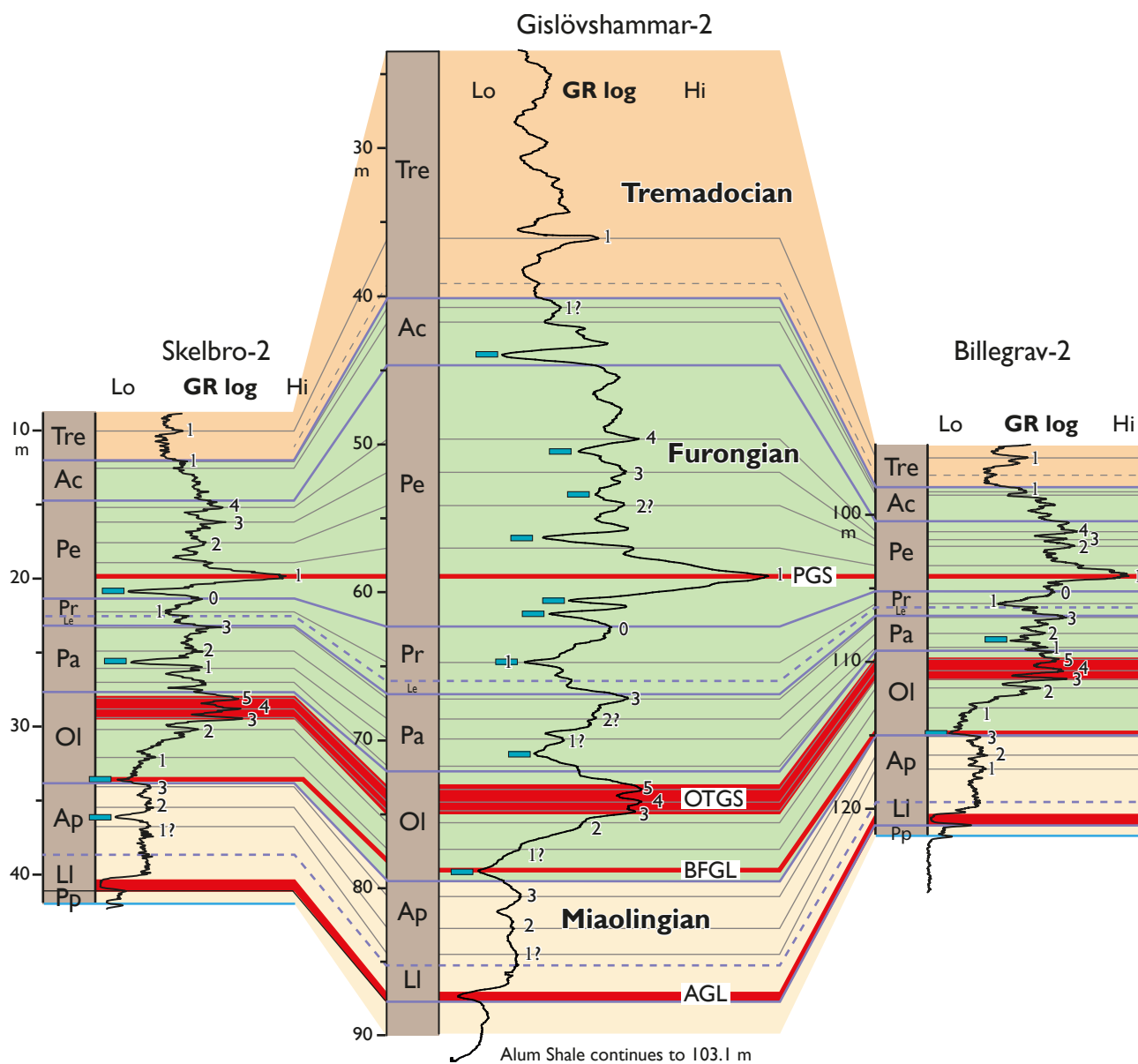


Fig. 15. Correlation of the Alum Shale in the Skelbro-2 and Billegrav-2 wells on Bornholm with the Gislövshammar-2 well in south-eastern Skåne, based on wireline GR logs. Logs for each of these wells are presented in Figs 8, 10 and 14. The small blue bars adjacent to the GR curves indicate limestone intercalations (producing GR lows). The thin grey lines trace minor GR oscillations, and the thicker light blue lines show superzone boundaries. Legend and abbreviations as in Fig. 6.

Alum Shale Formation are also identifiable using lithology-sensitive tools (sonic velocity, formation resistivity or density logs).

- The immediately overlying Alum Shale facies has a low and only slightly fluctuating gamma radiation (*Paradoxides paradoxissimus* Superzone).
- The combined Hyolithes + Andrarum Limestone Beds are signalled by a distinct low in the GR response, named the Andrarum Gamma Low (AGL) by Schovsbo *et al.* (2018) (lower part of the *Paradoxides forchhammeri* Superzone). However, due to averaging by the logging tool of the markedly different GR signal from the shale/limestone lithologies (the so-called shoulder-bed effect), the top and base of the amalgamated limestone are difficult to pick precisely on the GR logs. Better definitions of the limestone boundaries are typically obtained on the resistivity and/or the density log.
- The GR motif in the Miaolingian shale above the Andrarum Limestone Bed is rather uniform with only minor fluctuations. The boundary between the *L. laevigata* and *A. pisiformis* Zones is inconspicuous in terms of GR response, but comparison with the Gi-2 well suggests that it approximates a horizon with maximum GR values close above the Andrarum Limestone Bed. Despite being unremarkable, this minor peak is traceable in all wells (Fig. 16). The sonic logs available from the So-1 and Sk-2 wells show a decreasing p-wave velocity up through the interval excluding the peak velocities created by limestone intercalations.
- The lower boundary of the *Olenus* Superzone (i.e. base Furongian) is located immediately below (~0.1–0.2 m in the wells on Bornholm) a very distinctive GR minimum named the Base Furongian Gamma Low (BFGL) by Schovsbo *et al.* (2018). Identification of the lower boundary of the superzone is corroborated by findings of diagnostic fossils in Sk-1, Bi-2 and So-1 as well as Gi-2.
- The BFGL is upwards followed by a steep gradual increase in the GR level, leading up to the OTGS marker (see below). This very distinctive increase in gamma radiation is readily identified in all wells; it includes a couple of minor GR peaks labelled Ol-1 and Ol-2 (Fig. 16).
- The upper part of the *Olenus* Superzone is characterised by very high radiation levels with three intra-superzone GR peaks, numbered Ol-3 to Ol-5 and collectively termed the *Olenus* Triple Gamma Spike (OTGS) by Schovsbo *et al.* (2018).
- The lower boundary of the *Parabolina* Superzone is located on the falling limb of the OTGS marker and is well-defined in all wells (Fig. 16). The position of the boundary is corroborated by findings of fossils in Sk-1, Bi-2 and So-1 as well as Gi-2.
- The *Parabolina* Superzone is characterised by a general upwards increase in the GR intensity. However, the GR log pattern is usually rather fluctuating due to the common presence of limestone.
- The upper boundary of the *Parabolina* Superzone is located immediately above a conspicuous GR maximum labelled Pa-3 at the very top of the superzone (Fig. 16).
- The *Leptoplastus* Superzone is thin and only tentatively identified. It appears to be represented by just one GR ‘wiggle’ interspersed between the Pa-3 spike in the uppermost part of the *Parabolina* Superzone and a pronounced low forming the lower part of the *Protopeltura* Superzone.
- The *Leptoplastus/Protopeltura* superzone boundary seems to be marked by a minor GR peak. Despite being inconspicuous, it is traceable in all wells on Bornholm (Fig. 16).
- The *Protopeltura* Superzone, especially the lower part, is characterised by a lower GR level than the overlying *Peltura* Superzone (Pr-1, Fig. 16). In the uppermost part of the *Protopeltura* Superzone the GR readings increase rapidly upwards as an initial part of the rise leading to the PGS marker (see below).
- The *Protopeltura–Peltura* superzonal boundary is located at the Pe-0 spike perturbing the general GR rise leading to the PGS marker (see below). The boundary is occasionally obscured by the occurrence of limestone concretions with very low GR intensity.
- The *Peltura* Superzone is an overall high GR interval including the conspicuous PGS peak in the lower part (*Peltura* Gamma Spike, Schovsbo *et al.* 2018). This major peak represents the highest GR level in the entire Alum Shale Formation. From there the GR intensity decreases upwards but remains overall high in the *Peltura* Superzone; three smaller GR maxima can be traced consistently on Bornholm in the upper part of the superzone (labelled Pe-2–4 in Fig. 16).
- The boundary between the *Peltura* and *Acerocarina* Superzones is located on the falling limb of the GR log immediately above the Pe-4 spike that terminates the overall high GR level characteristic of the *Peltura* Superzone. Although being rather inconspicuous, this boundary is readily traceable between wells (Fig. 16). The sonic log (available from only So-1 and Sk-2) shows a gradually increasing p-wave velocity from that boundary and upwards.
- The *Acerocarina* Superzone is characterised by an overall upwards falling GR level intermediate between that of the underlying *Peltura* Superzone and the overlying Tremadocian interval. The lower half to two-thirds of the superzone is characterised by a fairly high GR level that abruptly falls to a lower

level in the upper part of the superzone (Fig. 16). In the Gi-2 well, this pronounced fall coincides broadly with the boundary between the fossiliferous lower part (*A. granulata* to *W. scanica* Zones) and the unfossiliferous upper part of the superzone (Fig. 14). The only exception to this pattern is the Bu-1 well, where the lower main part of the *Acerocarina* Superzone exhibits very high gamma radiation, almost as high as the PGS. This motif is also known from wells in central and western Skåne, but is less distinct in south-eastern Skåne and is not seen in the other Bornholm wells.

- The base of the Ordovician is located immediately above the small Ac-1 spike intersecting the general upwards fall in GR intensity that characterises the *Acerocarina* Superzone. In the Gi-2 well, where the Tremadocian is much expanded and stratigraphically more complete than on Bornholm, the Cambro-Ordovician boundary, identified by the FAD of graptolites, is located slightly above the Ac-1 peak (Fig. 14). The position of the boundary is constrained by the incoming of graptolites in the Bi-2 core (Fig. 8); graptolites have also been found in the Ordovician interval in the Sk-1 and So-1 cores (Figs 6, 11).
- Above the Cambro-Ordovician boundary, the GR intensity further decreases into the Ordovician and becomes clearly lower than in the *Acerocarina* Superzone. An omnipresent GR spike is labelled Tre-1 (Fig. 16). This maximum coincides with a graptolite-rich horizon within the *R. flabelliformis flabelliformis* Zone, known from the exposure at Limensgade and the Sk-1 core, as well as at various places in Skåne, e.g. the Flagabro well (Tjernvik 1958). The Tre-1 spike is also recognisable in the Gi-2 well (Fig. 14).
- The uppermost part of the Alum Shale, 0.5–0.6 m thick, exhibits an upwards increasing GR signal in most wells (and where it does not this may be due to the presence of a thin Tøyen Formation). This is likely associated with a high phosphorite content with raised levels of uranium (see Poulsen 1922 for description of the Limensgade section).
- The Tøyen Formation in the Bi-2 core cannot be identified on the logs, probably because it is too thin. The minor fall in GR intensity seen in the Sø-3 well, and especially in the Sø-4 well, immediately below the basal Komstad Limestone conglomerate peak (see below) may reflect the presence of a thin Tøyen Formation. In Sø-3, a marked low in the resistivity log is also seen at the same level, which is rather remarkable. However, without cores the presence of a thin Tøyen Formation remains speculative.
- The conglomerate at the base of the Komstad Limestone Formation is associated with a distinct maximum in the GR log and high formation resistivity readings (e.g. Fig. 10). The latter is related to

the carbonate matrix, whereas the high GR intensity reflects the common phosphorite nodules and elevated glauconite content. The underlying Alum Shale Formation is characterised by low resistivity values and this log type is best for picking the boundary precisely.

- The Komstad Limestone is characterised by low GR intensity associated with high resistivity readings. The top of the limestone is placed below a small GR spike that may reflect the phosphorite conglomerate at the base of the *Dicellograptus* Shale, an increased TOC level in the blackish uppermost part of the limestone (Nielsen 1995) or a combination of these factors.

Correlation and thickness variations of superzones on Bornholm

Paradoxides paradoxissimus Superzone

This superzone comprises the amalgamated Forsemølla and Exsulans Limestone Beds and the overlying Alum Shale up to the Hyolithes Limestone Bed (Fig. 3). The composite basal limestone, which is recognised in all investigated wells, is up to 0.25 m thick. The individual limestone beds cannot be discerned in wireline logs, but the composite unit is recognised by having very low GR values above the basal conglomerate GR peak, usually associated with a distinct spike in the resistivity log. A drop in resistivity coinciding with a rise in gamma radiation characterises the Alum Shale interval between the Exsulans and Hyolithes limestones. This shale is 0.5–1.95 m thick with minimum thickness in the Bi-2 well and maximum thickness in the So-1 well. Berg-Madsen (1985b) reported a thickness of only 0.1 m in Øleå below Ringborgen, but our re-measurement in 2017 showed this Alum Shale interval to be c. 0.5–0.6 m thick at this locality.

The entire *P. paradoxissimus* Superzone varies in thickness from 0.8–1.5 m in the Bu-1, Sk-1, Sk-2, Sø-3, Sø-4 and Bi-2 wells, to 2.15 m in the So-1 well (cored thickness). No systematic thickness variation across southern Bornholm is observed (Fig. 16, Table 4).

Paradoxides forchhammeri Superzone

This superzone comprises the Hyolithes and Andrarum Limestone Beds and the lower part of the overlying Alum Shale, assigned to the (traditional) *Lejopyge laevigata* and *Agnostus pisiformis* Zones (Fig. 3). The boundary between the latter zones is inconspicuous in the GR logs, but comparison with the log pattern in the Gi-2 well suggests a thickness of 0.9–1.6 m of the *L. laevigata* Zone on Bornholm (Table 5). This interpretation must be considered tentative, but it corresponds fairly well with the zonal thickness measured in the exposure at Borggård, Øleå,

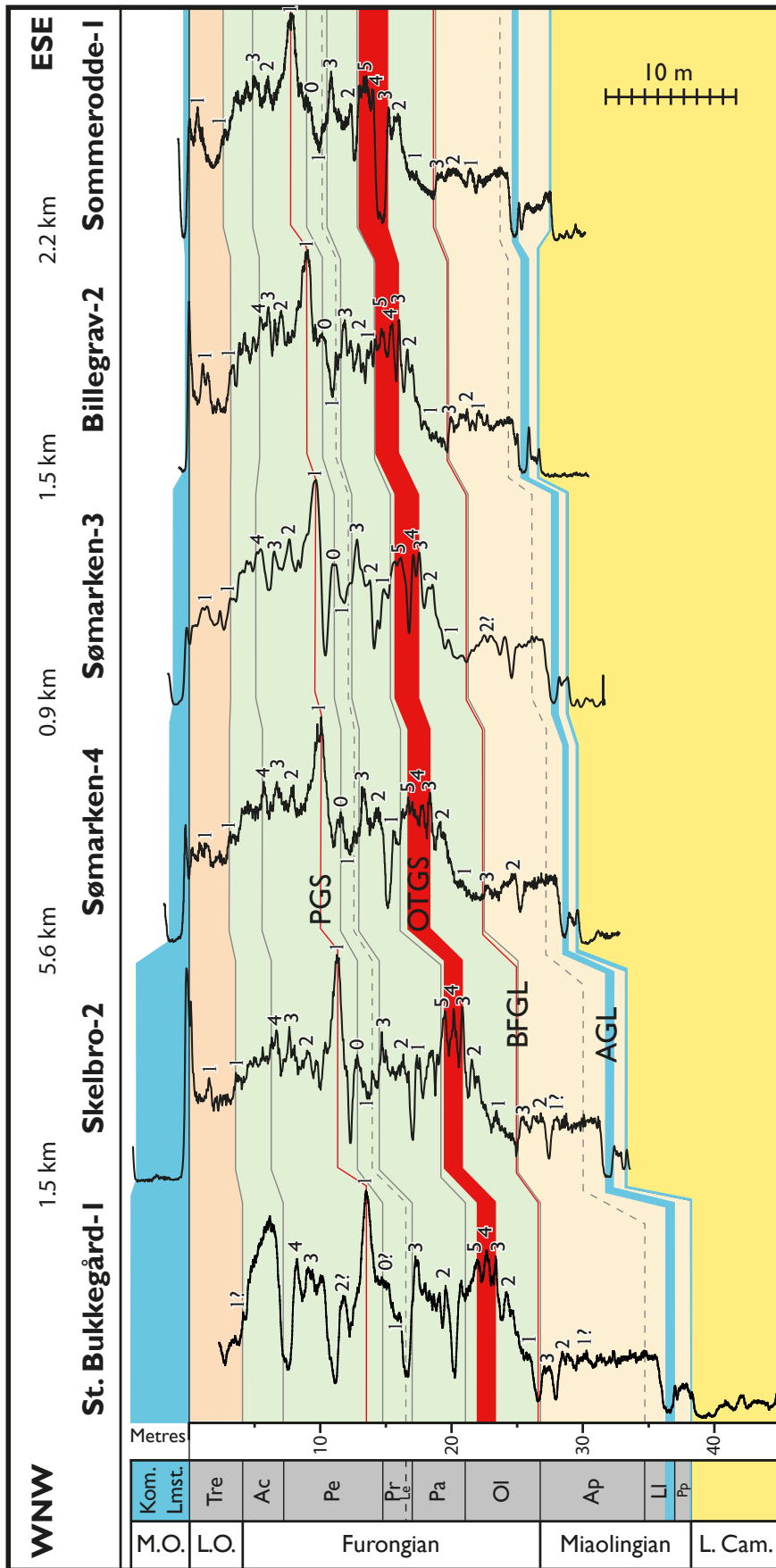


Fig. 16. Correlation of the Alum Shale interval in the St. Bukkegård-1, Skelbro-2, Sømarken-4, Sømarken-3, Billegrav-2, and Sommerødde-1, based on GR wireline logs. The distance in kilometres between the individual wells is indicated in the upper line. The numbers 1 and up to 5 adjacent to the logs indicate correlatable minor maxima or minima in the gamma-ray log, referred to by a prefix consisting of the first two letters in the superzone name and the number, e.g. Pa-2, OI-1 etc. Legend and abbreviations as in Figure 6 with the addition that M.O. = Middle Ordovician and Kom. Lmst. = Komstad Limestone. Logs for each well are shown in Figs 8, 10, 11, 12 and 13. Location of the correlation profile is indicated in Figure 2.

by Poulsen (1923) (boundary somewhere between 0.8 and 2.1 m above the Andrarum Limestone Bed) and Berg-Madsen (1986) (boundary between 1.5 and 1.6 m above the Andrarum Limestone Bed). However, there is no indication of a thinner development of the *L. laevigata* Zone in the Sk-2 and Bu-1 wells, on the contrary (Table 5). These wells are located close to the outcrop at Kalby, Læså, where the *L. laevigata* Zone was stated to be only ~0.65 m thick by Berg-Madsen (1986), based on findings of a conodont of assumed late Cambrian age (the same marker as used in the Øleå section). The Kalby section was the only site where Grönwall (1899, 1902) found *L. laevigata*, but he did not state the range and it is likely restricted to the anthraconite nodules immediately overlying the Andrarum Limestone Bed. The overlying *A. pisiformis* Zone is 4.6–5.0 m thick in most of the investigated wells and very thick, 7.8 m, in the Bu-1 well (Table 5).

The total thickness of the Miaolingian shale overlying the Andrarum Limestone Bed varies in thickness between 5.6 and 6.4 m except for the Bu-1 well, where it is 9.4 m. Overall, the *Paradoxides forchhammeri* Superzone shows no systematic thickness variation between wells (Table 4) and it is almost of the same thickness as in south-eastern Skåne. In fact, it is even thicker in the Bu-1 well, where the *A. pisiformis* Zone is remarkably thick. Note that the *L. laevigata*/*A. pisiformis* zonal boundary in the Gi-2 well (at 85.1 m) is defined by the LAD of *L. laevigata* following Axheimer *et al.* (2006); this boundary differs from the zonal definition used by Westergård (1942, 1944).

Olenus Superzone

Trilobites occur in great profusion in the lower part of the *Olenus* Superzone throughout Scandinavia (e.g. Westergård 1922; Lauridsen & Nielsen 2005 and references therein), and this fossiliferous level is usually recognisable in cores even without splitting. The GR log motif of the superzone is also very characteristic, and it is easily identified on wireline logs (see above).

The *Olenus* Superzone is 5.7–6.4 m thick across southern Bornholm and does not show notable thickness differences between the Læså and Øleå areas (Table 4). In the Gi-2 well, the *Olenus* Superzone is 7.4 m thick (Table 3), so the interval is slightly thinner on Bornholm. The GR log pattern is essentially similar between south-eastern Skåne and Bornholm (Fig. 15), strongly suggesting that the upper *Olenus scanicus*–*Olenus rotundatus* Zone with bradorid arthropods (*Polyphyma/Beyrichia* *sensu* Westergård 1922, 1942, 1944, 1947) is developed also on Bornholm, but the index trilobites have not been found. This upper part of the *Olenus* Superzone corresponds to the OTGS marker in the GR logs. The informal boundary between the lower and upper parts of the superzone (Fig. 3) is located approximately midway between the Ol-1 and Ol-2 spikes (Fig. 14).

Parabolina Superzone

This superzone comprises two zones (Fig. 3). The lower *Parabolina brevispina* Zone is 2.4 m thick in the Gi-1 well (Table 3) and seems to be characterised by low GR levels in the Gi-2 well, but the GR intensity

Table 4. Thicknesses and depth intervals (metres) of formations and superzones in wells on Bornholm.

	St. Bukkegård-1	Skelbro-2	Skelbro-16	Sømarken-3	Sømarken-4	Billegrav-2	Sommerodde-1
Komstad Limestone	[4.7] ¹	4.1 (4.4–8.5)	>3.9 (0–3.9)	1.3 (68.2–69.5)	1.5 (50.2–51.7)	0.1 (95.1–95.2) ³	0.6 (217.4–217.9)
Tøyen Formation	[0] ^{1,2}	0	0	Thin?	Thin?	0.2 (95.2–95.4) ³	0
Tremadocian	[4.0] ²	3.5 (8.5–12.0)	3.4 (3.9–7.4)	3.0 (69.5–72.5) ⁵	3.0 (51.7–54.7) ⁵	2.8 (95.4–98.2) ⁵	2.5 (217.9–220.4)
<i>Acerocarina</i> Superzone	≥3.0 (3.1–6.1)	2.7 (12.0–14.7)	2.9 (7.4–10.2)	2.0 (72.5–74.5)	2.5 (54.7–57.2)	2.2 (98.2–100.4)	2.2 (220.4–222.6)
<i>Peltura</i> Superzone	8.1 (6.1–14.3)	6.7 (14.7–21.4)	6.7 (10.2–16.9)	6.1 (74.5–80.7)	6.0 (57.2–63.2)	5.1 (100.4–105.5)	4.3 (222.6–226.9)
<i>Protopeltura</i> Superzone	1.2 (14.3–15.5)	1.1 (21.4–22.5)	1.1 (16.9–18.0)	1.1 (80.7–81.8)	1.0 (63.2–64.2)	0.9 (105.5–106.4)	1.2 (226.9–228.1)
<i>Leptoplastus</i> Superzone	0.5 (15.5–16.0)	0.6 (22.5–23.1)	0.6 (18.0–18.6)	0.4 (81.8–82.2)	0.5 (64.2–64.7)	0.5 (106.4–106.9)	0.5 (228.1–228.5)
<i>Parabolina</i> Superzone	4.1 (16.0–20.2)	4.5 (23.1–27.7)	4.2 (18.6–22.9)	2.6 (82.2–84.8)	2.9 (64.7–67.6)	2.3 (106.9–109.2)	2.0 (228.5–230.5)
<i>Olenus</i> Superzone total	5.8 (20.2–26.0)	6.1 (27.7–33.8)	6.3 (22.9–29.2)	6.4 (84.8–91.1)	6.4 (67.6–74.0)	5.8 (109.2–115.0)	6.3 (230.5–236.8)
<i>Paradoxides forchhammeri</i> Superzone	10.2 (26.0–36.2)	7.2 (33.8–41.0)	7.0 (29.2–36.2)	6.8 (91.1–97.9)	6.3 (74.0–80.3)	6.2 (115.0–121.2)	6.8 (236.8–243.6)
<i>Paradoxides paradoxissimus</i> Superzone	1.7 (36.2–37.8)	1.1 (41.0–42.1)	1.3 (36.2–37.5)	0.8 (97.9–98.7)	0.9 (80.3–81.2)	1.0 (121.2–122.1)	2.2 (243.6–245.8)
Total Alum Shale Fm: Logged thickness	38.9 ⁴	33.6	33.5	29.2 ⁵	29.5 ⁵	26.9	28.0
Total Alum Shale Fm: Cored thickness	–	33.5	33.5	–	–	26.8	27.9

¹Thickness in Vasagård-1. ²Thickness at Limensgade. ³Cored thickness. ⁴Incl. 4 m Tremadocian at Limensgade. ⁵A little thinner if Tøyen Fm is present.

⁶The GR log from this well is of low resolution; in particular the thickness of the *P. paradoxissimus* Superzone deviates from the drilled thickness (cf. Pedersen 1989).

The recorded drilled (isochore) thicknesses may be up to 2 % larger than the true stratigraphic thicknesses due to the dip of the strata, which on Bornholm and in SE Skåne typically is 5–10°. This concerns all thicknesses stated in this paper (Tables 3–5).

fluctuates due to the presence of limestone. The overlying *Parabolina spinulosa* Zone is 3.1 m thick in the Gi-1 core and is characterised by rising GR levels in the Gi-2 well, leading up to a quite prominent peak at the very top of the zone. The same log pattern with a marked reduction in GR intensity in the lower part of the superzone relative to the underlying OTGS marker, followed by an upwards rise culminating in an upper peak, also characterises the *Parabolina* Superzone on Bornholm (Fig. 16).

In the Sk-2 and Bu-1 wells, the total *Parabolina* Superzone is 4.5 and 4.1 m thick, respectively, which is thicker than the *P. spinulosa* Zone in the Gi-1 well (Table 3). Hence, since all Furongian zones and superzones on Bornholm are thinner than their counterparts in Skåne, and also because the GR log pattern of the superzone is very similar between the two areas (Fig. 15), we infer that the basal *P. brevispina* Zone is developed on Bornholm, at least in the Læså area. The *P. brevispina*/*P. spinulosa* zonal boundary approximates the Pa-1 spike in the Gi-2 well (Fig. 14) and adopting this boundary for Bornholm, the respective thicknesses of the two zones are shown in Table 5. The *Parabolina* Superzone shows a significant south-eastwards thinning from 4.1–4.5 m in the Bu-1, Sk-1 and Sk-2 wells to 2.0 m in So-1 (Table 4). The GR

log-correlation indicates that it is primarily the lower part of the superzone that becomes thinner (Fig. 16) and perhaps no *P. brevispina* Zone is developed in the So-1 well (Table 5).

Parts of the superzone are exposed in the Øleå and Læså streams (Poulsen 1923, locs 4, 5, 6, 19, 21; see also Hansen 1945). It contains very abundant orthid brachiopods (*Orusia lenticularis*), which occasionally form coquinoid limestone. Limestone is present in most of the investigated wells (Bu-1, Sk-1, Sk-2, Bi-2, Sø-3, Sø-4). Brachiopods have been found in this superzone in the cores from Sk-1 (20.6–20.8 m), Bi-2 (107.4–109.2 m) and So-1 (228.9–230.4 m).

***Leptoplastus* Superzone**

This superzone is the thinnest of all Furongian superzones and it is absent or incomplete at many sites in Scandinavia (Westergård 1922, 1947; Martinsson 1974, fig. 5). A full zonal suite is known only from Skåne (Ahlberg *et al.* 2006 and references therein). In the Oslo area, only the basal zone is missing (Rasmussen *et al.* 2015). On Bornholm, the *Leptoplastus* Superzone comprises only the upper two zones (Fig. 3). The entire superzone, 0.6 m thick, is exposed at Poulsen's (1923) locality 6 in the Læså section and the upper zone is also recorded from Poulsen's (1923) locality 22 in the

Table 5. Thicknesses and depth intervals (metres) of selected Furongian and Miaolingian zones in wells on Bornholm

	St. Bukkegård-1	Skelbro-2	Skelbro-1	Sømarken-3	Sømarken-4	Billegrav-2	Sommerodde-1
Peltura Superzone							
' <i>Parabolina megalops</i> ' Zone	0?	0?	0?	0?	0	0	0
<i>Parabolina lobata</i> Zone	2.0 (6.1–8.1)	1.5 (14.7–16.2)	1.6 (10.2–11.8)	1.5 (74.5–76.0)	1.1 (57.2–58.3)	0.8 (100.4–101.2)	0
' <i>Peltura scarabaeoides</i> ' Zone	4.5 (8.1–12.6)	3.7 (16.2–19.9)	3.6 (11.8–15.4)	3.2 (76.0–79.2)	3.4 (58.3–61.7)	2.9 (101.2–104.1)	3.0 (222.6–225.6)
<i>Ctenopyge tumida</i> Zone	1.7 (12.6–14.3)	1.5 (19.9–21.4)	1.5 (15.4–16.9)	1.5 (79.2–80.7)	1.5 (61.7–63.2)	1.4 (104.1–105.5)	1.3 (225.6–226.9)
Protopeltura Superzone							
' <i>Sphaerophthalmus angustus</i> ' Zone	0.3 (14.3–14.6)	0.3 (21.4–21.7)	Log	0.2? (80.7–80.9)	0.2 (63.2–63.4)	0.2 (105.5–105.7)	0.3 (226.9–227.2)
<i>Sphaerophthalmus flagellifer</i> Zone	0.4 (14.6–15.0)	0.5 (21.7–22.2)	too	0.5 (80.9–81.4)	0.5 (63.4–63.9)	0.5 (105.7–106.2)	0.6 (227.2–227.8)
' <i>Leptoplastus neglectus</i> ' Zone	0.5? (15.0–15.5)	0.3 (22.2–22.5)	crude	0.4 (81.4–81.8)	0.3 (63.9–64.2)	0.2 (106.2–106.4)	0.3 (227.8–228.1)
<i>Parabolina</i> Superzone							
<i>Parabolina spinulosa</i> Zone	2.7 (16.0–18.7)	2.9 (23.1–26.0)	2.9 (18.6–21.5)	2.3 (82.2–84.5)	2.4 (64.7–67.1)	1.9 (106.9–108.8)	2.0 (228.5–230.5)
<i>Parabolina brevispina</i> Zone	1.5 (18.7–20.2)	1.7 (26.0–27.7)	1.4 (21.5–22.9)	0.3 (84.5–84.8)	0.5 (67.1–67.6)	0.4 (108.8–109.2)	0
<i>Olenus</i> Superzone							
Upper <i>Olenus</i> Superzone	4.0 (20.2–24.2)	3.2 (27.7–30.9)	4.0 (22.9–26.9)	3.6 (84.8–88.4)	3.7 (67.6–71.3)	3.4 (109.2–112.6)	3.7 (230.5–234.2)
Lower <i>Olenus</i> Superzone	1.8 (24.2–26.0)	2.9 (30.9–33.8)	2.3 (26.9–29.2)	2.7 (88.4–91.1)	2.7 (71.3–74.0)	2.4 (112.6–115.0)	2.6 (234.2–236.8)
<i>Paradoxides forchhammeri</i> Superzone							
<i>Agnostus pisiformis</i> Zone	7.8 (26.0–33.8)	4.9 (33.8–38.7)	5.0 (29.2–34.1)	4.7 (91.1–95.8)	4.6 (74.0–78.6)	4.7 (115.0–119.7)	4.8 (236.8–241.6)
<i>Lejopyge laevigata</i> Zone	1.6 (33.8–35.4)	1.6 (38.7–40.3)	1.4 (34.1–35.5)	1.4 (95.8–97.2)	1.4 (78.6–79.9)	0.9 (119.7–120.6)	1.2 (241.6–242.7)
Andrarum Limestone	0.8 (35.4–36.2)	0.7 (40.3–41.0)	0.6 (35.5–36.2)	0.7 (97.2–97.9)	0.4 (79.9–80.3)	0.6 (120.6–121.2)	0.9 (242.7–243.6)

Øleå section. In the Læså section much of the superzone is made up of limestone; in the studied wells, limestone is present only in Bu-1. We presume that the *Leptoplastus* Superzone corresponds to the basal GR-cycle (low/high couplet) of the interval immediately above the *Parabolina* Superzone. Despite being rather unremarkable, this 'wobble' can be traced in nearly all wells (Fig. 16) and the interpretation is consistent with the GR log pattern and fossil distribution in the Gi-2 well in Skåne (Figs 14, 15). The tentative correlation suggests that the superzone is 0.4–0.6 m thick on Bornholm (Table 4), but due its thinness the relative measuring uncertainty is considerable.

Protopeltura Superzone

This superzone is 0.9–1.2 m thick in the investigated wells which is markedly thinner than in Skåne (Westergård 1944; Table 3). It shows no systematic thickness differences across southern Bornholm (Table 4). We prefer a simplified subdivision of the superzone into only three zones (Fig. 3), following Westergård (1944, 1947). In the Gi-2 well, the GR minimum labelled Pr-1 coincides with the '*Leptoplastus neglectus*'/*Sphaerophthalmus flagellifer* zonal boundary (Fig. 14) and this intra-superzone marker is also recognisable on Bornholm (Fig. 16), although limestone locally obscures the GR signal in the interval. In the Gi-2 well, the overlying *S. flagellifer* Zone is characterised by strongly upwards increasing GR intensity, in turn followed by the '*Sphaerophthalmus angustus*' Zone that has a fairly uniform GR level, increasing but very slightly upwards (Fig. 14). Applying this pattern to the GR logs from Bornholm, a tentative correlation of zones has been attempted (Table 5; see also individual logs).

The *Protopeltura* Superzone is exposed at Poulsen's (1923) locality 6 in the Læså section with a stated total thickness of *c.* 1.1 m, which conforms to the thicknesses encountered in wells (Table 5). The trilobites reported by Poulsen (1923) are only indicative of the *S. flagellifer* and '*S. angustus*' Zones; the precise ranges were not specified. However, the basal '*L. neglectus*' Zone is quite thin in Skåne (0.3–0.9 m; Westergård 1942, 1944) and if thinner on Bornholm, as must be anticipated, it requires high resolution sampling to locate it. Hence, the apparent absence in the Læså section may reflect lack of discovery of the diagnostic trilobites. The *Leptoplastus* cranidia found at 106.0 m in the Bi-2 core actually bring *L. neglectus* to mind, but need further study to be safely identified. '*Ctenopyge neglectus* var. *bornholmensis*' described by Poulsen (1923) is not an indicator for the '*L. neglectus*' Zone as hinted at by Poulsen (1923) and Martinsson (1974, fig. 5); the associated fauna clearly shows a derivation of this endemic species from the *Leptoplastus crassicornis*–*Leptoplastus angustatus* Zone (ATN unpublished data).

Assuming that the Pr-1 minimum marks the upper boundary of the '*L. neglectus*' Zone as in the Gi-2 well, the zone may be ~0.25–0.5 m thick on Bornholm (Table 5).

Peltura Superzone

This superzone thins south-eastwards from 6.7–8.1 m in wells in the Læså area to 4.3 m in So-1 (Table 4). Approximately half of this thinning is due to overall condensation of the interval and the remaining reduction is due to truncation of the upper part of the superzone (Fig. 16, Table 5).

The superzone is in this study, again essentially following Westergård (1944, 1947), subdivided into the *Ctenopyge tumida*, '*Peltura scarabaeoides*', *Parabolina lobata* and '*Parabolina megalops*' Zones, listed in ascending order (Fig. 3). In the Gi-2 well, the *C. tumida* Zone is characterised by rapidly upwards increasing GR readings culminating in the conspicuous PGS marker located at the boundary between the *C. tumida* and '*P. scarabaeoides*' Zones (Fig. 14). This pattern is readily identified in all wells on Bornholm (Figs 15, 16) where the *C. tumida* Zone thus delineated is 1.3–1.7 m thick (Table 5). In turn, the boundary between the overlying '*P. scarabaeoides*' and *P. lobata* Zones coincides with the Pe-3 peak in the Gi-2 well (Fig. 14), suggesting that the '*P. scarabaeoides*' Zone is 2.9 m–4.5 m thick on Bornholm (Fig. 16, Table 5; see also the individual logs). Finally, the boundary between the *P. lobata* and the '*P. megalops*' Zones in the Gi-2 well is located immediately above the Pe-4 peak (Fig. 14). Defined this way, the *P. lobata* Zone is 0.8–2.0 m across southern Bornholm except in the So-1 well, where it is thin or absent (Table 5). The Pe-4 peak (or lower levels) forms the top of the *Peltura* Superzone in all wells on Bornholm, and it is, accordingly, predicted that the rather thick '*P. megalops*' Zone (= *Peltura paradoxa* Zone in some schemes) of the Gi-2 well, totalling 4.9 m including the overlying trilobite-barren interval, has no counterpart on Bornholm. A similar gap is seen in all Alum Shale districts in south central Sweden (Martinsson 1974, fig. 5).

The *Peltura* Superzone is exposed at Poulsen's (1923) localities 6 and 7 in the Læså section near Vasagård and represents the *C. tumida*, '*P. scarabaeoides*' and *P. lobata* Zones according to Poulsen (1923, fig. 2) (*Parabolina longicornis* = *P. lobata*). The *C. tumida* Zone was stated to be 2.1 m thick at locality 6, whereas the overlying '*P. scarabaeoides*' and *P. lobata* Zones are allegedly only 1.8 m thick altogether in the section. The *C. tumida* Zone is thus a little thicker than in the closest wells, whereas the overlying '*P. scarabaeoides*' Zone is drastically thinner than in all well sections on Bornholm (Table 5). Investigation of locality 6 is in progress to disentangle this vexing discrepancy. A major problem seems to

be confident correlation between the main southern exposure and the northern part of the section, where the *P. lobata* Zone is exposed high up (see Poulsen 1923, fig. 2, his “G-level”). If, however, the limited thickness of the ‘*P. scarabaeoides*’ Zone reported by Poulsen (1923) by and large is correct, the *P. lobata* Zone must be significantly thicker on Bornholm than inferred in this study. Further speculations on the conflicting thicknesses should await re-investigation of the Læså section including hand-held gamma logging.

Acerocarina Superzone

The uppermost Cambrian superzone is absent across much of south central Sweden and is best known from Skåne (Westergård 1944, 1947; Martinsson 1974; Weidner & Nielsen 2013). The superzone is also developed on Bornholm, where the uppermost *Acerocare ecorne* Zone was described from Limensgade by Poulsen (1923). Lower parts of the superzone are not exposed, except possibly in the Risebæk, but those outcrops have never been investigated.

In Gi-2, a limestone nodule causes a drop in gamma intensity at 43.5–44.5 m (Fig. 14). This limestone yielded *Parabolina heres heres* and the level appears to match the lower boundary of the *Acerocarina* Superzone recorded in the adjacent Gi-1 well (Westergård 1942, 1944). Immediately above the limestone, the GR intensity is high, thence decreases upwards with an abrupt fall in the middle of the superzone. A comparable log pattern (without limestone) is observed in the wells on Bornholm (Fig. 16), except Bu-1 (discussed below), and the *Acerocarina* Superzone is, accordingly, inferred to encompass the interval with upwards waning GR intensity above the *Peltura* Superzone. Defined this way, the superzone includes 2.7–2.9 m of strata in the Sk-1 and Sk-2 wells, thinning south-eastwards to 2.0–2.5 m in the Øleå area (Fig. 16; Table 4).

The log pattern in the uppermost part of the Bu-1 well deviates markedly from this GR motif. Here the GR intensity is low immediately above the Pe-4 peak due to the presence of a rather thick limestone nodule (Fig. 12) and then becomes almost as high as in the PGS marker. In wells in western Skåne (e.g. Albjåra-1), a similar interval with very high gamma radiation is seen in the lowermost part of the *Acerocarina* Superzone.

The age of the limestone near the *Peltura/Acerocarina* Superzone boundary in the Bu-1 well can only be guessed at. Large limestone nodules are present in the *Parabolina lobata* Zone in the Læså section (Poulsen 1923, fig. 2) and limestone is also frequently encountered at the base of the *Acerocarina* Superzone in Skåne, as for instance in the Gislövshammar wells. Based on comparison with the zonal thicknesses in the Sk-1 and Sk-2 wells, and the observation that the Pe-4 spike is

double-peaked in Sk-2 and only single-peaked in Bu-1, we assume that the discussed limestone interval lies at the very top of the *Peltura* Superzone. If so, the *Acerocarina* Superzone is ~3.0 m in the Bu-1 well.

In the Gi-1 and Gi-2 wells, only the lowermost 1.6–2.1 m of the 4.6 m thick *Acerocarina* Superzone contains fossils and this basal part actually represents the three lower zones of the superzone (Table 3). In the Gi-2 well, the last occurrence of trilobites is shortly below the abrupt intra-superzone fall in GR intensity which is thus a rough proxy for the top of the *Westergardia illaenopsis*–*Westergardia scanica* Subzone *sensu* Westergård (1944). Then follows a thick unfossiliferous interval, and the *A. ecorne* Zone has not been identified in the Gislövshammar wells. Correlation of individual zones between Skåne and Bornholm based on the GR log pattern is not possible, but the upper part of the superzone, corresponding to the barren interval in the Gislövshammar wells, is comparatively much thinner on Bornholm.

Tremadocian

On Bornholm the Ordovician Alum Shale is best known from the abandoned quarry at Limensgade (Grönwall 1916; Poulsen 1922). The latter author reported a thickness of *c.* 2.5 m, which von Jansson (1979) later corrected to 4 m after finding graptolites at a lower level. The oldest dateable Tremadocian represents the *Rhabdinopora flabelliformis socialis* Zone (von Jansson 1979) and the basal *Rhabdinopora preparabola* Zone is either missing or not graptolitic (Fig. 3).

The Cambro–Ordovician boundary is indicated in wireline logs as a further and fairly significant drop of GR intensity above the small Ac-1 peak at the top of the *Acerocarina* Superzone. The general GR intensity is overall low in the Tremadocian interval relative to the Furongian, although not as low as in the Miaolingian. Identification of the lower boundary is corroborated by fossil evidence in the Bi-2 well, where graptolites turn up at 98.1 m (Fig. 8). In Gi-2, the graptolites appear slightly higher above the Ac-1 peak than on Bornholm (Fig. 14).

The small GR peak labelled Tre-1 is associated with a graptolite-rich horizon in the *Rhabdinopora flabelliformis flabelliformis* Zone in the middle of the Tremadocian (at 6 m in the Sk-1 core, Fig. 6; a densely graptolitic level at *c.* 2.5 m below the Komstad Limestone at Limensgade, corresponding to the base of the Ordovician identified by Poulsen 1922). This minor GR peak is readily identified in all wells on Bornholm (Fig. 16) and it is actually also recognisable in the expanded section in the Gi-2 well (Fig. 14).

The Tremadocian is 3.4–3.5 m thick in the Sk-1 and Sk-2 wells, thinning slightly south-eastwards to the Øleå area where the interval is *c.* 3 m in most wells

with a minimum of 2.5 m recorded in the So-1 well (Table 4). In south-eastern Bornholm, the Tremadocian comprises only the *Rhabdinopora* interval and no *Adelograptus tenellus* and *Bryograptus* Zones are developed.

Discussion

Stratigraphy

The biozonal boundaries often do not coincide precisely with obvious GR peaks or lows, but correlation of the log pattern between wells provides a very robust correlation of superzones (Fig. 16) and frequently even of zones, when they are more than ~0.5 m thick. The outlined correlation suggests that the *Olenus scanicus*–*O. rotundatus* and *Parabolina brevispina* Zones are developed on Bornholm although the latter may only occur in the Læså area. None of these zones have been proven to date by fossil findings. It is also likely that a thin '*Leptoplastus neglectus*' Zone is developed in the lower part of the *Protopeltura* Superzone. The fossiliferous lower part of the *Acerocarina* Superzone, known from the Gislövshammar wells, also seems to be developed on Bornholm, but it is unfeasible to differentiate the individual zones based on the GR log pattern. The '*Parabolina megalops*' Zone in the upper *Peltura* Superzone seems to be absent on Bornholm (or, at least, is very thin).

Depositional environment and uranium enrichment

The Alum Shale was deposited extremely slowly, which in combination with the prevailing low oxygen conditions at the seafloor caused a strong enrichment of many trace elements (e.g. Armands 1972; Andersson *et al.* 1985; Buchardt *et al.* 1997). Nielsen & Schovsbo (2015) concluded that the Miaolingian–Tremadocian oxygen crisis was a global phenomenon which seemingly was locally amplified in the epicontinental sea covering Scandinavia, likely due to uplift of the outer margins of Baltica, creating silled basin conditions. Coinciding with onset of the SPICE-event at the base of the Furongian (Fig. 6; Ahlberg *et al.* 2009; Hammer & Svensen 2017), the oxygen deficiency was intensified in the Alum Shale sea until even the distal inner shelf bottom environment became dysoxic (Nielsen & Schovsbo 2015). The cause is uncertain, but the intensified low-oxygen conditions may to some extent have been triggered by the lower sea level in the early Furongian hampering exchange of water masses across the submarine sills fringing Baltica. Whatever the case may be, a strong enrichment of trace elements is seen in

the Alum Shale from the early Furongian onwards, including uranium enrichment, and the GR intensity steadily increases through the *Olenus* Superzone to culminate in the OTGS marker horizon. Above this level, the GR intensity overall remains high throughout the Furongian but exhibits numerous fluctuations, creating a unique GR log pattern. The PGS marker in the *Peltura* Superzone signals maximum radiation levels. The reason(s) for the many fluctuations remains to be studied, but sea-level variations are undoubtedly an important controlling factor via the influence on sedimentary influx/condensation, storm-wave erosion and oxygen level at the seafloor (decreasing with depth); sea-level stand may also have regulated water exchange across the sills, thus affecting the general oxygen level in the basin as speculated above.

The GR intensity is closely linked to the uranium concentration in the Alum Shale which in turn is broadly linked to the TOC content (Fig. 5). Hence, the upwards fall in GR intensity above the PGS marker may signal gradually improved ventilation of the bottom environment, with reduced preservation of organic matter. This scenario is corroborated by the rarity of calcite-shelled fossils, notably trilobites, in the upper part of the *Acerocarina* Superzone as well as in the Tremadocian interval, which is ascribed to early dissolution of the skeletons in the near-surface sediment due to periodic oxygenation of pyrite (see Schovsbo 2001 for details). In effect, mainly the insoluble organic-walled graptolites and phosphatic brachiopods are preserved. Eventually the western margin of Baltica subsided in the late Tremadocian, restoring normal oxygen conditions in the Scandinavian epicontinental sea and terminating deposition of the Alum Shale (Nielsen & Schovsbo 2015).

Isostasy

The Miaolingian *Paradoxides paradoxissimus* Superzone is stratigraphically incomplete on Bornholm and very strongly condensed in comparison with Skåne (Fig. 17A; Table 3 vs. Table 4). We ascribe this to isostatic uplift of Bornholm that commenced in the latest 'early' Cambrian (Cambrian series 2), associated with the so-called Hawke Bay Event (Nielsen & Schovsbo 2015). We envisage that the uplift was a gentle broad crest aligned with the southern margin of Baltica, originally elevated some 150 m relative to the pre-uplift situation (Nielsen & Schovsbo 2015, fig. 56). The flanks of the crest were sloping merely ~2 m per kilometre northwards and southwards, and the submarine sill was by no means a prominent topographical feature in the seascape. Nonetheless, it had a marked influence on deposition due to the exceptional general flatness of the seafloor and the

overall strong clastic starvation of the epicontinental sea. The Hawke Bay uplift was initially accompanied by minor erosion that removed the uppermost lower Cambrian on Bornholm (for details, see Nielsen & Schovsbo 2011, 2015), but shortly into the Miaolingian the area appears to have been inundated again, despite the uplift, and then became characterised by sedimentary bypass. The renewed flooding was due to a combination of subsidence and a strongly rising sea level (Nielsen & Schovsbo 2015, fig. 56).

In addition to the missing upper 'lower' Cambrian and condensed Miaolingian strata on Bornholm, the outlined uplift scenario is corroborated by palaeontological evidence. The Miaolingian *Acidusus atavus* fauna described from Bornholm by Weidner & Nielsen (2014) contains a significantly higher percentage of polymerid 'normal' trilobites than the coeval strata in Skåne. Several of these 'normal' trilobite species are otherwise unknown from the Scandinavian Alum Shale Formation. This is clearly suggestive of a relatively well oxygenated local bottom environment, supporting the notion of a shallower position of Bornholm on the shelf relative to Skåne.

Due to the uplift, initial deposition in the Miaolingian consisted exclusively of autochthonous bioclastic limestone, formed by disintegrated calcite skeletons of the local shelly fauna. These limestone 'events' (Forsemölla, Exsulans and 'Atavus' Limestone Beds, but also the later Hyolithes and Andrarum Limestone Beds, see Fig. 3) record major sea-level lowstands that allowed a rich shelly fauna to temporarily invade the normally rather inhospitable oxygen-deficient Alum Shale seafloor. In detail, deposition took place during earliest sea-level rise after maximum lowstand; for more detailed remarks on these 'transgressive' limestones, see Nielsen & Schovsbo (2015, pp. 297–299). Eventually, deposition of Alum Shale facies began on Bornholm in the late part of the *A. atavus* Chron (Fig. 3). Nielsen & Schovsbo (2015) inferred that the recommencement of clastic sedimentation was due to a combination of sea-level rise and some measure of subsidence of the Bornholm area in the aftermath of the Hawke Bay uplift. However, it is inferred that Bornholm remained uplifted relative to Skåne all through to the Late Ordovician. As a result of the slightly higher topographical position of Bornholm on the shelf, erosion associated with the major sea-level lowstands that took place prior to deposition of the Hyolithes and the Andrarum Limestone Beds was intensive and removed most of the *Ptychagnostus punctuosus* Zone and virtually all of the *Goniagnostus nathorsti* Zone. The latter is represented only by a mixed lag deposit incorporated into the Hyolithes Limestone (Fig. 3). These erosive events in combination with the uplifted state of Bornholm are suggested

to be the main reason for the variable but overall insignificant thickness of the *Paradoxides paradoxissimus* Superzone on the island (Table 4), as the Alum Shale mud was readily winnowed and removed as a result of the lowered storm wave base during sea-level lowstands.

As can be seen from Figs 16 and 17 (and Table 4), the stratigraphic interval between the Andrarum Limestone Bed and the *Parabolina* Superzone is fairly uniformly developed across southern Bornholm. The *Agnostus pisiformis* Zone is also nearly of the same thickness as in south-eastern Skåne, locally even thicker (Bu-1, Table 4 vs. Table 3). This is suggestive of isostatic quiescence during this interval (Fig. 17A) after significant subsidence of the area. At the same time, the sea level rose strongly and reached a Cambrian maximum during the *A. pisiformis* Chron, at which stage deposition of Alum Shale facies reached as far east as Gotland (Ahlberg 1989). For these reasons, the seafloor in the Bornholm area came well out of reach of storm waves and no recycling of mud occurred.

The Furongian is reduced in thickness on Bornholm relative to Skåne, with condensation slowly commencing in the *Olenus* and *Parabolina* Superchrons, accelerating in the *Leptoplastus* Superchron and culminating in the *Protopeltura* and *Peltura* Superchrons (Fig. 17A). This is taken to indicate a new phase of mild isostatic uplift of the southern margin of Baltica, but maybe the slightly lower general sea level during the Furongian relative to the late Miaolingian highstand also played a part, as storm-driven winnowing may have removed mud during intermittent lowstand intervals. This is a plausible explanation for the absence on Bornholm of biozones in the basal *Leptoplastus* and uppermost *Peltura* Superzones (Fig. 3), as these zones are known only from deep outer shelf sites (Skåne and the Oslo region, see Martinsson 1974, fig. 5). The thinning of the lower part of the *Parabolina* Superzone from Sk-2 to So-1 may also relate to erosion or at least non-deposition during a transient sea-level lowstand (the *Parabolina brevispina* Zone is likewise developed only in marginal offshore facies of the Alum Shale, suggestive of a generally low sea level in the early *Parabolina* Superchron, cf. Martinsson 1974, fig. 5). This interpretation entails 1) that Bornholm was located higher on the shelf than Skåne during the Furongian and 2) that there must have been a slight difference in topographic elevation between the Læså and Øleå areas, and this also fits well with the general thinning of the *Protopeltura*, *Peltura* and *Acerocarina* Superzones towards south-east on Bornholm (Fig. 16, Table 4). Every Furongian superzone is thus as thick or thicker in the Bu-1, Sk-1 and Sk-2 wells compared with the four other wells treated

here, and the thinning takes place across a distance of only a few kilometres (Fig. 16). We ascribe this to rejuvenation of gentle isostatic uplift of the southern margin of Baltica during the Furongian (Fig. 17). The isostatic adjustments may be part of more widespread tectonic disturbances in Scandinavia at this time. The largest of the spectacular 'subsidence cones' in the lower Cambrian Hardeberga Formation, developed at many sites in south-eastern Skåne, thus has a core of disturbed Alum Shale (youngest preserved level: *Olenus truncatus* Zone), suggestive of Furongian earthquake activity (see Lindström 1967 for details). The 'subsidence cones' are associated with fractures striking WNW–ESE, an orientation essentially par-

allel with the southern margin of Baltica. Likewise, the youngest trilobites found in Alum Shale filled fissures in the basement in the Göteborg area are of early Furongian age (Martinsson 1968, Samuelson 1975). These fissures also strike WNW–ESE.

Within Baltica, the Ordovician Alum Shale has its thickest development in south-eastern Skåne and the Tremadocian is here four times thicker than in the Læså area of Bornholm (Tables 3 and 4). This is suggestive of local subsidence of south-eastern Skåne during the earliest Tremadocian. However, both south-eastern Skåne and Bornholm were uplifted later in the Tremadocian as the *Bryograptus* Zone is very thin or truncated in both areas and even the

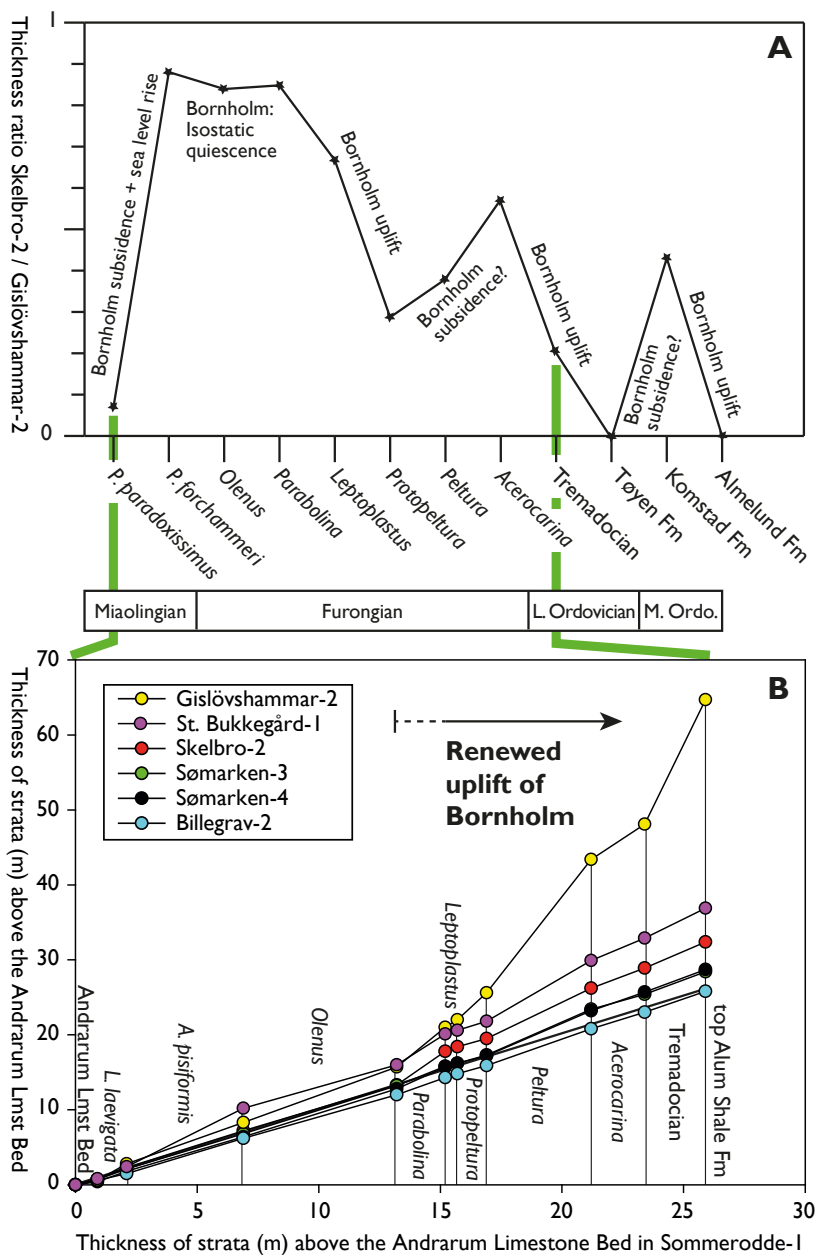


Fig. 17. Summary figure illustrating the isostatic movements of the Bornholm area through time. The plots are based on the thicknesses listed in Tables 3 and 4. **A:** Comparison of thicknesses in the Skelbro-2 and Gislövshammar-2 wells, revealing periods of uplift and subsidence of Bornholm relative to Skåne. The Almelund Formation is known from the Killeröd area (see Nielsen 1995 for references; in that paper the unit is referred to as the Upper Didymograptus Shale). **B:** Comparison of thicknesses between wells on Bornholm and Gislövshammar-2 in Skåne, relative to the succession in the Sommerodde-1 well. It is obvious that in the later part of the Furongian Skåne subsided more than Bornholm did. Sømarken-3 and -4 overlap and Sommerodde-1 and Billegrav-2 overlap, so that only Sømarken-4 and Billegrav-2 are visible on the figure.

Björkåsholmen Formation is locally absent in south-eastern Skåne (as on Bornholm). From then on, the Bornholm area appears to have been more extensively uplifted until the Late Ordovician and characterised by clastic by-pass, although the local presence of a thin veneer of Tøyen Formation in the Bi-2 well (and maybe also the Sø-3 and Sø-4 wells) indicates that the uplift history may be more complicated with periods of deposition alternating with periods of erosion (Fig. 17A). The sedimentary break is also interrupted by the Middle Ordovician Komstad Limestone that denotes a 2nd order sea-level lowstand (see Nielsen 1995, 2004) with increased ventilation of the seafloor, so that a shelly fauna could thrive and produce an autochthonous bioclastic limestone – as periodically in the Miaolingian (see above). However, deposition of the Komstad Limestone conceivably also reflects a transient subsidence of the Bornholm area (Fig. 17A). We note that limestone deposition here started earlier than in Skåne, again corroborating a higher position of Bornholm on the shelf, and the Komstad Limestone is also significantly thinner than in Skåne (Nielsen 1995). To complicate matters further regarding interpretation of the Komstad Limestone, climatic changes may also have favoured more prolific limestone formation during the Ordovician (C.M.Ø. Rasmussen *et al.* 2016 and references therein).

A Mid Ordovician phase of uplift after deposition of the Komstad Limestone was associated with increasing erosion of the unit in a south-eastwards direction on Bornholm; only the basal conglomerate is preserved in the Bi-2 well and the limestone is much thinner in all wells in the Øleå area compared with the Læså area. This uplift extended far into Skåne (Nielsen 1995, fig. 42) and seems to have been a quite prominent event only surpassed in magnitude by the terminal 'early' Cambrian Hawke Bay Event. The Komstad Limestone is everywhere on Bornholm overlain by Ordovician strata of Late Ordovician (Sandbian) age, and the extensive hiatus is indicative of a long period of uplift (~10 myr).

The general uplift of Bornholm from the latest early Cambrian to the Late Ordovician is the reason why the Miaolingian to Ordovician succession on the island is strongly condensed and stratigraphically incomplete relative to Skåne (Nielsen 1995, figs 41–42). The Alum Shale Formation is also comparatively thin in the German offshore well G-14 (Piske & Neumann 1993; Franke *et al.* 1994) and the Slagelse-1 well on Sjælland (Poulsen 1974), measuring, respectively, 32.3 m and 29 m in total, and the Ordovician is also thin in these wells (for location, see Fig. 1). This is taken to suggest that the uplift extended westwards from Bornholm along the southern margin of Baltica (see also Buchardt *et al.* 1997, fig. 7).

The recurrent isostatic adjustments of the southern margin of Baltica are surmised to have been triggered by stress changes related to contemporaneous plate tectonic processes in the adjacent Tornquist Sea (Nielsen & Schovsbo 2015).

The new data corroborate the suggestion of Nielsen (1995) and Nielsen & Schovsbo (2015) that the southern plate edge of Baltica was subjected to uplift through much of the Miaolingian, Furongian and Ordovician, eventually ending with the formation of a Caledonian foreland basin in the early Silurian (or latest Ordovician) involving major downwarp of the southern margin of the continent.

Conclusions

The Scandinavian Alum Shale Formation has a unique and highly characteristic GR log motif due to its generally very high but variable uranium content. Wireline GR logs obtained in boreholes are therefore extremely useful for correlation of the 'hot' formation locally as well as regionally. The present study has established a correlation of wells on Bornholm, Denmark, with the type section in south-eastern Skåne, Sweden.

The Miaolingian interval on Bornholm is characterised by relatively low GR radiation. Fluctuations are insignificant except for the ≤ 1 m thick amalgamated Hyolithes + Andrarum Limestone Beds that create a distinct GR low (the Andrarum Limestone Gamma Low, AGL), which is a fixed point for correlation. A conspicuous drop in GR intensity (the Base Furongian Gamma Low, BFGL) marks the Miaolingian/Furongian boundary. From this level upwards, the GR intensity increases very significantly, reaching a first high in the upper part of the *Olenus* Superzone (*Olenus* Triple Gamma Spike, OTGS). A second and even more prominent high, the *Peltura* Gamma Spike (PGS), is seen in the lower part of the *Peltura* Superzone. Above the PGS, the gamma radiation decreases slightly in the upper part of the *Peltura* Superzone and more strongly so in the *Acerocarina* Superzone. The general GR level of the Tremadocian is even lower, although not as low as in the Miaolingian. The upwards decrease in GR intensity reflects a lower TOC content that, in turn, probably signals an increasing oxygen concentration in the latest Furongian to Early Ordovician depositional environment.

The general thinning of the Alum Shale Formation from Skåne to Bornholm is inferred related to isostatic uplift of the southern margin of Baltica, which commenced in the latest 'early' Cambrian (Hawke Bay Event). The slow recommencement of sedimentation in the mid Miaolingian is taken to reflect a rise in sea level combined with some measure of subsidence

of the Bornholm area, which still was within reach of storm-wave reworking during sea-level lowstand events. As a result the local succession is very thin and stratigraphically incomplete. The late Miaolingian was a period of isostatic quiescence and high sea level without interludes of reworking, and shale of this age is uniformly distributed across southern Bornholm. The interval has, broadly speaking, the same thickness as in south-eastern Skåne. From the *Olenus* Superzone upwards, an increasing condensation of the succession is observed on Bornholm relative to Skåne. Within Bornholm, the Furongian strata are also consistently thicker in the Læså area compared with the Øleå area. This is suggestive of a Furongian phase of mild uplift of the southern margin of Baltica. Renewed uplift of the Bornholm area including parts of south-eastern Skåne also seems to have taken place in the late Tremadocian. The discovery of a thin Tøyen Formation in the Bi-2 core above the Alum Shale Formation indicates that yet another subsidence/uplift event took place in the late Early Ordovician prior to deposition of the Komstad Limestone, which started in the earliest Mid Ordovician. This longer-lasting depositional phase probably reflects a transient subsidence of the Bornholm area coinciding with a major sea-level lowstand, shifting (autochthonous) limestone deposition down-slope.

The recurrent small-scale isostatic adjustments probably relate to stress changes associated with ongoing plate tectonic processes in the adjacent Tornquist Sea, which was under closure.

Acknowledgements

The initial version of this paper was improved by suggestions by referees Jon Ineson and Mikael Calner and editor Lotte Melchior Larsen. This paper is a contribution to GeoCenter Danmark projects 2015–5 and 2017–3 awarded to Christian M.Ø. Rasmussen. CMØR further acknowledges the VILLUM Foundation's Young Investigator Programme for economical support (project no. 023452). This paper is a contribution to IGCP project 653: The Onset of the Great Ordovician Biodiversification Event.

References

Ahlberg, P. 1989: Cambrian stratigraphy of the När 1 deep well, Gotland. *Geologiska Föreningens i Stockholm Förhandlingar* 111, 137–148.
 Ahlberg, P. & Terfelt, F. 2012: Furongian (Cambrian) agnostoids of Scandinavia and their implications for intercontinental

correlation. *Geological Magazine* 149, 1001–1012.
 Ahlberg, P., Månsson, K., Clarkson, E.N.K. & Taylor, C.M. 2006: Faunal turnovers and trilobite morphologies in the upper Cambrian *Leptoplastus* Zone at Andrarum, southern Sweden. *Lethaia* 39, 97–110.
 Ahlberg, P., Axheimer, N., Babcock, L.E., Eriksson, M.E., Schmitz, B. & Terfelt, F. 2009: Cambrian high-resolution biostratigraphy and carbon isotope chemostratigraphy in Scania, Sweden: first record of the SPICE and DICE excursions in Scandinavia. *Lethaia* 42, 2–16.
 Andersson, A., Dahlman, B., Gee, D.G. & Snäll, S. 1985: The Scandinavian Alum Shales. *Sveriges Geologiska Undersökning Serie Ca* 56, 1–50.
 Armands, G. 1972: Geochemical studies of uranium, molybdenum and vanadium in a Swedish alum shale. *Stockholm Contributions in Geology* XXVII, 1–148.
 Axheimer, N., Eriksson, M.E., Ahlberg, P. & Bengtsson, A. 2006: The middle Cambrian cosmopolitan key species *Lejopyge laevigata* and its biozone: new data from Sweden. *Geological Magazine* 143, 447–455.
 Baumann-Wilke, M., Bauer, K., Schovsbo, N.H. & Stiller, M. 2012: P-wave traveltime tomography for a seismic characterization of black shales at shallow depth on Bornholm, Denmark. *Geophysics* 77, 53–60.
 Berg-Madsen, V. 1985a: The Middle Cambrian of Bornholm, Denmark: A stratigraphical revision of the lower alum shale and associated anthraconites. *Geologiska Föreningens i Stockholm Förhandlingar* 106 (for 1984), 357–376.
 Berg-Madsen, V. 1985b: A review of the Andrarum Limestone and the upper alum shale (Middle Cambrian) of Bornholm, Denmark. *Bulletin of the Geological Society of Denmark* 34, 133–143.
 Berg-Madsen, V. 1986: Oversigt over det reviderede Mellem Kambrium på Bornholm. *Dansk Geologisk Forening, Årsskrift for 1985*, 1–13.
 Bjerager, M., Kjøller, C., Olivarius, M., Olsen, D., Schovsbo, N.H. in press: Sedimentology, geochemistry and reservoir properties of Upper Jurassic deep marine sandstones (Hareelv Formation) in the Bloklev-1 borehole, Jameson Land Basin, East Greenland. *Geological Survey of Denmark and Greenland Bulletin* 42.
 Bruton, D.L., Erdtmann, B.-D. & Koch, L. 1982: The Nærnes section, Oslo Region, Norway: a candidate for the Cambrian – Ordovician boundary stratotype at the base of the Tremadoc Series. In: Bassett, M.G. & Dean, W.T. (eds), *The Cambrian–Ordovician boundary: Sections, Fossil Distributions and Correlations*. National Museum of Wales, *Geological Series* 3, 61–69.
 Bruton, D.L., Koch, L. & Repetski, J.E. 1988: The Nærnes section, Oslo Region, Norway: trilobite, graptolite and conodont fossils reviewed. *Geological Magazine* 125, 451–455.
 Buchardt, B. & Nielsen, A.T. 1985: Carbon and oxygen isotope composition of Cambro-Silurian limestone and anthraconite from Bornholm: evidence for deep burial diagenesis. *Bulletin of the Geological Society of Denmark* 33, 415–435.

- Buchardt, B., Clausen, J. & Thomsen, E. 1986: Carbon isotope composition of Lower Palaeozoic kerogen: Effect of maturation. *Organic Geochemistry* 10, 127–134.
- Buchardt, B., Nielsen, A.T. & Schovsbo, N.H. 1997: Alun skiferen i Skandinavien. *Geologisk Tidsskrift* 3, 1–30.
- Bulman, O.M.B. 1954: The graptolite fauna of the *Dictyonema* Shales of the Oslo region. *Norsk Geologisk Tidsskrift* 33, 1–40.
- Callisen, K. 1914: Tenformede Tungspatkrystaller ("Pseudo-Gaylussit" og "Pseudo-Pirssonit") i Alunskiferen. *Meddelelser fra Dansk Geologisk Forening* 4, 245–258.
- Clarkson, E.N.K. 2011: The life and times of the olenid trilobites. *Geologické výzkumy na Moravě a ve Slezsku* 18, 11–17.
- Clarkson, E.N.K. & Taylor, C.M. 1995: The lost world of the olenid trilobites. *Geology Today* 11, 147–154.
- Cooper, R.A. 1999: Ecostratigraphy, zonation and global correlation of earliest Ordovician planktic graptolites. *Lethaia* 32, 1–14.
- Egenhoff, S., Fishman, N.S., Ahlberg, P. & Petrowsky, M. 2015: Sedimentology of SPICE (Steptoean positive carbon isotope excursion): A high-resolution trace fossil and microfabric analysis of the middle to late Cambrian Alum Shale formation, southern Sweden. *Special paper of the Geological Society of America* 515, 87–102.
- Ellis, D.V. & Singer, J.M. 2007: Well logging for earth scientists. 2nd edition. Springer, Dordrecht, the Netherlands, 687 pp.
- Ericsson, M. 2012: Stratigraphy, facies and depositional history of the Colonus Shale Trough, Skåne, southern Sweden. Dissertation in Geology at Lund University, master thesis 310, 40 pp. Department of Geology, Lund University.
- Franke, D., Gründel, J., Lindert, W., Meissner, B., Schyult, E. & Zagora, I. 1994: Die Ostseebohrung G 14 – eine Profilübersicht. *Zeitschrift für Geologische Wissenschaften* 22, 235–240.
- Gautier, D.L., Schovsbo, N.H., Nielsen, A.T. 2014: Resource potential of the Alum Shale in Denmark. *Unconventional Resources Technology Conference (URTeC)*. SPE-2014-1931754-MS. DOI 10.15530/urtec-2014-1931754.
- Gill, B.C., Lyons, T.W., Young, S.A., Kump, L.R., Knoll, A.H. & Saltzman, M.R. 2011: Geochemical evidence for widespread euxinia in the Later Cambrian ocean. *Nature* 469, 80–83.
- Graversen, O. 2009: Structural analysis of superposed fault systems of the Bornholm horst block, Tornquist Zone, Denmark. *Bulletin of the Geological Society of Denmark* 57, 24–49.
- Grönwall, K.A. 1899: Bemærkninger om de sedimentære dannelser på Bornholm og deres tektoniske forhold. *Danmarks Geologiske Undersøgelse, II. række* 10, 1–52.
- Grönwall, K.A. 1902: Bornholms Paradoxideslag og deres fauna. *Danmarks Geologiske Undersøgelse, II. række* 13, 1–250.
- Grönwall, K.A. 1916: Palaeozoiske Dannelser. In Grönwall, K.A. & Milthers, V.: *Beskrivelse til Geologisk Kort over Danmark*. Kortbladet Bornholm. *Danmarks Geologiske Undersøgelse, I. Række* 13, 43–86.
- Hammer, Ø. & Svensen, H.H. 2017: Biostratigraphy and carbon and nitrogen geochemistry of the SPICE event in Cambrian low-grade metamorphic black shale, Southern Norway. *Palaeogeography, Palaeoclimatology, Palaeoecology* 468, 216–227.
- Hansen, K. 1945: The Middle and Upper Cambrian sedimentary rocks of Bornholm. *Danmarks Geologiske Undersøgelse, II. række* 72, 1–81.
- Henningsmoen, G. 1957: The trilobite family Olenidae with description of Norwegian material and remarks on the Olenid and Tremadocian Series. *Skrifter utgitt av Det Norske Videnskaps-Akademi i Oslo. I. Matematisk-Naturvitenskapelige Klasse* 1, 1–303.
- Hessland, I. & Armands, G. 1978: Alunskiffer: underlagsmateriale, geologi. *SIND*, vol. 3, 1–146. Utredning från statens industriverk, Stockholm.
- Hints, R., Soesoo, A., Voolma, M., Tarros, S., Kallaste, T. & Hade, S. 2014: Centimetre-scale variability of redox-sensitive elements in Tremadocian black shales from the eastern Baltic Palaeobasin. *Estonian Journal of Earth Sciences* 63, 233–239.
- Høyberget, M. & Bruton, D.L. 2012: Revision of the trilobite genus *Sphaerophthalmus* and relatives from the Furongian (Cambrian) Alum Shale Formation, Oslo Region, Norway. *Norwegian Journal of Geology* 92, 433–450.
- Johnstrup, F. 1874: Oversigt over de palaeozoiske Dannelser paa Bornholm. *Beretning 11'te skandinaviske Naturforsker møde i Kjøbenhavn* 1873, 1–10.
- Lauridsen, B.W. & Nielsen, A.T. 2005: The Upper Cambrian Trilobite *Olenus* at Andrarum, Sweden: a case of iterative evolution? *Palaeontology* 48, 1041–1056.
- Lecomte, A., Cathelineau, M., Michels, R., Peiffert, C. & Brouand, M. 2017: Uranium mineralization in the Alum Shale Formation (Sweden): evolution of a U-rich marine black shale from sedimentation to metamorphism, *Ore Geology Reviews*. doi: <http://dx.doi.org/10.1016/j.oregeorev.2017.04.021>.
- Leventhal, J.S. 1991: Comparison of organic geochemistry and metal enrichment in two black shales: Cambrian alum shale of Sweden and Devonian Chattanooga shale of United States. *Mineralium Deposita* 26, 104–112.
- Lindström, M. 1967: "Funnel Grabens" and Early Paleozoic Tectonism in South Sweden. *Geological Society of America Bulletin* 78, 1137–1154.
- Lindström, M. 1971: Vom Anfang, Hochstand und Ende eines Epikontinentalmeeres. *Geologische Rundschau* 60, 419–438.
- Maletz, J. & Erdtmann, B.-D. 1987: *Adelograptus tenellus* (Linnarsson 1871): its astogenetic development and its stratigraphical and palaeogeographical distribution. *Bulletin of the Geological Society of Denmark* 35, 179–190.
- Maletz, J., Egenhoff S. & Alonso, R. 2010: The Upper Tremadocian (Ordovician) graptolite *Bryograptus*: taxonomy, biostratigraphy and biogeography. *Palaeontology* 53, 59–75.
- Martinsson, A. 1968: Cambrian palaeontology of Fennoscandian basement fissures. *Lethaia* 1, 137–155.
- Martinsson, A. 1974: The Cambrian of Norden. In: Holland, C.H. (ed.), *Lower Palaeozoic Rocks of the World. 2. Cambrian of the British Isles, Norden, and Spitsbergen*, 185–283. London: John Wiley & Sons.

- Michelsen, O. & Nielsen, L.H. 1991: Well records on the Phanerozoic stratigraphy in the Fennoscandian Border Zone, Denmark. Hans-1, Sæby-1, and Terne-1 wells. *Danmarks Geologiske Undersøgelse Serie A* 29, 1–37.
- Moberg, J.C. 1898: En trilobit från Skånes Dictyograptus-skiffer. *Geologiska Föreningens i Stockholm Förhandlingar* 20, 317–324.
- Nielsen, A.T. 1995: Trilobite systematics, biostratigraphy and palaeoecology of the Lower Ordovician Komstad Limestone and Huk Formations, southern Scandinavia. *Fossils & Strata* 38, 1–374.
- Nielsen, A.T. 2004: Ordovician sea level changes: A Baltoscandian perspective. In: Webby, B.D., Paris, F., Droser, M.L. & Percival, L.G. (eds.), *the Great Ordovician Biodiversification Event*, 84–93. Columbia University Press.
- Nielsen, A.T. & Buchardt, B. 1994: Gislövshamar-2 shallow drill-hole in eastern Scania, Sweden: stratigraphy and geochemistry of the cored Lower Ordovician – Lower Cambrian strata. Unpublished Final report II, Pre-Westphalian Source Rocks in northern Europe, 1–30. Geological Institute, University of Copenhagen, Denmark.
- Nielsen, A.T. & Schovsbo, N.H. 2007: Cambrian to basal Ordovician lithostratigraphy in southern Scandinavia. *Bulletin of the Geological Society of Denmark* 53, 47–92.
- Nielsen, A.T. & Schovsbo, N.H. 2011: The Lower Cambrian of Scandinavia: depositional environment, sequence stratigraphy and palaeogeography. *Earth-Science Reviews* 107, 207–310.
- Nielsen, A.T. & Schovsbo, N.H. 2015: The regressive Early–Mid Cambrian ‘Hawke Bay Event’ in Baltoscandia: Epeirogenic uplift in concert with eustasy. *Earth-Science Reviews* 151, 288–350.
- Nielsen, A.T., Weidner, T., Terfelt, F. & Høyberget, M. 2014: Upper Cambrian (Furongian) biostratigraphy in Scandinavia revisited: definition of superzones. *GFF* 136, 193–197.
- Nikolaisen, F. & Henningsmoen, G. 1985: Upper Cambrian and lower Tremadoc olenid trilobites from the Digermul peninula, Finnmark, northern Norway. *Norges geologiske undersøkelse Bulletin* 400, 1–49.
- Owen, A.W., Bruton, D.L., Bockelie, J.F. & Bockelie, T. 1990: The Ordovician successions of the Oslo Region, Norway. *Norges geologiske undersøkelse, Special Publication* 4, 3–54.
- Pedersen, G.K. 1989: The sedimentology of Lower Palaeozoic black shales from the shallow wells Skelbro 1 and Billegrav 1, Bornholm, Denmark. *Bulletin of the Geological Society of Denmark* 37, 151–173.
- Pedersen, G.K. & Klitten, K. 1990: Anvendelse af gamma-logs ved korrelation af marine skifre i vandforsyningsboringer på Bornholm. *Dansk Geologisk Forening Årsskrift* 1987–89, 21–35.
- Peng, S.C., Babcock, L.E., Robison, R.A., Lin, H.L., Rees, M.N. & Saltzman, M.R. 2004: Global Standard Stratotype-section and Point (GSSP) of the Furongian Series and Paibian Stage (Cambrian). *Lethaia* 37, 365–379.
- Peng, S.C., Babcock, L.E. & Cooper, R.A. 2012: The Cambrian Period. In: Gradstein, M., Ogg, J.G., Schmitz, M.D. & Ogg G.M. (eds), *The Geologic Time Scale 2012*, 437–488. Elsevier.
- Petersen, H.I., Schovsbo, N.H. & Nielsen, A.T. 2013: Reflectance measurements of zooclasts and solid bitumen in Lower Palaeozoic shales, southern Scandinavia: Correlation to vitrinite reflectance. *International Journal of Coal Geology* 114, 1–18.
- Piske, J. & Neumann, E. 1993: Tektonische Gliederung des prävariszischen Untergrundes in der suedwestlichen Ostsee. *Geologisches Jahrbuch Reihe A-H* 131, 361–388.
- Poulsen, C. 1922: Om Dictyograptus-skiferen på Bornholm. *Danmarks geologiske Undersøgelse, IV. Række* 1, 1–28. (Also printed in *Meddelelser fra Dansk Geologisk Forening* 6:8).
- Poulsen, C. 1923: Bornholms Olenuslag og deres Fauna. *Danmarks geologiske Undersøgelse, II. række* 40, 1–83.
- Poulsen, C. 1974: Further Contributions to the Knowledge of the Palaeozoic of Slagelse No. 1, Western Sealand. *Danmarks geologiske Undersøgelse, II. Række* 101, 1–42.
- Poulsen, V. 1966: Cambro–Silurian stratigraphy of Bornholm. *Meddelelser fra Dansk Geologisk Forening (Bulletin of the Geological Society of Denmark)* 16, 117–137.
- Poulsen, V. 1978: *Dalmanitina* beds (late Ordovician) on Bornholm. *Danmarks geologiske Undersøgelse, Årbog* 1976, 53–87.
- Rasmussen, B.W., Nielsen, A.T. & Schovsbo, N.H. 2015: Faunal succession in the upper Cambrian (Furongian) *Leptoplastus* Superzone at Slemmestad, southern Norway. *Norsk Geologisk Tidsskrift* 95, 1–22.
- Rasmussen, B.W., Rasmussen, J.A. & Nielsen, A.T. 2016: Biozonation of the Furongian (upper Cambrian) Alum Shale Formation at Hunneberg, Sweden. *GFF* 138, 467–489.
- Rasmussen, B.W., Rasmussen, J.A. & Nielsen, A.T. 2017: Biostratigraphy of the Furongian (upper Cambrian) Alum Shale Formation at Degerhamn, Öland, Sweden. *GFF* 139, 92–118.
- Rasmussen, C.M.Ø., Ullmann, C.V., Jakobsen, K.G., Lindskog, A., Hansen, J., Hansen, T., Eriksson, M.E., Dronov, A., Frei, R., Korte, C., Nielsen, A.T. & Harper, D.A.T. 2016: Onset of the main Phanerozoic marine radiation sparked by emerging Mid Ordovician icehouse. *Nature Scientific Reports* 6, p. 18884, doi:10.1038/srep18884, 9 pp.
- Saltzman, M.R., Runnegar, B. & Lohmann, K.C. 1998: Carbon isotope stratigraphy of Upper Cambrian (Steptoean Stage) sequences of the eastern Great Basin: Record of a global oceanographic event. *Bulletin of the Geological Society of America* 110, 285–297.
- Samuelson, L. 1975: Palaeozoic fissure filling and tectonism of the Göteborg area, southwestern Sweden. *Sveriges Geologiska Undersökning Serie C* 711, 3–43.
- Schovsbo, N.H. 2000: Environmental fluctuations in the *Olenus* Zone (Upper Cambrian), southern Scandinavia: A geochemical approach. *Bulletin of the Geological Society of Denmark* 47, 53–62.
- Schovsbo, N.H. 2001: Why barren intervals? A taphonomic case study of the Scandinavian Alum Shale and its faunas. *Lethaia* 34, 271–285.
- Schovsbo, N.H. 2002a: Uranium enrichment shorewards in

- black shales: A case study from the Scandinavian Alum Shale. *GFF* 124, 107–116.
- Schovsbo, N.H. 2002b: Carbon isotope stratigraphy of Middle Cambrian to Lower Silurian shales from Baltoscandia: implications for presumed climatic stability. *Geochimica et Cosmochimica Acta* 66, p. A687.
- Schovsbo, N.H. 2003: Geochemical composition and provenance of Lower Palaeozoic shales deposited at the margins of Baltica. *Bulletin of the Geological Society of Denmark* 50, 11–27.
- Schovsbo, N.H. 2011: Completion report Billegrav-2 well (DGU 248.61), Part 1: Down-hole logs, core scanning data and core photos. Geological Survey of Denmark and Greenland Report 2011/53, 1–18.
- Schovsbo, N.H. 2012: Completion report Billegrav-2 well (DGU 248.61) Part 3: Results of core plug analysis. Geological Survey of Denmark and Greenland Report 2012/16, 1–52.
- Schovsbo, N.H., Nielsen, A.T., Klitten, K., Mathiesen, A. & Rasmussen, P. 2011: Shale gas investigations in Denmark: Lower Palaeozoic shales on Bornholm. Geological Survey of Denmark and Greenland Bulletin 23, 9–12.
- Schovsbo, N.H., Esbensen, K.H., Nielsen, A.T., Derbez, E., Gaucher, E.C., Poirier-Coutansais, X., Riou, A., Tallone, P. & Milton-Taylor, D. 2015a: Rock types in the Scandinavian Alum Shale resource play: Definitions and predictions. 77th EAGE Conference & Exhibition 2015, IFEMA Madrid, Spain 1–4 June 2015. Extended abstract Th N101 13, 5 pp.
- Schovsbo, N.H., Nielsen, A.T. & Klitten, K. 2015b: The Lower Palaeozoic now fully cored and logged on Bornholm, Denmark. Geological Survey of Denmark & Greenland Bulletin 33, 9–12.
- Schovsbo, N.H., Nielsen, A.T. & Erlström, M. 2016: Middle–Upper Ordovician and Silurian stratigraphy and basin development in southernmost Scandinavia. Geological Survey of Denmark and Greenland Bulletin 35, 39–42.
- Schovsbo, N.H., Nielsen A.T., Harstad, A.O. & Bruton D.L. 2018: Stratigraphy and geochemical composition of the Cambrian Alum Shale Formation in the Porsgrunn core, Skien-Langesund district, southern Norway. *Bulletin of the Geological Society of Denmark* 66, 1–20.
- Spjeldnæs, N. 1963: Some upper Tremadocian graptolites from Norway. *Palaeontology* 6, 121–131.
- Spjeldnæs, N. 1985: Excursion-Guide Oslo. Graptolite Working Group of the International Palaeontological Association, Copenhagen 1985, 13 pp.
- Terfelt, F. 2006: Review of uppermost Furongian trilobites from Scania, southern Sweden, based on type material. *Palaeontology* 49, 1339–1355.
- Terfelt, F., Eriksson, M.E., Ahlberg, P. & Babcock, L.E. 2008: Furongian Series (Cambrian) biostratigraphy of Scandinavia - a revision. *Norsk Geologisk Tidsskrift* 88, 73–87.
- Terfelt, F., Ahlberg, P. & Eriksson, M.E. 2011: Complete record of Furongian polymerid trilobites and agnostoids of Scandinavia – a biostratigraphical scheme. *Lethaia* 44, 8–14.
- Terfelt, F., Eriksson, M.E. & Schmitz, B. 2014: The Cambrian–Ordovician transition in dysoxic facies in Baltica – diverse faunas and carbon isotope anomalies. *Palaeogeography, Palaeoclimatology, Palaeoecology* 394, 59–73.
- Tjernvik, T.E. 1958: The Tremadocian beds at Flagabro in south-eastern Scania (Sweden). *Geologiska Föreningens i Stockholm Förhandlingar* 80, 259–276.
- von Jansson, C. 1979: Zur biostratigraphie des Tremadociums auf Bornholm, Dänemark. Unpublished diplom thesis, 51 pp. University of Hannover.
- Warming, B., Buchardt, B., Nielsen, A.T., Pukkonen, E., Schovsbo, N.H. & Wilken, U.G. 1994: Geochemical database for Lower Palaeozoic rocks in Baltoscandia. Final report VI, Pre-Westphalian Source Rocks in northern Europe, 1–91. Geological Institute, University of Copenhagen, Denmark.
- Weidner, T. & Nielsen, A.T. 2013: The late Cambrian (Furongian) *Acerocarina* Superzone (new name) on Kinnekulle, Västergötland, Sweden. *GFF* 135, 30–44.
- Weidner, T. & Nielsen, A.T. 2014: A highly diverse trilobite fauna with Avalonian affinities from the Middle Cambrian *Acidusus atavus* Zone (Drumian Stage) of Bornholm, Denmark, *Journal of Systematic Palaeontology* 12, 23–92.
- Westergård, A.H. 1909: Studier öfver Dictyograptusskiffern och dess gränslager. *Lunds Universitets Årsskrift N.F.* 2, 5(3), 1–79. (Also printed in *Meddelande från Lunds Geologiska Fältklubb serie B* 4).
- Westergård, A.H. 1922: Sveriges Olenidskiffer. *Sveriges Geologiska Undersökning Serie Ca* 18, 1–205.
- Westergård, A.H. 1942: Stratigraphic results of the borings through the Alum Shales of Scania made in 1941–1942. *Lunds Geologiska Fältklubb* 185, 1–20.
- Westergård, A.H. 1944: Borringar genom Skånes alunskiffer 1941– 42. *Sveriges Geologiska Undersökning Serie C* 459, 1–45.
- Westergård, A.H. 1946: Agnostidea of the Middle Cambrian of Sweden. *Sveriges Geologiska Undersökning Serie C* 477, 1–140.
- Westergård, A.H. 1947: Supplementary notes on the Upper Cambrian trilobites of Sweden. *Sveriges Geologiska Undersökning Serie C* 489, 1–34.
- Westergård, A.H. 1948: Non-agnostidean trilobites of the Middle Cambrian of Sweden. I. *Sveriges Geologiska Undersökning Serie C* 498, 1–32.
- Westergård, A.H. 1950: Non-agnostidean trilobites of the Middle Cambrian of Sweden. II. *Sveriges Geologiska Undersökning Serie C* 511, 1–56.
- Westergård, A.H. 1953: Non-agnostidean trilobites of the Middle Cambrian of Sweden. III. *Sveriges Geologiska Undersökning Serie C* 526, 1–58.
- Yuanlong, Z., Jinliang, Y., Babcock, L.E., Qingjun, G., Jin, P., Leiming, Y., Xinglian, Y., Chunjiang, W., Gaines, R.R., Esteve, J., Ruidong, Y., Yuning, Y., Haijing, S. & Tongsu, T., submitted: Proposed global standard stratotype-section and point for the base of the Miaolingian Series and Wuliuan Stage (Provisional Cambrian Series 3 and Stage 5). Submitted to the International Subcommittee on Cambrian Stratigraphy. 51 pp.

Instructions to authors

The Bulletin publishes articles normally not exceeding 30 printed pages, and short contributions not longer than 4 pages. Longer articles and monographs are also published, but in this case it is advisable to consult the chief editor before submitting long manuscripts. Short contributions may be comments on previously published articles, presentation of current scientific activities, short scientific notes, or book reviews.

Manuscripts with complete sets of illustrations, tables, captions, etc., should be submitted electronically to the chief editor (lml@geus.dk). The **main text** with references and figure captions should be in Word format, figures should be in either pdf, jpeg, or tiff format, and tables should be in Excel or Word format. Word tables should be ordinary text files with tab spacing between table columns; Word's 'table function' is discouraged. Compare published articles for table layout.

Manuscripts will be reviewed by two referees; suggestions of referees are welcome. The final decision on whether or not a manuscript will be accepted for publication rests with the chief editor, acting on the advice of the scientific editors. Articles will be published in the order in which they are accepted and produced for publication.

Manuscript

Language – Manuscripts should be in English. Authors who are not proficient in English should ask an English-speaking colleague for assistance before submission of the manuscript.

Title – Titles should be short and concise, with emphasis on words useful for indexing and information retrieval. An abbreviated title to be used as running title may also be submitted.

Abstract – An abstract in English must accompany all papers. It should be short, factual, and stress new information and conclusions rather than describing the contents of the manuscript. Conclude the abstract with a list of key words.

Main text – Use 1.5 or double spacing throughout, and leave wide margins. Italics should be used only in generic and species names and in some Latin abbreviations (e.g. c, et al., ibid., op. cit).

Spelling – Geological units named after localities in Greenland, formal lithostratigraphical units and intrusions named after localities in Greenland remain unchanged even if the eponymous locality names have since been changed in accordance with modern Greenlandic orthography.

References to figures, tables and papers – References to figures and tables in the text should have the form: Fig. 1, Figs 1–3, Table 3 or as (Smith 1969, fig. 3) when the reference is to a figure in a cited paper.

References to papers are given in the form Smith (1969) or (Smith 1969). Combined citations by different authors are separated by a semicolon; two or more papers by same author(s) are separated by commas. Citations are mentioned chronologically and then alphabetically. Use 'et al.' for three or more authors, e.g. Smith et al. (1985).

Reference list

Use the following style:

Smith, A.A. 1989: Geology of the Bulbjerg Formation. Bulletin of the Geological Society of Denmark 38, 119–144. [Note that name of journal is given in full].

Smith, A.A., Jensen, B.B. & MacStuff, C.C. 1987: Sandstones of Denmark, 2nd edition, 533 pp. New York: Springer Verlag. [For more than 10 authors, use first author followed by *et al.*].

Smith, A.A., Jensen, B.B. & MacStuff, C.C. 1992: Characterization of Archean volcanic rocks. In: Hansen, D.D. *et al.* (eds): Geology of Greenland. Geological Survey of Denmark and Greenland Bulletin 40, 1397–1438. [More than three editors – therefore *et al.* form is used].

Sorting – Danish letters æ, ø and å (aa) are treated as ae, o and a (aa), respectively.

References are sorted by:

- 1: Alphabetically by the first author's surname
- 2: Papers by one author: two or more papers are arranged chronologically
- 3: Papers by two authors: alphabetically after second author's name. Two or more papers by the same two authors: chronologically.
- 4: Papers by three or more authors: chronologically. Papers from the same year are arranged alphabetically after second, third, etc. author's name.

Authors themselves are responsible for the accuracy and completeness of their references. The reference list must include all, and only, the references cited in the paper (including figures, tables etc).

Illustrations

May be prepared in either black and white or colour. There is no colour charge. Horizontal illustrations are much to be preferred. Size of smallest letters in illustrations should not be less than 5.5 pt. Remember scale.

All figures (including photographs) should be submitted in electronic form ready for direct reproduction, i.e. having the dimensions of the final figure with a standard resolution of 300 dpi for photographs. Preferred formats are pdf, tiff and jpg.

Size – The width of figures must be 82 mm, 120–150 mm or 170 mm. Maximum height is 223 mm.

Captions – Captions to figures and plates must be delivered on separate pages, preferably at the end of the manuscript.

Supplementary data files

Supplementary files are accepted. Such files may provide e.g. analytical data tables, detailed data documentation, illustrations with special effects, or videos.

Proofs

Authors receive page proofs of the article after technical production. The cost of any alterations against the final manuscript will be charged to the author.

Content, vol. 66

<i>Schovsbo, N.H., Nielsen, A.T., Harstad, A.O. & Bruton, D.L.:</i> Stratigraphy and geochemical composition of the Cambrian Alum Shale Formation in the Porsgrunn core, Skien–Langesund district, southern Norway.....	1
<i>Marzola, M., Mateus, O., Milàn, J. & Clemmensen, L.B.:</i> A review of Palaeozoic and Mesozoic tetrapods from Greenland	21
<i>Cuny, G. & Stemmerik, L.:</i> New fossil fish microremains from the Upper Carboniferous of eastern North Greenland.....	47
<i>Hovikoski, J., Pedersen, G.K., Alsen, P., Lauridsen, B.W., Svennevig, K., Nøhr-Hansen, H., Sheldon, E., Dybkjær, K., Bojesen-Koefoed, J., Piasecki, S., Bjerager, M. & Ineson, J.:</i> The Jurassic–Cretaceous lithostratigraphy of Kilen, Kronprins Christian Land, eastern North Greenland.....	61
<i>Bennike, O. & Mortensen, M.F.:</i> A multi-disciplinary macrofossil study of late glacial to early Holocene sediments from Sønder Kobbendam, Hareskovene, Denmark.....	113
<i>Erlström, M., Boldreel, L.O., Lindström, S., Kristensen, L., Mathiesen, A., Andersen, M.S., Kamla, E. & Nielsen, L.H.:</i> Stratigraphy and geothermal assessment of Mesozoic sandstone reservoirs in the Øresund Basin – exemplified by well data and seismic profiles	123
<i>Hjuler, M.L., Hansen, V.F. & Fabricius, I.L.:</i> Interpretational challenges related to studies of chalk particle surfaces in scanning and transmission electron microscopy	151
<i>Souza, P.E., Kroon, A. & Nielsen, L.:</i> Beach-ridge architecture constrained by beach topography and ground- penetrating radar, Itilleq (Laksebugt), south-west Disko, Greenland – implications for sea-level reconstructions.....	167
<i>Milàn, J., Rasmussen, E.S. & Dybkjær, K.:</i> A crocodylian coprolite from the lower Oligocene Viborg Formation of Sofienlund Lergrav, Denmark.....	181
<i>Glad, A.C., Willumsen, M.E., Boldreel, L. O. & Clemmensen, L.B.:</i> Meandering river deposits in sediment cores, the Middle Jurassic Alma Field, Southern Danish Central Graben	189
<i>Myrvold, K.S., Milàn, J. & Rasmussen, J.A.:</i> Two new finds of turtle remains from the Danian and Selandian (Paleocene) deposits of Denmark with evidence of predation by crocodylians and sharks.....	211
<i>Bennike, O.:</i> Book review: Oceans of Archaeology	219
<i>Weidner, T. & Ebbestad, J.O.R.:</i> <i>Anoplenus henrici</i> Salter, a middle Cambrian (Drumian) centropleurid trilobite from the Alum Shale Formation of Scandinavia.....	223
<i>Malchyk, O. & Machalski, M.:</i> First record of <i>Epicymatoceras vaelsense</i> (Nautilida) from the Maastrichtian white chalk of northern Denmark	229
<i>Nielsen, A.T., Schovsbo, N.H., Klitten, K., Woollhead, D. & Rasmussen, C.M.Ø.:</i> Gamma-ray log correlation and stratigraphic architecture of the Cambro-Ordovician Alum Shale Formation on Bornholm, Denmark: Evidence for differential syndepositional isostasy	237